158
9/28/79

LA. 124
MASTER



METC/SP-79/6

PROCEEDINGS

THIRD EASTERN GAS SHALES SYMPOSIUM

October 1-3, 1979

Hilma Barlow, *Editor*

UNITED STATES DEPARTMENT OF ENERGY
Morgantown Energy Technology Center
Morgantown, West Virginia

TECHNICAL INFORMATION CENTER
UNITED STATES DEPARTMENT OF ENERGY

DISCLAIMER

This report was prepared as an account of work sponsored by an agency of the United States Government. Neither the United States Government nor any agency thereof, nor any of their employees, makes any warranty, express or implied, or assumes any legal liability or responsibility for the accuracy, completeness, or usefulness of any information, apparatus, product, or process disclosed, or represents that its use would not infringe privately owned rights. Reference herein to any specific commercial product, process, or service by trade name, trademark, manufacturer, or otherwise does not necessarily constitute or imply its endorsement, recommendation, or favoring by the United States Government or any agency thereof. The views and opinions of authors expressed herein do not necessarily state or reflect those of the United States Government or any agency thereof.

DISCLAIMER

Portions of this document may be illegible in electronic image products. Images are produced from the best available original document.

NOTICE

This report was prepared as an account of work sponsored by the United States Government. Neither the United States nor the United States Department of Energy, nor any of their employees, nor any of their contractors, subcontractors, or their employees, makes any warranty, express or implied, or assumes any legal liability or responsibility for the accuracy, completeness or usefulness of any information, apparatus, product or process disclosed, or represents that its use would not infringe privately owned rights.

This report has been reproduced directly from the best available copy.

Available from the National Technical Information Service, U. S. Department of Commerce, Springfield, Virginia 22161.

Price: Paper Copy $15.50
Microfiche $3.00

METC/SP-79/6
Distribution Category UC-92

NOTICE

This report was prepared as an account of work sponsored by the United States Government. Neither the United States nor the United States Department of Energy, nor any of their employees, nor any of their contractors, subcontractors, or their employees, makes any warranty, express or implied, or assumes any legal liability or responsibility for the accuracy, completeness or usefulness of any information, apparatus, product or process disclosed, or represents that its use would not infringe privately owned rights.

PROCEEDINGS

THIRD EASTERN GAS SHALES SYMPOSIUM

October 1-3, 1979
Lakeview Inn
Morgantown, West Virginia

SPONSORED BY

Morgantown Energy Technology Center
and
Eastern Section, American Association of Petroleum Geologists

Hilma Barlow, *Editor*

TABLE OF CONTENTS

GENERAL SESSIONS	Page
"The New Economics of Natural Gas Production in the Appalachian States" W. Gibson Jaworek	1
"Status Report of the Eastern Gas Shales Project" R.L. Wise	3
"Constraints and Problems in Producing Gas From Eastern Shales" Walter Rose	15
"Recovery of Energy From Michigan Antrim Shale by an In Situ Process" L.J. Washington	23
"A Suggested Origin for the Gas in Eastern Devonian Shales" Irving Breger	25
"Gas Content and Transport in Shale and Their Implications for Well Productivity" Paul Schettler, Jr.	27
"Exploration Strategy for an Unconventional Natural Gas Resource: Devonian Shale" C.S. Dean and W.K. Overbey, Jr.	35
"Digital Image Processing and Enhancement of Landsat Data for Lineament Mapping and Natural Gas Exploration in Appalachian Region" Thomas F. Wescott and Alan F. Smith	37
"Late-Tectonic Faulting in the Central Appalachians" P.S. Berger and R.L. Wheeler	51
RESOURCE CHARACTERIZATION SESSION	
"A Petrologic Evaluation of the Significance of Natural Fractures in Low Porosity Shale Gas Reservoirs - Results of Investigation in the Upper Devonian of Virginia and West Virginia" Robert Vinopal, Edward Nuhfer, and David Klanderman	63
"Pressure Coring of the Gas-Bearing Devonian Black Shales, Erie Co., Pennsylvania" R.E. Zielinski, J.A. Dixon, R.D. McIver, and A.E. Hunt	79
"Gas-Bearing Ohio Shale Along Lake Erie: Stratigraphy, Petrology, and Sedimentology" R.F. Broadhead, R.C. Kepferle, and P.E. Potter	81
"A Current Assessment of the Physiochemical Characterization Data for the Eastern Gas Shales" S.W. Nance, P.W. Seabaugh, and R.E. Zielinski	83
"Petrology and Maturation of Dispersed Organic Matter in the New Albany Shale Group of the Illinois Basin" Mary Barrows, Robert Cluff, and Richard Harvey	85

TABLE OF CONTENTS (con't.)

	Page
RESOURCE CHARACTERIZATION SESSION (con't.)	
"Devonian Shale - An In-Depth Analysis of Well EGSP NY No. 1 With Respect to Characterization, Hydrocarbon Gas Content and Wire-Log Data" R. S. Kalyoncu, J. P. Boyer, and M. S. Snyder	115
"Inorganic Geochemical Studies of Eastern Kentucky Gas Field(s) and Comparison with Gas Production" Jane Negus-de Wys, and John J. Renton	165
"Pyrolysis of Eastern Gas Shales: Effects of Temperature and Atmosphere on the Production of Light Hydrocarbons" Mei-In M. Chou and D. R. Dickerson	211
EXTRACTION TEHCNOLOGY R&D SESSION	
"Theoretical and Experimental Analyses of Hydraulic Fracturing" G.D. Anderson, M.E. Hanson, R. J. Shaffer	225
"Modeling of Devonian Shale Gas Reservoir Performance" Fikri Kucuk and Walter Sawyer	247
"Lineaments and Ground-Water Chemistry as Exploration Tools for Devonian Shale Gas in the Mid-way Extra Field of West Virginia" R. R. Beebe, and H. W. Rauch	277
"Interpretation and Statistical Analysis of Kentucky-West Virginia Open Flow Data, Incorporating Geochemical Information" P. W. Seabaugh, R. E. Zielinski, and C. A. Komar	291
"In Situ Testing of Well-Shooting Concepts" R. A. Schmidt, N. R. Warpinski, and D. A. Northrop	293
"Principle Considerations Governing Hydraulic Fracture Propagation in Eastern Gas Shales" S. H. Advani and C. A. Komar	303
"Cross-Strike Structural Discontinuities: Their Use in an Exploration Rationale for Eastern Plateau Province, Appalachian Basin" L. Wheeler	305
TECHNOLOGY TESTING SESSION	
"Cottageville Gas Field Correlation Analyses for Reservoir Modeling" T. E. Springer and E. B. Nuckols	317
"Lithology Studies of Upper Devonian Well Cuttings in the Eastern Kentucky Gas Field" Jane Negus-de Wys	331

TABLE OF CONTENTS (con't.)

TECHNOLOGY TESTING SESSION (con't.)	Page
"Unconventional Evaluation of the Cottageville Devonian Shale Field, Jackson and Mason Counties, West Virginia" **W.M. Hennington**	371
"Projection of Favorable Gas-Producing Areas from Paleoenvironmental Areas" **R.E. Zielinski, J.A. Dixon, and R.D. McIver**	385
"The Characterization of the Production Mechanism in the Devonian Shale and Its Sensitivity to Change in Various Reservoir Parameters" **W.K. Ford**	387
"The Interaction of Proppants with Crack Formation and Propagation in Hydraulic Fracturing" **S.L. McHugh, P.E. Senseny, D.D. Keough, and A.L. Florence**	401
"Past & Current Developments for Drilling New Albany Shale Gas in Western Kentucky" **Julian Duffy and Howard Schwalb**	403
OTHER PAPERS	
"The Parsons Cross Strike Structural Discontinuity as an Exploration Area for Fractured Gas Reservoirs" Jeanette M. Dixon and Thomas H. Wilson	407
"The Effect of Explosive Gases on the Fracture Process in Geologic Solids" S. McHugh and D. Keough	415
"Cross-Polarization Carbon -13 NMR of Kerogens from Devonian Shale and Coal" Stephen K. Beer and Larry C. Headley	425
"Compositional Variations in a Fabric-Element Based Lithologic Type Classification for Devonian Shale David S. Klanderman and Michael Ed. Hohn	433
"Regional Survey of Surface Joints in Eastern Kentucky" Brian R. Long	445
"Parameters of Geologic Structure Which Affect Devonian Gas Shale Production in West Virginia and Eastern Kentucky - A Progress Report 1978-1979" R. C. Shumaker, R. R. Beebe, J. Negus-de Wys, J. M. Dixon, M. A. Evans, K. G. Kirk, K. D. Lee, H. W. Rauch, J. E. Ruotsala, W. W. Schaffer, R. L. Wheeler, R. T. Williams, T. H. Wilson.	451

TABLE OF CONTENTS (con't.)

OTHER PAPERS (con't.)	Page
"Effects of Aqueous Carbon Dioxide on Devonian Shales" J. F. Miller, J. P. Boyer, S. J. Kent, M. J. Snyder, and J. C. Sharer	473
"A Fabric-Element Based Classification for Low-Porosity-Shale Gas Reservoirs" E. B. Nuhfer and R. J. Vinopal	485
"The Elucidation of Geomatrices by Laser Pyrolysis/Gas Chromatography and Pyrolysis/Mass Spectrometry" N. E. Vanderborgh and C. R. Johns	499
"Distribution and Geochemical Characterization of the Hannibal Member of the New Albany Shale in Indiana" P. J. Lechler, N. R. Hasenmueller, J. L. Bassett, and R. K. Leininger	511
"Acoustic and Mechanic Analysis of a Transverse Anisotropy in Shale" D.D. Miller and R.J.E. Johnson	527

THE NEW ECONOMICS OF NATURAL GAS PRODUCTION IN THE APPALACHIAN STATES

W. Gibson Jaworek
Consultant
Washington, D.C.

ABSTRACT

Since at least 1920, production of natural gas in the Appalachian states has fluctuated between 400 and 500 billion cubic feet per year. Among the factors limiting expansion in drilling, recompletion of old wells, and introduction of new technology, such as that applicable to Devonian shale, has been the adverse wellhead prices paid to producers by purchasers under regulations applied by the federal government under the Natural Gas Act of 1938.

After long debate and apparent deadlock, the Congress passed The Natural Gas Policy Act of 1978. The provisions of the Act include incentive pricing for stripper wells, for deep drilling, and the deregulation of all sales of gas from Devonian shale beginning November 9, 1979. Other aspects of the legislation, when fully implemeted, should allow greater freedom to producers to bargain fairly with purchasers of natural gas in most curcumstances.

An analysis of the Act is presented from the point of view of its potential impact in spurring research efforts to commercialize natural gas production from Devonian shale and other unconventional sources, as well as accelerating exploration and development from conventional reservoir targets in the Appalachian region.

Finally, projections are presented comparing future prices and costs of Appalachian gas with costs of supplies from the Southwest, the Arctic and foreign LNG, together with synthetic fuels. It is concluded that the "new economics" of Appalachian natural gas can revitalize the industry within the next decade, and provide a regional solution to the predicted national energy supply deficit in the 1980's.

Note: Paper not available at time of publication.

STATUS REPORT OF THE

EASTERN GAS SHALES PROJECT

Robert L. Wise
Acting Project Manager

Eastern Gas Shales Project
Morgantown Energy Technology Center, WV



ABOUT THE AUTHOR

Robert L. Wise is the Project Manager for the Methane Recovery from Coalbeds and the Eastern Gas Shales projects at the Department of Energy's Morgantown Energy Technology Center, Morgantown, West Virginia. The Center is engaged in the management, research and development of projects associated with the recovery of energy values from oil, gas and coal resources.

Mr. Wise earned a Bachelor of Science degree in Chemical Engineering from the University of Wyoming. Prior to joining the Morgantown Energy Technology Center, he worked as a consulting engineer with the Denver Research Institute and as a senior engineer with the Laramie Energy Technology Center. He was also involved in oil shale research and was a plant metallurgist for the molybdenum and uranium minerals industries.

Mr. Wise is a past member of the Veterans Honorary Society. He is the author of many technical articles dealing with unconventional gas and oil shale research activities.

ABSTRACT

Unconventional sources of natural gas already provide over 1 TCF annually to domestic gas production and could ultimately provide a much larger share of the natural gas supply. As a result of the studies being carried out through the Eastern Gas Shales Project (EGSP), the eastern Devonian Shales should make a significant, near-term contribution to the nation's natural gas supply.

This paper presents project progress and status of field and laboratory studies for the Resource Characterization, Extraction Technology R&D, Technology Testing and Verification and Project Integration aspects of the EGSP.

INTRODUCTION

Natural gas accounts for about one-fourth of the nation's energy requirements. In recent years, demand for natural gas has been restrained to the level of available supply by non-market factors such as residential hook-up moratoria, regulations on industrial and electric utility use and, in extreme cases, curtailments. Recent projections agree that while constrained gas demand will remain at the current level of about 20 TCF at least through the 1990s, unconstrained demand could reach 25-30 TCF by 1990. Thus, gas consumption is expected to hold constant or to increase, depending on availability of supply and gas-use regulations.[1]

However, domestic production and reserves--dominated by conventional gas resources--have declined steadily. Production in 1978 was 19.3 TCF, down from the 1973 peak of 22.6 TCF. Reserves have dropped to 200 TCF from their 1967 peak of 293 TCF. Reserve additions (excepting Prudhoe Bay) have replaced only 46% of withdrawals during the 1970s.[1]

This serious decline in production and reserves has continued despite a nearly tripling of average natural gas price (in real terms) since 1973, the emergence of still higher price intrastate markets, and a corresponding doubling of exploratory effort.

The four Unconventional Gas Recovery projects (Eastern Gas Shales Project, Western Tight Gas Sands, Methane Recovery from Coalbeds Project, and Geopressured Aquifers) carried out by US DOE may contribute to near-term domestic gas supply while the longer term alternatives are being developed by government and industry. Approximately 0.1 TCF/year is already being produced from the eastern Devonian Shale formations. The outcome of the EGSP should be a substantial increase in both yearly production and proved reserves.

The EGSP is beginning the fourth full year of a planned eight year program. The primary objective of the project is to stimulate the private sector to develop the gas resource contained in the shales of the Appalachian, Illinois and Michigan Basins (Figure 1). US DOE, USGS, state geological surveys, universities, national laboratories, private industry and oil and gas operators are cooperating to establish and exploit the gas potential of the Devonian Shales.

The Eastern Gas Shales Project is a planned sequence of activities divided into the following four categories:

Resource Characterization and Inventory

- Geological, geochemical, and physical characterization of the shale.
- Inventory of natural gas and other hydrocarbon resources and determination of the economically recoverable resource.
- Identification of new exploration techniques for fractured shale reservoirs.

Extraction Technology Research and Development

- Laboratory research and modeling to predict technology required for effective gas recovery.
- Development of stimulation and extraction methods for improving the rate of gas recovery and ultimate gas recovery.

Technology Testing & Verification

- Field testing to demonstrate viability of new exploration and extraction technologies in various geologic provinces.

Project Integration

- Economic analysis of new technologies.
- Assessment of potential environmental effects.
- Transfer of technology.

The discussion of technical progress in each of these four categories will be directed primarily toward the significance of accomplishments. More detailed technical discussions will be presented by the investigators in reports either formally published or in the open file.

DISCUSSION OF TECHNICAL PROGRESS

Resource Characterization and Inventory

Approximately 16,906 feet of Devonian Shale core has been collected for physical and geochemical analysis and stratigraphic interpretations (Figure 2)--seven WV cores, eight Tennessee cores (non-oriented), four in KY, three in OH, two in PA, one in NY, one in VA, four in IL, and two in IN.[2] Initial efforts have been completed to define the logging suite which will yield optimum formation evaluation data at a minimum cost. This preliminary suite consists of the following logs:[3]

- Gamma ray
- Compensated bulk density
- Induction
- Temperature
- Sibilation* (*Trademark of Birdwell Division of Seismograph Service Corp.)

This suite is presented as only a preliminary attempt at defining the most useful logs available to the operator. The suite is, of course, subject to modification by the individual operator and investigator, future analysis of additional log data, and the proven utility of other logging tools and techniques.

All basic geologic mapping is nearing completion in the Appalachian and Illinois Basins. In the Michigan Basin, the geologic mapping efforts are being directed under a study separate from the EGSP by Dow Chemical Company and the mapping is scheduled for completion by the end of Fiscal Year 1980.

State geological surveys and the USGS have been cooperating in the generation of both interlocking state-specific geologic cross sections and more regional cross sections over the entire Appalachian and Illinois Basins and part of the Michigan Basin. Six regional cross sections covering the Appalachian Basin have been completed and put on open file. Over sixty additional sections have been completed in the three basins. Nine state-specific cross sections have been published for western Pennsylvania and are available through the Morgantown Energy Technology Center. All cross sections and maps are being published for distribution as they become available from the various contractors.

State-specific isopach maps of the main radioactive shale units in the Appalachian and Illinois Basins are approximately seventy-five percent completed and should be finished by the end of this fall. These maps will then be compiled into basin-wide maps and used in conjunction with the determination of the gas volume present in the Devonian Shale to identify regions of high production potential.

Results of structural studies as done at the Cottageville Gas Field in western West Virginia indicate that the development of fracture facies, so critical in gas production from the shales, may be related to fault movements in the basement (Rome Trough) structure.[4] If this relationship is

subsequently proven, the occurrence of porous fractions associated with these features (slickensides and natural fractures) may be predicted. Natural porous fracture systems are primary exploration targets in maximizing gas production from the Devonian Shales.

Preliminary interpretations of the relationship of gas occurrence to various geologic parameters in the eastern Kentucky Gas Fields (Big Sandy) are being developed. Initial results indicate that production from the fields is related to preferential fracture directions. The preferential fracture directions suggest that they could be related to tensional stresses associated with thrust faulting and faulting in the basement rocks.[5]

Bulk density of an individual shale sample shows an inverse correlation to gas volume and gamma ray intensity.[6] Therefore, high gas zones in the shale may be indicated by a combination of gamma ray intensity and bulk density logs. However, inspection of just these two logs will not, in most cases, indicate the presence of natural fractures that are needed for the economic production of the gas.

The mineralogy of the shale is relatively constant on samples and wells tested to date. The major components are quartz and the clay material illite.[2] Organic rich intervals have been shown to be relatively insensitive to water contact for short contact times but organic lean shale intervals are sensitive. In the latter case, usually a 2% KCl solution is required for logging or fracturing.

Approximately twelve analytical tests have been identified as providing the most useful data to measure the gas resource. These tests include: outgassing volume, kinetics, C_1-C_7, visual kerogen, TAI, Ro, density, four elements - U, Th, V, Ni, adsorption isotherms, permeability, total carbon, and organic carbon.[7]

Mean gas content for the wells tested ranged from 0.003 to 1.110 cu. ft. gas per cu. ft. shale and averages 0.42 cu. ft. gas per cu. ft. shale in the Appalachian Basin and 0.36 in the Illinois Basin. The Illinois Basin wells have less gas and a lower percentage of lighter hydrocarbons than the Appalachian Basin wells.[8,9]

An EGSP contractor has determined that gas well and water well yields in the Midway-Extra Field study area of West Virginia are related to photolineament density. Short lineaments may represent near-surface zones of enhanced permeability that are about 400 feet wide, with permeability becoming greater as a photolineament's center line is approached.[10] A completed study shows that photo traces or lineaments are also indicators of better well locations in the Big Sandy extension field of Eastern KY.[11] Therefore, pilot data suggest that fracture traces from photolineaments should be considered for increasing the likelihood of encountering reservoir capacity.

Future plans include collecting up to twenty-one cores from selected sites in the Appalachian, Illinois, and Michigan Basins (Figure 3); concluding the basic geologic mapping of the shales; continuing to run selected physical and geochemical analyses on the retrieved cores; modifying existing and developing new exploration techniques to locate gas-filled natural fracture systems; and determining a realistic resource estimate for the Devonian Shale gas. It is currently anticipated that all geologic mapping and structural evaluations will be completed by the end of FY80, although the majority of this work will be completed by the end of FY79. The remaining activities are scheduled through the middle of FY81.

Extraction Technology Research and Development

The EGSP deviated well, drilled by Consolidated Gas Supply Corp., in the Cottageville Field, WV was completed in late 1978. The well tested an IOF of 1.5 million SCFPD after penetrating only 30 feet vertically into the Lower Huron zone. Subsequent drilling operations resulted in an influx of water believed to be from a lower formation which drowned out the gas. Workover activities to shut off the water have not been successful and the well has been classified as a non-economical gas well.

The use of directional drilling in the shales at this point needs several more tests to establish definitely the techniques for drilling. After the technology is established, the economics can be projected with some degree of assurance. A potentially useful application of directional drilling in the shale is to drill in areas where other complications preclude conventional stimulation technology application.

Research continued during FY79 to evaluate conventional stimulation techniques (hydrofrac and borehole shooting) and to compare these treatments with newer techniques (foam frac and cryogenic frac). The work includes fluids, treatment sizes, injection rates, proppant injection rates, proppant sizes, cleanup rates and initial open flow rates before and after stimulation and second year production rates.

The early goal established for the stimulation evaluation work was to increase the initial production rate from about 100 MCFPD to 300 MCFPD. While the much needed knowledge base was being built over the last 3½ years, which would allow more intelligent stimulation design, a number of tests were conducted in different areas to collect pilot data and to assess the difficulty of the problem. During this period, 42 stimulations have been conducted in 26 wells. The results of these stimulations are summarized in Table 1. Additional stimulation tests will be carried out during FY80.

As a result of this stimulation evaluation work, several problems were identified and some significant conclusions have been reached:[12]

- Hydraulically fractured wells will produce considerably more gas than conventional shot wells (perhaps 200 to 300 MMCF additional in 30 years).
- Energy assist fracturing fluids are warranted for low pressure fractured reservoirs.
- Limited entry in selected intervals with an energy assisted fracturing fluid is the preferred stimulation design.
- Large volume treatments do not necessarily increase production proportionately.
- Results of liquid explosive technology are encouraging but as yet require further development.
- Directionally deviated well technology is achievable but additional demonstrations are warranted in other regions to complete an economic assessment.
- Organic lean intervals can restrict induced fracture growth vertically at low propagating pressures.
- Stress ratio (minimum horizontal/vertical) is an estimator of reservoir fracture intensity.
- Effectiveness of Landsat and U-2 imagery is of little consequence in siting wells.
- Clay swelling in the shale may be effectively minimized by the use of non-wetting foam.[13]
- Location of regions of increased fracture intensity is required to assure likelihood of a commercial well.
- Normal reservoir pressure tests provide little useful data on hydraulically fractured shale well effectiveness.
- Factors affecting shale production appear to be strongly associated with frac length and formation permeability.

The effectiveness of a dual completion scheme to enhance the economics of shale gas production is being tested in Trumbull County, OH. One well was drilled to evaluate both the Devonian Shale and the Clinton Sandstone. The well was tested in the shale, but completed only in the Clinton since the shale section was non-productive. A detailed exploration program to optimize exploration locations is now being carried out, prior to the resumption of drilling.

Modeling of the Devonian Shale production mechanisms and overall reservoir behavior continued to make progress during the past year. The main effort has been toward interpreting production, diffusion and adsorption isotherm data to resolve the question of whether single or multiple porosity systems control reservoir production and particularly to determine the timing and amount of the contribution of matrix gas to cumulative production during the life of a well.

Technology Testing and Verification

During FY79, large scale field programs to test the most promising exploration and stimulation techniques for Devonian Shale gas were initiated. Four contractors are currently carrying out these DOE-industry cost-sharing programs:

Columbia Gas System Service Corp. - A total of ten wells will be drilled in Lorain and Trumbull Counties, OH. This contract is a test of the relative effectiveness of stimulation techniques in increasing gas production. The testing of two stimulation techniques per area is planned. Drilling of the first well began in late summer, 1979.

Donohue, Anstey and Morrill - This contract will test a new exploration technique using surface measurements of seismic velocity to locate zones (velocity lows) of natural fractures in the Devonian Shales of south-eastern Ohio. A total of three wells will be drilled and completed to test the technique. The velocity analysis has been completed. Drilling of the first well is scheduled for the late summer or early fall, 1979.

Mitchell Energy Corp./Columbia Gas System Service Corp. - This contract will test a new exploration theory for locating gas-filled fractured reservoirs. The theory being tested proposes that the locations of naturally fractured reservoirs in the shale are related to the structure at the time of deposition. This concept is based on the depositional model for clastic sedimentation. During deposition, sediment sorting by wave action leaves coarser, less compactible material on the depositional highs, with finer more compactible muds and organic debris being washed onto the flanks and into the lows. In this situation, differential compaction will create "natural compaction fractures" along the flanks of the depositional highs. The new exploration technique consists of two steps: (1) the approximate depositional structure will be obtained through a subtle process termed "Reconstruction of Depositional Structure". This process interrelates subsurface structure, porosity and production information in order to determine and remove from the present day structure the distortion which has occurred from the time of deposition to the present; (2) the resulting depositional structure is analyzed and areas with high potential for natural fractured reservoir development are located.

A total of 11 wells will be drilled, and a program recommended for large scale, economical development of the Ohio Devonian Shale reserves. To date, a seismic survey of the study area, the depositional structure reconstruction, and well site selection have been completed. The first wells are scheduled to be drilled in late summer, 1979.

Thurlow Weed and Associates, Inc. - This contract will result in the drilling, coring and completion of a well in Knox County, OH, and the stimulation of an additional three existing wells to test various stimulation techniques. The test well has been drilled and is awaiting stimulation. A total of 700 feet of Devonian Shale core was recovered from the well, and is now being analyzed. The three existing wells have been logged and stimulation treatments are being designed.

Project Integration

An environmental impact study for the entire EGSP has been completed. The assessment of potential environmental effects which could result from individual well site activities continues to be made as needed.

Economic analyses are being carried out by the EGSP in order to determine the best combination of exploration and extraction techniques for the Appalachian, Illinois and Michigan Basins.

The technology being developed through the EGSP is continually being transferred to the private sector through symposia, the Unconventional Gas Recovery Open File, Semi-Annual Reports, Technology Information newsletters, professional publications, and by presentations to state oil and gas associations.

SUMMARY

The Resource Characterization of the Devonian Shales will be largely completed by the end of FY80. A detailed geological, geochemical and physical data base will have been established for the eastern Devonian Shales. These data will be used to develop new exploration rationales and techniques for locating gas-filled, fractured shale reservoirs and to determine the amount of the tota gas resource and recoverable reserves of the shale formations.

The Extraction Technology R&D studies are determining the production mechanisms for shale gas production and a quantitative description of the effects of stimulation treatments.

Field activities of the Technology Testing and Verification portion of the EGSP are currently validating exploration and stimulation schemes for the Ohio Devonian Shale formations. The schemes should be directly applicable to most other areas underlain by the eastern Devonian Shales.

Project Integration activities are ensuring that the environmental effects of shale gas exploration and extraction are minimized, as well as providing analyses to determine the most cost-effective means of exploiting the shale gas.

As a result of the studies being carried out through the EGSP, the eastern Devonian Shales should make a significant, near-term contribution to the nation's natural gas supply.

REFERENCES

1. "Draft US DOE Resources RD&D Management Plan", 1979.

2. "EGSP Facts, Update No. 14, August 1, 1979", DOE/Morgantown Energy Technology Center, 1979.

3. Curtis, J. B. and Fingleton, W. G.: "A Preliminary Evaluation of Various Log Analysis Techniques for the Eastern Devonian Shales", Paper I, Society of Professional Well Log Analysts 20th Annual Logging Symposium, Tulsa, Oklahoma, June 3-6, 1979.

4. Nuckols, E. B.: "The Cottageville Gas Field, Jackson County, West Virginia: a Case Study of Devonian Shale Gas Production", West Virginia University draft report submitted to DOE/METC under Contract No. DE-AC21-76MC05194, 1978.

5. de Wys, J. N., and Shumaker, R. C.: "Relations of Gas Occurrence to Geologic Parameters in Eastern Kentucky Gas Fields", abstract, American Association of Petroleum Geologists, Vol. 63, No. 3, March 1979, p. 502.

6. "Eastern Gas Shales Project Annual Report, Fiscal Year 1977", DOE/Morgantown Energy Technology Center, 1978, p. 40.

7. Streib, D. L., Personal communication, Science Applications, Inc., August 1979.

8. "Draft Semi-Annual Report for the Unconventional Gas Recovery Program, Period Ending September 30, 1978", DOE/Morgantown Energy Technology Center, 1978, p. 59-121.

9. Howard, J. F.: "Devonian Shale Production in the Illinois Basin", manuscript presented at the Kentucky Oil and Gas Association, June 1978.

10. Shumaker, R. C., de Wys, J. N., Dixon, J. M., Evans, M. A., Kirk, K. G., Lee, K. D., Long, B. R., Rauch, H. W., Routsala, J. E. and Wilson, T. H.: "Structural Parameters that Influence Devonian Shale Gas Production in West Virginia and Eastern Kentucky", West Virginia University monthly report submitted to DOE/METC under Contract No. DE-AC21-76MC05194, February 1979.

11. Howard, J. F.: Final report submitted to DOE/METC under Contract No. EY-78X210139, April 1979.

12. Komar, C. A.: "Eastern Gas Shales Project, Extraction Technology R&D", presented at the Fossil Energy Unconventional Gas Recovery Project Review, US DOE, Morgantown, West Virginia, June 12-14, 1979.

13. Komar, C. A., Yost, A. B., and Sinclair, A. R.: "Practical Aspects of Foam Fracturing in the Devonian Shale", SPE Paper 8345, 54th Annual Fall Technical Conference and Exhibition, SPE, Las Vegas, Nevada, September 23-26, 1979.

TABLE 1

RESULTS OF DOE STIMULATION
TESTS IN DEVONIAN SHALE WELLS

	Treatment	Well	Zones Treated	Total Treatment Size (gal)	Open Flow Potential After Test (MCFPD)
		LIMITED ZONE PROCESSES			
1	Hydrofrac	Minard Run	1	N/A	Mech Failure
2	MHF	CGS 20401	4	837,000	322
3	MHFF	CGS 20403	4	1,263,000	381
4	MHFF	CGS 20402	2	300,000	145
5	MHFF	Peoples Gas	1	N/A	Mech Failure
6	MHFF	Consol 12041	1	163,000	173
7	CO_2	Reel Energy	2	N/A	Made Water
8	CO_2	MERC 1	2	155,000	N/A
9	CO_2	CGS 11236	2	231,000	36
10	CO_2	CGS 20338T	2	210,000	150
11	CO_2	CGS 20337	2	83,300	133
12	CO_2	CGS 20336	2	126,000	620
13	CO_2	CE Power	1	80,000	25
14	Foam	KWV 7239	4	183,000	60
15	Foam	KWV 7246	1	50,000	337
16	Foam	Ray Clark 1	1	50,800	2
17	Foam	KWV 1627	1	50,800	103
18	Foam	Welch 1-15	1	46,000	550
19	Foam	Consol Deviated	1	50,000	12[1]
20	Foam	Ashland 3-RS	1	18,750	43
21	Foam	Tetra Tech Shaf 1	1	N/A	0
		UNLIMITED ZONE PROCESS			
22	CEF	PTC 686-1	Open Hole	3,000	260
23	CEF	PTC 686-2	Open Hole	3,000	300
24	CEF	PTC 686-3	Open Hole	3,000	310
25	CEF	PTC 685-2	Open Hole	3,000	350
26	CEF	PTC 685-3	Open Hole	3,000	350

[1]Formation water influx. IOF pre-stimulation was 1.5 MMCFD (See text).

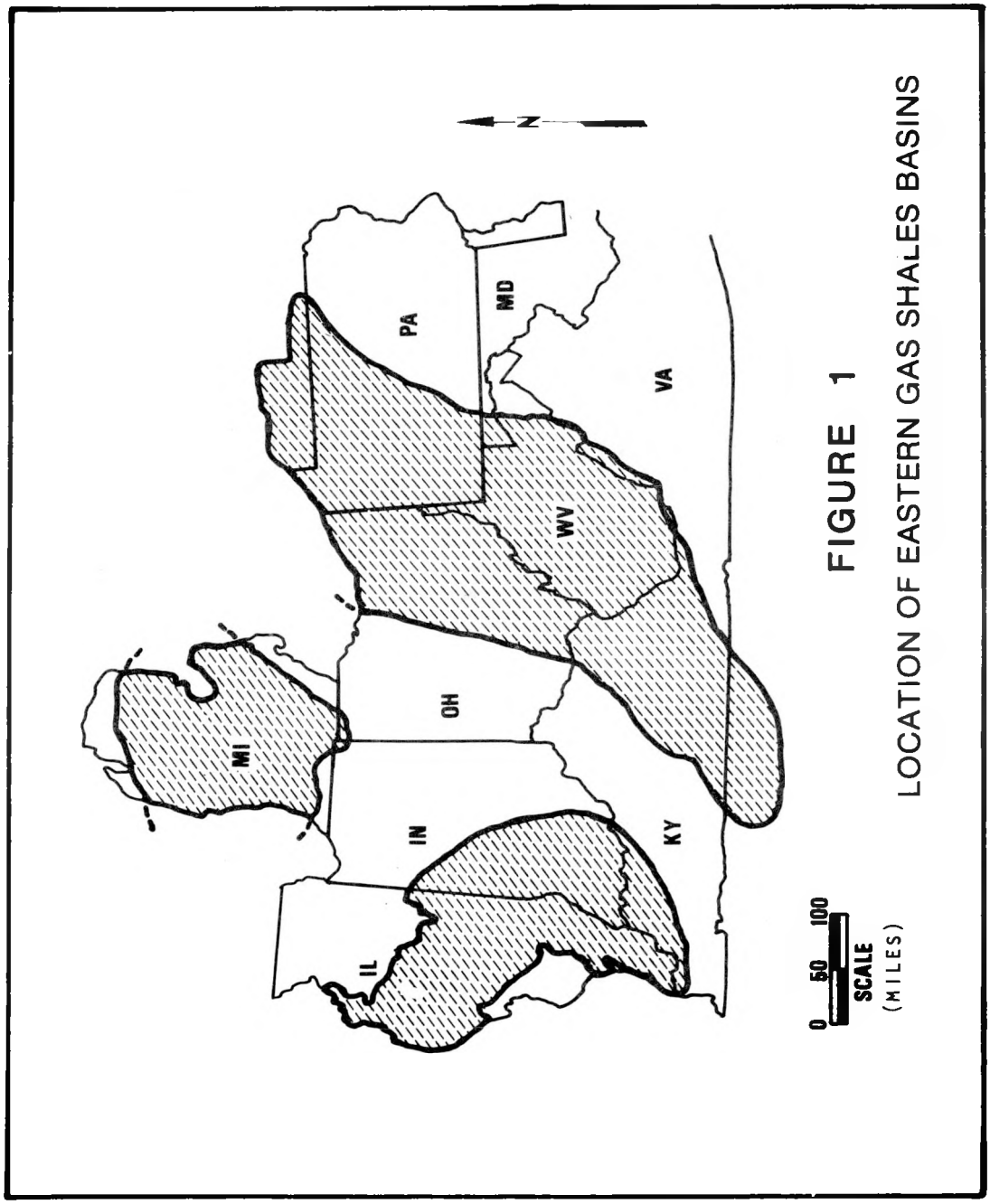
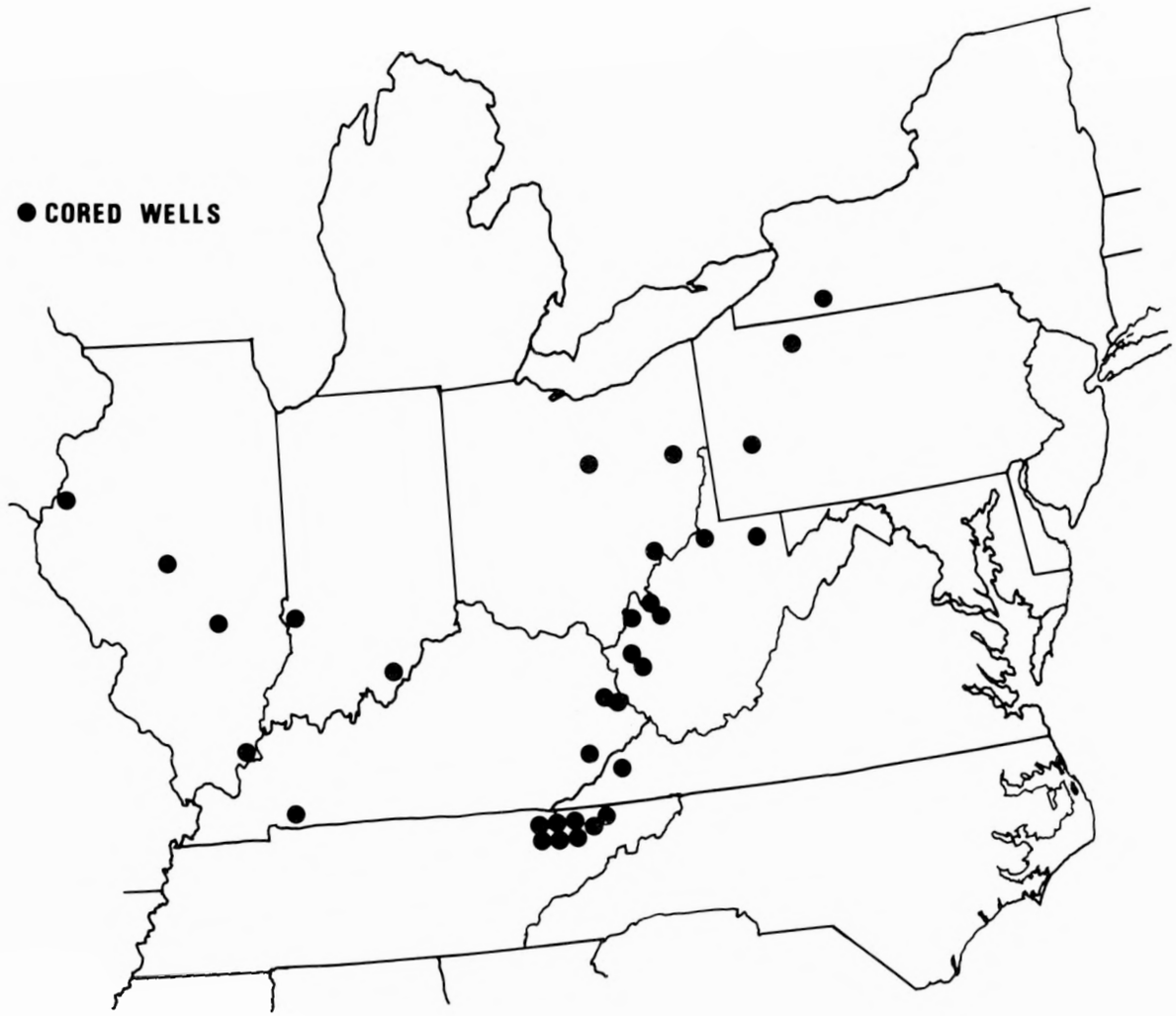


FIGURE 1

LOCATION OF EASTERN GAS SHALES BASINS

FIGURE 2

EGSP CORE WELL LOCATIONS



EGSP PLANNED OR PROPOSED CORE LOCATIONS

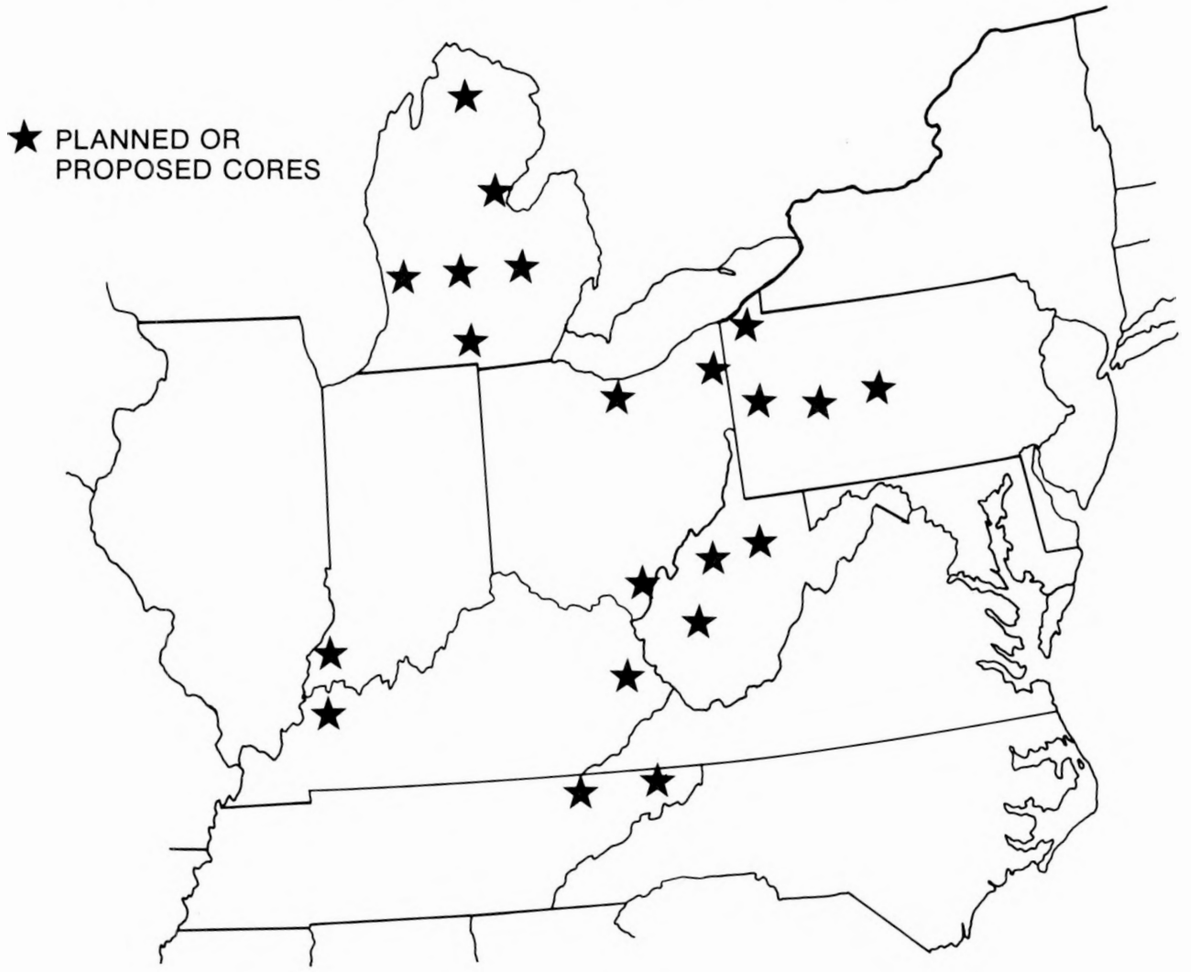
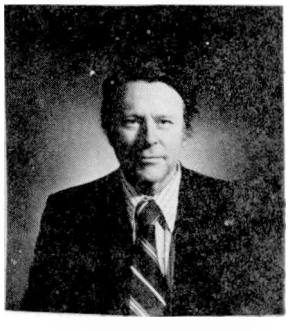


FIGURE 3

CONSTRAINTS AND PROBLEMS IN PRODUCING GAS FROM EASTERN SHALES

Walter Rose

Science Applications, Inc.



ABOUT THE AUTHOR

Mr. Rose has been writing papers on petroleum economics and reservoir engineering since the 1940's. Only lately has he had the opportunity to study the question of gas production from the Eastern shale provinces, and the present paper is a statement of some of the conclusions reached in that inquiry.

2 CONSTRAINTS AND PROBLEMS IN PRODUCING GAS FROM EASTERN SHALES

ABSTRACT

The enormous gas resource locked in the various Devonian and Mississippian shale layers of the major Eastern geologic basins naturally attracts the interest of energy policy makers and commercial entrepreneurs who are motivated to see and participate in the exploitation of that fraction which can be easily recovered. To succeed in this endeavor, however, certain bothersome constraints have to be faced, and other nagging problems have to be resolved. The aim of this paper is to classify the constraints and to identify the problems so that they can be dealt with systematically. The mode selected for doing this is the classical one of describing outcomes of events such as the drilling of exploratory wells as probability distributions which are conditional on the underlying factors.

INTRODUCTION

The fact that the Eastern shale gas resource is widespread, and indeed reasonably evenly-spread, must be weighed against the circumstance that so far very few ways have been found to achieve high levels of prolonged production even from the historical reservoir locations. In many cases the obstacle that appears to most limit recovery has to do with the fact that the shale matrix which holds much (most) of the gas as a sorbed phase, has the character of a molecular sieve. This means that somehow transport paths must be induced by enhancing the in situ fractures and/or by creating new rubblizations so that the gas can more easily move towards the wellbore sinks.

Three consequences of the ongoing work to increase in one way or another the effective wellbore radii (surfaces of drainage) are remarkable:

- The insitu "states-of-Nature" conditions themselves are not well-defined; hence it is not always clear what constitutes an improvement in specific cases.
- Until a mineback (or equivalent) experiment is undertaken in the Eastern shales, no one will really know if improvements have been achieved by the new well-stimulation techniques under test and development.
- In the meantime, those engaged in the mathematical modeling of well and reservoir performance, somehow feel justified in postulating well-stimulation outcomes that are not verified, in order to assess economic impact through quasi-sensitivity runs.

The consequence is that no one knows for sure whether or not operators of Eastern gas shale wells ever will be able to improve on the "states-of-Nature," and thus remove or mitigate this major obstacle to commercialization. There are other obstacles also to be dealt with, however. One has to do with minimizing the skin damage resulting from the drilling, completing and stimulation processes. Another has to do with the economics (cost-effectiveness) of the exploration and exploitation procedures that are followed in particular cases. Unfortunately, none of these classes of obstacles so far have been dealt with in previous EGSP papers with any degree of completeness (as can be verified, for example, by scanning the abstracts of the papers presented at the previous DOE-sponsored shale gas symposiums).

If this were to be a paper about what is known or should be known, instead of being a paper about what is not known, there would be a justification to attempt to expand the analysis started above. A different (and more modest) approach will be followed, however, where certain critical questions will be asked as the first step towards finding the answers for them.

Specifically, the purpose of this paper is to talk in a somewhat new way about a somewhat old subject (viz. exploratory drilling to add substantial natural gas reserves to the Nation's inventory). In fact, some unfamiliar terminology will be introduced to facilitate a compact discussion. The account will be brief, moreover, since it is a formalistic problem-statement that is wanted rather than the achievement of specific problem-solving capability.

As mentioned, attention will be directed here to the Eastern shale gas resource provinces. The topic being addressed has to do with finding and stipulating the requirements for a methodology to assess the risk-adjusted expectations when wells are to be drilled according to some specified exploration rationale. The need for a suitable methodology is particularly acute for the case of the subject shale gas reservoirs. This is because while the target is enormous (e.g. hundreds of tcf of high quality natural gas in Appalachia alone) the attending problems of extraction technology are complex and far from being enough understood to be resolved.

Simplistically (but conveniently) the various outcomes from drilling exploratory wells can be expressed in terms of a probability distribution function. The mean value of the distribution then can be converted to the risk-adjusted net present worth of the project--or indeed to other fruitful measures of expectation. Similarly, the standard deviation of the distribution will provide information about how much confidence can be put in the statistical inferences. In any case, it is clear that the values associated with the various outcomes following an exploratory drilling program, are easier to assign than are the associated probabilities that measure the frequency of occurence of these values.

For example, a limiting outcome is that a given exploratory well will discover no gas reserves at all (that is, it will be a dry hole). To assign a value (cost) to this event is entirely straightforward, but to stipulate the probability of drilling one or more dry holes is complex because of uncertainties about the role played by the conditional dependencies between the event and the antecedent governing factors.

Accordingly, the goal to be achieved is to develop a methodology for specifying the probability distributions that characterize the outcomes of exploratory drilling programs in the Eastern gas shales. The optimum methodology is the one that yields best-estimates against the prevailing background of uncertainty

ANALYSIS

Let V_i denote the value of one of the several outcomes from drilling an exploratory well according to some specified explorational rationale, R. Then, the notation: $p(V_i)$ expresses the probability of that outcome. Simplistically, outcomes might be restricted to a few possibilities (e.g. V_1 could refer to the present worth of a dry hole; V_2 could refer to the present worth of a well that discovered X Mcf of gas; and V_3 could refer to the present worth of a well that discovered Y Mcf of gas, with $Y > X$).

Since it is most likely that the outcomes achieved in the drilling of an exploratory well will depend upon the nature of the exploration rationale followed, we avoid addressing that question in what follows by focusing attention on a base case exploration rationale, R_B. Specifically, we say that the exploratory well under consideration has been sited at a random location, and then drilled to a depth such that the target shale beds have been completely penetrated. The choice of this base case rationale is for convenience only, and not because it is one that can be recommended as a general approach. The merit of it for analytical purposes, however, is in the fact the concept of a randomly sited well is well-set and unambigious.

If the $p(V_i)$ for each particular well-drilling opportunity were known a priori, there would be no risk associated with the drilling of exploratory wells. This is because an operator would be free to choose only those opportunities where the mean value of the distribution and the variance would guarantee profit in the venture suitable to the operator's economic requirements. On the other hand, all that is known a priori is that the probability of the outcomes are dependent upon what may be referred to as the prevailing situation. Symbolically we say $p(V_i) \neq p(V_i/S_k)$, where the second term of this inequality is to be read: the probability of V_i given the particular condition, S_k.

The situations, S_k, include all of those influential ones that can be expected when the exploratory well is drilled at a particular location (say, as sited by the stipulated exploration rationale). To make the discussion more precise, we distinguish between the real situations (denoted by ${}^{R}S_k$) and the assumed situations (denoted simply by S_k). Since some prevailing situations will be more favorable than others to the prospect of obtaining desirable outcomes from the drilling of exploratory wells, it follows that if ${}^{R}S_k$ were known a priori, the operator again could avoid risk in the venture by only choosing opportunities where the predicted outcomes would meet the economic objectives.

In real world situations, however, $S_k \neq {}^{R}S_k$, which is to say that risk always will be associated with basing expectations on $p(V_i/S_k)$. Even so, we shall find it convenient, indeed mandatory, to deal with and to establish:

$$p(V_i/S_k) = p(V_i)\ p(S_k/V_i)\ /\ p(S_k) = p(V_i S_k)/p(S_k)$$

where

$$p(S_k) = \Sigma\ p(S_k/V_i)\ p(V_i)$$

according to Bayes Theorem.

What is the nature of the situations under discussion? Let us say that situations can be thought of as comprised of, in fact defined by, a set of prevailing factors $\{F_j\}$. Some of these factors will be favorable to the prospects of achieving wanted outcomes in the drilling of exploratory wells, while others will be in the nature of constraints. For example, a low in situ fracture density will be a constraint, while a well stimulation operation by which a 500 foot induced fracture is achieved will be a favorable factor. Similarly, a low selling price for the gas will be a constraint.

In other words, constraint-factors may be offset by advantage-factors in the sense that a constraint can be thought of as a negative advantage. In any case, some constraints (e.g. low in situ fracture density) represents a State-of-Nature that is not subject to control when wells are sited at random locations.* Others (e.g. induced fracture geometry) have to do with the imposed technology which to one degree or another is subject to control. And still others (e.g. environmental impact, depletion allowances, gas price) reflect prevailing socio-econo-political situations.

The probability of being faced with a particular factor, $p(F_j)$, ideally also must be expressed as a probability distribution. For example, the factor: in situ fracture density, can range from very low values (in fact, zero) to very high values. If such distributions are unimodal, and display a peaked central tendency with a negligible variance, then each F_j factor can be more simply thought of as a statement which asserts either that the central tendency condition prevails, or that it does not. In other words, we say: $p(F_j) + p(f_j) = 1$, where the upper case notation, F_j, is reserved for affirmative statements, and the lower case notation, f_j, is reserved for the contradictory negative (denial) statements.

The approximate way of dealing with factors described above to some extent is justified by the fact that we are only able to visualize and manipulate with assumed situations, S_k, rather than with the real situations, $^{R}S_k$, that are hidden by the so-called background of uncertainty. To illustrate, let us suppose that we are dealing with situations where there are two dominant factors, F_1 and F_2, needed to approximately (but adequately) define these situations. Thus, F_1 could be the statement: The in situ fracture spacing is 10 centimeters on the average or less, but seldom larger, while f_1 would be the denial of this statement. Additionally, F_2 could be the statement: The prevailing price of gas will average around $4 per Mcf over the next five years, while f_2 could be the converse statement: A gas price greater than $4 per Mcf is most unlikely over the next five years.

Figure 1 depicts the joint (and implicitly the conditional probabilities) for this two-parameter problem. There it is seen that there are four situations to be dealt with, namely: $S_k = \{F_1F_2, F_1f_2, f_1F_2, f_1f_2\}$. By way of illustration, suppose that $p(F_1) = 0.2$ and $p(F_2) = 0.33$, then it follows that the probabilities of the four derivative situations will be: $p(S_1) = 0.067$; $p(S_2) = 0.133$; $p(S_3) = 0.267$; and $p(S_4) = p(f_1f_2) = 0.533$. Obviously, in general, there will be 2^j situations where j is the number of factors chosen to define the S_k. That the situation, S_4, is dominant is obvious (meaning, for example, that S_1 and perhaps S_2 and S_3 can be ignored in the above example).

To be more realistic, however, more than two factors usually will be required to define the range of likely situations that should be dealt with when attempting to assess the outcomes of exploratory drilling ventures. For example, in a five parameter model there will be 32 situations to be dealt with explicitly ($= 2^5$), and so forth. Ultimately, what is wanted is the information depicted graphically (but schematically) by Figure 2. There it is suggested tnat $p(V_i/S_k)$ distributions vary according to the prevailing values of S_k. The ones where $p(S_k)$ are dominant deserve special attention, of course.

Referring back to Bayes Theorem as expressed analytically above, in order to obtain the desired $p(V_i/S_k)$, the following steps must be taken:

- The exploration rationale, R (e.g. R_B) must be stipulated and held fixed for the well(s) being drilled.
- The allowed V_i must be set (e.g. V_1 is the present worth of a dry hole, V_2 is the present worth of an exploratory well that finds X Mcf of producible gas reserves, and so forth).

*Obviously, given some exploration rationale, R, where wells are sited on the basis of inferrential information about where in situ fractures are, can lead to a way to circumvent the influence of an adverse fracture density factor.

- Statements about the j controlling factors, F_j, must be formulated, and judgement-probabilities must be assigned to them, and to the converse statements, f_j.

- The derivative situations, S_k, of which there will be 2^j in number, must be listed along with the associated probabilities, $p(S_k) = \Pi p(F_j)$, where the notation $\Pi p(F_j)$ is to be read: the product of $[p(F_1)\ p(F_2). \ . \ . \ . \ p(F_j)]$, et cetera. In these connections, it is instructive to note that it is only the probabilities but not the associated values (magnitudes) of the S_k that are wanted and needed in the analysis.

- Judgement-statements* about the unconditional values of the $p(V_i)$, and about the conditional values of the $p(S_k/V_i)$, additionally are required in order to obtain the associated $p(V_i/S_k)$ from Bayes Theorem.

In the end, one wants to know the most likely value of the outcome of the exploratory well(s) being drilled, V_j, associated with the most likely prevailing situation, S_k. In this way a risk-adjusted net present worth of the venture can be assigned as a decision-criterion that will be useful when the investment-venture is first being considered. Obviously, as time elapses, the amount of available information increases; hence uncertainty about the input probabilities to assess the most-likely outcomes gradually vanishes. To suppose, however, that uncertainty (viz. risk) can be avoided in exploratory ventures (except in an after-the-fact way), is to ignore the logical implications of Bayesian statistics. Even so, linear programming provides a way to put bounds on an otherwise indeterminate situation.

A SIMPLIFIED EXAMPLE

Suppose that previous (basin-wide) experience shows that the mean value of the distribution of outcomes, V_i, is $\langle V \rangle$, where $\langle V \rangle = \Sigma\ V_i\ p(V_i)$, (by definition); and** $p(V_i) = e^{-\beta V_i}/\Sigma\ e^{-\beta V_i}$, where β is the so-called Lagrangian Multiplier that measures the strength of the information. These probabilities, as will be recalled, are the least-prejudiced estimates subject to the prevailing constraints (namely, that $\langle V \rangle$ is given, and that $\Sigma\ p(V_i) = 1$).

To find the $p(V_i)$, we need only to stipulate the allowed levels of the V_i themselves, and then to solve the resulting polynomial. Thus, in the simplified example under discussion, we choose arbitrarily to limit the V_i to the two values as follows: $V_1 = -\ 10^5$ dollars (a dry hole); and $V_2 = +\ 10^6$ dollars (a well that has discovered reserves). We also arbitrarily choose to say that $\langle \tilde{V} \rangle = 0$ in the example under discussion, therefore we have as the local rule of experience that: $p(V_i) = 10/11 = 0.9091$ and $p(V_2) = 1/11 = 0.0101$.

Now referring back to Figure 1, we further assume that we are dealing with a simple two-factor situation where the $p(S_k)$ of the most likely one is $[p(f_1)\ p(f_2)] = p(S_4) = 0.533$. This corresponds to an unfavorable situation since the probability of finding a close in situ fracture spacing at the sited well location, $p(F_1)$, is low, and since the probability of having a high gas price incentive, $p(F_2)$, also is low. Note again, that the probabilities of the three other possible situations, S_1, S_2 and S_3, are all substantially lower than $p(S_4)$. This tells us intuitively that: $p(S_4/V_1) > p(S_4) > p(S_4/V_2) = [1 - p(S_4/V_1]$.

We now make an intuitive value-assessment, and say that the most likely influence of the constraints as measured by $p(F_1)$ and $p(F_2)$ provoke us to assign values such as: $p(S_4/V_2) = p(S_4)/(1.05) = 0.508$ $(=<0.533)$, hence $p(S_4/V_1) = 0.536$ $(=>0.533)$. Then, by Bayes Theorem, we have: $p(V_1/S_4) = 0.913$ and $p(V_2/S_4) = 0.087$, or $\langle V/S_4 \rangle = -4{,}762$ dollars.

The conclusion: The well in this example should not be drilled since a negative expected value (i.e. a loss) is the most likely outcome. The result, of course, is predictable since the mean value of the unconditional outcome was set at zero, and since S_4 inherently was unfavorable (i.e. constraint-laden).

---

*For example, as based in the past history (experience) of success ratios for exploratory wells in the region under consideration.

**See for example: M. Tribus, Rational Descriptions, Decisions and Designs Pergamon Press (1969).

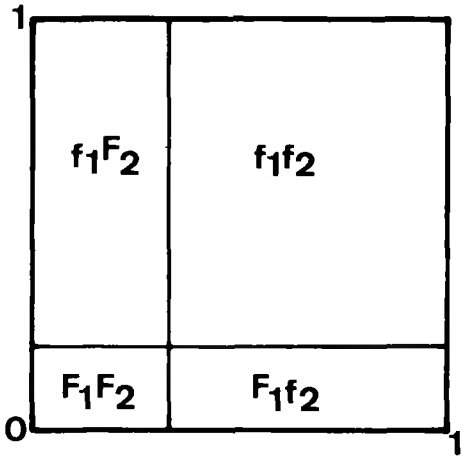
CONCLUSIONS

- The outcome from drilling an exploratory well (or wells) to some extent depends upon the exploration rationale that led to the siting of the well location (N.B. The fact that some well-sitings are made on the basis of logistics, for example proximity to pipelines, as well as technical factors, also must be taken into account in any complete analysis of the problem).

- The outcome under discussion most directly depends on the prevailing (site-specific, time-specific) situation. The latter reflects and is defined in terms of the prevailing positive (advantageous) and negative (constraint) factors. While the situation itself cannot be quantified (e.g. given a scalar or vector magnitude), the underlying factors usually can be expressed in terms of numbers. More than that, since probabilities, $p(F_j)$ can be assigned to the factors on the basis of judgment, the $p(S_k)$ can be immediately derived (as needed for manipulating with Bayes Theorem).

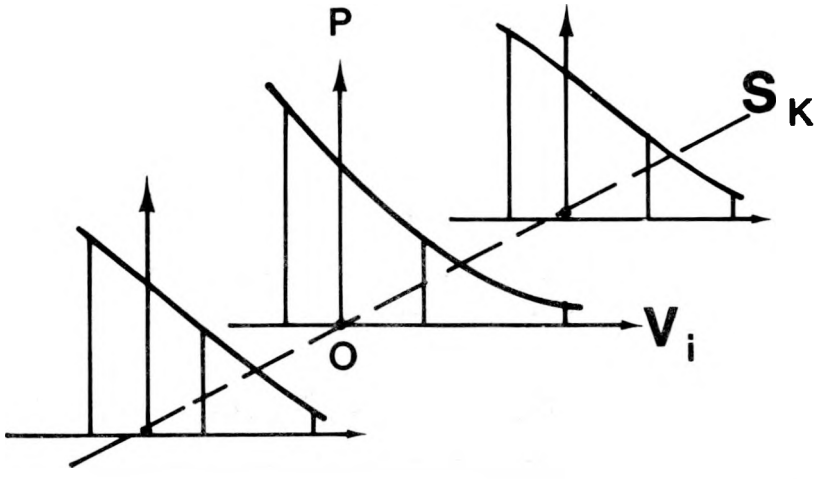
- If at the present stage the Bayesian approach does not offer the prospect of obtaining a practical problem-solving capability, this is because problem-statement is still in a primative stage. In other words, the limitations exposed by this paper provide a focus by which the remaining problems to be solved can be clearly seen.

- While the approach followed in this paper has been classically Bayesian, it is represented as a conclusion that the way of describing situations in terms of factors, and for handling the apriori judgement probabilities, $p(V_i)$ and $p(S_k/V_i)$, are novel and deserving of special attention (see above simplified example).



TWO - FACTOR JOINT PROBABILITIES

Figure 1



PROBABILITY DISTRIBUTIONS

$$P(V_i / S_K)$$

Figure 2

RECOVERY OF ENERGY FROM MICHIGAN ANTRIM SHALE BY AN IN SITU PROCESS

L. J. Washington

Dow Chemical Company

ABSTRACT

A twelve member team at The Dow Chemical Company has completed three years of a four-year, $14 million contract* with DOE to assess the feasibility of recovering energy from Antrim oil shale. The contract has four tasks specifically identified, as follows:

1) Shale Characterization
2) In Situ Fracturing and Assessment
3) In Situ Extraction Trials
4) Environmental, Public Policy and Legal Assessment

At Dow's experimental site in Sanilac County, Michigan, the Antrim formation is about 200 feet thick at 1200-1400 feet below the surface. Under Task 2, several wells have been drilled into the Antrim layer in three 10-acre plots. Each plot has been subjected to a different fracturing procedure and the results have been evaluated.

a) Hydraulic fracturing followed by explosive fracturing
b) Explosive underreaming followed by explosive fracturing
c) Chemical underreaming followed by explosive fracturing

The plot which appeared, on the basis of permeability studies, well-to-well communications, and various downhole logging studies, to offer the best chance of success in Task 3 was chosen for an in situ extraction trial. This trial was scheduled to begin in August, 1979.

This paper will outline the fracturing experiments and the evaluation process which led to the choice of the preferred site for the extraction experiment. It will also summarize the results of the in situ extraction trials as they have been obtained to date.

*DOE Contract No. EX-76-C-01-2346

Note: Paper not available at time of publication.

A SUGGESTED ORIGIN FOR THE GAS IN EASTERN DEVONIAN SHALES

Irving A. Breger



ABOUT THE AUTHOR

Irving Breger received his B.S. degree in Chemistry from Worcester Polytechnic Institute in 1941. He received his S.M. degree in Organic Chemistry and his Ph.D. in Geochemistry from M.I.T. in 1947 and 1950 respectively. He is presently employed by U.S. Geological Survey in Reston, VA.

2 A SUGGESTED ORIGIN FOR THE GAS IN EASTERN DEVONIAN SHALES

ABSTRACT

Kerogen of the Chattanooga Shale in eastern Tennessee and adjacent areas is known to be of predominantly terrestial origin. In effect, the Chattanooga Shale may be viewed as high-ash, low-rank coal. Recent detailed studies of peat from The Everglades of Florida have led to the observation that the rate at which cellulose is degraded is reduced as the mineral content increases. Knowing of the contribution of terrestial plant material to the sediments that later became the Chattanooga Shale, which consists of 75 to 85 percent mineral matter, we believe that those sediments probably contained an accumulation of cellulose. Slow, anaerobic degradation of that cellulose by methanogenic bacteria would be expected to result in the formation of methane that would then dissolve in other organic components of the sediment. Only in those regions where the contribution of aquatically derived organic detritus to the sediment was significant would appreciable amounts of ethane, propane, and higher gaseous hydrocarbons be expected, perhaps as products of low-temperature thermal processes.

These considerations suggest that study of the composition of kerogen in the Chattanooga Shale and its correlatives could delineate those regions of the Eastern Devonian Shales most likely to be the best sources of methane.

NOTE: Paper not available at time of publication.

GAS CONTENT AND TRANSPORT IN SHALE

AND THEIR IMPLICATIONS FOR WELL PRODUCTIVITY

by

Paul D. Schettler, Jr.
Department of Chemistry
Juniata College
Huntingdon, Pennsylvania 16652

ABSTRACT

Attention is directed at the role that gas in the rock matrix plays in the production of gas from a well in tight shale. The assumptions of several different theoretical models which include matrix gas transport are examined in terms of their predicted well productivity curves. Among other parameters these models utilize laboratory-obtained data of gas content and transport in shale. The average values, standard deviations, and a variety of correlations of these data with other parameters is discussed

INTRODUCTION

The purpose of this paper is to report progress that has been made toward understanding the basic kinetic processes involved in gas well production in tight formations as represented by the Devonian shales. It is to be believed that as this knowledge is obtained it can be applied to practical problems such as determining well location, deciding on the stimulation procedure, and the estimation of reserves.

Two basic models have been proposed that are designed to account for production in tight shales. The earliest model assumes that the gas is located in fractures in the shale and that the gas is produced by venting these fractures. In this fracture gas model the ultimate source of the gas is organic matter entrapped in the rock which is released over geologic time to the fractures; the rate of this release is presumed to be so slow, however, as to contribute only negligibly to production. Thus the parameters that determine the total gas available for production are the volume associated with the fractures and the pressure of the gas in them. In addition, the parameters that determine the rate of production include the fracture permeability and the fracture geometry.

The second model assumes that the fractures serve only as conduits between the well bore and the source of the gas which is bulk rock. In this matrix gas model, gas is presumed to diffuse through bulk shale in a manner that obeys the laws of diffusion. Upon reaching a fracture the gas can flow relatively freely to the well bore. In this model the bulk rock is the reservoir, and the volume of rock, its capacity to sorb methane, and the gas pressure are the parameters that determine reservoir capacity. The parameters that determine the rate of production include in addition the extent of the fracture system, its geometry and permeability, as well as the intrinsic rate of diffusion of gas through the rock matrix.

Prepared for DOE under Contract No. DE-AS05-76MC05197.

The differences between the two models are considerable. Since the volume of rock is much larger than the volume of fractures within the rock the volume of gas associated within any given region will be different by orders of magnitude depending on which model is used. In the first model fracture properties alone determine both the amount of gas obtained and the particular shape of the productivity decline curve. In the second model, rock matrix properties must be considered in conjunction with fracture properties. For example, there will still be considerable resistance to flow in the case where the fracture permeability is low because of the effect of matrix diffusion

Neither model makes any a priori statement about the geometry of the fracture system and different geometries will generally give different productivity decline curves for each model. Thus the shape of productivity decline curves is in general not a definitive test of either model because the possibility exists that for some fracture geometry the other model can give a similar decline curve. Nevertheless, for a given fracture geometry the two models will generally predict very different productivity decline curves. For example, for the average geometric and matrix parameters that appear to be present in Appalachian Devonian shales, the matrix gas model predicts about 3 orders of magnitude greater amount of gas than for a fracture gas model during the lifetime of a typical well.

Unfortunately the pattern of natural fractures is not completely known for any reservoir. Cores will give information as to frequency and direction of fractures and transient analysis will permit the calculation of a permeability given simplifying assumptions. However, the extent, width, and interconnectedness of fractures are more difficult to measure. Further, if there is matrix gas participation in the production, the permeability measured by transient analysis cannot be interpreted in terms of fracture geometry alone. In particular, questions such as the radius of drainage of a well become difficult to calculate. The problem is much simplified if one can assess the extent of matrix participation by some other means such as independent measurement of the extent and rate of methane desorption from bulk rock by laboratory analysis of core.

In this paper we first review our progress in this latter area of methane desorption from bulk shale. Second, we discuss the implication of these measurements for a set of prototype models involving matrix diffusion into a fracture with a variety of constrictive effects.

EXPERIMENTAL RESULTS

Juniata has been involved in an experimental program to directly measure the amounts of methane dissolved in shale as a function of pressure and the rate of its release through shale surfaces upon release of pressure. Table I summarizes the data to date for methane [1]. The column marked isotherm records the amount of gas (volume STP) sorbed into a unit volume of shale upon increase of pressure from zero to 1 atm. It is clear that adsorption onto clay minerals or solution into kerogen make the shales under consideration significant reservoirs of methane given sufficient pressure [2]. It should be noted that there are significant variations in the ability of Devonian shale to sorb gas both in respect to well site and with respect to depth at a given well site reflecting the different rock properties.

The second column shows the rate of gas release through the surface of shale particles upon a sudden decrease in external pressure. The rate of release follows the equation

$$1) \quad \frac{M_T}{A} = 2G\Delta P t^{\frac{1}{2}}$$

where ΔP is the pressure change (atm.), t is the time (sec.), and $\frac{M_T}{A}$ is the amount of gas released from a unit surface of shale (vol. gas (STP)/cm^2 surface) [3].

It is of major interest to compare this rate of gas release with the amount of gas originally in the fracture. This comparison allows one to choose between the fracture gas and matrix gas models. If one assumes a fracture width of .01 cm., the amount of resident gas that can be produced is .01 ΔP ml per sq. cm. of fracture, where ΔP is the pressure drop. The amount of gas that will consequently be produced by diffusion through the surfaces of this same fracture will be .00074 $\Delta P t^{\frac{1}{2}}$ where t is the time in seconds and the coefficient refers to average release kinetics. The amount of matrix gas equals the amount of fracture gas originally produced in about 3 minutes and becomes 100 times the fracture gas within a month. The amount of matrix gas produced in

various parts of the well depends upon the variation of the degasibility which in turn typically varies by more than an order of magnitude. For equivalent fracture systems and equivalent initial rock pressures, one would expect a variation in well productivity from one zone to another that would be proportional to the specific degasibility of that zone.

We have made some attempts in several directions to determine the mechanism responsible for sorption and transport of gas through shale. One such study has been to measure isotherm/degasibility parameters as a function of temperature. The data is summarized in Table II. One standard use of this type of data is to estimate the strength of the adsorbate/adsorbent interaction. The magnitude of interaction obtained is in the range of weak physical attraction between the methane and the clay minerals of the induced dipole type. It is about 1% of chemical bonding energies but nevertheless sufficient to reversibly concentrate methane within the shale.

In a second area of investigation we have observed a significant degree of correlation between isotherm/degasibility data and radioactivity counting data [4]. Table III shows the results obtained using 30 samples from a variety of wells. The uranium isotherm/degasibility correlations are, however, larger than the total organic carbon isotherm/degasibility correlations. Since the clay minerals are known sorbents of both ionic and non-ionic materials, both methane and uranium can be sorbed onto sites on clay minerals as well as dissolve in kerogen. If it is the total sorptive capacity of shale that is important rather than the sorptive capacity of the kerogen alone, then the observed correlational effects can be explained.

The magnitude, rates and temperature dependence of desorption are consistent with a microporous structure of shale wherein very fine channels exist between the mineral grains. These pores account for no more than 25% of reservoir capacity of shale but rather serve primarily as conduits between sites of condensed methane. These sites can be the surface and interior of both kerogen and clay mineral crystals.

Methane is presumably formed by the maturation process of shales over geologic time. However, the magnitude of diffusion that we have measured indicates that gas formed at the end of the Devonian age would have diffused a mean distance of between 1100 and 3000 feet (using averaged diffusion constants from the degasibility data for the wells in Table I). This permits the possibility that gas formed in one location with low isotherm/degasibility parameters may migrate over a considerable distance to locations with high values of isotherm parameters and be more readily produced there than at the original source by virtue of a high degasibility parameter. (There is a strong positive correlation between degasibility and isotherm slope.)

A second area of implication of the matrix gas model is the calculation of fracture area to be associated with a given well. This is most easily accomplished wherein n = .5 as is roughly the case for some of the Cottageville wells. Assuming averaged values of the matrix rock parameters we calculate 1.18×10^6 m^2 fracture area or $.59 \times 10^6$ m^2 fracture extent corresponding to a total fracture void volume of about 2000 cubic feet.[1/] A single radial fracture would have a drain radius of 435 meters or a single linear fracture would be 14.8 km. Fracture branching and multiple fractures would cut the linear estimates considerably.

A third area of implication of the matrix gas model has to do with the calculation of reserves. On the one side estimation of gas reserves from the fracture volume will greatly underestimate the amount of gas obtainable because of the major contribution of matrix gas. On the other hand its estimation from the total amount of matrix gas will greatly overestimate reserves because much of the gas will be too distant from the fractures necessary for it to be produced. One possible procedure is to calculate the amount of gas that can be produced per unit area of fracture over, say, 50 years, assuming that well placement is such that it can degas in the open fracture mode. With these assumptions and taking a fracture spacing of 100 feet, a rock pressure of 16 atm, a well lead pressure of 3 atm, $G = 2 \times 10^{-7}$ cm/torr/sec$^{\frac{1}{2}}$, one estimates that about 10^6 MCF can be produced from a square mile of formation thickness of 1000 feet.

MODELS

Given that the experimental results above lend support to the matrix gas model as compared to the fracture gas model, one can proceed to interpret the productivity decline curves of individual wells in terms of the geometry of the fracture system. Certain geometries are capable of extracting

[1/] This calculation assumes fracture width = .01 cm, $G = 4 \times 10^{-7} \frac{cm^3 \text{ gas (STP)}}{cm^2 \text{ torr sec}^{\frac{1}{2}}}$, and ΔP = 400 psi.

gas from the matrix more rapidly than others. Generally the more fracture area that is accessible to the well bore the greater the production. A rather important geometric factor is the width of the fractures involved and the question arises as to the effects of fracture width and constrictions upon productivity decline curves. Effects due to constricted fracture width may be expected to be particularly important close to the well bore where the pressure gradients are greatest. This is also the area in which fracture modification by stimulation and propping will be most effective. To approach these problems we have constructed some simple prototype models with a limited number of parameters from which productivity decline curves can be calculated. The first of these models is a linear fracture flow/matrix diffusion model wherein a single uniform fracture of .001 cm width, 40 meters heighth, and of indefinite length intersects the well bore [5]. The rock is assumed to have a specific degasibility of 4×10^{-7} and a rock pressure of 500 psi. The second model is a single horizontal fracture of the same width that is intersected by the vertical well bore [1]. The rock matrix is assumed to have the physical chemical properties as in the linear case. The third prototype model is a large fracture connected to the well bore through some low permeability opening such as a partially plugged fracture. The plugging is assumed to be complete enough so that the effect of matrix diffusion can be neglected. The final model is an open fracture system of finite size, degasibility 2×10^{-7} and large enough fracture widths so that the effects of fracture permeability can be neglected. These models are prototypes in the sense that they may serve as diagnostic tools toward the identification of some predominant fractures of real fracture systems and their relationship to decline curves. For example well production is the summation of the production of the multiple fractures that normally intersect the well bore. However the total production of a well may have certain features that signatures the predominance of one or another of the prototype model fractures.

Figure 1 shows the production decline curves for these four cases. It should be noted that the open fracture model has the greatest slope, and the plugged fracture has the least with the constant fracture cores coming out between the two extreme cores. The curve for the radial core is flatter than that for the linear core reflecting the decreased fracture circumference and consequent "necking down" of the fracture close to the well bore.

Figure 2 shows pressure profiles for the linear and radial cores. For the open fracture core the pressure is at the well bore pressure along the entire fracture whereas for the constricted fracture core the entire pressure crop is at the fracture exit. This in conjunction with Figure I suggests the association of flattened productivity decline curves with a pressure gradient that is close to the well bore. In such cases artificially increasing the permeability close to the well bore will increase production.

All of these cores fit the equation

$$M_T = At^n$$

where M_T and t are the cumulative production and the time respectively and A and n are fitted constants that can be determined from a log plot of cumulative production versus time. Flattened production curves correspond to n close to 1 while the open fracture case corresponds to n = 1/2. For the linear and radial cores n = .75 and .96 respectively. Actual production data is often approximately linear on log-log plots with curve slopes in the 1/2 to 1 range. This suggests the interpretation that the wells with large slopes are (or were) prime candidates for increased production by (further) stimulation. On the other hand, for wells which have slopes close to 1/2, stimulation procedures can have increased effectiveness only if they access new fractures. Further propping of existing fractures should have little effect.

CONCLUSIONS

We have long stressed that the key to increased understanding of gas production from shale wells is greater quantitative knowledge of certain key parameters of the matrix rock. With this knowledge the productive behavior of a well becomes a powerful instrument too for assessing fracture geometry. This assessment is in turn necessary to determine the effect of stimulation, to establish optimal well spacing, to make predictions of productivity, and to estimate reserves.

Production rates can be correlated with the amount of fracture surface area given knowledge of kinetics of gas flow through the surface. Further, the slope of production decline curves can be interpreted in terms of the degree of localization of the pressure gradient along the fracture near the well bore. Short wide fractures give very different decline curves from long narrow fractures or fractures that have been constricted close to the bore, perhaps by drilling mud. An implication from this is that the greatest potential for increased production by stimulation is fracture geometries that are yielding production decline curves that are flat because of the association of these curves with extensive fractures and/or plugged exits. On the other hand, fracture geometries that yield steep decline curves are probably already flowing with minimal fracture resistance.

REFERENCES

1. A more complete data summary can be found in Schettler, P. D., and Wampler, D. L., "Study of Hydrocarbon-Shale Interaction," Report #14 (ORO-5197-14), submitted to Morgantown Energy Technology Center under DOE Contract No. DE-AS05-76MC05197.

2. Schettler, P. D., Wampler, D. L., Sipling, P. J., Mitchell, D. J., "The Relationship of Thermodynamic and Kinetic Parameters to Well Production in Devonian Shales," Proceedings of the First Annual EGSP Symposium, Morgantown, 1977.

3. Schettler, P. D., "The Concept of Specific Degasibility and Its Application to Gas-bearing Tight Formations as Represented by the Devonian Shales of Appalachia," Proceedings of the Fourth Annual DOE Symposium, Tulsa, 1978.

4. The samples were obtained through Eric Smith of Columbia Gas System Service Corporation. The radioactivity decay data had been done by David Coles of Lawrence Livermore Laboratory.

5. Schettler, P. D., Wampler, D. L.,"Study of Hydrocarbon-Shale Interaction," Report #13 (ORO-5197-13), submitted to Morgantown Energy Technology Center under DOE Contract No. DE-AS05-76MC05197.

Table I. Summary Average of Isotherm and Kinetic Parameters for Several Wells.

Well	Isotherm Slope V gas/V rock/atm.	Degasibility x 10^5 (G) V gas/cm^2 rock/atm./$sec.^{\frac{1}{2}}$
IL#1	.33 ± .18	5.39 ± 3.72
IL#2	.47 ± .09	1.52 ± .91
IL#3	.44 ± .16	.83 ± .04
NY#1	.25 ± .13	8.82 ± 6.54
WV#5	.24 ± .06	12.8 ± .90
WV#6	.93 ± .72	61.0 ± 52.6
WV#7	.34 ± .25	23.7 ± 23.1
20336	.22 ± .08	7.14 ± 4.71
20338	.57 ± .58	44.7 ± 43.9
20403	.20 ± .09	14.59 ± 15.5

Table II. Change of Isotherm and Degassing Parameters As Function of Temperature

Well	% Change in Isotherm slope/degree	% Change in Degasibility/degree	ΔH_{ads} Kcal/mole
WV#5:2935	-2.83	-1.02	-2.55 ± .13
20403:2926	-1.58	-1.19	-2.78 ± .23
WV#6:7474	-1.37	-1.19	-3.44 ± .13
20403:3416	- .70	---	---
20403:3716	-1.03	---	---

Table III. Correlation of Radioactivity with Isotherm/Degasibility Parameters

Element	Methane Isotherm	Methane Degasibility
U_{238}	.760	.484
U_{235}	.771	.486
Pb_{210}	.667	.428
Total Organic Carbon	.550	.372

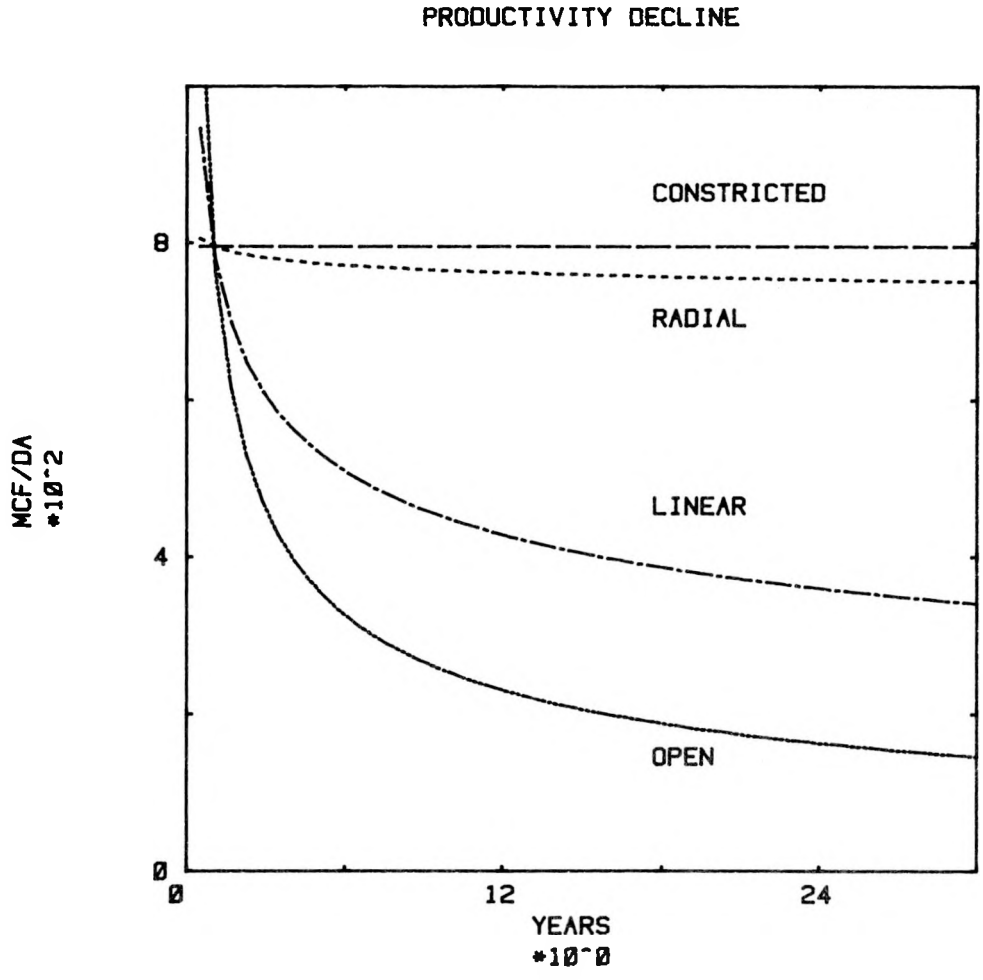


FIG # 1

FIGURE 1. PRODUCTIVITY DECLINE OF VARIOUS MODELS

Values of parameters used: $G = 4 \times 10^{-7} \frac{cm}{torr\ sec^{\frac{1}{2}}}$; rock pressure = 500 psi; well lead pressure = 100 psi; viscosity of methane = 102.6×10^{-6} poise. Linear--vertical fracture = .086 cm x 50 m and of indefinite extent. Radial--horizontal fracture = .01 cm wide and of indefinite extent; well bore radius = 10 cm. Open--fracture area (total of both sides of fracture) = 1.77×10^{7} m^2. Constricted--small opening with large fracture system behind it.

Parameters were chosen so as to give some production rate after 1 year for each model. Stimulation of constricted case would increase production and shift it to lower times.

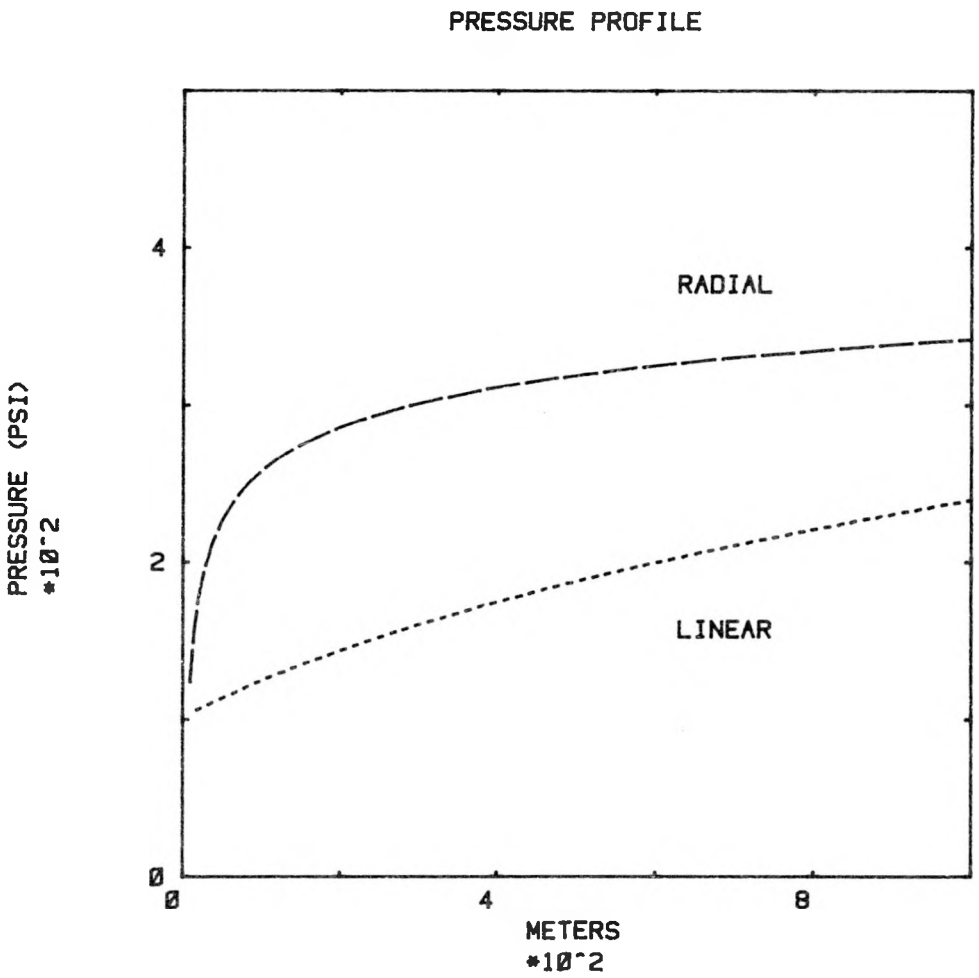


FIGURE 2. PRESSURE PROFILE

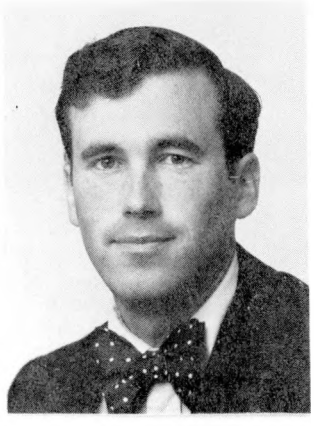
Same parameters used as in Figure 1 except linear has a .01 cm fracture width. A larger fracture width would further decrease the slope of the pressure profile. A constricted fracture would have (almost) constant pressure up to X = 0 where the pressure would drop to 100 psi quickly. An open fracture would have a fracture pressure that was (almost) uniformly = 100 psi.

EXPLORATION STRATEGY FOR AN UNCONVENTIONAL NATURAL GAS RESOURCE: DEVONIAN SHALE

Claude S. Dean and William K. Overbey Jr.

Morgantown Energy Technology Center, WV





ABOUT THE AUTHORS

The senior author received two S.B. degrees from M.I.T., the first in Mechanical Engineering (1964) and the second in Earth Sciences (1968). He went on to receive an A.M. (1970) and a Ph.D. (1976) in Geology from Harvard University. He served two years (1965-66) active duty as an officer in the Navy. Dr. Dean has been three years in the employment of U.S. DOE's Morgantown Energy Technology Center. He is assigned as a geologist to the Oil, Gas, and In Situ Coal R&D Branch, where he coordinates the Eastern Gas Shale Project's exploration R&D effort.

Upon completion of a B.S. degree in Geology at West Virginia University in 1959, Mr. Overbey went on to work for the West Virginia Geological Survey as a petroleum geologist, remaining there until 1963, when he joined the petroleum and natural gas research group at the U.S. Bureau of Mines, Morgantown Energy Research Center. Mr. Overbey served as project geologist for the Oil and Gas Reservoir Evaluation Project from 1963 to 1969, when he was promoted to Project Leader. He initiated projects to study the effects of earth fracture systems of fossil fuel extraction processes. From 1969 to 1973 he served as Project Leader of Earth Fracture Systems Project and the Deviated Well Project. In 1973 he helped plan and served as Project Leader for the In Situ Coal Gasification Project to test the use of deviated wells in underground coal conversion processes. In 1975 he initiated planning for the Eastern Gas Shales Project and served as Project Manager from December, 1975 to June, 1978. Mr. Overbey is currently serving as Senior Scientist for the Oil, Gas, and In Situ Coal Division at Morgantown Energy Technology Center. He has authored or coauthored more than forty publications on energy research topics.

2 EXPLORATION STRATEGY FOR AN UNCONVENTIONAL NATURAL GAS RESOURCE: DEVONIAN SHALE

ABSTRACT

Exploration rationales, exploration techniques, and prospects are the key elements of EGSP's ideal exploration strategy for the Devonian shales of the Appalachian, Illinois, and Michigan Basins. An exploration rationale is a theory of how several known or suspected geological circumstances may combine to create a favorable environment for the generation and accumulation of the producible hydrocarbons. The unconventional nature of the Devonian shales as a natural gas resource demands shale specific rationales. These are characterized by a hypothesized geological mechanism for the creation of a natural fracture system, because fracture permeability is essential to shale production. Fractures are a necessary, but not sufficient, condition; hence, shale specific rationales include supporting information: black shale thickness, kerogen content, thermal maturity, reported shows, production history, etc. Exploration rationales are area specific, but generally not site specific. Prospect development is the process by which site specific prospects issue from area specific rationales. Exploration techniques are the means employed to evaluate rationales short of drilling and optimize local geologic factors in site selection. An inventory of conceivable exploration rationales and techniques for the Devonian shales is presented.

The development of seven exploration prospects associated with the Newman Ridge and Greendale Synclines in eastern Tennessee and southwestern Virginia serves as a case study illustration of EGSP's exploration strategy.

OUTLINE

I. Exploration Strategy and Definitions

- A. Exploration rationale
- B. Exploration technique
- C. Shale specific rationales and techniques
- D. Prospect development
- E. Regional screening

II. Inventory of Promising Exploration

Rationales and Techniques Directed Toward the Devonian Shales-Discussion (see below)

III. Case Example: Development of Prospects Associated with the Greendale and Newman Ridge Synclines of Eastern Tennessee and Southwestern Virginia

- A. Background review
  1. Regional geology
  2. Tennessee Division of Geology's contract research project
     - a. Reflection seismic survey
     - b. NX core hole drilling program
- B. Exploration rationale and techniques
  1. Statement and explanation of rationale
  2. Techniques
  3. Supporting factors
- C. Prospect development/identification

EGSP EXPLORATION INVENTORY

I. Exploration Rationales

A. Basement tectonics related
1. Major basement faults with evidence or suspicion of post-Devonian reactivation.
a. Faults of the Eastern Interior Aulacogen (Rome Trough in WV)
i. Cottageville - like situations
ii. Southeast boundary fault in Kanawha and Boone Counties, West Virginia (7000 ft. of structural relief in a lateral distance of 2 mi.; see Kulander & Dean, 1978, fig. 10)
iii. Rough Creek Fault System, western Kentucky
b. Faults of the newly discovered aulacogen underlying the Michigan Basin
c. New York - Alabama aeromagnetic lineament (I. Zietz, USGS)

2. Basement warps
a. Related to aulacogens
b. Related to Acadian through Allegheny orogeny (if such exist)

3. Tectonically relaxed areas (isotropic stress in the horizontal plane)
a. Related to aulocogens (Rome Trough)
b. Associated with deep interior basins (Michigan Basin)

B. Detachment tectonics related
1. Ramping detachment thrusts
a. Pine Mountain thrust related
b. Valley & Ridge Province
i. Greendale and Newman Ridge Synclines, eastern Tennessee and western Virginia (southern Appalachians)
ii. West Virginia, Maryland and Pennsylvania (northern Appalachians)
c. Folded Plateau
i. Chestnut Ridge Anticline
ii. Warfield Anticline

2. Detachment related folds
a. Growth folds: Mann Mtn. Anticline (W. Perry)
b. Controlled by stratigraphic facies changes: Burning Springs Anticline (Silurian salt pinch out; possibly incipient salt tectonics)

3. Cross-strike structural discontinuities
a. Bounding faults of the Pine Mountain thrust block
i. Russell Fork Fault
ii. Jacksboro Fault
b. Parsons and Petersburg Lineaments (R.L. Wheeler)
c. Breezewood - Shippensburg fault system (S.I. Root and D.M. Hoskins)

4. Central-Southern Appalachian orocline, Greenbrier Co., WV (See Dean and Kulander, 1978)

5. Detachment influenced by underlying basement structure
a. Isolated area bypassed by detachment, Cumberland, TN
b. Burning Springs Anticline and similar structures
c. Basement highs and lows

C. Astroproblems and Crypto-explosion structures

D. Glacial loading and unloading
1. Lake Erie Devonian shale producing area
2. Other areas along the southern margin of the Wisconsin ice sheet
3. Areas along the southern margin of the Illinoian ice sheet

E. Dilatency due to uplift and erosional unloading

F. Stratigraphic
   1. Onondaga reefs, NY
   2. Silurian reefs, MI
   3. Bioherms in the Pokejoy Member of the Manhantango Formation (Hasson and Dennison)
   4. Vertically versus alternately stacked Pennsylvania fluviatile sandstones (A.C. Donaldson)

G. Diagnetic
   1. Dewatering with lithification
   2. Volume shrinkage with compaction

II. Exploration Techniques

A. Non-penetrative (surface)
   1. Remote sensing
      a. Detection of structural features (lineaments, faults, folds, circular structures, etc.)
      b. Detection of buried structures through drainage analysis (entrenched meanders)
      c. Detection of more densely fractures areas via multi-temporal/spectral analysis

   2. Field fracture investigations
      a. Fracture trend survey
      b. Fracture density survey

   3. Water well production survey

   4. Analysis of regional magnetic and gravity surveys

   5. Geologic mapping
      a. Conventional (Valley and Ridge Province)
      b. Pennsylvanian fluviatile sandstones

   6. Geochemical surveying

B. Penetrative (subsurface)
   1. Subsurface data analysis and mapping
      a. Structure contours
      b. Isopachs
      c. Gas shows
      d. Production
      e. Black shale organic content
      f. Shale gas BTU content

   2. Reflection seismic
      a. Structural analysis
      b. Velocity analysis

   3. Resistivity and related geophysical techniques

DIGITAL IMAGE PROCESSING AND ENHANCEMENT OF LANDSAT DATA FOR LINEAMENT MAPPING AND NATURAL GAS EXPLORATION IN APPALACHIAN REGION

Thomas F. Wescott
Digital Image Processing Specialist

and

Alan F. Smith
Remote Sensing Specialist/Geologist

ABOUT THE AUTHORS

Mr. Wescott received his B.A. degree in Physics from the State University of New York. He serves as systems engineer and as applications engineer for the Digital Image Analysis Laboratory (DIAL). As system engineer, he develops techniques in advancing the state-of-the-art of the DIAL facility in image enhancements and image classification. Recently, he was instrumental in the implementation of an image convolution/spatial enhancement program at DIAL. As an applications engineer, he has applied satellite and aircraft data processing technology to projects in mineral exploration, forestry, land use and wetlands.

Mr. Smith received his B. S. degree in Geology from the University of North Carolina at Chapel Hill, North Carolina. Mr. Smith participates in many facets of the remote sensing applications program at General Electric. He is directly associated with the Digital Image Analysis Laboratory (DIAL), a facility involved in the commercial application of digital image processing and analysis technology of Landsat and other data for Earth resources studies. As a geologist, he is currently involved in the ASVT program at NASA/Goddard Space Flight Center. He recently completed a project for the Bureau of Land Management involving the detection of and correlation between lineaments and hydrothermally altered areas in the California Desert using digitally enhanced Landsat data.

2

DIGITAL IMAGE PROCESSING AND ENHANCEMENT OF LANDSAT DATA FOR LINEAMENT MAPPING AND NATURAL GAS EXPLORATION IN APPALACHIAN REGION

ABSTRACT

A project is currently underway to prepare digitally enhanced Landsat images covering test sites in the Appalachian region and to evaluate their application for lineament mapping and natural gas exploration.

Digitally enhanced products were prepared using seasonal Landsat data covering test sites located in seven states (New York, Pennsylvania, Ohio, W. Virginia, Virginia, Kentucky and Tennessee). At least ten different types of digital enhancements were applied to each test site for each season for review and analysis. The optimum four products (per season, per test site) have been forwarded to the participating state users for evaluation and assessment.

Digital enhancements are displayed and specific enhancement procedure are explained and illustrated. The differences in edge enhancements and in linear and non-linear contrast stretches for the same season and for different seasons are described. The digital processing methodology used for processing, evaluating, and selecting the optimum contrast stretches and edge enhancements is discussed. The role of the interactive digital computer in image processing and enhancement is illustrated.

INTRODUCTION

General Electric's Digital Image Analysis Laboratory (DIAL) is currently participating in a joint NASA (Goddard Space Flight Center)/ARC (Appalachian Regional Commission) project involving the preparation of Landsat digital enhancements covering areas in Appalachia.

This particular project is part of a larger effort - the Appalachian Lineaments Application System Verification and Transfer (ASVT) Project - the purpose of which is to conduct a Landsat-based lineament analysis for selected areas in Appalachia underlain by Devonian shales. These shales show considerable promise for natural gas finds and as such are of considerable interest to the energy exploration community.

This paper pertains to one aspect of this ASVT project, the description of the image processing procedures and techniques utilized to prepare the Landsat digital enhancements.

Figure 1 shows the test sites that were selected for preparation of digital enhancements. The areas are: (Site 1) southeastern Ohio/eastern Kentucky/western West Virginia; (Site 2) southwestern New York/northwestern Pennsylvania; (Site 3) southeastern Kentucky/northeastern Tennessee/southwestern Virginia. The size of each test site is approximately 80 x 90 miles (130 x 145 km). The New York/Pennsylvania site covers an area approximately 120 x 90 miles (192 x 145 km). Seasonal Landsat data (fall, winter, and spring) were selected for each test site.

The counties included in the Appalachian project are indicated by number on Figure 1. These counties are:

Test Site #1	Test Site #2	Test Site #3
Ohio:	New York:	Kentucky:
Lawrence (7)	Chautaugua (1)	Harlan (12)
Kentucky:	Cattaraugas (2)	Bell (13)
Boyd (8)	Pennsylvania:	Virginia:
Lawrence (9)	Warren (3)	Lee (14)
West Virginia	McKean (4)	Tennessee
Wayne (10)	Forest (5)	Claiborne (15)
Cabell (11)	Elk (6)	Hancock (16)
		Union (17)
		Grainger (18)

The project can be summarized as follows: A set of twelve digitally enhanced, seasonal Landsat photographic 1:250,000 scale prints covering each of the three test sites have been produced. These enhanced images were generated using such techniques as contrast stretch and edge enhancement. Prior to preparation of the final products, examples of enhancement techniques for each season and for each site were delivered to the NASA Technical Officer for the final selection process. The final product,

a set of twelve cibachrome photographic 1:250,000 scale Landsat prints were delivered by NASA/GE representatives to each state user for image assessment.

BACKGROUND

The goal of image enhancement is to improve the quality of and/or accentuate selected features for subsequent human viewing and interpretation. Although original Landsat data provide a relatively good radiometric representation of surface features, they are not necessarily the most desirable from of image data for further processing and interpretation. Further enhancement may be necessary to aid either human or automated photointerpretation. Enhancement techniques modify radiometric values to achieve this goal.

Both mathematical and heuristic techniques are utilized to achieve desired results. Visual rather than machine-oriented interpretative techniques represent the primary method of extracting information from an enhanced image. Moreover, a human interpreter using images enhanced for a specific purpose can in many cases perform successful analyses of pictorial data without relying on time-consuming mathematical-statistical pattern recognition procedures. In some applications, such as lineament analysis, human interpretation of imagery is far superior to automated interpretation.

Heuristic techniques attempt to attenuate or discard irrelevant information while, at the same time, emphasizing (enhancing) features of interest. Attenuation is achieved by contrast reductions or by smoothing (filtering) operations, both of which tend to blur image detail. Enhancement is accomplished by increasing contrast or by feature sharpening. Since both of these techniques tend to accentuate noise, development of the optimum enhancement usually requires a trade-off between these two effects. Thus, the most efficient method for evaluating and selecting an enhancement consists of the subjective evaluation of the value of a specific product for satisfying a given task. Use of an interactive image analysis system provides a distinct advantage in that an enhancement can be developed, reviewed, improved and tailored to the desired application in a near real-time environment. Ideally, the person who will actually interpret the enhancement will participate in the interactive enhancement selection process.

DIGITAL CORRECTION TECHNIQUES

Banding Removal (Destriping)

Some Landsat images, particularly those from the earlier days of the Landsat program, contain a cyclic 6th line intensity artifact referred to as banding or striping. Since the eye is particularly adept at detecting periodic variations of this type, the artifact is very objectionable and interferes with photointerpretation. This banding characteristic is due to the manner in which Landsat data are acquired. Six different detectors are used for each of the four specified Landsat bands. Each of these detectors (a total of 24 detectors) has a unique transfer (response) characteristic; the variations in radiometric sensitivity between detectors results in banding.

NASA applies a standard correction technique to all Landsat data in an attempt to remove banding. The procedure consists of the application of a linear transfer function to each detector. The transfer function is based on time-averaging of calibration data acquired between mirror scans. The technique has proven to be less than perfect for several reasons. First, a linear correction will never perfectly equalize detector outputs because of non-linearities in detector characteristics and amplifier gain. Secondly, evidence suggests that calibration data are noisy, resulting in the introduction of variations within an image that are of longer term than 6th line banding. Finally, it should be noted that in this type of an operation more than one original digital data level can be mapped into a single digital output level resulting in an irretrievable loss of one of the original levels along with its associated information.

Several methods for minimizing banding have been implemented by various Landsat data users. They range from applying linear transfer functions to the six subsets of data corresponding to each sensor, to line by line filtering, and to cumulative distribution function matching. These processing techniques vary in effectiveness and in the effort required to process the data. All the mentioned techniques provide satisfactory results in most cases, but all will also produce unsatisfactory results when the original data have been subjected to poor ground data processing. The best method of acquiring debanded images consists simply of visually screening and selecting images that contain no undesirable banding characteristics. This approach is preferable to indiscriminate application of debanding algorithms, as it eliminates any information loss through smoothing or co-

incident digital level mapping. It should be noted that the availability of Landsat images containing little or no noticeable banding continues to improve due to the considerable refinement in Landsat ground data processing techniques during the past four years.

Geometric Correction

At least thirteen (13) sources of geometric distortion have been identified in Landsat MSS data. Geometric correction techniques currently in use that consider all of these error sources require 30 or more ground control points per Landsat scene as well as relatively elaborate computer processing techniques. Positional accuracies of a small fraction of a pixel have been achieved using this technique. The cost effectiveness of this approach is questionable, considering the extensive computer processing effort necessary and the considerable manual effort required to locate a sufficient number of ground control points. For most applications, mapping accuracies of this order of magnitude are generally unnecessary and far too expensive in terms of current technology capabilities.

A considerably simpler processing technique can be utilized for geometric correction of a geographic area smaller than the full Landsat scene. Two primary reasons account for this. First, a typical requirement consists of the fitting of the digital enhancements to the 1:250,000 scale USGS topographic map. In this case, geometric processing errors having the same magnitude as those evident in these maps would be acceptable. The standard USGS map specification requires that features be plotted within .02 inches on the map. Nominal mapping errors of 128 meters (i.e., 250,000 x .02 inches x 1m/39.4 inches) on the ground would be expected by this specification. Geometric correction techniques having an accuracy of $\pm$ 1 pixel would therefore be sufficient to satisfy the image/map registration requirement. A second reason justifying the simpler approach considers the fact that only four (4) geometric error sources inherent on Landsat data are significant if an area of two-thirds (or less) of a Landsat scene is to be geometrically corrected to fit a 1:250,000 scale USGS map. These four sources of error are:

	Error Source	Error Type
1.	Skew caused by Earth rotation	Systematic
2.	Mirror scan	Systematic
3.	Roll, yaw	Scene dependent
4.	Dynamic pitch, roll, yaw	Scene dependent

Image skew can be calculated from scene latitude. The mirror scan/panoramic distortion error must be corrected by a nonlinaar correction based on angular velocity measurements of the scanning mirror. Scene dependent errors must be corrected either by a dynamic model or by ground control points.

DIGITAL ENHANCEMENT TECHNIQUES

Digital Contrast Enhancements (Stretches)

Contrast enhancements are defined as a transformation of original image intensity levels into a redistributed set of intensity levels for the enhanced version. Intensity levels associated with features of particular interest are redistributed on the output scale to increase contrast in the selected areas. If the desired contrast is high, or if the dynamic range of interest in large, the result may be a loss of contrast in other relatively less important portions of the input scale.

Reflectance characteristics of Landsat scenes can be displayed by the construction of histograms which illustrate the relationship between pixel brightness values (digital numbers - DN) and their frequency of occurrence. Examples of histograms produced on the GE DIAL IMAGE 100 for one MSS band of a sample Landsat subscene are displayed on Figure 2.

Dashed lines on the graph indicate the spectral range of the data within that band. For example, the histogram indicates that the original data are clustered within relatively limited brightness value ranges. Contrast stretching is employed to expand the distribution of digital numbers of 0 and 255 (corresponding to black and white, respectively, on a positive image). The percentage of the total picture elements saturated to white or black is controlled by the computer analyst. These reassigned data have been "truncated" from the end portions of the histograms. The points at which truncation has occurred are termed "stretch limits." The result of truncating the histogram and thereby saturating portions of the data to white and black is the creation of a greater range of brightness levels for a selected portion of the contrast stretched scene.

Linear contrast stretching involves operating on brightness values using a linear transfer function. Stretch parameters are determined from histograms and/or analyst decisions. The main disadvantage of linear stretching is that truncation (or loss of input levels at the high and low ends of the brightness scale) usually occurs when applying extreme contrast stretches. The optimum linear stretch is therefore a compromise between desired constrast and objectionable truncation. With Landsat images, linear stretches work particularly well when the radiometric (brightness) range of pixel values is relatively small. This is commonly the case with low sun angle images or with images covering heavily vegetated areas. Figure 3 shows the slope of the input/output curve for a linear stretch.

Histogram equalization stretching is generally a non-interactive technique in which a non-linear transfer function is defined from histograms of brightness values. The stretch rearranges levels to create a uniform distribution of intensities and is sometimes referred to as "equal area stretch" or "cumulative distribution stretch" (Figure 3). The technique is particularly effective in images which possess a wide range of intensities or which have a high variance in intensities. It is also useful for images characterized by heavily skewed distributions where mean brightness values are biased toward one end of the scale. The technique has been widely and effectively used on Landsat scenes covering areas with little or no vegetation. This technique is not as effective in forested areas or in areas with significant farming activity because it tends to overenhance images with low signal distribution variance. A reasonable compromise for use in vegetated areas is to prepare a distribution weighted stretch in which maximum contrast is kept to an acceptable level.

Piecewise linear contrast stretching is an extension of linear contrast stretching. It allows user specification of break point or line segments to define the desired transfer function. Virtually any linear or non-linear stretch can be transformed into a piecewise linear stretch. A common use of this technique is to modify a linear stretch to achieve higher contrast in the heavily populated mid-range intensities with contrast tapering off at the gray scale extremes to prevent truncation. The shape of the piecewise linear input/output curve is shown in Figure 3.

EDGE ENHANCEMENT

Landsat data often have subtle brightness variations which are difficult to detect, particularl in an original unenhanced image. These brightness variations are related in part to topographic relief characteristics, including landforms and drainage patterns. Since lineaments are directly expressed or enhanced by topographic relief, some form of enhancement to exaggerate selected topographic patterns can be especially useful.

The edge enhancement technique improves or enhances brightness variations of Landsat data. Edge enhancements intensify radiometric (brightness) patterns which have a certain spatial frequency; both low and high frequency filters are typically used. A high frequency filter examines the average brightness value of a small number of pixels surrounding the specific pixel to be enhanced. After the filter has been applied to these test data the new brightness values are then applied to the appropriate pixels within the test site. The edge enhancement technique utilized by GE consists of the use of a weighting mask (or kernel) to determine the local pixel average; the enhancement process involves convolution of an image to prepare the new enhancement. The edge enhanced product is achieved by extracting high frequency spatial image information and then recombining this information with the original image.

The edge enhancement technique produces a sharper image, but it may introduce artifacts ("noise") into the data. Thus, there is some trade-off in deciding to what extent edges should be enhanced. Usually, the optimum edge enhancement is both scene and task dependent. Because of this, the capability to perform convolution on an interactive video display system is highly desirable in that it allows real-time viewing and modification of the weighting mask factors.

A description of the three edge enhancement techniques used by GE--Laplacian, MTF compensation and "fast filter"--are described in the following section.

Laplacian Enhancement

A relatively simple mathematical operation ideally suited to image enhancement is the two dimensional second derivative of image intensity, often called the Laplacian. Its effect on an image is to make edges or intensity discontinuities appear sharper than they actually are. Basically, the first derivative (gradient), (or rate of change of image intensity) locates edges in an image; the

2nd derivative (or rate of change of the gradient) exaggerates these edges. The output of a true Laplacian operation has a mean value of zero, and zero output occurs at those points where no edges are found. When the operation passes over an edge of decreasing intensity the output shifts first positive, then negative, and vice versa. By applying an additive offset to the output, positive values are maintained, thus allowing the output to be displayed pictorially. This operation extracts information associated only with edges, and completely subdues non-edge, low spatial frequency information.

A typical application of the Laplacian operation as an enhancement technique consists of the summation of the output with the original image. This technique preserves low spatial frequency information and accentuates the higher spatial frequency information extracted by the operator.

Fast Filter

A family of spatial filters called "VICAR fastfill" have been designed for rapid execution on a general purpose computer. These filters have the unique property that all elements in the kernel are either plus 1 or minus 1. Thus, the need for the large number of multiplicative operations usually required to perform convolution is eliminated. The coefficients are arranged so that the portion of the kernel surrounding the central element sums to zero. The summation of the kernel value with the central element value brings the total sum to unity. The original image for any area of uniform intensity is then output and a non zero component is added if the area contains either an edge or any texture information.

MTF Compensation

The Modulation Transfer Function (MTF) is a mathematical description of the accuracy of reproduction by some imaging device, of an idealized sinusoidally varying object as a function of spatial frequency. For typical images, the MTF is nearly perfect for low spatial frequencies and falls off as the resolution limit of the image is approached. MTF compensation is one of the most commonly used spatial frequency restoration techniques and its purpose to increase the modulation or reproduction brightness of higher spatial frequencies correcting the inevitable attenuation of these frequencies caused by an imperfect atmosphere and by the use of an imaging device with finite resolution.

Compensation for the MTF of an imaging system (MTFC) is performed by convolving an image with a two dimensional kernel, with the characteristic form of the kernel being defined on a theoretic basis. The form is such that elements near the central element are heavily weighted with a sign opposite that of the central element. Elements farther from the center are weighted less heavily and therefore have a less pronounced effect on the output, see Figure 2-10.

Exact determination of the MTFC kernel on a theoretical basis is a difficult task involving the modeling or measuring of imaging system characteristics. However, the task can be circumvented if we consider only the characteristics of the specific image and the problem of correcting its edges to approximate step functions as closely as possible. The amount of sharpening required by any specific image can be determined by investigations of the degree of edge smoothing present in that image. If image processing hardware capable of performing high speed convolution is available, then kernel element weighting can be determined through iterations with the analyst adjusting the amount of sharpening necessary to approximate perfect edge reproduction.

For the purpose of enhancement, it is sometimes not particularly advantageous to restore edges to a theoretic optimum, but to exaggerate them by creating edges which exceed (overshoot) true edge sharpness. Again this is best performed interactively to achieve a well balanced enhancement.

Photographic Film and Exposure Considerations

GE utilizes a DICOMED digital-to-film recording system for preparation of film enhancements. The DICOMED system utilizes Kodak Ektachrome film processed with the E6 chemistry as the standard input. In utilizing Landsat data it is necessary to relate the digital input values to both the specific recorder and to the related film density. The minimum and maximum digital values must be limited to remain within the linear range of the recorder/film/processing combination. In this manner Landsat pixel digital values can be correlated and matched as necessary via a look-up table with the linear range of the recording system.

With this empirically derived information, the GE DIAL IMAGE 100 can process Landsat imagery to stretch (or compress) and shift the digital values to the appropriate linear range of the recording process. In this manner optimum use is made of the dynamic range of the recorder/film combination while avoiding undesirable data truncation (and possible loss of desired data) which would occur if the Landsat pixel values exceeded certain limits.

METHODOLOGY

The methodology employed to produce the enhanced products was developed after careful consideration of all of the factors that might affect product quality, overall image utility, and scene content.

The project began with the review and selection of seasonal Landsat data over the three sites. After image selection, the respective computer compatible tapes were preprocessed to remove undesirable banding characteristics and to geometrically correct the tapes to a Universal Transverse Mercator projection. Subsequently the data were processed on the GE Digital Image Analysis Laboratory (DIAL) IMAGE 100 to interactively process and select the optimum contrast stretch and edge enhancements. A variety of products were then generated for the most promising combinations and reviewed by the NASA Technical Officer for final selection. Final products at 1:250,000 scale were then prepared and forwarded to the state users for evaluation. This effort is described in more detail in the following sections.

Selection of Landsat Computer Compatible Tapes (CCTs)

Upon project start, the NASA/GSFC Technical Officer developed a preliminary listing of high quality, cloud-free and seasonal, Landsat data covering the three Appalachian test sites. These data were reviewed at the GSFC Browse Library for final selection. Where possible, scenes having minimal striping characteristics and cloud cover were selected.

Preprocessing of Landsat Tapes

This initial task consisted of the extraction of test sites from the CCTs onto a digital file containing only the test site area. These test site files were checked for data "drop" lines and striping characteris ics; new files were created as required.

Landsat Scene Merging

Two of the selected test sites (Kentucky-Tennessee and Ohio-Kentucky-West Virginia) were located in an undesirable position on their respective Landsat scenes. That is, although the test sites were considerably smaller in area than the average of one Landsat scene, their specific scene location was such that two adjacent Landsat scenes were needed to fully cover each test site. Tape merging was necessary to reduce the necessary digital processing effort.

The solution to this problem was to merge the Landsat CCTs to form new digital files which were centered on each test site. Digital mergins of the Landsat scenes presented no significant problem because in each case the data required for the merged composite came from the same down-track spacecraft orbital path.

Debanding

Only one of the twelve Landsat images used in this project had undesirable banding characteristics. This image (ID #2600-15094, New York/Pennsylvania test site) was debanded using look-up tables generated from a linear correction transfer function.

Geometric Correction Procedure

This project required geometric correction of Landsat data for each test site. Specifically, the requirement was that the geometry of the resulting enhanced photographic products should conform to the geometric characteristics of relevant 1:250,000 scale Transverse Mercator maps published by USGS.

Interactive digital image processing was conducted to identify ground control points (GCPs) within the test sites that were evident on both the USGS map and Landsat data. The geographic location of each GCP on the Landsat scene was determined by using a special purpose "scaled cursor" routine that enabled the operator to determine the location of the GCP by pixel line and column. Using this information the operator was then able to digitally correct the Landsat data so that the GCPs evident on the Landsat data had the same geometric and spatial relationships as evident on the USGS map. A nearest neighbor resampling technique was used for the geometric correction procedure.

Preparation of Digital Contrast Enhancements (Stretches)

After tape merging, extraction of test sites, replacement of bad data lines, debanding and geometric correction, the Landsat data files were then in the proper format for selection of optimum contrast enhancements.

The interactive capability of the DIAL IMAGE 100 was utilized to allow the analyst to prepare, evaluate, modify and tailor a contrast stretch to each test site in a real-time environment. This capability insured that maximum scene contrast was attained while scene detail was preserved.

In this project both interactive and non-interactive techniques were utilized to develop contrast enhancements. The specific procedure varied according to the type of stretch desired. Typically, development of the non-linear stretches required more interactive processing than did the linear stretch.

As described in Section 2.3, the contrast stretch technique involves the acquisition of input values and the selection of output values for a given test site. To achieve a contrast stretch, the specific input value for each MSS band was output at a different brightness value.

Input values were acquired in the following manner. Upon storing and displaying the given test site on the television screen, a cursor was positioned on the screen to include the entire image. Histograms for each of the four MSS bands were produced by training on the cursored area and printing out brightness value on a cathode ray tube. This printout showed, on a gray level scale of from 0-127, the number of pixels for each gray level.

Output values were acquired using either of two approaches. Contrast stretches were prepared interactively and displayed in real-time on the DIAL IMAGE 100 television screen. The computer analyst selected the desired stretch by modifying brightness values (truncating, etc.), as explained previously. Output values were then printed out for the new stretched enhancement. A new set of brightness values were acquired by training on a cursored area. Based on these two sets of data, a contrast stretch input/output curve was developed.

The second technique utilized was primarily non-interactive in that the design of the stretch input/output line was accomplished by using the input values to develop a candidate input/output curve. These data were then used to process a candidate enhancement for subsequent evaluation.

Preparation of Edge Enhancements

After an initial series of test products were generated and evaluated, several edge enhancements were found to produce consistently good results and were standardized for the project. Assessment of the quality of edge enhancements was based primarily on a visual inspection of the film product. Then if the edges were evaluated to be over emphasized or not sharp enough additional interactive work was conducted.

For VICAR fast filter, several enhancements were produced with both 3 x 3 and 7 x 7 kernels. Since it was felt that some edges were overenhanced, a few enhancements were run with modified kernels. Modified kernels were made by changing each element in the adjacent area to $\pm$ .5 and leaving the central element set at unity. The net effect of this change was to make the edge enhancement a little more subtle by weighting the central kernel element more heavily than the others.

Generation of DICOMED Digital Film Enhancements

A variety of digital enhancements were prepared using the DICOMED digital-to-film-recorder. It is evident that quite a variety of enhancements could have been produced, based on the number of en-

hancement options (at least three basic types stretches, three basic types of edge enhancements, plus a choice of two film gammas). In actuality, the most promising enhancements were prepared based in part on the experience of computer analyst plus the results of experimentation. Approximately eight different types of enhancements were prepared for each test site, for each season. 8 x 10 inch prints were made of the most promising. Film transparencies and prints were studied in more detail for final selection.

The bulk of the digital enhancements produced for this study used gamma values = 1 (no tonal contrast increase) or ≈ 2 (considerable tonal contrast increase). It was found that better results were always achieved using the higher gamma value for Kodak vericolor negative film. Better results were also noted in most cases using the higher gamma value for the Ektachrome-Cibachrome enhancements.

The NASA/GSFC Technical Officer selected four digital film transparencies for each test site per season for printing on Cibachrome paper at a scale of 1:250,000; the USGS 1:250,000 scale maps were used as a guide to insure exact enlargement. The size of each print was 20 x 24 inches at this scale. Only the New York/Pennsylvania test site required two (2) prints to cover the required area; the other two sites were fully covered by one 20 x 24 inch print. Two (2) of these copies were then delivered to each of the state users.

Evaluation of Enhanced Landsat Images

The enhanced Landsat data were delivered to the participating state users beginning in early 1979. The users are (at the data of preparation of this paper) currently evaluating the application of these data for lineament mapping and for natural gas exploration. Each product will be evaluated for its advantages/disadvantages for geologic mapping. A summary report indicating the relative value of each product for lineament mapping and other geologic applications will be prepared and provided to NASA for further evaluation.



Figure 1. Test Sites.

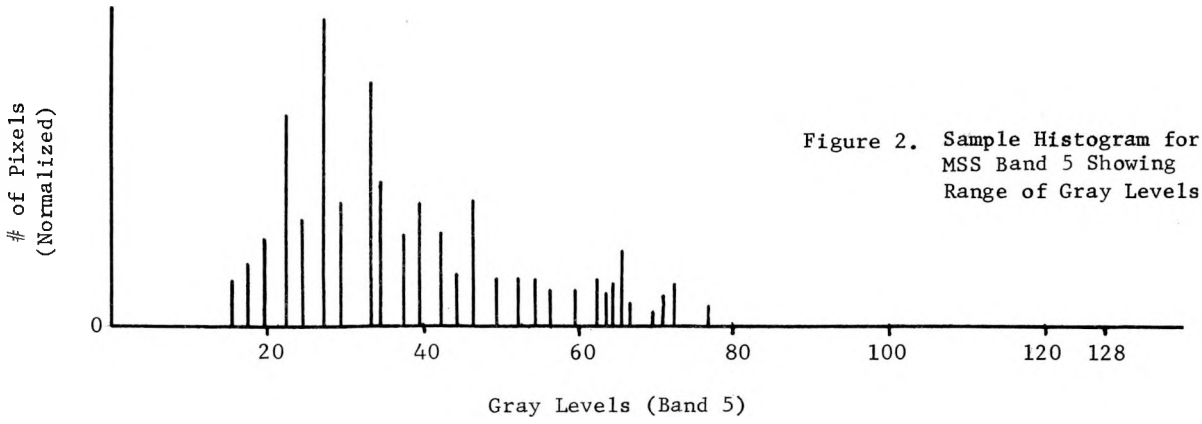
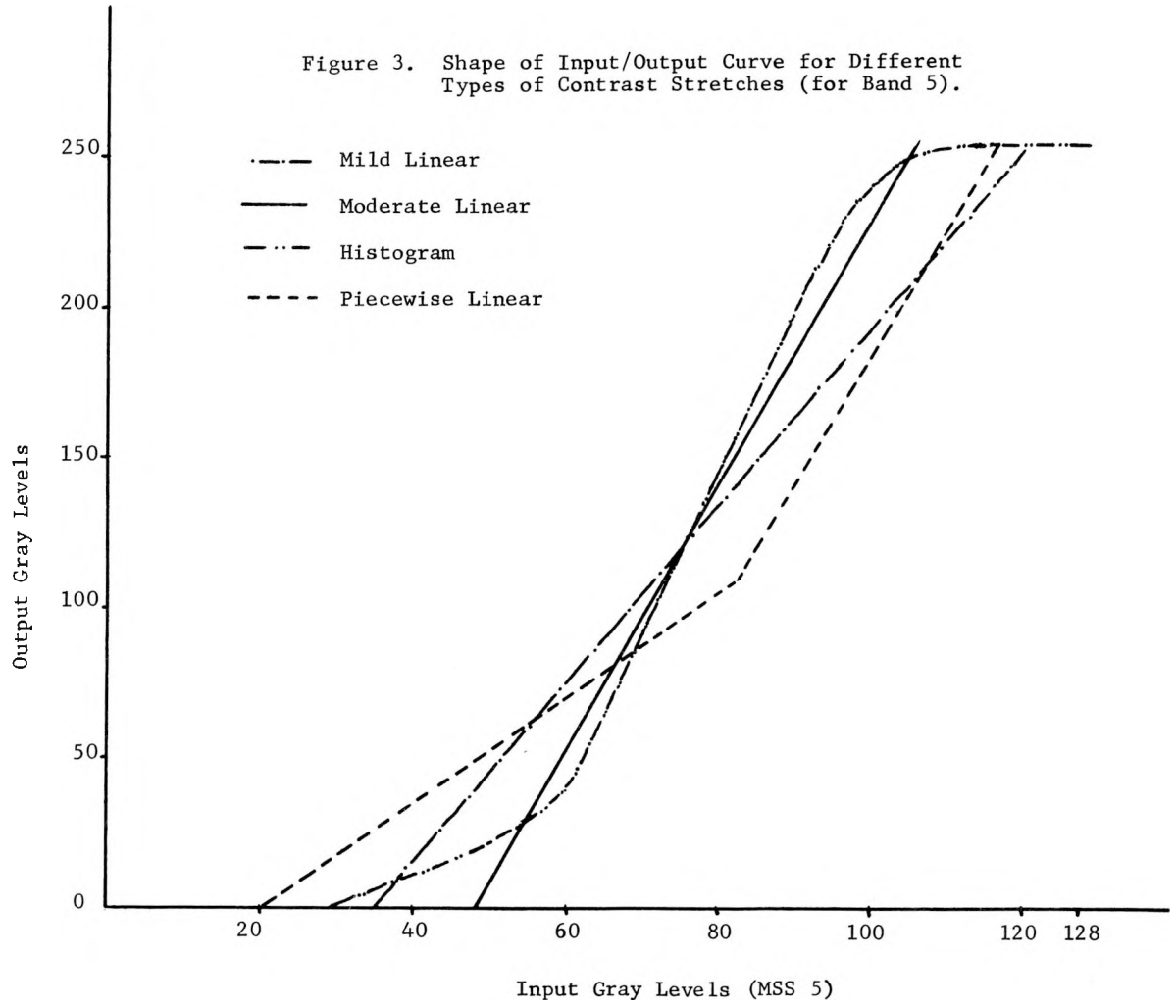


Figure 2. Sample Histogram for MSS Band 5 Showing Range of Gray Levels.

Figure 3. Shape of Input/Output Curve for Different Types of Contrast Stretches (for Band 5).

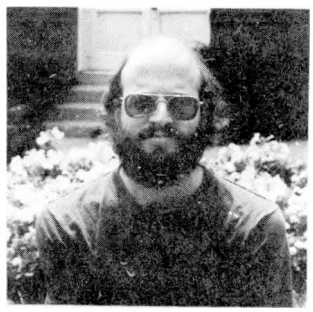


LATE-TECTONIC EXTENSION FAULTING IN THE CENTRAL APPALACHIANS

Philip S. Berger
Department of Geology
University of Cincinnati, OH

and

Russell L. Wheeler
Department of Geology
West Virginia University



ABOUT THE AUTHORS

Mr. Berger received his B.S. in Geology (1976) from the University of Maryland and his M.S. in Geology (1978) from West Virginia University. He is presently employed by the Branch of Tectonophysics, Office of Earthquake Studies, U.S.G.S., while pursuing his Ph.D. full-time at the University of Cincinnati.

His Ph.D. research concerns analytical, experimental and field studies of the formation of contraction faults in a multilayered sequence.

Dr. Wheeler received his B.S. in Geology from Yale University and his Ph.D. from Princeton University (1973). He was formerly an Associate Professor of Structural Geology at West Virginia University and is presently employed by the Branch of Tectonophysics, Office of Earthquake Studies, U.S.G.S. in Denver, Colorado.

His research interests include spacing and sequencing of rock fractures, geologic characterization of cross-strike structural discontinuities in the central Appalachians, applications of statistics to tectonics and structural geology, and regional geology of the Caledonides.

ABSTRACT

Extension faulting was an important mechanism of layer-parallel elongation in folded rocks in parts of the western Valley and Ridge and eastern Allegheny Plateau provinces of Maryland, Pennsylvania, Virginia, and West Virginia. The faults formed late during folding, when beds were dipping steeply, and contributed to growth of anticlines. The faults are particularly abundant in the Brallier Formation (Upper Devonian) on the steep, northwestern limb of Wills Mountain anticline, where the Brallier Formation is thinned by as much as 75 percent. We suggest that the thinning is partly due to late-tectonic extension faulting in multilayers of sandstone and shale and to flowage in thick shale units, rather than to splay faults rising from detachment surfaces. Sequences of extended multilayers may contribute fracture permeability to a gas reservoir.

INTRODUCTION

This study is based on examination of bed-parallel extension structures, primarily faults. Extension faults can form at any bed orientation, depending on the attitude of the local maximum principal compressive stress (Norris, 1958, 1964). However in the central Appalachians, analysis of structural style and field investigation indicates that extension faults form when bed dip exceeds 45 degrees (Berger, 1978; Berger, Perry and Wheeler, 1979) serving to thin the beds. Cloos and Broedel (1943), Root and Wilshusen (1977) and Nickelsen (1979) describe similar faults elsewhere in the central Appalachians. Perry (1971) and deWitt and Dennison (1972) describe similar faults in the study area. Perry and deWitt (1977), Perry (1978), and Berger, Perry and Wheeler (1979) recognize these reverse faults as extension faults, analogous to those in the Canadian Rockies described by Norris (1958, 1964) and Price (1964, 1967).

With the possible exception of some systematic joints, these extension faults are the latest effects of brittle but fold-related deformation in the central Appalachians (Berger, Perry and Wheeler, 1979; Nickelsen, 1979). Because the faults are formed late during deformation, they are least likely to be filled by vein material or closed during later deformation. If sufficiently numerous and extensive and assuming the presence of a gas-bearing source and reservoir seal, they are an excellent target for gas exploration. In particular, they may form permeable fractured reservoirs in the Middle and Upper Devonian clastic sequence. The purposes of this paper are threefold: 1) to examine the lithostructural distribution of extension faults, 2) to document map-scale thinning by extension faulting and shale flowage, and 3) to interpret these data for fractured reservoir potential.

FIELD OBSERVATIONS

More than 100 large exposures of steeply dipping or overturned beds were examined for extension faulting in the western Valley and Ridge and eastern Allegheny Plateau provinces (Fig. 1). Of these exposures, 24 were intersected by at least one extension fault where horizontal separation could be measured. Measureable extension faults and associated slip surfaces are particularly well developed on the steep to overturned northwest limb of the Wills Mountain anticline. Twelve of the exposures with measureable extension faults occur there.

Some extension faults occur singly. Others are conjugate pairs. Some have associated synthetic and antithetic extension faults. Extension faults may terminate against each other, or against a thick bed of siltstone or limestone. In some places the thick bed is broken by a fracture zone along the continuation of the extension fault, and the fractures may show small amounts of slip. An extension fault may die out as a single fault or by distributing its slip among several splays in shales. Many extension faults curve upwards or downwards into surfaces of bedding-plane slip (Price, 1964).

Numerous other fractures were observed, especially in the shaly parts of the Upper Devonian Brallier Formation, many with slickenside, slickenline, or apparent dip orientations similar to those of nearby extension faults but not showing drag folding or matchable beds. The number of extension faults recognized (Table 1), as well as the numerous undifferentiated fractures, indicates to us that extension faulting is an important and little recognized mechanism of deformation. Indeed, this mechanism is characteristic of certain stratigraphic units like the Brallier Formation where those units are rotated to steep dips.

Other extension structures found include boudinage of thin siltstone or limestone beds, abundant lenticular extension fractures oriented roughly perpendicular to bedding, and three normal faults of small displacement. In predominantly thick shales steep siltstone beds show abrupt terminations, indicating that the vertical continuations of the beds are somewhere updip.

We suggest that steep interbedded sequences of siltstone and shale (such as the Brallier Formation)

responded to continued horizontal shortening by extension faulting in the stiff beds and shale flowage in the soft beds. The amount of extension accomplished by faulting in the stiff beds will approximate the amount of shale flowage in the soft beds. For thick shales with minor siltstone interbeds, we suggest hingeward flow of the shales, substantially thinning the sequence.

FOLD GROWTH BY EXTENSION FAULTING AND TECTONIC THINNING

The major anticlines of the central Appalachians are active structures generated mainly by duplication of strata by ramping of underlying detachment faults, by splay faulting, and by ductile flow of shale or evaporite sequences into anticlinal crests (Gwinn, 1964; Faill, 1969; Wheeler, 1975). The major synclines are passive structures resulting from anticlinal growth in adjacent rocks, rather than from active downbuckling (Gwinn, 1964). In most places in the central Appalachians, the detachment surface r splay fault does not reach the surface. We propose that extension faulting in stiff beds and aulting and flowage of soft beds late during folding provides a contribution to anticlinal growth.

'ectonic thinning of measured stratigraphic sequences has been reported on the steep northwest limb of the Wills Mountain anticline (Dennison and Naegele, 1963; Dennison, Travis and Ferguson, 1966; deWitt and Dennison, 1972; deWitt, 1974) and was used as a guide by us in locating exposures that have undergone extension faulting. We hoped to be able to recognize enough extension faults to account for a large proportion of the tectonic thinning. Table 2 summarizes Berger's measurements of extension faults in outcrop. For each identifiable extension fault, the horizontal separation was measured. The amount of tectonic thinning (T) is approximately

$$T \cong H/ET \qquad (1)$$

where H = the sum of the amounts of horizontal separation of measured extension faults. ET = thickness of the exposure, measured perpendicular to bedding.

We emphasize that fault separation measurements reported here are probably minimum values. Only definite extension faults were measured. All measurements were taken in 2 to 3 m high strips along the accessible basal segments of exposures. The larger the displacement along the fault the less the chance of matching beds across the fault.

At Station 4, near Ketterman's Knob, Pendleton County, West Virginia (Fig. 1, Table 2), Dennison and Naegele (1963) report that approximately 60 m of the Brallier formation is absent (about 25 percent tectonic thinning). Outcrop examination at Station 4 indicates a minimum of 0.1 percent tectonic thinning by extension faulting. Here Dennison and Naegele (1963) write that tectonic thinning was probably accomplished by minor faulting within a fault zone in the Brallier Formation. We suggest that here thinning occurred predominantly by shale flowage rather than by extension faulting.

To the Northeast along strike, Dennison, Travis and Ferguson (1966) infer the presence of four major fault zones in the Brallier Formation (Kittlelick, Dawson, Cresaptown [station 3], and Hyndman [station 21] faults) from geomorphic evidence of a narrowed strike valley and from measured stratigraphic sections. Dennison, Travis and Ferguson (1966) infer that these fault zones are splay faults rising from a deep detachment, probably located in the Ordovician Reedsville Formation. deWitt (1974 and written communication, 1978) proposes from seismic data that the Hyndman fault is a large splay fault with associated extension faults in the fault zone, particularly near the village of Hyndman.

We believe that the tectonic thinning reported by Dennison and Naegele at our Stations 3 (La Vale) and 4 (Ketterman's Knob) was accomplished more by small and medium size extension faults and shale flowage than by the single splay faults envisioned by Dennison and Naegele (1963) and deWitt and Dennison (1972) (Fig. 2). Our arguments are three. First, all four inferred splay faults occur on the northwest limb of the Wills Mountain anticline and crop out in and thin the Brallier Formation. This requires a fortuitous coincidence of erosion level with the intersection of the Brallier Formation and the fault surface and must occur for all four faults. If a fault is a splay and thus not confined to the Brallier, then it is about equally likely to crop out stratigraphically above, within, or below that unit. Second, as shown in Table 1, the Brallier Formation shows more extension faults than does any other Devonian unit examined. Third, as noted above under "Field Observations", the Brallier contains more minor faults, many unclassifiable, than does any other unit examined. We suggest a simpler explanation that the Brallier Formation localizes extension faulting and shale transport in our study area (Fig. 2B).

We suggest that the Dawson thrust of Dennison and Naegele (1963) and deWitt and Dennison (1972) may be a zone of shale flowage because we observed few minor extension faults in the outcrop belt of the fault zone (station 21 and in exposures near station 1).

The thinning in the Hyndman fault zone is more likely to be due to splay faulting than to the associated

extension faults (deWitt, written communication, 1978) on the basis of confidential seismic data available to deWitt. However, the thinning mapped at the surface (deWitt, 1974) may not be clearly connected with the splay fault observed on the seismic section at depth because poor reflections are usually received in such areas of steep dips.

The Kittlelick fault is described as a fault zone by Dennison, Travis and Ferguson (1966). We agree but suggest that the thinning along the Kittlelick fault is due to a zone of extension faulting and shale flowage similar to the zone of numerous extension faults observed along the Cresaptown fault [station 3] and near Ketterman's Knob [station 4]. We also suggest that thinning of stratigraphic units adjacent to the Kittlelick and Hyndman faults as reported by Dennison and others (1966) and deWitt and Dennison (1972) may also be due in part to extension faulting as well as to branches from splay faults.

MAP-SCALE FOLDING AND GAS POTENTIAL

Anticlines in the central Appalachians can grow by crestward flowage of shale and mudstone units (Wheeler, 1975; Perry and deWitt, 1977; Kulander and Dean, 1978). In stiffer units extension faults can thin and extend beds on steep limbs of asymmetrical anticlines. The presence of gravity lows on the northwest (steeper dipping) limbs of the Wills Mountain, Blackwater, Browns Mountain and Glady anticlines (Kulander and Dean, 1978, Plate 2) indicates to us: (1) flowage of low density shale from low on the steep limbs to high on those limbs, (2) thickened or repeated shale sections due to detachment-related, pre-folding thrusting (Kulander and Dean, 1978; stage I of Berger and others, 1979), (3) vertically dipping low density shales (B. Kulander, oral communication, 1978), or (4) combination of the above.

We would expect gravity lows caused by (2) or (3) to extend parallel to the anticlinal axis. Thus the relatively long, linear gravity lows on the northwest limbs of the Wills Mountain and Browns Mountain anticlines (Kulander and Dean, 1978, plate 2) are probably more the result of detachment related repetition and thickening of the Ordovician Martinsburg Formation and Devonian shales than to ridge-shaped crestward transport of ductile rocks (B. Kulander, oral communication, 1978). In contrast, the circular lows on the northwest limbs of the Blackwater and Glady anticlines are more likely due to lobes of uplimb flowage in the ductile units of the Middle and Upper Devonian clastic sequence. Those inferred thickened shale lobes suggest that there exists a thinned Brallier Formation lower on the limb that is subjected to extension faulting in the stiff units and faulting and flowage in the soft units (Fig. 3). This thinning would be similar to that observed in outcrop in the Devonian Brallier Formation (Dennison and Naegle, 1963) and could indicate gas potentially in a permeable fractured reservoir. The source beds could be the Devonian black shales (the Marcellus and Harrell Formations) and the flowed, thickened, perhaps heavily slickensided shale updip could seal the reservoir. We suggest further exploration for thinned and fractured shales down-dip of the buried, thickened shales that we infer to lie beneath the observed gravity lows. For steep or overturned northwestward limb dips, the suggested exploration target would lie roughly under the northwestern boundary of a circular gravity low. Additional gravity measurements and modeling of the gravity lows mapped by Kulander and Dean (1978), guided by construction of balanced cross sections (Dahlstrom, 1969; Perry, 1971), should define those targets more exactly.

ACKNOWLEDGMENTS

We acknowledge financial support to the senior author from the U.S. Department of Energy through its Eastern Gas Shales Project Contract nos. EY-75-C-05-5194 and EY-77-C-21-8087. Additional support was received from the American Association of Petroleum Geologists as a Research Grant-in-Aid and from Sigma Xi. Comments of A. Johnson, B. Kulander, R. C. Shumaker, M. T. Heald, W. deWitt, W. J. Perry, Jr., and T. Wilson improved the manuscript. Most of the research by the senior author was accomplished while a student at West Virginia University.

REFERENCES

1. Berger, P. S.: "Extension Structures in the Central Appalachians", Morgantown, W. Va., West Virginia Univ., M.S. Thesis, 1978, 97 p. [University Microfilms, Ann Arbor, MI].

2. Berger, P. S., Perry, W. J., and Wheeler, R. L.: "Three Stage Model of Brittle Deformation in the Central Appalachians", Southeastern Geology, v. 20, n. 2, 1979, pp. 59-67.

3. Cardwell, D.: "Deep Well and Structural Geologic Map of West Virginia", W. Va. Geol. and Econ. Sur., 1973.

4. Cloos, E., and Broedel, C.: "Reverse Faulting North of Harrisburg, Pennsylvania", Geol. Soc. Amer. Bull., v. 54, 1943, pp. 1375-1398.

5. Dahlstrom, C.: "Balanced Cross Sections", Canadian Jour. Earth Sci., v. 6, 1969, pp. 743-757.

6. Dennison, J. M., and Naegele, O. D.: "Structure of Devonian Strata along Allegheny Front from Corriganville, Maryland, to Spruce Knob, West Virginia, West Virginia Geol. and Econ. Survey, Bulletin 24, 1963, 63 pp.

7. Dennison, J. M., Travis, J. W., and Ferguson, J. H.: "Kittlelick Thrust: A New Fault in Mineral and Grant Counties, West Virginia, Proceedings of the West Virginia Academy of Science, 1966, v. 38, pp. 177-185.

8. de Witt, W.: Geologic Map of the Beans Cove and Hyndman Quadrangles and part of the Fairhope Quadrangle, Bedford County, Pennsylvania, U.S.G.S. Map I-801, 1974.

9. de Witt, W., and Dennison, J. M.: "The Allegheny Front from Bedford County, Pennsylvania to Grant County, West Virginia": In Dennison, J. M., ed., Stratigraphy, Sedimentology, and Structure of Silurian and Devonian Rocks along the Allegheny Front in Bedford County, Pennsylvania, Allegheny County, Maryland, and Mineral and Grant Counties, West Virginia, Harrisburg, Pa., Pennsylvania Bur. Topog. and Geol. Survey, Guidebook for 37th Ann. Field Conf. of Pennsylvania Geologists, 1972, pp. 14-32.

10. Faill, R. "Kink Band Structures in the Valley and Ridge Province, Central Pennsylvania", Geol. Soc. Amer. Bull., v. 61, 1969, pp. 857-876.

11. Gwinn, V.: "Thin-skinned Tectonics in the Plateau and Northwestern Valley and Ridge Provinces of the Central Appalachians", Geol. Soc. Amer. Bull., v. 85, 1964, pp. 863-900.

12. Kulander, B., and Dean, S.: "Gravity and Structural Reconnaissance across Browns Mountains, Wills Mountain, and Warm Springs Anticlines - Gravity Study of the Folded Plateau, West Virginia, Virginia, and Maryland": In: Appalachian Structures, Origin, Evolution, and Possible Potential for new Exploration Frontiers, Morgantown, W. Va., W. Va. Geol. and Econ. Sur., 1972.

13. Kulander, B., and Dean, S., 1978: "Gravity, Magnetics, and Structure, Allegheny Plateau/Western Valley and Ridge in West Virginia and Adjacent States, West Virginia Geol. and Econ. Sur., Rept. of Investigation RI-27, 1978, 61 p.

14. Nickelsen, R., "Sequence of Structural Stages of the Allegheny Orogeny at the Bear Valley Strip Mine, Shamokin, Pennsylvania", Amer. Jour. Sci., v. 279, 1979, pp. 225-271.

15. Norris, D. K.: "Structural Conditions in Canadian Coal Mines", Canada Geol. Survey Bull. 44, 1958, 54 pp.

16. Norris, D. K.: "Microtectonics of the Kootenay Formation near Fernie, British Columbia", Bull. Canadian Petroleum Geologists, v. 12, 1964, pp. 383-398.

17. Perry, W., Jr.: "Structural Development of the Nittany Anticlinorium, Pendleton County, West Virginia", New Haven, Conn., Yale University, Ph.D. Dissert., 1971, 227 pp.

18. Perry, W., Jr.: "Sequential Deformation in the Central Appalachians", Am. Jour. Sci., v. 278, 1978, pp. 518-542.

19. Perry, W., Jr., and de Witt, W.: "A Field Guide to Thin-Skinned Tectonics in the Central Appalachians", Annual AAPG/SEPM Convention, Washington, D.C., June 12-16, 1977, 56 pp.

20. Price, R.: "Flexural-slip Folds in the Rocky Mountains, Southern Alberta and British Columbia", Seminars in Tectonics-IV, Dept. Geol. Sciences, Queen's University, Kingston, Ont., 1964, pp. 6-17.

21. Price, R.: "The Tectonic Significance of Mesoscopic Subfabrics in the Southern Rocky Mountains of Alberta and British Columbia", Can. Jour. Earth Sciences, v. 4, 1967, pp. 39-70.

22. Root, S., and Wilshusen, J.: "Structure and Engineering Geology at the Rockville Cut", Pennsylvania Geology, v. 8, no. 1, 1977, pp. 2-6.

23. Wheeler, R. L.: "Geometric and Kinematic Analysis of Folds in the Upper Devonian Chemung Group, and Relationships to Processes Forming Major Structures of the Eastern Plateau Province" [abs.], Abstracts with Programs, Geol. Soc. Amer., v. 7, no. 4, 1975, pp. 548-549.

Table 1.

STRATIGRAPHIC UNIT	NO. EXT. FAULTS SEEN	NO. MEASURABLE EXT. FAULTS	SECTION THICKNESS: EXPOSURES WITH MEAS. EXT. FAULTS	FAULTS PER M OF SECTION
Mississippian				
Pocono Formation	9	4	266 m	0.034
Devonian				
Hampshire Formation	1	0	--	--
Chemung Group	8	6	308 m	0.026
Brallier Formation	104	43	1251 m	0.083
Millboro Formation	1	1	75 m	0.01
Marcellus Formation	4	0	--	--
Silurian				
Tonoloway Formation	35	24	200 m	0.175
Wills Creek Formation	1	1	159 m	0.006
Bloomsburg Formation	7	2	94 m	0.074
McKenzie Formation	27	17	148 m	0.182
Rochester Shale	14	14	139 m	0.101
Keefer Sandstone	2	1	6 m	0.3
Rose Hill Formation	4	2	7 m	0.6
Tuscarora Formation	7	4	82 m	0.08
Ordovician				
Juniata Formation	3	2	40 m	0.08
Total	227	115		

Table 2.

STATION	T/R	LOCATION	UNIT(S)
1 Pinto, Md	1.6%	NW limb, Wills Mt. ant.	Rose Hill/Keyser
2 Woodmont, Md	0.4%	NW limb, Cacapon Mt. ant.	Mahantango/Brallier
3 La Vale, Md	0.5%	NW limb, Wills Mt. ant.	Mahantango/Hampshire
4 Ketterman's Knob, WV	0.1%	NW limb, Wills Mt. ant.	Brallier
5 Parsons, WV	3.5%	axial region, Deer Park ant.	Chemung
6 White Sulfur Springs, WV	0.1%	NW limb, Brown Mt. ant.	Chemung/Pocono
7 Judy Gap-a, WV	0.2%	NW limb, Wills Mt. ant.	Tonoloway
8 Ryder Gap, Va	3.7%	NW limb, Wills Mt. ant.	Brallier/Chemung
9 Cedar Cliffs, Md	0.6%	SE limb, Wills Mt. ant.	Bloomsburg/McKenzie
10 Rose Hill, Md	0.2%	SE limb, Wills Mt. ant.	Rose Hill/McKenzie
11 Teeter Hollow, WV	0.1%	NW limb, Wills Mt. ant.	Rochester
12 Snowy Mt. Rd.-a, WV	0.4%	NW limb, Wills Mt. ant.	Rochester/Keefer
13 Snowy Mt. Rd.-b, WV	2.9%	NW limb, Wills Mt. ant.	Rochester/Keefer
14 Snowy Mt. Rd.-c, WV	1.9%	NW limb, Wills Mt. ant.	Rochester/Keefer
15 Huntersville, WV	<.1%	NW limb, Browns Mt. ant.	Bloomsburg
16 Rte. 39, WV	<.1%	axial region, Browns Mt. ant.	Tuscarora
17 Minnehaha Springs, WV	0.8%	SE limb, Browns Mt. ant.	Juniata/Tuscarora
18 I-64-a, WV	0.1%	SE limb, Browns Mt. ant.	Brallier
19 I-64-b, WV	0.2%	axial region, Browns Mt. ant.	Harrell/Brailler
20 North Fork Gap, WV	0.3%	NW limb, Wills Mt. ant.	Tuscarora
21 Wolf Camp Run, Pa	0.1%	NW limb, Wills Mt. ant.	Mahantanto/Brallier
22 Martin Mt., Md	0.3%	NW limb, Patterson Ck. Mt. ant.	Tonoloway
23 Hancock, Md	0.1%	SE limb, Cacapon Mt. ant.	Bloomsburg
24 Judy Gap-b, WV	3.1%	NW limb, Wills Mt. ant.	Brallier

T = tectonic thinning; R = structural relief

Estimates of structural relief are: Wills Mountain anticline - 4000 m (Perry, 1971), Browns Mountain anticline - 3000 m (Kulander and Dean, 1972), Deer Park anticline, 3000 m (Gwinn, 1964), Cacapon Mountain anticline - 4000 m (Perry and deWitt, 1977), and Patterson Creek Mountain anticline - 2500 m (Cardwell, 1973).

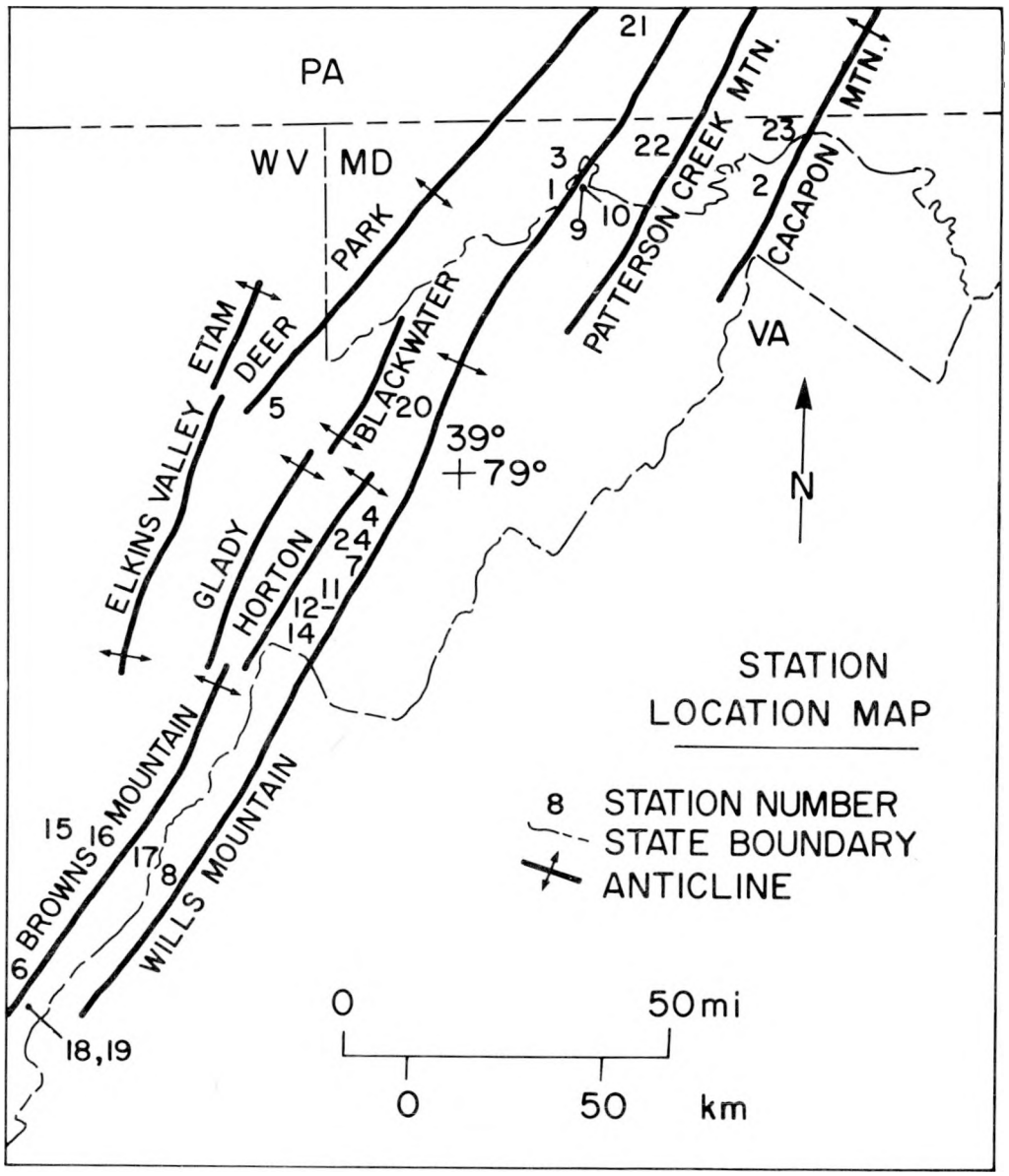


Fig. 1. Map showing major anticlines in the study area. Numbers show locations of stations listed in Table 2.

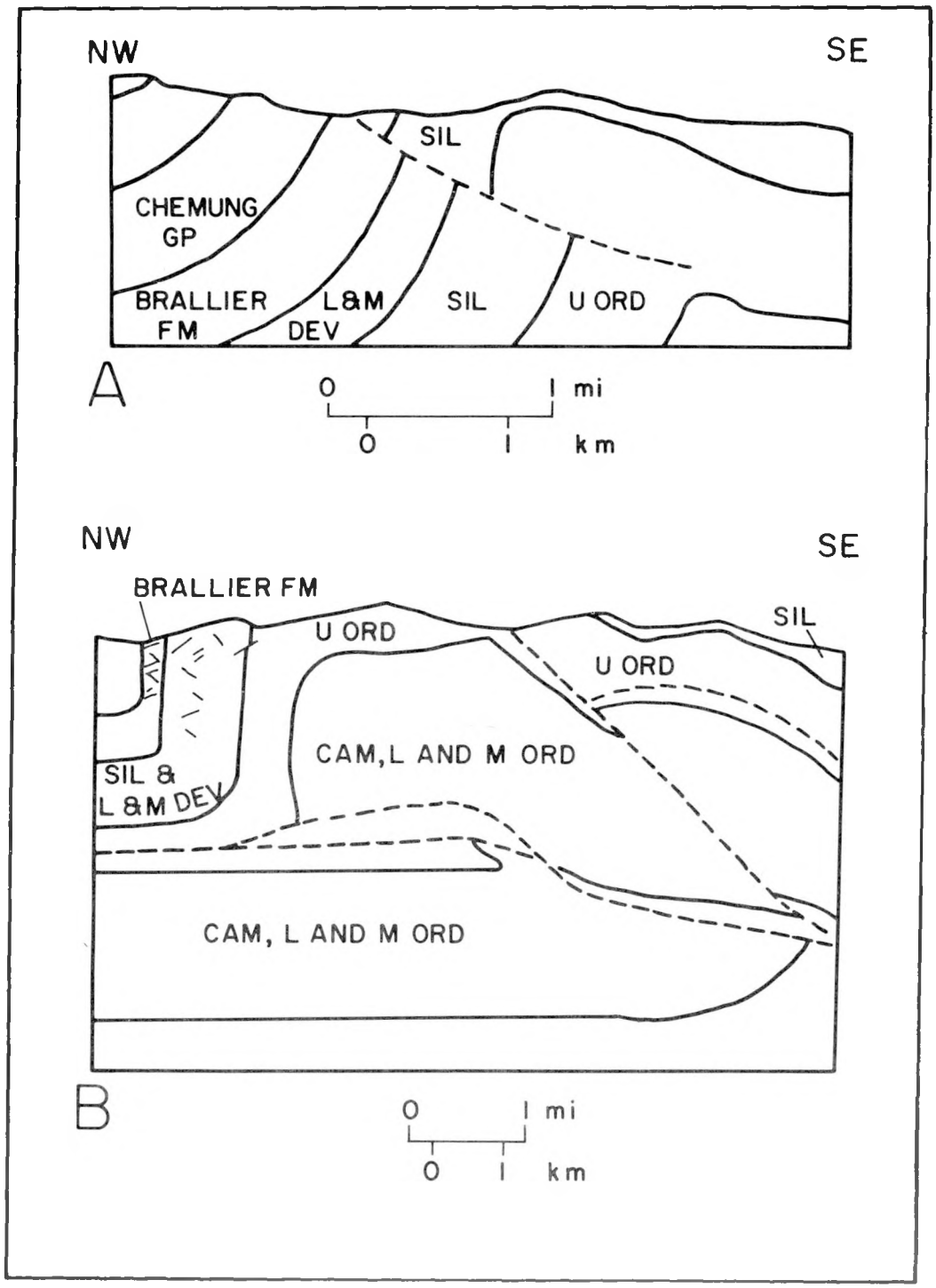


Fig. 2. Contrasting models of tectonic thinning by faulting on the northwest limb of the Wills Mountain anticline. No vertical exaggeration. A. Splay fault interpretation modified from Dennison and Naegele (1963), Dennison and others (1966) and de Witt and Dennison (1972). B. Extension fault interpretation modified from Perry (1971). Dashed lines are decollement or splay faults. Short solid lines in upper left are extension faults. Cross-sections are not to the same scale.

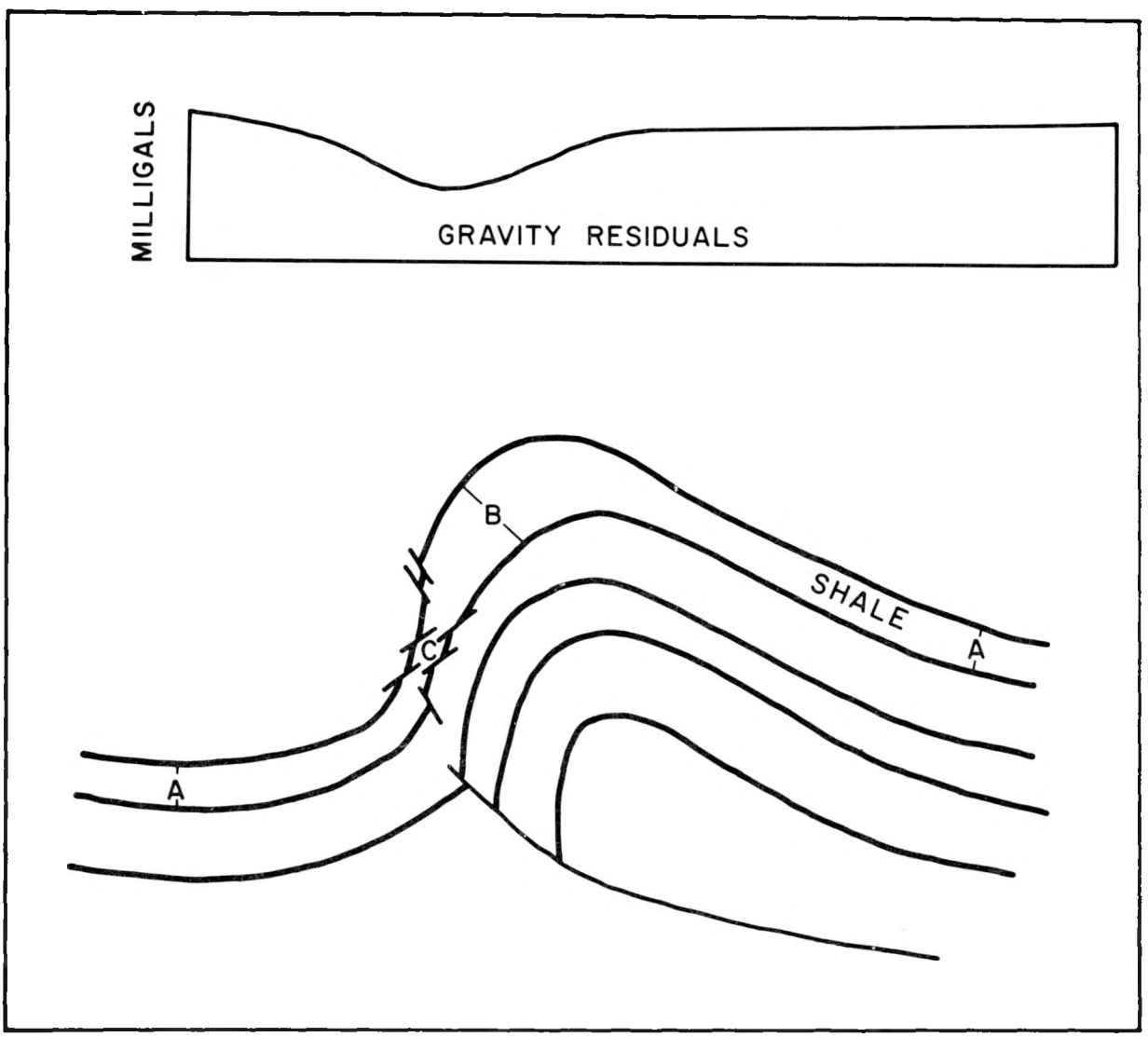


Fig. 3. Suggested relationship of gravity low to anticline. A. Original thickness. B. Siltstone and shale thickned by uplimb flow of shale. C. Siltstone and shale thinned by uplimb flow of shale and thinning by extension faulting of siltstones and shales.

A PETROLOGIC EVALUATION OF THE SIGNIFICANCE OF NATURAL FRACTURES IN LOW-POROSITY SHALE GAS RESERVOIRS-RESULTS OF INVESTIGATION IN THE UPPER DEVONIAN OF VIRGINIA AND WEST VIRGINIA

by

Robert J. Vinopal, Edward B. Nuhfer*, and David S. Klanderman

West Virginia Geological and Economic Survey
PO Box 879 Morgantown, WV 26505

About The Authors



Vinopal



Nuhfer



Klanderman

Robert Vinopal received his B.S. and M.S. degrees in geology from Kent State University and is working on a doctorate at West Virginia University. Research interests include petrology of clastic rocks and coal. He was employed for one year as a petroleum geologist for Earth Resources Consultants and is presently a sedimentary petrologist with the Easter Gas Shales Project at the West Virginia Geological and Economic Survey.

Edward Nuhfer received his B.S. and M.S. degrees in geology from West Virginia University and is completeing PhD requirements at the University of New Mexico. He taught for two years at Marietta College and is presently teaching at the University of Wisconsin. His principal research interests and publications are in geochemistry and petrology of recent muds, determinative mineralogy, analytical geochemistry, well log evaluation, and economic geology. Professional experience includes two years as a petroleum geologist with Chevron Oil Company and four years as an economic geologist and sedimentary petrologist with the West Virginia Geological and Economic Survey.

David Klanderman received his B.S. degree in geology from N. Arizona University, and an M.S. degree in geology from Oregon State University. He has worked for Amax Exploration Inc., Exxon, and the Oregon Department of Geology and Mineral Industries. At present, he is a research associate (sedimentary petrology) with the West Virginia Geological Survey/Eastern Gas Shales Project and is working on a doctorate at West Virginia University.

* Present address-Geosciences Department, University of Wisconsin, Plattsville, WI 53818

2 A PETROLOGIC EVALUATION OF NATURAL FRACTURES

Abstract

Economic production of gas from the Devonian shales of the Appalachian Basin is dependent on the presence of natural or induced fracturing. Investigation of natural fractures in five cored wells of varying productivity indicates that fracture frequency alone is not the sole control of well productivity. A one to one relationship between natural fracture seen in cores and gas shows indicated by temperature and sibilation logs is not present. This is attributed to degrees of permeability enhancement by different fracture types. No system of abundant microfractures was documented after study of nearly 400 shale samples by radiography, thin section and SEM. Thus, only macroscopic fractures are of importance. Horizontal to subvertical slickensided fractures, even with frequencies of 2 to 3 per foot, are not associated with gas shows in organic-rich, laminated shales. Examination of their surfaces by SEM shows complete obliteration of grain to grain boundaries and a uniform, glassy surface of low permeability. High angle vertical fractures, associated with higher gas productivity, retain some openness and permeability in the subsurface due to mineralization and slight movement between fracture hackles. The most productive well, final open flow of 1007 MCFPD, possessed high angle vertical fractures in its pay zone of organic-rich laminated shale. Slight offsetting along fracture hackles opened widths up to 28mm. Vertical fractures with no mineralization, indication of offsetting along hackles or gas shows are interpreted as being closed at depth.

Introduction

The presence of natural or induced fractures intersecting the wellbore has been stressed by many investigators (for example, de Wys and Shumaker, 1977; Bagnall and Ryan,1976; Schettler, 1976; Hunter and Young, 1953) as one of the factors necessary for economic Devonian hale gas production. Fractographic logging of Devonian hale cores revealed that there was not a one to one relationship between gas shows recorded by temperature,sibilation logs and natural fractures found in cores (B Kulander - personal communication) which suggested that fracture frequency alone is not the sole control of well productivity. The purpose of this paper is to describe the characteristics of natural fractures associated with productive and non productive shale intervals.

Five wells (Linclon 1637, Jackson 1369, Jackson 1371, Mason 196, Wise 253)provided approximately 2200 feet of shale core which served as the sample base for this study. The wells had varying natural open flows: 1) Lincoln 1637 - 198 MCFPD, 2) Wise 253 -0 MCFPD, 3) Jackson 1371-0 MCFPD , 4) Jackson 1369 - 1007 MCFPD 5) Mason 196 - 200 MCFPD. As such, they presented an opportunity to compare the nature of natural fractures found in wells of high and low natural open flow. The structural setting of the cored wells also varied, providing examples of fractures in shales associated with: (1) Pine Mt. Thrust plate, (2) Rome Trough, and (3) regional fracturing not related to any major detached or basement structure (Fig.1). None of the wells were located on anticlines. Only one well (Lincoln 1637) was cored through the entire shale section present in western West Virginia and Virginia, but all wells had cores of intervals which proved productive before or after stimulation.

Microscopic Fractures and Macroscopic Fractures

Macroscopic natural fractures in core samples were distinquished from induced fractures using the criteria of Kulander, Dean, and Barton (1977) and were intially classified into three groups on the basis of fracture dip; high angle fractures (dip 90-80°), inclined fractures (dip 79-45°) and low angle fractures (dip 44-0°). Of the 94 samples collected, only eight had dips between 79 and 45° which may be related to the style of fracturing in the areas cored, or it may simply reflect removal or distruction of samples prior to when we viewed the core. Although this classification does result in three well defined classes, the presence of gas shows are not strictly delineated by these classes. Thus, for the purpose of disscussion in this paper, macroscopic natural fractures are broken up into 2 classes: those associated with gas shows and those not associated with gas shows.

Current models of shale gas production invoke a dual porosity reservoir in which the fracture porosity system is recharged by diffusion from the matrix. Microfractures were postulated to contain readily removable gas and to serve as corduits to recharge the macroscopic fractures (Science Applications Inc., 1977). Examination of natural fracture surfaces and broken surfaces adjacent to natural fractures by scanning electron microscopy, transmitted light microscopy and x-ray radiography failed to detect any significant microfracture system. No intragranular fractures, microdisplacement along grain boundaries mineralized microfractures, or prefered orientation of grains suggestive of microstructural features were observed. At the termination of the fracture front of some macroscopic fractures, minor microfractures were noted, but they commonly extended only a few millimeters and did not consitute a microfracture system. Dingler (1978), in a microfracture study of tight sandstones stimulated by nuclear blasts, found macroscopic fracturing dominant with only slight deformation (intragranular cracks and clay lath orientation) observed in the rock matrix adjacent to the macrpscopic fractures.

Matrix porosity and permeability determinations on core samples do not support the existence of a microfracture system. The mean matrix porosity of the productive lower portion of the Huron Member is significantly higher in Lincoln 1637 (85 MCFPD natural open flow) than in Jackson 1369 (1007 MCFPD natural open flow). Permeability tests by Core Laboratories for selected samples from Jackson 1369 were not significantly different from shale wells characterized by lower productivity. If a microscopic fracture system capable of containing or transmitting significant quantities of gas was present, it should have been reflected in higher matrix porosity and permeability values. These tests are in agreement with the visual observations that no microscopic fracture enhancement of porosity and permeability exists. Thus,only macroscopic fractures are of importance.

Natural Macroscopic Fractures Associatied With Gas Shows

Fractures associated with gas shows must be partially open to enhance permeability and porosity. Mechanisms for keeping fractures open at depth include pore fluid pressure (Currie, 1977) and mechanical propping. Since the Devonian Shales are not overpressured, mechanical propping probably plays a major role in keeping fractures open.

Mineralization is a common form of propping, and mineralized fractures do at times correlate with gas shows, but there is not a strict one to one correspondence. Gas production (natural open flow -105 MCFPD) from the upper-middle portion of the Huron Member in Lincoln 1637 is associated with a zone of vertical fractures 1 to 2mm in width mineralized by dolomite and barite (Fig. 2). However, individual fractures showed varying degrees of mineralization. Porosity measurements of fracture fillings ranged from 3% to 20%. Attempts to impregnate fractures with resin in order to study pore geometry failed in the case of low porosity fillings. When viewed in thin section, these fillings were seen to be tightly cemented by a mosaic of anhedral dolomite crystals (Fig. 2). They are interpreted as possessing permeability no higher than that of the shale matrix. No contractor, to the best of our knowledge, has ever performed permeability tests on mineralized fractures. The higher porosity fracture fillings did yield pore casts after dissolving the fracture matrix. Pores were interconnected, resulting in higher permeability (Fig. 2).

A good example of partial mineralization was found in the lower portion of the Huron Member in Mason 196. A vertical fracture 1.5mm in width in the pay zone (200 MCFPD) had scattered euhedral dolomite rhombs on its surface (Fig. 2). Where interbedded silt lenses were present, the dolomite crystals were lined up along them. Examination of the silt lenses in thin section revealed that they are tightly cemented by dolomite. The silt lenses probably acted as conduits by which water and ions (Ca, Mg, CO_3) necessary for dolomite formation were expelled from the compacting shale (Curtis, 1978). Mineralized vertical fractures in the shale fit the model of Secor (1965) who postulated that some vertical fractures are natural hydraulic fractures formed by high fluid pressure in the rock matrix.

Offset along irregular fracture surfaces is interpreted as being a second major process in maintaining open fractures at depth in Devonian Shales. Fracture surfaces reveal a variety of features related to the fracture event (Kulander, Dean, and Barton, 1978). Depending on the relief of the surface hackles, varying amounts of void space can be produced by slight vertical offsetting (Fig. 3). For offsetting to occur, it is necessary for the fracture to interconnect laterally with other fractures, producing fracture-bounded blocks which would be able to shift position. Perhaps these fractures are similar to the master joints of Hodgson (1976).

Offsets marked by slickensided portions of fracture hackles are present in Lincoln 1637 in the upper-middle portion of the Huron Member (Fig. 4) and lower portion of the Huron Member. The vertical fractures in the productive zone of the lower Huron (87 MCFPD) are not mineralized (Fig.5) indicating that mineralized fractures are not necessary for production. Scanning electron microscopic examination of the natural fracture surfaces showed that the microfabric of the shale surface is not deformed; grain boundaries of the clay laths are well defined (Fig.5). Cut and ground samples showed destruction of the microfabric indicating that samples prepared in this manner are not suitable for permeability tests or microfabric studies.

The best developed example of offset vertical fractures was seen in Jackson 1369. In the productive lower portion of the Huron member (natural open flow 1007 MCFPD) numerous, natural fractures were observed (Fig. 6). Some were completely mineralized and probably did not contribute to the high productivity of this well. Others showed some evidence of offsetting and were only partially mineralized. Depending on how wide the fracture opened and the angle of movement, certain areas of the irregular fracture surface ground against each other, producing slickensides at points of contact and propping the fracture open. In Jackson 1369, the maximum observed relief of the hackles on the fracture surfaces was 14mm. If the fracture was opened and offset so that these hackles abutted against each other, vugs with a width of 28mm would be formed. These large,laterally extensive voids were not completely filled by mineralization and thus greatly enhanced reservoir permeability. Werner (1977) states that this well was not located near photolineaments. Examples of offsetting were observed in core samples in a 20 foot section of the productive interval. However, due to poor core recovery (Martin and Nuchols, 1976) and destruction of samples in characterization tests prior to viewing by us,only portions of fracture surfaces were found.

The presence of mineralized and unmineralized natural vertical fractures within the same stratigraphic unit is interpreted as reflecting at least two periods of fracturing in the Devonian shales. The first period produced the mineralized fractures and is probably related to high fluid pressures in a dewatering shale (Secor, 1965). The second period of fracturing occured after the shales were essentially dewatered and may be related to a decrease in overburden pressure (Overby, 1976). Cursory measurements of samples collected from Mason 196 did not reveal a great difference in the orientation of mineralized and unmineralized fractures.

Natural Macroscopic Fractures Not Associated with Gas Shows

Smith (1978) indicates that the average grey shale contains .1 cf gas /cf shale and the average Devonian block shale .6 cf gas/cf shale. Natural fractures not associated with gas shows in gas bearing rocks must be closed at depth or have little permeability due to complete mineralization. One core sample from Wise 253 contained three mineralized vertical fractures (1.5 mm in width) which were seen in thin section to be tightly cemented by carbonates and sulfates (Fig.7). Many of the individual crystals in the filling extend across the entire width of the fracture, effectively sealing it. (Fig.7). This growth habit may be due to single crystals preferentially growing until they reach the other side of the fracture, or may be related to syntectonic crystal growth as described by Durney and Ramsay (1973). Other crystal fabrics, commonly a mosaic of anhedral crystals, are also associated with non produtivity in Lincoln 1637 and Mason 196 (Fig.7).

Examples of unmineralized natural vertical fractures in grey and block shales with no corresponding gas shows were present in Lincoln 1637 and Mason 196. None showed any evidence of offsetting. A possible explanation for the lack of offsetting may be fracture length. If the fractures are of limited lateral and vertical extent and do not intersect other fractures, then it would be difficult for offsetting movements to occur.

No natural fractures with low dips (less than 60°) were associated with gas shows. All were slickensided. Low angle fractures were found in every core, but were most common in the Wise 253 core from the Pine Mt. Thrust plate. Veins of fibrous dolomite and ferroan dolomite accompanied many slickensided fractures (Fig.8). Ramsay and Barnes (1973) interpreted elongate fibrous or needlelike crystal habits as forming in "tectonic veins filled synchronously with fissure dilation and that there are no actual spaces available for vuglike crystal growths". Little porosity and permeability can be expected when individual crystals span the entire width of the fracture.

Scanning electron microscopic examination of slickensided surfaces showed complete obliteration of grain to grain boundaries due to crushing and grinding producing a surface of low permeability which greatly restricts gas migration from the matrix into the fracture. Scattered euhedral sulfate and carbonate crystals occur on the surfaces of some slickensided fractures. Although some intercrystalline porosity is associated with the fracture, no apparent increase in permeability is associated with these samples. The amount of movement necessary to produce a slickensided surface (virtual obliteration of grain to grain boundaries) could not be measured in the majority of samples. One radiograph of a closely spaced set of inclined, slickensided fractures from Lincoln 1637 showed that movements as small as 2mm could produce a slickensided surface (Fig. 8).

Low angle fractures possess a variety of surface markings. Some have well developed fine striae and mirror-like surfaces,while hackles typical of high angle fractures are formed on others (Fig.9). The hackles are slickensided, but apparently not enough movement occured to destroy them. Mineralized en echilon tension fractures were observed in close proximity to some low angle fractures (Fig.9). A fault breccia from Lincoln 1637 contained long pieces of shale rotated at least 90° but cementation by pyrite prevented any increase in permeability (Fig.9).

Natural Fracture Permeability and Porosity

The contribution of open fractures to the permeability of the shale reservoir is high, given the low permeability of the rock matrix, but contribution to porosity is not accurately known. Schettler (1978) maintains that gas contained in natural fractures is depleted in a short time (hours to weeks) and that most gas eventually produced migrates from the shale matrix into permeable fractures which connect with the wellbore. The total fracture surface area is a major control of productivity.

Other researchers, Hunter and Young (1953) and de Wys and Shumaker (1977), suggest that large volumes of gas exist in fracture systems. The fracture gas is postulated to take several years to drain off before gas migration from the matrix begins. The fractures examined in the naturally productive intervals of the wells studied do not appear to contribute greatly to porosity. As discussed previously, mineralized fractures (1.5-2mm wide) with 20% intercrystalline porosity and unmineralized fractures of approximately the same width are correlated with productivity. Jackson 1369 did contain fractures interpreted as being open to a greater extent.

Although the amount of fracture porosity present in Devonian shales can never be directly measured, limits on the value can be approached. For example, from a cube of shale cut by two sets of vertical fractures (each fracture open 1mm) the amount of fracture porosity can be calculated. If a fracture frequency of four feet is assumed, fracture porosity is approximately 0.16%. A fracture

frequency of two feet yields a fracture porosity of 0.32%. Such a model (Fig. 10) assumes a much higher frequency of open fractures than is seen in cores and outcrops, and probably overestimates the amount of fracture porosity. Drummond (1964),in a summary of estimates of fracture porosity in various reservoirs, states that "bulk fractured porosities in fractured reservoirs range down from three percent." Murry (1968) reported a fracture porosity of less than one percent for the Spanish pool, North Dakota, and concluded that the major role of fractures is enhancement of permeability. A similar situation seems to exist for the Devonian shales of western West Virginia.

Conclusions

1. Microscopic fractures are rare in Devonian shales and do not significantly contribute to permeability or porosity. Only macroscopic fractures are of importance. Gas shows correlate with natural macroscopic fractures observed in core samples. Many macroscopic fractures have no corresponding shows due to tight mineralization or closure at depth.

2. Low angle slickensided fractures are not associated with productively. High angle fractures which remain open due to partial mineralization or propping caused by offsetting of irregular fracture surfaces are productive.

3. The close spatial relationship between mineralized and unmineralized high angle fractures suggest at least two generations of fractures.

4. Fracture porosity is apparently minor in Devonian shales. The major role of fractures is enhancement of permeability.

Acknowledgements

The assistance of Byron Kulander in fracture identification and Jeff Clagett in sample preparation is appreciated.

References

Bagnall, W.D., and Ryan, W.M., 1976, The geology, reserves, and production characteristics of the Devonian Shale in Southwestern West Virginia: in Devonian Shale Production and Potential; R.C. Shumaker and W.K. Overby eds., NTIS, MERC/SP-76/2, p. 41-53.

Currie, J.B., 1977, Significant geologic processed in development of fracture porosity: Amer. Assoc. Petrol. Geol. Bull, V. 61, p.1086-1089.

Curtis, C.D., 1978, Possible links between sandstone diagenesis and depth-related geochemical reactions occurring in enclosing mudstones: Jour. Geol. Soc. London, v. 135, p.107-117.

Dengler, L.A., 1978, Microcracks and matrix deformation in stressed gas-bearing sandstones: in Scanning Electron Microscopy, v.1, A. O'Hare ed., p.603-608.

Drummond, J.M., 1964, An appraisal of fracture porosity in reservoir rocks at depth: Bull. Can. Petrol. Geol., v.22, p.42-58.

Durney, D.W., and Ramsay, J.G., 1973, Incremental strains measured by syntectonic crystal growths: in Gravity and Tectonics, K.A. De Jong ed., Wiley and Sons, New York, p. 67-96.

De Wys, T.N., and Shumaker, R.C., 1978, Pilot study of gas production analysis methods applied to Cottageville field, NTIS, MERC/CR -78/6, 45 p.

Hodgson, R.A., 1976, Fracture systems: characteristics and origin: in Devonian Shale Production and Potential, R.C. Shumaker and W.K. Overby eds ., NTIS, MERC/SP-76/2, p. 41-53.

Hunter, C.D., and Young, D.M., 1953, Relationship of natural gas occurrence and production in eastern Kentucky (Big Sandy gas field) to joints and fractures in Devonian bituminous shale: Amer. Assoc. Petrol. Geol. Bull., v. 37, p. 282-299.

Hulander, B.R., 1977, Fractography workshop short course notes, June 28 and 29, Morgantown, WV.

Kulander, B.R., Dean, S.L., and Barton, C.C., 1977, Fractographic logging for determination of pre core and core-induced fractures-Nicholas Combs #7239 well, Hazard Kentucky, NTIS, MERC/CR-77/3 44 p.

Martin, P., and Nuckols, E.B., 1976, Geology and oil and gas occurrence in the Devonian shales:

northern West Virginia: in Devonian Shale Production and Potential, R.C. Shumaker and W.K. Overby eds. NTIS, MERC/SP-76/2, p.20-40.

Murry, G.H., 1968, Quantitative fracture study- Spanish pool, McKenzie county, North Dakota: Amer. Assoc. Petrol. Geol. Bull., v.52, p.57-65.

Overby, W.K., 1976, Effect of in situ stress on induced fractures: in Devonian Shale Production and Potential, R.C. Shumaker and W.K. Overby eds., NTIS, MERC/SP-76/2, p.182-211.

Science Applications Inc., 1977, Increasing U.S. natural gas reserves from eastern gas-bearing shales, MERC/SP-77/3, 24p.

Secor, D.T., 1965, Role of fluid pressure in jointing: Amer. Jour. Sci., v 263, p.633-646.

Schettler, P.D., Wampler, D., Mitchell, D., and Russey, W., 1976, Degrassification of Devonian shales: in Devonian Shale Production and Potential, R.C. Shumaker and W.K. Overby eds., NTIS, MERC/SP-76/2, p. 239-264.

Shettler, P.D, 1978, The relationship of thermodynamic and kinetic porometers to well production in Devonian shale: Proceedings first eastern gas shales symposium, NTIS, MERC/SP-77/5, p. 608-619.

Werner, E., 1978, Interrelationships of photolineaments, geological structures, and fracture production of natural gas: Proceedings first eastern gas shales symposium, NTIS, MERC/SP-77/5 p. 474-483.

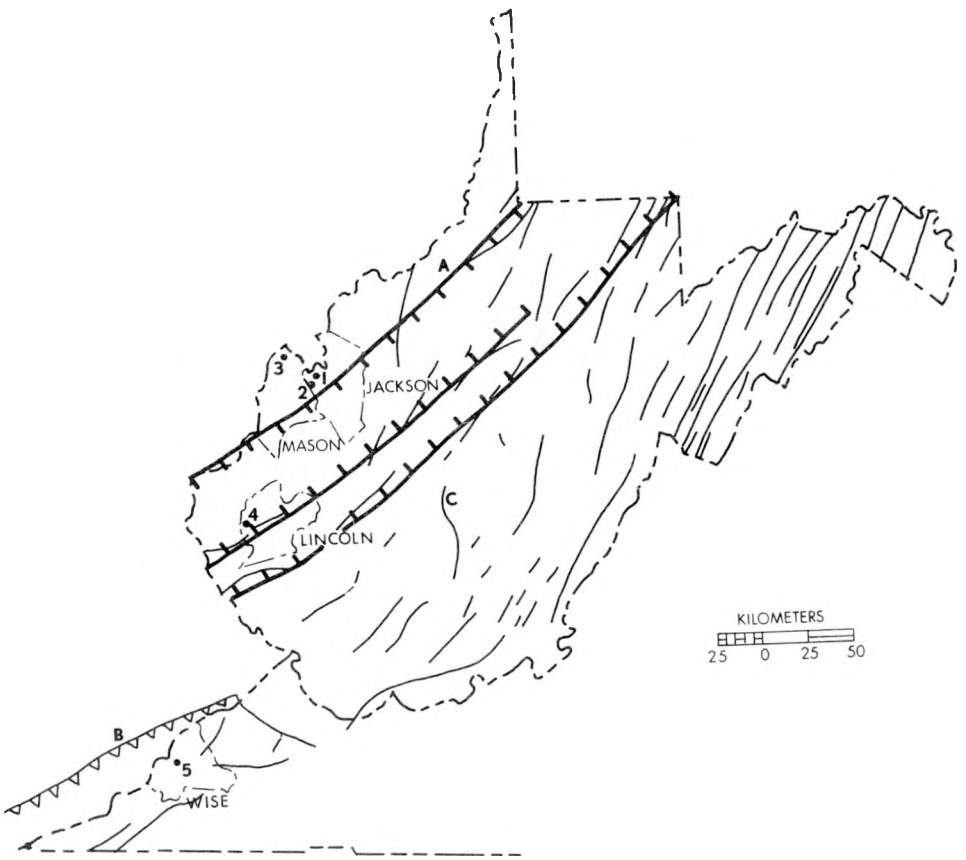


Figure 1. Structural setting of five cored Devonian shale wells utilized in this study: A) Rome Trough, B) Pine Mt. Thrust, C) anticline axes. County permit numbers and company numbers of wells: 1) Jackson 1371 (CGTC #12041), 2) Jackson 1369 (CGTC #11940), 3) Mason 196 (Reel Energy D&K #3), 4) Lincoln 1637 (CGTC #20403), 5) Wise 253 (CGTC #20338).

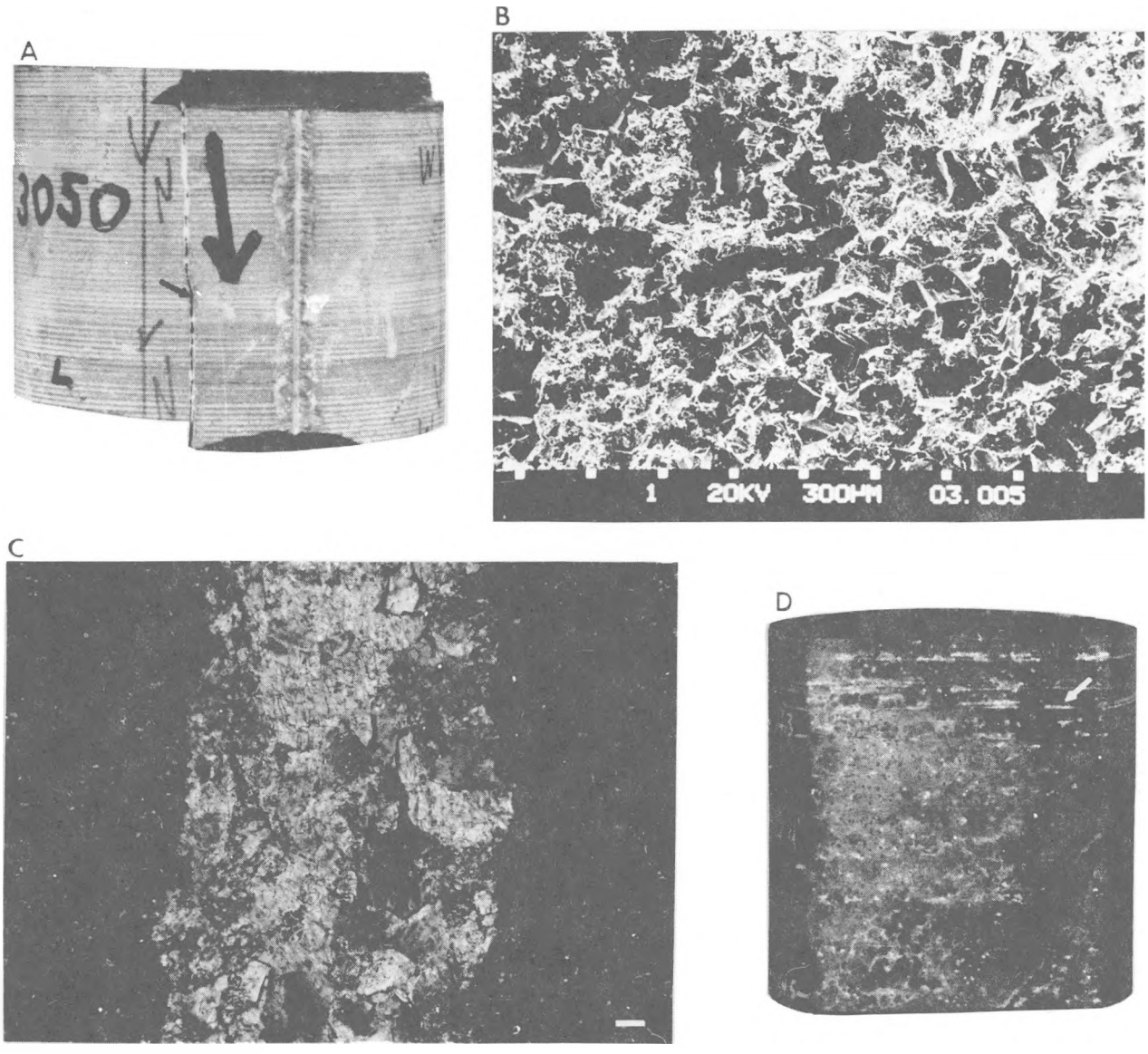


Figure 2. Mineralized fractures from productive intervals. A) Vertical mineralized fracture from upper-middle Huron in Lincoln 1637. Apparent vugs (arrow) are produced by plucking during coring. From a core depth of 3050'. Diameter of core is 4 inches. B) SEM micrograph of pore cast (20% porosity) from A showing connecting nature of porosity. Amount of porosity (light areas) is exaggerated by oblique view. C) Thin section photomicrograph of tightly mineralized fracture from upper-middle Huron in Lincoln 1637. Intercrystalline porosity of 3% exists in the mosaic of anhedral dolomite crystals. Attempts to impregnate filling were unsucessful, suggesting little permeabilty exists. From a core depth of 3068'. Scale bar is .25mm. D) Partially mineralized fracture from productive portion of lower Huron in Mason 196. Euhedral dolomite crystals are approximately 1mm wide. Note lineation of crystals (arrow) along interbedded silt lenses. From a core depth of 2734'. Diameter of core is 3.5 inches.

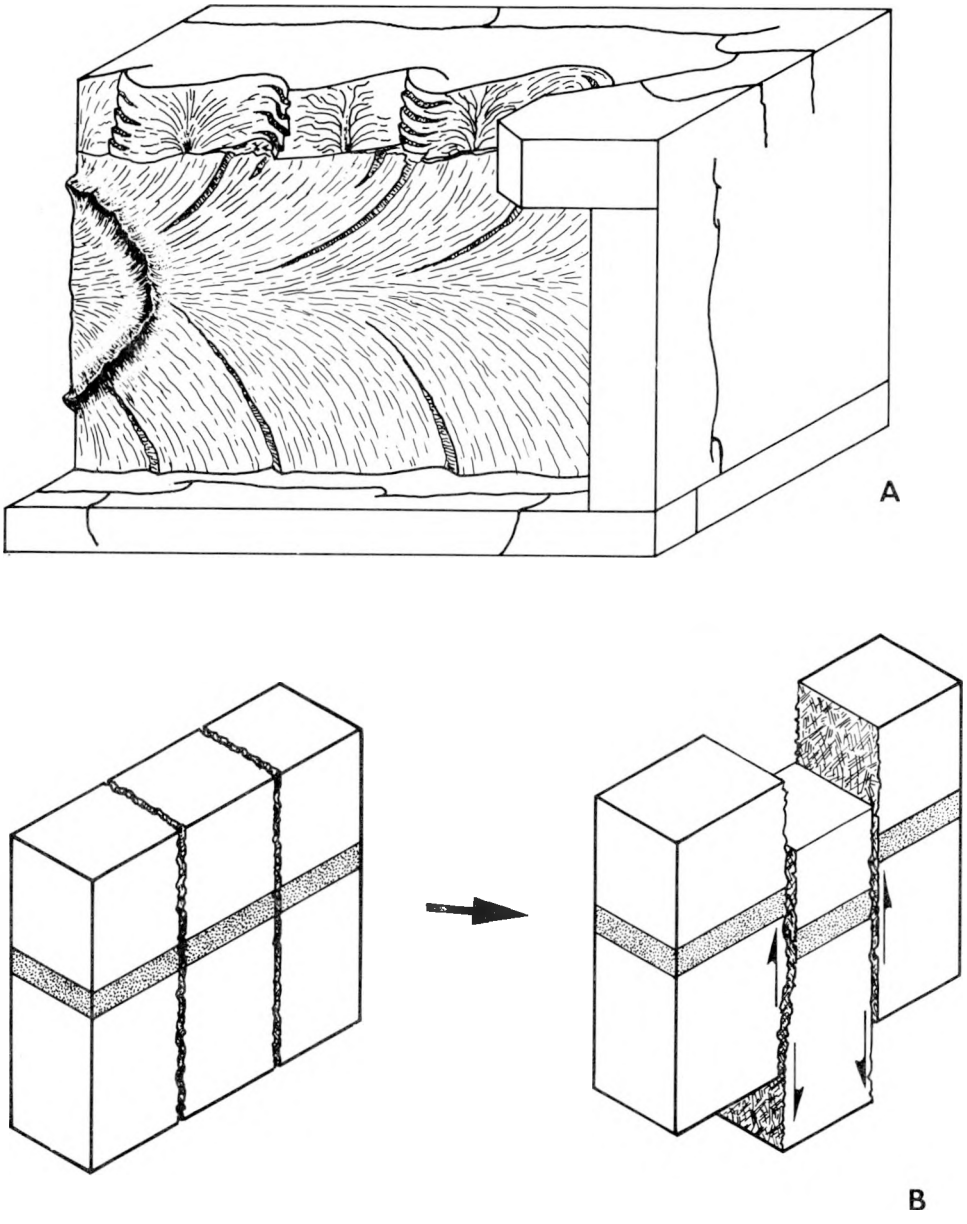


Figure 3. Illustration of offsetting creating permeability and porosity. A) Surface features of a fracture surface (Kulander, 1977). The relief of fracture hackles observed in Devonian shales ranges from 14mm to less than 1mm. B) If offsetting movement occurs, fractures can be held open by mechanical propping. Slickensides or ground surfaces will be produced at points of contact. Amount of open space produced depends on the relief of the fracture surface and the extent of later mineralization.

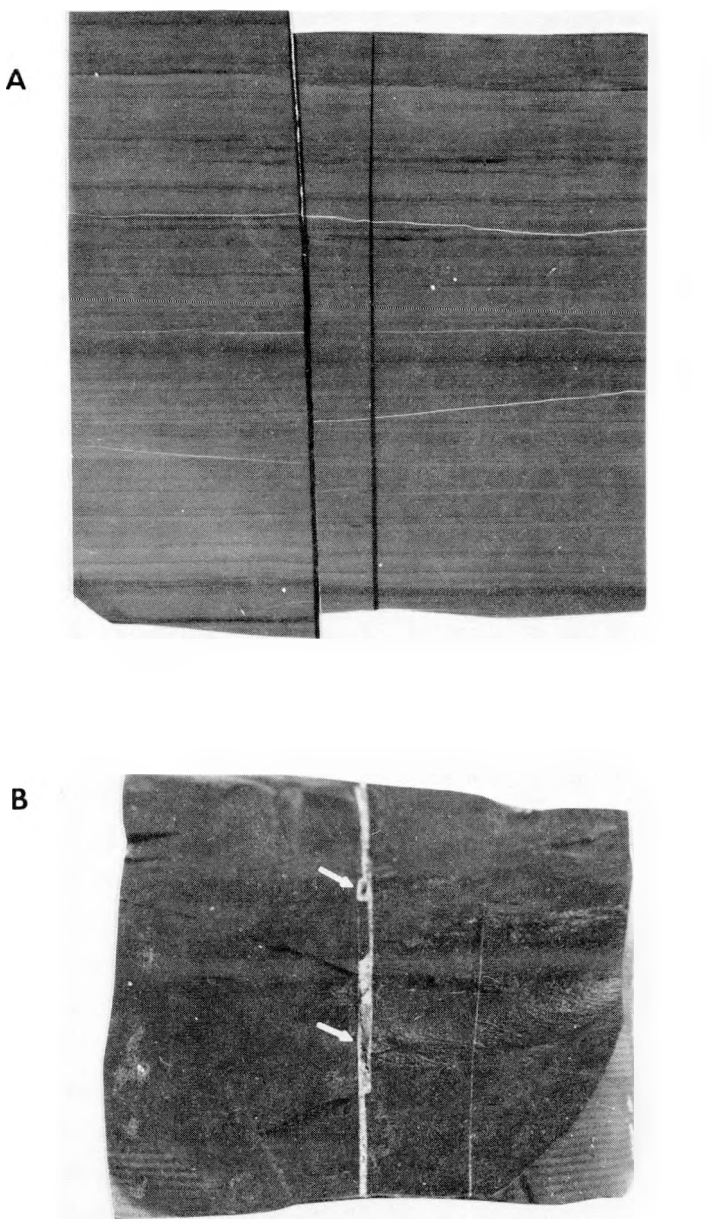


Figure 4. Vertical fracture offsets in upper-middle Huron of Lincoln 1637. A) X-radiograph showing offset prior to mineralization. Dolomite mineralization appears to be holding fracture open, but propping along irregular surfaces may be present outside the limited area sampled by the core. Voids in center of fracture are due to sample preparation. Porosity of filling is 3%, see Fig. 1C. From a core depth of 3068'. Diameter of core is four inches. B) Slight vertical offset between two closely spaced vertical fractures joined along bedding surface produced small vugs (arrows) which were only partially mineralized. They do not have great lateral extent and will constitute closed porosity if the connecting fractures are tightly mineralized. From a core depth of 3052'. Diameter of core is four inches.

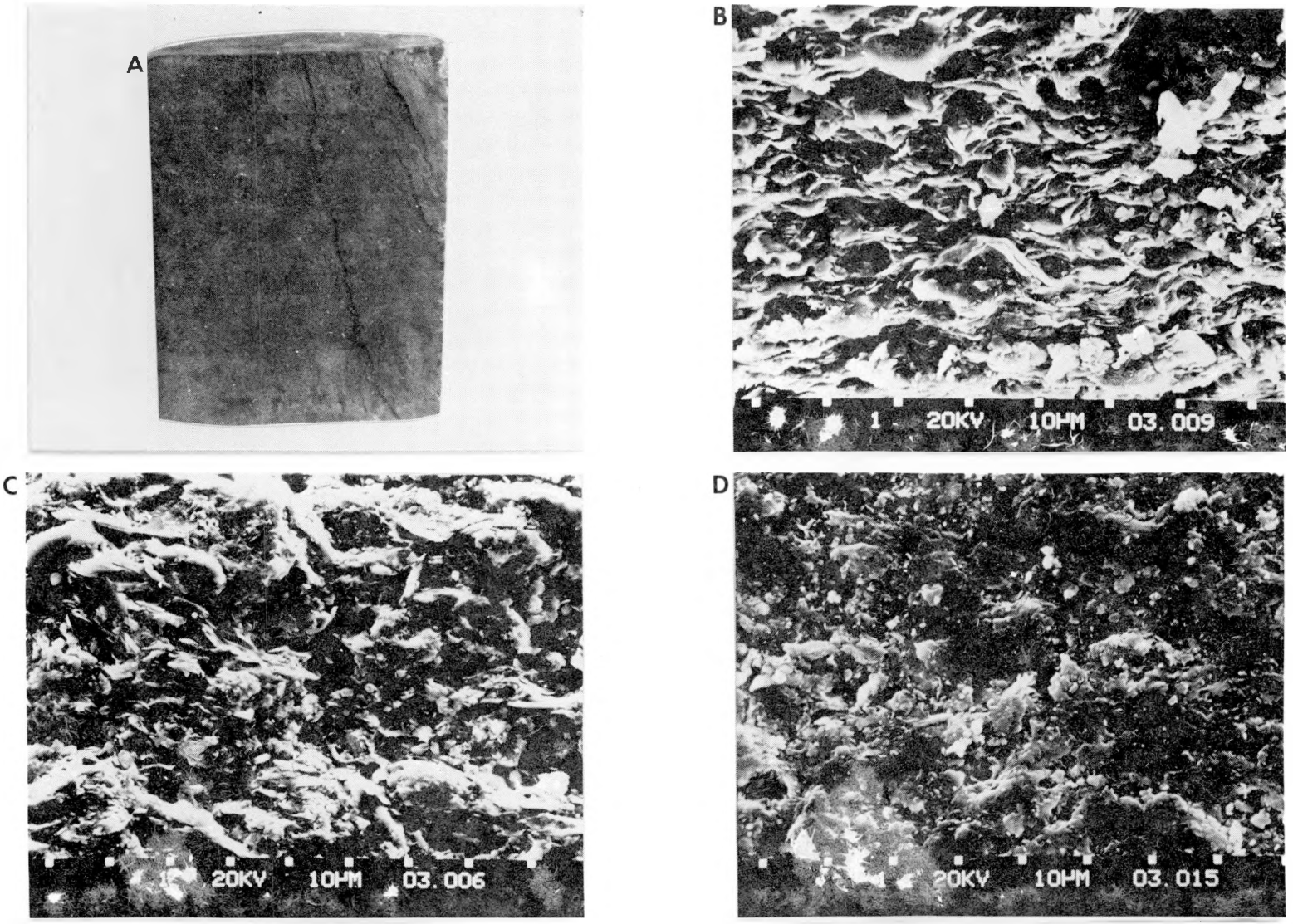


Figure 5. A) Unmineralized natural vertical fracture with prominent hackles from productive portion of lower Huron interval in Lincoln 1637. From a core depth of 3585'. Diameter of core is four inches. B) SEM micrograph of A showing nature of shale microfabric on natural farcture surface. Grain to grain boundaries are sharply defined. C) SEM micrograph of broken surface of core sample from A showing microfabric similar to B. D) SEM micrograph of sample from A after it was cut and ground. Destruction of many grain to grain boundaries will likely result in lower permeability. Artifacts in the shale microfabric are easily produced by sample preparation.

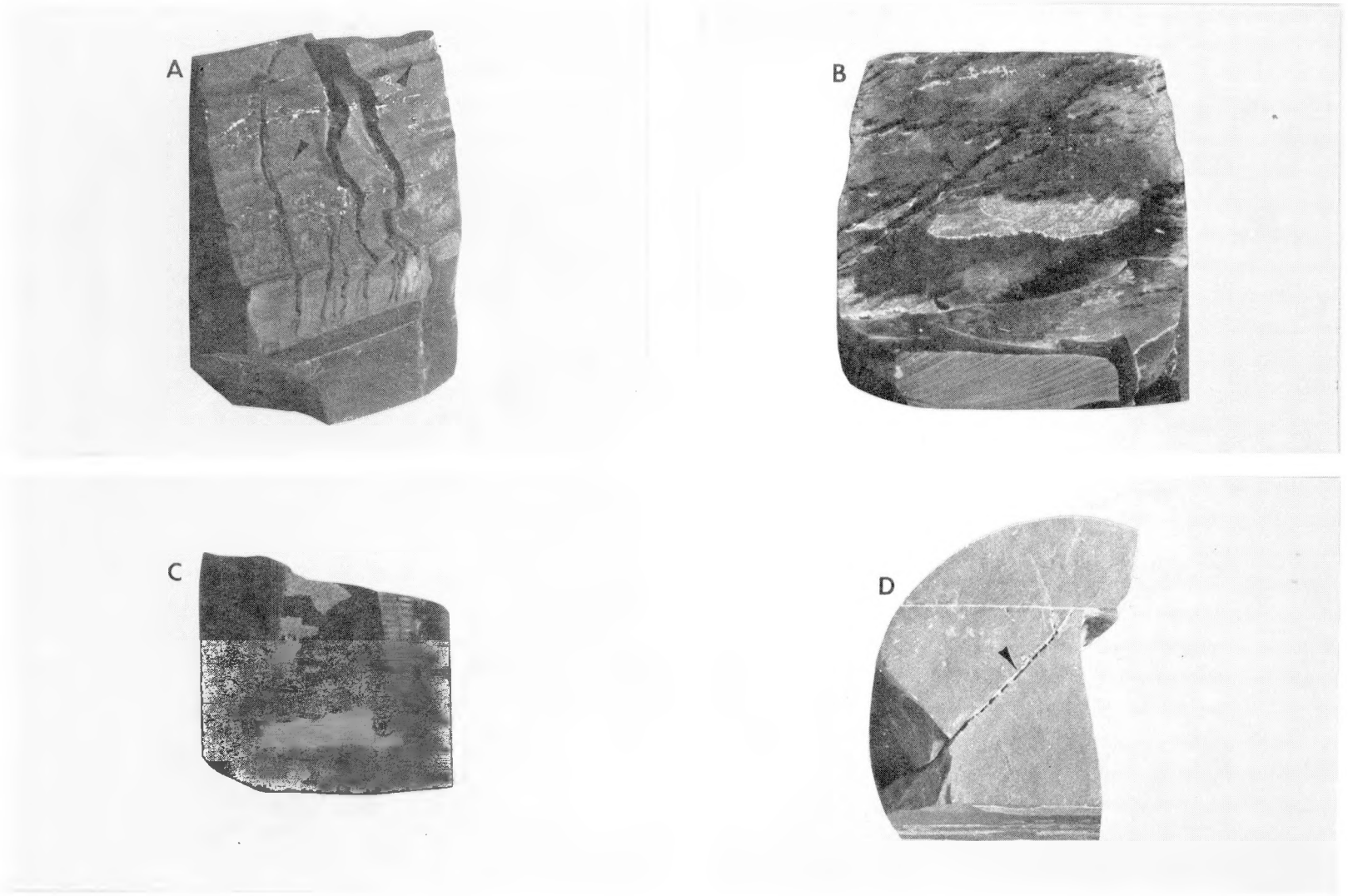


Figure 6. Natural fractures from the productive zone of the lower Huron in Jackson 1369. Diameter of all cores is four inches. A) High angle vertical fracture with coarse hackles. Slickensides (arrows) are evidence of later vertical offset. From a core depth of 3720', B) Steeply inclined fracture with slickensided hackles (arrow). Void space was more infilled with dolomite than previous sample. From a core depth of 3729'. C) Vertical fracture with low relief hackles. Fracture was tightly cemented by dolomite (spalled off in handling) and apparently contributed little to permeability or porosity. From a core depth of 3726'. D) Open cross fracture (arrow) between two mineralized vertical fractures. Fracture is held open by slight offsetting along irregular surface and is partially infilled by dolomite. From a core depth of 3724'.

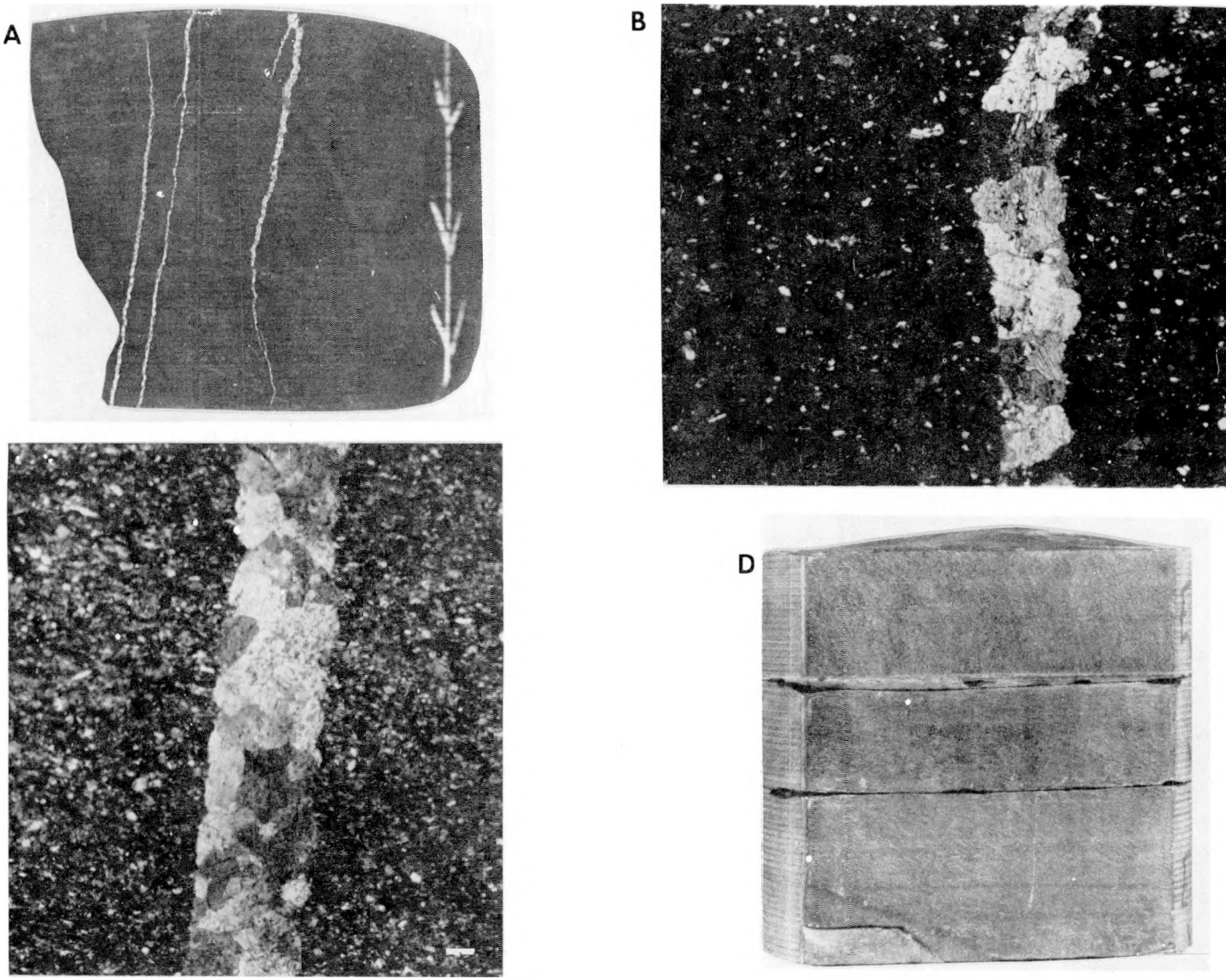


Figure 7. Vertical fractures not associated with productivity. A) Mineralized vertical fractures in brown shale of Three Lick Bed. From Wise 253 at a core depth of 4914'. B) Photomicrograph of fracture filling from A. Many of the individual dolomite crystals extend completely across the fracture, effectively sealing it. Scale bar is .5 mm. C) Photomicrograph of mineralized fracture from lower portion of Huron Member in Mason 196. Anhedral mosaic of dolomite crystals has little porosity and is interpreted to possess little permeability. From a core depth of 2842'. Scale bar is .5mm. D) Unmineralized natural vertical fracture from upper-middle Huron. Low relief hackles are present and show no evidence of offsetting. This fracture is interpreted as being closed at depth. From a core depth of 3008' in Lincoln 1637. Photos reduced 20%

Figure 8. Characteristics of low angle fractures. A) Photomicrograph of fibrous dolomite crystals commonly associated with low angle fractures. Little porosity or permeability exists due to tightly interlocking crystal habit. From a core depth of of 5305' in Wise 253. Scale bar is .5 mm. B) SEM micrograph of natural slickensided surface (right) adjacent to artificial fracture surface showing complete destruction of shale microfabric and sealing of matrix. From a core depth of 5331' in lower Huron interval of Wise 253. C) SEM micrograph of euhedral sulfate crystals on apparently unmineralized slickensided surface indicating that some porosity is present, but is probably not interconnected. From a core depth of 5325' in lower Huron interval of Wise 253. D) X-radiograph of a set of slickensided fractures (arrows) with small offsets. Large voids reflect paring along slickensides after cutting. From a core depth of 3923' in Lincoln 1637.

Figure 9. Other examples of natural fractures not associated with productivity. A) Slickensided fracture with fine striae. From a core depth of 5393 in lower Huron of Wise 253. Diameter of core is 3.5 inches. B) Inclined slickensided fracture possessing hackles which indicate that the fracture propagated upwards. From a core depth of 3865' in Rhinestreet Member of Lincoln 1637. Diameter of core is four inches. C) En echilon tension fractures tightly cemented by dolomite. From a core depth of 4931' in Three Lick Bed of Wise 253. D) X-radiograph of fault breccia cemented by pyrite (arrow). Scale bar is 1 cm. From a core depth of 3757' in Java Fm. of Lincoln 1637.

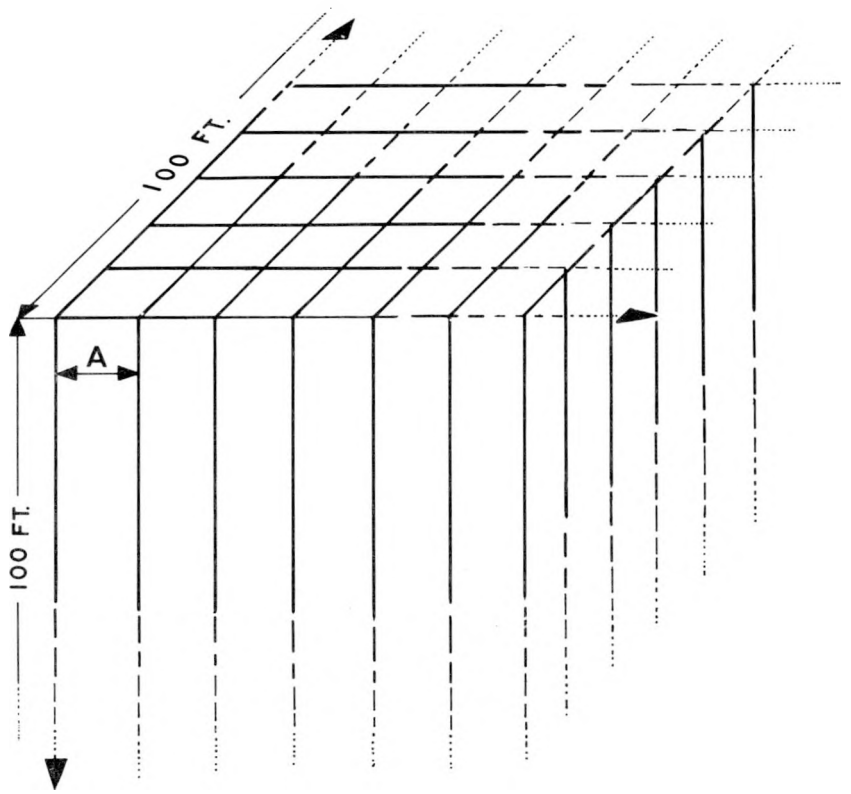


Figure 10. Model of possible limits to fracture porosity in Devonian shale. A 100 foot block of shale is assumed (a larger cube gives the same results) to be cut by two sets of vertical fractures intersecting at ninety degrees with each fracture open one millimeter. If A (fracture spacing) is four feet, calculated fracture porosity is 0.16%. If A is two feet, fracture porosity is 0.32%. This model assumes a much higher frequency of open fractures than has ever been documented in cores or outcrops. The main contribution of fractures is probably enhancement of permeability and not storage of large volumes of gas.

PRESSURE-CORING OF THE GAS-BEARING DEVONIAN BLACK SHALES, ERIE COUNTY, PENNSYLVANIA

R. E. Zielinski, J. A. Dixon,
Mound Facility*

R. D. McIver
Geochem Research

and

A. E. Hunt
Morgantown Energy Technology Center

ABSTRACT

A Christiansen model pressure-retaining core barrel (the Pressure Core Barrel) was used in the drilling of an EGSP research well in Erie County, Pennsylvania, the well being a joint Mound Facility-METC effort. Results from the pressure cores taken from the this research well are presented in this paper.

Off-gassing of cores begins as soon as air-drilled cores are cut, and large quantities of gas are lost while such a core is being brought to the surface. Drilling mud was used to minimize gas loss during core cutting, and the Pressure Core Barrel allowed as complete as possible recovery of the total in-place hydrocarbons in the dark shale.

Note: Paper not available at time of publication.

*Mound Facility is operated by the Monsanto Research Cororporation for the U. S. Department of Energy under Contract No. DE-ACo4-76-DP00053

GAS-BEARING OHIO SHALE ALONG LAKE ERIE: STRATIGRAPHY, PETROLOGY, AND SEDIMENTOLOGY

Ronald F. Broadhead[1], Roy C. Kepferle[2], and Paul Edwin Potter[1]

ABOUT THE AUTHORS

Ronald F. Broadhead received a B.S. in geology in 1977 from the New Mexico Institute of Mining and Technology in Socorro where he also worked as a petrographer at the New Mexico Bureau of Mines and Mineral Resources studying thermal metamorphism in southwestern New Mexico. He is currently completing his Master's program at the University of Cincinnati where he has been a research assistant on the Eastern Gas Shales Project for two years. Ron will start work in October for Cities Service Company in Tulsa, Oklahoma.

Dr. Roy C. Kepferle received his B.A. at the University of Colorado, 1950; M.S. at South Dakota School of Mines and Technology, 1954; Ph.D. at the University of Cincinnati, 1972. He has been with the U.S. Geological Survey since 1950 working on projects that include: strippable lignite and uraniferous lignite, Williston basin; uraniferous shale, trace elements, South Dakota and Nebraska; Far East geology; areal geology in Kentucky; stratigraphy and sedimentology of Lower Mississippian and Devonian rocks, Illinois and Appalachian basins.

Dr. Paul Edwin Potter received his Ph.D. in geology from the University of Chicago in 1952. Since that time he has been a National Science Foundation senior fellow and a Guggenheim fellow. He has worked for the Illinois State Geological Survey, has been a Professor of Geology at Indiana University, and is currently Professor of Geology at the University of Cincinnati.

1. Department of Geology, University of Cincinnati, Cincinnati, Ohio 45221
2. U.S. Geological Survey, University of Cincinnati, Cincinnati, Ohio 45221

ABSTRACT

Increased interest in low-yield gas-bearing strata has led to our reexamination of the Ohio Shale in the vicinity of Lake Erie where it has had a history of marginal commercial production for more than a century. These strata thin depositionally westward from a maximum of 2000 ft (600 m) at the Pennsylvania-Ohio border to less than 600 ft (180 m) near Sandusky. West of Sandusky, they are truncated by recent erosion on the Findlay arch.

The rocks were subdivided into six major types based on thin section petrology: Claystone, clayshale, mudshale, black bituminous shale, siltstone, and siltshale. Claystone and siltstone are unlaminated and clayshale, mudshale, black bituminous shale, and siltshale are laminated. The average modal compositions of these rocks are tabulated below.

The most common lithotopes are the black and gray rocks composed of clay- and silt-sized detritus. Carbonate rock and sandstone are rare. Black bituminous shale is most abundant in the west. The gray clayshale, claystone, mudshale, siltstone, and siltshale are most abundant in the east where they constitute 75 percent of the section, the remainder being predominantly black bituminous shale.

Stratigraphic and sedimentologic studies indicate that these rocks were deposited as Upper Devonian prodeltaic mud and turbidites in an episodically euxinic basin.

Gas productivity and gas shows are localized in interbedded gray and black shale lithotopes in the west, and in the gray shale lithotopes in the east.

Average modal composition of rock types in the Ohio Shale
(T, trace)

ROCK TYPE	QUARTZ AND FELDSPAR	CLAY	MICA	ORGANIC MATTER	SPORES	PYRITE	CARBONATE MINERALS	*OTHER
Claystone	10.4	79.2	2.5	3.3	T	2.2	2.1	T
Clayshale	13.8	71.3	2.5	5.0	T	4.8	2.5	T
Mudshale	31.2	50.2	3.5	7.2	1.0	5.0	1.5	T
Black bituminous shale	13.0	50.3	2.5	24.3	1.4	5.8	2.2	T
Siltstone and siltshale**	68.5	6.1	3.9	T	0	T	19.1	1.0

*Includes heavy minerals, rock fragments, chert, chalcedony, and bone fragments.
**Siltstone and siltshale are grouped in table because of their great lithologic similarity and similar content of detrital quartz.

NOTE: Paper not available at time of publication.

A CURRENT ASSESSMENT OF THE PHYSIOCHEMICAL CHARACTERIZATION DATA FOR THE EASTERN GAS SHALES

S. W. Nance, P. W. Seabaugh, R. E. Zielinski
Mound Facility

Mound Facility

ABSTRACT

Detailed physiochemical properties are determined for Devonian Gas Shales. These results are used to assess the total natural gas potential of this resource, to define significant exploration and production parameters, and to develop effective methods for determining these parameters.

To date, over 600 core and drill cutting samples have been evaluated. These samples were selected from the upper Devonian interval of eight, Illinois Basin and eleven, Appalachian Basin wells.

Geochemical characteristics are determined for the organic material and whole rock sample. For the organic material, the composition and contents are determined for the gaseous hydrocarbons, bitumen, and kerogen fractions. The thermal maturity of the samples are primarily evaluated by visual kerogen (thermal alteration indices) and vitrinite reflection analyses. The sample hydrocarbon potential is assessed from the sample; C_1 to C_7 gas contents, organic carbon content, pyrolysis-gas chromatography analysis and material balance assay results. Major and select minor elemental concentrations are determined for the kerogen and whole rock sample. The source of organic material is determined by kerogen analysis.

The organic carbon content, thermal maturation, and organic mattertype primarily determine the natural gas potential of the Devonian Shales. A minimum organic carbon content is required to provide an adequate gas source. For a given well, gas contents generally increase with organic carbon content. Illinois Basin shales have not reached a stage of thermal maturation sufficient for intense hydrocarbon generation.

Appalachian Basin shales are more mature with thermal maturation tending to increase with depth. The shales from the wells nearest the Devonian Appalachian highlands have matured to the stage of metagenesis. Algalamorphous material increases and woody-coaly material decreases with the distance from the Devonian Appalachian Basin clastics.

Biostratigraphic analysis indicates the presence of a relatively high gas potential organic facies. This facies, predominantly algal-amorphous and herbaceous material was deposited with a restricted marine environment.

2 A CURRENT ASSESSMENT OF THE PHYSIOCHEMICAL CHARACTERIZATION DATA FOR THE EASTERN GAS SHALES

The double ratio vandium:nickel to uranium:thorium is an effective indicator of organic carbon content. In addition, analyses using the double ratio vandium:nickel to uranium:thorium show that the ratio provides a cut-off threshold which differentiates between organic material deposited within a restricted marine environment and other biostratigraphically determined environments.

Note: Paper not available at time of publication

PETROLOGY AND MATURATION OF DISPERSED ORGANIC MATTER IN THE NEW ALBANY SHALE GROUP OF THE ILLINOIS BASIN

Mary H. Barrows, Robert M. Cluff, and Richard D. Harvey

Illinois State Geological Survey, Urbana, ~~Illinois~~



ABOUT THE AUTHORS

Mary H. Barrows received her B.S. in geology from the University of Illinois. She worked as a geologist for a civil engineering firm in Chicago, Illinois, prior to becoming a research assistant for the Illinois State Geological Survey in January 1978. She is now employed by the Survey to do reflected light microscopy and scanning electron microscopy for the Eastern Gas Shales Project.

Robert M. Cluff received his B.S. in geology from the University of California at Riverside and his M.S. from the University of Wisconsin at Madison. He joined the Illinois State Geological Survey in 1976 and has worked extensively on the sedimentology and depositional environment of the New Albany Shale.

Dr. Harvey studied geology at Indiana University at Bloomington, Indiana, where he specialized in mineralogy and petrography and received a Ph.D. degree in 1960. He has been with the Illinois State Geological Survey since 1960. He had conducted research on carbonate rocks in the Industrial Minerals Section, with emphasis on the use of carbonates in SO_2 sorption from flue gases. In 1976 he transferred to the Coal Section and now directs research on the petrography of Illinois coals. He is in charge of the petrographic studies of the New Albany Shale at the Survey.

ABSTRACT

The New Albany Shale Group of the Illinois Basin is being studied to evaluate its potential for yielding hydrocarbons. As part of this study, coal petrographic techniques have been employed to evaluate the composition and thermal maturity of dispersed organic matter in the shales.

Vitrinite reflectance was measured on acid-macerated kerogen separates from 11 cores and 126 cuttings from drill holes through the New Albany Shale in Illinois, Indiana, and western Kentucky. No significant variations in reflectance values were observed within the New Albany at any single location with respect to either depositional facies or depth. An isoreflectance map prepared from the data shows large areas of the Illinois Basin where reflectance is uniformly low (<0.5% $\bar{R}_o$) and the organic matter has not yet reached the stage of petroleum generation. Several areas of higher reflectance are also present: (1) near the northern erosional truncation of the New Albany in central Illinois; (2) in east-central Illinois, within a broad southward plunging syncline immediately west of the Clay City Anticlinal Belt; (3) in Wayne and Hamilton Counties, Illinois, the present-day area of maximum burial depth; and (4) in extreme southeastern Illinois, where the highest reflectances yet observed (>1.0% $\bar{R}_o$) correspond to a complexly faulted and mineralized area with nearby igneous intrusions. Changes in color and intensity of UV fluorescence of liptinites are generally in good agreement with reflectance data.

Occurrence and abundance of amorphous organic matter, alginites (mainly *Tasmanites*), vitrinites, and exinites are facies dependent. Solid hydrocarbons that occur as pore fillings in fusinite are found mainly in samples from southeastern Illinois. Their presence suggests that hydrocarbon generation and expulsion have occurred in the New Albany in southeastern Illinois.

INTRODUCTION

Geologists have long regarded most dark-colored, fine-grained sedimentary rocks in which abundant organic matter has been preserved as probable petroleum source rocks. The New Albany Shale Group (Devonian-Mississippian), the thickest and most continuous black shale in the Illinois Basin (fig. 1), therefore has been suspected of having played a major role in petroleum generation throughout the basin. Suprisingly few data have been collected and published, however, to evaluate the quality of source beds in the New Albany and to identify areas where petroleum generation is likely to have occurred.

A potential petroleum source rock must have the following characteristics: (1) abundant organic matter must have been deposited and preserved in the sediment (*quantity*); and (2) the organic matter must be of an appropriate type or composition for oil and/or gas to be generated (*quality*). For a potential source rock to then generate and expel significant quantities of hydrocarbons two additional conditions must be met: (1) the organic matter must be thermally degraded during burial, over sufficient time, to form various petroleum compounds (*maturation*); and (2) pathways for effective *primary migration* must exist for expulsion of the hydrocarbons generated.

Previous studies

Lamar, Armon, and Simon (1956) determined the quantity of oil present in many samples of dark-colored (organic) shales. The samples were taken from various outcrops in Illinois and included several from the New Albany Shale Group. Their data showed that some shales of Pennsylvanian age associated with coal strata commonly contained between 5 and 15 gallons of oil per ton of shale, but shales from the New Albany Group (Devonian) only contained between 0 and 6.4 gallons.

The quantity of organic matter in the New Albany Shale was investigated by Stevenson and Dickerson (1969). They examined core samples and drill cuttings of the lower 15 meters of the shale from approximately 350 drill holes throughout Illinois. They found the total organic carbon contents of the samples to range from slightly less than 1 percent to more than 9 percent. Lineback (1970) reported organic carbon contents as high as 20 percent by weight in some beds of the New Albany in Indiana. Stevenson and Dickerson (1969) also determined the amount and composition of benzene-extractable organic matter in a limited number of core samples. They found the benzene extractables to be only a small fraction of the total organic carbon (about .05), but the amount of extractable compounds correlated very closely with the total organic carbon contents (fig. 2). This type of relationship is believed to indicate that the extracted oil is indigenous to the source rock.

Schrayer and Zarrella (1963) found a relationship between areas of high organic carbon content in the Mowry Shale and the locations of Lower Cretaceous oil pools in Wyoming. Essentially all of the proven reservoirs are in areas where the average organic carbon content exceeds 1.5 percent in the

shale. Stevenson and Dickerson (1969), however, were unable to demonstrate a similar relationship for the New Albany Shale. Various lines of evidence suggested that most of the oil in the underlying carbonate and sandstone reservoirs of the Hunton Megagroup (Silurian-Devonian) originated in the New Albany; however, no simple relationship between carbon content and oil accumulation was found (fig. 3). One possible explanation of this is that the New Albany contains sufficient organic matter to be a potential source rock throughout its extent.

The critical lower limit of organic carbon required for significant quantities of petroleum generation in detrital rocks is widely accepted to be somewhere between 0.5 and 1.0 percent (Tissot and Welte, 1978). Because the organic carbon content of almost all of the samples studied by Stevenson and Dickerson (1969) exceeded 1.0 percent, it must be concluded that throughout its extent in Illinois at least some beds in the New Albany are potential source rocks.

Purpose of this investigation

In 1976 the Illinois State Geological Survey, with partial support from the U.S. Department of Energy, began an intensive study of the New Albany Shale to evaluate its potential as a source of hydrocarbons, especially natural gas. As part of this overall effort, a study of the petrography of organic matter in the shales was initiated.

This study has two major goals: to characterize the types of organic matter in the shales and their stratigraphic and areal distribution; and to characterize the degree of organic metamorphism, or maturation, of organic matter in the New Albany Shale by vitrinite reflectance analyses and other means. This study primarily relies on reflected light microscopy of acid insoluble organic residue (kerogen) of samples of the New Albany Shale in Illinois. A few samples from the Illinois Basin portions of Indiana and western Kentucky have also been included.

The relative likelihood of oil or gas generation and the role of the New Albany Shale as a petroleum source rock will be evaluated in this paper on the basis of organic content, kerogen type, and degree of maturation. Those areas of the Illinois Basin where petroleum generation is most likely to have occurred will be identified. Primary migration of generated hydrocarbons is assumed to have occurred and the mechanism of migration is not an object of this investigation. Some preliminary results of this study were published as a contract report (Harvey, Cluff, and White, 1977) and an abstract (Hansman (Barrows) et al., 1978).

METHODS

Sample selection

Samples for organic petrographic analysis were selected from approximately 150 drill holes penetrating the New Albany Shale Group in Illinois, Indiana, and western Kentucky (fig. 4). No samples were included in this study from areas where the New Albany crops out or from areas where the shale has been deeply eroded and is overlain by Pennsylvanian or Pleistocene sediments. The density of sampled drillings is greatest in Illinois and is least in western Kentucky. More than 350 samples of the shale and associated sediments were collected; at the time of this writing (July 1979), the study of more than 75 percent of these samples has been completed.

To evaluate variations in the types of organic matter and maturation with respect to depth, stratigraphic position, and depositional facies, 12 New Albany Shale cores in Illinois, 1 core in Indiana, and 2 in western Kentucky were sampled in detail. These cores were generally sampled at 2 to 3 meter intervals; fewer samples were selected from those cores in which organic-lean greenish-gray shales were the predominant lithology.

The remainder of the samples studied were obtained from washed drill cuttings in the files of the Illinois State Geological Survey and the Indiana Geological Survey. A visual sample study was made of the entire New Albany interval for each drill hole, and the samples were hand picked to minimize contamination from overlying strata. Approximately 20 to 30 grams of shale were picked from a 1 to 5 meter interval every 30 meters (100 feet) throughout the shale. Samples of organic-rich black shales were chosen whenever possible. For most wells only one or two samples were obtained; in areas where the New Albany Shale is thickest, three to four samples per well were selected. All of the sampled wells have been linked through a basin-wide network of stratigraphic cross sections (Reinbold, 1978; Cluff and Reinbold, in preparation; Bassett and Hasenmuller, in preparation).

Sample preparation

All shale samples used in this study required special processing to isolate and concentrate the organic matter from the mineral matrix. The separation techniques used are similar to those used in palynological investigations, except no oxidants were used (Gray, 1965). The procedures are outlined in table 1. In addition to the acid-macerated kerogen separates, several polished blocks of shale were prepared from core samples to observe the distribution of organic matter within the rock. A few samples of vitrain (mostly *Callixylon* stems and fragments) were obtained from bedding plane surfaces in cores. These vitrain samples were not chemically treated, but were mounted in epoxy, polished, and examined to evaluate the effect, if any, of acid maceration on reflectance.

Reflected light microscopy

Modified coal petrographic techniques were used to evaluate the hydrocarbon potential of the New Albany Shale. Reflected light microscopy of kerogen concentrates was used to characterize the type of the organic matter. The well-established tool of vitrinite reflectance and the more recently employed technique of blue light fluorescence were used to determine the degree of thermal maturation.

Types of organic matter

Visual estimations of the occurrence and abundance of organic matter types were made to determine whether the organic matter incorporated in the New Albany Shale is of the appropriate type or composition for oil and/or gas to have been generated. Estimates of percentages of the abundance of amorphous organic matter, liptinites, vitrinites, and inertinites were made using a Leitz Orthoplan MPV II microscope with the 50x/0.85p achromatic oil immersion objective during vitrinite reflectance analysis. Special notations about particle size, organic matter preservation, and the inclusion of unusual particles were also made.

Vitrinite reflectance

Vitrinite originates from the woody tissues of plants. It occurs as sand- and silt-sized particles dispersed in shales and other sedimentary rocks. The vitrinite group of macerals is distinguished from other macerals by its reflectivity and morphology. Figure 5 illustrates a typical piece of vitrinite as seen in an acid-macerated separate. Vitrinite particles generally are minor constituents in the black shales (figs. 6 and 7) and may be totally absent in the greenish-gray shales that contain little organic matter.

The relative amount of normally incident light that is reflected from polished surfaces of vitrinite particles in coals has been recognized as a reliable guide to the degree of metamorphism or rank of the coal. This method of analysis has also been successfully applied to many clastic sediments to evaluate the relative maturity of the organic matter that is dispersed in the rock. Figure 8 illustrates the relationships between vitrinite reflectance and other measures of organic metamorphism as they relate to the generation of oil and gas.

The vitrinite reflectance analyses were carried out on polished pellets made from the kerogen separates. The measurements were made using a Leitz Orthoplan MPV II microscope-photometer. A 50x/0.85p achromatic oil immersion objective was used for all reflectance measurements. In addition, a 32x/0.65p oil immersion objective was used for general observation and photography. A 12-volt 100-watt halogen tungsten-filament lamp using a stabilized power supply provided illumination.

The microscope-photometer was standarized prior to and after measuring each sample using at least two glass standards of known reflectance (0.302, 0.532, and 1.000 % $\bar{R}_o$). Reflectance measurements were made through a 547 nm monochromatic filter. The variable measuring diaphragm was set to read a spot approximately 2.5 μm square. Each sample was scanned manually in a rectangular search pattern. Vitrinite particles were visually identified, and the measuring spot was carefully centered by hand on a uniform area of each particle large enough for an accurate reading. The reflectance was read directly from a digital voltmeter and entered on a programmable desk calculator. It is impractical to rotate the microscope stage to obtain maximum reflectance values because the vitrinite particles are usually very fine silt sized, and it is impossible to keep them centered under the measuring spot during rotation. Therefore, all reflectance values reported are randomly oriented values. According to Dow (1977), mean random reflectance values are actually preferred for kerogen studies having reflectance values of less than about 1 percent.

Fifty readings were made on each sample or, if there was insufficient vitrinite for 50 measurements, the entire pellet was scanned. The mean of the reflectance and the standard deviation of the readings were calculated, and a reflectance-class histogram was plotted for each sample. Samples having fewer than 20 readings or having large standard deviations (generally >0.15) were considered to be unrepresentative and were excluded in the final compilation of the data.

Fluorescence

Recent work by van Gijzel (1967) and Ottenjahn, Teichmüller, and Wolf (1975) has suggested that the fluorescence of liptinites may also be used as a guide to the rank of coals and/or the maturity of organic matter dispersed in sedimentary rocks. These studies, and others, report that both the intensity and the color of fluorescence change with increasing maturation. Fluorescence intensity was found to decrease with increasing diagenesis and catagenesis until fluorescence disappears at the end of the oil generation zone. The color of the fluorescence moves from the blue wavelength range to the red range as catagenesis increases (Tissot and Welte, 1978). Most recent work is aimed at quantitative rather than qualitative measures of this parameter.

The visual fluorescence has been assessed on many samples of New Albany Shale (limitations in equipment would not allow quantitative fluorescence assessment). The fluorescence of the liptinitic fraction of 109 of the shale samples was examined with a Leitz Ortholux microscope using a 25x/0.65 oil immersion objective. An XBO 150w/1 Xenon lamp, a BG 12 (blue) excitation filter, and a yellow barrier filter were used for the fluorescence work. Each pellet was scanned in a rectangular search pattern over a period of 10 to 15 minutes.

The color and intensity of the fluorescence of the different liptinite group macerals were noted for each sample and were recorded. Because *Tasmanites* (an alginite) was the most easily recognized of the liptinite group, the final evaluation of this data was made on the fluorescence of only the *Tasmanites*.

RESULTS

Types of organic matter

Estimates of the percentage of abundance of various types of organic matter have been completed for 142 samples thus far. These estimates indicate that 90 to 95 percent of the organic constituents of the poorly laminated brownish-black and well-laminated black shale facies is amorphous (sapropelic) organic matter. This amorphous material is probably predominantly marine algal in origin although small, unrecognizable fragments of humic material are undoubtedly also included. This material surrounds and is not clearly distinguishable from the mineral constituents in a polished block, but is clearly visible after the acid-maceration processes. Figure 9 illustrates the spongy network of amorphous sapropelic matter, generally dark to medium gray, that is preserved in most of the samples examined. In the southeastern portion of Illinois, however, this network is not often observed; here a lighter gray hash of unidentifiable fragments is more commonly observed (fig. 10). The remaining 5 to 10 percent of the organic constituents throughout the study area are divided among silt-sized, detrital macerals of the vitrinite group (vitrodetrinite, fig. 5), the inertinite group (fig. 11), and the liptinite group (fig. 12).

The alginite (*Tasmanites*) is the most commonly recognized liptinite maceral; its abundance appears to vary randomly. Vitrinite is generally more common than inertinite except in the southeastern part of Illinois where the inertinite maceral, semifusinite, commonly is observed. This mixed assemblage of predominantly marine and some nonmarine organic matter constituents is typical of Type II kerogen as defined by Tissot and Welte (1978).

The greenish-gray shale facies contains little organic matter. Acid-maceration treatment of these shales often results in insufficient material to characterize the types of organic matter that are present. The network of amorphous organic material, so common in the laminated brownish-black and black shale facies, is not generally observed in these samples. Inertinites and vitrinites generally are predominant in the meager acid residues of the greenish-gray shale facies. This assemblage is typical of Tissot and Welte's (1978) Type III kerogen (predominantly nonmarine in origin).

The notations that were made about particle size and preservation of organic matter also have been useful in evaluating reflectance results. For example, samples having very fine, silt-sized particles, or zoned or fractured particles indicative of weathering, were scrutinized to determine the reliability of the mean random reflectance.

Occurrence of solid hydrocarbons

During the examination of the occurrence and abundance of the organic constituents, a dark- to medium-gray material was observed as fillings in a number of fusinite pores (fig. 13). Figure 14 illustrates the locations of samples where such fillings appear. This figure also illustrates the locations where large amounts of similar material were also observed. These latter particles appear to have been fillings of material which has been dissolved by the acid-maceration process. The angular nature of these particles is illustrated in figure 15. These particles may be solid hydrocarbons (Castaño, personal communications). Other workers have referred to similar particles as meta-bituminite (Teichmüller *in* Stach et al., 1975), pyrobitumen (Alpern, 1970), or bitumen (Robert, 1973). This type of particle is thought to be one of the residues produced during the maturation (bituminization) process (Stach et al., 1975). The presence of these particles suggests that hydrocarbon generation and expulsion have occurred in the New Albany of southeastern Illinois.

Vitrinite reflectance

Data from 70 samples taken from 8 cores whose locations are shown in figure 4 indicate no significant increase in vitrinite reflectance with depth. The plots of mean random vitrinite reflectance (% $\bar{R}_o$) versus depth shown in figure 16 and 17 illustrate this observation. Although vitrinite reflectance generally increases with depth through several hundred meters of strata, it is not unusual that this relationship is not observed through the relatively thin (140 meters or less) New Albany Shale. The reflectance of vitrinite in the New Albany is about the same as the overlying Pennsylvanian coals, even though the New Albany occurs some 400 to 1200 meters deeper. The reasons for this apparent anomaly are not, as yet, known.

A map of average vitrinite reflectance, by sample locations, for the New Albany Shales (fig. 18) shows distinct regional patterns of increasing reflectance similar to the patterns of regional Pennsylvanian coalification (Damberger, 1971). The maturation trends illustrated in figure 18 can be related to structural controls, as will be discussed later. This map is based on data collected from 218 samples that represent 94 wells. If more than one sample was examined per well, the $\bar{R}_o$ values were averaged because, as mentioned earlier, no pattern of increasing reflectance with depth was observed.

Four untreated vitrain bands (large compressed pieces of coalified wood—principally *Callixylon* in the New Albany Shale) were examined to determine if the acid-maceration treatment significantly altered reflectance results. The vitrinite reflectance values of the vitrain bands differed only slightly from the reflectance values of closely associated acid-macerated samples. These differences were not systematic and were within the normal standard deviations for the treated samples. These differences can be largely attributed to the difficulty in distinguishing between vitrinite and other macerals in the kerogen separates because the particles are often fine silt-sized. For such small particles, the distinguishing characteristics of reflectance and morphology may not be clearly shown. Furthermore, since 90 to 95 percent of the sample is amorphous organic matter, the comparision of particles often necessary for maceral identification may be hampered because two or more macerals may not appear in the same field of view. Such difficulties rarely arise for vitrain samples because vitrinite is generally the only constituent and the particle size is larger than fine sand.

In samples having relatively large amounts of liptinite, the reflectance values of vitrinite may be low if the small liptinite fragments are easily confused with vitrinite fragments. Likewise, in samples having relatively high amounts of semifusinite, reflectance values may be slightly high because some confusion between fragments of semifusinite and vitrinite is unavoidable. By carefully evaluating the reflectance histogram for each sample some, but not all, of this type of error may be eliminated.

High reflectance values that cannot be attributed to misidentification may be due to weathering of the vitrinite particles. Stach et al. (1975) warn that cracked, corroded, or mottled particles may be oxidized and should not be measured.

Fluorescence

Although visual fluorescence studies are not as precise as vitrinite reflectance studies, the patterns observed (fig. 19) tend to support patterns of increasing reflectance and maturity illustrated earlier. Figure 19 is based on data from 109 samples representing 79 wells. Generally the fluorescence color grades from yellow through yellow-orange and finally to orange toward the southeast in Illinois. In extreme southern Illinois an absence of fluorescence is evident. Note that in

the east-central portion of the state fluorescence ranges from yellow-orange and orange to absent. This area corresponds closely to the area of 0.7 percent reflectance illustrated in figure 18.

DISCUSSION

Types of organic matter

The predominant type of organic matter in the black shale facies of the New Albany is amorphous (sapropelic) kerogen; minor amounts of liptinites, vitrinites, and inertinites are also present. This assemblage is characterisitic of the Type II kerogen of Tissot and Welte (1978) and is typical of many cratonic black shales around the world. The greenish-gray shale facies in the New Albany contains small amounts of vitrinite and fusinite and is almost totally lacking in amorphous kerogen. This assemblage corresponds to the Type III kerogen of Tissot and Welte (1978) and is typical of fine-grained sedimentary rocks deposited in oxygenated environments.

Numerous studies on the chemical composition of kerogens and their pyrolysis products have shown that Type II kerogen is capable of generating large quantities of oil and gas and is a favorable source rock material. Type III kerogen, because of its chemical composition and structure, is much less likely to generate oil but may generate gas. Type II kerogens are therefore said to be "oil prone," and Type III kerogens are "gas prone."

The high organic-carbon contents documented by Stevenson and Dickerson (1969), combined with the predominance of Type II kerogen in black shales of the New Albany, demonstrate that the New Albany contains both sufficient *quantity* and *quality* of organic matter to be a prolific petroleum source rock.

Vitrinite reflectance

Many studies by geologists and organic geochemists have shown that petroleum is generated by the thermal transformation of kerogen during burial. In recent years it has been recognized that oil is generated within a relatively narrow maturation range (the "oil window"), and natural gas is formed over a much broader range. The range of vitrinite reflectances corresponding to the oil generation window is between 0.5 and 1.3 percent $\bar{R}_o$ (fig. 8); peak oil generation and expulsion occur at maturation levels corresponding to reflectances greater than 0.6 to 0.7 percent $\bar{R}_o$ (Hood, Gutjahr, and Heacock, 1975; Dow, 1977).

The range of reflectances observed in the New Albany Shale correspond to the immature and initially mature stages of petroleum generation (fig. 8). Potential source rocks that are still in the immature stage have not yet generated hydrocarbons by thermal processes, although some biogenic gas (principally methane) may have been formed by bacterial processes during early burial. Biogenic methane can be differentiated from later formed thermogenic methane by its isotopic composition (Stahl, 1977).

Much of the New Albany Shale in the Illinois Basin is still within the immature stage. Those areas on figure 18 where the reflectance is less than 0.5 percent $\bar{R}_o$ are unlikely to have generated petroleum, although small amounts of gas may be present within the shale. Isotopic analysis of released gases from several core samples in one of these low maturity areas (Christian County, Kentucky) indicates a low maturity thermogenic origin for the gas (Dickerson and Coleman, 1977).

Those areas (fig. 18) where the reflectance lies between 0.5 and 0.7 percent $\bar{R}_o$ are within the earliest stage of oil generation (for Type II kerogen, Tissot and Welte, 1978). Oil and gas generation may have occurred, but there is some question as to whether sufficient amounts have been generated for expulsion of the hydrocarbons to begin (Hood, Gutjahr, and Heacock, 1975). In addition, in some areas of the New Albany Shale this increased reflectance range may not be due solely to increased thermal maturation. The New Albany is truncated along most of its northern margin in Illinois by the major sub-Pennsylvanian unconformity. This deeply and subaerially eroded surface truncates progressively older strata towards the north and east (Bristol and Howard, 1971). All along the subcrop of the New Albany Shale beneath Pennsylvanian sediments, and in areas in relatively close proximity to the subcrop, the reflectance values are slightly higher than in areas distant from the subcrop. The increased reflectance in areas proximal to the subcrop is attributed to oxidation of the organic matter in the shales during circulation of ground water in the Pennsylvanian or to weathering, not to increased thermal maturation. The geophysical characteristics (especially resistivity) of the New Albany in these areas become flat and undifferentiated, also suggesting alteration of the shale by groundwater or weathering. The reflectance levels in these areas, therefore, are unreliable indicators of maturity and petroleum generation.

Oil generation and expulsion are most likely to have occurred in areas where vitrinite reflectance exceeds 0.7 percent $\bar{R}_o$ (fig. 18). Three areas of the New Albany Shale lie within the mature stage. The northernmost of these is centered in Cumberland and Jasper Counties, Illinois, and coincides with a broad southward plunging syncline on the west flank of the Clay City Anticlinal Belt (fig. 20). The sediments in this syncline have been buried by 300 to 600 meters of additional sediments compared to the structurally high areas immediately to the east and west. Therefore, the sediments have probably been subjected to slightly higher burial temperatures since the mid-Paleozoic time.

The second area of increased reflectance is represented by a narrow finger of the 0.7 percent $\bar{R}_o$ contour extending northward into Wayne and Hamilton Counties, Illinois (fig. 18). This area is the present day area of maximum burial of the New Albany Shale (fig. 20) and, like the area discussed previously, has been subjected to slightly elevated burial temperatures.

The highest reflectances in the New Albany Shale are in extreme southern Illinois, predominantly south of the Rough Creek Lineament. The maximum reflectances yet obtained are approximately 1.0 percent $\bar{R}_o$ and were observed in Saline County and vicinity. Although the New Albany is not buried to great depths in this region, southern Illinois is characterized by extensive faulting, mineralization, and scattered small igneous intrusions. Damberger (1971, 1974) noted a similar anomalous increase in the rank of Pennsylvanian coals in southern Illinois and postulated two possible explanations that could separately, or in combination, account for this unusual coalification pattern. He suggested that if the former greatest depth of burial is solely responsible for the degree of coalification, then the maximum depth of burial must have occurred in this region rather than in the present region of deepest burial. He furthermore suggested that the existence of a deep-seated igneous intrusion would have also provided the higher heat flow necessary for increased coalification. This area of high maturation is presumed to extend eastward into the Moorman Syncline area of western Kentucky; however, we have not yet collected any data in that region.

Nowhere within the Illinois Basin have levels of maturation corresponding to the main zone of gas generation been observed. Although the reflectance map of figure 18 indicates large areas where petroleum generation has likely occurred, the only gas that is likely to have been formed is relatively small amounts of biogenic gas and gas associated with oil generation. Indeed, most oil fields in Illinois have relatively small amounts of associated gas production, and no major gas fields are present in the Illinois Basin portions of Illinois or Indiana. There are several large gas fields in western Kentucky; this suggests that high maturation levels may be found within the Moorman Syncline.

Relationship of New Albany Shale to known oil reservoirs

The distribution of abundant oil-prone types of kerogen, high thermal maturation ($\bar{R}_o$ >0.7 percent), and solid hydrocarbon pore fillings suggest that the hydrocarbons were generated and expelled from the New Albany Shale in southeastern and southern Illinois. The occurrence of commercial accumulations of oil and gas, however, shows no simple relationship to those areas where petroleum generation was likely to have occurred.

Stevenson and Dickerson (1969) cited several reasons for suspecting the New Albany as the source of oil and gas in reservoirs in the underlying Silurian-Devonian Hunton Megagroup. Figure 21 shows the distribution of known oil and gas fields in the Hunton Megagroup in Illinois. Except for a few small Dutch Creek (Devonian) pools in southeastern Illinois, most of the production has been oil from areas far removed from probable source areas in the New Albany. This suggests either long distance migration of oil from the New Albany or a deeper and older source bed.

The occurrence of oil and gas in Mississippian and Pennnsylvanian reservoirs is shown on figures 22 and 23. Together, these reservoirs account for more than 90 percent of the total reserves in Illinois and a similarly large proportion in Indiana and western Kentucky. Although the distribution of Mississippian oil generally coincides with probable source areas in the New Albany, it is much more strongly controlled by the areal distribution of suitable reservoir rocks (mostly Chesterian sandstones and Valmeyeran oolitic limestones). No casual relationship can be shown between the limit of oil in Mississippian strata and proximity to source beds in the New Albany. Similarly, the distribution of Pennsylvanian oil bears little, if any, relationship to the areas of generation in the New Albany Shale.

Most disturbing, perhaps, is the absence of oil accumulations in extreme southern Illinois, where the maturation is highest and black shale facies is thickest. One reason for this is that most of the porosity in Chesterian sands has been destroyed by mineralization, so that their quality as a reservoir

is greatly diminished. There are many tests into prospective carbonate strata, however, and no satisfactory explanation is known for the lack of oil in them.

If oil and gas were generated in the New Albany in southern Illinois, they have apparently migrated long distances away from the locus of generation. Possible migration pathways include: (1) northward toward the Rough Creek Lineament and thence upward along the faults into younger carrier beds and reservoirs north of the lineament; (2) southward, updip and out of the basin towards the Pascola Arch, where the oil was eventually lost at the surface or destroyed by pre-Cretaceous erosion; and (3) eastward into the Moorman Syncline and thence updip into younger reservoirs in western Kentucky and possibly Indiana.

CONCLUSIONS

Considerations of (1) the occurrence and abundance of amorphous-sapropelic organic matter, (2) the thermal maturation as determined by vitrinite reflectance and the character of fluorescence, and (3) the occurrence of solid hydrocarbon pore fillings and isolated angular solid hydrocarbons, strongly suggest that active petroleum generation and expulsion occurred within the New Albany Shale in southern and southeastern Illinois. Nowhere within the Illinois Basin is the thermal maturation known to reach the mature and post-mature zone of gas generation. Gas within the New Albany is therefore thought to be primarily biogenic or early thermogenic (generated concurrently with oil).

The time of the oil generation, the migration pathway, and the ultimate fate of petroleum formed in the New Albany Shale remain a mystery. The distribution of oil accumulations in Mississippian and Pennsylvanian strata is consistent with the New Albany as its source, but it cannot be demonstrated that the New Albany is the sole source on the basis of available data. Unless long-distance migration of petroleum was a major factor in the accumulation of underlying Silurian and Devonian oil, it now seems unlikely that the New Albany was the principal source for these oils as has been previously supposed. The validity of current models for petroleum generation might be questioned because of the absence of commercial accumulations in southern Illinois, where all of the established indicators of source rock potential are most favorable.

At the present time, there are essentially no data on which to base correlations between source rocks and crude oil accumulations in the Illinois Basin. Many of the questions arising from this study will remain unanswered until such data are available.

ACKNOWLEDGMENTS

This investigation is supported by U.S. Department of Energy Contract DE-AC21-76-MC05203 with the Illinois State Geological Survey. The manuscript was critically reviewed by Heinz Damberger, Richard Howard, Elwood Atherton, Robert Bergstrom, and Jack Simon. Much credit is due the drafting, clerical, editorial, and photographic staffs of the Survey for their help and patience in producing the final draft of the paper.

REFERENCES

Alpern, B., 1970, Classification pétrographique des constituants organiques fossiles des roches sedimentaires: Reve de L'institut Français du Pétrole et Annales des Combustibles Liquides, v. 25, no. 11, p. 1233-1266.

Bassett, J. L., and N. R. Hasenmueller, 1978, The New Albany Shale and correlative strata in Indiana: Proceedings of First Eastern Gas Shales Symposium, October 17-19, 1977, Morgantown, WV, U.S. Department of Energy MERC/SP-77/5, p. 183-194.

Bristol, H. M., and R. H. Howard, 1971, Paleogeologic map of the sub-Pennsylvanian Chesterian (Upper Mississippian) surface in the Illinois Basin: Illinois State Geological Survey Circular 458, 16 p.

Damberger, H. H., 1971, Coalification pattern of the Ilinois Basin: Economic Geology, v. 66, p. 488-494.

Damberger, H. H., 1974, Coalification patterns of Pennsylvanian coal basins of the Eastern United States, *in* Carbonaceous materials as indicators of metamorphism: Geological Society of America Special Paper 153, p. 53-74.

Dickerson, D. R., and D. D. Coleman, 1977, Mode of occurrence and relative distribution of hydrocarbon phases in shale, *in* R. E. Bergstrom and N. F. Shimp [principal investigators], Geologic and geochemical studies of the New Albany Group (Devonian black shale) in Illinois: Illinois State Geological Survey, Annual Report ORO-E-(40-1)-5203-12 to U.S. Energy Research and Development Administration, p. 115-135.

Dow, W. G., 1977, Kerogen studies and geological interpretations: Journal of Geochemical Exploration, v. 7, p. 79-99.

Gray, J., 1965, Extraction techniques, *in* B. Kummel and D. Ramp [eds.], Handbook of paleontological techniques: W. H. Freeman and Company, San Francisco, p. 530-587.

Hansman (Barrows), M., R. M. Cluff, R. D. Harvey, and D. A. Burke, 1978, Organic maturity of the New Albany Shale Group (Devonian-Mississippian) in Illinois: Geological Society of America Abstracts with Programs, v. 10, no. 7, p. 416.

Harvey, R. D., R. M. Cluff, and W. A. White, 1977, Mineralogic and petrographic characterization of New Albany in Illinois, *in* R. E. Bergstrom and N. F. Shimp [principal investigators], Geologic and geochemical studies of the New Albany Group (Devonian black shale) in Illinois: Illinois State Geological Survey, Annual Report ORO-E-(40-1)-5203-12 to U.S. Energy Research and Development Administration, p. 40-79.

Hood, A., C.C.M. Gutjahr, and R. L. Heacock, 1975, Organic metamorphism and the generation of petroleum: American Association of Petroleum Geologists Bulletin, v. 59, no. 6, p. 986-996.

Howard, R. H., 1967, Oil and gas pay maps of Illinois: Illinois State Geological Survey, Illinois Petroleum 84, 64 p.

Lamar, J. E., W. J. Armon, and J. A. Simon, 1956, Illinois oil shales: Illinois State Geological Survey Circular 208, 22 p.

Lineback, J. A., 1970, Stratigraphy of the New Albany Shale in Indiana: Indiana Geological Survey Bulletin 44, 73 p.

Ottenjahn, K., M. Teichmüller, and M. Wolf, 1975, Spectral fluorescence measurements of sporinites in reflected light and their applicability for coalification studies, *in* Petrographie de la matière organique des sédiments, relations avec la paléotempérature et le potentiel pétrolie: Centre National de la Recherche Scientifique, Paris, p. 49-65.

Reinbold, M. L., 1978, Stratigraphic relationships of the New Albany Shale Group (Devonian-Mississippian) in Illinois: Preprints, Second Eastern Gas Shales Symposium, Oct. 1978, Morgantown, WV, U.S. Department of Energy Morgantown Energy Technology Center METC/SP-78/6, v. 1, p. 443-454.

Robert, P., 1973, Analyse microscopique des charbons et des bitumes dispersés dans les roches et mesure de leur pourvoir réflecteur: Advances in Organic Geochemistry, 1973, Editions Technip, Paris, p. 549-569.

Schrayer, G. J., and W. M. Zarrella, 1963, Organic geochemistry of shales - I. Distribution of organic matter in the siliceous Mowry Shale of Wyoming: Geochim. et Cosmochim Acta, v. 27, p. 1033-1046.

Schwalb, H. R., and P. E. Potter, 1978, Structure and isopach map of the New Albany-Chattanooga-Ohio Shale (Devonian and Mississippian) in Kentucky: western sheet: Kentucky Geological Survey, Series X, map.

Stach, E., M.-Th. Mackowsky, M. Teichmüller, G. H. Taylor, D. Chandra, and R. Teichmüller, 1975, Stach's textbook of coal petrology: Gebrüder Borntraeger, Berlin, 428 p.

Stahl, W. J., 1977, Carbon and nitrogen isotopes in hydrocarbon research and exploration: Chemical Geology, v. 20, p. 121-149.

Stevenson, D. L., and D. R. Dickerson, 1969, Organic geochemistry of the New Albany Shale in Illinoi Illinois State Geological Survey Illinois Petroleum 90, 11 p.

Stevenson, D. L., and L. L. Whiting, 1967, Geologic structure of the Devonian-Silurian Hunton Limestone Megagroup in Illinois: Illinois State Geological Survey Illinois Petroleum 87, 5 p.

Tissot, B. P., and D. H. Welte, 1978, Petroleum formation and occurrence, a new approach to oil and gas exploration: Springer-Verlag, Berlin, 538 p.

van Gijzel, P., 1967, Autofluorescence of fossil pollen and spores with special reference to age determination and coalification: Leidse Geologische Mededelingen, v. 40, p. 263-317.

TABLE 1

Sample preparation procedure for organic petrographic analysis.

I. Chemical disaggregation

A. Crush sample (in small jaw crusher) to <0.5 cm.

B. Pulverize sample (in disc pulverizer) to -35 mesh (<0.5 mm).

C. Place samples in acid resistant polyethelyene or teflon containers resting in a hot water bath (∿50°C) under fume hood.

D. Dissolve carbonate minerals in 10 percent HCl (1 to 3 days). Decant, and rinse with water (3 rinses).

E. Dissolve silicate minerals in 48 percent HF (1 to 3 days). Decant into Na_2CO_3 solution to neutralize unspent acid. Rinse with water (7 rinses).

F. Dissolve fluoride reaction products in 10 percent HCl (1 day). Decant, and rinse samples with water (3 rinses).

II. Mechanical separation

A. Transfer samples to centrifuge tubes. Centrifuge. Decant water.

B. Float kerogen in $ZnBr_2$ solution (sp gr = 2.0) with short centrifuge. Decant $ZnBr_2$ solution and kerogen.

C. Discard heavy fraction (unreacted shale, pyrite, and other acid insoluble minerals).

D. Dilute $ZnBr_2$ with water. Centrifuge to sink kerogen and decant.

E. Rinse kerogen with water. Centrifuge. Decant water (3 rinses).

III. Pellet preparation

A. Transfer to glass bottles and dry kerogen in vacuum oven at ∿50°C (1 day).

B. Scraped dried kerogen from bottles and carefully grind in small mortar and pestle.

C. Mix kerogen powder with Armstrong C4 epoxy. Cast in a small plastic mold if sample is large; coat thin layer on 1-inch square plexiglas block if sample is small. Cure 1 day at room temperature.

D. Polish on automatic polisher to 0.5 μm.

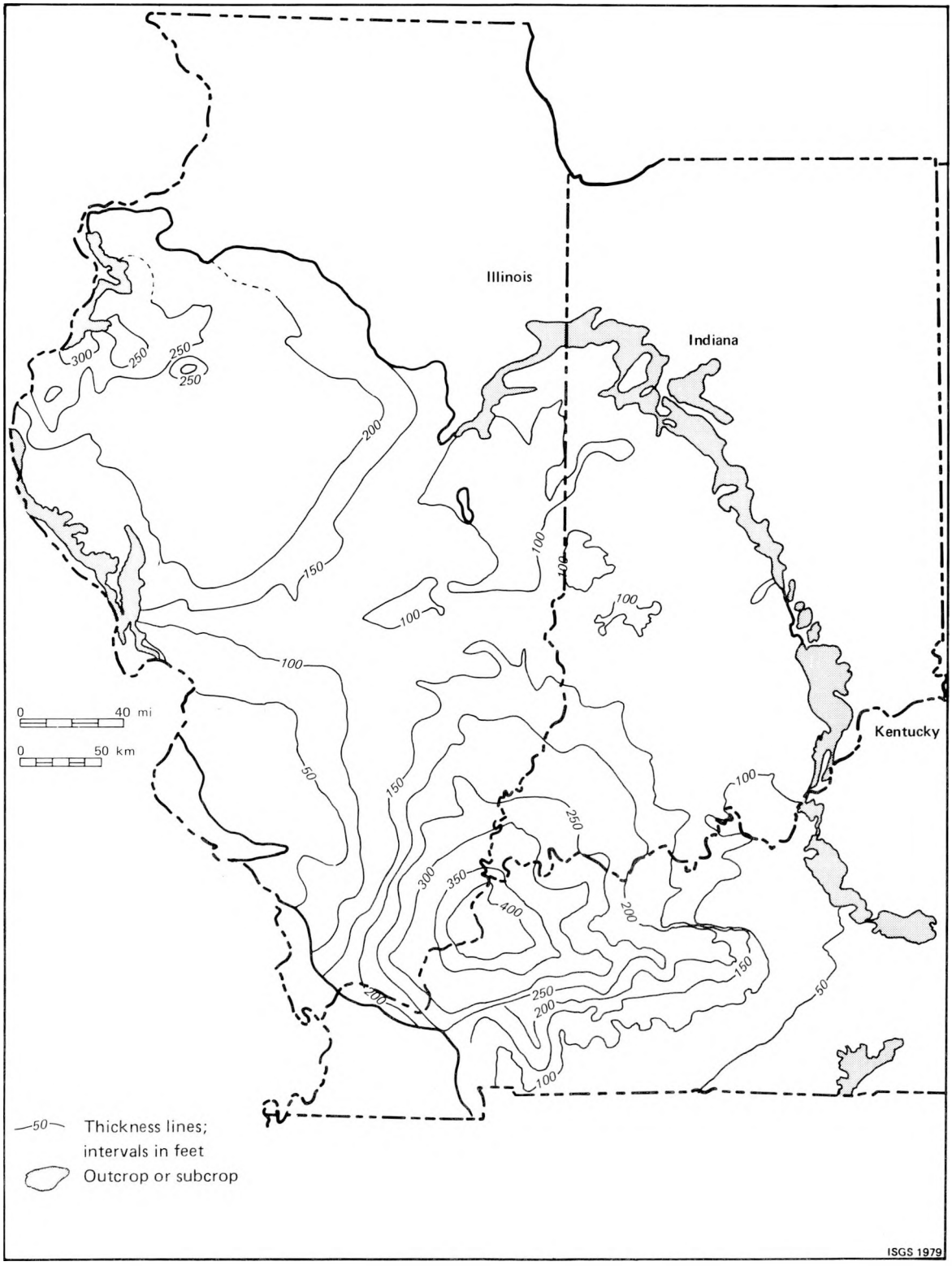


Figure 1. Thickness of the New Albany Shale Group in the Illinois Basin (after Reinbold, 1978; Bassett and Hasenmueller, 1978; Schwalb and Potter, 1978).

Figure 2. Percentage of organic carbon versus percentage of benzene-extractable organic matter (from Stevenson and Dickerson, 1969, fig. 4).

Figure 3. Contour map showing organic carbon content of the bottom 15 meters of the New Albany Shale (from Stevenson and Dickerson, 1969, fig. 5).

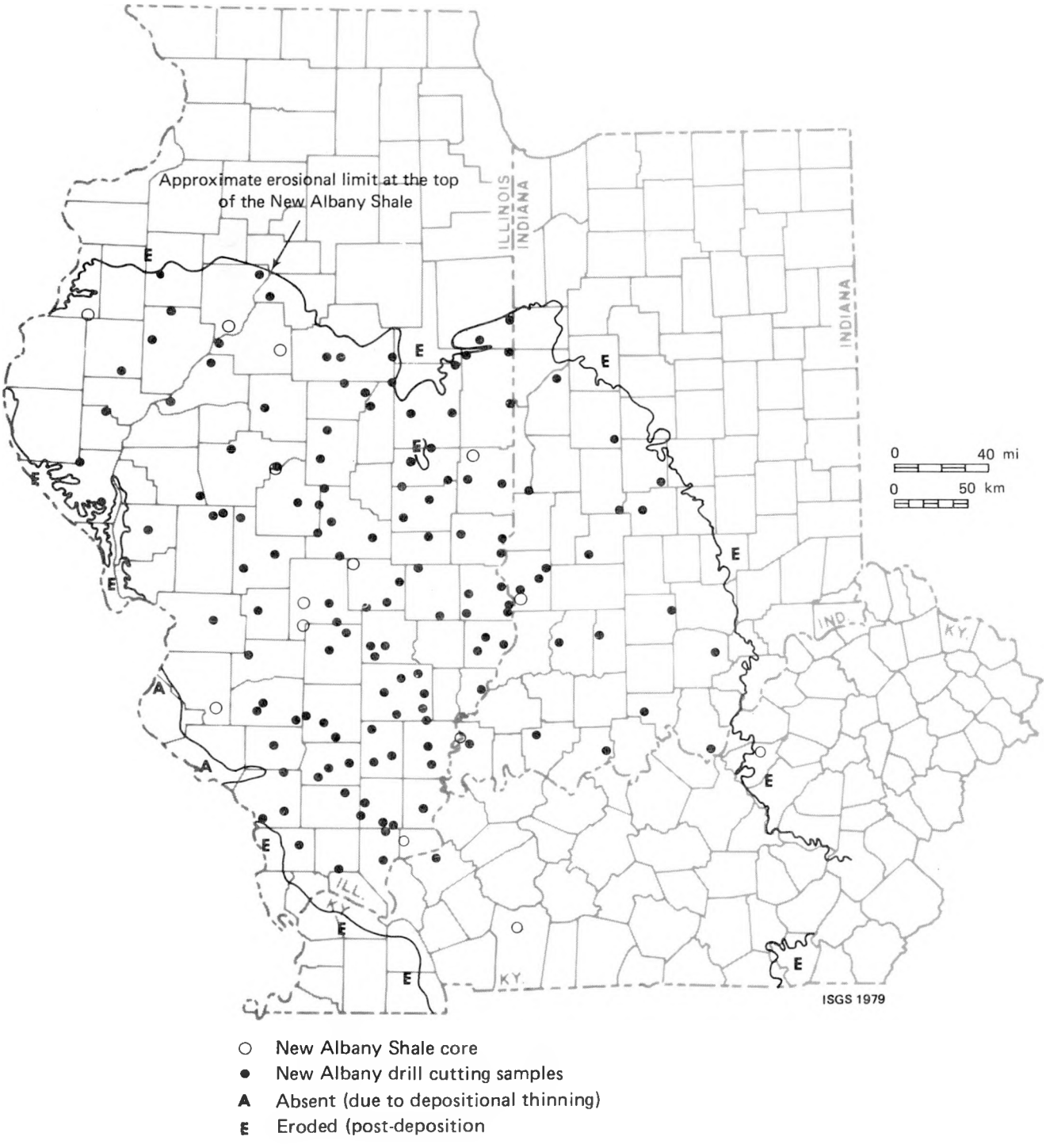


Figure 4. Locations of New Albany Shale samples used in this study.

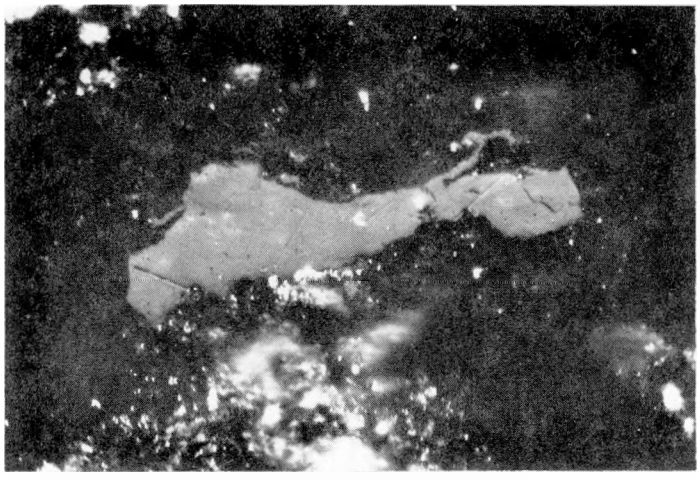


Figure 5. This irregularly shaped particle without cellular structures is typical of the vitrinite found in the acid-macerated kerogen separates of the New Albany Shales. This sample (NAS-148) from Clark County, Illinois, has a mean random reflectance of 0.54 percent. Within any one sample, vitrinites are higher in reflectance than liptinites and lower in reflectance than inertinites.

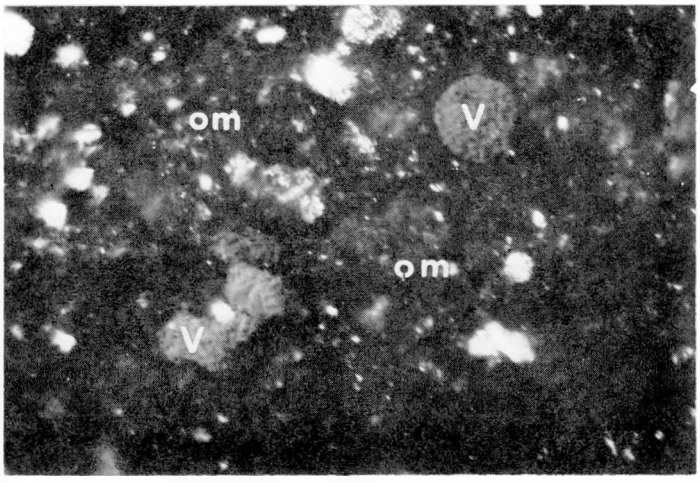


Figure 6. Pieces of vitrinite (V) and some amorphous organic matter (OM) are easily identified in this polished block of brownish-black shale (01KY02C1) from Christian County, Kentucky.

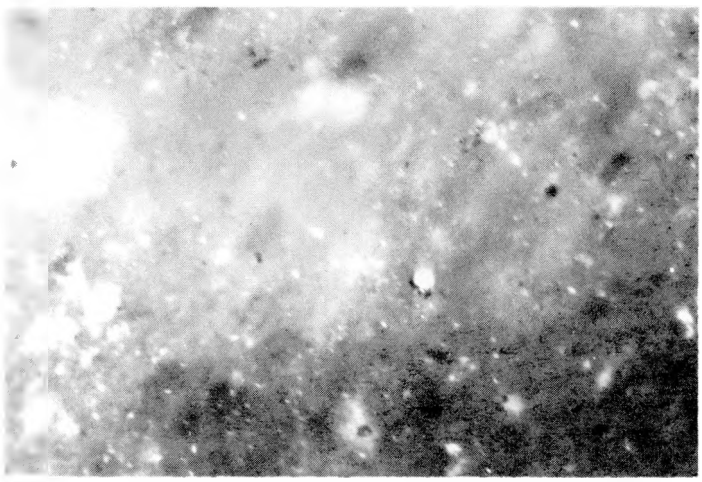


Figure 7. A paucity of dispersed organic matter is evident in this polished block of greenish-gray shale (01KY06L1) from Christian County, Kentucky.

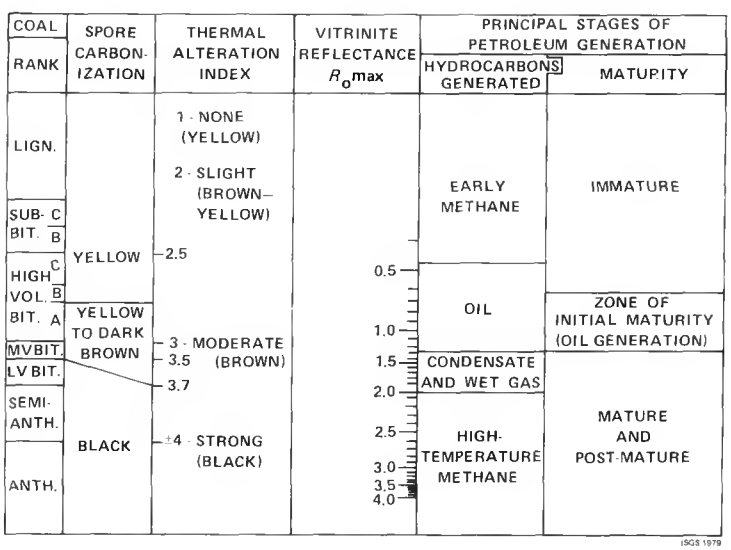


Figure 8. Relation of coal rank, vitrinite reflectance, and other measures of rank in sediments to the principal stages of oil and gas generation (after Hood, Gutjahr, and Heacock, 1975). Note that the reflectance scale is for maximum reflectance readings, not mean random reflectances as used in this study. At low maturity levels ($< 1.0\%$ $\bar{R}_o$) the difference between the two methods is negligible (Dow, 1977).

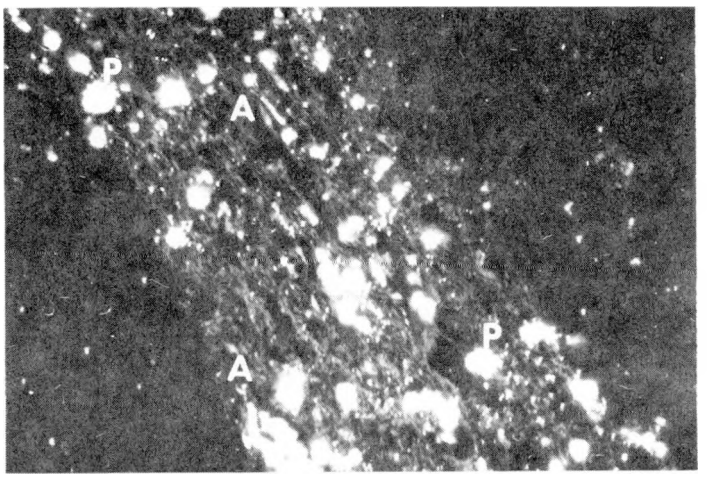


Figure 9. For most samples examined, a spongy network of amorphous organic material was clearly visible in pellets made from the acid-macerated kerogen separates. Pyrite (P) and alginite (A) are often included in the network structure as illustrated by this sample (NAS-131) from Wabash County, Illinois. Vitrinites and inertinites are also commonly incorporated in these structures.

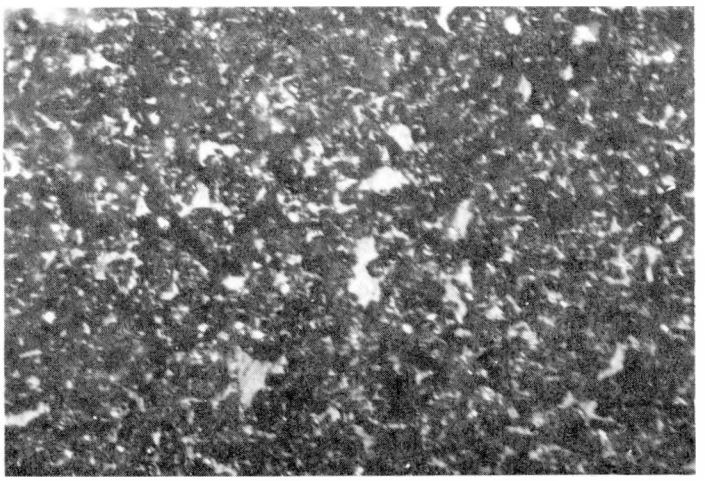


Figure 10. As the maturity of the organic matter increases, the amorphous organic material appears as a gray hash of unidentifiable fragments rather than a distinct network, as is illustrated by this sample from Johnson County, Illinois. This sample (NAS-360) has a mean random reflectance of 0.89 percent.

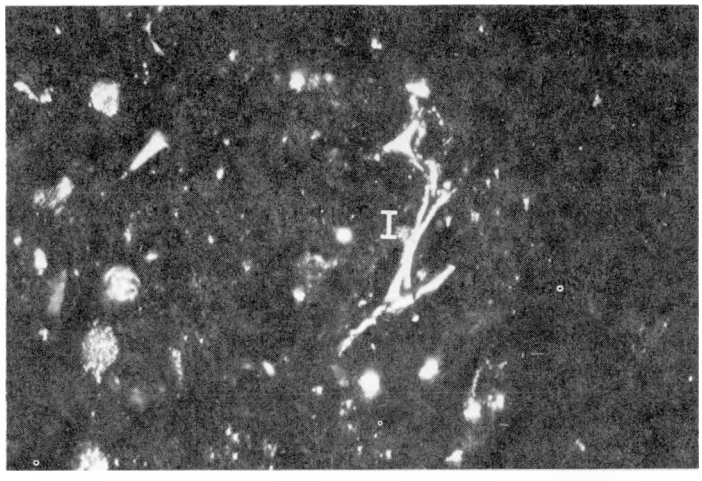


Figure 11. Inertinites (I) most often appear as high reflecting shards. These fragments from a sample (NAS-151) in Coles County, Illinois, are typical of inertinites observed in the New Albany Shale.

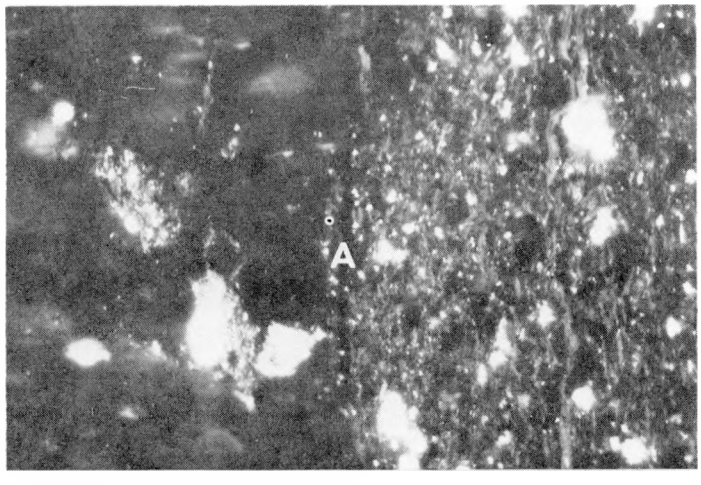


Figure 12. The dark gray particle is an alginite (A) (*Tasmanites*). These particles are reddish brown to dark gray in ordinary reflected light and are frequently difficult to distinguish from the surrounding amorphous organic material. In samples with reflectance values less than 0.70 percent, these alginites are easily identified in blue light by their characteristic fluorescence.



Figure 13. This sample (NAS-176) from Edgar County, Illinois, illustrates the fillings in inertinite pores that were observed in some samples, particularly in southeastern Illinois.

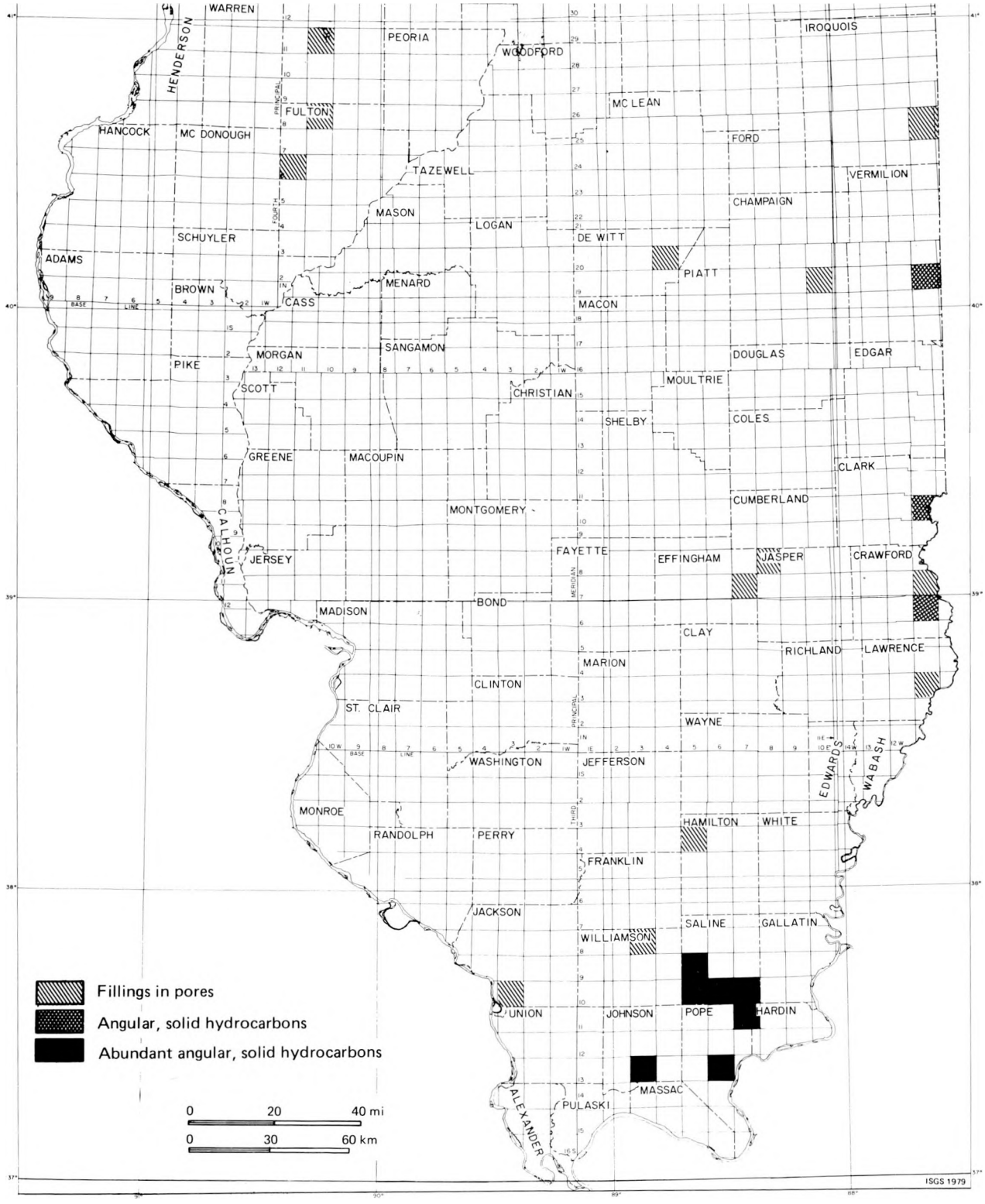


Figure 14. Areas where samples contained solid hydrocarbons as fillings or isolated angular particles.

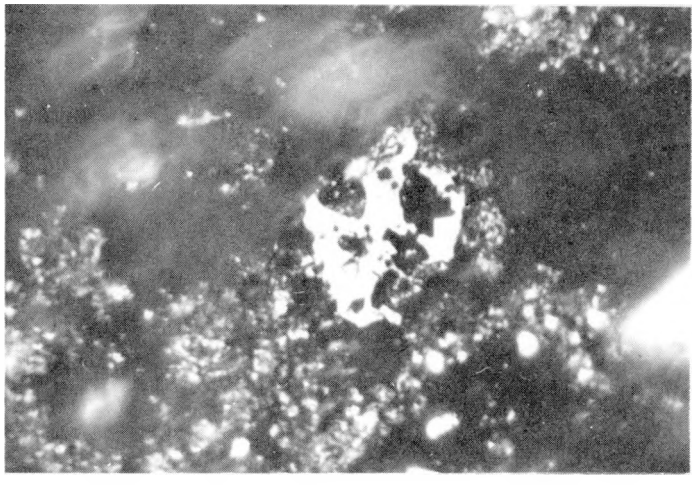


Figure 15. In the region where the highest mean random vitrinite reflectances were recorded, we observed a number of isolated angular fragments like this particle in a sample (NAS-360) from Johnson County, Illinois. These particles are probably solid hydrocarbons.

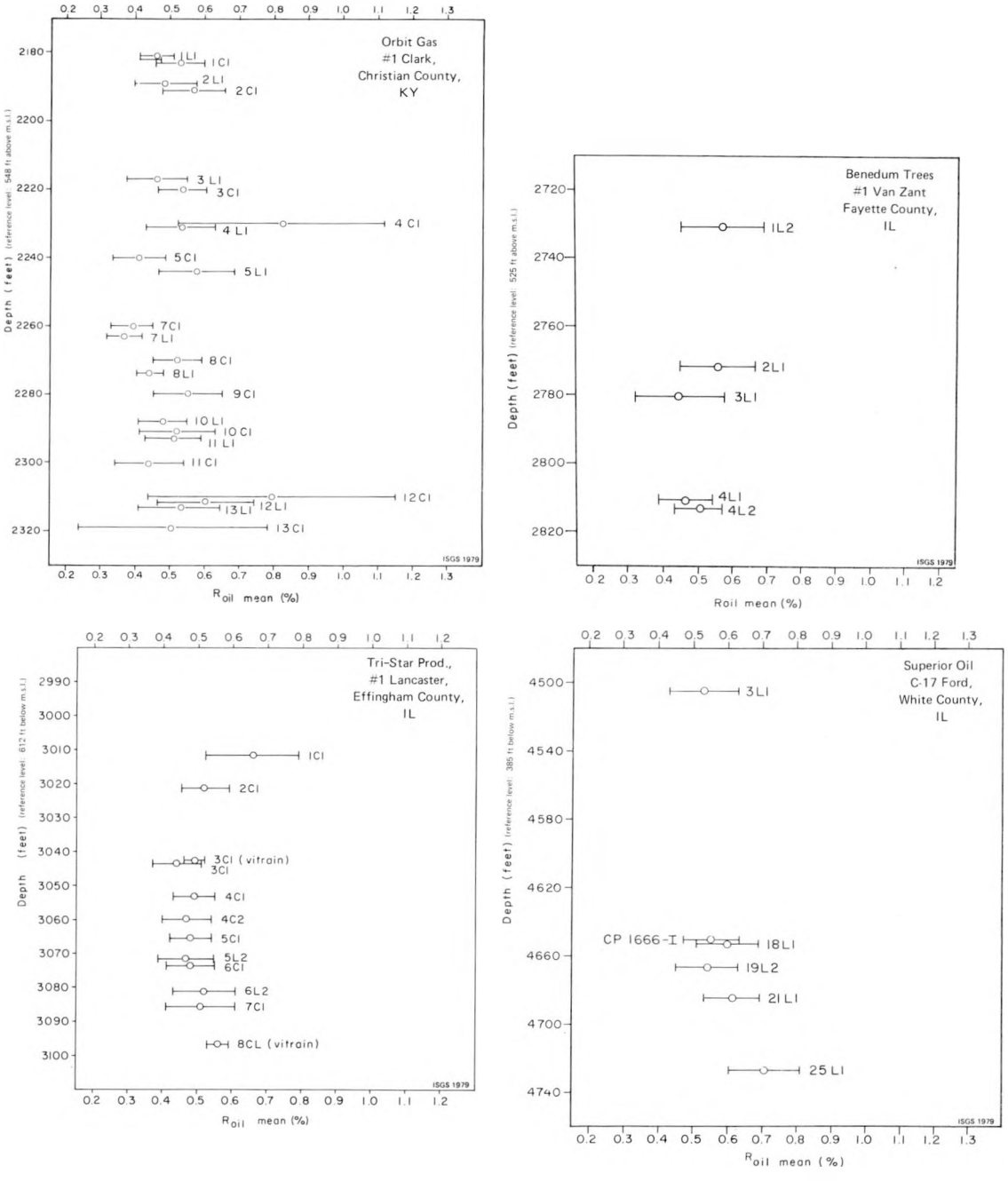


Figure 16. Variation of vitrinite reflectance with depth for four New Albany Shale cores in the central and southern portions of the Illinois Basin.

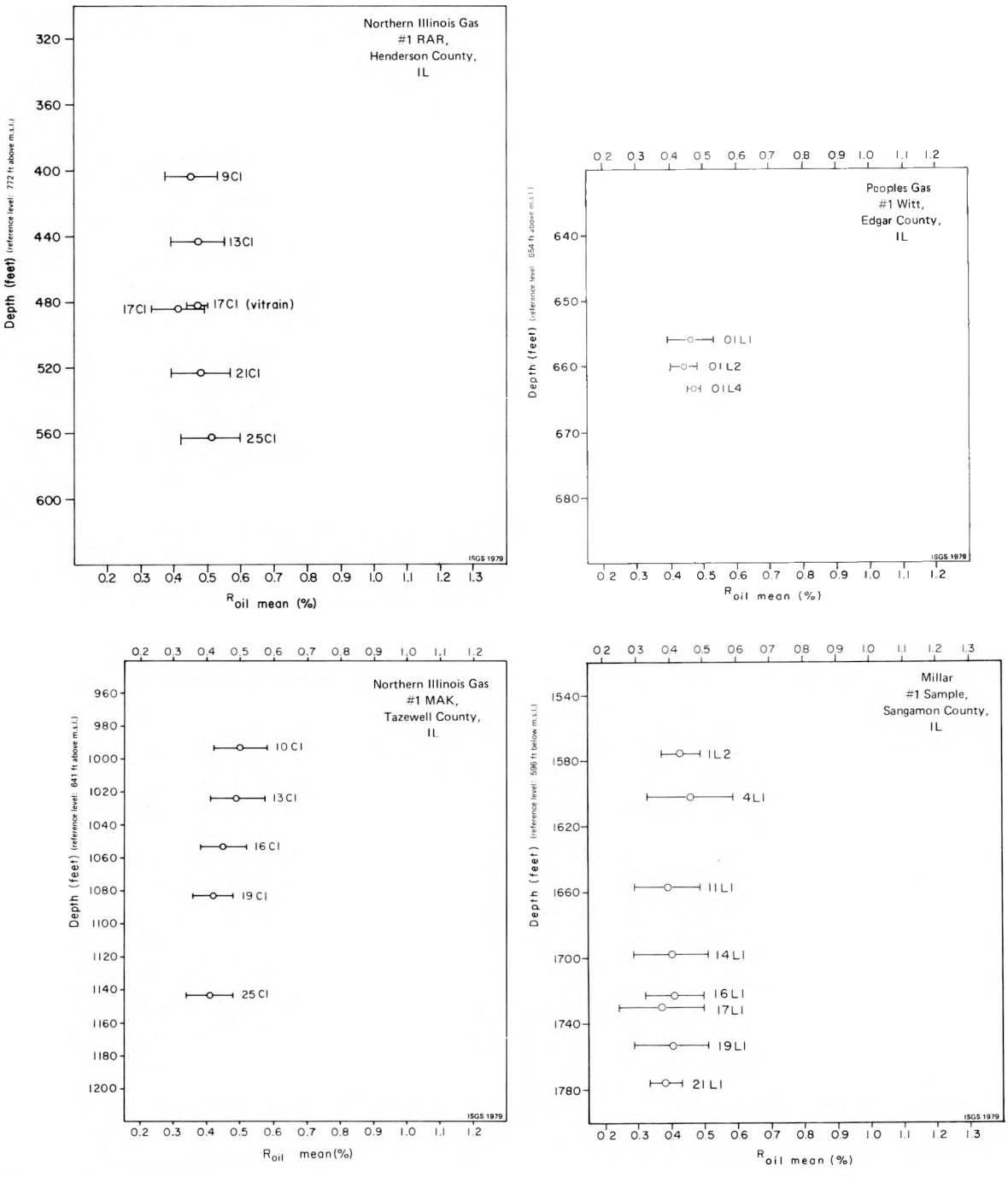


Figure 17. Variation of vitrinite reflectance with depth for four New Albany Shale cores in the northwestern and northern areas of the Illinois Basin.

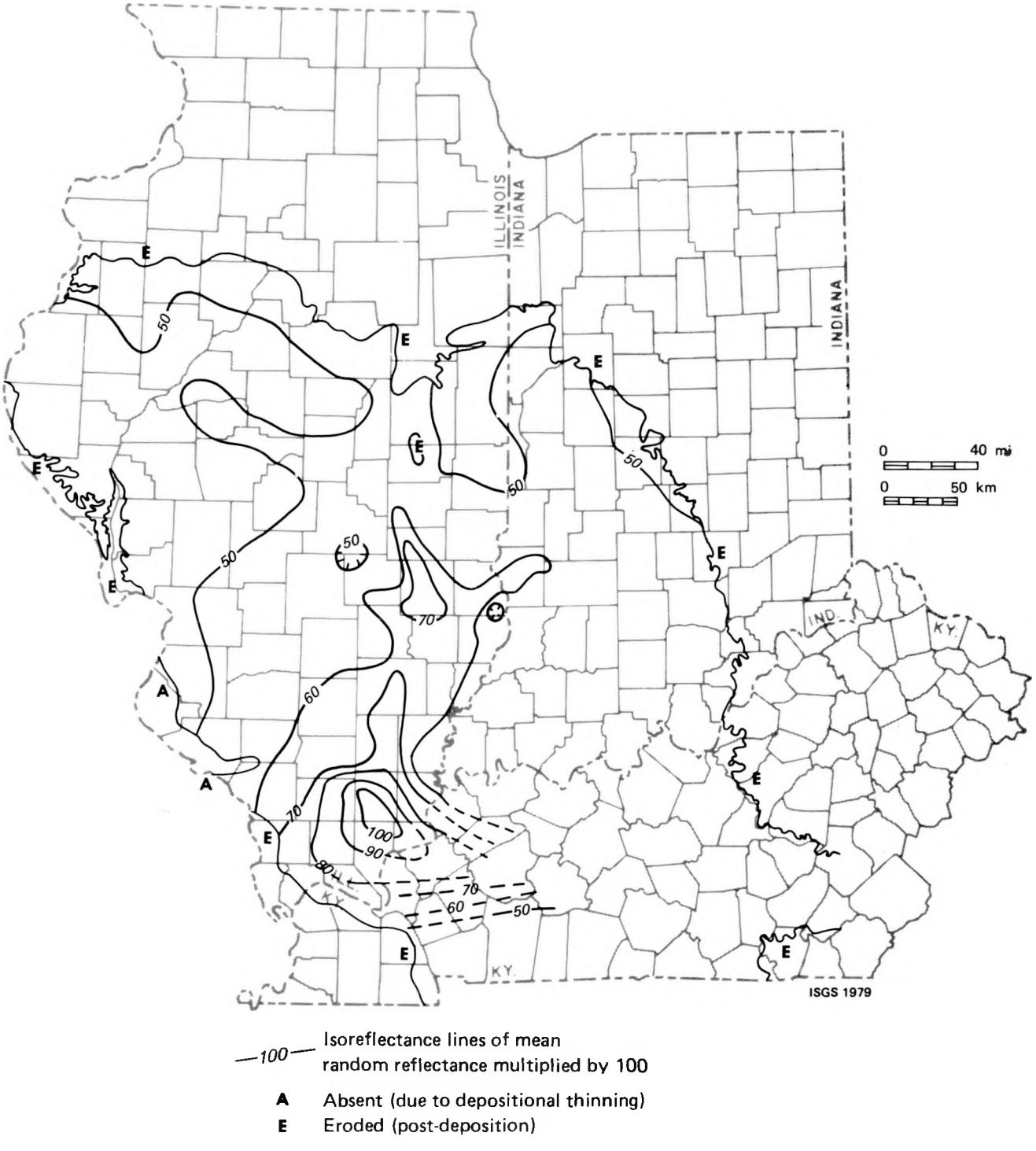


Figure 18. Mean random reflectance of vitrinite in the New Albany Shale (R_o percent x 100).

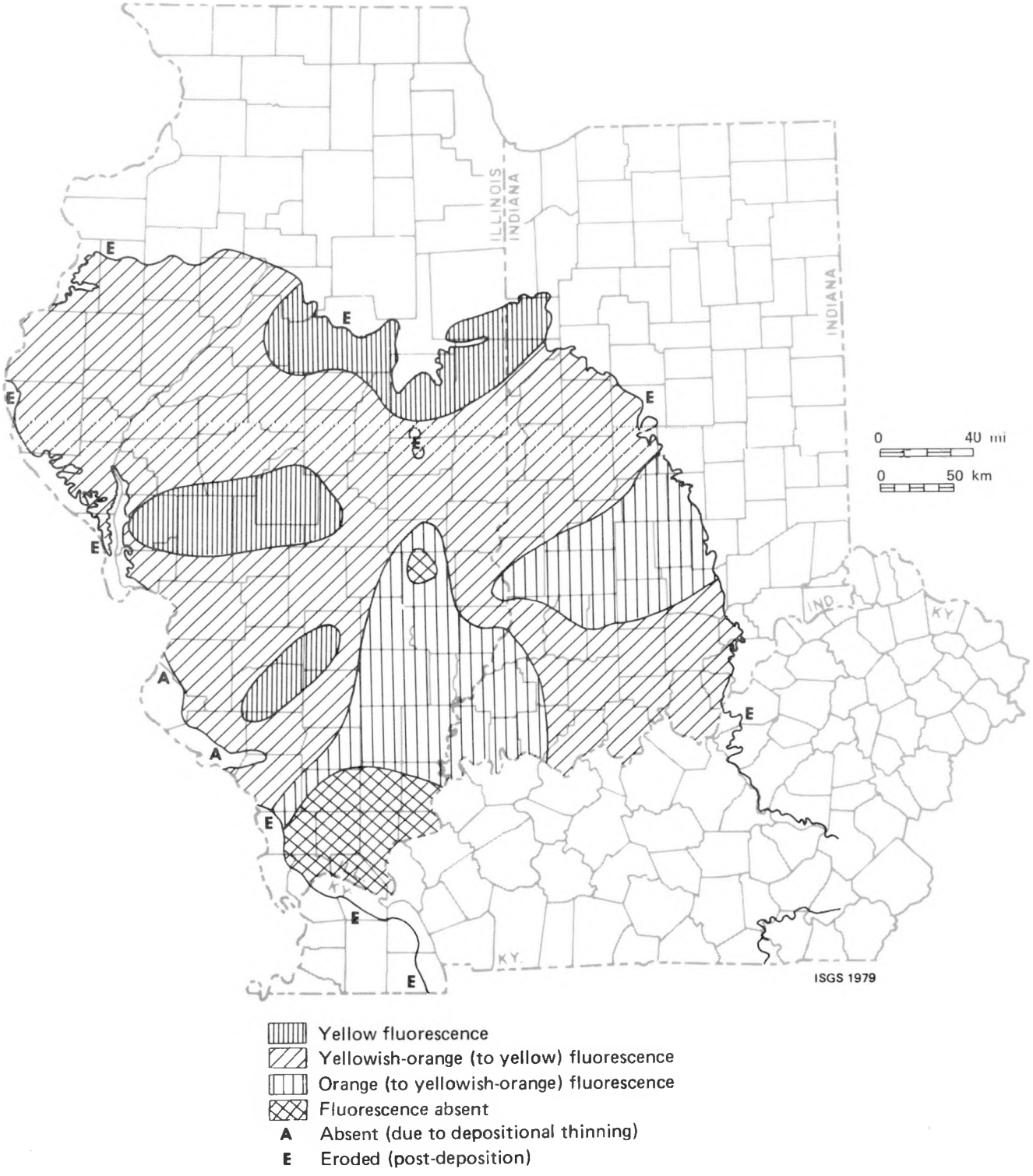


Figure 19. Variation of observed visual fluorescence.

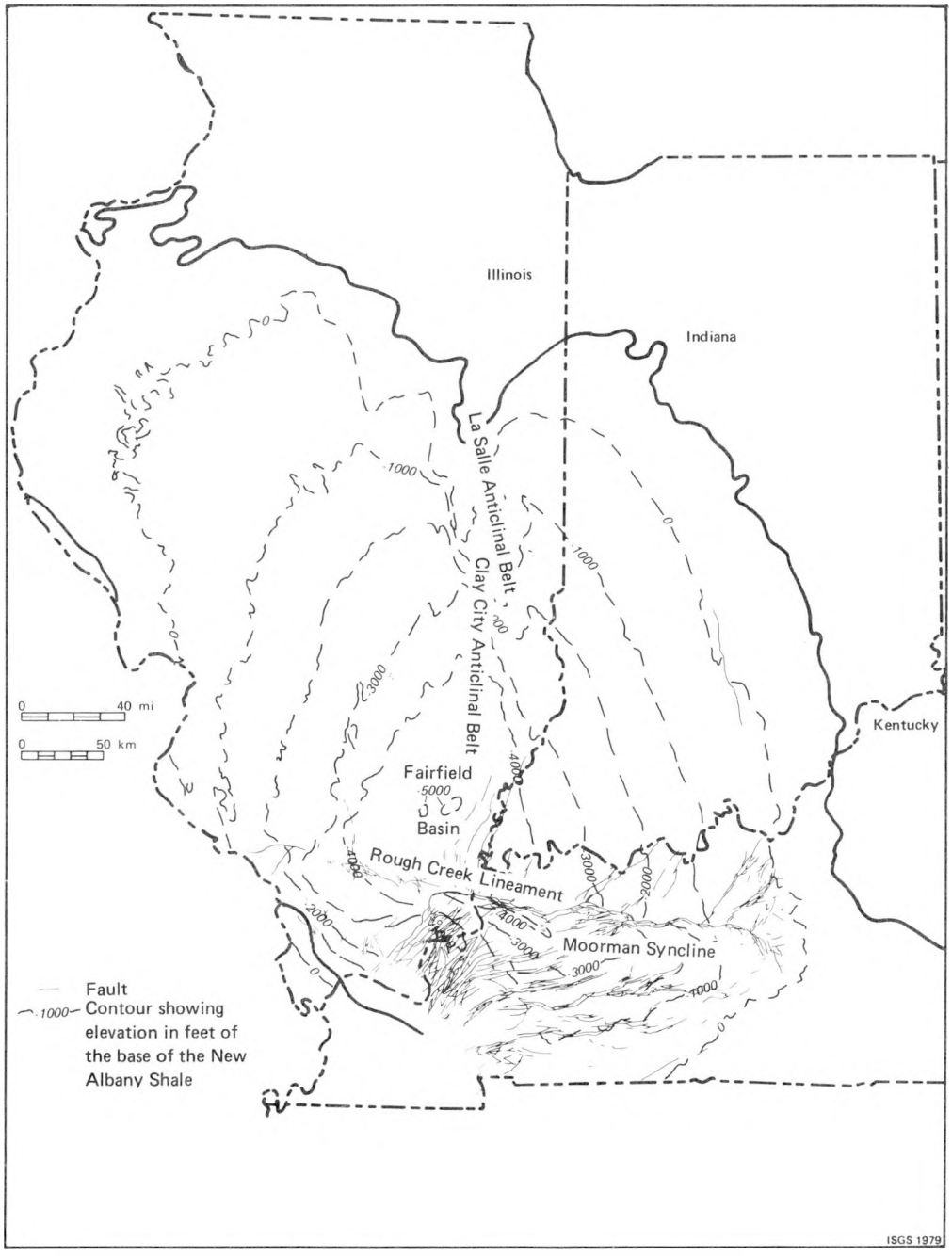


Figure 20. Geologic structure on the base of the New Albany Shale (after Stevenson and Whiting, 1967; Bassett and Hasenmueller, 1978; Schwalb and Potter, 1978).

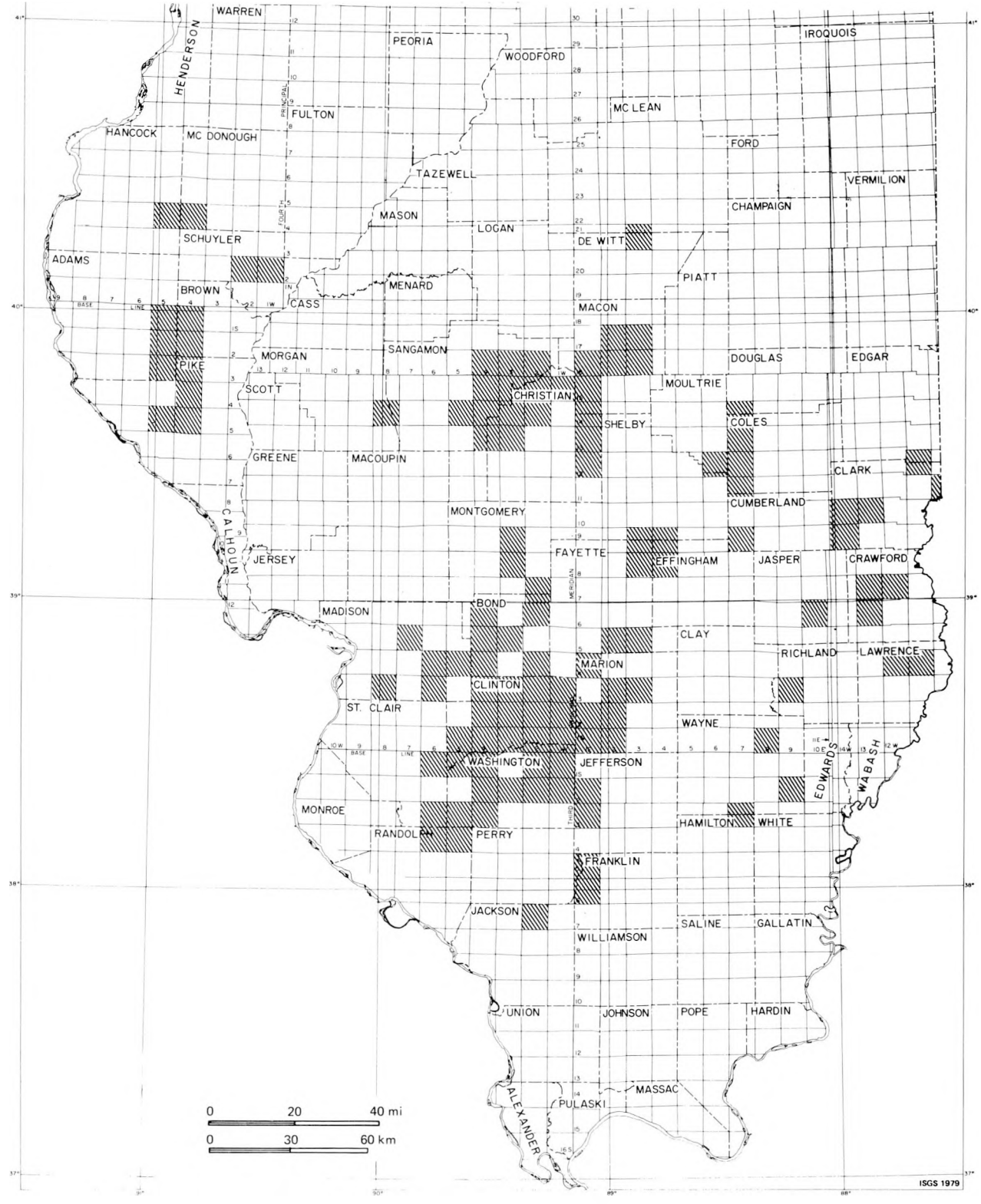


Figure 21. Devonian and Silurian oil and gas productive areas in Illinois (after Howard, 1967).

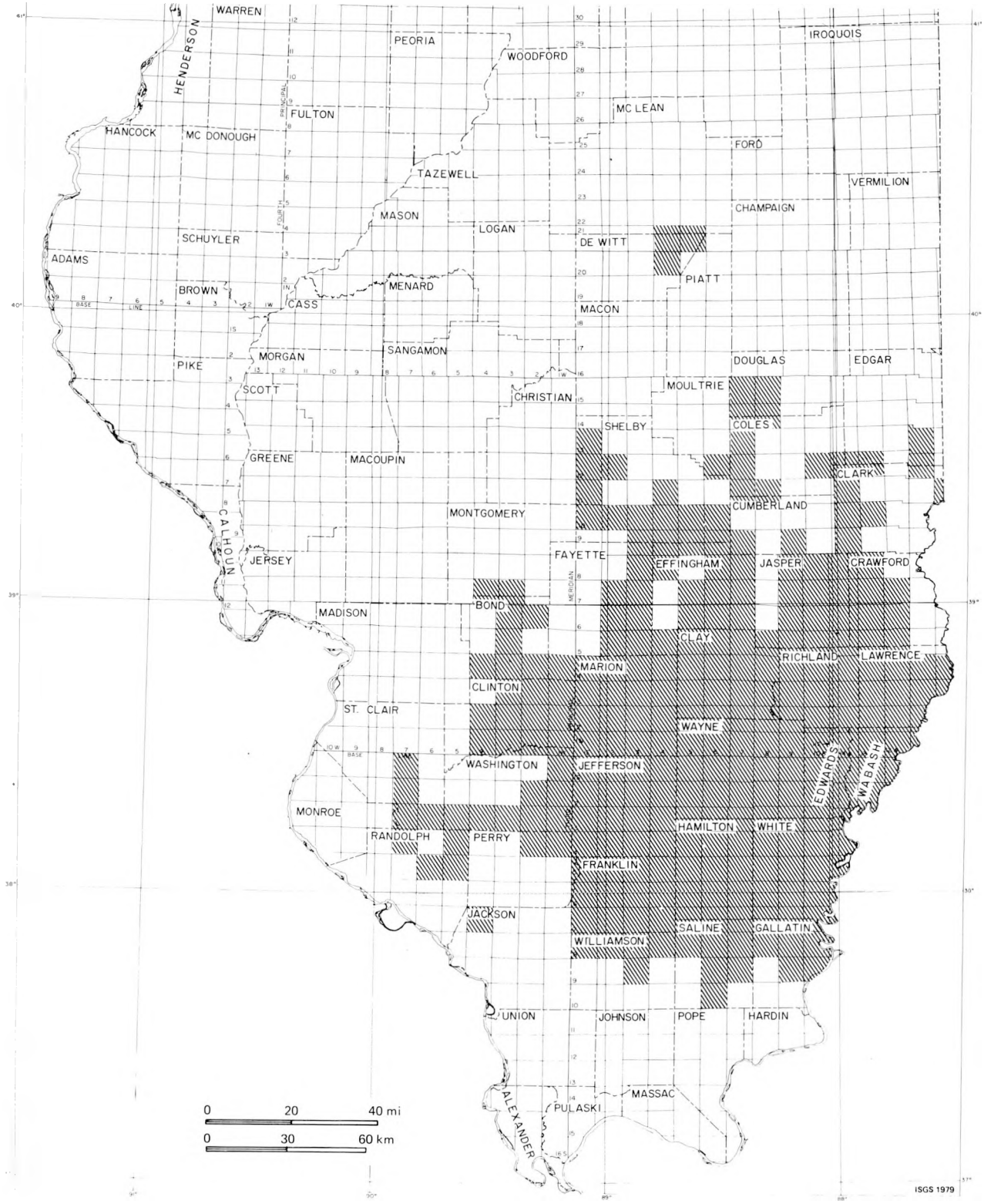


Figure 22. Mississippian oil and gas produtive areas in Ilinois (after Howard, 1967).

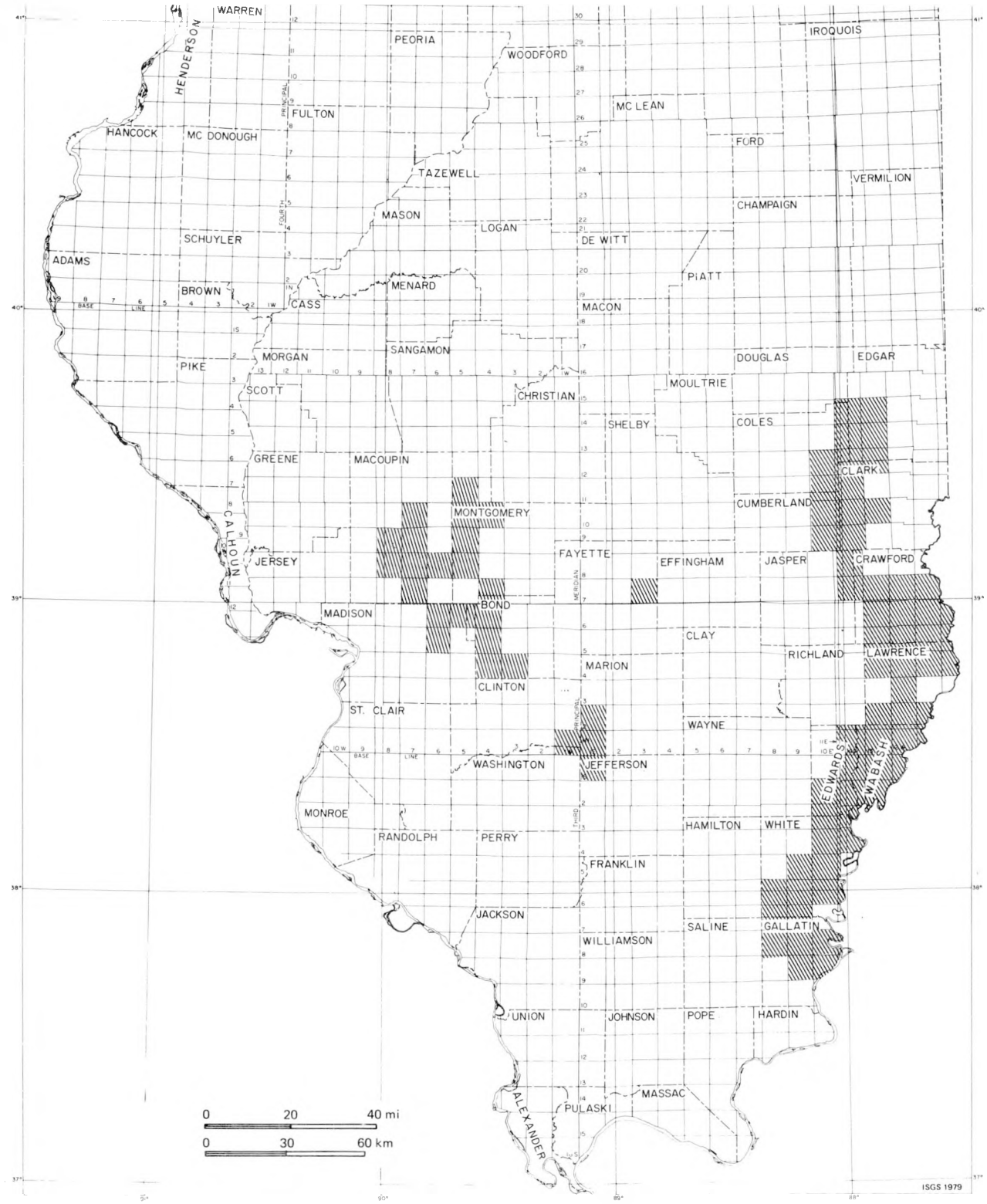


Figure 23. Pennsylvanian oil and gas productive areas in Illinois (after Howard, 1967).

DEVONIAN SHALES - AN IN-DEPTH ANALYSIS OF WELL EGSP NY NO. 1 WITH RESPECT TO SHALE CHARACTERIZATION, HYDROCARBON GAS CONTENT AND WIRE-LOG DATA

R. S. Kalyoncu, J. P. Boyer, and M. J. Snyder

Battelle Columbus Laboratories, OH

ABSTRACT

The objective of the Battelle portion of the Eastern Gas Shale Program has been to determine the relationships between shale characteristics, hydrocarbon gas content, and wire-log information in order to establish a sound basis for defining the productive capacity of this reserve and to provide guidance for continuing research, development, and demonstration projects designed to enhance the recovery of gas from shale deposits.

Historically, efforts to determine interrelationships have been hampered by the lack of data bases large enough for meaningful statistical interpretations. During the coring of Well EGSP NY No. 1 over 160 core samples were taken and over 12 wire-log runs were made. This data base has provided a sound foundation from which possible correlations and conclusions can be made.

INTRODUCTION AND SUMMARY

The Eastern Gas Shales Project at Battelle was initiated in September 1976, with the objective and scope of determining the relationships between the shale characteristics, hydrocarbon gas contents, and well location, and thereby provide a sound bases for (1) assessing the productive capacity of the Eastern Devonian gas shale deposits and, (2) guiding research, development, and demonstration projects to enhance the recovery of natural gas from the shale deposits. Included in the scope of the program ara a number of elemental tasks as a part of Resource Inventory and Shale Characterization subprojects of DOE's Eastern Gas Shales Project, designed to provide large quantities of support data for current and possibly future needs of the project.

Battelle Columbus Laboratories have thus far analyzed approximately 900 cored shale specimens from 20 different locations covering seven states in Appalachian and Illinois Basins. This article concerns itself with the characterization results on Allegany County, New York well (Y-1) and the data correlation analysis conducted, employing the Automatic Interaction Detection (AID) technique. Among the characterization data are free gas contents, gas release kinetics, chemical analysis (carbon, hydrogen, nitrogen, and sulfur), physical characteristics (densities, porosities, permeabil ities), and lithology of shales.

Analysis of the hydrocarbon gases in Y-1 samples indicates that the longer chain hydrocarbon gases (ethane, propane, butane) in these shales are significantly higher than in the previous wells studied. Because these hydrocarbons have significantly higher heats of combustion than methane, the methane equivalent of the hydrocarbon gas contents in New York shales is considerably higher.

The carbon contents of the Y-1 well, on the other hand, are somewhat lower than one would predict from the hydrocarbon gas contents. There is still a positive relationship between the carbon and hydrocarbon gas contents, however; that is, higher carbon contents are associated with increasing hydrocarbon-gas content in the shales. A similar relationship is also apparent between the sulfur and hydrocarbon gas contents.

No unusual trends are observed in the porosity values, and a reasonable agreement exists between the measured Hg-intrusion values and those calculated from the density data.

From limited lithological observations New York shales exhibit variable clay mineral and quartz contents. Generally, low levels of pyrite and carbonate minerals are observed. The low pyrite and carbonate contents noted in the powder examination of the samples are supported by the EDAX results showing low Ca and S contents.

The use of statistical methods (Automatic Interaction Detection) has shown that approximately 70-80 percent of the variance found in the gas contents of the core samples from this well can be explained through the variability in density, carbon content, and sulfur values. Based on these analyses no significant correlations between wire-log data and gas contents have been found.

EXPERIMENTAL FINDINGS

Characterization data were obtained on 165 cored shale samples from Allegany County, New York. Free gas contents, gas release kinetics, chemical analysis (C-H-N and sulfur), physical properties, such as densities, porosity, surface area, permeabilities, and lithological characteristics were determined.

Total carbon, hydrogen, nitrogen, and sulfur contents are summarized in Table 1. The measured carbon contents are somewhat low compared with the hydrocarbon gas contents (Table 5). This observation is somewhat contrary to the findings in the studies of the previous wells where the general trends have been the association of high carbon contents with high values of hydrocarbon gas contents. The positive relationship between carbon and hydrocarbon gas contents, however, is still apparent, as illustrated in Figure 8. The Y-1 well shows higher H/C atomic ratios than the previous wells, indicating that inorganic minerals (mostly clay minerals such as illite and kaolinite) are also sources of hydrogen (in the form of water) in addition to organic compounds (such as kerogen). Additional one-to-one correlations between chemical composition and gas contents are depicted in Figures 2 and 3.

The physical characterization data are summarized in Table 2. For the 165 samples characterized the bulk densities have a mean value of 2.62 and true density of 2.77. One-to-one relationships between the bulk densities and various other data (hydrocarbon gas, carbon, and hydrogen contents) are illustrated in Figures 4 through 6. Similar relationships between carbon, hydrogen, nitrogen, and porosities are shown in Figures 7 through 9. Figure 10 is a plot of bulk density versus porosity.

Porosities measured with mercury intrusion method (Table 3) compare reasonably well with porosities obtained from the density data.

Helium permeabilities measurements were made on several shale specimens. No significant permeation of gas took place after 60 minutes of subjecting the samples (1-inch diameter and 1-1/4-inch thick) to 1 atmosphere pressure gradient.

Allegany County, New York shales are characterized by variable clay mineral and quartz contents, and generally low in pyrite, carbonate minerals, and organic materials contents. Chemical and physical characterization data support the low organic contents observed microscopically. Quartz grain sizes vary from 10 to 80 μm. Pyrite grain sizes, which are generally sparse, range mostly in the 5 to 10 μm.

In Table 4 are presented EDAX results obtained using the SEM. With one exception these results are in good agreement with microscopic observations of powder samples. Samples Y-1-1440 and Y-1-1909 appear to be very low in illite and very high in quartz contents. This is reflected in the low K and high Si contents, or low K/Si ratios, shown in Table 4. The low pyrite and carbonate mineral contents noted in the powder examinations are supported by the low S and Ca contents. Occasionally Cl is noticeable in small amounts in EDAX results and is thought to be attributable to contamination from handling the specimen. However, the contents detected in samples Y-1-1440 and particularly Y-1-1592 were listed in Table 9 because care was taken in handling the sample.

FREE GAS CONTENTS AND GAS RELEASE KINETICS

The initial quantities of hydrocarbon gases, "free" gas contents, and release kinetics are presented in Table 5. A wide variation in the total hydrocarbon gas contents among the core samples is quite apparent from the table. The mean value of hydrocarbon gas contents is approximately 28.7 percent of the total gas mixture occupying the free space surrounding the shale samples in the sealed containers. This translates to an average hydrocarbon gas content of approximately 0.4 cubic foot per cubic foot of shale.

Some of the shale specimens exhibit significant amounts of longer chain hydrocarbon gases (ethane, propane, butane). These long chain hydrocarbons have considerably higher heats of combustion than that of methane. For example, the heat of combustion for ethane (373 kCal/mol) is about 1.75 times that of methane (212 kCal/mol). The values for propane (531) and butane (688) are 2.5 and 3.2 times higher than that of methane, respectively. With the heat of combustion value in mind the total hydrocarbon gas contents could be converted to methane equivalent by simply multiplying the high hydrocarbon gas values by the ratio of the heats of combustion. Table 6 summarizes the methane equivalent of the hydrocarbon gas contents obtained in this manner. High hydrocarbons to methane ratio (2 + 3 + 4 + 5/1) is also given. This ratio could be looked at as a measure of gas quality. The higher this ratio the higher would be the BTU content of the gas. As indicated in Table 6, the ratio varies between zero (no hydrocarbons other than methane) and 2.73 for direct ratio, and zero to 7.5 for the methane equivalents.

Gas release rates were determined for five Y-1 shales. This work was performed by rapidly evacuating the shale containers, and then monitoring the pressure buildup over a period of about 65 days. Data for these samples are shown in Table 7.

These data were analyzed using the methods of Wilson[1]. Accordingly, the following equation applies:

$$\frac{P}{P_\infty} = 1 - \Sigma \frac{4a\ (1 + a)}{4 + 4a + a^2 q_n^2} e^{-Dq_n^2\ t/r^2} \qquad (1)$$

where r is the sample radius (4.4 cm), a is the ratio of the capacity of the shale to that of the free space in the container, and q_n's are the positive non-zero roots of the equation

$$aq_n J_o\ (q_n) + 2J_1\ (q_n) = 0 \qquad (2)$$

where the J's are zero and first order Bessel functions. Solutions for the q_n's are available in standard tabulations for various values of a, the capacity parameter. The latter parameter must be determined by fitting the data to Equation (1). For cases where there is little sorption of the gas by the shale, a is small and is determined by bulk volume of the shale and its porosity. However, when appreciable sorption occurs, the value of a can be quite large. At values of a > 10, Equation (1) becomes insensitive to this parameter. Within the range of a values of 0-10, the shape of the pressure response curve is fairly sensitive to the value of a, and a preliminary judgment of the appropriate value of a can be made by comparison of the pressure curve to curves given by Wilson[1].

Application of Equation (1) to the data cited above yields the results tabulated in Table 8.

Calculated curves for samples Y-1-1939, 2119, and 2538 are shown along with the experimental data in Figures 11, 12, and 13. Data for the other two samples are not plotted due to lack of sufficient data points.

In principle, it should be possible to assess the total gas content per unit volume of shale from knowledge of a. However, because of the insensitivity of the results when a > 10, only qualitative comparisons can be made for the case discussed here. For these samples, the value of a, based solely on the physical dimensions of the sample and its container, is 0.25. Thus, all of these samples display at least some capacity for hydrocarbon gas sorption.

It is interesting to compare the derived values of P_∞ with the hydrocarbon pressures initially present in the containers before the experiment was begun. This comparison is illustrated in Table 9.

Except for the case of sample 1939, values of P_∞ are less than the initial hydrocarbon pressures. This is to be expected if any appreciable gas was lost during the pump-out procedure. Samples 1939 and 2538 have large "a" values indicating relatively large gas capacities. Sample 1939, however, has a very small diffusion coefficient and 2538 has a relatively large diffusion coefficient. Thus, most of the gas present in 1939 was retained during the handling and experimental procedures, but it appears that much of the gas originally present in sample 2538 could have been lost. This comparison is significant because it indicates possible errors in judgment of gas capacity by the usual procedure of measuring pressures after some period of time (usually 30 days). In the case of sample 1939, this time is obviously not long enough; for sample 2538, a significant portion of the gas could have been lost before it was sealed into the container. In any case, the variation of real capacities (as opposed to the physical dimensions of the sample) make the initial pressure measurement less meaningful. Although this measurement probably reflects the amount of gas readily available under the current sampling conditions, it does not reflect the fact that more efficient fracture of sample 1939 would result in release of much more gas than could be obtained from sample 2119. For example, if the sample radius for 1939 had been 2.2 cm, the pressure expected after 65 days would be 355 torr. Furthermore, the simple pressure measurement probably underestimates the true original gas content of sample 2538.

Long-term diffusion study was conducted with sample Y-1-2538 at temperatures of 25 and 80 C using the continuous flow total hydrocarbon technique[2]. Data for the 80 C run are shown in Figure 14. These data are interesting in that they display a departure from expected bahavior during the initial portion of the run, and suggest a modified approach that should enable us to extract additional information from similar samples.

Our customary analysis of the diffusion data is based on the assumption that only methane contributes significantly to the observed total hydrocarbon signal. Treating the core sample as a cylinder having "easy" diffusion in the radial direction, the average concentration of gas in the cylinder at any time is

$$\bar{C} = 4C_o \sum_i \frac{1}{\xi_i} 2 \exp\left[-\frac{\xi_i^2 Dt}{r^2}\right] \quad (3)$$

where C_o is the initial concentration, ξ_i are zero-order Bessel function roots, D is the diffusion coefficient, and r is the radius of the cylinder. With the technique used, we do not measure the concentration in the sample, but determine the total hydrocarbon concentration in a stream of nitrogen flowing over the sample. Thus, the gas phase concentration, C_g, is given by

$$C_g = (V_s/F)(d\bar{C}/dt) \quad (4)$$

or

$$C_g = 4C_o DV_s/r^2F \sum_i \exp\left[-\frac{\xi_i^2 Dt}{r^2}\right] \quad (5)$$

For values of $Dt/r^2 > 0.15$, only the first term of the series in Equation (5) is significant and a plot of $\ln C_g$ versus t yields a straight line having a slope proportional to D and an intercept proportional to the initial concentration in the cylinder.

Figure 14 shows the data for the subject sample plotted in this manner, with an apparent D of 1.6×10^{-6} cm^2/sec. and an apparent gas to shale ratio of 0.80 V/V. However, the early portion of the experimental curve does not conform to Equation (5) (it suggests a higher diffusion coefficient). The most probable reason for this behavior is the inclusion of higher molecular weight ($>C_1$) in the escaping gas early in the experiment. The initial gas analysis for this sample indicate an average of about 1.8 carbons per molecule, which agrees well with the approximately 2:1 disparity between the observed and predicted response curves.

General hydrocarbon gas diffusion coefficients determined at 28 and 80 C are shown in Figure 15. The diffusion coefficient measured at temperatures of 28 and 80 C are 5.0×10^{-7} and 1.1×10^{-6} cm^2/sec., respectively. Concentration values extrapolated to zero times in Figure 15 are 0.7 V/V and 2.9 V/V, respectively. Analysis of the individual components of the hydrocarbon gas mixtures during diffusion studies showed that the residual gas in the 80 C specimen was primarily propane, with small amounts of butane and pentane. The 28 C specimen showed some methane, but was again primarily propane. Thus, the apparent temperature dependencies for the two branches of the response curve are different, with the early portion having the greater coefficient. This too would be expected if the excess signal is due to higher molecular weight hydrocarbons.

One way to resolve this question while simultaneously obtaining additional information about the gas release process is to analyze the effluent gas for individual hydrocarbons rather than measuring the total carbon content. This was accomplished by modifying the existing set-up.

Figure 16 illustrates the type of results obtained with the modified method. A shale sample from another location was used for this purpose. In the figure the numbers refer to the number of carbon atoms in the species detected (e.g., 1 stands for methane). For purposes of clarity in presenting the data some data points have been omitted in Figure 16.

Although there is some scatter in these data, the diffusion coefficients appear to be, for the most part, inversely proportional to the square root of molecular weight for the various species. This suggests a Knudsen or molecular diffusion process for flow of the hydrocarbons through the shale matrix. With sample K-4-1280, the apparent activation energy for the process is 3.1 ± 0.4 kCal/mol.

DATA INTERPRETATION AND CORRELATION

In attempting to develop a clear understanding of how the hydrocarbon gas is distributed within the shale formation and, more importantly, in identifying the tools available to predict this distribution extensive use has been made of a computer technique referred to as Automatic Interaction Detection (AID). This method does not rely upon the assumption of a model, an assumption inherent to regression analysis; rather, it relies on a partition of the variation in the data base. The end result is a decision tree that is used to establish the mean value and standard deviation of the dependent variable for a given set of predictor variables. Since this tree is model independent, it provides a more reliable prediction than regression analysis.

Originally developed in 1963 by Sonquist and Morgan at the Institute for Social Research[3], AID focuses on problems associated with the analysis of survey data. In this situation, the problem is one of determining which of the variables, for which data has been collected, are related to the phenomena in question (in this case the hydrocarbon gas content), and how they may be used to predict changes in the criterion (dependent) variable. The objective is to explain the variance of the criterion variable. Where the number of predictors is small, the problem of isolating the relationships is manageable, but when the number of potential predictors is large, which is typical of the shale program, then an analysis of the joint affects presents serious problems. The AID program uses an algorithm to ask the question. "Given the units of analysis under consideration, what predicts values of the dependent variable?". Using the algorithm the AID program divides the sample, through a series of binary splits, into a mutually exclusive series of subgroups. Every observation is a member of exactly one of these subgroups. They are chosen so that at each step in the procedure their means account for more of the total sum of squares (reduce predictive error) than the means of any other groups established by other possible splits.

Figure 17 shows a typical tree structure from one of these analyses. In this case the question was which of the various laboratory, physical and chemical parameters can best predict the values of the criterion -- hydrocarbon gas content. The answer in this case is that with a combination of true density, total carbon and sulfur the variance in the data base is 86.4 percent accounted for. The apparently unusual feature of this predictive structure is found in the first split in which high values of density are found to be associated with high gas release. (It should be noted that the actual values of all variables have been transformed into integers ranging from 0-63 so that the statistics are not biased by the actual value of the mean of a particular variable.) Although apparently anomalous this feature of the data is found for many of the EGSP wells. In fact, as seen in Figure 18, the trend also occurs with wire-log data.

In Figure 18, after splitting on total carbon and sulfur both the high and the low gas content groups are split on Coriband porosity and true density, respectively, with low porosity and high density being associated with higher gas content. Although the explanation for this behavior is uncertain it is postulated that the behavior arise from the fact that the low gas samples have porosity which is truely "open" or unfilled whereas the original pores in the high gas samples are now primarily filled with a mixture of gas and residue of organic material which decayed to create the gas. Support for this postulate can be found in the fact that when AID analyses are made with porosity as the criterion variable the data is split on the basis of total carbon with high carbon being associated with low porosity.

The AID program has also been extensively used to determine which, if any, of the wire-log data is most useful in predicting gas contents. Figure 19 illustrates the result of this analysis for Y-1. As this analysis shows the wire-log data alone is not particularily useful as a predictive tool. The initial split, for instance, explains only 24 percent of the variability whereas total carbon and true density explain 58.6 percent and 41.5 percent, respectively, in the previous analyses. It has been suggested by researchers at Columbia Gas that because of sampling uncertainties (i.e., gasless prior to canning, depth correlation errors) the data should be grouped in some fashion as an aid to predictability. Table 10 illustrates the changes in predictability of the first split when single samples are analyzed, when adjacent samples are averaged or when all samples over a 50 foot interval are averaged. In general, this averaging appears to improve predictability. Although a part of this improvement is due to the reduction in the variance of the original data base the indication is that if a valid manipulation of the raw data can be made then predictability is enhanced.

Table 10 also illustrates how much more refinement of logging techniques is necessary before these tools can be truly useful. Although other researchers have reported that gamma radiation has proven useful in determining density and organic content, these results do not show any correlation between this variable and gas contents in the shale.

CONCLUSIONS

The analysis of the characterization data on well Y-1 and data correlation analysis lead us to the following conclusions:

(1) Logging techniques employed in the EGSP are not suitable in predicting potential gas contents in the Devonian Shales. There is need for the development of logging methods and instrumentation for use in natural gas exploration.

(2) Inordinately large varieties and quantities of characterization data are not necessarily useful in predicting the gas potential of shale formations. More emphasis should be given to quality and relevance of the laboratory investigations.

(3) Laboratory investigations should be geared toward understanding the state of the organic matter in shale as related to microstructure and mechanism and kinetics of gas release rates in the shale formations.

BIBLOGRAPHY

(1) Wilson, A. H., "A Diffusion Problem in Which the Amount of Diffusing Substance is Finite - I", Phil. Mag., 39 (7) pp 48-58 (1948).

(2) Kalyoncu, R. S., and Snyder, M. J., "Characterization and Analysis of Devonian Shales as Related to Release of Gaseous Hydrocarbons", Quarterly Technical Progress Reports to DOE/METC for FY-1978.

(3) Sonquist, J. A., and Morgan, J. H., "The Detection of Interaction Effect, A Report on a Computer Program for the Selection of Optimum Combinations of Explanatory Variables", Mongraph 35, Survey Research Center, Institute for Scoial Research, The University of Michigan, Ann Arbor, Michigan.

TABLE 1. CHEMICAL CHARACTERIZATION DATA, 02/02/79

SAMPLE ID	TOTAL CARBON PERCENT	TOTAL HYDROGEN PERCENT	TOTAL NITROGEN PERCENT	TOTAL SULFUR PERCENT	CARD CODE	SEQ NO.
Y 1- 372.	.6	.5	.1	.1	5	1
Y 1- 382.	.3	.4	.1	.1	5	2
Y 1- 392.	1.1	.5	.1	.2	5	3
Y 1- 402.	.2	.4	.1	.4	5	4
Y 1- 412.	.3	.4	.1	.3	5	5
Y 1- 422.	.3	.5	.1	.3	5	6
Y 1- 431.	.4	.4	.1	.9	5	7
Y 1- 441.	.3	.3	.1	.2	5	8
Y 1- 451.	.3	.4	.1	.6	5	9
Y 1- 461.	.1	.3	.1	.4	5	10
Y 1- 471.	.3	.3	.1	.4	5	11
Y 1- 481.	.6	.3	.1	.5	5	12
Y 1- 491.	.3	.3	.1	.8	5	13
Y 1- 501.	.4	.4	.1	.5	5	14
Y 1- 521.	.3	.4	.1	.7	5	15
Y 1- 530.	.1	.2	.1	.1	5	16
Y 1- 565.	.5	.3	.1	.1	5	18
Y 1- 575.	1.0	.4	.1	.4	5	19
Y 1- 585.	.5	.4	.1	.3	5	20
Y 1- 595.	1.4	.5	.1	1.5	5	21
Y 1-1014.	.6	.2	.1	1.0	5	23
Y 1-1530.	1.0	.5	.1	1.6	5	24
Y 1-1540.	1.1	.5	.1	1.6	5	25
Y 1-1550.	.4	.3	.1	1.6	5	26
Y 1-1560.	.3	.5	.1	.2	5	27
Y 1-1570.	.2	.5	.1	.1	5	28
Y 1-1580.	.2	.5	.1	1.3	5	29
Y 1-1590.	.4	.3	.1	.1	5	30
Y 1-1600.	.6	.4	.1	.1	5	31
Y 1-1610.	.3	.5	.1	.1	5	32
Y 1-1620.	1.2	.5	.1	1.3	5	33
Y 1-1630.	.1	.5	.1	.2	5	34
Y 1-1640.	.4	.2	.1	.1	5	35
Y 1-1649.	.3	.3	.1	.1	5	36
Y 1-1659.	.6	.5	.1	.3	5	37
Y 1-1669.	.5	.3	.1	.1	5	38
Y 1-1679.	.3	.4	.1	.1	5	39
Y 1-1684.	.3	.5	.1	.1	5	40
Y 1-1694.	.2	.4	.1	.2	5	41
Y 1-1704.	1.2	.5	.2	1.4	5	42
Y 1-1714.	.6	.5	.1	2.4	5	43
Y 1-1724.	.3	.5	.1	.6	5	44
Y 1-1733.	.1	.6	.1	.1	5	45
Y 1-1743.	.3	.5	.1	.2	5	46
Y 1-1753.	.3	.5	.1	.1	5	47

TABLE 1. (Continued)

SAMPLE ID	TOTAL CARBON PERCENT	TOTAL HYDROGEN PERCENT	TOTAL NITROGEN PERCENT	TOTAL SULFUR PERCENT	CARD CODE	SEQ NO.
Y 1-1563.	.2	.4	.1	.1	5	48
Y 1-1573.	.4	.6	.1	.1	5	49
Y 1-1583.	.3	.4	.1	.1	5	50
Y 1-1592.	.5	.3	.1	.2	5	51
Y 1-1602.	.2	.5	.1	.1	5	52
Y 1-1612.	.3	.4	.1	.2	5	53
Y 1-1622.	.1	.4	.1	.1	5	54
Y 1-1632.	.2	.5	.1	.4	5	55
Y 1-1642.	.7	.5	.1	.1	5	56
Y 1-1652.	.2	.4	.1	.2	5	57
Y 1-1662.	.3	.5	.1	.2	5	58
Y 1-1672.	.6	.5	.1	.2	5	59
Y 1-1682.	.3	.5	.1	.2	5	60
Y 1-1692.	.3	.5	.1	.3	5	61
Y 1-1703.	.5	.5	.1	.7	5	62
Y 1-1711.	.5	.3	.1	.1	5	63
Y 1-1721.	.6	.5	.1	.4	5	64
Y 1-1731.	.4	.5	.1	.2	5	65
Y 1-1741.	.5	.5	.1	1.2	5	66
Y 1-1751.	.4	.6	.1	.3	5	67
Y 1-1761.	.2	.3	.1	.5	5	68
Y 1-1770.	.3	.5	.1	.3	5	69
Y 1-1780.	.9	.6	.1	1.4	5	70
Y 1-1790.	.5	.5	.1	.4	5	71
Y 1-1800.	.5	.6	.1	1.3	5	72
Y 1-1810.	.9	.6	.1	1.9	5	73
Y 1-1820.	.8	.6	.1	2.9	5	74
Y 1-1830.	1.1	.6	.1	2.4	5	75
Y 1-1840.	.7	.5	.1	1.8	5	76
Y 1-1850.	3.5	.6	.1	.2	5	77
Y 1-1860.	.4	.3	.1	1.4	5	78
Y 1-1870.	.7	.5	.1	1.6	5	79
Y 1-1880.	1.1	.6	.1	1.6	5	80
Y 1-1889.	.9	.6	.1	.2	5	81
Y 1-1899.	.7	.6	.1	.5	5	82
Y 1-1909.	1.0	.2	.1	.9	5	83
Y 1-1919.	.5	.3	.1	.2	5	84
Y 1-1929.	.8	.6	.1	2.8	5	85
Y 1-1939.	1.2	.5	.2	1.8	5	86
Y 1-1947.	.3	.5	.1	.5	5	87
Y 1-1957.	1.0	.5	.1	1.5	5	88
Y 1-1967.	1.6	.5	.1	.1	5	89
Y 1-1977.	.4	.5	.1	1.8	5	90
Y 1-1987.	2.8	.6	.1	.3	5	91
Y 1-1997.	.4	.6	.1	.5	5	92

TABLE 1. (Continued)

SAMPLE ID	TOTAL CARBON PERCENT	TOTAL HYDROGEN PERCENT	TOTAL NITROGEN PERCENT	TOTAL SULFUR PERCENT	CARD CODE	SEQ NO.
Y 1-2606.	.4	.6	.1	.7	5	93
Y 1-2616.	.3	.4	.1	3.0	5	94
Y 1-2626.	.4	.5	.1	.4	5	95
Y 1-2636.	.3	.6	.1	.2	5	96
Y 1-2646.	.4	.6	.1	.1	5	97
Y 1-2656.	.3	.6	.1	.4	5	98
Y 1-2665.	1.1	.5	.1	1.9	5	99
Y 1-2675.	.4	.5	.1	1.1	5	100
Y 1-2685.	.5	.4	.1	.2	5	101
Y 1-2695.	.3	.5	.1	.3	5	102
Y 1-2705.	1.3	.5	.1	1.2	5	103
Y 1-2715.	.7	.5	.1	1.9	5	104
Y 1-2719.	2.0	.5	.2	1.8	5	105
Y 1-2725.	.7	.5	.1	.2	5	106
Y 1-2735.	.5	.4	.1	1.7	5	107
Y 1-2745.	.6	.5	.1	2.6	5	108
Y 1-2755.	1.9	.5	.1	1.9	5	109
Y 1-2765.	1.0	.4	.4	5.3	5	110
Y 1-2775.	.3	.5	.1	.3	5	111
Y 1-2784.	.5	.5	.2	.2	5	112
Y 1-2794.	.7	.4	.2	1.0	5	113
Y 1-2804.	.4	.5	.1	.3	5	114
Y 1-2814.	.5	.5	.2	.7	5	115
Y 1-2824.	.3	.4	.2	.7	5	116
Y 1-2834.	.6	.3	.2	.3	5	117
Y 1-2843.	.5	.6	.5	.3	5	118
Y 1-2853.	.6	.5	.6	.2	5	119
Y 1-2863.	.4	.5	.5	.2	5	120
Y 1-2873.	.4	.5	.5	.1	5	121
Y 1-2883.	.6	.6	.6	.7	5	122
Y 1-2893.	.4	.5	.4	.6	5	123
Y 1-2902.	.5	.5	.5	.1	5	124
Y 1-2912.	.7	.5	.1	1.2	5	125
Y 1-2922.	.4	.5	.1	.9	5	126
Y 1-2932.	1.0	.5	.1	1.5	5	127
Y 1-2942.	.4	.4	.2	1.9	5	128
Y 1-2952.	.4	.5	.1	.1	5	129
Y 1-2966.	.6	.5	.1	1.1	5	130
Y 1-2978.	.7	.5	.1	1.2	5	131
Y 1-2986.	.6	.5	.1	1.6	5	132
Y 1-2996.	.6	.5	.1	1.7	5	133
Y 1-3006.	.7	.4	.1	1.5	5	134
Y 1-3016.	2.0	.5	.1	1.5	5	135
Y 1-3026.	.6	.5	.1	1.2	5	136
Y 1-3036.	1.6	.6	.1	1.6	5	138

TABLE 1. (Continued)

SAMPLE ID	TOTAL CARBON PERCENT	TOTAL HYDROGEN PERCENT	TOTAL NITROGEN PERCENT	TOTAL SULFUR PERCENT	CARD CODE	SEN NO.
Y 1-2576.	.7	.5	.1	1.7	5	139
Y 1-2586.	1.2	.5	.2	1.6	5	140
Y 1-2596.	.9	.5	.1	1.7	5	141
Y 1-2607.	1.6	.5	.1	2.1	5	142
Y 1-2617.	4.0	.6	.1	1.8	5	143
Y 1-2627.	2.0	.5	.1	2.6	5	144
Y 1-2637.	1.3	.5	.1	1.4	5	145
Y 1-2647.	.8	.4	.1	1.6	5	146
Y 1-2657.	1.3	.4	.1	.6	5	147
Y 1-2725.	2.0	.4	.1	.9	5	148
Y 1-2735.	2.1	.5	.1	.9	5	149
Y 1-2745.	2.1	.4	.1	.9	5	150
Y 1-2755.	3.1	.4	.1	1.0	5	151
Y 1-2765.	2.2	.4	.1	.9	5	152
Y 1-2775.	2.3	.4	.1	.5	5	153
Y 1-2784.	2.4	.5	.2	2.4	5	154
Y 1-2794.	1.9	.4	.1	.7	5	155
Y 1-2804.	2.6	.4	.2	.6	5	156
Y 1-2814.	1.0	.4	.1	.7	5	157
Y 1-2824.	1.6	.5	.1	1.0	5	158
Y 1-2834.	3.1	.5	.1	1.3	5	159
Y 1-2844.	1.8	.5	.1	1.4	5	160
Y 1-2854.	3.8	.5	.1	1.6	5	161
Y 1-2864.	6.5	.3	.1	.4	5	162
Y 1-2874.	6.6	.3	.1	.7	5	163
Y 1-2884.	4.8	.5	.1	1.0	5	164
Y 1-2894.	5.1	.6	.1	1.0	5	165

TABLE 2. SUMMARY OF PHYSICAL CHARACTERIZATION DATA, 02/12/79

SAMPLE ID.	BULK DENSITY, G/CC	TRUE DENSITY, G/CC	POROSITY, PCT	SURFACE AREA, M2/G	SEQ NO.
Y 1- 372.	2.305	2.763	16.584	4.122	1
Y 1- 382.	2.676	2.603	0.000	3.649	2
Y 1- 392.	2.539	2.845	10.766	.903	3
Y 1- 402.	2.448	2.619	6.511	1.013	4
Y 1- 412.	2.609	2.774	5.945	1.746	5
Y 1- 422.	2.621	2.657	1.372	2.982	6
Y 1- 431.	2.643	2.567	0.000	3.605	7
Y 1- 441.	2.689	2.584	0.000	2.477	8
Y 1- 451.	2.388	2.673	10.670	4.052	9
Y 1- 461.	2.600	2.739	5.060	4.124	10
Y 1- 471.	2.508	2.547	1.517	3.372	11
Y 1- 481.	2.681	2.751	2.532	3.194	12
Y 1- 491.	2.633	2.665	1.206	1.747	13
Y 1- 501.	2.634	2.902	9.233	1.462	14
Y 1- 521.	2.538	2.767	8.264	2.363	15
Y 1- 530.	2.543	2.811	9.532	2.430	16
Y 1- 965.	2.543	2.588	1.740	1.521	18
Y 1- 975.	2.568	2.790	7.968	2.284	19
Y 1- 985.	2.684	2.038	0.000	1.188	20
Y 1- 995.	2.508	2.793	10.193	2.241	21
Y 1-1014.	2.548	2.680	4.927	1.145	23
Y 1-1330.	2.614	2.688	2.738	1.079	24
Y 1-1340.	2.642	2.634	0.000	1.542	25
Y 1-1350.	2.618	2.638	.751	1.563	26
Y 1-1360.	2.563	2.818	9.054	2.507	27
Y 1-1370.	2.645	2.669	.902	3.387	28
Y 1-1380.	2.612	2.809	7.029	1.003	29
Y 1-1390.	2.534	2.685	5.614	3.706	30
Y 1-1400.	2.586	2.663	2.893	1.090	31
Y 1-1410.	2.645	2.781	4.895	5.833	32
Y 1-1420.	2.621	2.629	.304	2.515	33
Y 1-1430.	2.628	2.774	5.265	3.934	34
Y 1-1440.	2.561	2.614	2.009	2.012	35
Y 1-1449.	2.655	2.709	1.995	4.291	36
Y 1-1459.	2.669	2.727	2.119	4.216	37
Y 1-1469.	2.635	2.578	0.000	1.022	38
Y 1-1479.	2.629	2.628	0.000	1.997	39
Y 1-1484.	2.659	2.652	0.000	5.197	40
Y 1-1494.	2.590	2.683	3.484	2.681	41
Y 1-1504.	2.614	2.646	1.226	3.322	42
Y 1-1514.	2.587	2.770	6.602	1.997	43
Y 1-1524.	2.472	2.748	10.057	5.069	44
Y 1-1533.	2.622	2.974	11.825	1.973	45
Y [illegible]543.	2.630	2.717	3.189	2.179	46
Y [illegible]553.	2.697	2.772	2.720	1.598	47

TABLE 2. (Continued)

SAMPLE ID.	BULK DENSITY, G/CC	TRUE DENSITY, G/CC	POROSITY, PCT	SURFACE AREA, M2/G	SEQ NO.
Y 1-1563.	2.653	2.641	0.000	1.996	48
Y 1-1573.	2.656	2.851	6.849	1.109	49
Y 1-1583.	2.651	2.684	1.237	.932	50
Y 1-1593.	2.642	2.736	3.443	1.053	51
Y 1-1603.	2.607	2.685	2.918	4.265	52
Y 1-1613.	2.587	2.632	1.724	1.616	53
Y 1-1623.	2.685	2.676	0.000	2.581	54
Y 1-1633.	2.609	2.679	2.609	2.487	55
Y 1-1643.	2.652	2.719	2.473	3.749	56
Y 1-1653.	2.426	2.663	8.898	2.314	57
Y 1-1663.	2.681	2.824	5.053	2.303	58
Y 1-1673.	2.686	2.753	2.429	.934	59
Y 1-1683.	2.654	2.887	8.081	3.527	60
Y 1-1693.	2.608	2.656	1.810	2.716	61
Y 1-1703.	2.638	2.732	3.452	2.967	62
Y 1-1711.	2.667	2.591	0.000	1.659	63
Y 1-1721.	2.593	2.825	8.212	3.893	64
Y 1-1731.	2.521	2.645	4.678	3.542	65
Y 1-1741.	2.642	2.732	3.287	3.980	66
Y 1-1751.	2.646	2.680	1.276	2.641	67
Y 1-1761.	2.640	2.602	0.000	2.853	68
Y 1-1775.	2.628	2.594	0.000	2.490	69
Y 1-1780.	2.635	2.651	.602	3.126	70
Y 1-1790.	2.648	2.634	0.000	1.874	71
Y 1-1800.	2.638	2.803	5.882	4.459	72
Y 1-1810.	2.613	2.682	2.574	3.144	73
Y 1-1820.	2.615	2.896	9.716	1.336	74
Y 1-1830.	2.599	2.762	5.912	1.015	75
Y 1-1840.	2.583	2.701	4.374	3.779	76
Y 1-1850.	2.646	2.947	10.226	2.443	77
Y 1-1860.	2.623	2.629	.234	2.018	78
Y 1-1870.	2.563	2.755	6.956	.947	79
Y 1-1880.	2.570	2.662	3.453	1.198	80
Y 1-1889.	2.675	2.746	2.573	2.635	81
Y 1-1899.	2.594	2.716	4.484	2.858	82
Y 1-1909.	2.650	2.646	0.000	1.027	83
Y 1-1919.	2.624	2.677	1.974	2.295	84
Y 1-1929.	2.594	2.718	4.559	1.717	85
Y 1-1939.	2.624	2.962	11.423	1.628	86
Y 1-1947.	2.698	2.710	.458	2.065	87
Y 1-1957.	2.633	2.661	1.067	2.338	88
Y 1-1967.	2.671	2.888	7.514	1.230	89
Y 1-1977.	2.672	2.690	.679	4.319	90
Y 1-1987.	2.689	2.882	6.703	2.531	91
Y 1-1997.	2.555	2.646	3.431	4.733	92

TABLE 2. (Continued)

SAMPLE ID.	BULK DENSITY, G/CC	TRUE DENSITY, G/CC	POROSITY, PCT	SURFACE AREA, M2/G	SEQ NO.
Y 1-2006.	2.645	2.780	4.850	2.436	93
Y 1-2016.	2.626	2.669	1.617	2.876	94
Y 1-2026.	2.663	2.724	2.233	1.809	95
Y 1-2036.	2.700	2.580	0.000	.968	96
Y 1-2046.	2.633	2.792	5.693	1.502	97
Y 1-2056.	2.695	2.663	0.000	1.324	98
Y 1-2065.	2.681	2.633	0.000	2.306	99
Y 1-2075.	2.647	2.687	1.492	1.982	100
Y 1-2085.	2.661	2.664	.129	2.443	101
Y 1-2095.	2.603	2.696	3.456	2.004	102
Y 1-2105.	2.561	2.773	7.635	2.371	103
Y 1-2115.	2.620	2.738	4.324	2.351	104
Y 1-2119.	2.596	3.101	16.285	2.517	105
Y 1-2125.	2.610	2.914	10.439	4.043	106
Y 1-2135.	2.571	2.684	4.197	1.958	107
Y 1-2145.	2.609	2.770	5.823	3.554	108
Y 1-2155.	2.642	2.737	3.475	1.734	109
Y 1-2165.	2.677	3.112	13.986	2.036	110
Y 1-2175.	2.665	2.714	1.809	1.892	111
Y 1-2184.	2.668	2.998	11.020	2.823	112
Y 1-2194.	2.665	2.764	3.592	2.592	113
Y 1-2204.	2.676	2.889	7.368	2.885	114
Y 1-2214.	2.672	2.777	3.786	1.958	115
Y 1-2224.	2.647	2.800	5.450	2.284	116
Y 1-2234.	2.681	2.821	4.971	1.285	117
Y 1-2243.	2.672	2.848	6.186	2.631	118
Y 1-2253.	2.664	2.801	4.881	1.643	119
Y 1-2263.	2.537	2.967	14.492	2.433	120
Y 1-2273.	2.687	2.855	5.885	3.755	121
Y 1-2283.	2.588	3.148	17.799	2.207	122
Y 1-2293.	2.608	2.908	10.325	1.666	123
Y 1-2302.	2.669	2.593	0.000	2.759	124
Y 1-2312.	2.464	3.016	18.301	1.652	125
Y 1-2322.	2.665	2.801	4.863	3.622	126
Y 1-2332.	2.633	2.988	11.880	3.027	127
Y 1-2342.	2.640	2.904	9.099	2.005	128
Y 1-2352.	2.672	3.063	12.765	3.486	129
Y 1-2488.	2.636	2.882	8.542	3.516	130
Y 1-2498.	2.651	2.800	5.317	1.447	131
Y 1-2508.	2.655	2.822	5.928	2.966	132
Y 1-2518.	2.667	2.904	8.155	1.612	133
Y 1-2528.	2.636	2.884	8.584	2.804	134
Y 1-2538.	2.542	2.813	9.632	1.685	135
Y 1-2548.	2.622	2.980	12.017	.947	136
Y 1-2568.	2.624	2.622	0.000	1.685	138

TABLE 2. (Continued)

SAMPLE ID.	BULK DENSITY, G/CC	TRUE DENSITY, G/CC	POROSITY, PCT	SURFACE AREA, M2/G	SEQ NO.
Y 1-2578.	2.668	3.166	15.724	3.523	139
Y 1-2588.	2.653	2.914	8.965	2.777	140
Y 1-2598.	2.581	2.964	12.914	3.004	141
Y 1-2607.	2.692	3.021	10.881	2.320	142
Y 1-2617.	2.524	2.766	8.762	2.812	143
Y 1-2627.	2.560	2.957	13.413	1.869	144
Y 1-2637.	2.651	2.884	8.074	2.568	145
Y 1-2647.	2.658	3.037	12.467	1.784	146
Y 1-2657.	2.642	2.875	8.094	1.864	147
Y 1-2725.	2.686	2.704	.668	2.569	149
Y 1-2735.	2.651	2.619	0.000	1.016	152
Y 1-2745.	2.636	2.948	10.594	2.658	148
Y 1-2755.	2.644	2.851	7.252	2.395	150
Y 1-2765.	2.650	2.901	8.637	.941	151
Y 1-2775.	2.661	2.834	6.100	1.945	153
Y 1-2784.	2.610	2.879	9.347	2.341	154
Y 1-2794.	2.630	3.086	14.764	3.851	155
Y 1-2804.	2.669	2.823	5.449	1.364	156
Y 1-2814.	2.641	2.637	0.000	3.170	157
Y 1-2824.	2.621	2.918	10.174	2.669	158
Y 1-2832.	2.613	2.848	8.253	1.758	159
Y 1-2844.	2.563	2.786	8.016	1.819	160
Y 1-2854.	2.522	2.870	12.125	1.132	161
Y 1-2864.	2.625	2.791	5.931	1.422	162
Y 1-2874.	2.541	2.832	10.284	1.075	163
Y 1-2884.	2.553	2.760	7.513	1.270	164
Y 1-2894.	2.533	2.718	6.792	2.483	165

TABLE 3. MERCURY INTRUSION POROSITY RESULTS FOR WELL Y-1 SHALES

Sequence No.	Sample ID	Porosity, percent
1	Y-1-372	4.73
3	-392	4.75
5	-412	4.62
9	-451	4.25
11	-471	3.94
13	-491	4.61
15	-521	5.00
19	-975	3.57
21	-995	3.79
23	-1014	8.31
27	-1360	6.64
29	-1380	4.39
31	-1400	4.50
33	-1420	4.14
35	-1440	5.25
37	-1459	6.70
41	-1494	2.59
43	-1514	4.86
45	-1533	5.87
47	-1553	2.23
49	-1573	9.93
51	-1592	5.76
53	-1612	9.52
55	-1632	5.40
57	-1652	2.28
59	-1672	6.88
61	-1692	5.63
65	-1731	4.56
67	-1751	5.66
73	-1810	7.19
75	-1830	8.08
77	-1850	10.32
79	-1870	9.41
81	-1889	9.55
85	-1929	3.35
87	-1947	5.37
89	-1967	9.19
91	-1987	6.78
93	-2006	8.20
95	-2026	9.40

TABLE 3. (Continued)

Sequence No.	Sample ID	Porosity, percent
97	Y-1-2046	5.19
101	-2085	6.39
103	-2105	4.79
105	-2119	3.87
107	-2135	2.44
109	-2155	2.85
111	-2175	6.69
113	-2194	6.08
115	-2214	4.41
117	-2234	5.82
119	-2253	11.59
121	-2273	5.97
123	-2293	5.06
125	-2312	7.37
127	-2332	7.58
129	-2352	8.50
131	-2498	5.91
133	-2518	8.29
135	-2538	4.37
139	-2578	11.50
141	-2598	9.63
143	-2617	2.68
145	-2637	7.66
147	-2657	3.06
149	-2725	4.92
151	-2765	6.20
153	-2775	6.23
155	-2794	3.18
159	-2832	7.26
161	-2854	5.14
163	-2874	7.17
165	-2894	5.17

TABLE 4. ENERGY DISPERSIVE ANALYSIS OF Y-1 SHALES

	Element Count Per 100 Counts													
Shale Sample	Na	K	Ca	Mg	Al	Si	Fe	S	Cl	Ti	Fe/S	K/Al	K/Si	Al/Si
Y-1-372	-	8.9	1.6	2.0	21.3	55.6	9.4	-	-	1.2	∞	0.42	0.14	0.38
-975	-	11.8	-	-	24.5	54.2	8.0	0.2	-	1.3	40	0.48	0.22	0.45
-1440	-	3.9	3.5	-	11.5	73.7	6.1	-	0.5	0.8	∞	0.34	0.05	0.16
-1592	-	6.5	2.0	-	16.7	61.0	9.1	-	3.3	1.4	∞	0.39	0.11	0.27
-1751	-	8.7	-	-	18.9	59.0	9.6	2.4	-	1.4	4.0	0.46	0.15	0.32
-1909	-	3.7	7.1	1.7	9.8	71.1	5.3	0.4	-	0.9	14.0	0.37	0.05	0.14
-2085	-	8.1	-	2.8	25.1	58.4	4.4	-	1.2	-	∞	0.32	0.14	0.43
-2253	-	9.7	-	2.6	23.9	55.4	6.8	0.4	1.2	-	16.5	0.41	0.17	0.43
-2548	-	7.9	21.1	1.4	14.8	42.7	8.5	1.4	0.9	1.3	5.94	0.53	0.18	0.34
-2794	-	7.5	9.9	2.8	16.5	57.7	3.7	0.8	1.1	-	4.59	0.45	0.13	0.28
-2894	-	6.2	8.5	1.8	16.4	61.5	3.5	1.7	0.9	-	2.01	0.40	0.10	0.27
Illite grain	-	17.2	-	-	25.5	57.3	-	-	-	-	-	0.67	0.30	0.45
Pyrite grain	-	-	-	-	-	-	27.5	72.5	-	-	0.38	-	-	-
Quartz grain	-	-	-	-	-	100.0	-	-	-	-	-	-	-	-

TABLE 5. INITIAL GAS RELEASE DATA: WELL Y-1, 02/05/79

SAMPLE ID	PRESSURE TORR	FREE VOLUME CC	CORE VOLUME CC	POROSITY PCT.	GAS COMPOSITION, VOLUME PERCENT METHANE	ETHANE	PROPANE	BUTANE	PENTANE	TOTAL HYDROC.	NITROGEN	OXYGEN	CARBON DIOXIDE	GAS RELEASED/ UNIT VOLUME OF SHALE	SEQ NO.
Y 1- 372.	725.	624.	826.	16.58	.59	.19	.16	.01	0.00	.95	79.76	16.82	2.45	.01	1
Y 1- 382.	725.	754.	696.	0.00	.67	0.00	0.00	0.00	0.00	.67	78.63	20.34	.38	.01	2
Y 1- 392.	720.	546.	904.	10.77	.93	.09	.03	.01	0.00	1.06	80.13	18.14	.68	.01	3
Y 1- 402.	720.	568.	882.	6.51	.73	.06	0.00	0.00	0.00	.79	79.68	18.74	.82	.00	4
Y 1- 412.	730.	721.	729.	5.95	.58	.13	.18	.03	0.00	.92	79.23	19.41	.46	.01	5
Y 1- 422.	725.	817.	633.	1.37	.42	.11	.05	.01	0.00	.59	78.80	20.33	.26	.01	6
Y 1- 431.	740.	955.	495.	0.00	.40	.17	.13	.03	0.00	.73	77.87	20.72	.65	.01	7
Y 1- 441.	735.	807.	643.	0.00	1.29	.45	.14	.04	0.00	1.92	78.36	19.16	.53	.02	8
Y 1- 451.	735.	558.	892.	10.67	1.95	.50	.21	.05	0.00	2.71	78.12	18.17	.99	.02	9
Y 1- 461.	730.	731.	719.	5.06	.82	.17	.14	.02	0.00	1.15	78.38	19.93	.50	.01	10
Y 1- 471.	740.	663.	787.	1.52	1.61	.34	.23	.03	0.00	2.21	77.55	19.81	.39	.02	11
Y 1- 481.	745.	782.	668.	2.53	1.86	.44	.27	.04	0.00	2.61	76.54	20.56	.29	.03	12
Y 1- 491.	725.	905.	545.	1.21	1.09	.25	.15	.03	0.00	1.52	77.14	20.80	.56	.02	13
Y 1- 501.	725.	823.	627.	9.23	2.06	.40	.12	.04	0.00	2.62	76.29	18.75	2.33	.03	14
Y 1- 521.	730.	512.	938.	8.26	35.84	5.44	2.12	.69	.15	44.24	47.45	6.57	1.63	.23	15
Y 1- 530.	840.	2363.	717.	9.53	13.57	1.64	.73	.26	.05	16.25	66.60	16.78	.38	.59	16
Y 1- 965.	740.	802.	648.	1.74	3.10	.30	.16	.02	0.00	3.58	76.90	18.80	.69	.04	18
Y 1- 975.	740.	682.	768.	7.97	5.56	0.00	.39	.08	0.00	6.03	76.30	16.00	.99	.05	19
Y 1- 985.	745.	659.	791.	0.00	5.65	.30	.30	.05	0.00	6.30	75.20	17.50	.64	.05	20
Y 1- 995.	1100.	627.	823.	10.19	31.30	4.81	1.96	.52	.12	38.71	51.30	9.28	.73	.43	21
Y 1-1014.	950.	734.	716.	4.93	8.39	6.32	8.63	5.74	2.21	31.29	61.53	3.75	3.47	.40	23
Y 1-1330.	1200.	650.	800.	2.74	33.52	7.34	3.14	.93	.25	45.18	49.30	4.30	1.25	.58	24
Y 1-1340.	1225.	582.	868.	0.00	35.90	6.92	2.17	.59	.15	45.73	46.30	7.41	.66	.49	25
Y 1-1350.	1060.	474.	976.	.75	30.63	4.92	2.16	.70	.12	38.53	54.40	6.26	.87	.26	26
Y 1-1360.	750.	666.	784.	9.05	6.20	.13	.24	.03	0.00	6.60	74.10	18.05	.72	.06	27
Y 1-1370.	750.	616.	834.	.90	6.45	0.00	0.00	0.00	0.00	6.45	74.80	18.00	.74	.05	28
Y 1-1380.	900.	579.	871.	7.03	19.60	2.21	1.15	.27	.03	23.26	63.60	12.40	.65	.18	29
Y 1-1390.	700.	688.	762.	5.61	5.10	.25	.24	.03	0.00	5.62	76.10	17.40	.63	.05	30
Y 1-1400.	780.	711.	739.	2.89	12.00	2.30	.57	.05	.02	14.94	72.60	13.60	1.20	.15	31
Y 1-1410.	750.	716.	734.	4.90	5.07	.55	.15	.02	0.00	5.79	75.58	18.04	.62	.06	32
Y 1-1420.	1500.	426.	1024.	.30	29.67	5.63	1.85	.43	.11	37.69	50.78	11.24	.31	.31	33
Y 1-1430.	750.	695.	755.	5.27	5.10	.57	.21	.02	0.00	5.90	75.89	17.80	.45	.05	34
Y 1-1440.	750.	623.	827.	2.01	6.96	.92	.50	.21	.11	8.70	78.80	11.91	.57	.06	35
Y 1-1449.	350.	559.	891.	2.00	15.64	1.79	.77	.14	0.00	18.34	67.93	12.78	.95	.05	36
Y 1-1459.	900.	548.	902.	2.12	19.18	2.42	.74	.14	.39	22.87	64.23	12.24	.97	.16	37
Y 1-1469.	800.	495.	955.	0.00	10.63	.99	.37	.07	0.00	12.06	70.27	17.03	.64	.07	38
Y 1-1479.	750.	715.	735.	0.00	3.86	.39	.16	0.00	0.00	4.41	75.33	19.54	.67	.04	39
Y 1-1484.	750.	835.	615.	0.00	4.38	.57	.27	.02	0.00	5.24	76.53	17.59	.66	.07	40
Y 1-1494.	800.	600.	850.	3.48	8.58	1.02	.44	.09	.01	10.14	73.39	15.75	.75	.08	41
Y 1-1504.	900.	722.	728.	1.23	20.33	3.02	1.09	.27	.07	24.78	63.06	11.05	1.11	.29	42
Y 1-1514.	1100.	654.	796.	6.60	33.00	3.99	1.62	.37	.11	39.09	51.28	9.20	.44	.46	43
Y 1-1524.	800.	719.	731.	10.06	11.11	1.74	.79	1.82	.05	15.51	73.33	10.86	1.95	.16	44
Y 1-1533.	750.	602.	848.	11.83	8.19	.92	.39	.04	0.00	9.54	73.40	16.37	.68	.07	45
Y 1-1543.	800.	593.	857.	3.19	12.37	1.93	1.00	.20	.05	15.55	71.75	11.59	1.08	.11	46
Y 1-1553.	750.	597.	853.	2.72	6.57	.73	.33	.04	0.00	7.67	62.29	14.06	.42	.05	47

TABLE 5 (Continued)

	SAMPLE ID	PRESSURE TORR	FREE VOLUME CC	CORE VOLUME CC	POROSITY PCT.	GAS COMPOSITION, VOLUME PERCENT METHANE	ETHANE	PROPANE	BUTANE	PENTANE	TOTAL HYDROC.	NITROGEN	OXYGEN	CARBON DIOXIDE	GAS RELEASED/ UNIT VOLUME OF SHALE	SEQ NO.
Y	1-1563.	750.	721.	729.	0.00	4.90	.58	.20	.03	0.00	5.71	75.45	18.60	.27	.06	48
Y	1-1573.	650.	534.	916.	6.85	10.78	1.78	.42	.04	0.00	13.02	71.91	14.89	.79	.06	49
Y	1-1583.	750.	697.	753.	1.24	8.12	.94	.30	.06	0.00	9.42	74.54	15.14	.89	.09	50
Y	1-1592.	750.	656.	794.	3.44	5.77	.88	.60	.10	0.00	7.35	77.66	14.06	.89	.06	51
Y	1-1602.	750.	741.	709.	2.92	8.37	1.12	.86	.16	.04	10.57	74.51	14.13	.77	.11	52
Y	1-1612.	750.	632.	818.	1.72	9.12	1.17	.80	.15	.04	11.28	74.46	13.61	.63	.09	53
Y	1-1622.	750.	576.	874.	0.00	9.84	1.43	.95	.15	.04	12.41	72.87	14.36	.35	.08	54
Y	1-1632.	800.	484.	966.	2.61	8.01	1.13	.55	.10	.03	9.82	72.16	17.74	.28	.05	55
Y	1-1642.	850.	511.	939.	2.47	18.71	2.47	1.09	.25	.06	22.58	66.02	9.60	1.79	.14	56
Y	1-1652.	750.	849.	601.	8.90	7.23	1.53	.86	.26	.08	9.98	76.71	11.95	1.39	.14	57
Y	1-1662.	800.	676.	774.	5.05	16.49	3.30	1.74	.48	.15	22.16	69.60	6.70	1.54	.20	58
Y	1-1672.	1300.	611.	839.	2.43	40.92	6.64	3.90	.93	.25	52.64	45.01	1.53	.83	.66	59
Y	1-1682.	750.	614.	836.	8.08	6.40	1.64	1.03	.20	.06	9.33	77.19	12.04	1.41	.07	60
Y	1-1692.	750.	743.	707.	1.81	1.00	.16	.38	.02	0.00	1.56	76.96	21.37	.11	.02	61
Y	1-1703.	800.	673.	777.	3.45	9.64	1.47	1.07	.11	.02	12.31	71.61	15.55	.48	.11	62
Y	1-1711.	950.	485.	965.	0.00	4.65	.58	.41	.10	.03	5.77	73.83	20.21	.20	.04	63
Y	1-1721.	750.	764.	686.	8.21	7.93	1.12	.75	.07	0.00	9.87	73.58	15.70	.84	.11	64
Y	1-1731.	800.	763.	687.	4.68	13.63	1.60	.60	.11	.01	15.95	67.97	15.40	.68	.19	65
Y	1-1741.	1350.	513.	937.	3.29	43.97	7.31	2.76	.62	.16	54.82	39.72	4.19	1.26	.53	66
Y	1-1751.	750.	579.	871.	1.28	11.38	1.51	.66	.09	.01	13.65	70.70	15.23	.43	.09	67
Y	1-1761.	750.	733.	717.	0.00	3.85	.60	.44	.06	.01	4.96	75.73	18.80	.51	.05	68
Y	1-1770.	800.	682.	768.	0.00	22.97	3.87	2.43	.61	.19	29.87	63.36	4.52	2.27	.28	69
Y	1-1780.	800.	641.	809.	.60	22.75	2.67	2.39	.57	.18	28.56	64.64	4.74	2.03	.24	70
Y	1-1790.	750.	519.	931.	0.00	6.76	1.09	.74	.07	0.00	8.66	73.92	17.01	.40	.05	71
Y	1-1800.	800.	591.	859.	5.88	13.83	2.56	1.25	.34	.10	18.08	72.14	7.86	1.87	.13	72
Y	1-1810.	900.	638.	812.	2.57	19.22	3.71	1.54	.35	.09	24.91	63.53	10.67	.89	.23	73
Y	1-1820.	850.	711.	739.	9.72	13.92	2.76	1.56	.34	.11	18.69	68.91	10.84	1.57	.20	74
Y	1-1830.	900.	574.	876.	5.91	22.22	3.58	3.53	1.01	.29	30.63	65.33	1.30	2.74	.24	75
Y	1-1840.	800.	603.	847.	4.37	21.92	2.62	2.24	.58	.17	27.53	62.35	8.58	1.51	.21	76
Y	1-1850.	800.	781.	669.	10.23	12.10	2.36	.75	.18	0.00	15.39	70.09	13.87	.67	.19	77
Y	1-1860.	750.	573.	877.	.23	21.62	3.93	1.41	.34	.03	27.33	60.57	10.88	1.18	.18	78
Y	1-1870.	850.	633.	817.	6.96	18.59	3.83	2.14	.36	.10	25.02	63.76	10.29	.91	.22	79
Y	1-1880.	1300.	611.	839.	3.45	34.37	10.84	2.93	.67	.16	48.97	45.12	4.41	1.51	.61	80
Y	1-1889.	800.	538.	912.	2.57	14.39	3.00	1.18	.17	.03	18.77	72.29	7.56	1.34	.12	81
Y	1-1899.	800.	725.	725.	4.48	15.71	4.18	1.48	.36	.10	21.83	71.72	3.23	3.21	.23	82
Y	1-1909.	750.	552.	898.	0.00	4.12	.95	.43	.10	.01	5.61	75.04	18.86	.47	.03	83
Y	1-1919.	750.	660.	790.	1.97	23.48	4.95	2.01	.62	.18	31.24	61.33	5.09	2.36	.26	84
Y	1-1929.	750.	522.	928.	4.56	21.29	6.62	2.36	.67	.21	31.15	64.19	2.47	2.22	.17	85
Y	1-1939.	915.	2410.	670.	11.42	16.94	2.64	1.45	.38	.11	21.52	62.88	15.20	.39	.93	86
Y	1-1947.	850.	517.	933.	.46	24.26	4.85	1.75	.54	.19	31.59	62.05	5.40	.97	.20	87
Y	1-1957.	950.	666.	784.	1.07	39.71	10.15	4.18	1.05	.32	55.41	41.91	1.82	.87	.59	88
Y	1-1967.	850.	501.	949.	7.51	20.51	4.44	1.22	.30	.06	26.53	64.08	8.50	.92	.16	89
Y	1-1977.	800.	562.	888.	.68	16.53	3.23	.98	.24	.03	21.01	67.63	9.87	1.49	.14	90
Y	1-1987.	850.	642.	808.	6.70	19.65	3.74	1.09	.25	.03	24.76	64.96	8.20	2.09	.22	91
Y	1-1997.	750.	549.	901.	3.43	12.04	2.06	.58	.08	0.00	14.76	73.18	10.05	1.99	.09	92

TABLE 5. (Continued)

	SAMPLE ID	PRESSURE TORR	FREE VOLUME CC	CORE VOLUME CC	POROSITY PCT.	GAS COMPOSITION, VOLUME PERCENT METHANE	ETHANE	PROPANE	BUTANE	PENTANE	TOTAL HYDROC.	NITROGEN	OXYGEN	CARBON DIOXIDE	GAS RELEASED/ UNIT VOLUME OF SHALE	SEQ NO.
Y	1-2006.	800.	566.	884.	4.85	14.68	3.00	.78	.14	.01	18.61	72.60	6.84	1.91	.13	93
Y	1-2016.	750.	643.	807.	1.62	12.49	3.04	1.06	.20	.05	16.84	71.18	10.96	1.03	.13	94
Y	1-2026.	800.	497.	953.	2.23	22.14	5.64	1.85	.52	.15	30.30	65.53	1.29	2.92	.17	95
Y	1-2036.	750.	584.	866.	0.00	14.48	3.61	1.10	.23	.05	19.47	72.20	7.69	.62	.13	96
Y	1-2046.	800.	611.	839.	5.69	9.79	1.40	.44	.03	0.00	11.66	71.65	16.12	.59	.09	97
Y	1-2056.	750.	629.	821.	0.00	18.19	4.29	1.21	.30	.09	24.08	65.08	9.73	1.12	.18	98
Y	1-2065.	900.	589.	861.	0.00	41.95	8.97	4.73	1.41	.38	57.44	40.52	.53	1.48	.47	99
Y	1-2075.	1250.	594.	856.	1.49	38.42	8.97	2.98	.80	.23	51.40	44.73	2.32	1.59	.59	100
Y	1-2085.	950.	541.	909.	.13	22.72	3.44	.94	.23	.03	27.36	59.85	11.92	.85	.20	101
Y	1-2095.	800.	749.	701.	3.46	10.82	1.64	.51	.06	0.00	13.23	71.57	13.77	1.40	.15	102
Y	1-2105.	1000.	782.	668.	7.64	30.59	6.98	2.04	.53	.15	40.29	51.20	7.89	.67	.62	103
Y	1-2115.	850.	690.	760.	4.32	19.18	4.10	1.23	.32	.10	24.93	65.47	7.94	1.65	.25	104
Y	1-2119.	750.	2543.	537.	16.29	18.92	6.43	2.71	.82	.13	29.01	57.56	13.37	.06	1.36	105
Y	1-2125.	750.	563.	887.	10.44	21.32	5.74	1.86	.49	.14	29.55	62.91	5.66	1.92	.18	106
Y	1-2135.	900.	601.	849.	4.20	33.45	9.56	3.06	.91	.28	47.26	50.12	.74	1.84	.40	107
Y	1-2145.	750.	588.	862.	5.82	25.62	8.49	3.09	.87	.25	38.32	57.44	3.10	1.12	.26	108
Y	1-2155.	1050.	608.	842.	3.48	46.55	14.90	6.28	1.77	.50	70.00	28.66	.64	.71	.70	109
Y	1-2165.	700.	725.	725.	13.99	18.27	6.67	4.17	1.40	.54	31.05	61.82	2.39	4.70	.29	110
Y	1-2175.	700.	553.	897.	1.81	24.83	6.13	1.85	.27	0.00	33.08	58.39	1.89	6.66	.19	111
Y	1-2184.	1250.	665.	785.	11.02	30.96	8.42	4.92	1.51	.19	45.80	52.38	.71	1.13	.64	112
Y	1-2194.	800.	788.	662.	3.59	15.60	4.58	2.03	.51	.07	22.79	68.76	7.44	.97	.29	113
Y	1-2204.	750.	621.	829.	7.37	12.98	3.39	1.35	.29	.03	18.04	69.86	11.34	.76	.13	114
Y	1-2214.	1250.	540.	910.	3.79	39.94	8.90	4.41	1.08	.15	54.48	43.98	.66	.90	.53	115
Y	1-2224.	750.	638.	812.	5.45	20.92	7.00	2.99	.82	.13	31.86	61.07	4.74	2.31	.25	116
Y	1-2234.	750.	623.	827.	4.97	20.21	4.44	1.97	.58	.20	27.40	61.29	8.36	2.92	.20	117
Y	1-2243.	850.	586.	864.	6.19	25.17	4.14	1.21	.20	0.00	30.72	64.24	2.82	2.18	.23	118
Y	1-2253.	750.	502.	948.	4.88	21.30	4.01	1.22	.15	0.00	26.68	66.13	5.01	2.17	.14	119
Y	1-2263.	750.	691.	759.	14.49	14.01	1.67	.53	.53	0.00	16.54	68.32	14.29	.82	.15	120
Y	1-2273.	750.	725.	725.	5.89	6.26	1.37	.36	.04	0.00	10.03	74.93	13.62	1.48	.10	121
Y	1-2283.	850.	583.	867.	17.80	23.58	3.97	.87	.14	0.00	28.56	63.71	6.11	1.61	.21	122
Y	1-2293.	750.	829.	621.	10.53	4.51	.70	.16	0.00	0.00	5.37	76.54	17.38	.68	.07	123
Y	1-2302.	750.	584.	866.	0.00	8.57	1.57	.45	.07	0.00	10.66	72.60	15.96	.79	.07	124
Y	1-2312.	800.	696.	754.	18.30	15.42	4.42	0.00	0.00	0.00	19.84	68.57	10.22	1.33	.19	125
Y	1-2322.	1200.	505.	945.	4.86	30.71	12.40	4.03	.66	0.00	55.80	42.09	1.08	1.06	.47	126
Y	1-2332.	1500.	613.	837.	11.88	43.12	11.52	5.02	1.19	.37	61.22	28.66	9.56	.56	.68	127
Y	1-2342.	1050.	507.	943.	9.10	34.01	7.41	1.79	.37	.12	43.70	50.23	4.39	1.71	.32	128
Y	1-2352.	750.	742.	708.	12.77	2.18	.21	.05	0.00	0.00	2.44	76.25	21.15	.14	.03	129
Y	1-2488.	750.	497.	953.	8.54	29.13	13.09	5.62	1.69	.57	50.10	46.32	2.48	1.10	.26	130
Y	1-2498.	750.	742.	708.	5.32	27.80	13.24	4.08	1.04	.31	46.47	47.41	4.89	1.22	.48	131
Y	1-2508.	750.	583.	867.	5.93	25.23	15.71	6.34	1.64	.48	49.40	45.39	4.57	.63	.33	132
Y	1-2518.	950.	577.	873.	8.16	45.18	15.06	4.98	1.24	.39	66.85	31.49	.52	1.16	.55	133
Y	1-2528.	750.	496.	954.	8.58	37.07	15.13	6.70	1.61	.55	61.06	23.52	14.66	.78	.31	134
Y	1-2538.	1140.	2368.	712.	9.63	23.00	8.73	4.10	1.37	0.00	37.20	52.17	10.16	.01	1.85	135
Y	1-2548.	750.	523.	927.	12.02	28.48	14.55	5.96	1.73	.57	51.29	44.72	3.07	.90	.29	136
Y	1-2568.	1250.	557.	893.	0.00	43.70	18.20	8.55	2.54	.69	73.68	25.98	.34	.04	.76	138

TABLE 5. (Continued)

	SAMPLE ID	PRESSURE TORR	FREE VOLUME CC	CORE VOLUME CC	POROSITY PCT.	GAS COMPOSITION, VOLUME PERCENT METHANE	ETHANE	PROPANE	BUTANE	PENTANE	TOTAL HYDROC.	NITROGEN	OXYGEN	CARBON DIOXIDE	GAS RELEASED/ UNIT VOLUME OF SHALE	SEQ NO.
Y	1-2578.	750.	545.	905.	15.72	26.68	21.04	9.41	2.60	.83	60.56	37.21	1.76	.49	.36	139
Y	1-2588.	750.	804.	646.	8.97	30.54	18.44	8.16	2.28	.74	60.16	37.51	2.09	.26	.74	140
Y	1-2598.	850.	598.	852.	12.91	51.17	15.59	4.68	1.15	.39	72.98	25.78	.61	.67	.57	141
Y	1-2607.	750.	762.	688.	10.88	36.96	22.25	11.53	3.54	1.11	75.39	23.75	.53	.37	.82	142
Y	1-2617.	1500.	609.	841.	8.76	32.83	19.62	10.41	2.99	.74	66.59	32.27	.41	.69	.95	143
Y	1-2627.	750.	671.	779.	13.41	28.97	18.13	11.93	4.16	1.21	64.40	33.98	.58	1.03	.55	144
Y	1-2637.	850.	662.	788.	8.07	53.07	16.42	4.91	1.20	.46	76.06	21.96	.90	1.09	.71	145
Y	1-2647.	1500.	640.	810.	12.47	45.22	16.31	6.74	1.73	.56	70.56	28.50	.74	.20	1.10	146
Y	1-2657.	750.	577.	873.	8.09	40.53	14.46	4.75	1.08	.32	61.14	33.85	4.53	.49	.40	147
Y	1-2725.	1250.	603.	847.	.67	43.50	16.70	6.29	1.57	.40	68.46	30.61	.55	.35	.80	148
Y	1-2735.	1500.	520.	930.	0.00	54.94	13.45	4.54	1.22	.31	74.46	24.25	1.04	.21	.82	149
Y	1-2745.	750.	624.	826.	10.59	17.79	16.80	9.64	2.81	.83	47.87	47.42	4.28	.43	.36	150
Y	1-2755.	750.	646.	804.	7.25	41.33	24.77	11.59	3.22	.99	81.90	17.39	.45	.27	.65	151
Y	1-2765.	1500.	478.	972.	8.64	57.00	11.19	3.66	.90	.24	72.99	24.52	2.22	.22	.71	152
Y	1-2775.	750.	498.	952.	6.10	35.59	14.34	5.29	.92	.13	56.27	35.97	7.56	.20	.29	153
Y	1-2784.	750.	892.	558.	9.35	6.77	7.02	5.42	1.64	.56	21.43	61.80	13.61	3.17	.34	154
Y	1-2794.	750.	694.	756.	14.76	39.79	14.43	5.66	1.37	.37	61.62	34.61	3.50	.26	.56	155
Y	1-2804.	750.	589.	861.	5.45	32.43	15.98	6.08	1.61	.45	56.55	37.85	5.38	.18	.38	156
Y	1-2814.	1500.	651.	799.	0.00	53.64	11.87	4.79	1.34	.39	72.03	26.88	1.04	.03	1.16	157
Y	1-2824.	750.	608.	842.	10.17	23.44	20.96	18.45	7.74	3.46	74.05	25.38	.47	.13	.53	158
Y	1-2832.	775.	2435.	645.	8.25	2.28	2.23	5.13	3.10	1.18	13.92	75.90	10.03	.19	.54	159
Y	1-2844.	750.	583.	867.	8.02	12.49	16.15	10.97	3.40	1.12	44.13	47.27	3.62	4.97	.29	160
Y	1-2854.	800.	714.	736.	12.13	8.97	18.19	17.32	6.45	1.77	52.70	44.59	.74	1.95	.54	161
Y	1-2864.	750.	626.	824.	5.93	32.09	11.18	5.65	.95	.34	48.21	42.36	8.78	.67	.36	162
Y	1-2874.	750.	626.	824.	10.28	9.06	12.29	9.17	3.28	1.02	34.82	60.27	4.40	.52	.26	163
Y	1-2884.	950.	505.	945.	7.51	5.96	12.46	15.72	6.35	1.84	42.33	56.42	1.24	0.00	.28	164
Y	1-2894.	700.	654.	796.	6.79	10.39	9.56	11.53	5.82	2.08	39.38	58.31	2.27	.02	.30	165

TABLE 6. COMPARATIVE HYDROCARBON GAS ANALYSIS WELL Y-1, 01/09//9

SAMPLE NO.	METHANE (1)	ETHANE (2)	PROPANE (3)	BUTANE (4)	PENTANE (5)	MOLAR BASIS TOTAL HYDROCARB	MOLAR BASIS (2+3+4+5)/1	METHANE EQUIVALENTS TOTAL HYDROCARB	METHANE EQUIVALENTS (2+3+4+5)/1
372	.59	.19	.16	.01	0.00	.95	.61	1.35	1.30
382	.67	0.00	0.00	0.00	0.00	.67	0.00	.57	0.00
392	.93	.09	.03	.01	0.00	1.06	.14	1.19	.26
402	.73	.06	0.00	0.00	0.00	.79	.08	.84	.14
412	.58	.13	.18	.03	0.00	.92	.59	1.35	1.34
422	.42	.11	.05	.01	0.00	.59	.40	.77	.83
431	.40	.17	.13	.03	0.00	.73	.82	1.12	1.80
441	1.29	.45	.14	.04	0.00	1.92	.49	2.56	.98
451	1.95	.50	.21	.05	0.00	2.71	.39	3.51	.80
461	.82	.17	.14	.02	0.00	1.15	.40	1.53	.87
471	1.61	.34	.23	.03	0.00	2.21	.37	2.88	.79
481	1.86	.44	.27	.04	0.00	2.61	.40	3.43	.85
491	1.09	.25	.15	.03	0.00	1.52	.39	2.00	.83
501	2.06	.40	.12	.04	0.00	2.62	.27	3.19	.55
521	35.84	5.44	2.12	.69	.15	44.24	.23	53.70	.50
530	13.57	1.64	.73	.26	.05	16.25	.20	19.37	.43
541	41.60	6.58	5.31	3.30	1.33	58.12	.40	84.23	1.02
965	3.10	.30	.16	.02	0.00	3.58	.15	4.09	.32
975	5.56	0.00	.39	.08	0.00	6.03	.08	6.79	.22
985	5.65	.30	.30	.05	0.00	6.30	.12	7.09	.25
995	31.30	4.81	1.96	.52	.12	38.71	.24	46.95	.50
1005	35.46	7.14	2.49	.70	.17	45.96	.30	57.36	.62
1014	8.39	6.32	8.63	5.74	2.21	31.29	2.73	71.50	7.52
1330	33.52	7.34	3.14	.93	.25	45.18	.35	58.57	.75
1340	35.90	6.92	2.17	.59	.15	45.73	.27	56.15	.56
1350	30.63	4.92	2.16	.70	.12	38.53	.26	47.55	.55
1360	6.20	.13	.24	.03	0.00	6.60	.06	7.12	.15
1370	6.45	0.00	0.00	0.00	0.00	6.45	0.00	6.45	0.00
1380	19.60	2.21	1.15	.27	.03	23.26	.19	27.38	.40
1390	5.10	.25	.24	.03	0.00	5.62	.10	6.23	.22
1400	12.00	2.30	.57	.05	.02	14.94	.25	17.72	.48
1410	5.07	.55	.15	.02	0.00	5.79	.14	6.47	.28
1420	29.67	5.63	1.85	.43	.11	37.69	.27	46.13	.55
1430	5.10	.57	.21	.02	0.00	5.90	.16	6.69	.31
1440	6.96	.92	.50	.21	.11	8.70	.25	11.09	.59
1449	15.64	1.79	.77	.14	0.00	18.34	.17	21.15	.35
1459	19.18	2.42	.74	.14	.39	22.87	.19	27.82	.45
1469	10.63	.99	.37	.07	0.00	12.06	.13	13.51	.27
1479	3.86	.39	.16	0.00	0.00	4.41	.14	4.94	.28
1484	4.38	.57	.27	.02	0.00	5.24	.20	6.12	.40
1494	8.58	1.02	.44	.09	.01	10.14	.18	11.81	.38
1504	20.33	3.02	1.09	.27	.07	24.78	.22	29.59	.46
1514	33.00	3.99	1.62	.37	.11	39.09	.18	45.82	.39
1524	11.11	1.74	.79	1.82	.05	15.51	.40	22.28	1.01

TABLE 6. (Continued)

SAMPLE NO.	MOLAR BASIS METHANE (1)	ETHANE (2)	PROPANE (3)	BUTANE (4)	PENTANE (5)	TOTAL HYDROCARB	(2+3+4+5)/1	METHANE EQUIVALENTS TOTAL HYDROCARB	(2+3+4+5)/1
1533	8.19	.92	.39	.04	0.00	9.54	.16	10.30	.33
1543	12.37	1.93	1.00	.20	.05	15.55	.26	19.16	.55
1553	6.57	.73	.33	.04	0.00	7.67	.17	8.60	.34
1563	4.90	.58	.20	.03	0.00	5.71	.17	6.51	.33
1573	10.78	1.78	.42	.04	0.00	13.02	.21	15.07	.40
1583	8.12	.94	.30	.06	0.00	9.42	.16	10.71	.32
1592	5.77	.88	.60	.10	0.00	7.35	.27	9.13	.58
1602	8.37	1.12	.88	.16	.04	10.57	.26	13.26	.58
1612	9.12	1.17	.80	.15	.04	11.28	.24	13.87	.52
1622	9.84	1.43	.95	.15	.04	12.41	.26	15.42	.57
1632	8.01	1.13	.55	.10	.03	9.82	.23	11.85	.48
1642	18.71	2.47	1.09	.25	.06	22.58	.21	26.89	.44
1652	7.23	1.53	.88	.26	.08	9.98	.38	13.38	.85
1662	16.49	3.30	1.74	.48	.15	22.16	.34	28.98	.76
1672	40.92	6.64	3.90	.93	.25	52.64	.29	66.64	.63
1682	6.40	1.64	1.03	.20	.06	9.33	.46	12.82	1.00
1692	1.00	.16	.38	.02	0.00	1.56	.56	2.29	1.29
1703	9.64	1.47	1.07	.11	.02	12.31	.28	15.35	.59
1711	4.65	.58	.41	.10	.03	5.77	.24	7.18	.54
1721	7.93	1.12	.75	.07	0.00	9.87	.24	11.99	.51
1731	13.63	1.60	.60	.11	.01	15.95	.17	18.34	.35
1741	43.97	7.31	2.76	.62	.16	54.82	.25	66.53	.51
1751	11.38	1.51	.66	.09	.01	13.65	.20	16.02	.41
1761	3.85	.60	.44	.06	.01	4.96	.29	6.25	.62
1770	22.97	3.67	2.43	.61	.19	29.87	.30	38.46	.67
1780	22.75	2.67	2.39	.57	.18	28.56	.26	36.21	.59
1790	6.76	1.09	.74	.07	0.00	8.66	.28	10.74	.59
1800	13.83	2.56	1.25	.34	.10	18.08	.31	23.07	.67
1810	19.22	3.71	1.54	.35	.09	24.91	.30	31.18	.62
1820	13.92	2.76	1.56	.34	.11	18.69	.34	24.34	.75
1830	22.22	3.58	3.53	1.01	.29	30.63	.38	42.14	.90
1840	21.92	2.62	2.24	.58	.17	27.53	.26	34.90	.59
1850	12.10	2.36	.75	.18	0.00	15.39	.27	18.69	.54
1860	21.62	3.93	1.41	.34	.03	27.33	.26	33.28	.54
1870	18.59	3.83	2.14	.36	.10	25.02	.35	32.35	.74
1880	34.37	10.84	2.93	.67	.16	48.97	.42	63.69	.85
1889	14.39	3.00	1.18	.17	.03	18.77	.30	23.30	.62
1899	15.71	4.18	1.48	.36	.10	21.83	.39	28.43	.81
1909	4.12	.95	.43	.10	.01	5.61	.36	7.23	.76
1919	23.48	4.95	2.01	.62	.18	31.24	.33	40.14	.71
1929	21.29	6.62	2.36	.67	.21	31.15	.46	42.07	.98
1939	16.94	2.64	1.45	.38	.11	21.52	.27	27.01	.59
1947	24.26	4.85	1.75	.54	.19	31.59	.30	39.89	.64
1957	39.71	10.15	4.18	1.05	.32	55.41	.40	73.04	

TABLE 6. (Continued)

SAMPLE NO.	METHANE (1)	ETHANE (2)	PROPANE (3)	BUTANE (4)	PENTANE (5)	MOLAR BASIS TOTAL HYDROCARB	MOLAR BASIS (2+3+4+5)/1	METHANE EQUIVALENTS TOTAL HYDROCARB	METHANE EQUIVALENTS (2+3+4+5)/1
1967	20.51	4.44	1.22	.30	.06	26.53	.29	32.62	.59
1977	16.53	3.23	.98	.24	.03	21.01	.27	25.57	.55
1982	19.65	3.74	1.09	.25	.03	24.76	.26	29.89	.52
1997	12.04	2.06	.58	.08	0.00	14.76	.23	17.35	.44
2006	14.68	3.00	.78	.14	.01	18.61	.27	22.39	.52
2016	12.49	3.04	1.06	.20	.05	16.84	.35	21.38	.71
2026	22.14	5.64	1.85	.52	.15	30.30	.37	39.12	.77
2036	14.48	3.61	1.10	.23	.05	19.47	.34	24.56	.70
2046	9.79	1.40	.44	.03	0.00	11.66	.19	13.44	.37
2056	18.19	4.29	1.21	.30	.09	24.08	.32	30.18	.66
2065	41.95	8.97	4.73	1.41	.38	57.44	.37	76.08	.81
2075	38.42	8.97	2.98	.80	.23	51.40	.34	65.59	.70
2085	22.72	3.44	.94	.23	.03	27.36	.20	31.99	.41
2095	10.82	1.84	.51	.06	0.00	13.23	.22	15.51	.43
2105	30.59	6.98	2.04	.53	.15	40.29	.32	50.43	.65
2115	19.18	4.10	1.23	.32	.10	24.93	.30	31.00	.62
2119	18.92	6.43	2.71	.82	.13	29.01	.53	40.30	1.13
2125	21.32	5.74	1.86	.49	.14	29.55	.39	38.35	.80
2135	33.45	9.56	3.06	.91	.28	47.26	.41	62.28	.86
2145	25.62	8.49	3.09	.87	.25	38.32	.50	52.36	1.04
2155	46.55	14.90	6.28	1.77	.50	70.00	.50	96.74	1.08
2165	18.27	6.67	4.17	1.40	.54	31.05	.70	47.81	1.62
2175	24.83	6.13	1.85	.27	0.00	33.08	.33	41.05	.65
2184	30.96	8.42	4.92	1.31	.19	45.80	.48	63.25	1.04
2194	15.60	4.58	2.03	.51	.07	22.79	.46	30.72	.97
2204	12.99	3.39	1.35	.29	.03	18.04	.39	23.39	.80
2214	39.94	8.90	4.41	1.08	.15	54.48	.36	70.84	.77
2224	20.92	7.00	2.99	.82	.13	31.86	.52	44.00	1.10
2234	20.21	4.44	1.97	.58	.20	27.40	.36	35.86	.77
2243	25.17	4.14	1.21	.20	0.00	30.72	.22	36.09	.43
2253	21.30	4.01	1.22	.15	0.00	26.68	.25	31.95	.50
2263	14.01	1.67	.53	.33	0.00	16.54	.18	19.32	.38
2273	8.26	1.37	.36	.04	0.00	10.03	.21	11.59	.41
2283	23.58	3.97	.87	.14	0.00	28.56	.21	33.15	.41
2293	4.51	.70	.16	0.00	0.00	5.37	.19	6.14	.36
2302	8.57	1.57	.45	.07	0.00	10.66	.24	12.67	.48
2312	15.42	4.42	0.00	0.00	0.00	19.84	.29	23.16	.50
2322	38.71	12.40	4.03	.66	0.00	55.80	.44	72.62	.88
2332	43.12	11.52	5.02	1.19	.37	61.22	.42	81.67	.89
2342	34.01	7.41	1.79	.37	.12	43.70	.28	53.30	.57
2352	2.18	.21	.05	0.00	0.00	2.44	.12	2.67	.23
2488	29.13	13.09	5.62	1.69	.57	50.10	.72	74.62	1.56
2498	27.80	13.24	4.08	1.04	.31	46.47	.67	66.20	1.38
2508	25.23	15.71	6.34	1.64	.48	49.40	.96	76.46	2.03

TABLE 6. (Continued)

SAMPLE NO.	MOLAR BASIS METHANE (1)	ETHANE (2)	PROPANE (3)	BUTANE (4)	PENTANE (5)	TOTAL HYDROCARB	(2+3+4+5)/1	METHANE EQUIVALENTS TOTAL HYDROCARB	(2+3+4+5)/1
2518	45.19	15.06	4.98	1.24	.39	66.85	.48	90.10	.99
2528	37.07	15.13	6.70	1.61	.55	61.06	.65	88.47	1.39
2538	23.00	8.73	4.10	1.37	0.00	37.20	.62	52.95	1.30
2548	28.48	14.55	5.96	1.73	.57	51.29	.80	77.51	1.72
2558	38.66	27.46	12.68	3.25	1.07	83.12	1.15	134.69	2.48
2568	43.70	18.20	8.55	2.54	.69	73.68	.69	108.86	1.49
2578	26.68	21.04	9.41	2.60	.83	60.56	1.27	99.90	2.74
2588	30.54	18.44	8.16	2.28	.74	60.16	.97	94.57	2.10
2598	51.17	15.59	4.68	1.15	.39	72.98	.43	95.97	.88
2607	36.96	22.25	11.53	3.54	1.11	75.39	1.04	122.15	2.30
2617	32.83	19.62	10.41	2.99	.74	66.59	1.03	106.84	2.25
2627	26.97	16.13	11.93	4.16	1.21	64.40	1.22	110.49	2.81
2637	53.07	16.42	4.91	1.20	.46	76.06	.43	100.44	.89
2647	45.22	16.31	6.74	1.73	.56	70.56	.56	99.22	1.19
2657	40.53	14.46	4.75	1.08	.32	61.14	.51	82.93	1.05
2725	43.50	16.70	6.29	1.57	.40	68.46	.57	95.68	1.20
2735	54.94	13.45	4.54	1.22	.31	74.46	.36	95.44	.74
2745	17.79	16.80	9.64	2.81	.83	47.87	1.69	84.85	3.77
2755	41.33	24.77	11.59	3.22	.99	81.90	.98	129.40	2.13
2765	57.00	11.19	3.66	.90	.24	72.99	.28	89.94	.58
2775	35.59	14.34	5.29	.92	.13	56.27	.58	77.58	1.18
2814	53.64	11.87	4.79	1.34	.39	72.03	.34	92.82	.73
2832	2.28	2.23	5.13	3.10	1.18	15.92	5.11	35.39	14.52

TABLE 7. GAS RELEASE RATES OF Y-1 SHALES
(GAS PRESSURES, TORR)

	Sample Identification (EGSP-NYL Series)				
Time, days	530	1939	2119	2538	2832
0	22	22	22	22	20
1	33	36	46	91	58
5	32	49	52	240	63
15	34	83	61	345	72
40	34	137	69	318	*
65	37	193	76	318	*

* Air accidentally admitted to container

TABLE 8. DIFFUSION COEFFICIENTS OF HYDROCARBON GASES IN Y-1 SHALES (PARAMETERS FOR EQUATION 1)

Sample No.	P_∞, torr	D, cm^2/sec	a
530	34	2×10^{-6}	0.3
1939	1650	8.5×10^{-9}	large
2119	77	1×10^{-6}	0.43
2538	319	4×10^{-6}	large
2832	(120)	(1×10^{-6})*	(2)*

* Insufficient data; values cited are rough estimates

TABLE 9. INITIAL AND ULTIMATE PRESSURES IN THE SEALED CANISTERS

Sample No.	P_∞, torr	P_{HC}, torr
Y-1-530	34	150
Y-1-1939	1650	200
Y-1-2119	77	249
Y-1-2538	319	430
Y-1-2832	(120)	108

TABLE 10. PERCENT VARIABILITY REDUCTION FOR VARIOUS PREDICTORS AND AVERAGING TECHNIQUES

CRITERION - HYDROCARBON GAS CONTENT

Predictor	Variability Reduction for Initial Split		
	10' Samples	Averaged Over 20'	Averaged Over 50'
Wire-log Data			
Neutron Porosity	1.4	3.3	4.4
Bulk Density	14.2	23.2	17.8
Gamma Ray	4.1	7.3	1.6
Medium Resistivity	14.0	17.0	30.6
Deep Resistivity	16.9	18.4	42.7
Lateral Resistivity	11.4	24.6	44.1
Transit Time	7.8	8.0	17.1
Total Porosity*	22.1	24.2	21.4
Clay*	11.1	17.0	31.1
Kerogen*	1.2	0	0
Saturation Water*	2.7	6.5	0
Average Grain Density*	9.4	16.8	30.4
Laboratory Data			
Total Carbon	21.9	41.5	54.5
Total Nitrogen	7.2	2.3	0
Sulfur	22.1	41.1	57.5
Surface Area	1.5	12.5	14.8
Open Porosity	5.1	7.6	12.9
Bulk Density	4.1	9.1	14.6
True Density	6.4	33.2	58.6
Total Porosity	6.6	21.5	44.4

* Coriband

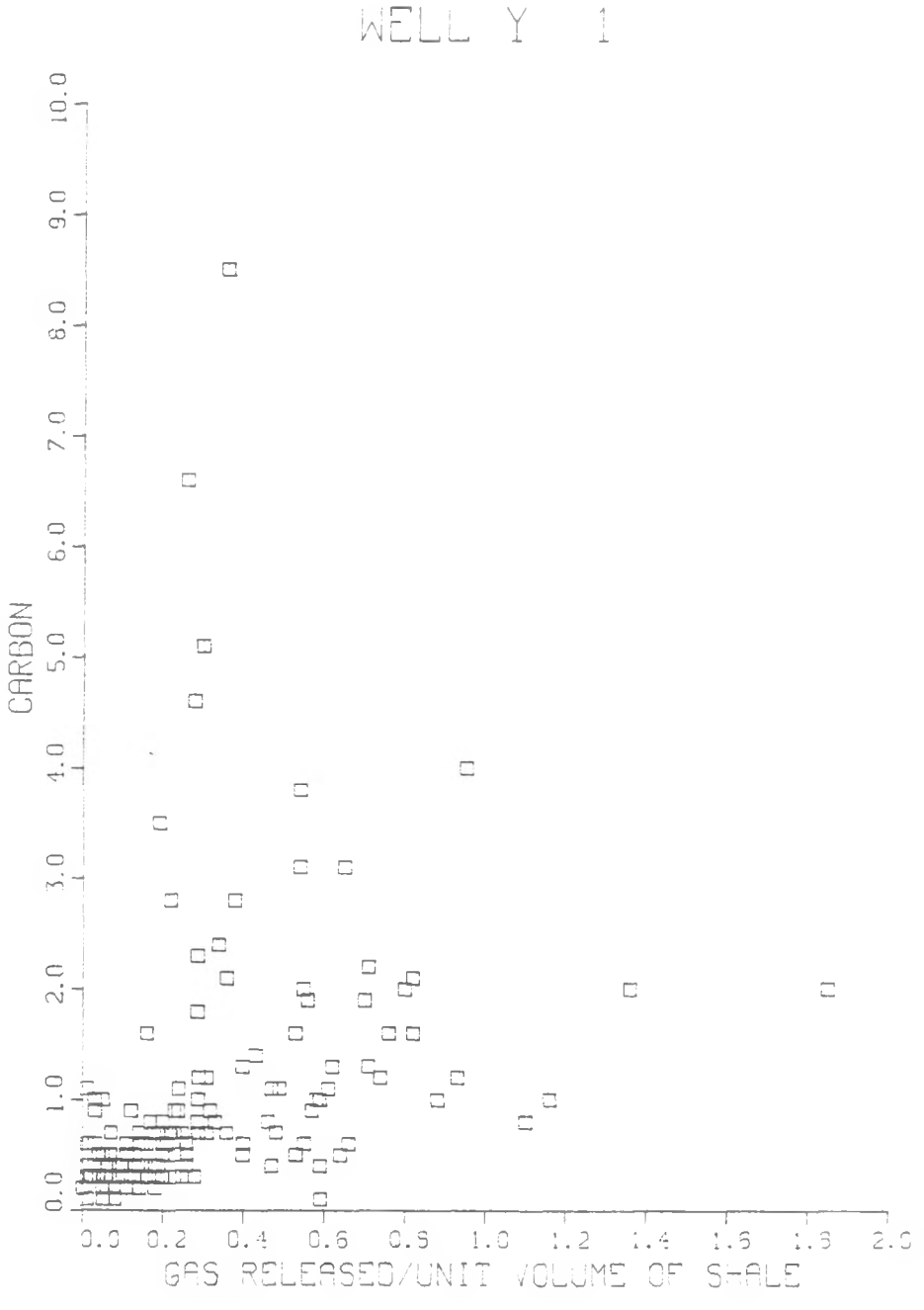


FIGURE 1. CARBON VERSUS HYDROCARBON GAS

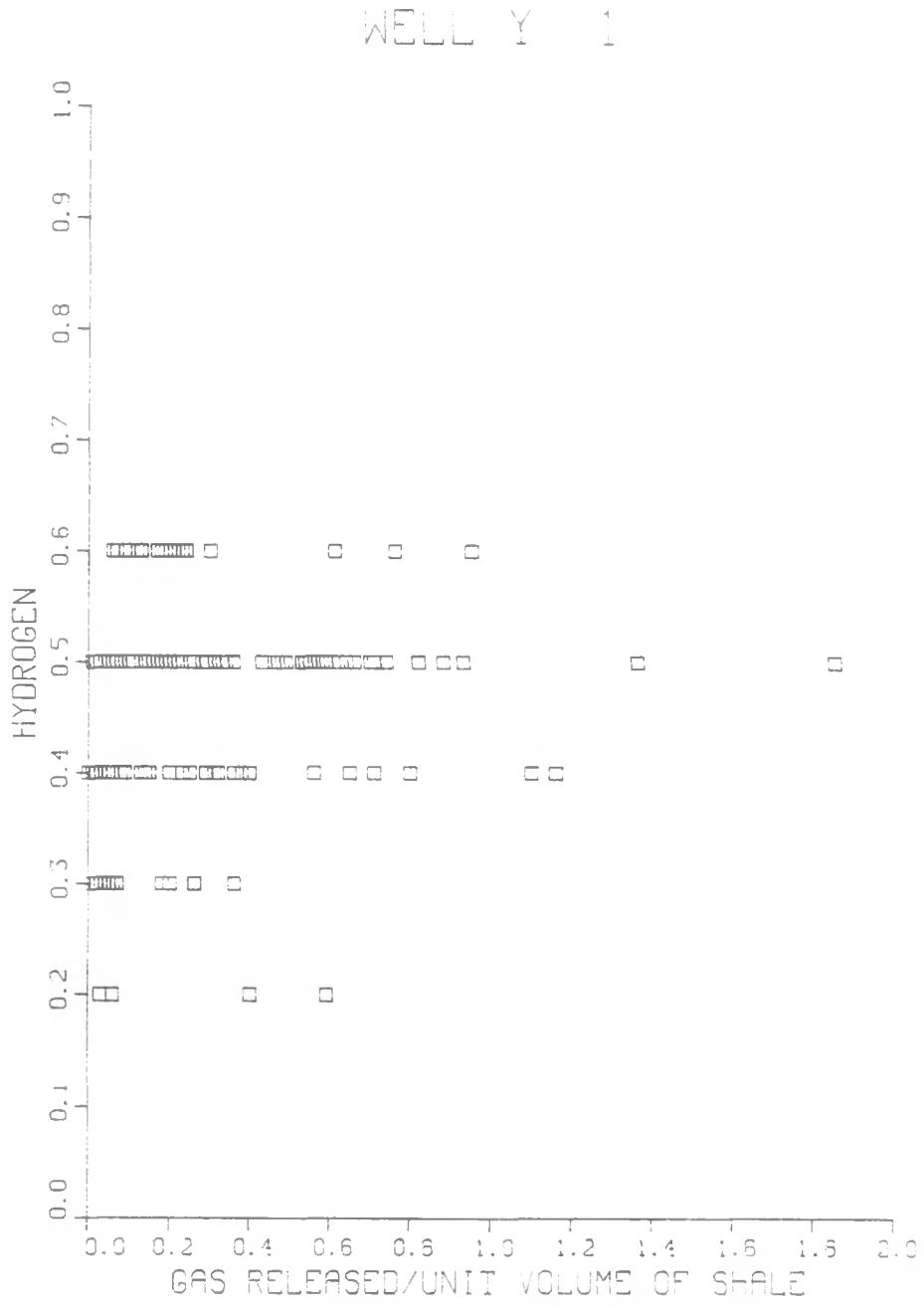


FIGURE 2. HYDROGEN VERSUS HYDROCARBON GAS

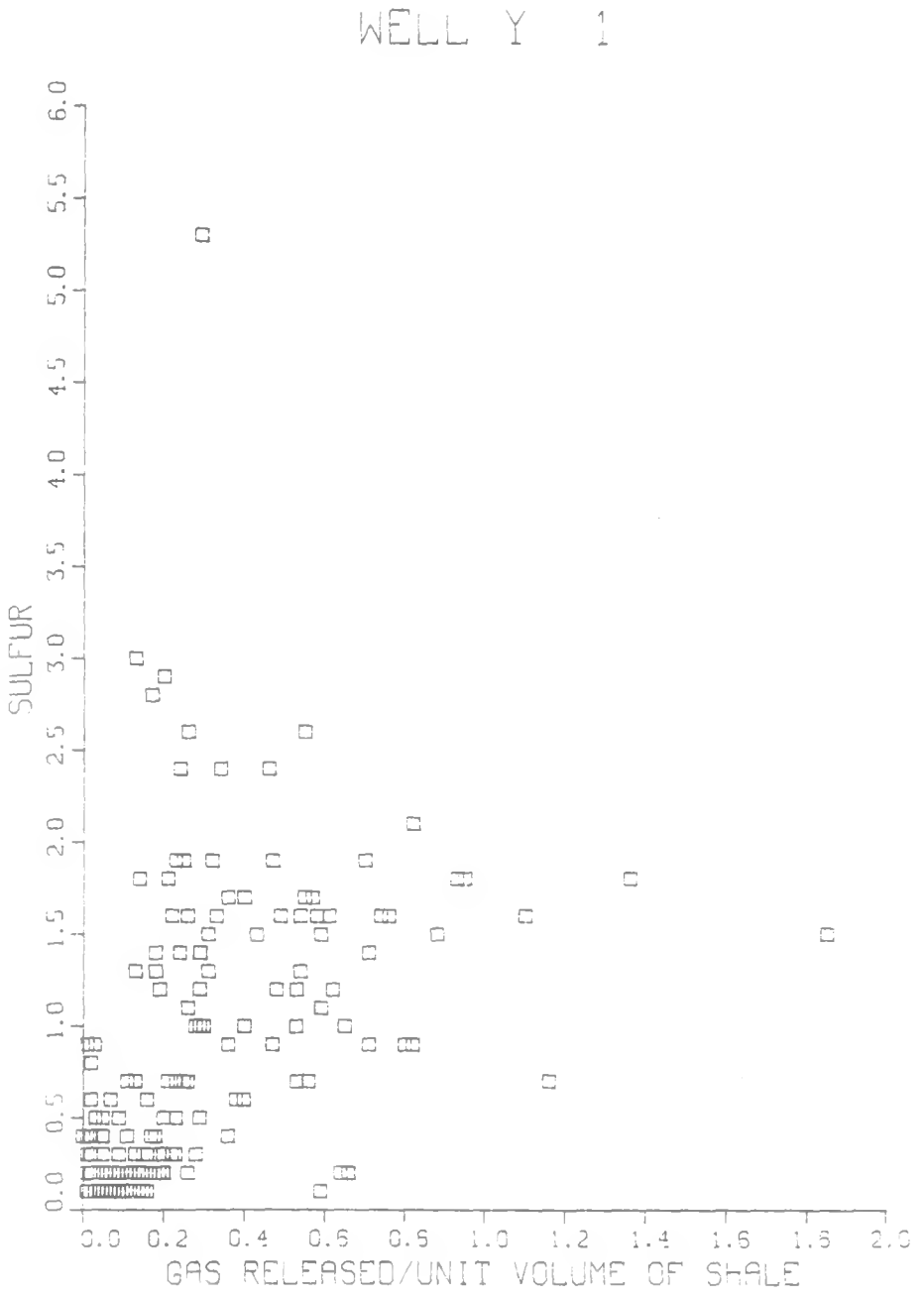


FIGURE 3. SULFUR VERSUS HYDROCARBON GAS

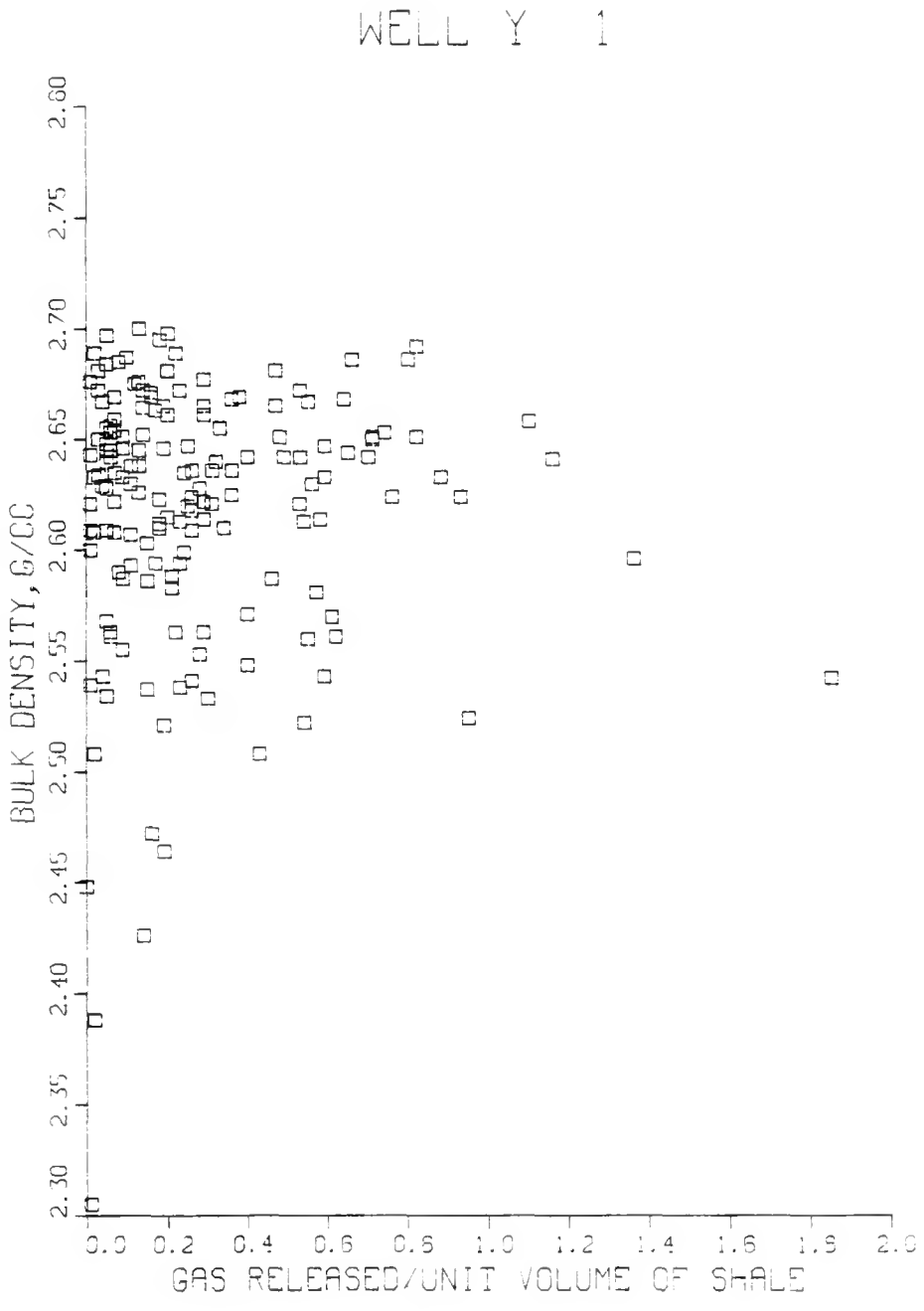


FIGURE 4. BULK DENSITY VERSUS GAS RELEASED

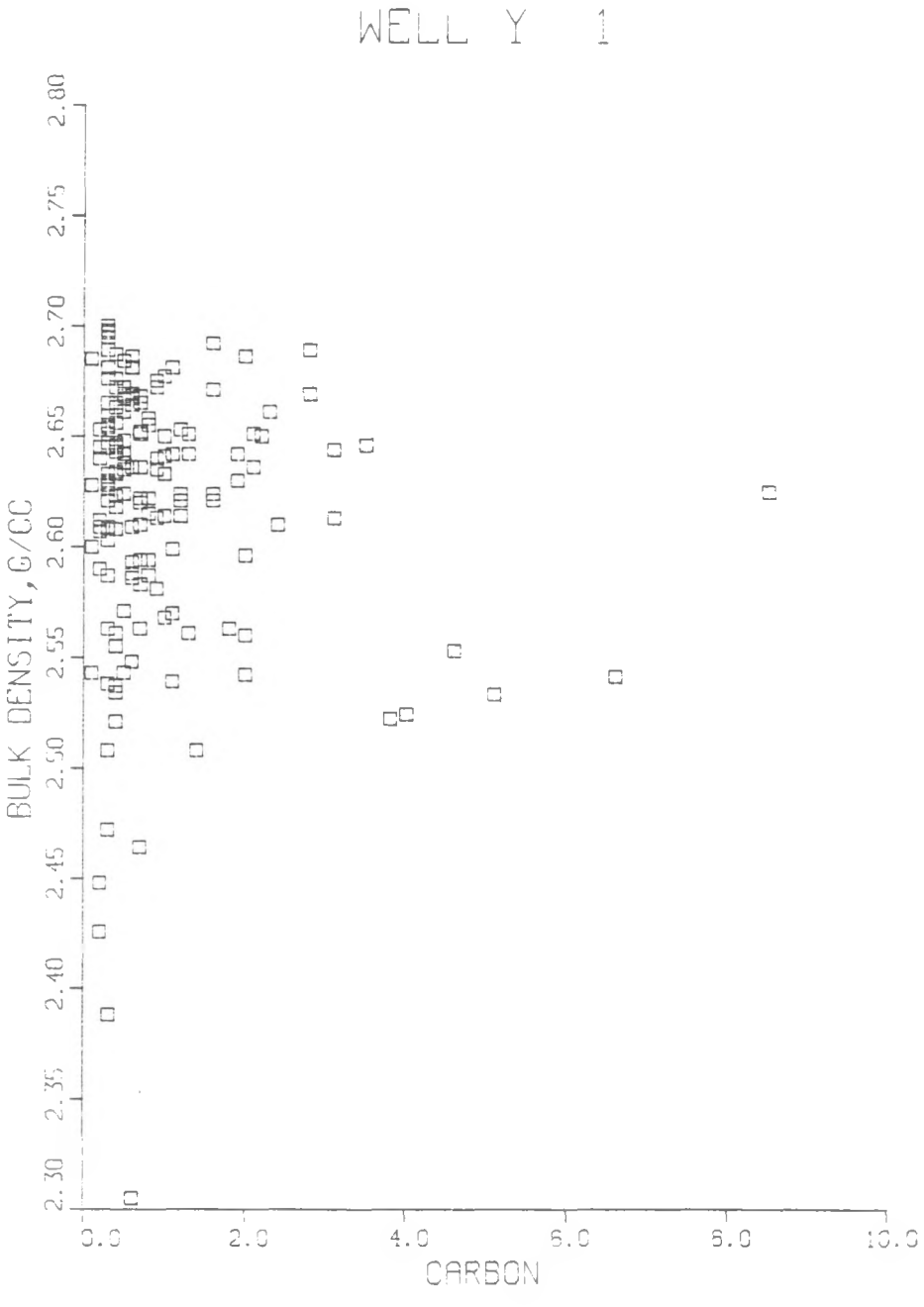


FIGURE 5. BULK DENSITY VERSUS CARBON

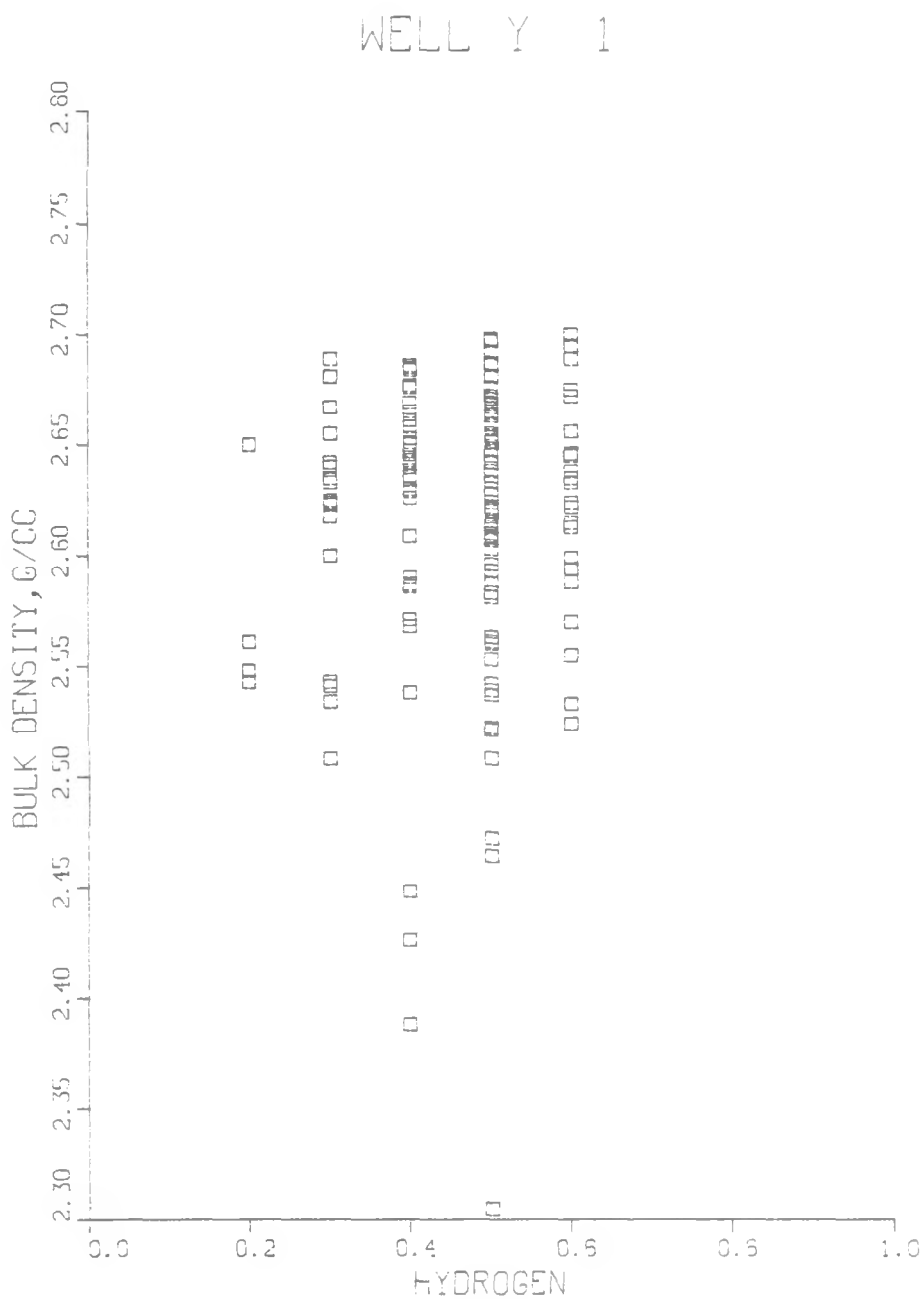


FIGURE 6. BULK DENSITY VERSUS HYDROGEN

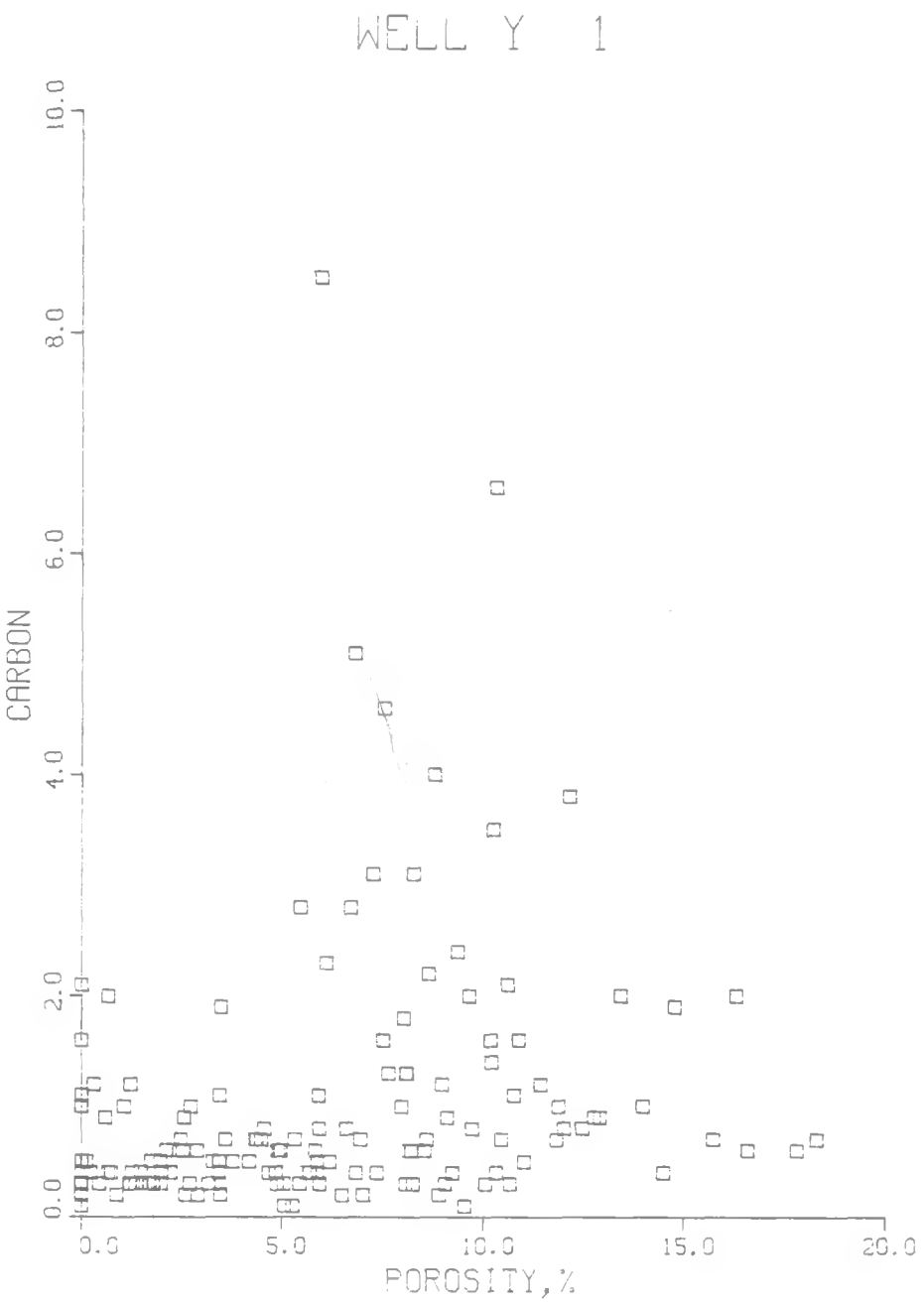


FIGURE 7. CARBON VERSUS POROSITY

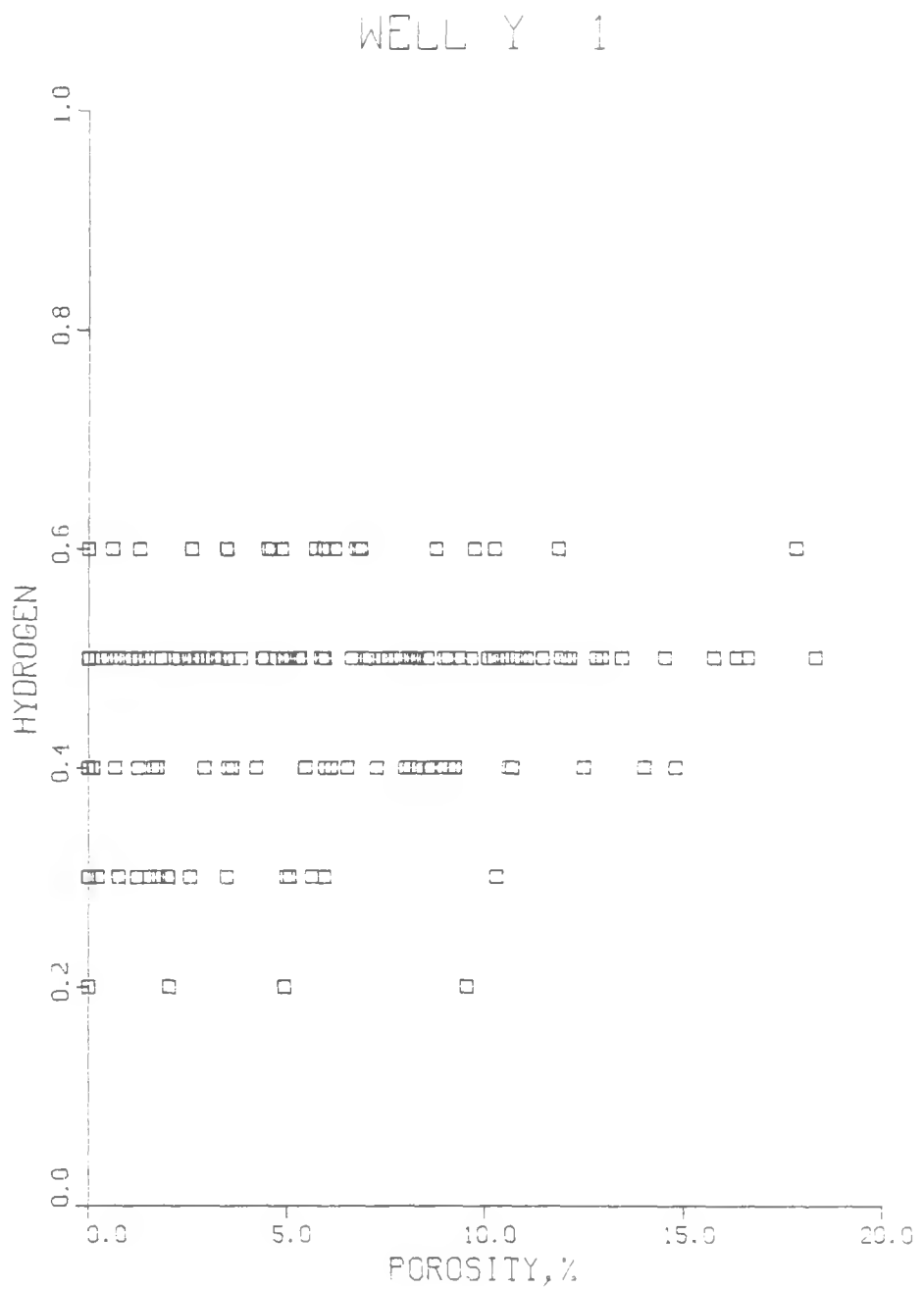


FIGURE 8. HYDROGEN VERSUS POROSITY

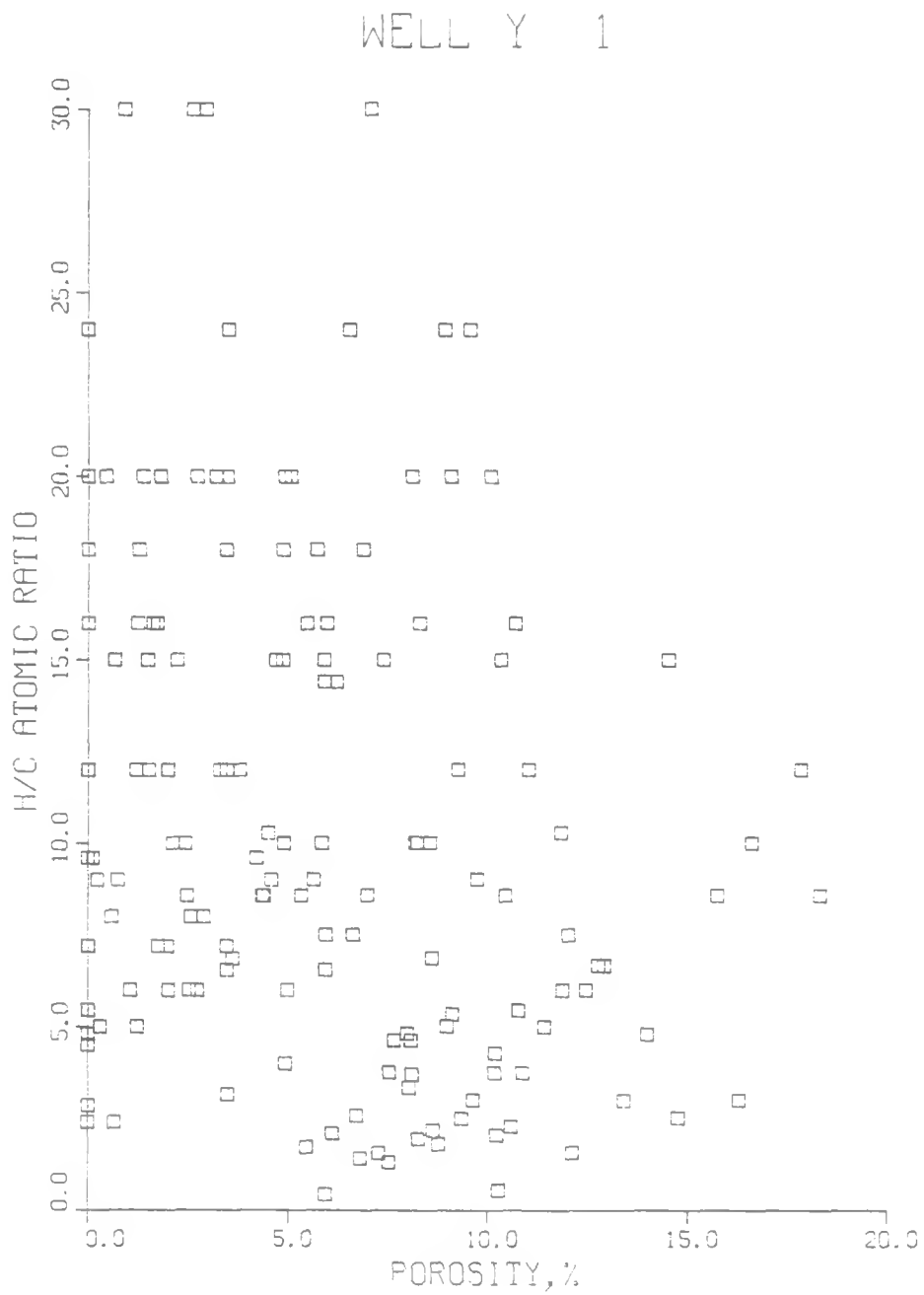


FIGURE 9. HYDROCARBON VERSUS POROSITY

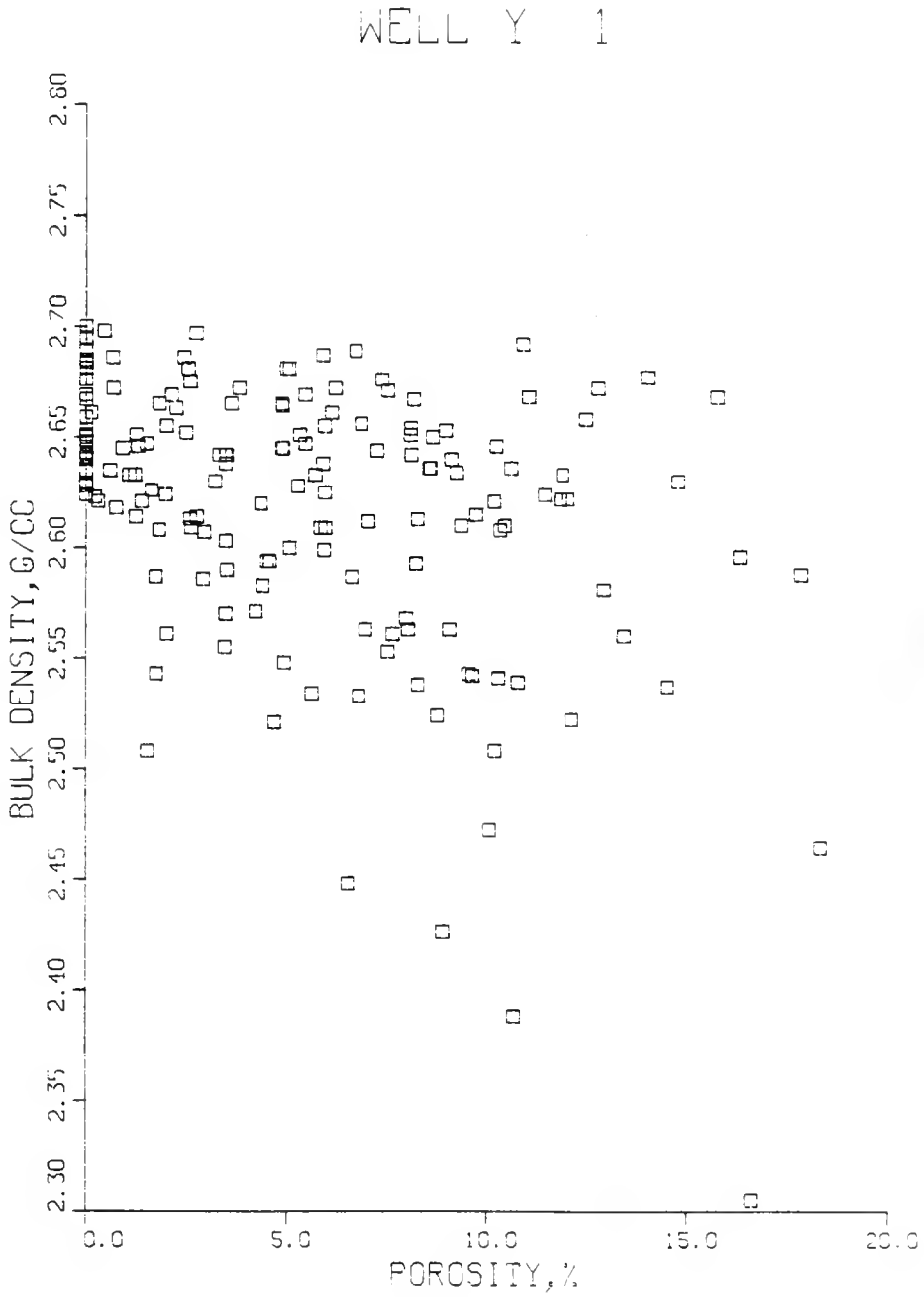


FIGURE 10. BULK DENSITY VERSUS POROSITY

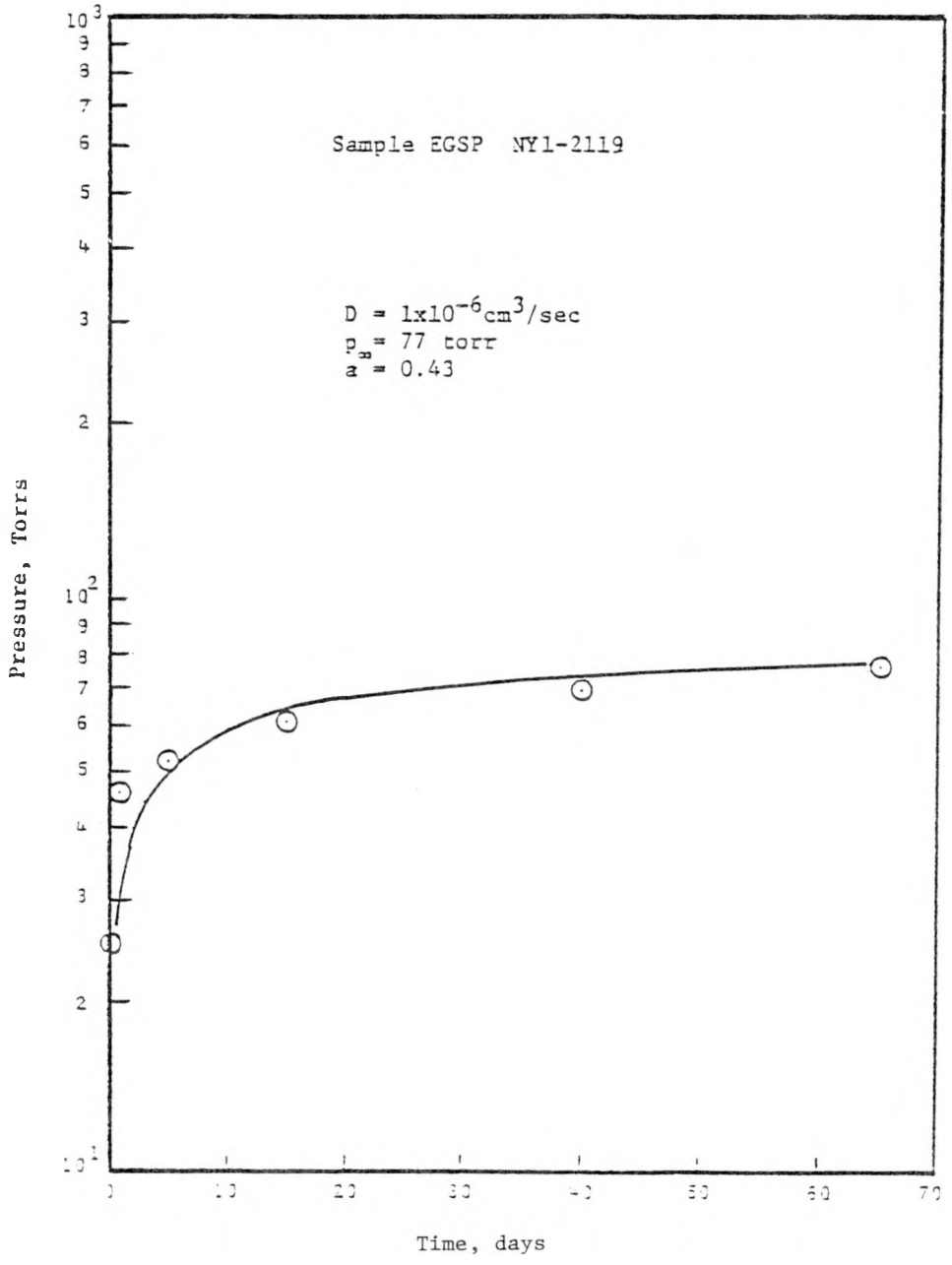


FIGURE 11. EXPERIMENTAL AND CALCULATED GAS RELEASE RATES

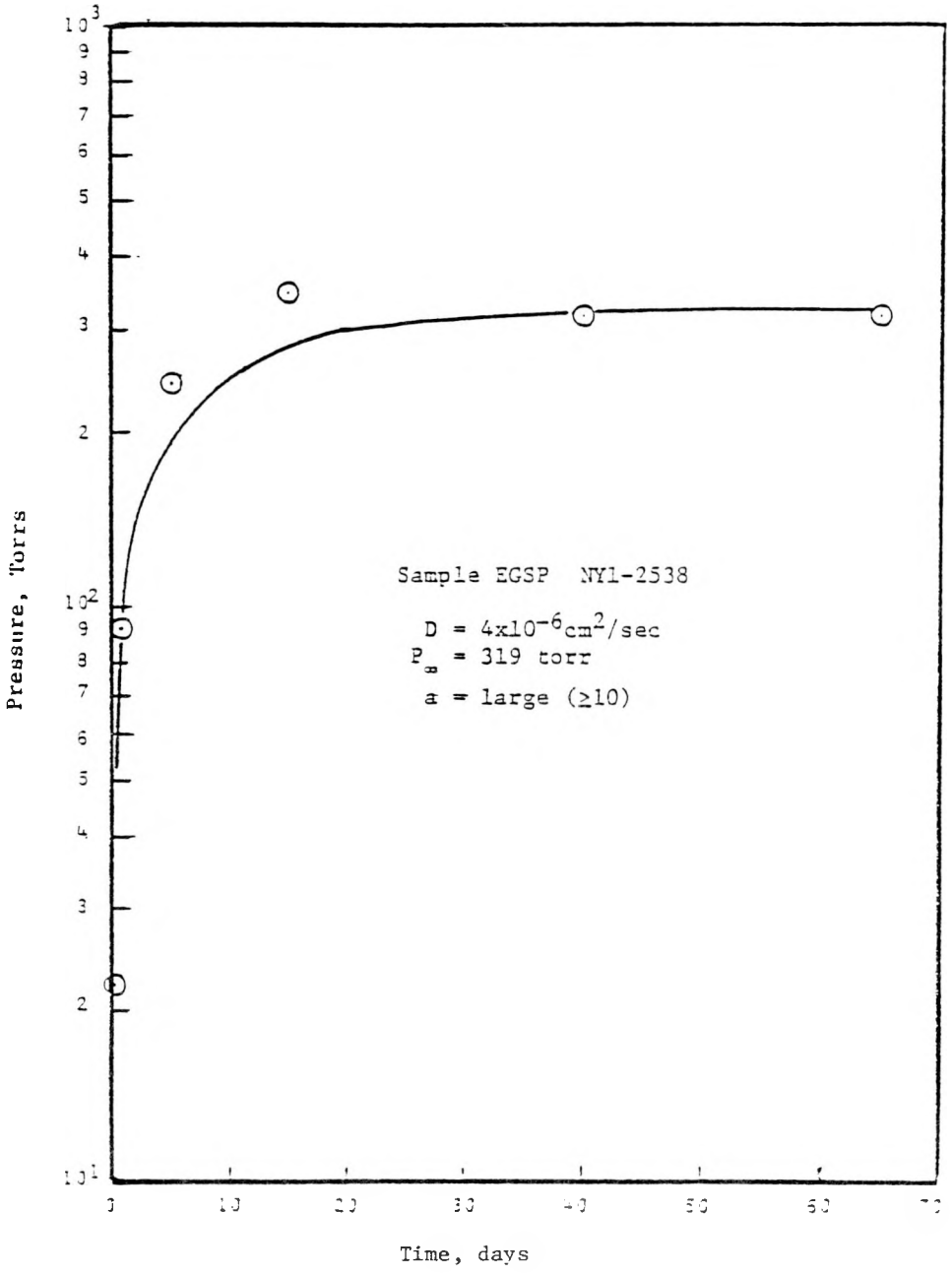


FIGURE 12. EXPERIMENTAL AND CALCULATED GAS RELEASE RATES

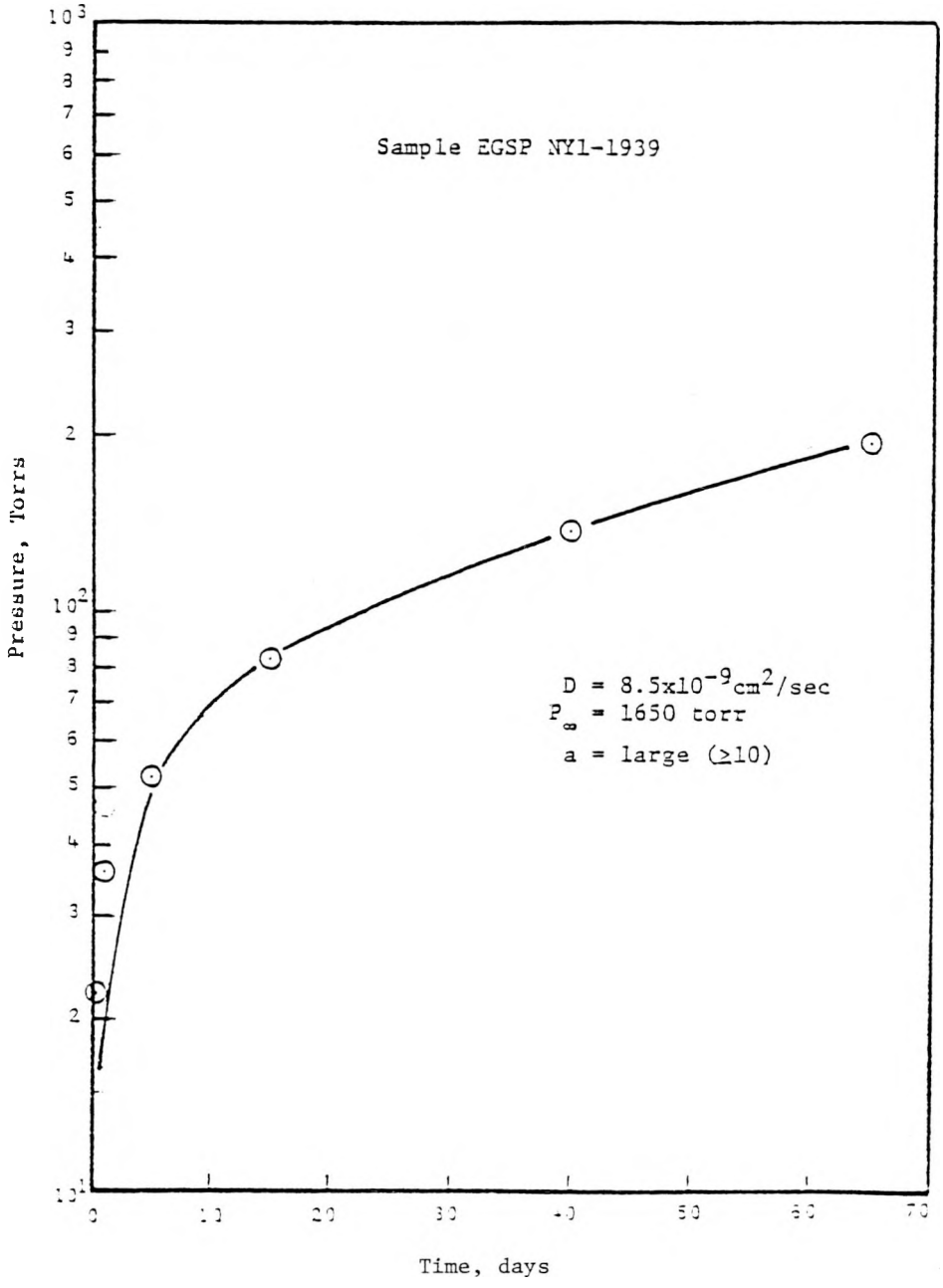


FIGURE 13. EXPERIMENTAL AND CALCULATED GAS RELEASE RATES

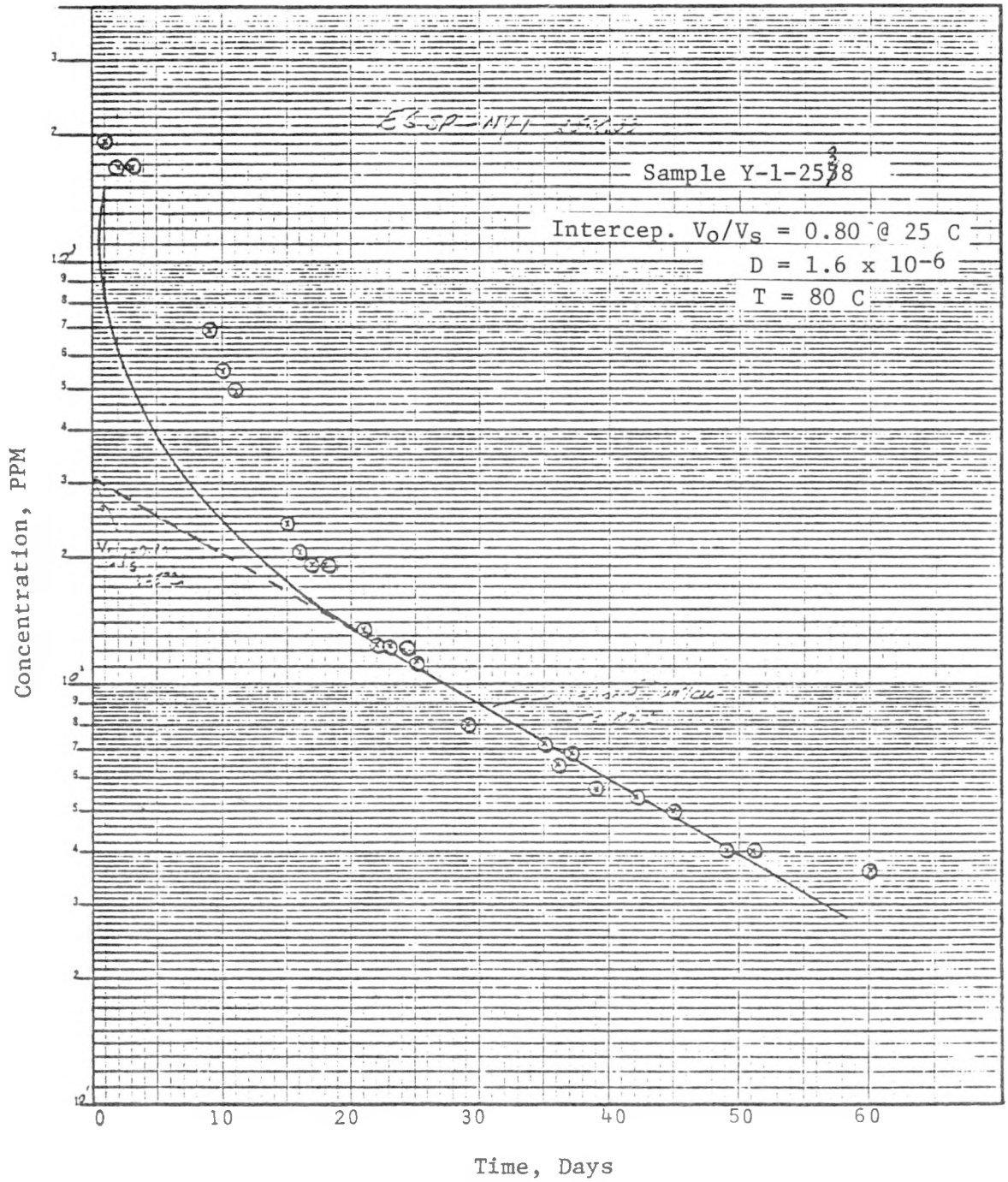


FIGURE 14. RELEASE KINETICS CURVE FOR Y-1-2538

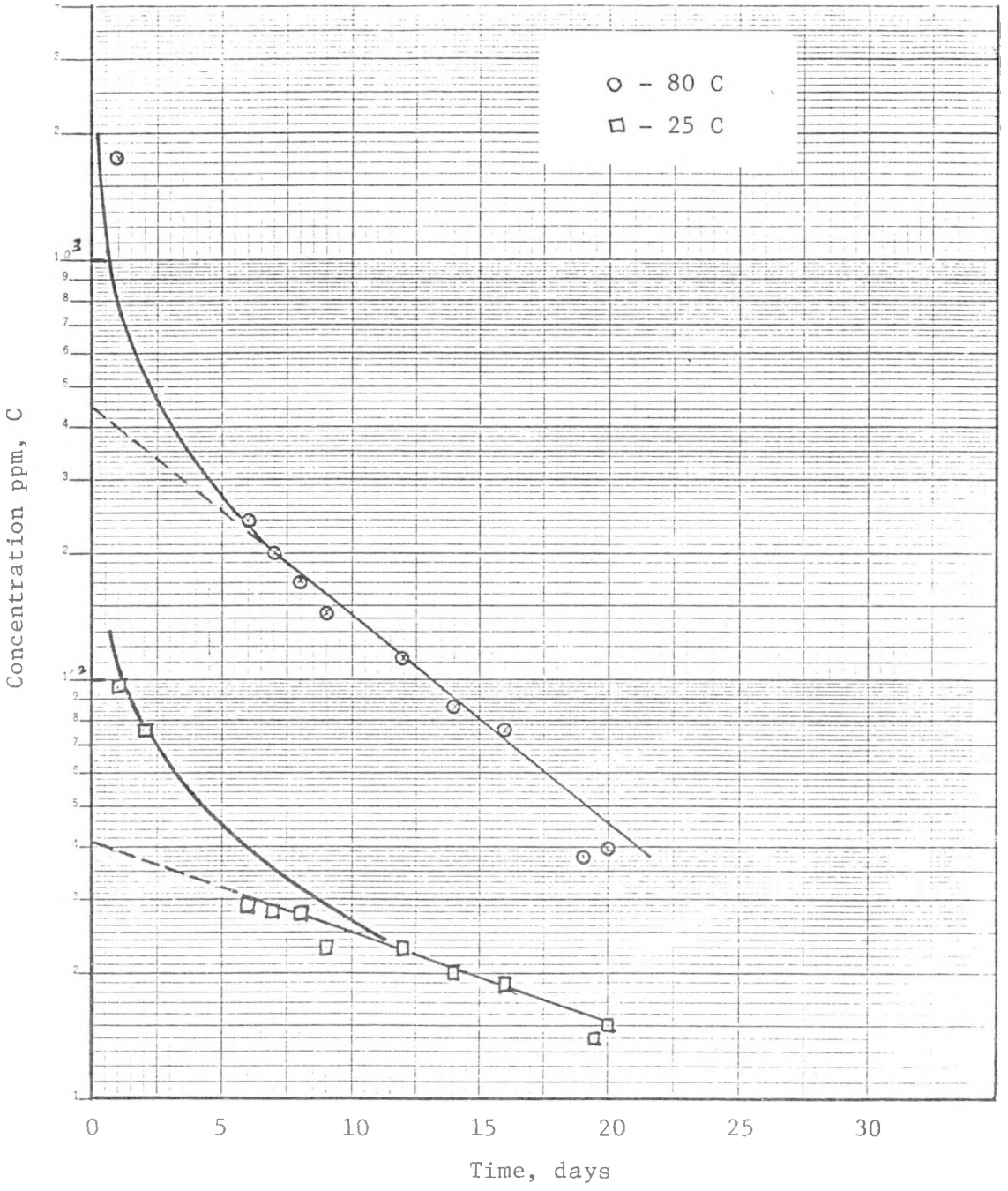


FIGURE 15. Hydrocarbon Effusion from Shale K-4-1069

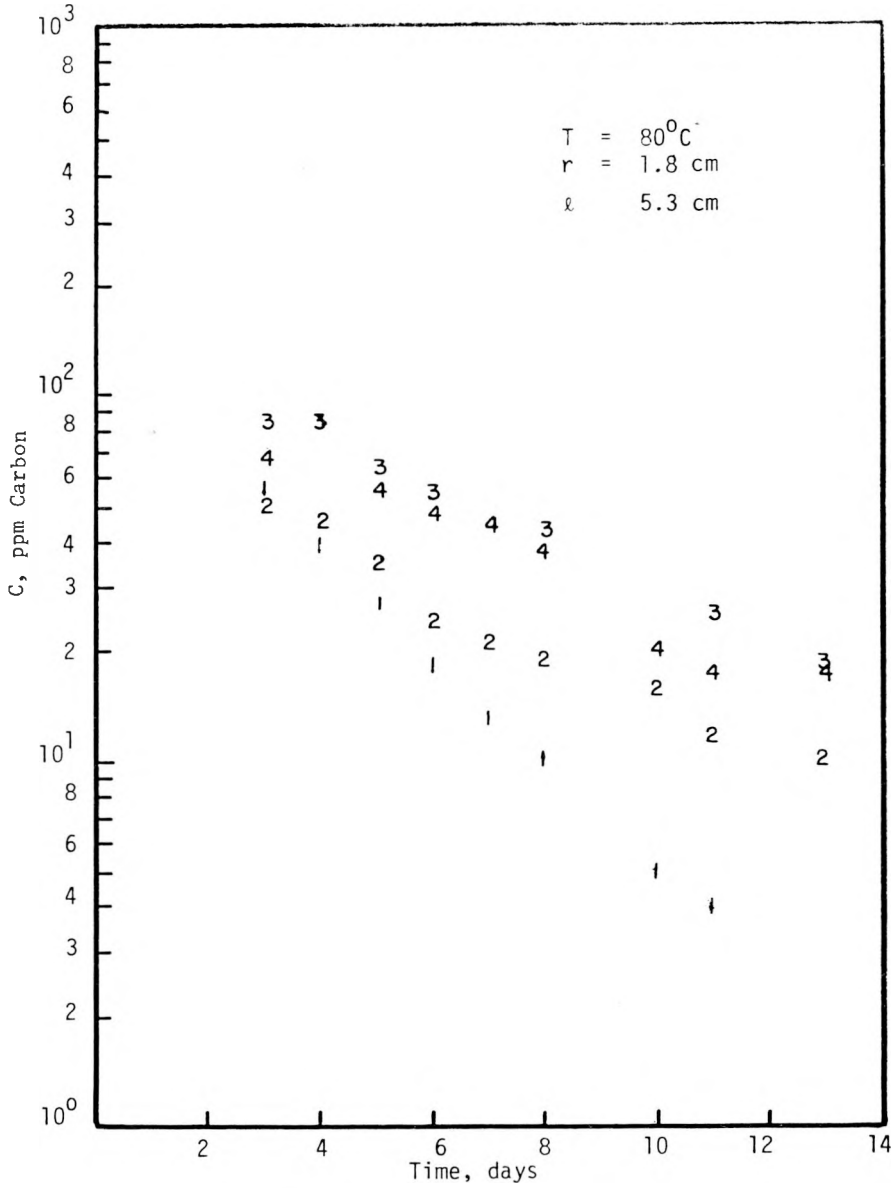


FIGURE 16. Hydrocarbon Effusion from Shale Ky4 1280

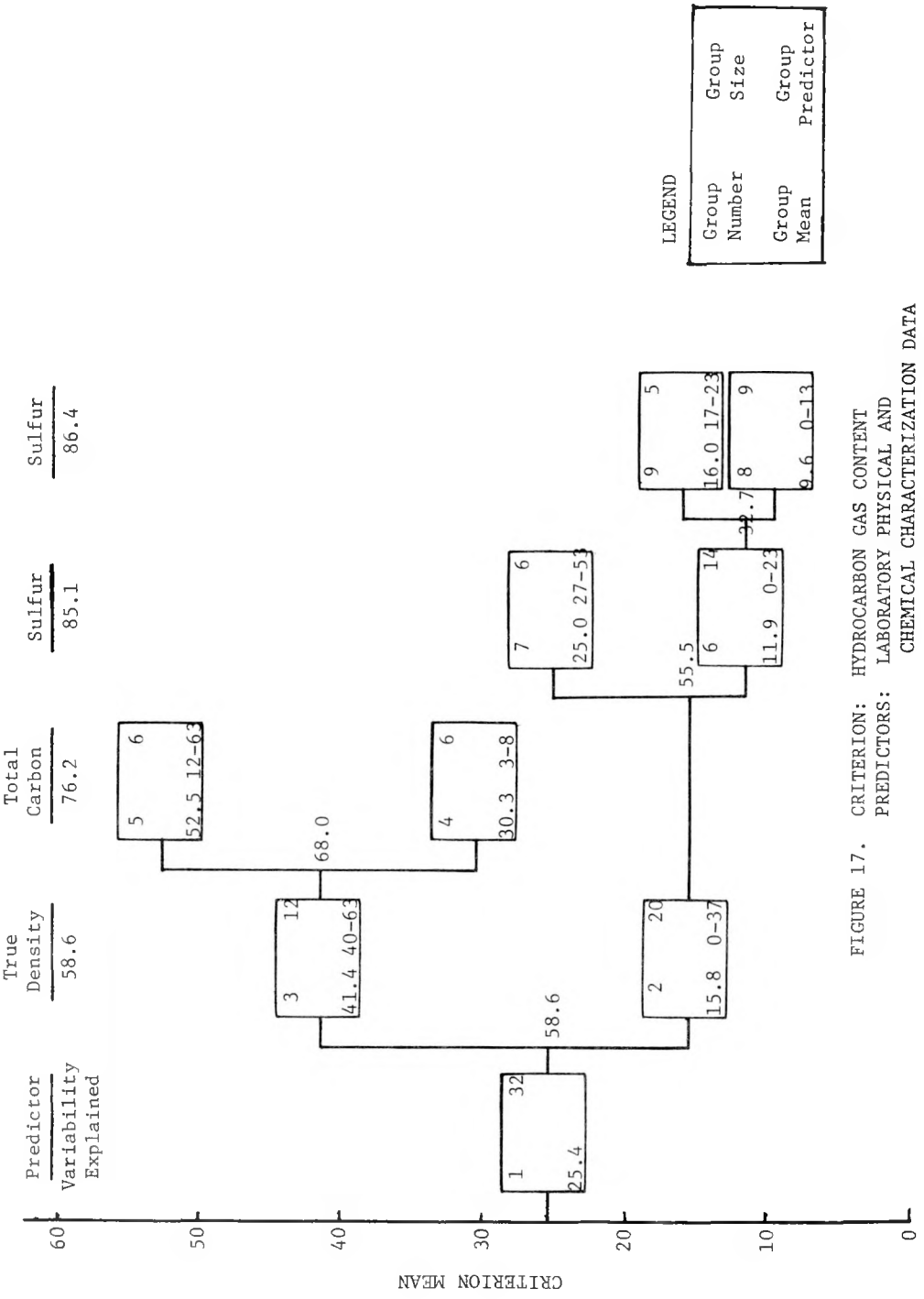


FIGURE 17. CRITERION: HYDROCARBON GAS CONTENT
PREDICTORS: LABORATORY PHYSICAL AND CHEMICAL CHARACTERIZATION DATA

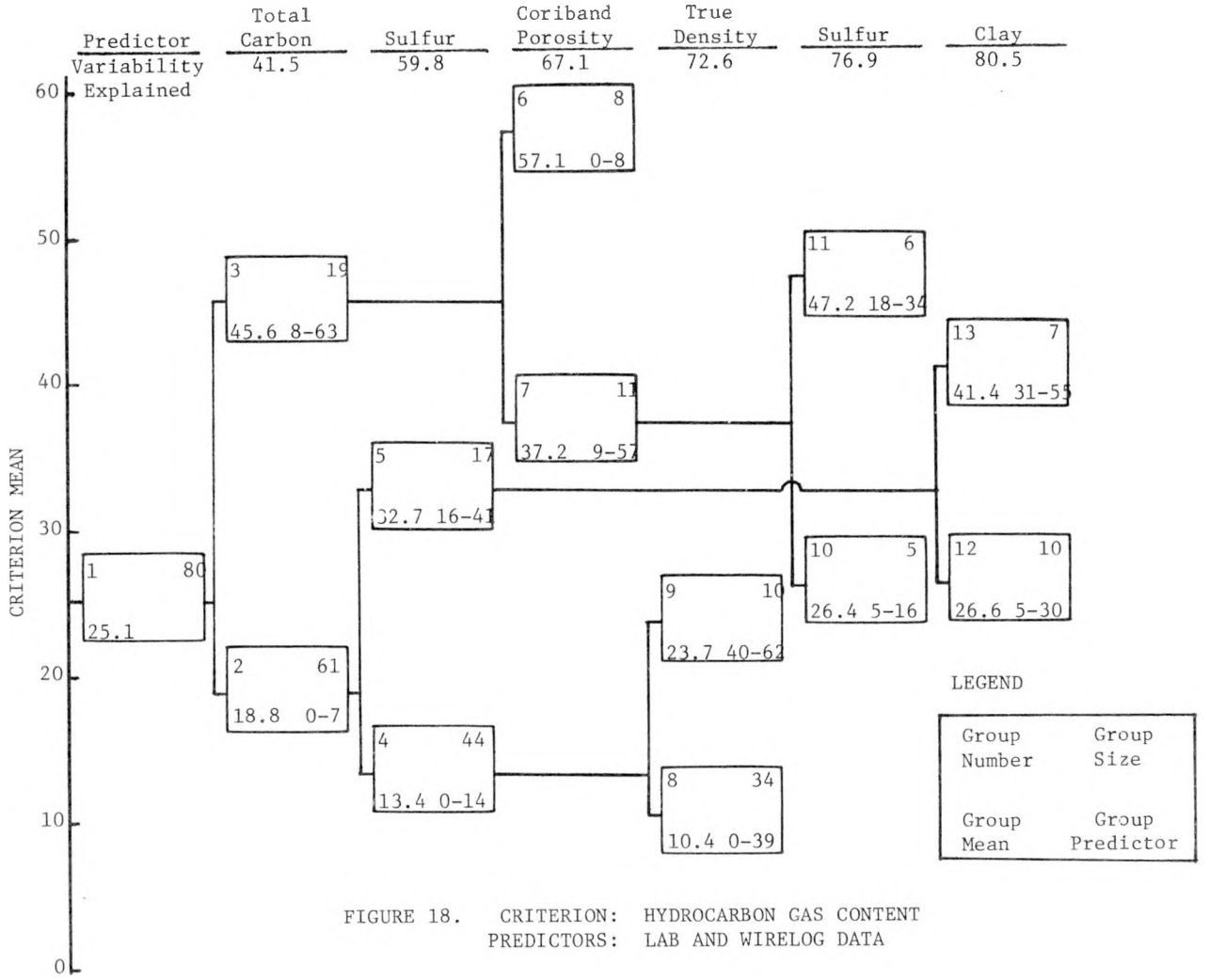


FIGURE 18. CRITERION: HYDROCARBON GAS CONTENT
PREDICTORS: LAB AND WIRELOG DATA

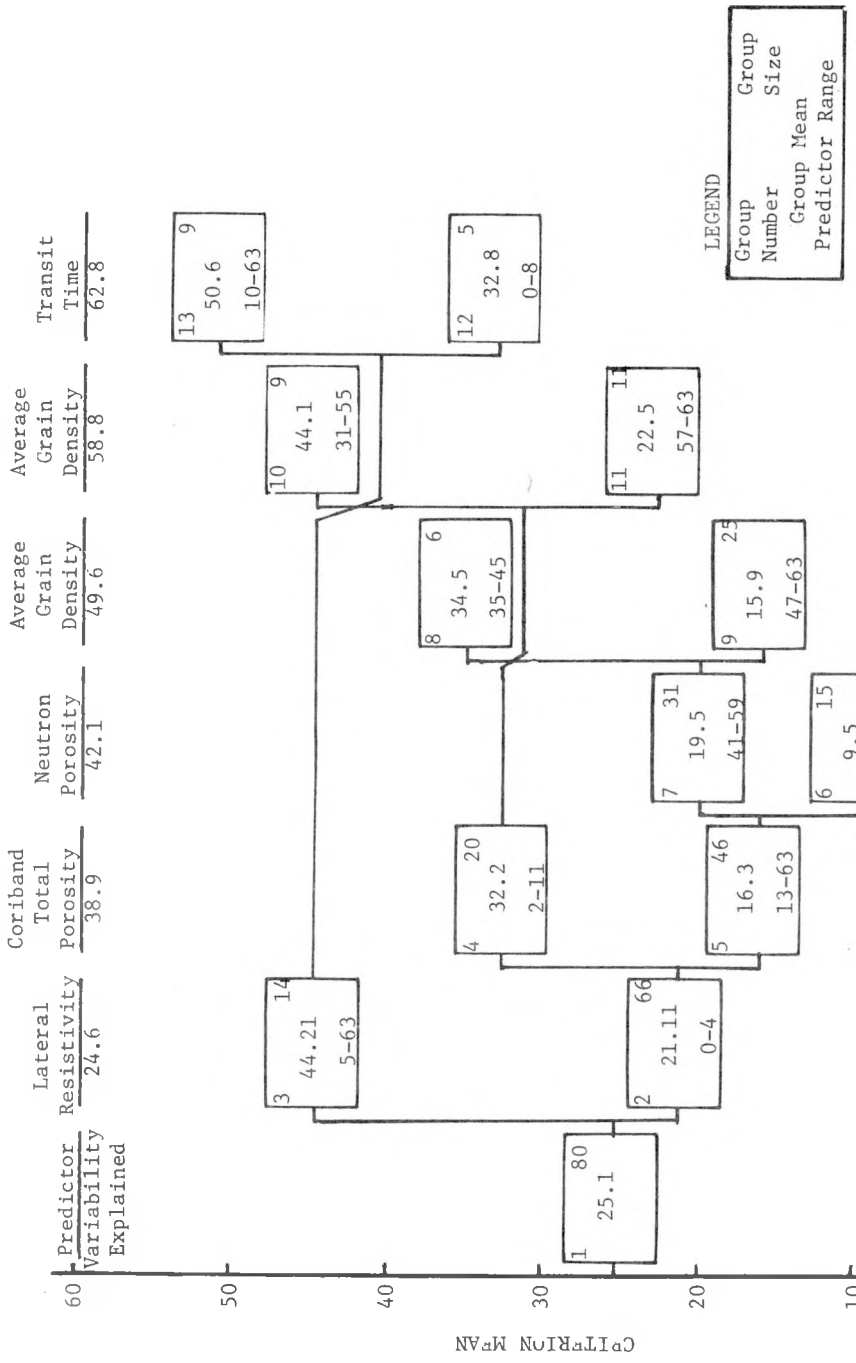


FIGURE 19. CRITERION: HYDROCARBON GAS CONTENT
PREDICTORS: WIRELOG DATA

INORGANIC GEOCHEMISTRY STUDIES OF THE EASTERN KENTUCKY GAS FIELD

by

J. Negus-de Wys and J. J. Renton
West Virginia University
Department of Geology and Geography
425 White Hall
Morgantown, West Virginia 26506



ABOUT THE AUTHOR

Ms. Negus-de Wys received her BA with honors in geology from Miami University, Oxford, Ohio. She attended graduate school at the University of Wisconsin, Ohio State University, and U.C.L.A., in Los Angeles, and Law School at Texas Tech University. She is completing her doctorate in Geology at West Virginia University and expects to receive the degree in December, 1979.

Ms. Negus-de Wys taught Geology at Case Western Reserve University; was Curator of the Geology Museum in Madison, Wisconsin; worked with Shell Oil in Midland, Texas, and Mene Grande Corporation in Venezuela; was Research Associate in the Ohio State Research Foundation Mapping and Charting Laboratories (Radar Interpretation); was Senior Scientist and Surveyor Experimenter at Cal-Tech Jet Propulsion Laboratory (Magnet Experiment); was Assistant to Director of Research at the University of Utah Research Institute. Ms. Negus-de Wys has, in addition, worked in top level business management for six years in Jackson, Wyoming. She is included in 1978- Who's Who in the West.

In August of 1977, Ms. Negus-de Wys joined the staff on the Devonian Shale Program as Research Associate in the Geology Department at West Virginia University. Her Ph.D. dissertation is STUDY OF THE EASTERN KENTUCKY GAS FIELD(S): GEOLOGICAL PARAMETERS AND POSSIBLE RELATIONSHIPS TO GAS OCCURRENCE AND PRODUCTION.

John Renton received his B.S. in Chemistry from Waynesburg College in 1956 and his M.S. and Ph.D. in Geology from West Virginia University in 1959 and 1965 respectively. Between 1960 and 1963 he was a Research and Development Officer, Solid State Physics Group, Wright Patterson AFB, Ohio.

He was appointed to the faculty of the Department of Geology in 1965 and now holds the rank of Professor. He is also on the staff of the West Virginia Geological Survey where he is acting head of the Analytical Section.

His specialty area is sedimentary geochemistry. His emphasis during the past 8 years has been the geochemistry of coal and the enclosing rock sequence with special emphasis upon the systematic variability of mineral matter in coal. These investigations have recently involved the study of modern peats and their relationship to the genesis of coal.

His investigation into the geochemistry of the black shales involves the same spatial characterization used in coal studies, tying the observed compositional patterns to both stratigraphy and structure with the over-riding hypothesis that the depo-system of the black shales is similar to that of coal: namely, a shallow water, plant dominated swamp environment.

2 INORGANIC GEOCHEMISTRY STUDIES OF THE EASTERN KENTUCKY GAS FIELD

ABSTRACT

The Upper Devonian Ohio Shale sequence including the Cleveland, Three Lick, and Upper, Middle, and Lower Huron, and the Mississippian Berea-Bedford sequence are studied by using XRF and XRD on >500 samples from 14 wells from the Eastern Kentucky Gas Field. Elements studied are Mg, Al, Si, P, K, Ca, Ti, Mn, Fe, S, Cu, Zn, Sr, Na. Minerals included in the study are chlorite, illite, kaolinite, anhydrite, szomolnokite ($FeSO_4 \cdot H_2O$), quartz, orthoclase, plagioclase, calcite, dolomite, siderite, pyrite, and bassanite ($CaSO_4 \cdot 1/2H_2O$). Ratios studied were Si/Al and five mineralic ratios: 1) kaolinite/kaolinite + illite; 2) quartz/quartz + kaolinite + illite + chlorite; 3) siderite/calcite + dolomite + siderite; 4) calcite/calcite + dolomite, and 5) chlorite/chlorite + kaolinite.

The data are examined in terms of average values for total producing sequence, for Ohio Shale sequence and for each stratigraphic unit. Computer-drawn maps, using six contour levels, are compared with final open flow data patterns from a hand-contour map using ~4750 data points and with maps showing density contours of high-producing wells.

A striking pattern match is shown by several elemental maps with the high-producing well density maps. The mineralic ratios run are perhaps best used as paleoenvironmental indicators and interpreters of the elemental complexes.

The predictive and exploration value of such an investigation is obvious.

Changes of given elements and minerals, within and between wells, are shown for comparison across the Eastern Kentucky Gas Field. The pattern relationships are not obvious from the graphs, nor are they from the formation density logs of the wells.

Further refinements of this work are in process. Seventy-two maps on the elemental analysis have been run to date. Mineralic data is in the process of analysis. Further studies will refine data tops and integrate this work with the more comprehensive study of the Eastern Kentucky Gas Field.

INTRODUCTION

The unique puzzle of the occurrence and recovery of gas from the Upper Devonian shales has long been an enigma to geologists. The depositional environment of the highly organic black shale has aroused considerable debate. Preservation of concentrated organic material is of prime importance. This could occur in a wide range of water depths. Source of organics could be terrestrial, marine, or a combination of both. The necessary anoxic bottom conditions are also derived by a variety of models. Swager (1978) has suggested that the pycnocline theory of Byers (1977) and the thermocline (quasi-estuarine circulation) theory of Heckel (1977) could be modified to fit paleoenvironmental conditions for the Devonian-Mississippian shale sequence.

Recovery of the gas once formed appears closely related to fractures, other factors being equal (Hunter and Munyan, 1935; McFarlan, 1943; Shumaker, 1978; Negus-de Wys, 1979). Many fractures are filled or partially filled with predominantly calcite or pyrite.

The differences in paleoenvironment and fracture filling may be reflected in well cutting analyses. With this concept in mind well cuttings from fourteen wells in the Eastern Kentucky Gas Field are being analyzed for sixteen elements, one elemental ratio, thirteen minerals, and five mineralic ratios.

The structural setting of the Eastern Kentucky Gas Field is shown in Figure 1. (Shumaker, 1977; Negus-de Wys and Shumaker, 1978) Figure 2 shows the basement structure for the field area only. The Rome Trough is the dominant basement feature cutting across the northern section of the field in an east-northeasterly direction. The Floyd County Channel extends from the south in a northerly direction between the Perry County Uplift on the west and the Pike County Uplift on the east. Figure 3 shows the basement interpretation from Bouguer gravity, suggesting an intersection of the Rome Trough by the channel or aborted graben (Ammerman and Keller, 1979).

The stratigraphic units included in the study are Berea-Bedford through Lower Huron (Figure 4).

Structure on the Top of the Ohio Shale is shown in Figure 4 (Provo, 1977) and structural-stratigraphic sections through the field in Figures 6, 7, and 8 (Negus-de Wys and R. C. Shumaker, 1978). The latter were constructed from formation density logs. Other sections as noted on the location map are available in the 1978 paper referenced.

Thus the setting for the Upper Devonian shales in the Eastern Kentucky Gas Field is a gentle doming structure, the Paint Creek Uplift, extending south-southeastward into the field, with the Devonian strata thickening to the east.

From 1935-1962 Coleman Hunter studied well cuttings from several counties and published average values for quartz, pyrite, kerogen and bitumen (Hunter and Munyan, 1935). Iso-value lines on these data are shown in Figures 9, 10, 11, and 12. Hunter's estimated ultimate recovery per well is shown by county in Figure 13. The quartz map shows high values to the east; pyrite is high in Floyd County and may extend north; kerogen is higher in Floyd and on to the north as well as in Perry County and to the northwest; bitumen is higher to the northwest and low to the east-southeast; and the estimated recovery contours show an elongate oval configuration with a northeast-southwest axis.

The purpose of the present study is to ascertain whether meaningful geochemical parameters can be identified to better understand the paleoenvironment of deposition of the shale sequence, the relationships within the field, and relate such evidence to gas occurrence and recovery.

DATA

The locations of the wells from which cuttings were analyzed are shown in Figure 14. Analysis was by x-ray fluorescence and x-ray diffraction (Renton, 1979). All elements except sulfur are analyzed as oxides. Figure 15 shows the elements analyzed with Minimum, Maximum, and Mean Values, Variance, and Coefficient of Variance. Variance is the average of the square of the deviations of the measurements about their mean; coefficient of variance is the standard deviation ($\sqrt{\text{variance}}$) divided by its related mean, and is a relative measurement of deviation.

A comparison of Si and Al oxide graphs for the Berea-Bedford through Huron sequence are shown in Figure 16. The wells are arranged from west to east. Figure 17 shows the Si Oxide graphs in the well positions. Field cross sections of the Si-Al oxide ratios are shown in Figures 18, 19, and 20 with stratigraphic units noted.

From these data computer maps were run on the average values of individual stratigraphic units, for the total sequence, and for the Ohio Shale. The map for the Si oxide in the Three Lick unit is shown in Figure 21. As will be seen from production maps (Figure 38), this map correlates very closely with the contoured configuration of density of high producing wells.

A comparison of computer drawn map miniatures is shown in Figure 22 for all units for Si/Al, Al, Si, S, Mg, K, Fe, and Ca. The darkest shade is the highest values, the lightest represents the lowest value. All were run with six levels, not always representing equal increments, due to data range differences.

The maps showing the greatest similarity to the production maps (Figure 38) show highest values in the central area with a northeast trend. A reverse correlation of very light values in this area could also be significant. One of the closest parallels is observed in the Si/Al series for the stratigraphic units as well as Total Sequence and Total Ohio Shale (Figure 23).

The minerals analyzed are shown in Figure 24. Chemical formulas are shown in Figure 25 and the ratio combinations in Figure 26.

The basic environmental interpretations for the ratios are tabulated in Figure 27.

KAOLINITE/KAOLINITE + ILLITE RATIO #1: Based upon our work with coal, the ratio of kaolinite to illite changes depending upon the inferred depositional environment. Kaolinite is an indication of fresh water environments while illite becomes increasingly dominant as the environment becomes more "marine" (alkaline). In the southern Appalachian Basin coals or the western coals that we interpreted as having fresh water origins (lacustrine, alluvial plain), kaolinite makes up 70% or more of the clays. In the northern Appalachian basin, interpreted as being more "brackish," the ratio is about 50:50, while in the Illinois Basin where the coals accumulated in a more "marine" influence, the kaolinite represents about 30-40% of the clays. It might be pointed out that the terms "brackish" and "marine" are relative terms; the most marine conditions under which coal could be preserved would actually be brackish at best. The Kaolinite/Kaolinite + Illite ratio in the shale study is being monitored as a possible indicator of marine influence, the shales being considered the product of a poorly preserved peat type environment.

QUARTZ/QUARTZ + KAOLINITE + CHLORITE + ILLITE RATIO #2: This is basically a quartz-clay ratio. The relative abundance of quartz would be expected to increase as the clastic source is approached, i.e., greater proximity to land. This ratio will be so tested.

SIDERITE/CALCITE + DOLOMITE + SIDERITE RATIO #3: Again referring to the coal studies, siderite is correlative with a fresh water dominated environment. This ratio parallels the Kaolinite/Kaolinite + Illite ratio, the siderite only appearing as a dominant carbonate phase when kaolinite represents 70% or more of the clays.

CALCITE/CALCITE + DOLOMITE RATIO #4: The classic carbonate ratio with increased dolomite reflecting near shore (evaporative) environments.

CHLORITE/CHLORITE + KAOLINITE RATIO #5: Based upon the coal studies, chlorite is a marine indicator. There does seem to be a variation in the relative abundance of the chlorite and kaolinite depending upon the depositional geochemistry. This ratio monitors the chlorite portion of the clay suite.

Computer drawn maps for these ratios for the average values for the total stratigraphic sequence are shown in Figures 28, 29, 30, 31, and 32. Interpretation of these maps is in the initial stages at the time of writing this paper. Figures 33 and 34 show stages of interpretation.

Comparison of these maps is made with Final Open Flow data based on 4750 wells (Figure 35). Hand contoured this data presents a highly complicated pattern (Figure 36). When a trend surface analysis program is run on these data, the 4th order polynomial yields Figure 37. This is similar to the contours resulting from Hunter's 1962 prediction of ultimate recovery per well by county. When the data is contoured by density of wells > .5 MMcf/day/25 square miles and > 1 MMcf/day/25 square miles, Figure 38 results. Comparison with one of the computer maps considered to closely resemble the production configurations is shown in Figure 39, the Si/Al map for the Three Lick unit.

Figure 40 shows a table of the element maps run to date and correlation with contours of density of high producing wells. This is a visual comparison. A statistical analysis is in progress. The Sulfur, Magnesium oxide, Si/Al oxides ratio and Aluminum oxide maps show the highest number of correlations. The Sulfur maps and the combination of Si/Al ratio and Aluminum oxide maps show correlations with all units.

Of the ratio maps, only mineral Ratio 4 shows similarities with the production configurations.

CONCLUSIONS

Based on studies to date:

1) Elemental geochemistry shows promise as an exploration tool for field development.

2) The Si/Al ratio of oxides, Al oxide, Sulfur, and Magnesium oxide maps show the highest number of correlations with contoured density of high producing wells.

3) The Lower Huron shows the highest number of correlations of elemental data with production; the Upper Huron is a close second. The Three Lick shows the least correlation.

4) Mineralic ratios are best used for paleoenvironment interpretation. Refinement of interpretation is ongoing. Figures 33 and 34 show the present level of interpretation.

We are presently seeking funding to continue this innovative and promising research. It is hoped that complete mineralic analyses, application of refinement of tops from lithological studies (Negus-de Wys, 1979), further well sample analyses and data analysis will be funded.

This work was initiated with no funding and has received subsequent interim support under DOE contract #DE-AC21-76MC05194 (formerly EY-76-C-05-5194).

ACKNOWLEDGMENTS

The authors wish to express their appreciation to Ernie Jenkins and Bob Hager of Kentucky-West Virginia Gas in Prestonsburg, Kentucky, for their cooperation in supplying well cuttings and giving valuable assistance and consultation; and to Jean Cheng who has patiently and persistently programmed the statistical and mapping procedures.

REFERENCES

Ammerman, M. L. and G. R. Keller, 1979, Delineation of Rome Trough in eastern Kentucky by gravity and deep drilling data: AAPG Bulletin, v. 63, no. 3 (March), p. 341-353.

Byers, C. W., 1977, Biofacies patterns in euxinic basins: a general model: S.E.P.M. Special Publication, no. 25, p. 5-17.

Heckel, P. H., 1977, Origin of phosphatic black shale facies in Pennsylvanian cyclothems of mid-continent North America: A.A.P.G. Bulletin, v. 61, no. 7, p. 1045-1068.

Hunter, C. D., and A. C. Munyan, 1935, Black shales, in Devonian shales: A Symposium by Appalachian Geological Society, v. 1, Charleston, W. Va.

McFarlan, A. C., 1943, Geology of Kentucky: University of Kentucky, Lexington, Ky.

Negus-de Wys and R. C. Shumaker, 1978, Study of the geology and gas occurrence in the Eastern Kentucky Gas Field: Eastern Devonian Gas Shales Symposium, Lakeview Country Club, Morgantown, W. Va. (October).

Negus-de Wys, J., 1979, Lithology studies of Upper Devonian well cuttings in the Eastern Kentucky Gas Field: Preprints ES/AAPG-DOE/EGSP Symposium, Lakeview Country Club, Morgantown, W. Va. (October).

Provo, L., 1977, Stratigraphy and sedimentology of radioactive Devonian-Mississippian shales of the Central Appalachian Basin: Ph.D. Dissertation, University of Cincinnati, Cincinnati, Ohio.

Renton, J. J., 1979, Use of weighted x-ray diffraction data for semi-quantitative estimation of minerals in low temperature ashes of bituminous coal and in shale: Dept. of Energy, METC/CR-79/5, Morgantown Energy Technology Center, Morgantown, W. Va.

Shumaker, R. C., 1977, Unpublished basement map.

Shumaker, R. C., 1978, Porous fracture facies in the Devonian shales of eastern Kentucky and West Virginia: Preprints 2nd Eastern Gas Shales Symposium, U.S. Dept. of Energy, METC/SP-78, v. 6, no. 1, p. 360-365.

Swager, D. R., 1978, Stratigraphy of the Upper Devonian-Lower Mississippian shale sequence in the eastern Kentucky outcrop belts: Master's Thesis, University of Kentucky, Lexington, Ky., 116 p.

CORRELATION OF COMPUTER MAPS WITH CONTOURED DENSITY OF HIGH PRODUCING WELLS

Units	Oxides of Si/Al Ratio	Elements (all oxides except Sulfur)							Totals
		Al	Si	S	Mg	K	Fe	Ca	
Berea-Bedford	+	+		+	+	+			5
Cleveland	0	+		+	+	+			5
Three Lick		0	+	+					3
Upper Huron	+	0	+	+	0	0			6
Middle Huron		+		0	+			+	4
Lower Huron	+	0		+-	+	0	0	+	7
Total Sequence	+			+-	+		0	+	5
Ohio Shale	+			+-	+		0	+	5
Totals	6	6	2	8	7	4	3	4	

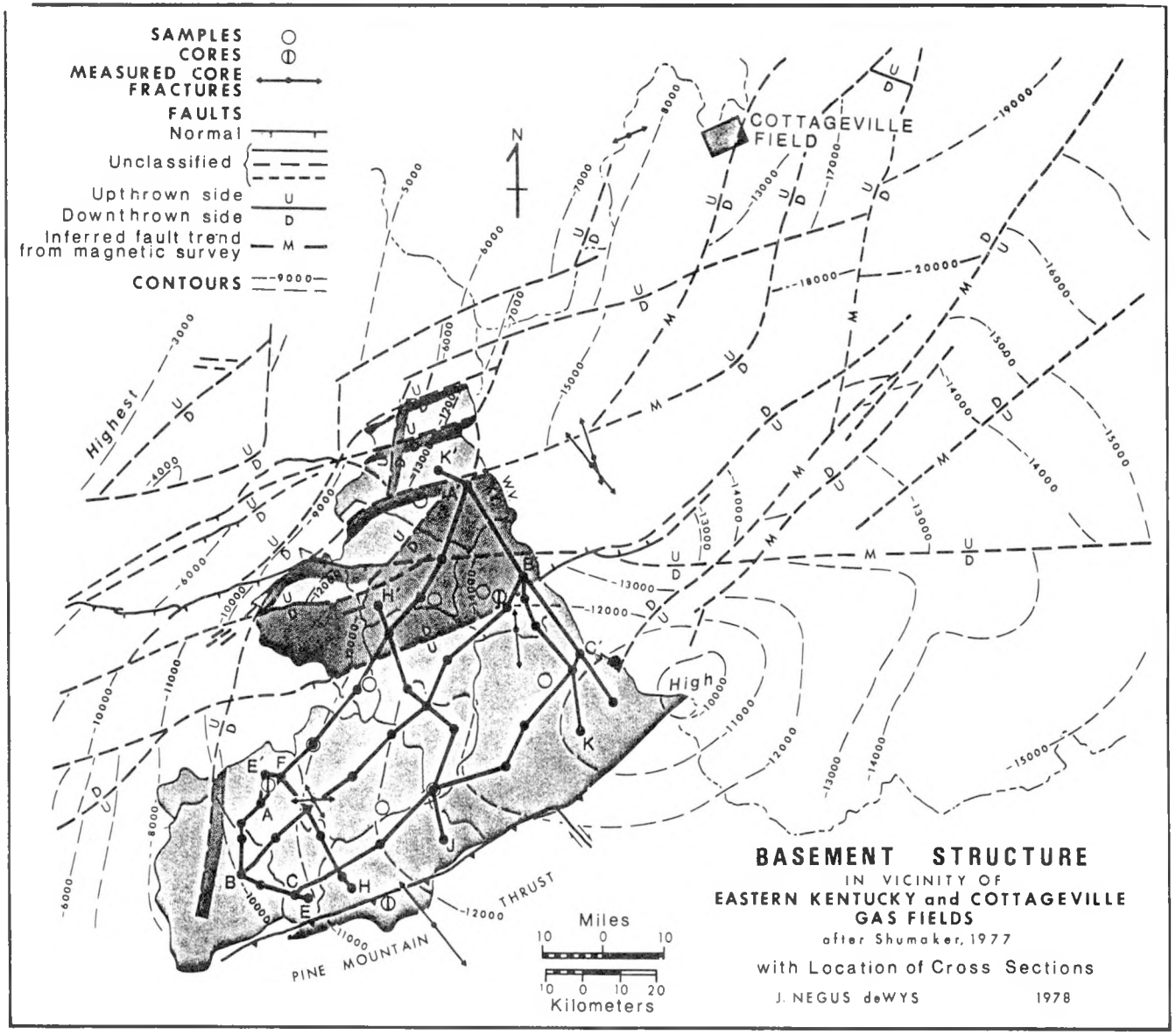


Figure 1 Structural setting of the Eastern Kentucky Gas Field showing the Rome Trough cutting across the northern part of the field and the Floyd County Channel extending from the south into the center of the field.

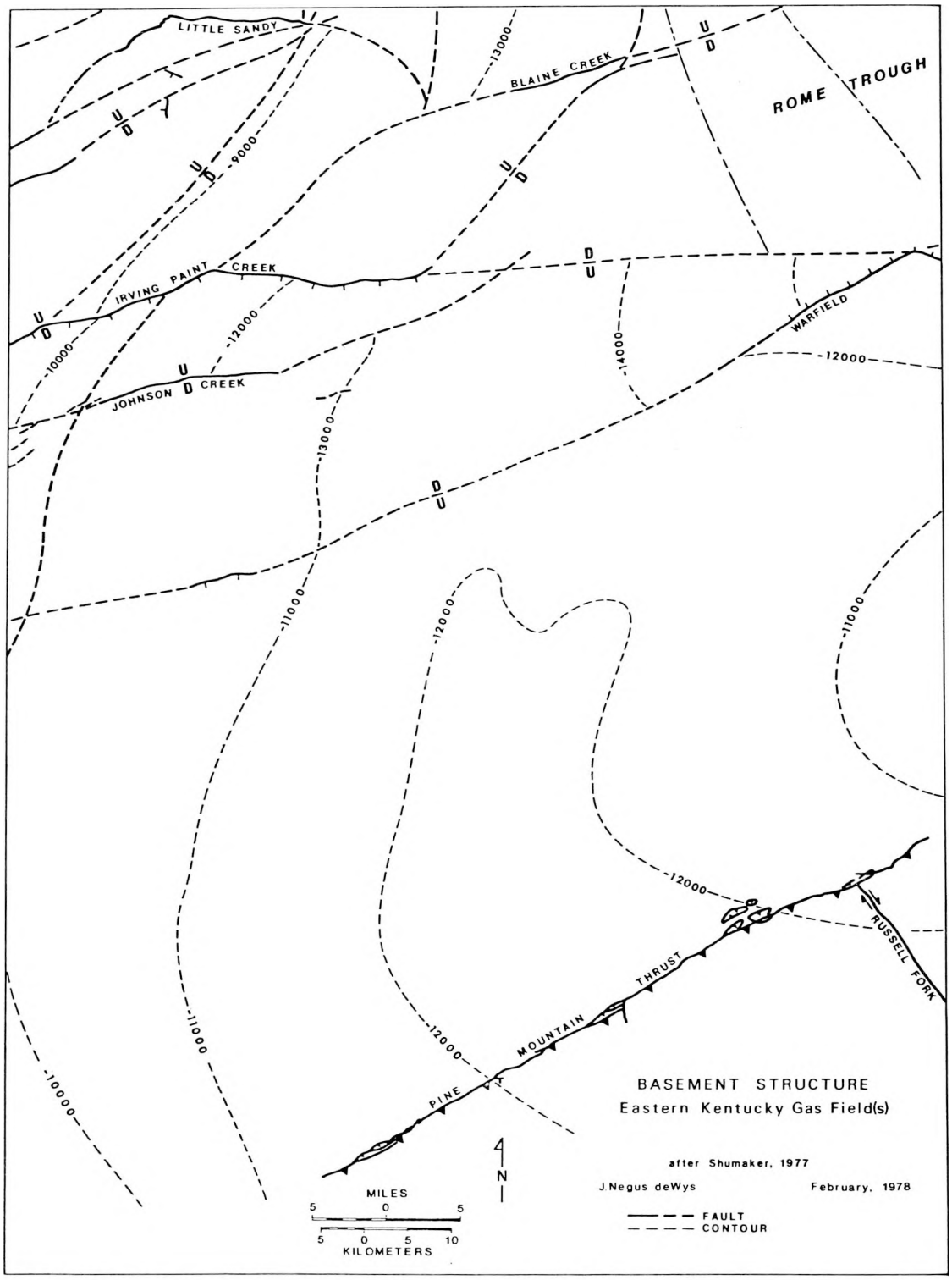


Figure 2 Basement structure of the area studied (after Shumaker, 1977).

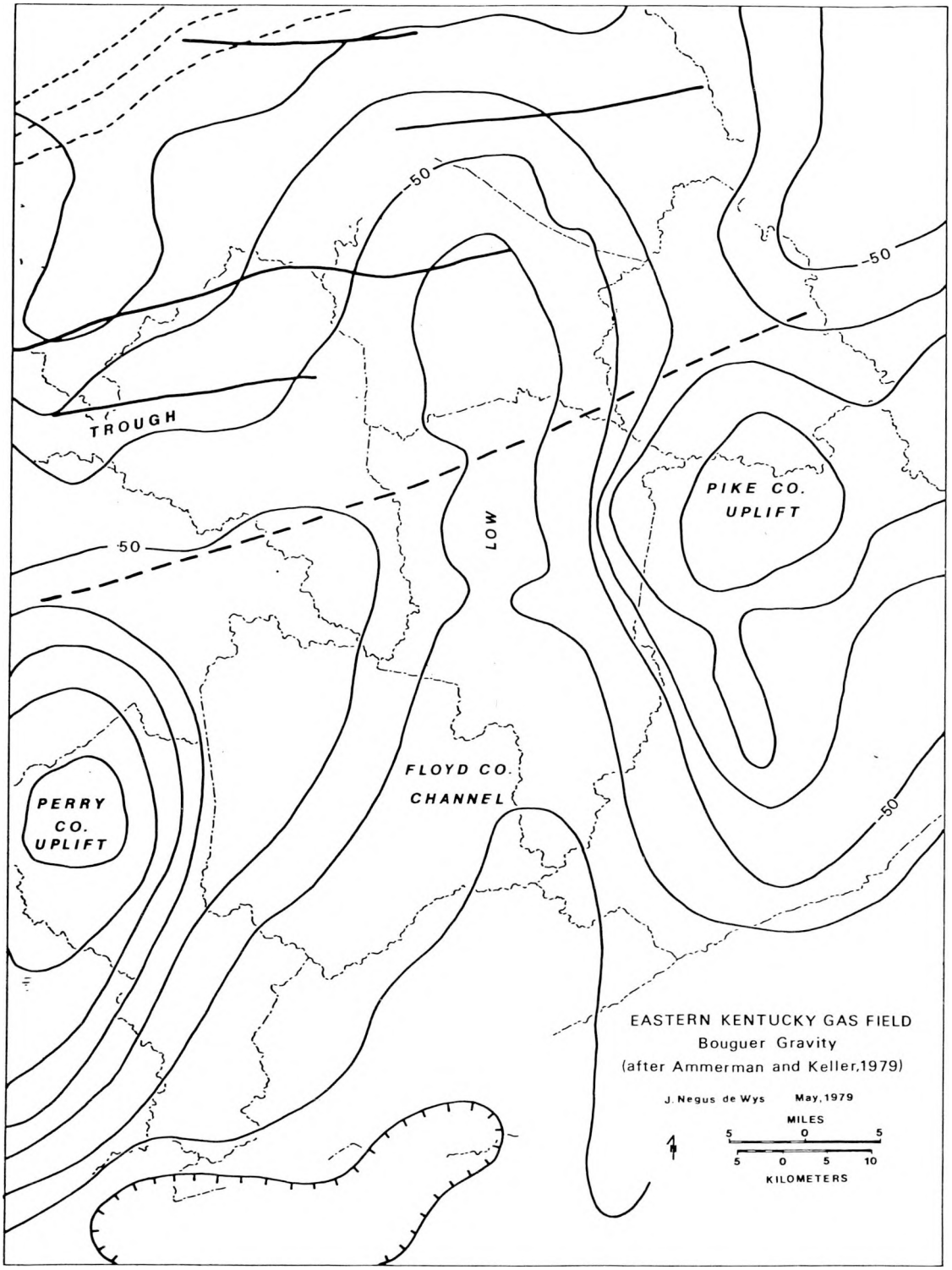


Figure 3 Basement structure of the area studied from Bouguer gravity (after Ammerman and Keller, 1979). Note extension of Floyd County Channel to intersect the Rome Trough.

STRATIGRAPHIC SEQUENCE	
BEREA/BEDFORD	Berea Sandstone and Bedford Shale, undivided
CLEVELAND	Cleveland Member of Ohio Shale of Ohio
THREE LICK	Three Lick Bed of Provo, Kepferle, and Potter, 1977
UPPER HURON	Upper Part of Huron Member of Ohio Shale of Ohio
MIDDLE HURON	Middle Part of Huron Member of Ohio Shale of Ohio
LOWER HURON	Lower Part of Huron Member of Ohio Shale of Ohio

Figure 4 Stratigraphic Units included in study.

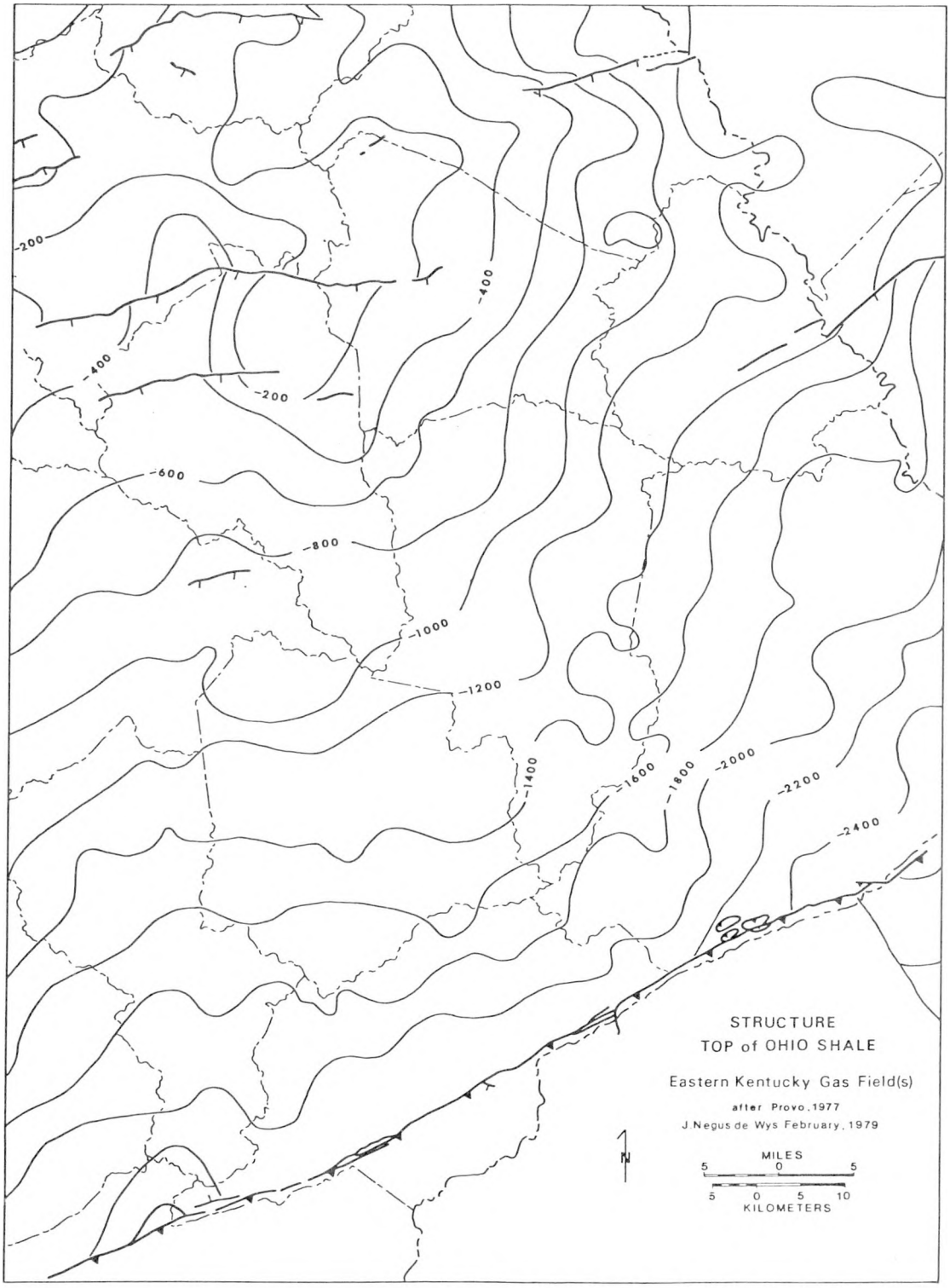


Figure 5 Structure on Top of the Ohio Shale (after Provo, 1977).

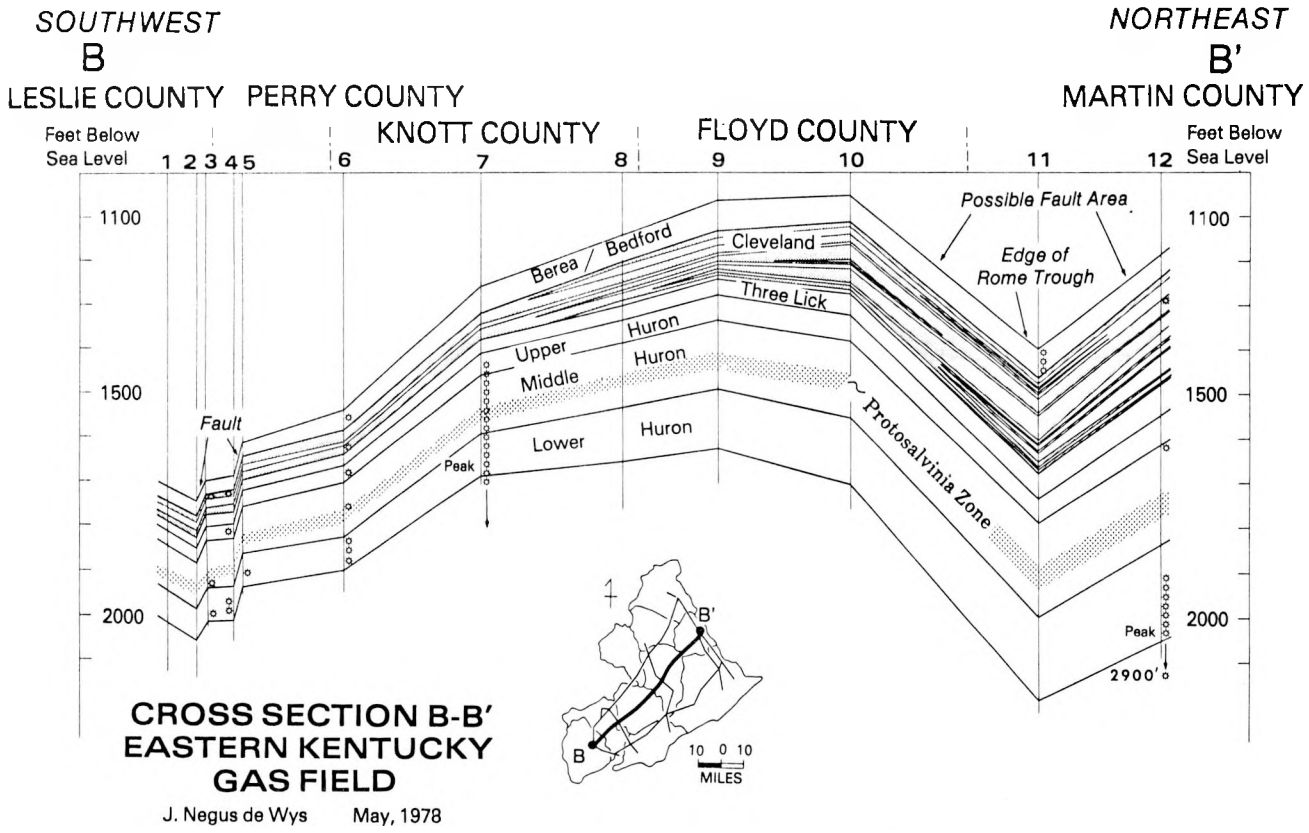


Figure 6 Structural-stratigraphic section B-B' through the center of the field, southwest to northeast.

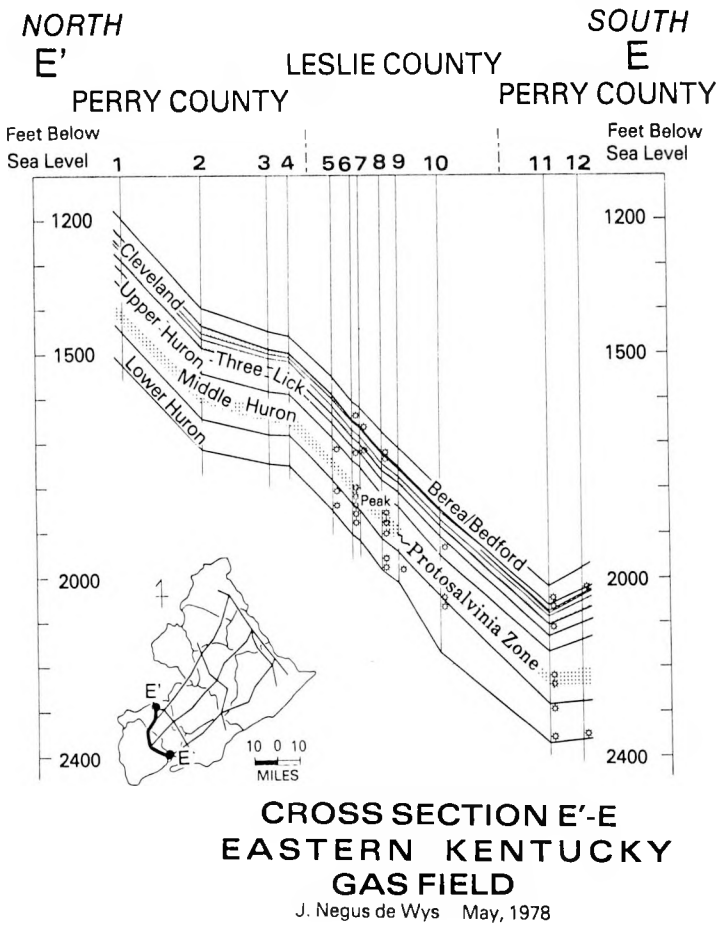


Figure 7 Structural-stratigraphic section E'-E through the southwest end of the field, north to south.

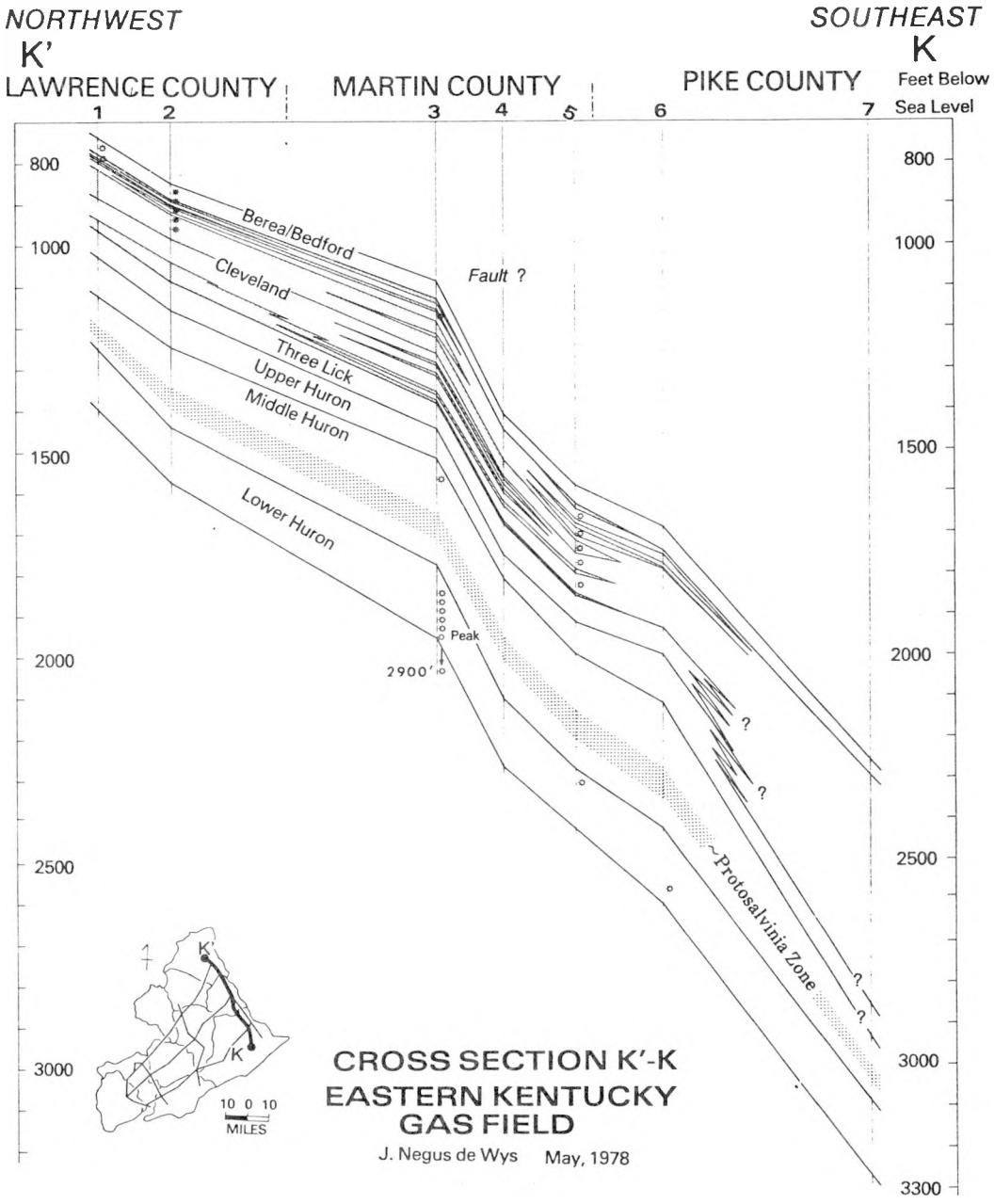


Figure 8 Structural-stratigraphic section K'-K through the northeastern part of the field, north to south.

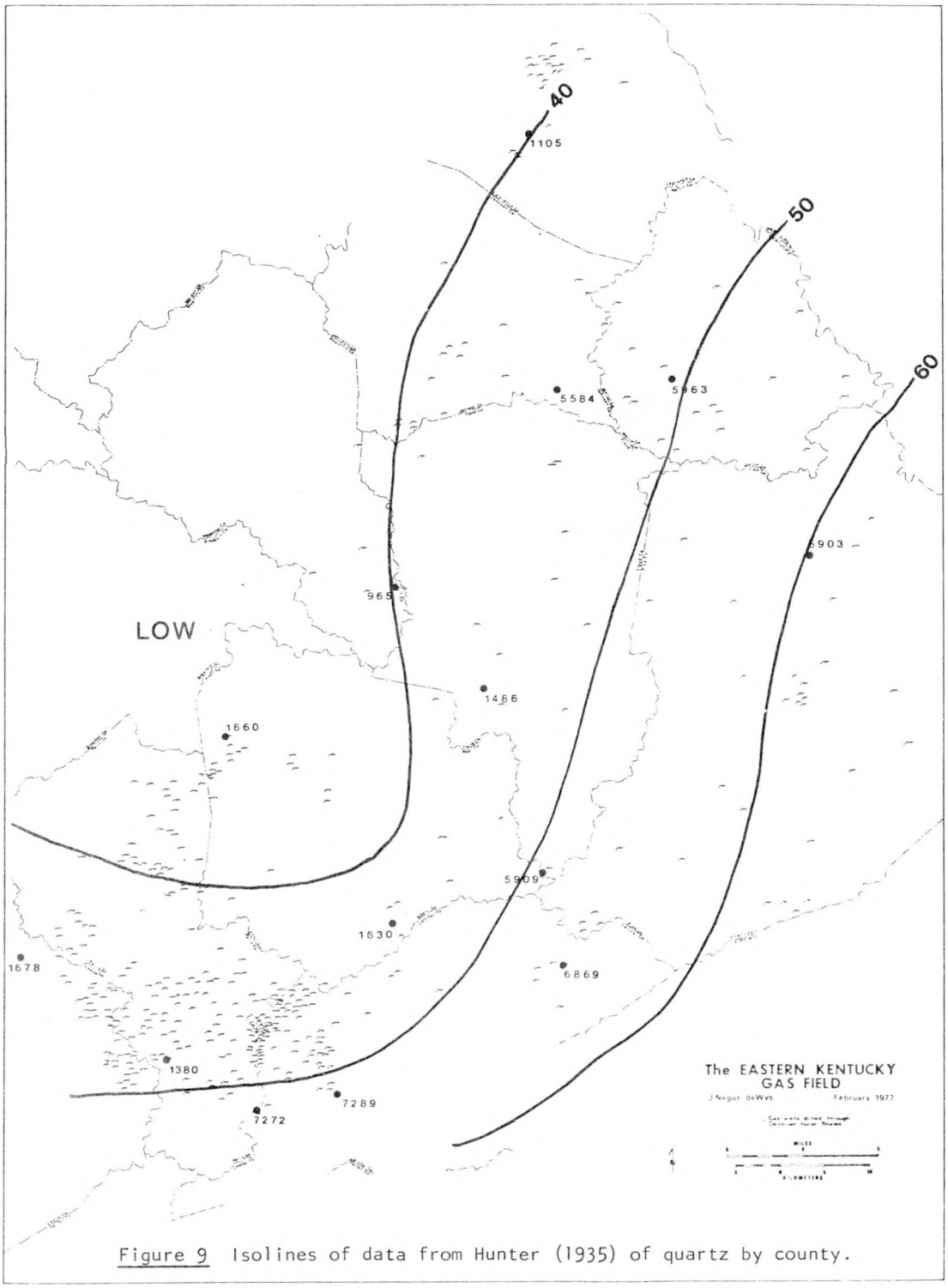


Figure 9 Isolines of data from Hunter (1935) of quartz by county.

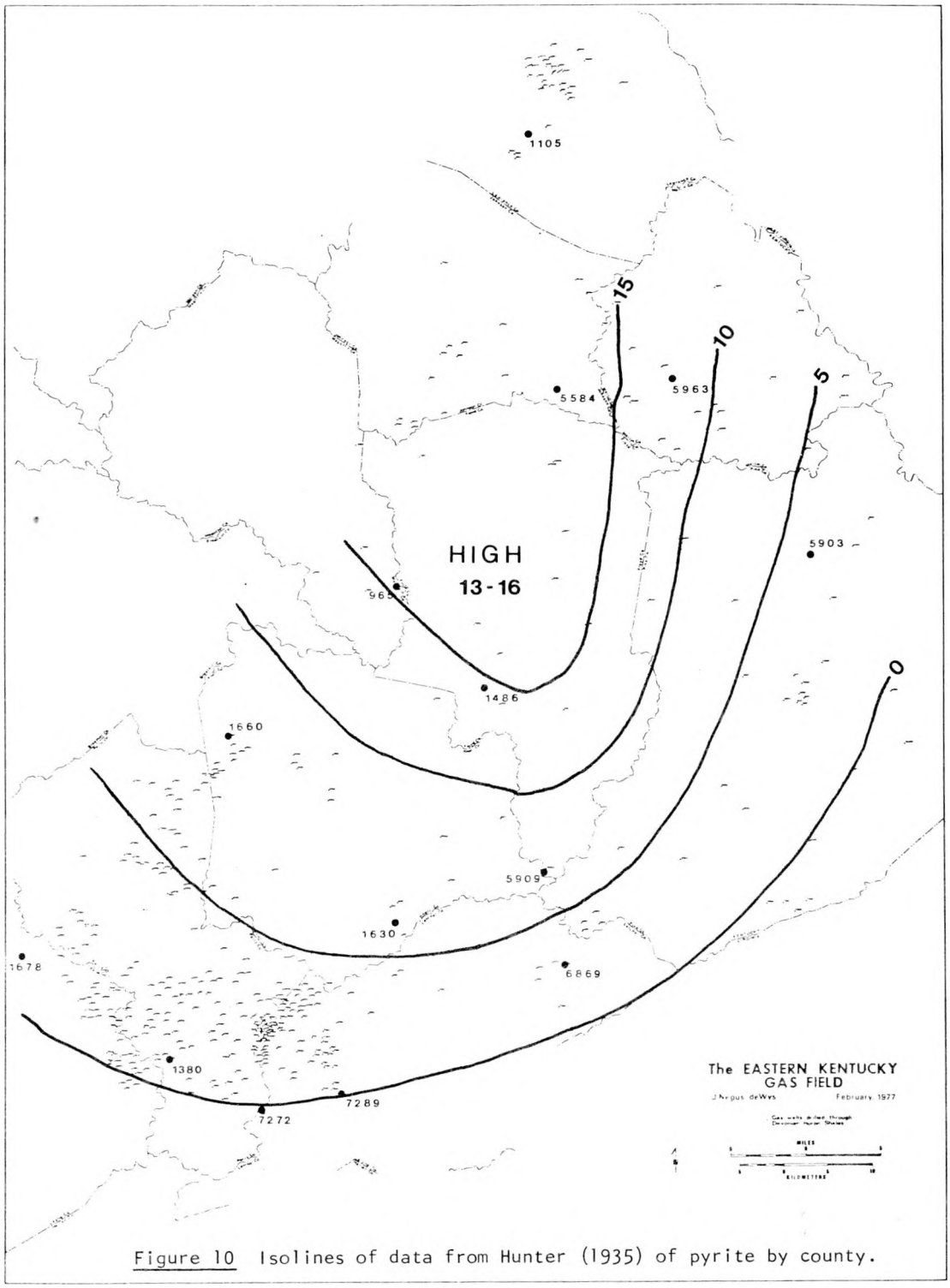


Figure 10 Isolines of data from Hunter (1935) of pyrite by county.

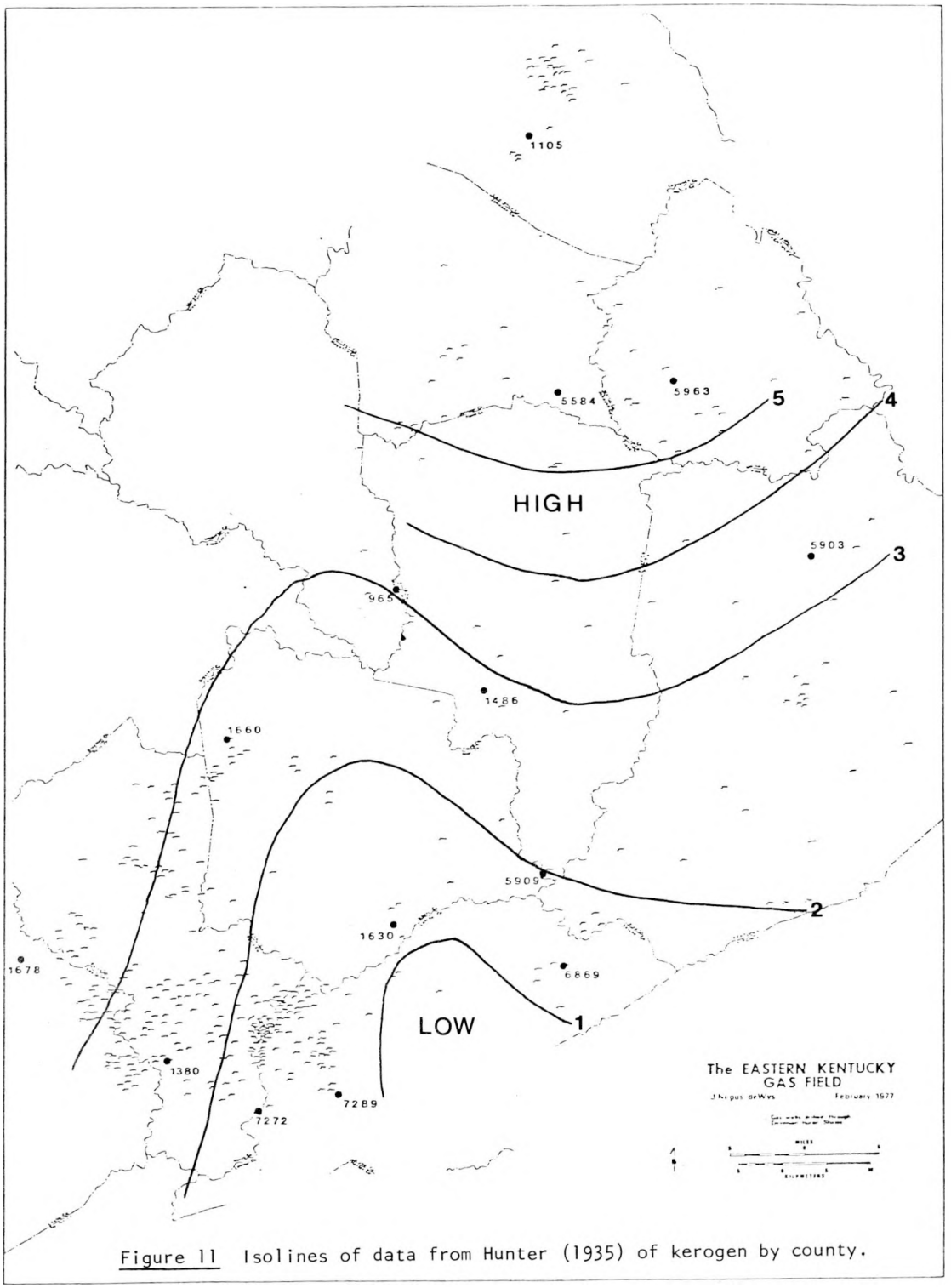


Figure 11 Isolines of data from Hunter (1935) of kerogen by county.

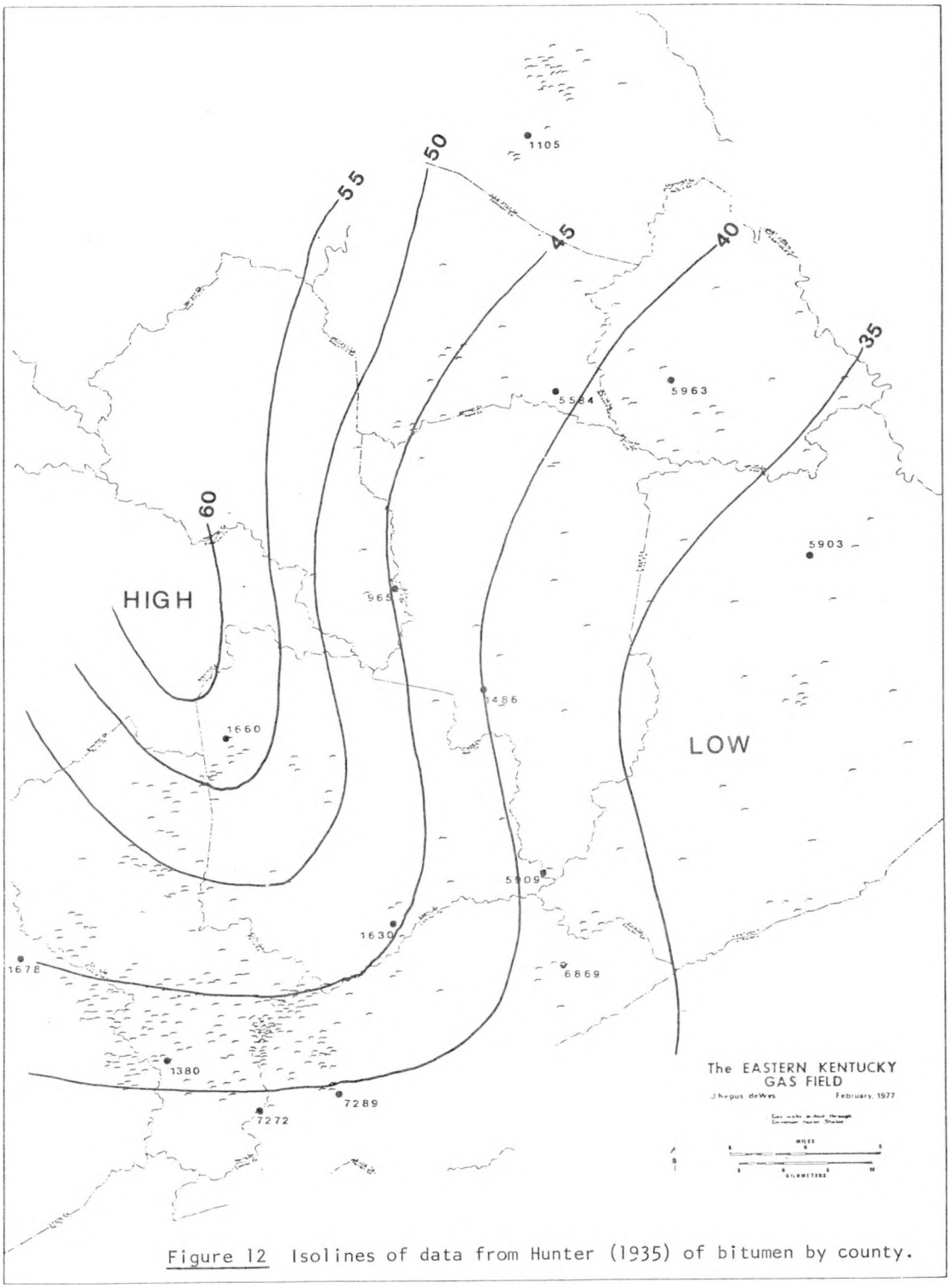


Figure 12 Isolines of data from Hunter (1935) of bitumen by county.

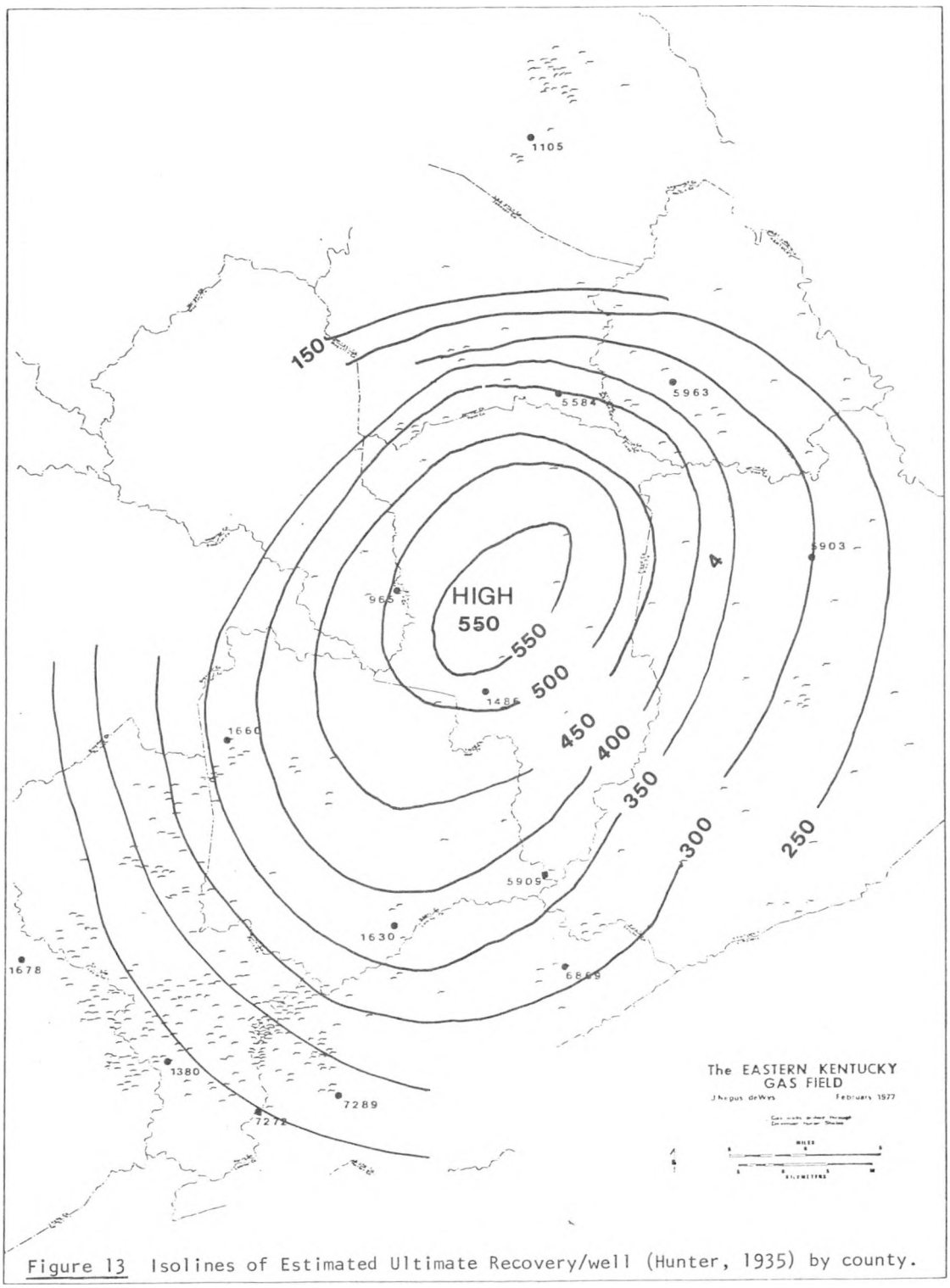


Figure 13 Isolines of Estimated Ultimate Recovery/well (Hunter, 1935) by county.

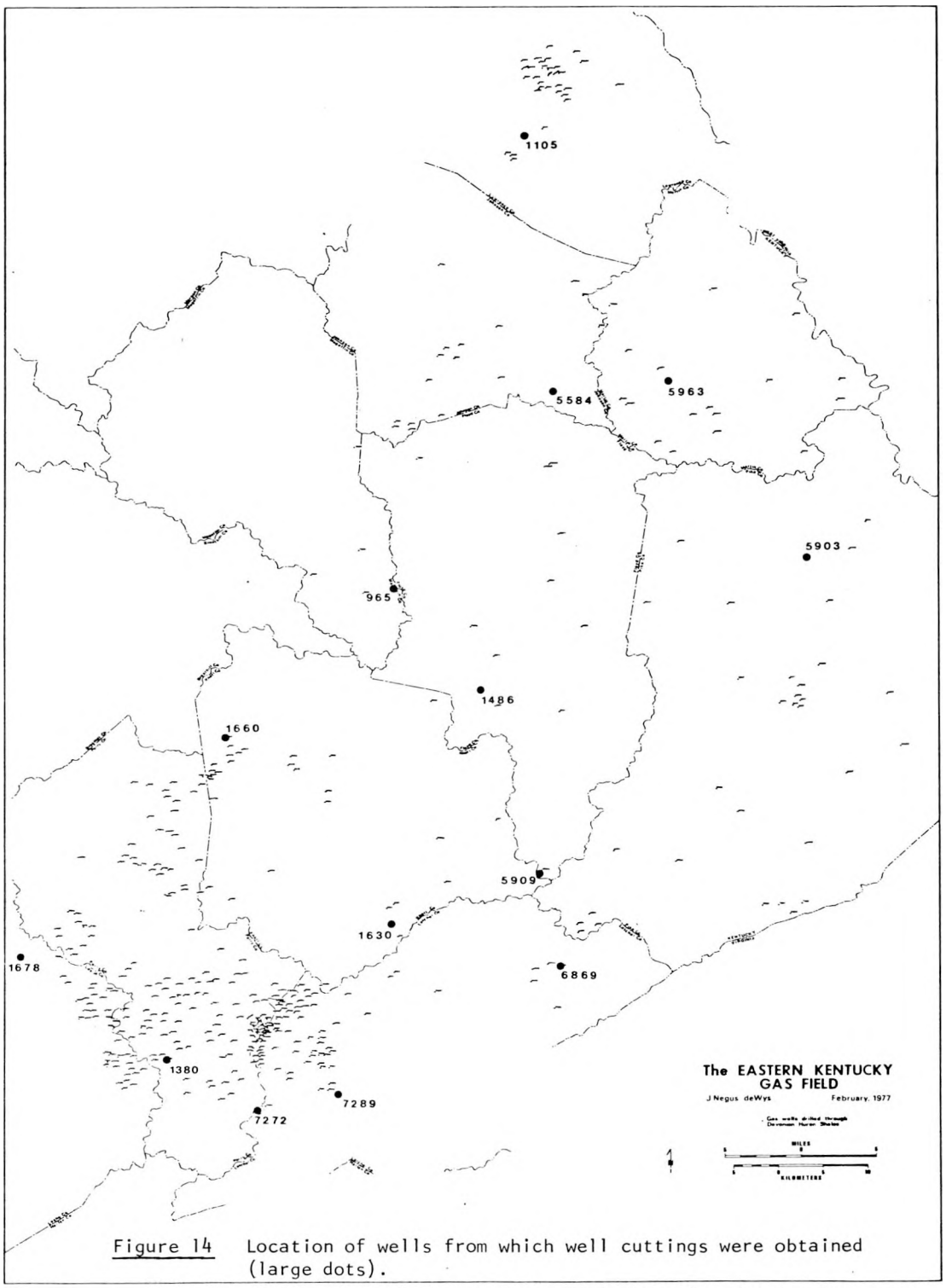


Figure 14 Location of wells from which well cuttings were obtained (large dots).

Small points are wells from which formation density logs were available.

SIMPLE STATISTICS FOR CHEMICAL ELEMENTS

Variable	Weight Percent oxide (except Sulfur)			Variance	Coefficient of Variance
	Minimum	Maximum	Mean		
MN	0.016	0.500	0.051	0.001	66.789
FE	3.590	20.150	8.519	2.679	19.214
S	0.051	8.258	2.364	0.907	40.272
ZN	0.001	0.106	0.013	0.000	72.342
SR	0.000	0.064	0.004	0.000	109.953
NA	0.149	0.730	0.661	0.004	9.660
MG	0.733	4.157	1.428	0.171	29.007
AL	6.000	18.120	14.206	3.333	12.851
SI	48.000	78.300	55.103	7.912	5.105
P	0.102	0.962	0.138	0.009	70.618
K	0.401	8.460	3.354	0.438	19.720
CA	0.155	32.985	1.252	12.565	283.140
TI	0.230	1.160	0.931	0.020	15.043
Si/Al RATIO	2.829	12.102	3.982	0.776	22.113

Figure 15 Table of Simple Statistics for Elements and Ratio Si/Al analyzed.

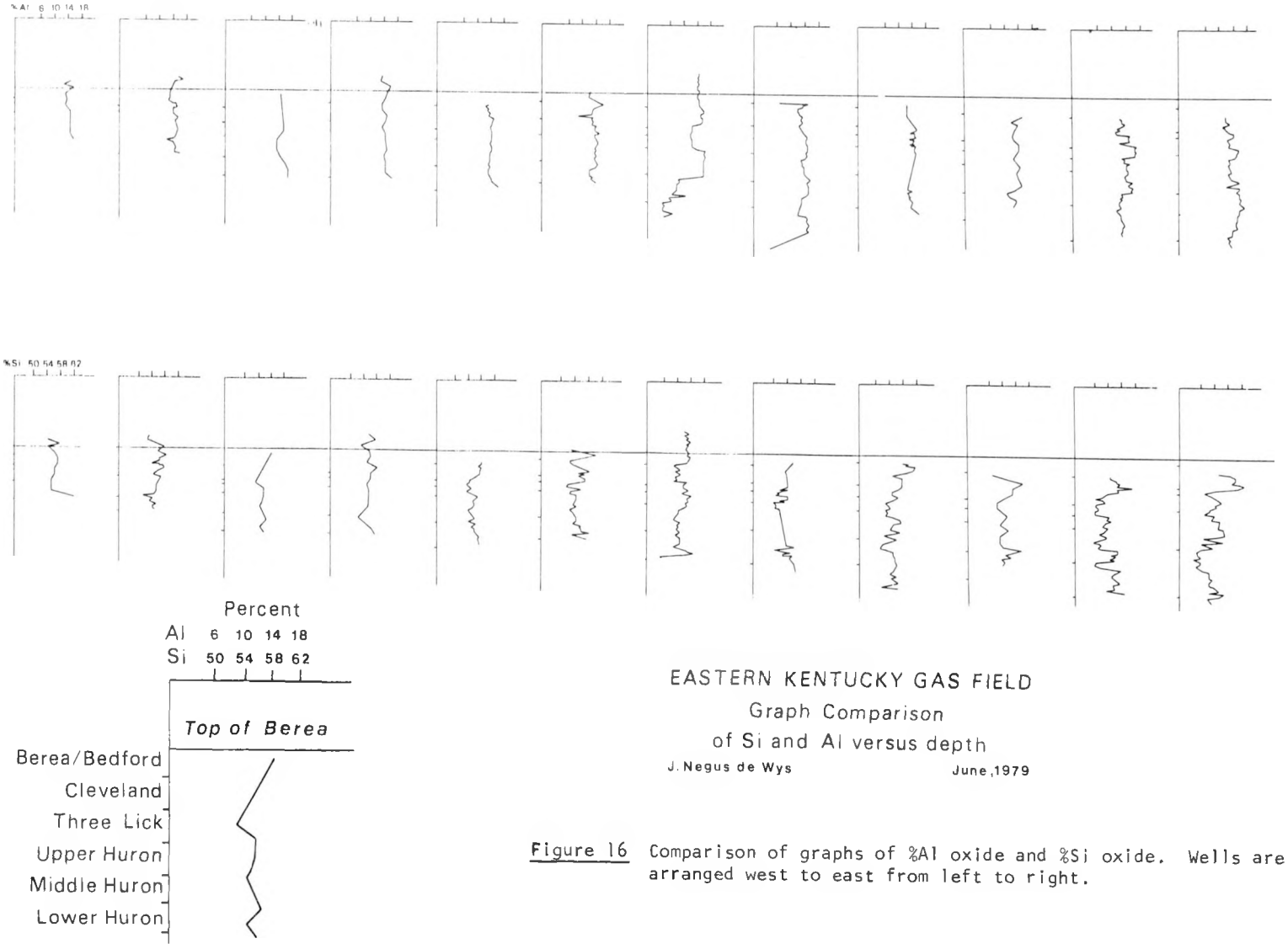


Figure 16 Comparison of graphs of %Al oxide and %Si oxide. Wells are arranged west to east from left to right.

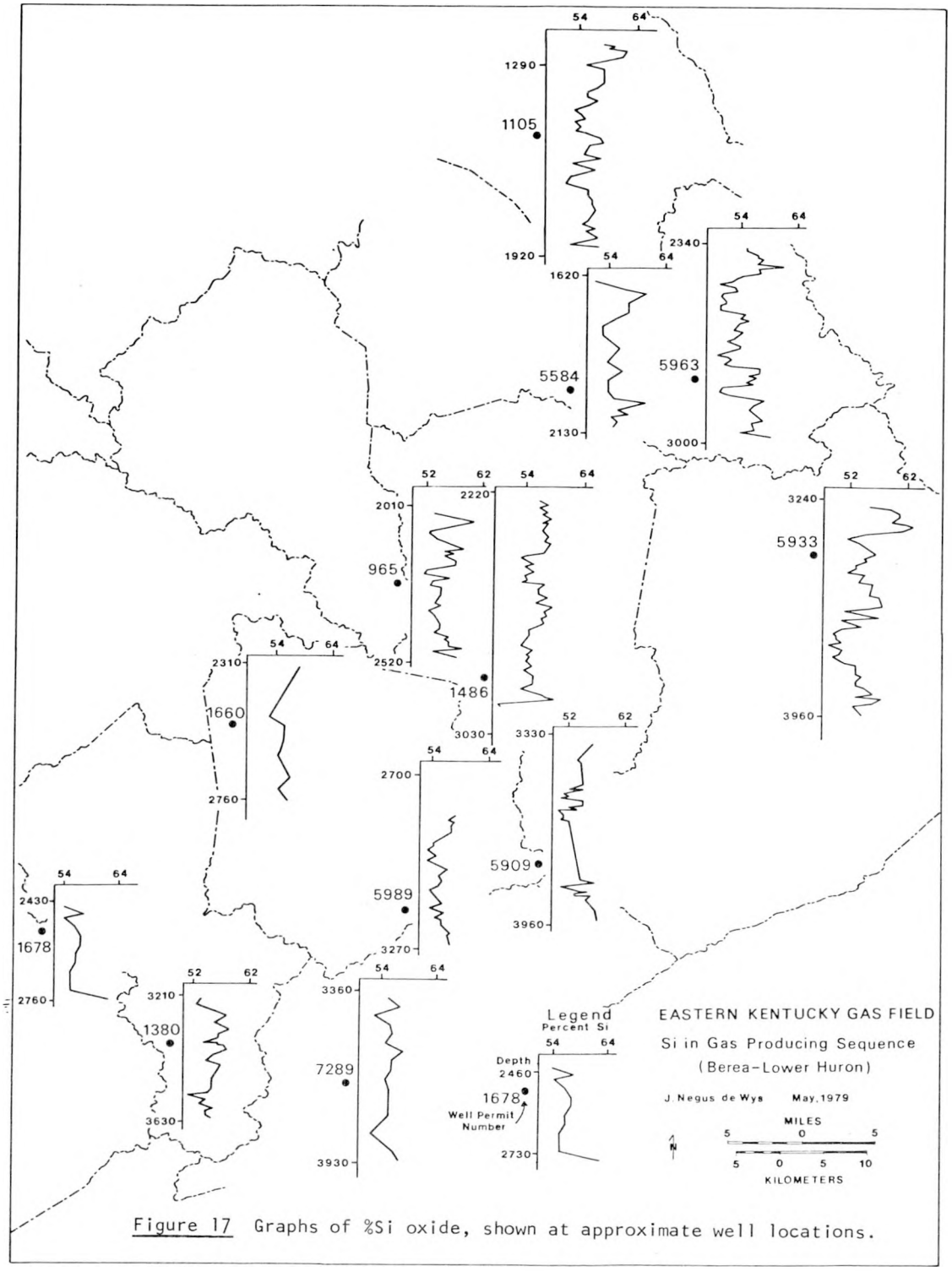


Figure 17 Graphs of %Si oxide, shown at approximate well locations.

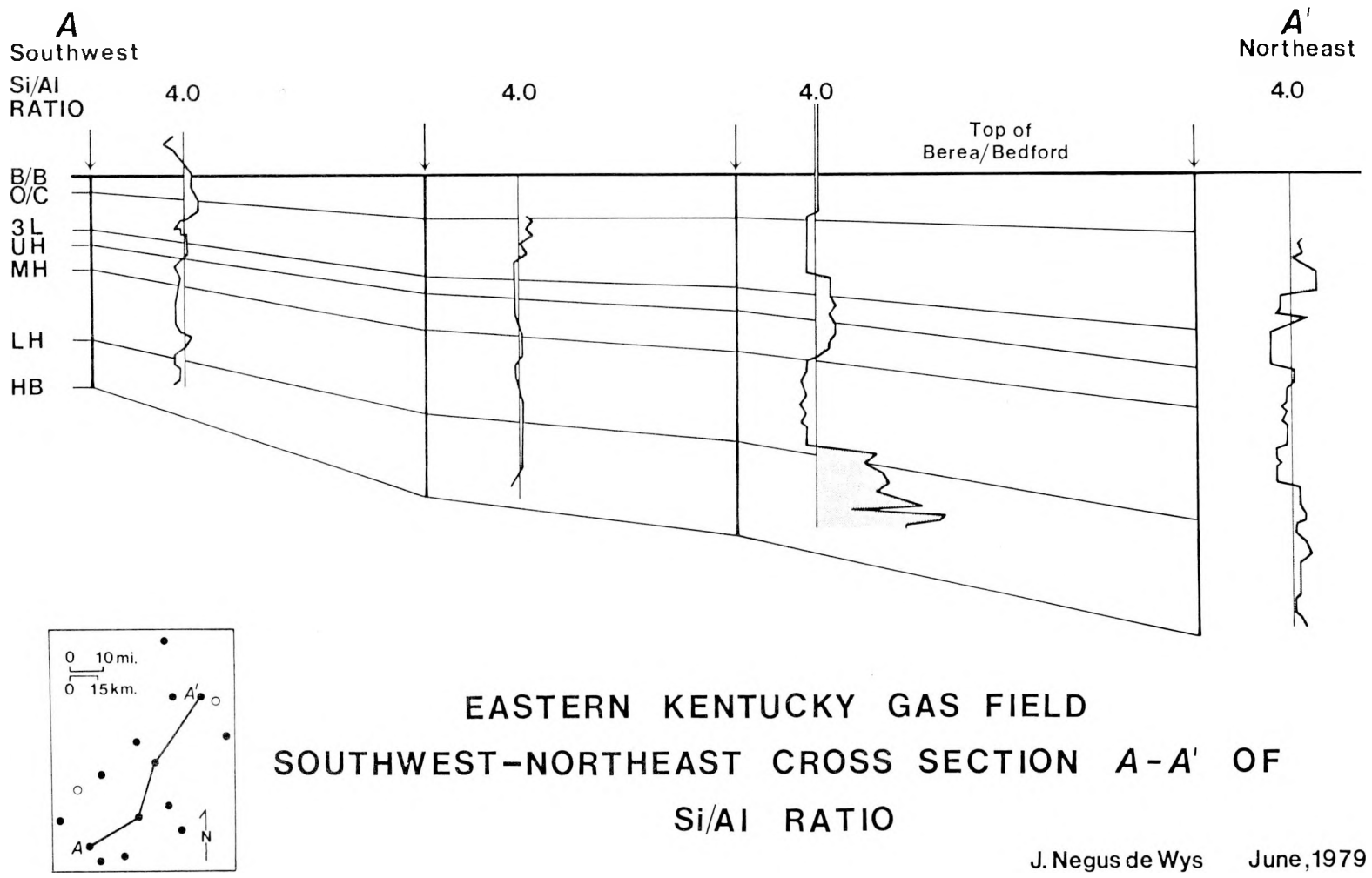


Figure 18 Southwest-northeast cross section A-A' through the field with Si/Al oxide ratio graphs. Compare with Figure 6.

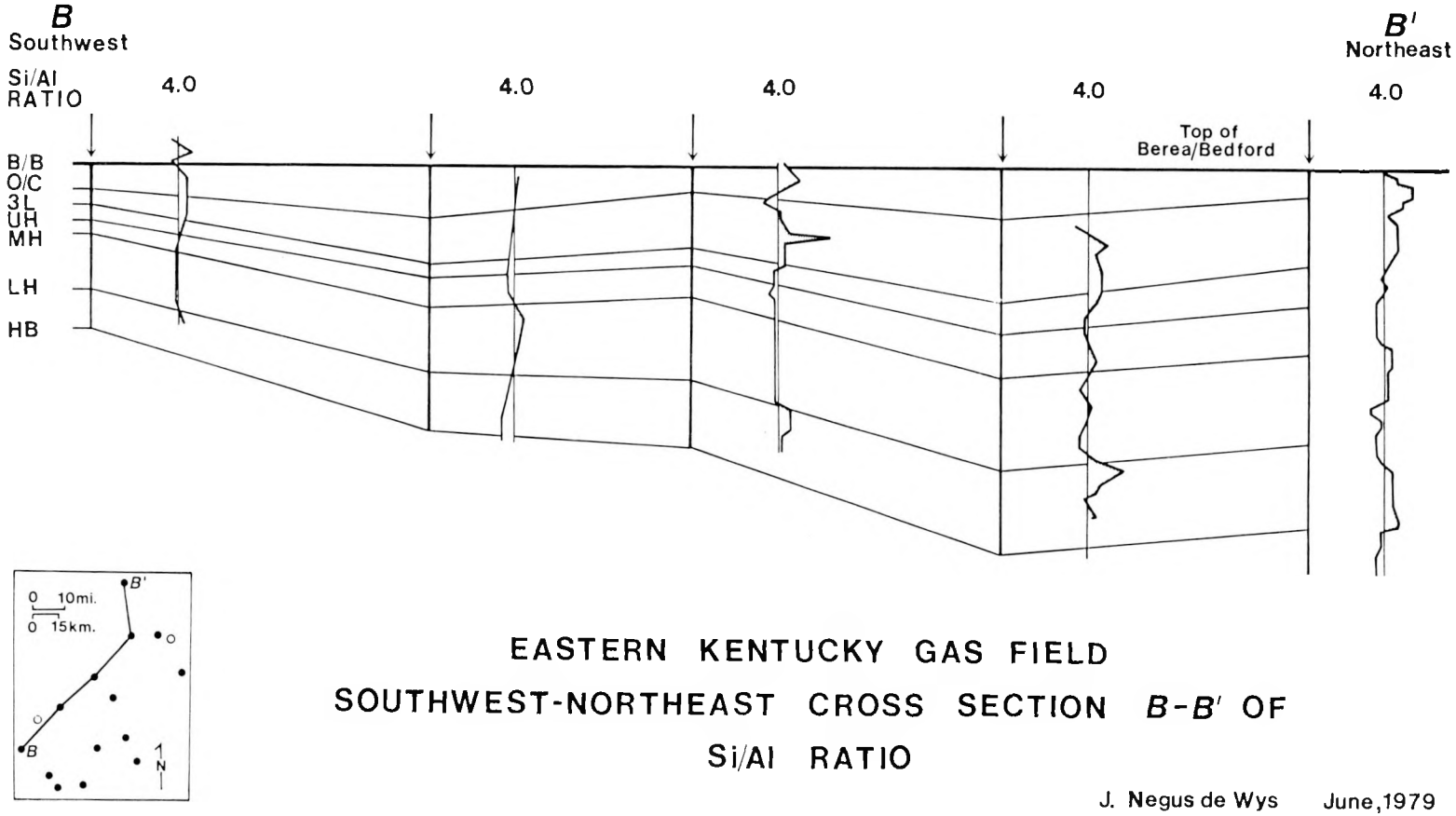


Figure 19 Cross sections of %Si/Al oxide ratio southwest-northeast B-B'. Compare with Figure 6.

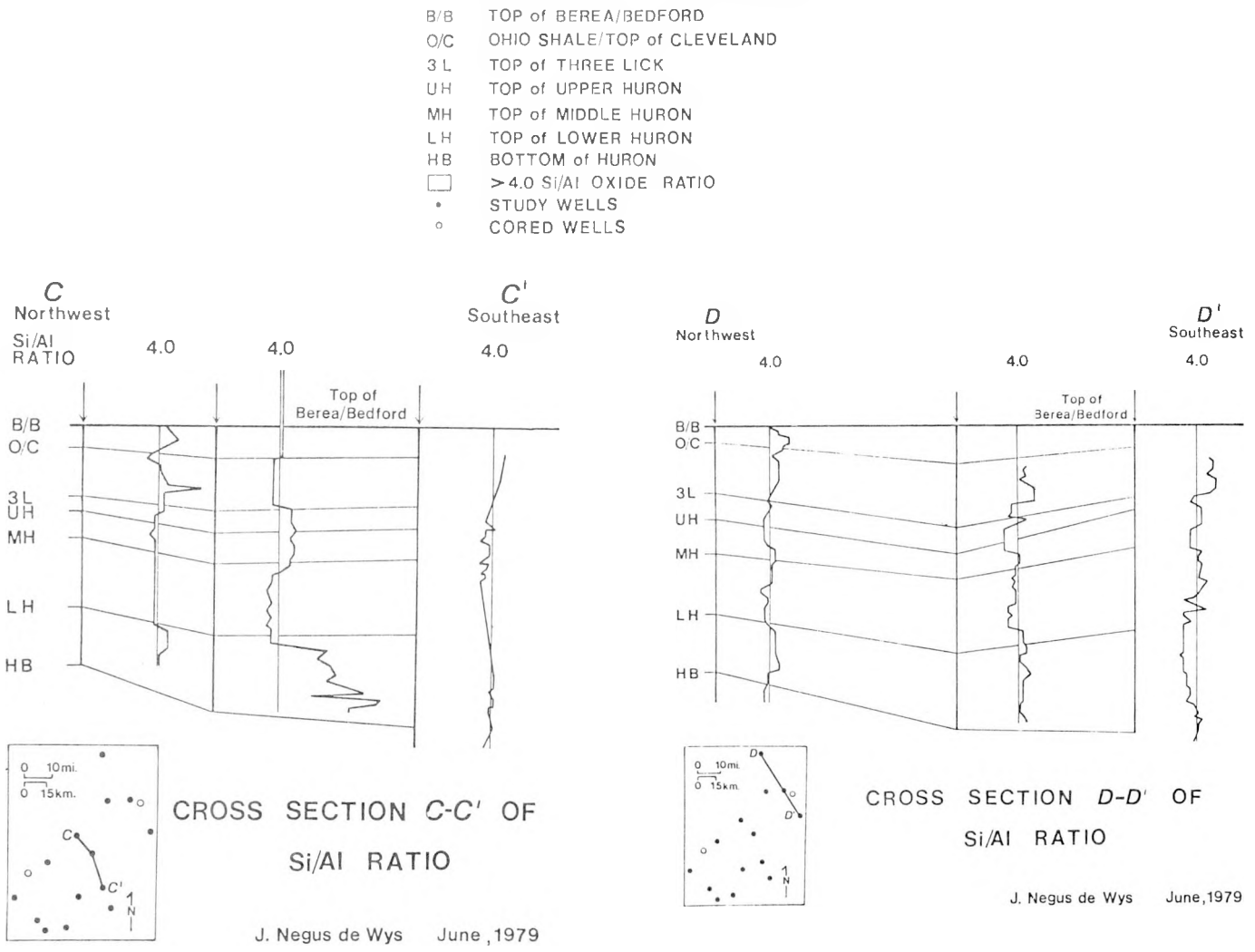


Figure 20 Cross section of %Si/Al oxide ratios northwest-southeast C-C' and D-D'. Compare with Figure 8.

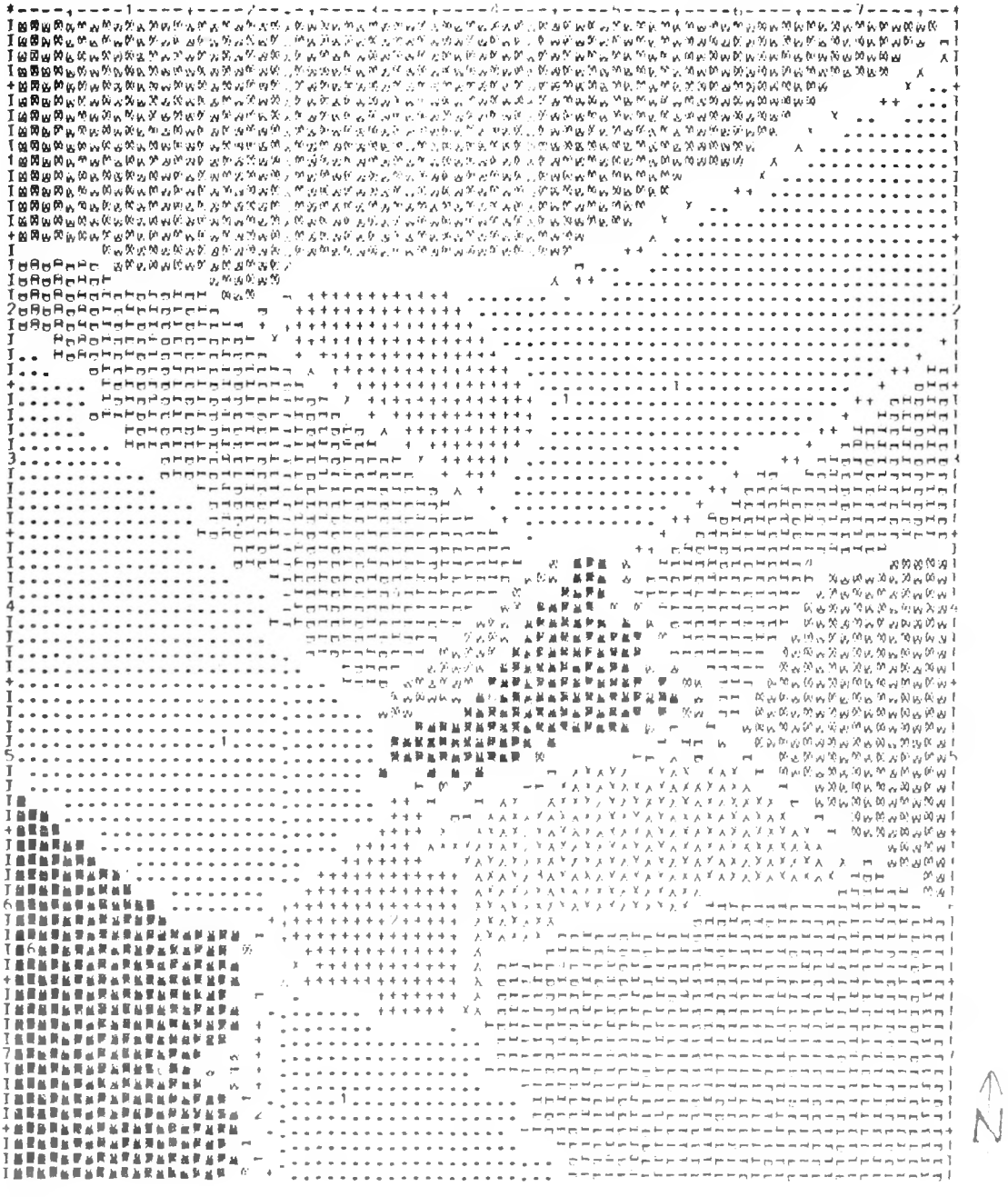
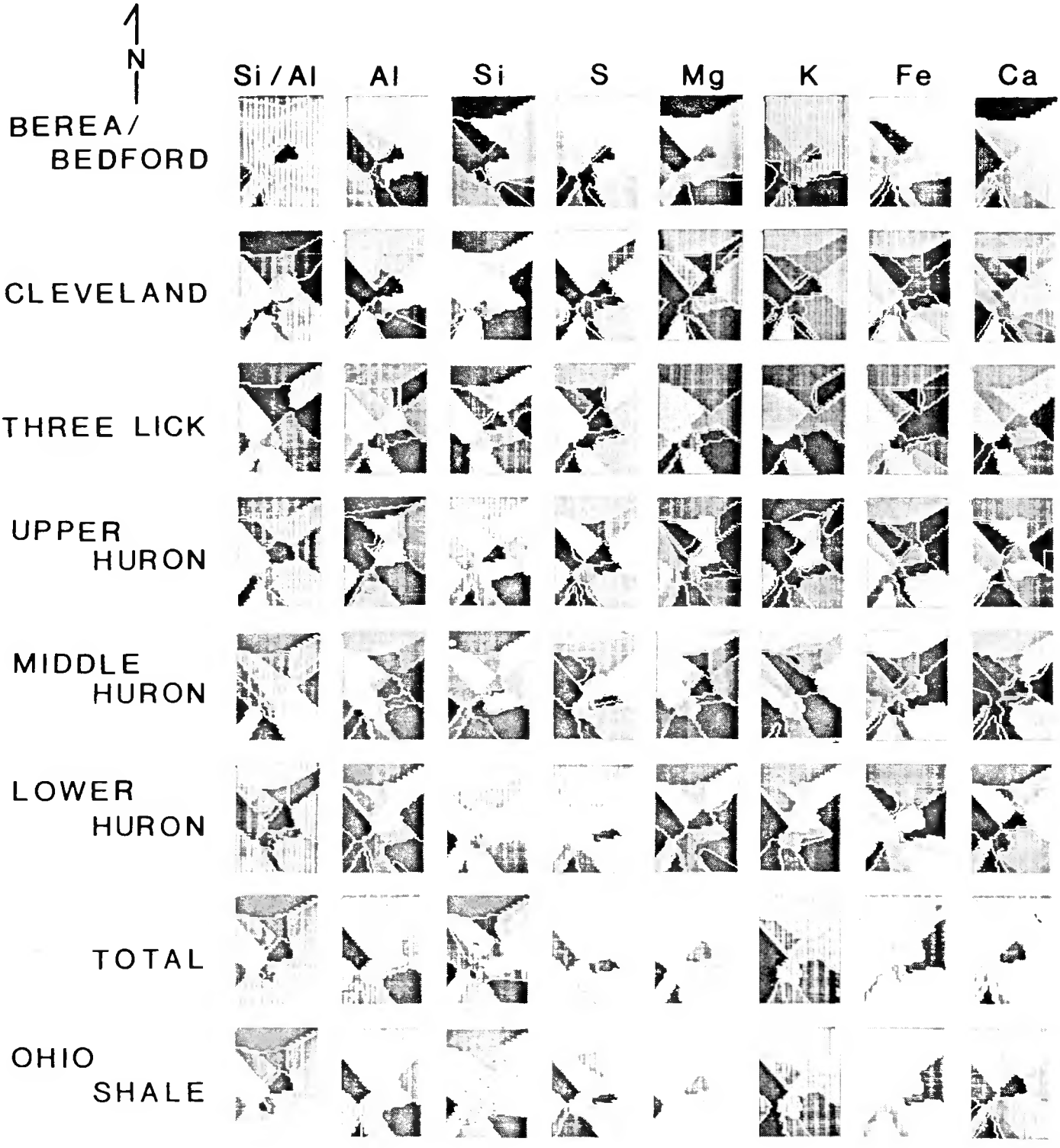


Figure 21 Computer-drawn map for %Si oxide for the Three Lick unit. Highest concentration are the darkest (center and southwest) with second highest to the north-northwest and east central. Lowest areas of concentration are the lightest (west central, northeast, and south central).



*All elements in oxides except Sulfur

Chart of
COMPUTER DRAWN MAPS
Eastern Kentucky Gas Field

J.Negus deWys July, 1979

Figure 22

Computer-drawn maps for Si/Al oxide ratio, Al oxide, Si oxide, Sulfur, Mg oxide, K oxide, Fe oxide, and Ca oxide arranged in a table with stratigraphic units and sequences represented.

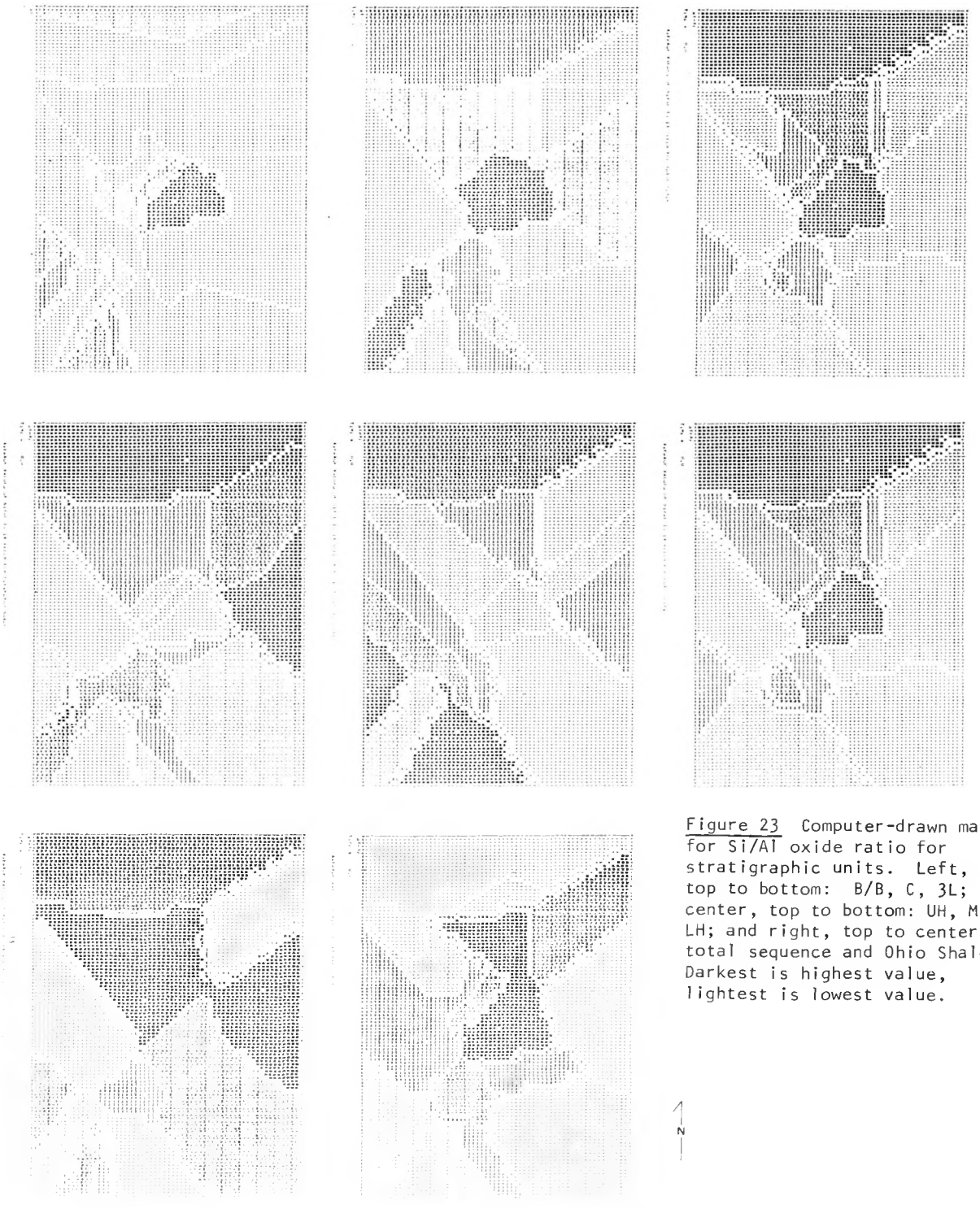


Figure 23 Computer-drawn maps for Si/Al oxide ratio for stratigraphic units. Left, top to bottom: B/B, C, 3L; center, top to bottom: UH, MH, LH; and right, top to center: total sequence and Ohio Shale. Darkest is highest value, lightest is lowest value.

SIMPLE STATISTICS FOR MINERAL DATA

VARIABLE	Percent Total Integrated Intensity*			Variance	Coefficient of Variance
	Minimum	Maximum	Mean		
ILLITE	0.0	91.4	52.3	189.2	26.308
CHLORITE	0.0	1.9	0.7	0.1	50.586
QUARTZ	4.0	83.3	33.7	119.6	31.085
KAOLINITE	0.0	13.0	0.5	3.2	374.000
SZOMOLNOKITE	0.0	2.2	0.0	0.1	664.617
CALCITE	0.0	68.9	1.3	42.9	522.579
ORTHOCLASE	0.0	2.0	0.0	0.0	469.630
ANHYDRITE	0.0	1.1	0.1	0.1	277.298
PLAGIOCLASE	0.0	2.7	0.9	0.2	42.371
BASSANITE	0.0	4.0	1.9	0.5	36.698
DOLOMITE	0.0	70.5	1.7	67.1	475.066
SIDERITE	0.0	17.5	2.2	2.6	72.945
PYRITE	0.0	13.1	4.8	15.6	49.622
RATIO 1	0.0	100.0	1.3	42.8	515.179
RATIO 2				717.6	34.045
RATIO 3	0.0	100.0	78.7	585.3	267.249
RATIO 4	0.0	100.0	9.1		
RATIO 5					

*May be considered numerically equivalent to weight percent

Figure 24 Table of Simple Statistics for Minerals and Mineral Ratios analyzed.

CHEMICAL FORMULAS FOR MINERALS

ILLITE	$(H_30,K)_y$ $(Al_4 \cdot Fe_4 \cdot Mg_6)$ $(Si_8 - Aly)$ $0_{20}(OH)_4$
	where y <2, usually y =1-1.5
CHLORITE	$(Mg, Fe^{+2}, F^{+3})_6AlSi_30_{10}(OH)_8$
QUARTZ	SiO_2
KAOLINITE	$Al_2Si_2O_5(OH)_4$
SZOMOLNOKITE	$FeSO_4 \cdot H_2O$
CALCITE	$CaCO_3$
ORTHOCLASE	$KAlSi_3O_8$
ANHYDRITE	$CaSO_4$
PLAGIOCLASE	$(Na, Ca)Al(Si,Al)Si_2O_8$
BASSANITE	$CaSO_4 \cdot 1/2H_20$
DOLOMITE	$CaMg(CO_3)_2$
SIDERITE	$FeCO_3$
PYRITE	FeS_2

Figure 25 Chemical formulas for minerals analyzed.

RATIO DEFINITIONS

RATIO 1 $$\frac{\text{KAOLINITE}}{\text{KAOLINITE + ILLITE}}$$

RATIO 2 $$\frac{\text{QUARTZ}}{\text{QUARTZ + KAOLINITE + ILLITE + CHLORITE}}$$

RATIO 3 $$\frac{\text{SIDERITE}}{\text{CALCITE + DOLOMITE + SIDERITE}}$$

RATIO 4 $$\frac{\text{CALCITE}}{\text{CALCITE + DOLOMITE}}$$

RATIO 5 $$\frac{\text{CHLORITE}}{\text{CHLORITE + KAOLINITE}}$$

Figure 26 Ratio definitions.

	RATIO	ENVIRONMENT	RATIO MEANING
1.	$\frac{Ka}{Ka + Ill}$	>Ka = fresh water >Ill = marine or alkaline influence	>Ratio - fresher water <Ratio marine alkaline
2.	$\frac{Q}{Q + Ka + Ill + Chl}$	>Q = clastic source	>Q >Ratio >Ratio - closer to clastic source
3.	$\frac{Sid}{Cal + Dol + Sid}$	>Sid = fresh water	>Ratio - fresher water
4.	$\frac{Cal}{Cal + Dol}$	>Dol = near shore evaporative environment	<Ratio - near shore evaporative environment
5.	$\frac{Chl}{Chl + Ka}$	Chl = marine indicator	>Ratio - more marine

Figure 27 Interpretation of Ratios.



Figure 28 Computer-drawn map of Ratio 1.

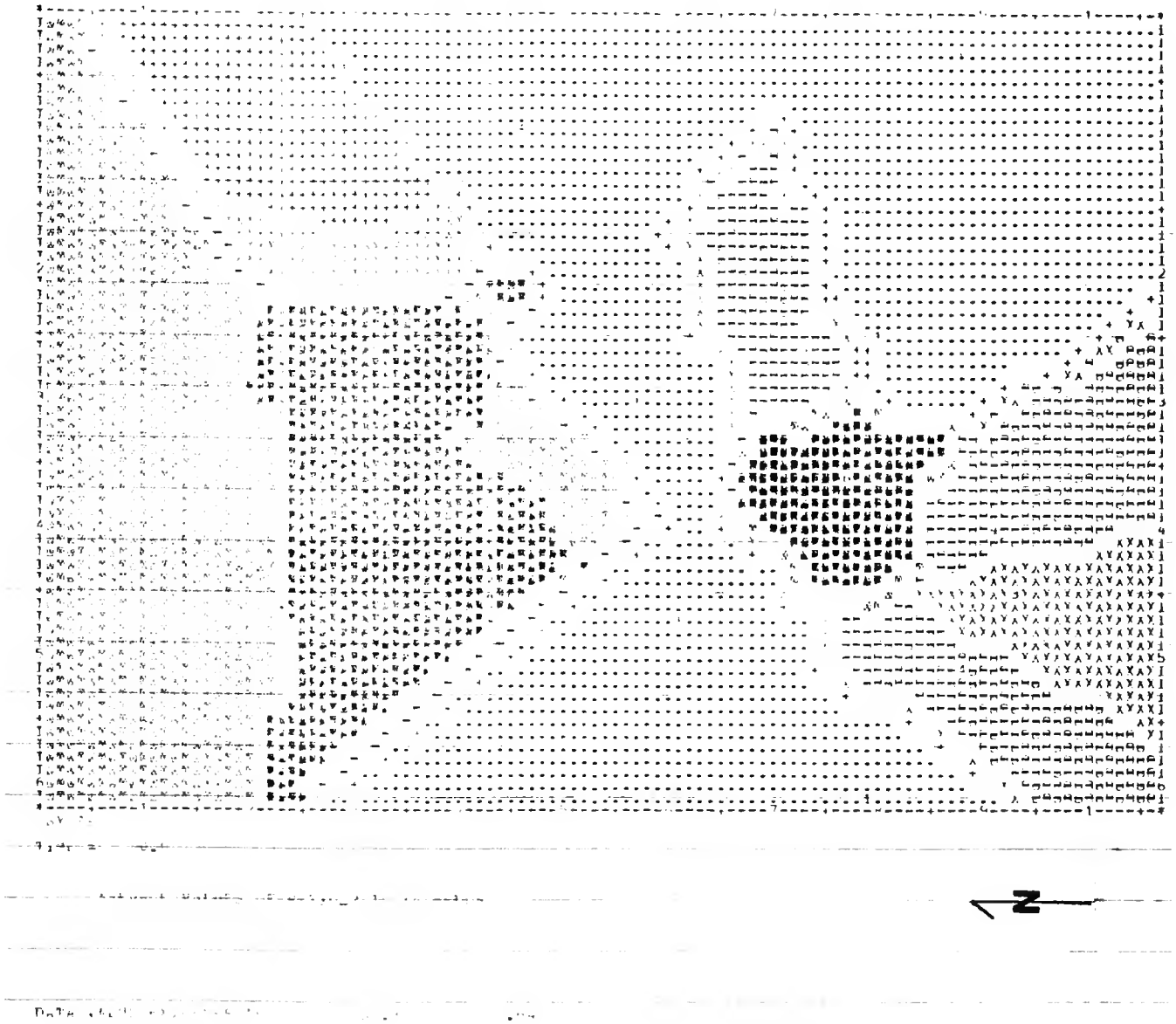


Figure 29 Computer-drawn map of Ratio 2.



Figure 30 Computer-drawn map of Ratio 3.



Figure 31 Computer-drawn map of Ratio 4.

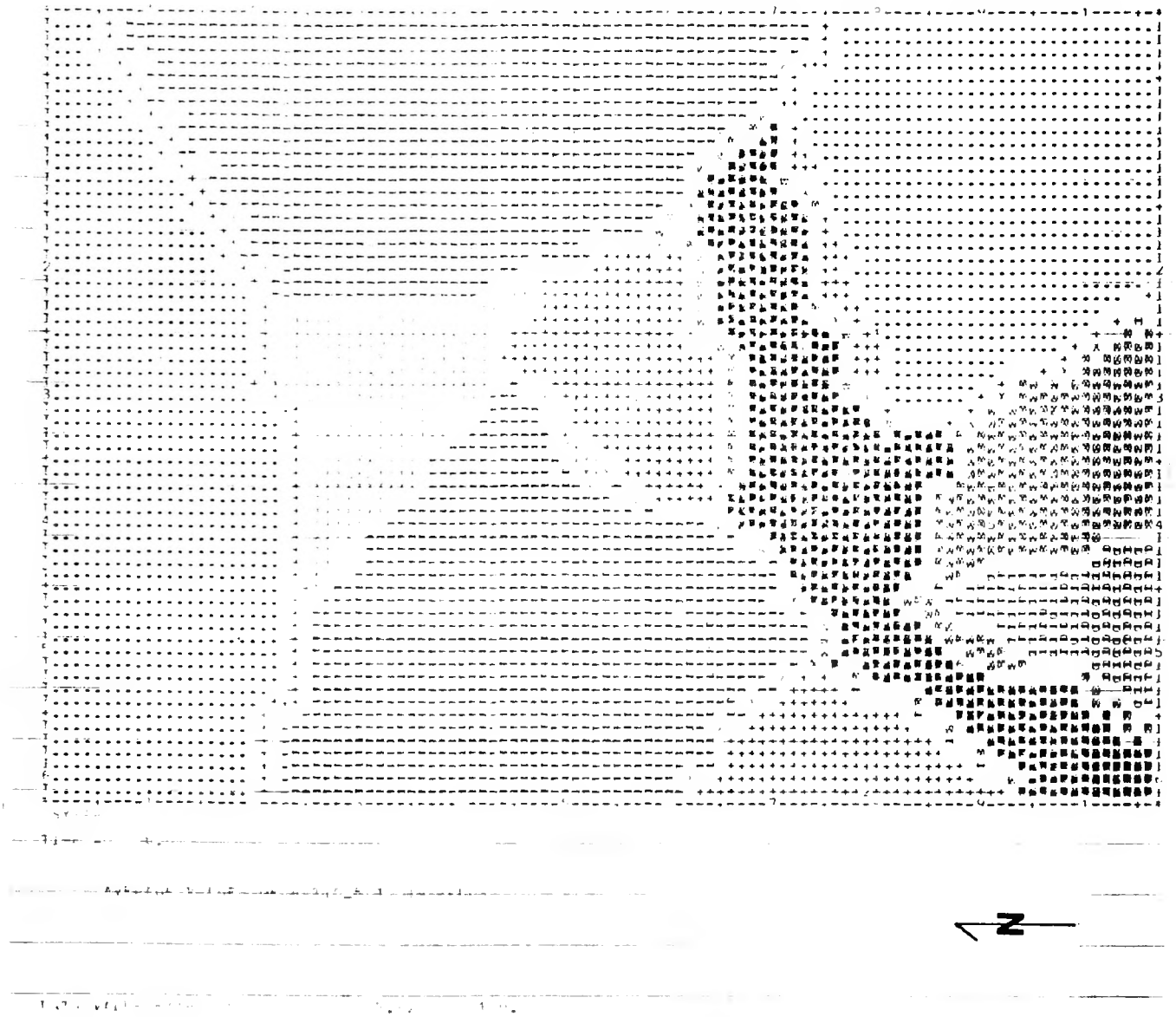


Figure 32 Computer-drawn map of Ratio 5.

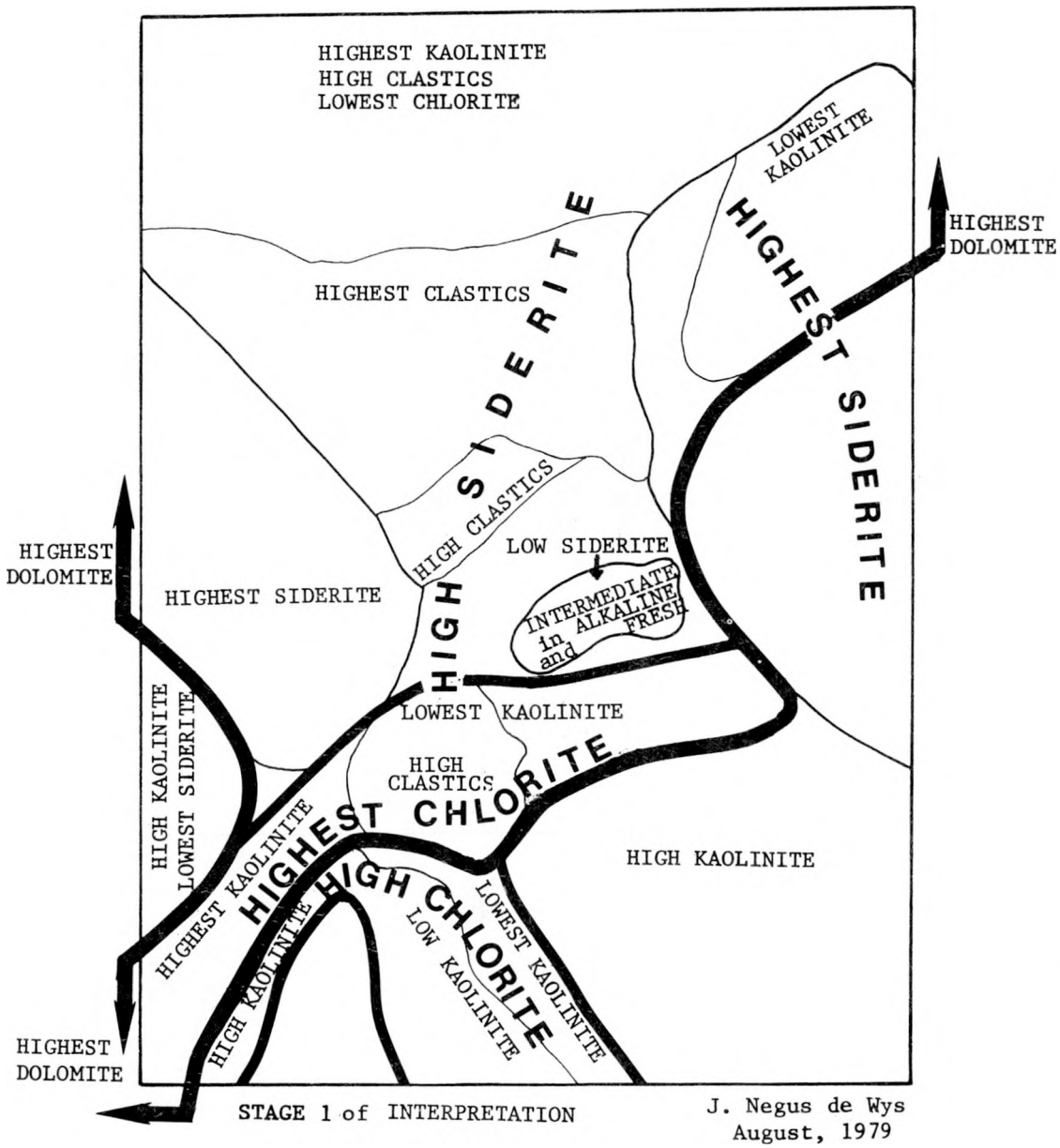
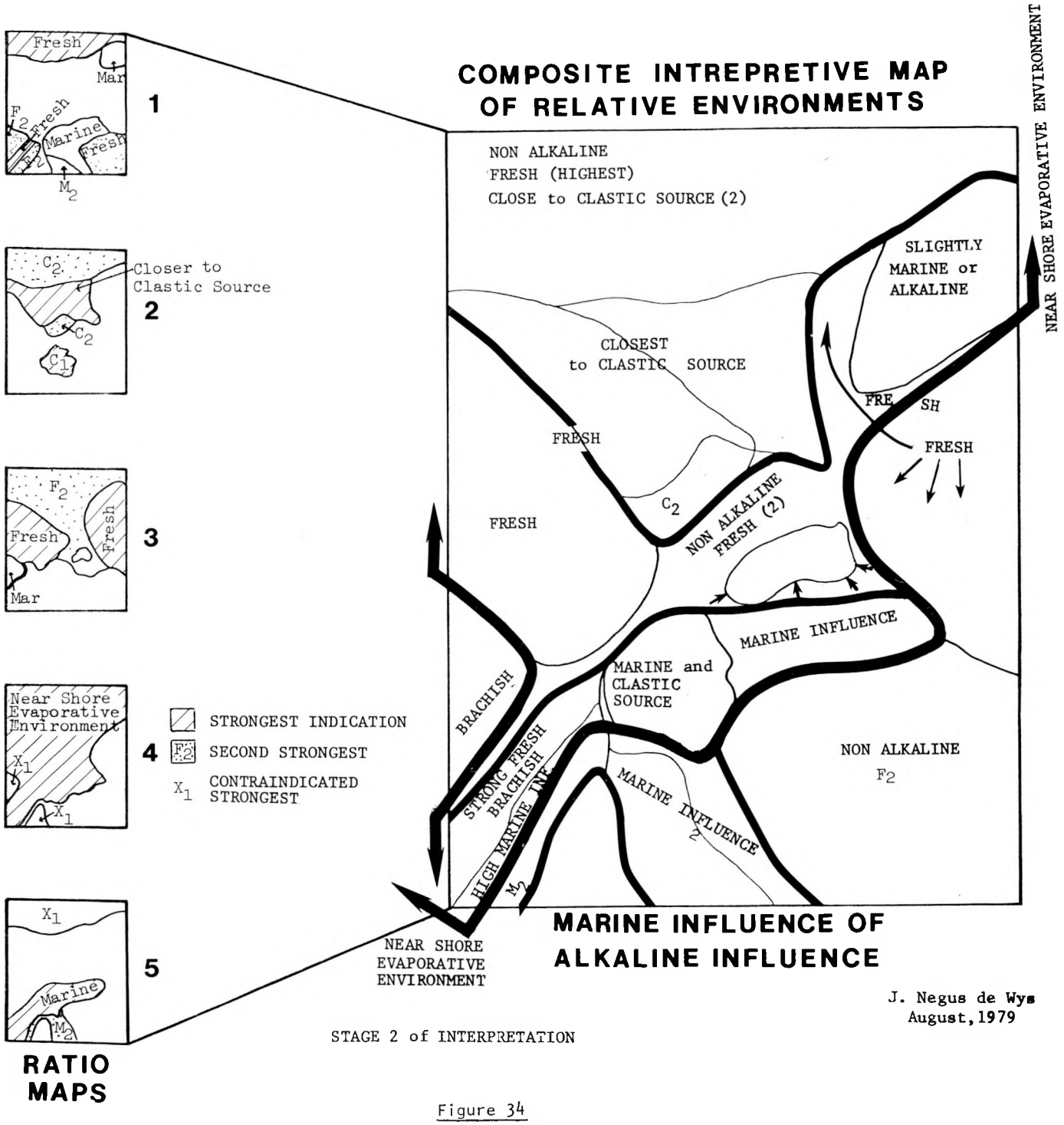

HIGHEST KAOLINITE
HIGH CLASTICS
LOWEST CHLORITE
LOWEST KAOLINITE
HIGHEST DOLOMITE
HIGHEST CLASTICS
HIGHEST SIDERITE
HIGH SIDERITE
HIGH CLASTICS
LOW SIDERITE
HIGHEST DOLOMITE
HIGHEST SIDERITE
INTERMEDIATE in ALKALINE and FRESH
HIGH KAOLINITE LOWEST SIDERITE
LOWEST KAOLINITE
HIGH CLASTICS
HIGHEST CHLORITE
HIGHEST KAOLINITE
HIGH KAOLINITE
HIGH CHLORITE
LOW KAOLINITE
LOWEST KAOLINITE
HIGH KAOLINITE
HIGHEST DOLOMITE
STAGE 1 of INTERPRETATION
J. Negus de Wys
August, 1979

Figure 33



STAGE 2 of INTERPRETATION

Figure 34

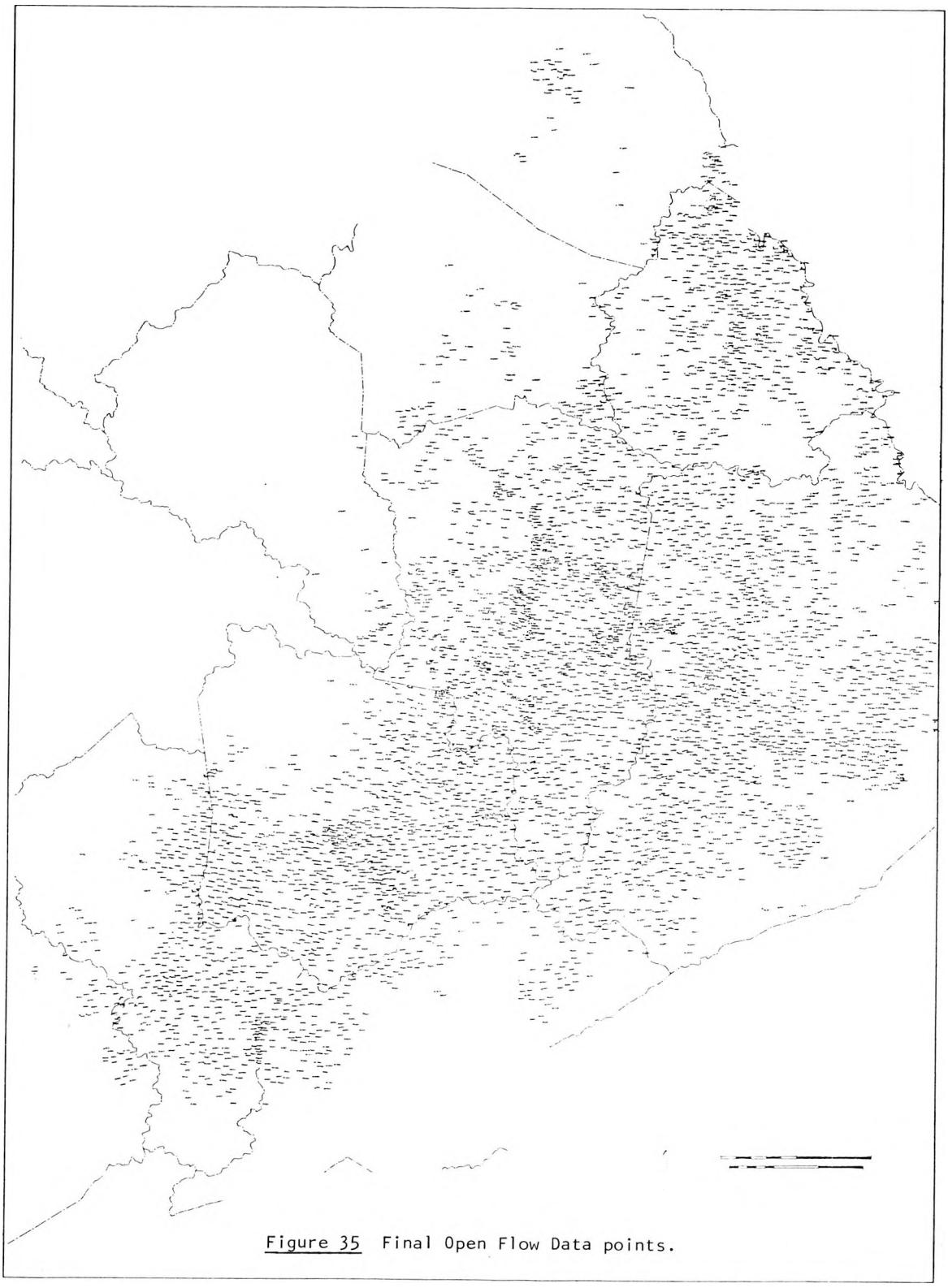


Figure 35 Final Open Flow Data points.

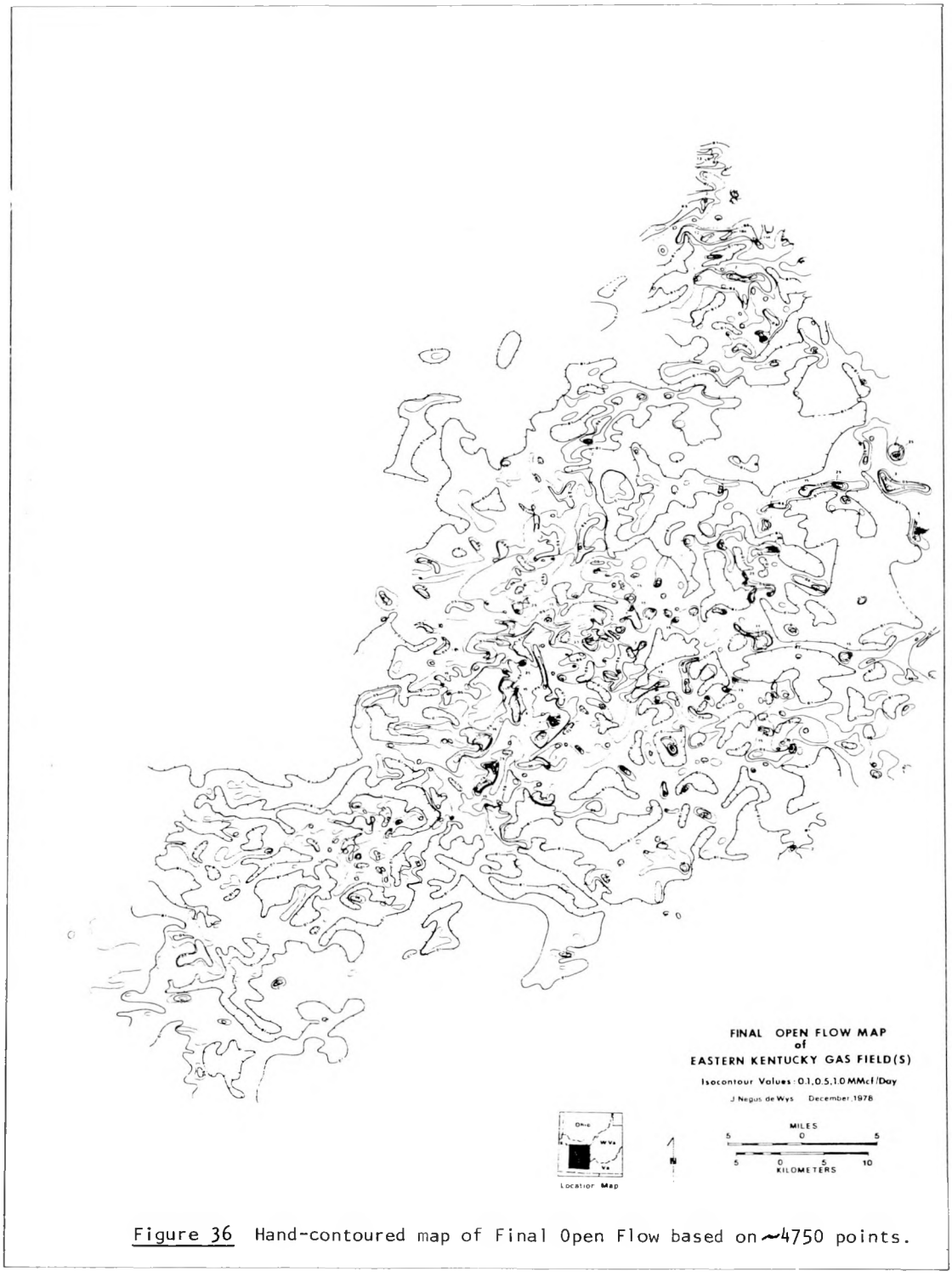


Figure 36 Hand-contoured map of Final Open Flow based on ~4750 points.



TREND SURFACE ANALYSIS, 4th order polynomial. Contour level = 0.05 MMcf/day, contour increment = 0.05 MMcf/day.

Key

etc
3
2
1 } >.05 increasing

. datum .05

A
B
C } <.05 decreasing
etc

Figure 37 Trend Surface Analysis (4th order polynomial) of ~4000 Final Open Flow data points.

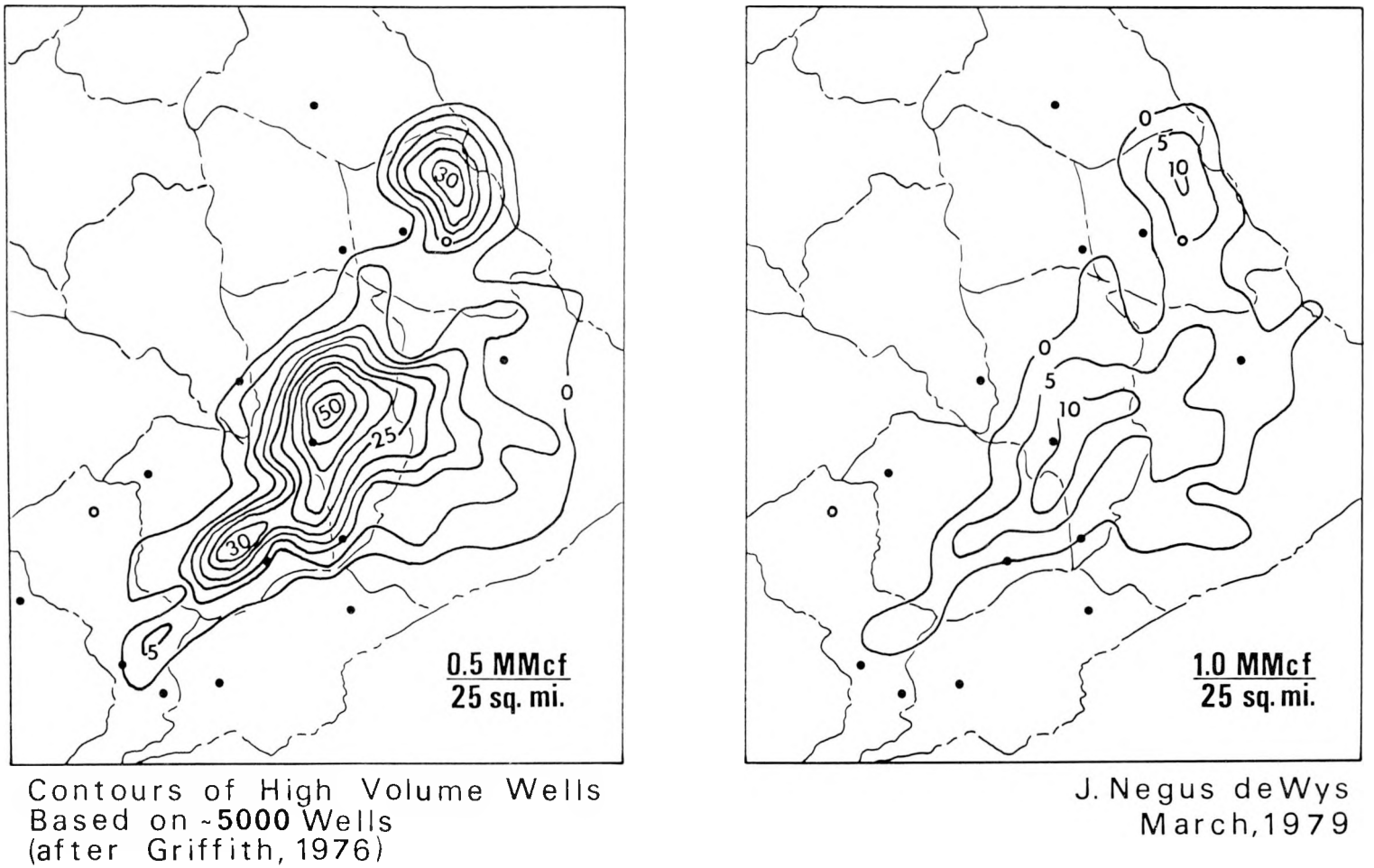
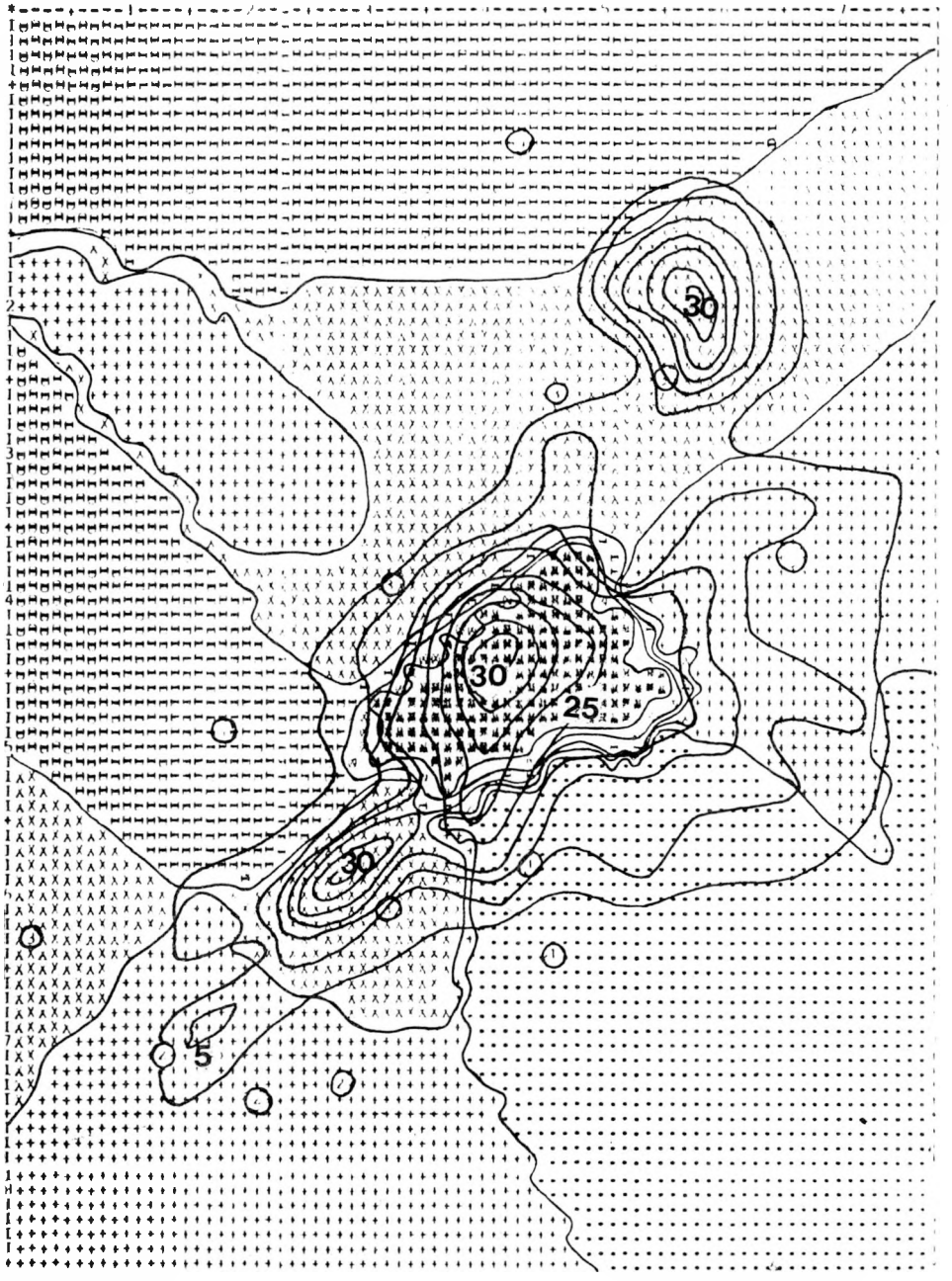


Figure 38 Isolines of density of high producing wells: left - >.5 MMcf/day/25 square miles, and
right - > 1 MMcf/day/25 square miles (after Griffith, 1976).

Si/Al



(GRIFFITH, 1976-77)

0.5/25 sq. mi.

CONTOUR OF HIGH VOLUME WELLS

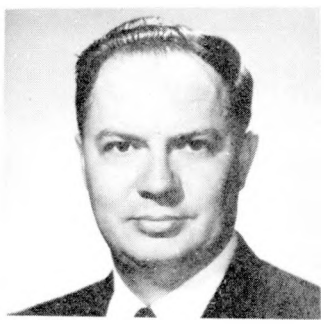
Figure 39 Comparison of Si/Al oxide ratio map with density of high producing wells.

PYROLYSIS OF EASTERN GAS SHALE-EFFECTS OF TEMPERATURE AND ATMOSPHERE ON THE PRODUCTION OF LIGHT HYDROCARBONS

Mei-In Melissa Chou and Donald R. Dickerson

Illinois State Geological Survey, Urban, IL 61808





ABOUT THE AUTHORS

Mei-In M. Chou received her B.S. in chemistry at National Taiwan Normal University and her Ph.D. in organometallic chemistry from Michigan State University (1977). Currently she is employed by the Illinois State Geological Survey as Research Associate. She is conducting part of U.S. DOE granted projects "Characterization of Chemical and Physical Properties of Hydrocarbon-bearing Eastern U.S. Shales" and "Characterization of Coal and Coal Residues". Experienced in organic and organometallic chemistry, she is specializing in high vacuum system, atmosphere controlling reaction technique, simple hydrocarbon gas analysis, organic synthesis, transition metal catalysis reaction, and instrumental and method development on the analysis of chemical composition in shale and coal.

Donald R. Dickerson received his B.S. and M.S. degrees in Chemistry and his Ph.D. in Food Chemistry from the University of Illinois. He has had experience as a microanalyst in a commercial microanalytical laboratory. He has been employed at the Illinois State Geological Survey for 26 years, first as an organic microanalytical chemist and later as a research chemist in the synthesis of organic fluorine containing compounds. For the past 10 years, he has been doing research and is the author of several publications dealing with the organic chemistry of petroleum and coal. He is a member of the American Chemical Society and the Illinois State Academy of Science. He has held a number of council offices in the Illinois State Academy of Science and is presently serving as president of the Academy.

ABSTRACT

Samples of black shale from four cores of the New Albany Shale Group (Devonian-Mississippian) from the Illinois Basin in Kentucky and Illinois were used in this study. Sections measuring 4 inches (9 cm) in length were taken from the 4-inch (9-cm) diameter cores and were sealed in canisters for study of released gas. Following the study of released gas, the shale was crushed to <100 mesh for use in the study of the effects of temperature and atmosphere on the pyrolysis of shale.

The correlation coefficients between the quantity of gas released at room temperature from the "canistered" core sections and the organic carbon content, and between the gas released and the total porosity of the shale samples were calculated for the individual cores. The coefficients for the quantity of gas released and the organic carbon content of the four cores were 0.7018(06IL), 0.0023(02IL), 0.8034(04IL), and 0.7531(01KY).

A study was made of the gaseous hydrocarbons produced by pyrolysis of shale at 600°C. Two regression lines could be drawn on the graph of the hydrocarbon gas produced versus the original organic carbon content, one (r^2=0.96) fitting data points for the Illinois cores and the other (r^2=0.92) fitting data points for the Kentucky core.

The composition of the noncondensable hydrocarbon gases produced by heating selected black shale samples at four different temperatures was studied. The formation of alkanes was favored over that of alkenes, particularly at low temperature. Methane, ethane, and ethylene from thermal cracking and higher carbon number alkenes were positively identified in the gases from shale heated to above 120°C.

A study was made of the effect of the pyrolysis atmosphere on the yield of light hydrocarbons (C_1 to C_8), carbon dioxide, carbon monoxide, acetaldehyde, and acetone during thermal degradation of a gram amount of selected shale samples. The effect of various amounts of oxygen in the pyrolysis atmosphere was monitored. The yield of an individual hydrocarbon generally increased with the increase in the oxygen content of the pyrolysis atmosphere until the oxygen content reached the 10 percent level; when the oxygen content was increased above 10 percent, there was a decrease in yield. The yield of carbon dioxide and carbon monoxide increased with the increase in oxygen content of the pyrolysis atmosphere.

Results reported in this study may increase the ability to predict the potential for production of gas from the black shale in the New Albany Group. The study may also provide information useful for improving the quality of the gas produced by pyrolysis of shale.

INTRODUCTION

As part of the Eastern Gas Shale Project of the U.S. Department of Energy, the Illinois State Geological Survey (ISGS) is conducting a number of geologic and geochemical studies[1] of the New Albany Shale Group (Devonian-Mississippian) in the Illinois Basin to evaluate its potential as a source of hydrocarbons. The amount of volatile materials in the shale, their origin, and their continuous formation are of considerable interest with regard to the history and current alteration of shale formation. The present study was undertaken in order to determine the relationships between the light hydrocarbons (C_1 to C_5) released from the shale and the organic carbon content, the pyrolysis temperature, and the molecular oxygen content of the pyrolysis atmosphere. Through observation of the changes—changes that occur when conditions for pyrolysis are changed—in the amounts of CO_2, CO, CH_3CHO, CH_3COCH_3, alkanes, alkenes, and in the alkane to alkene ratios, an insight may be gained into the oxidative processes taking place in the shale during pyrolysis.

EXPERIMENTAL PROCEDURE

Gas released from shale at room temperature

The quantity and composition of gas released at room temperature from specially canned core sections were measured. Ten of the core sections were from drill holes in Christian County, Kentucky (01KY); nine from Effingham County, Illinois (02IL), twenty-nine from Henderson County, Illinois (04IL), and twenty-five from Tazewell County, Illinois (06IL). The locations of these holes are shown in figure 1.

The shale core sample (approximately 4 inches (9 cm) in height and 4 inches (9 cm) in diameter) was sealed in a 2800-mL aluminum resealable canister as soon as possible after the core had been brought to the surface and the sample cut. Each canister was equipped with a rubber septum-sealed valve. The canistered samples were stored in a room with a constant temperature of 21°C for approxi-

mately 3 to 4 months. Hydrocarbons that had been formed by natural processes, e.g., by microbial degradation of organic matter, and had remained trapped in the shale until the core was cut were released to the headspace of the canister. The pressure inside the canisters was monitored periodically with a mercury manometer. The gas yield was calculated from the volume of the canister headspace and the pressure of the gas. The composition of the gases was determined with a Beckman GC-4 gas chromatograph equipped with a hot wire detector and a flame ionization detector. A CTR column (Alltech Associates, Inc.), with the injector at 100°C, and temperature programmed from 60° to 180°C at 16°C/min was used with the hot-wire detector at 185°C. A Chromosorb 102 column with the injector at 100°C and temperature programmed from 50° to 150°C at 16°C/min was used with the flame-ionization detector at 175°C.

Yield of gaseous hydrocarbons (C_1 to C_5) from pyrolysis of shale

Thirty shale samples were studied. Eight of the samples were from the core from Christian County, Kentucky, six were from Effingham County, eight were from Henderson County, and eight were from Tazewell County, Illinois.

A 250-mg sample of pulverized shale (<100 mesh) was weighed into a custom-made pyrex tube (7 in. x 0.7 in. ID). The tube was sealed with a rubber serum cap secured with a wire band. The sample was degassed with a small hypodermic needle, and the tube was then placed in a pre-heated (600°C) electric tube furnace for 5 minutes. A known amount of pure cyclopropane was injected into each sample tube for use as an internal standard. The gases that were noncondensable at 29 ± 1°C were sampled from the headspace and analyzed on a Perkin-Elmer 3920B gas chromatograph equipped with a flame ionization detector and interfaced with a Perkin-Elmer Sigma 10 data system. A stainless steel column (6 ft x .125 in. [2M x 3 mm ID]) packed with Chromosorb 102 (80/100 mesh) was used. The inlet and detector temperatures were 200° and 250°C, respectively, and the column temperature was programmed from 40°C to 180°C at 8°C/min and was held at the upper temperature for 8 minutes. The flow of helium carrier gas was 20 mL/min.

A blank was run to be certain that all the gas in the tube came from the shale. A small amount, however, may have come from indigenous gas trapped in the pore structure of the shale. Figure 2 shows the gas chromatogram of a representative gas sample separated on the Chromosorb 102 column. The yield of pyrolysis products was determined by integration of the chromatograms and was calculated by using the Sigma 10 data system.

Effect of temperature on the pyrolysis of shale

A shale sample taken from a section of the drill hole in Christian County, Kentucky, which was 2182 to 2249 ft below the surface, was used in this study.

The temperatures selected for pyrolysis were 60°, 145°, 300°, and 450°C. Small portions (0.5 to 1 g) of pulverized shale sample (<100 mesh) were weighed into pyrex tubes. Each tube was sealed with a rubber serum cap secured with a wire band as previously described.

A silicon oil bath was used to heat the samples to 60° and 145°C, and an electric furnace was employed for higher temperatures. The heating time was always 18 hours. The gas compositions were analyzed by gas chromatography using a Chromosorb 102 column and were checked with a Carbopack C/ 0.2 percent CW 1500 column; operating conditions were the same as described in the preceding section. Figure 3 shows a typical GC trace of a gas sample separated on the Carbopack C/ 0.2 percent CW 1500 column.

Effect of molecular oxygen on the pyrolysis of shales

A shale sample taken from the core from the drill hole in Effingham County, Illinois, at 3,053 ft below the surface was used in this study.

One-gram amounts of samples of pulverized shale were weighed into pyrex tubes and sealed as described above. The bulk of the air in the sample tube was exchanged for a gas mixture of known composition by evacuating the tube and filling it with oxygen and nitrogen in the desired proportions. The percentage of oxygen in the sample tube was checked by gas chromatography before pyrolysis.

All samples were pyrolyzed at 450°C for 15 minutes. The headspace gases, with an added internal standard, were measured by gas chromatography on both a Chromosorb 102 and a Carbopack C/

0.2 percent CW 1500 column. The operating conditions were as described previously. A 5A Molecular Sieve column was also used for separation of the hydrocarbons and the products of oxidation. Conditions for the chromatography were: injection port at 200°C; column oven with initial hold of 3 minutes at 40°C and then programmed from 40° to 260°C at 20°C/min and held at 260°C for 10 minutes; hot wire detector at 300°C; helium carrier gas at 30 mL/min flow rate. The identification of the components of the gas was confirmed by GC-MS analysis.

RESULTS AND DISCUSSION

Gas released from shale at room temperature

For the four cores studied, correlation coefficients were calculated for the relationship of the quantity of gas released from the "canistered" core sections at room temperature to the organic carbon content and total porosity of the shale. The correlation coefficients (r^2) of the organic carbon content with the quantity of gas released, for the four cores, were 0.70(06IL), 0.002(02IL), 0.80(04IL), and 0.75(01KY). The Illinois State Geological Survey made porosity measurements (at 100°C) on some of the 77 samples, and the results have been reported elsewhere[2] (see table 1). The correlation coefficients between the porosity and the released gas for the four cores were 0.19, 0.30, 0.16, and 0.02, respectively. The amount of gas released from shale at room temperature did not appear to be related to the porosity of the shale.

For the Effingham County core (02IL), there is considerable scatter to the points in the plot of the data for the released gas yield versus the organic carbon content (fig. 4). This may be explained in part by the fact that in this area the black shale overlies an oil pool. The composition of the gas released from the shale was essentially identical to that of the gas released from a producing oil well nearby. This indicates that most of the gas migrated into the shale rather than being indigenous to it.

There was good correlation between the amount of gas released and the organic carbon content for the other three cores; however, the correlation was not as good as that between the organic carbon content and the gas released upon pyrolysis of the shales, as established in the next section of results. The poorer correlation between indigenous volatile material and organic carbon content may be due, in part, to the fact that the amount of gas in the core is a function not only of the amount of gas formed over geologic time periods, but also of the amount that remained trapped in the shale. It is also possible that the trapped gases may have originated elsewhere and migrated into the shale in question. Other geologic factors may be operative as well.

The correlation of the gas released with the organic carbon content and the lack of correlation between the gas released and the porosity is in agreement with the findings of Kalyoncu et al.[3] and Snyder et al.[4]

Yield of gaseous hydrocarbons (C_1 to C_5) from pyrolysis of shales

The relationship of the gas yield from the pyrolysis of shale at 600°C with the organic carbon content of shales is shown in figure 5. There is a direct correlation between the gaseous hydrocarbon yield and the organic carbon content. Despite some scatter of data points, two regression lines can be drawn through the points in figure 5. One (r^2=0.96) closely fits data points for Illinois drilling hole cores and the other (r^2=0.92) follows data points for the Kentucky drill hole core only. For all data points the correlation coefficient (r^2) is 0.86. The reason that the Kentucky core produced more hydrocarbon gas than the Illinois cores per unit of organic carbon content has not been accounted for. A difference in the nature of the organic matter or the existence of a special mineral-surface catalytic reaction may be the cause. Of these four drilling holes, only the one in Kentucky appeared to have the potential to be an economical gas-producing well.

Effect of temperature on the pyrolysis of shale

Samples of shale from the core from a drilling hole in Christian County, Kentucky, were pyrolyzed at 60°, 145°, 300°, and 450°C for 18 hours. The long pyrolysis time was chosen in order to accumulate a sufficient amount of gas for analysis at a comparatively low temperature (60°C). Pyrolyses over an eighteen-hour period could not be carried out at temperatures higher than 450°C because of possible damage to the rubber septum seal. The average values of the relative hydrocarbon yields from several determinations at each temperature are presented in table 2. Typical GC traces obtained at 60° and at 300°C are shown in figure 6. At 60°C the hydrocarbon products were mostly alkanes; alkenes were in trace amounts only. The yields of C_1 and C_2 hydrocarbons from thermal cracking and of higher carbon number alkenes are substantially increased as the temperature of

pyrolysis is raised to 300°C. The alkane/alkene ratios for C_2 to C_5 hydrocarbons as a function of pyrolysis temperature are shown in figure 7. The ratios for C_2, C_3, C_4, and C_5 hydrocarbons show that conditions for the formation of these alkenes are more favorable at high temperatures[3].

The total yield of gases (C_1 to C_5) increases fairly rapidly as the temperature of pyrolysis is increased (fig. 8). The increase in yield is dramatic at a pyrolysis temperature of 450°C.

The trends observed in this study can be related to the trends observed in the study of the effects of molecular oxygen on pyrolysis (see fig. 9). The data may also provide information on the type of hydrocarbons that exist in the shale.

Effect of molecular oxygen on the pyrolysis of shale

The yields of products obtained from heating shale at 450°C for 15 minutes with various percentages of oxygen in the pyrolysis atmosphere are presented in table 3. The products are comprised of C_1 to C_8 hydrocarbons and include CH_3COCH_3, CH_3CHO, CO, and CO_2. The yield of each hydrocarbon generally increases with an increase in oxygen content of the pyrolysis atmosphere until the oxygen content reaches 10 percent.

Figure 9 shows the ratio of alkanes to alkenes produced for carbon numbers 2 through 6, as a function of the oxygen content in the pyrolysis atmosphere. The plot of the alkane to alkene ratio for C_2 shows that the alkene formation becomes relatively more favorable as the oxygen content increases. For C_3, C_4 C_5, and C_6, alkene formation becomes only slightly more favorable relatively, as the oxygen content becomes higher in the pyrolysis atmosphere.

The higher oxygen levels will result in higher surface temperature because of oxidation. Thus an effect of oxygen is to lower the pyrolysis temperature at which the maximum level of evolution of organic gases occurs. Whether the trends in yields observed are the same at different temperatures is under investigation. Information concerning the effect of controlling both the temperature and the quantity of molecular oxygen on the pyrolysis of shale should prove very helpful for optimizing shale retorting operations.

The yields of CO_2, CO, CH_3CHO, and CH_3COCH_3 as a function of the oxygen content of the pyrolysis atmosphere are given in figure 10. The yields of CO_2, CO, and CH_3COCH_3 increase significantly as the percentage of oxygen increases in the pyrolysis atmosphere.

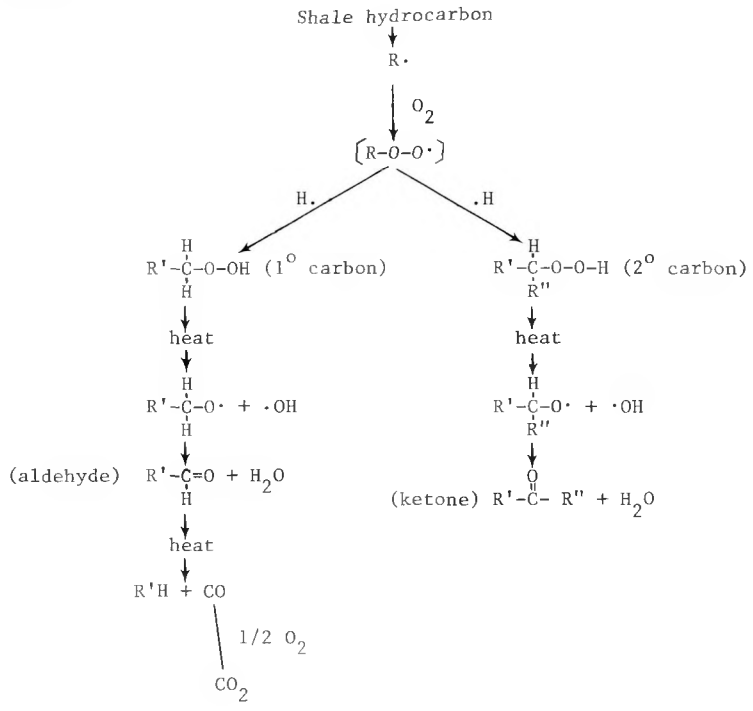
Many details of the complex reaction involved in the oxidation of hydrocarbons by moleuclar oxygen have not yet been elucidated. It is commonly accepted that a chain mechanism is operative[5,6] and that one of the first products formed is a hydroperoxide that may be oxidized further or decomposed thermally, thereby to initiate new chains. It is also known that these intermediates are responsible for the increased yield of oxygenated compounds in the thermolysis of hydrocarbons in higher oxygen concentrations.[5,6] Most likely, oxidation proceeds by the pathways shown on the diagram at the top of the next page. In the initial reaction hydroperoxide radicals are formed by combination of the organic free radicals (formed by thermolysis from shale hydrocarbons) and molecular oxygen, and further thermolysis reactions produce aldehyde and ketone molecules.

CONCLUSIONS

Our study of the gas released from shale at ambient temperature shows that the amount of gas released is highly dependent on the organic carbon content and is not limited by the porosity of the shale. For the shales studied, the organic carbon content of a given shale appears to be a much better indicator of the potential for gas production from shale than does porosity data. There may be other geological factors, however, that play an important role in the production of gas from shale.

About twenty times more gas was produced from the shale by high temperature pyrolysis than was obtained by natural release at ambient temperature. The yield of hydrocarbons in pyrolysis showed a higher degree of dependence on the organic carbon content of a given shale than was found for ambient temperature gas release. This may be true, in part, because the gas produced by pyrolysis was not affected by geologically controlled factors.

In the study of the effects of temperature on pyrolysis, data showed that the yield of the total quantity of light hydrocarbons (C_1 to C_5) was increased the most for pyrolysis temperatures above 300°C, and the relative proportion of alkene to alkane produced for a given carbon number increased as the pyrolysis temperature was increased. The same trend was observed in the study of



the effect of the presence of molecular oxygen on the pyrolysis of shale. The proportion of alkenes to alkanes that were produced for a given carbon number increased as the oxygen content of the atmosphere was increased; however, except for C_2, the increase in the relative production of alkene to alkane was not very significant. The quantity of any individual hydrocarbon that was produced generally increased as the oxygen content increased in pyrolysis atmosphere until the oxygen content reached 10 percent; thereafter there was a decrease in yield as the process of combustion became more significant. A plot of the effect of oxygen on the formation of CO and CO_2 had a point of inflection at about the 10 percent oxygen level. Possibly, the presence of some molecular oxygen could lower the pyrolysis temperature needed to produce a gas of desired composition. The study of the effect of molecular oxygen at different temperatures of pyrolysis and the determination of gases other than hydrocarbons formed in pyrolysis of shale at different temperatures would be helpful in order to test this conclusion. Moreover this additional study could be used to determine the changes that occur in the composition of the light gases produced from the organic matter in shales as temperature and atmosphere of pyrolysis are varied.

ACKNOWLEDGEMENTS

The authors thank Drs. R. A. Griffin, D. D. Coleman, and J. K. Frost for their helpful suggestions during the preparation of this paper. Appreciation is also expressed to JoAnn Eidsmore for drafting the figures. This research was supported in part by the United States Energy Research and Development Administration under Contract No. DE-AC21-76-MC05203.

REFERENCES

1. Harvey, R. D., W. A. White, R. M. Cluff, J. K. Frost, and P. B. DuMontelle, 1977, Petrology of New Albany Shale Group (Upper Devonian and Kinderhookian) in the Illinois Basin, a preliminary report: First Eastern Gas Shales Symposium, WV, Oct. 17-19, 1977, Morgantown Energy Research Center, EGS-18.

2. Thomas, Josephus, Jr., and Robert R. Frost, 1977, Internal surface area and porosity in eastern gas shales from the sorption of nitrogen, carbon dioxide, and methane—A status report: First Eastern Gas Shale Symposium, WV, Oct. 17-19, 1977, Morgantown Energy Research Center EGS-37.

3. Kalyoncu, R. S., W. G. Coppins, D. T. Hooie, and M. J. Snyder, 1977, Characterization and analysis of Devonian shales: I. Physical characterization: First Eastern Gas Shales Symposium, WV, Oct. 17-19, 1977, Morgantown Energy Research Center, EGS-14.

4. Snyder, M. Jack, M. P. Raush, J. O. Ogden, and R. W. Coutant, 1977, Characterization and analysis of Devonian shales: Gas composition and release rates: First Eastern Gas Shales Symposium, WV, Oct. 17-19, 1977, Morgantown Energy Research Center EGS-34.

5. Sieg, L., [ed.] W. Gordon Jost, 1965, Low temperature oxidation: Breach Science Publishers, New York, 191 p.

6. Allara, D. L., T. Mill, D. G. Hendry, and F. R. Mayo, 1968, Oxidation of organic compounds: Advanced Chemistry Series, v. II, no. 76, 40 p.

TABLE 1

Linear regression analysis on the amount of gas released from shale at room temperature and the porosity of shale.

Core and sample #	Depth to top of sample (ft)	Y Gas released, cu ft/cu ft$_{shale}$	X Porosity (%)	$y = a_2 + bx$ r^2*
06IL-16C1	1053.15	0.0067	11.8	
19C1	1083.20	0.0321	11.3	
20C1	1093.35	0.0277	6.8	0.19
02IL-01C1	3011.4	0.30	7.0	
04C1	3033.0	0.29	4.6	
07C1	3085.5	0.57	7.0	
08C1	3096.5	0.51	6.66	0.30
04IL-10C1	413.5	0.0089	15.7	
20C1	513.4	0.0329	13.4	
29C1	604.5	0.0013	9.1	0.16
01KY-01C1	2182.25	1.47	3.6	
04C1	2230.20	0.39	4.2	
05C1	2240.10	0.76	2.7	
06C1	2250.00	0.09	2.9	0.02
			Overall	0.35

*r^2 = the correlation coefficient

TABLE 2

Relative percentages of hydrocarbons (C_1 to C_5) produced in the pyrolysis of shale from a drill hole at Christian County, Kentucky, at selected temperatures for 18 hours.

	Pyrolysis temperature (°C)			
Composition	60° (%)	145° (%)	300° (%)	450° (%)
methane	1.7	1.8	20.2	18.8
ethylene	-	1.1	7.0	6.6
ethane	0.1	2.0	13.8	15.8
propylene	0.1	1.7	10.7	11.7
propane	12.7	12.9	15.6	15.9
i-butane	5.0	8.7	6.4	3.5
1-butene	-	0.7	3.0	8.0
n-butane	51.0	40.9	16.9	18.2
1-pentene	-	0.3	0.5	0.5
n-pentane	29.4	29.8	6.0	1.4

TABLE 3

Composition of product obtained from heating shale at 450°C for 15 minutes with various percentages of oxygen in the pyrolysis atmoshpere.

Constituent	Yield of hydrocarbons (X 10^{-5} g/g shale) O_2 in pyrolysis atmosphere				
	1.48%	5.1%	10.11%	15.16%	20.0%
methane	78.93	91.60	119.56	81.76	86.29
ethylene	17.96	21.01	27.97	21.66	23.80
ethane	68.20	75.94	92.61	67.42	68.03
propylene	35.86	40.89	50.19	38.73	38.87
propane	47.77	50.84	60.04	45.92	44.77
butenes	22.97	24.77	29.26	23.25	22.15
i-butane	4.00	4.29	5.01	3.86	3.66
n-butane	24.19	26.00	30.04	23.08	21.76
cyclopentane	0.56	0.63	0.65	0.55	0.43
pentenes	11.54	12.72	14.70	10.97	9.90
i-pentane neo-pentane	7.82	8.67	10.40	7.58	6.95
n-pentane	7.45	7.73	8.33	6.44	5.78
cyclohexane methyl-cyclohexane	0.70	0.73	0.62	0.56	0.44
hexenes	3.73	4.00	4.05	3.25	3.05
i-hexane & isomers	3.67	3.81	3.71	3.19	2.93
n-hexane	2.41	2.45	2.44	1.96	1.86
benzene	1.72	1.72	1.71	1.44	1.37
C_7's	5.70	5.62	4.59	6.48	3.75
C_8's	1.98	1.54	0.73	1.05	0.89
acetone	0.41	0.59	1.27	1.57	2.27
CH_3CHO	11.17	14.13	15.86	37.70	33.49
CO	6.03	9.77	37.29	70.09	84.27
CO_2	14.16	21.78	84.05	140.23	161.96
Total	378.93	431.23	605.08	598.74	628.67

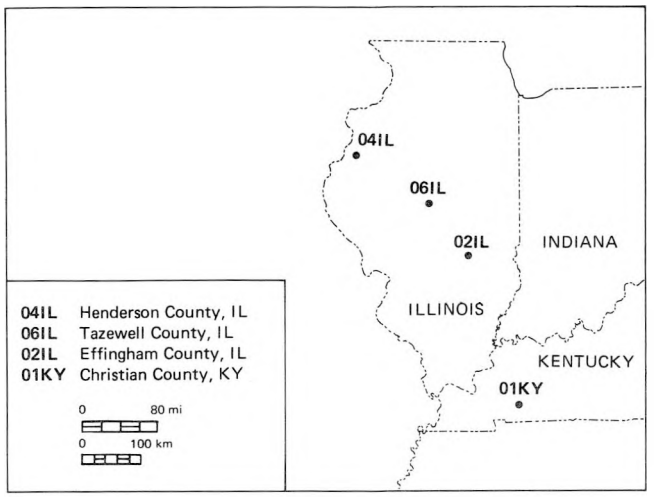


Figure 1. Location of wells.

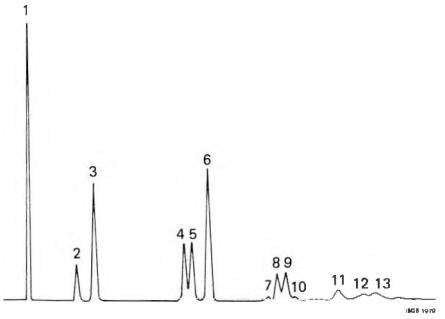


Figure 2. GC trace of light hydrocarbon gases from shale pyrolysis. Column: stainless steel 2m x 3mm I.D. Chromasorb 102. Temperature programmed from 40°C to 180°C (held at 180°C for 8 minutes). Hydrocarbon gases: (1) Methane, (2) Ethylene, (3) Ethane, (4) Propylene, (5) Propane, (6) Cyclopropane (std.), (7) iso-Butane, (8) 1-Butene, (9) Butane, (10) 2-Butenes, (11) Acetone, (12) 1-Pentene, and (13) Pentane.

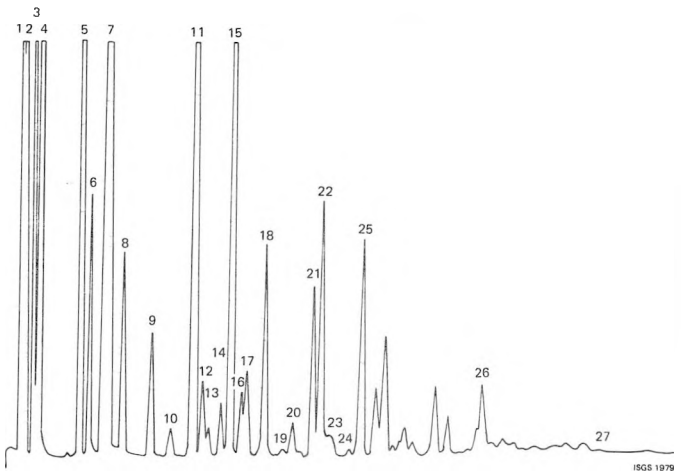


Figure 3. GC trace of light hydrocarbon gases from shale pyrolysis. Column: stainless steel 2m x 3mm I.D. Carbopack C/0.2 percent CW 1500. Temperature programmed from 40°C to 180°C (held at 180°C for 10 minutes). Hydrocarbon gases: (1) Methane, (2) Ethane and Ethylene, (3) Cyclopropane (std.), (4) Propane and propylene, (5) iso-Butane, (6) 1-Butene, (7) n-Butane, (8) Neopentane, (9) Cyclopentane, (10) saturated C_5, (11) iso-Pentane, (12) 1-Pentene, (13) cis-2-Pentene, (14) trans-2-Pentene, (15) n-Pentane, (16) iso-Pentene, (17) Cyclohexane, (18) Methyl-Cyclopentane, (19), (20) saturated iso-Hexane isomers, (21) iso-Hexane, (22) Benzene, (23) 1-Hexene, (24) trans-2-Hexene, (25) n-Hexane, (26) n-Heptane, and (27) n-Octane.

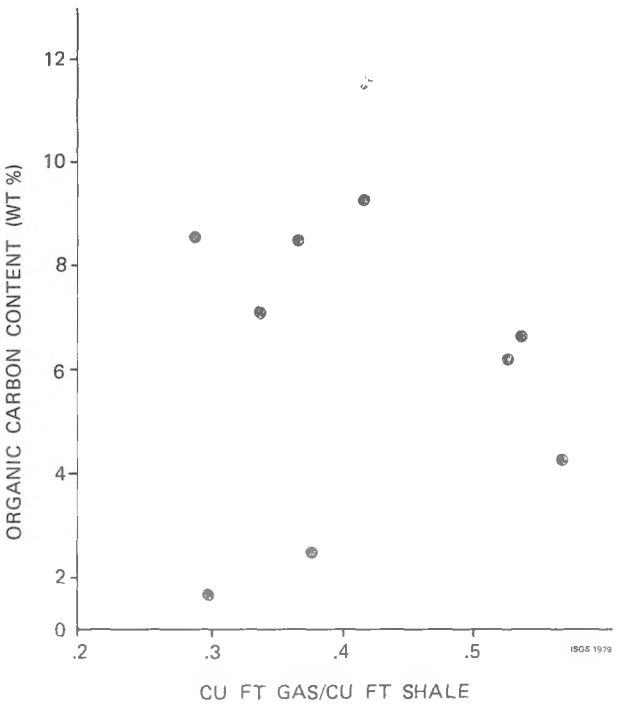


Figure 4. The organic carbon content versus the volume of gas released at room temperature from shale samples taken at 10-foot intervals from the core at Effingham County, Illinois.

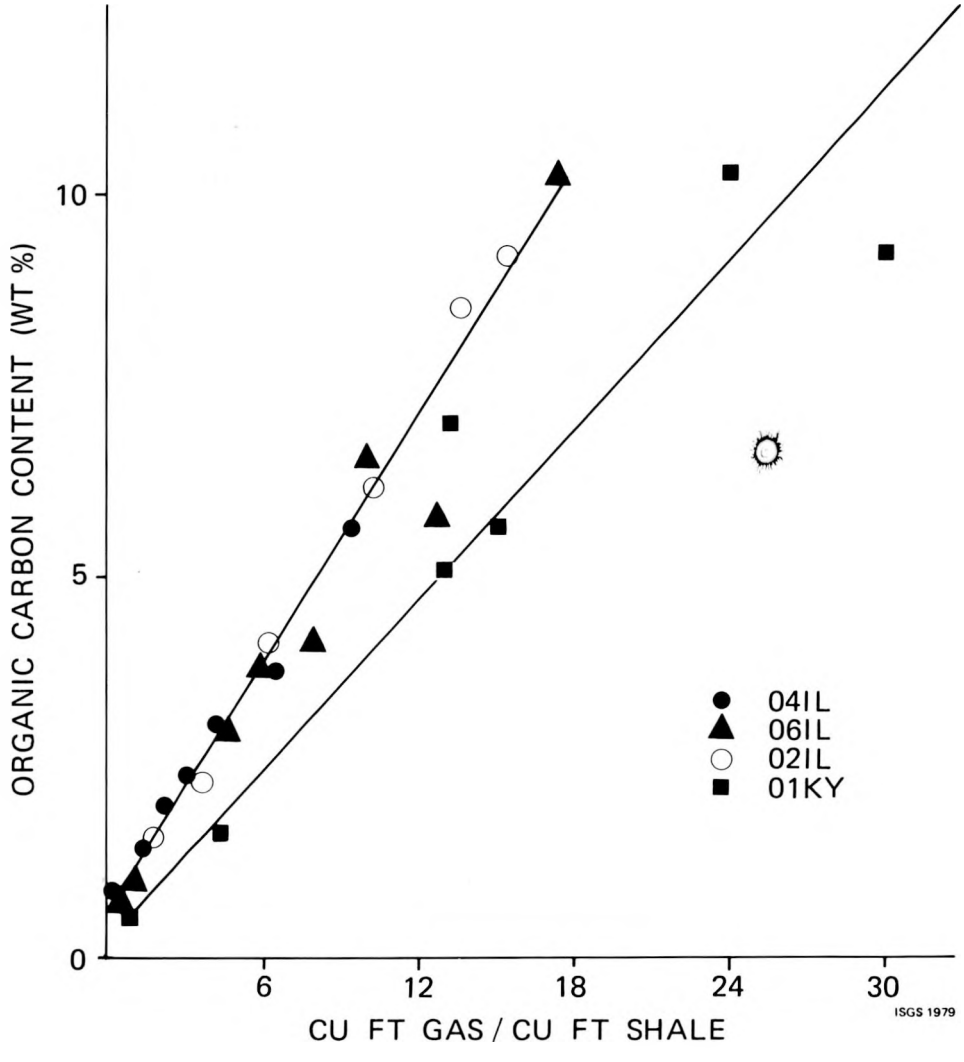


Figure 5. The relationship of the gas yield from pyrolysis of shale at 600°C to the organic carbon content of the shale.

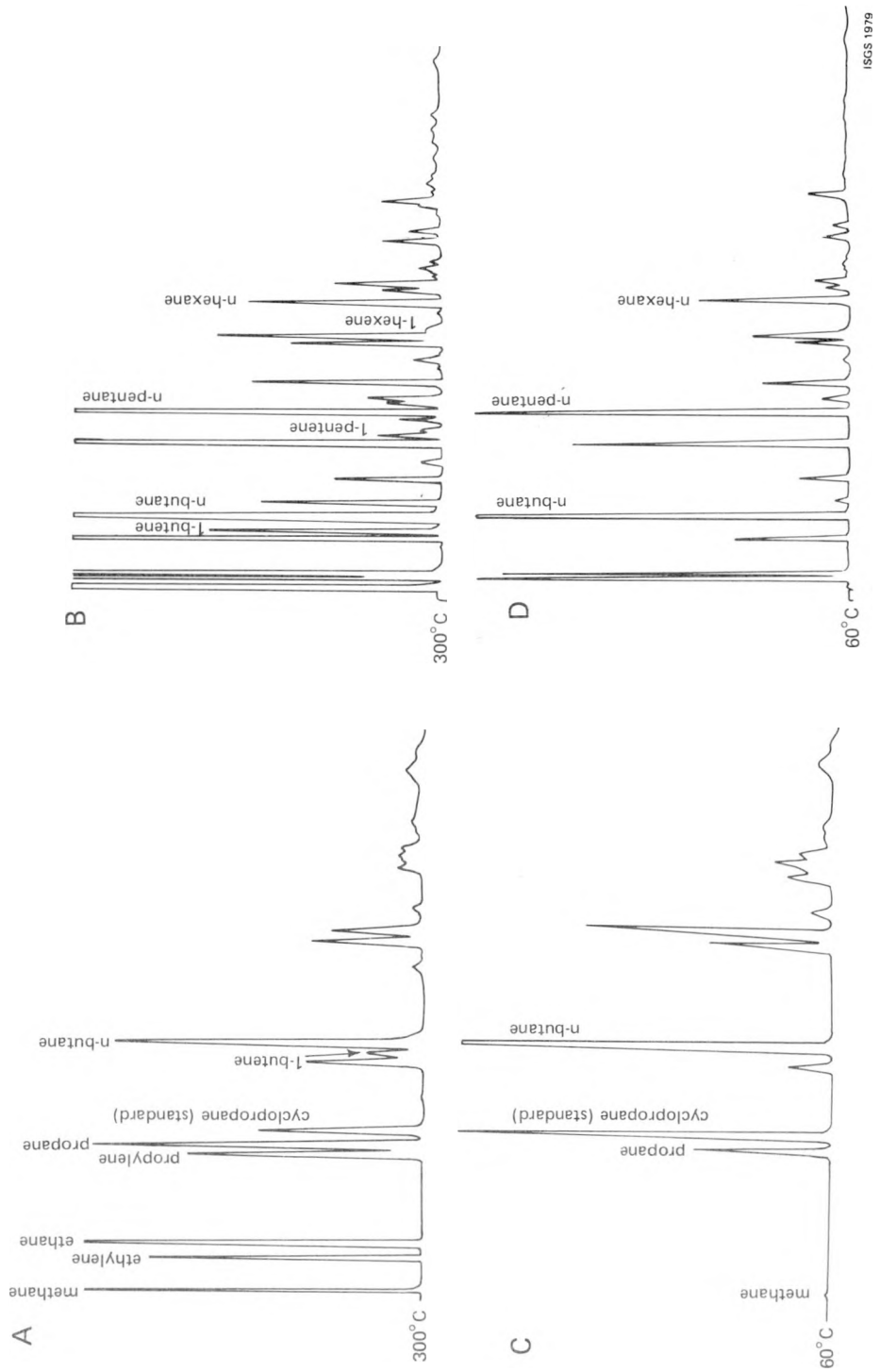


Figure 6. Typical GC trace of gaseous products from shale pyrolysis at 60°C (C, D) and at 300°C (A, B). A and C—Chromasorb 102 column; B and D—Carbopack C/0.2 percent CW 1500 column.

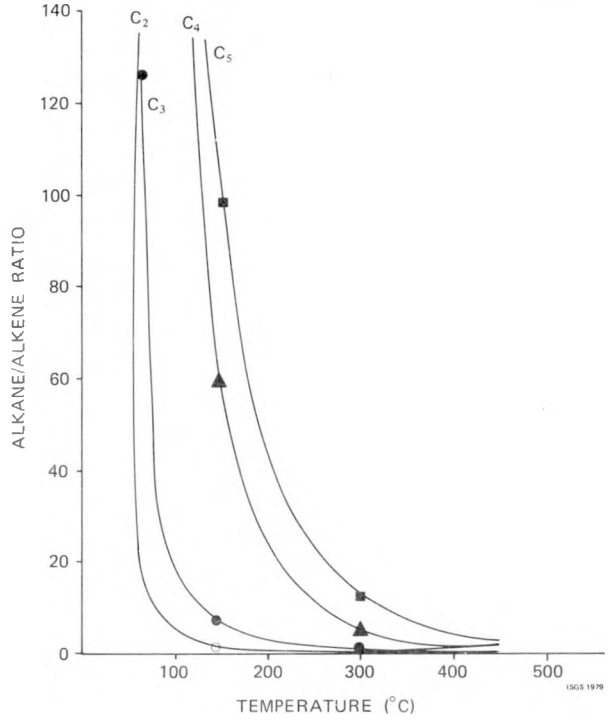


Figure 7. The alkane/alkene ratio of the hydrocarbons produced by pyrolysis of shale as a function of temperature.

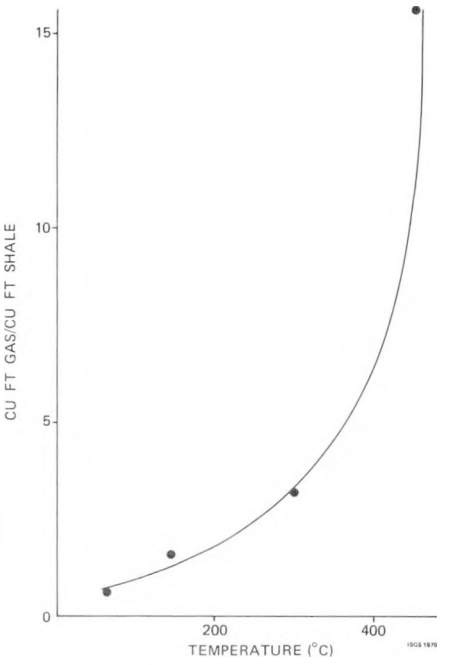


Figure 8. The total yield of hydrocarbons (C_1-C_5) produced from shale as a function of pyrolysis temperature.

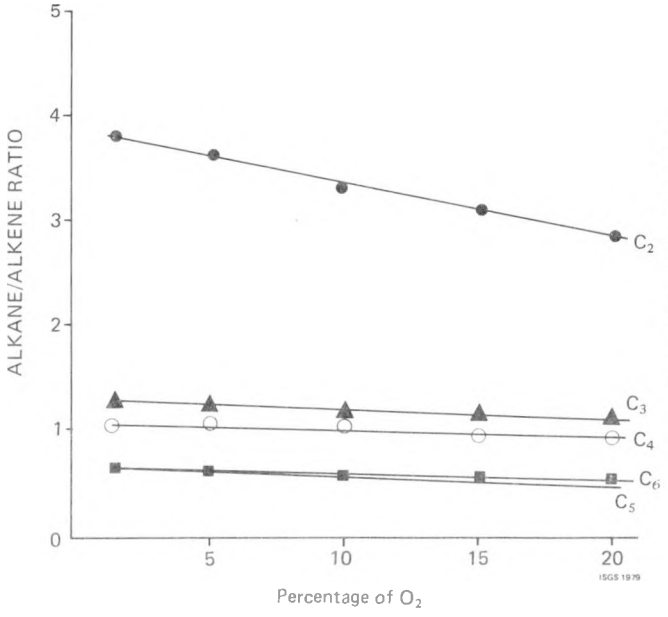


Figure 9. The alkane/alkene ratio of hydrocarbons produced by the pyrolysis of shale as a function of the percentage of oxygen in the pyrolysis atmosphere.

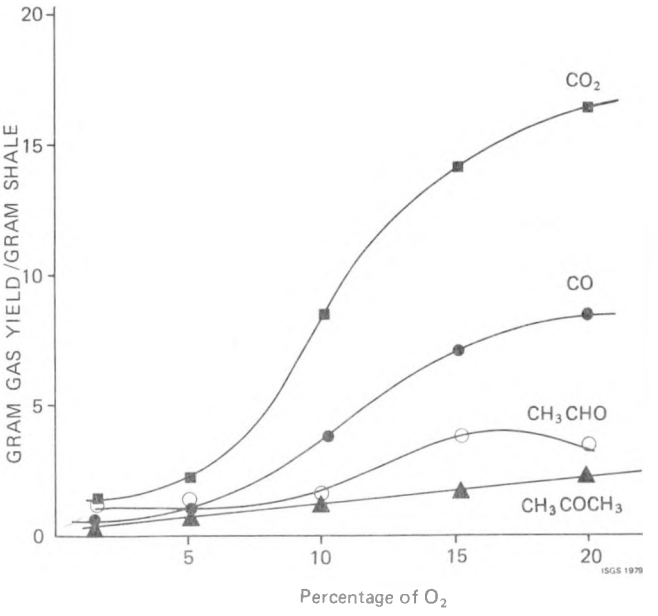


Figure 10. The yield ($X10^{-4}$) of CO_2, CO, CH_3CHO, and the yield ($X10^{-5}$) of CH_3COCH_3 produced by the pyrolysis of shale as a function of the percentage of oxygen in the pyrolysis atmosphere.

THEORETICAL AND EXPERIMENTAL ANALYSES OF HYDRAULIC FRACTURING*

by
Dr. Gordon D. Anderson
Dr. Merle E. Hanson
Dr. Ronald J. Shaffer

Lawrence Livermore Laboratory
Livermore, California



ABOUT THE SPEAKER

Dr. Gordon D. Anderson received a BS degree in physics from Iowa State University and MS and PhD degrees in physics from Washington State University. For ten years he was with Stanford Research Institute where he conducted experimental research in hypervelocity impact, high pressure equation of state of solids, and shock wave propagation in solids. For three and one half years he was with Systems, Science and Software where he conducted experimental and theoretical research on stress wave propagation in the ground in support of underground nuclear testing. Since joining Lawrence Livermore Laboratory in 1974 he has conducted experiments to study shock wave propagation in geological materials and more recently began conducting small scale laboratory experiments to study the hydraulic fracture process.

*This work was performed under the auspices of the U.S. Department of Energy by the University of California Lawrence Livermore Laboratory under contract number W-7405-ENG-48.

THEORETICAL AND EXPERIMENTAL ANALYSES OF HYDRAULIC FRACTURING

ABSTRACT

We are conducting a joint theoretical/experimental research program on hydraulic fracturing. Experiments are being performed to study the growth of hydraulically driven cracks in the vicinity of an unbonded interface in rocks. Blocks of the rock materials which are to be studied are held adjacent to one another in a hydraulic press so that a normal stress is set up across their mutual interface. A hydraulically driven crack is initiated in one of the blocks. It is found that the major parameters which affect hydraulic crack penetration into the adjacent block are the relative values of the mechanical strength and moduli of the rocks on either side of the interface, the finish of the interface surfaces, and the magnitude of the normal stress across the interface. To gain a better understanding of the mechanisms which control the growth of cracks across the interfaces, experiments are being performed to study the frictional properties of these interface surfaces. The experiments involve the simultaneous measurement of the normal force across the interface and the applied force necessary to overcome friction to initiate displacement. These experiments indicate that in addition to the normal force, the frictional force depends upon the surface finish and the presence of water in the rock.

Newly developed numerical models have been applied to analyze some aspects of fracture propagation near well bonded material interfaces to determine if these interfaces can inhibit propagation. Results from these calculations indicate that, for fractures propagating from a lower modulus material toward an interface with a higher modulus material, the stress intensity factor at the tip near the interface decreases significantly as the tip approaches the interface. However, upon penetration of the interfaces into the higher modulus material, the stress intensity factor is seen to increase abruptly and arrive at a higher value than in the lower modulus material. Conversely, when the fracture is propagating from a lower modulus material toward a higher modulus material, the situation is reversed. The presence of existing fractures near the interface is seen to significantly reduce the effects of these phenomena.

INTRODUCTION

Hydraulic fracturing and a variant, massive hydraulic fracturing (MHF), are primary candidates for stimulating production from the tight gas reservoirs in the United States. Hydraulic fracturing has been used as a well-completion technique for about 30 years with more than three--quarters of a million applications. Massive hydraulic fracturing is a recent application which obviously differs from hydraulic fracturing in that much larger quantities of fluid and proppant are pumped to create extensive fractures in the reservoir. Application of MHF to increase production from the tight gas reservoirs has provided mixed and, in many cases, disappointing results.

For hydraulic fracturing or MHF to be successful in enhancing the production of gas from the tight reservoirs, it is important that the fractures be emplaced in productive reservoir rock providing large drainage surfaces and conductive channels back to the well bore. Hydraulic fracturing, when used as the standard well-completion technique, results in fractures driven a few tens of feet into the formation to overcome the damage due to drilling. Although the concept of MHF is to drive extensive fractures in the reservoir, we are faced with the problem of containing those fractures in a given formation. There are several reservoir properties that have been proposed as having an effect on the control of the created fracture geometry. These include the in-situ stresses, stratigraphic layering, and preexisting faults and fractures.

From theories implied[1] and demonstrated,[2-4] hydraulic fractures propagate perpendicular to the least principal stress. Hence, the azimuthal orientation of the fracture is approximately controlled by the in-situ stress field. We also know that, except for very shallow applications, the created hydraulic fractures will be primarily vertical. The vertical gradient in the horizontal stresses could also be a factor in the control of the shape or the vertical extent of the fractures. There have also been speculations that the stratigraphy, especially where the elastic material properties vary from layer to layer, could be effective in containing the vertical extent of the fractures. Additionally, interfacial properties such as the extent of bonding, normal load, and friction will also play an important part in

inhibiting or enhancing the growth of the created fractures across the interfaces. Existing fractures and faults can also be important to the growth and final geometry of the propped fracture. To determine if and to what extent these effects are operative in controlling the geometry of the created fractures requires both theoretical and experimental analyses.

Lawrence Livermore Laboratory (LLL) is conducting a research program, funded by the Department of Energy (DOE), that includes small scale laboratory experiments on hydraulic fracture and development of theoretical models to analyze pressure driven fractures under various conditions. In the laboratory program small scale experiments are performed in which hydraulically driven cracks are initiated in polymethylmethacrylate (PMMA), limestone, and sandstone. The parameters which govern the growth of hydraulically driven cracks are: (1) the mechanical properties of the solid (i.e., elastic moduli, strength, etc.), (2) the physical state of the solid (i.e., presence of preexisting cracks, porosity, pore fluid, layering, etc.), (3) boundary conditions (i.e., free surfaces, externally applied stresses such as overburden), (4) the manner in which the driving fluid is injected into the solid, (5) the characteristics of the fluid itself (i.e., viscosity), and (6) any chemical reaction between the solid and the fluid.

At present we have been able to study the effects on crack growth of only a few of these parameters. It has been shown that the stress intensity factor influences whether or not a crack will cross a boundary between two materials and that the mechanical properties of the materials on either side of the interface and the shear strength of the interface itself determine whether or not a crack will cross the interface.[5-7] We have concentrated recently on the study of crack growth across unbonded interfaces. This work has involved observation of the conditions of normal stress and surface finish under which cracks will cross interfaces and measurement of the frictional properties of these interface surfaces. Although our work is still in progress and not complete, our results indicate that a normal threshold stress exists for crack growth across interfaces and the threshold stress may depend upon surface finish as well as mechanical properties of the rock.

Two-dimensional numerical models have been constructed to analyze fracturing in an elastic, layered, jointed continuum. Pore-pressure effects and changes in pore pressure resulting from previous flow have been coupled to the elastic calculations[7] using the descriptions due to Terzaghi.[8] The elastic part of the model was formulated using bilnear forms[9] with the fractures simulated in the elements using techniques similar to that of Hanson and Sanford,[10] Hanson[11] and Shaffer et al.[12] The model can accommodate more than one elastic material so that the effects of layering, and changes in elastic properties from layer to layer can be studied. In many of the studies, wave propagation effects are ignored to speed up the calculations. Fracture propagation in these cases is then analyses as a succession of equilibrium states. We assume that this approximation is valid in the continuum sense because the wave speed is much larger than the macroscopic propagation velocity of a hydraulically driven fracture. For example, a fracture is driven on the order of 2000 ft (610 m) in 5 to 8 h, while an elastic wave traverses this distance in 200 ms. Therefore, we assume that at a given time the elastic continuum is in a quasi-equilibrium state with the fracture.

EXPERIMENTS

EXPERIMENTAL TECHNIQUES

The materials we have used in our unbonded interface experiments are Indiana limestone and Nugget sandstone. Indiana limestone, from Bedford, Indiana, was chosen because it is a homogeneous, isotropic rock of about 15% porosity. The Nugget sandstone was chosen because it is a high strength, low porosity rock. It is anisotropic with the tensile strength as measured by Brazil tests being approximately 50% greater ($\sim$ 7.5 MPa) along the bedding planes than perpendicular to them. The test specimens of these rocks were generally cubes or rectangular blocks of varying size ranging from 5 to 10 cm on a side. The mechanical properties of these two rocks are summarized in Table 1.

Hydraulic fracture - interface experiments. The fluid used to initiate and drive hydraulic fractures in all experiments was a medium heavy weight oil. The oil was injected into the test specimen through a steel injection tube (0.635-cm o.d. by .125-cm wall) which was

bonded by epoxy to the interior of a 0.711-cm i.d. injection hole. A small diameter section at the bottom of the borehole (∿ 0.635-cm i.d. x 1.25-cm long), which is near the center of the block, was left uncased so that the pressurized oil may press directly against the rock. A small O-ring was glued on the bottom of the injection tube to aid in preventing pressurized oil from escaping between the outer surface of the injection tube and the inner surface of the borehole. In no case was oil found to escape. In each experiment, prior to connecting the injection tube to the hydraulic pressure line, the injection tube and the open section of the borehole were filled with oil so that all air was displaced. The oil was then pressurized by a motor driven pressure intensifier. The oil pressure was monitored by a transducer and recorded on a strip chart recorder. The fluid pressure can be read to a precision of about 0.3 MPa on a full scale of 100 MPa.

To study how hydraulic fractures initiated by this system behave near unbonded interfaces under a normal stress, a 100 ton laboratory press was used. Two or more blocks, one of which contains the fluid injection tube, were stacked between the platens of the press with their unbonded interface parallel to the platens of the press as shown in Fig. 1. The outer block surfaces, to which the load is applied, were separated from the loading platens by thin (0.5 mm thick) Teflon sheets to reduce friction at the platens and to distribute the load more uniformly. The remaining sides of the blocks were unconfined. The lower platen rested on a calibrated load cell whose output was recorded by a chart recorder. The block faces to which loads were applied were ground flat and parallel to within 0.0025-cm to provide as uniform loading across the interface surfaces as possible.

Static-friction measurements. The static frictional properties of interface surfaces of the rocks used in the hydraulic fracture experiments were studied using a sandwich geometry as shown in Fig. 2. In this geometry one block of the rock to be studied is held under an applied load (W) between two other blocks of the same material. The load W, which was applied by a horizontal hydraulic press, was recorded by a pressure transducer and recorded on a strip chart recorder. A vertical driving force (F) was applied to the center block by a vertical hydraulic press. The upper platen for this press rode on a calibrated load cell whose output was displayed on the same chart as the load W. The apparatus is shown in Fig. 3. All blocks used in these experiments were precision machined so that adjacent faces were perpendicular and opposite faces are flat and parallel to within 0.0025-cm. In a typical frictional experiment the load W was increased in a step-wise manner from 0 to full scale and at each step the driving force F was increased until motion was initiated. The actual values of the normal and shear frictional stresses attained at full scale depend upon the block size since the maximum forces are fixed by the pressues and the full scale recording capability of the instrumentation. Typically these stresses ranged from 0-10 MPa which covered our range of interest at present. A typical record for a friction test on smooth Indiana limestone surfaces is shown in Fig. 4. The stair-step record is that of the normal load W. At a given value of W, the frictional driving force F was seen to increase until slip occurs at which time the force relaxes. As soon as slip initiates the force F was allowed to relax so that no further displacement occurs. During an entire run of the type shown in Fig. 4, less than 0.63 cm of displacement occured. However, even with this small total displacement, in a relatively soft rock like Indiana limestone, significant comminution can occur along the interfaces.

EXPERIMENTAL RESULTS

Fractures near interfaces. Two types of interface surface finishes have been used to study crack growth in Indiana limestone and Nugget sandstone. One of the surface finishes was ground smooth while the other was roughened by sandblasting. It was found that the threshold normal stress across the interface for hydraulic cracks to cross the interface was about 4.5 MPa for dry Indiana limestone and did not appear to vary significantly with surface finish. However when the limestone block adjacent to the dry block into which oil was injected was saturated with water, the threshold stress for crack growth across the interface dropped to about 3.4 MPa. Two blocks of dry Indiana limestone from such an experiment are shown in Fig. 5. The block on the left was loaded in the press such that the stress across the interface was greater than the threshold stress. The crack is seen to have crossed the interface and passed completely through both blocks. The block on the right was loaded below the threshold stress

and the crack terminated at the interface. Whereas there was no discernable effect of the surface finish on the threshold stress in Indiana limestone, the same was not true for Nugget sandstone. In Nugget sandstone it was found that the threshold for cracks to cross a smooth surface was about 5.5 MPa and for roughened surfaces about 3.4 MPa. The result of a Nugget sandstone experiment in which the applied stress load was 4.2 MPa, between the two thresholds, is shown in Fig. 6. The crack, which was initiated in the center block, has crossed the upper interface which was roughened and terminated at the lower interface which was smooth. The results for experiments of this type for dry Nugget sandstone in which there is a rough and a smooth interface are summarized in Fig. 7. The abscissa is breakdown pressure at which hydraulic fracture initiated and the ordinate is applied load. The breakdown pressure is a random quantity which is controlled by flaws near the borehole. Above the upper threshold the cracks cross both interfaces, below the lower threshold they cross neither interface and in between they cross only the roughened interface. When experiments were performed in which cracks were initiated in a dry Nugget sandstone block which was adjacent to a water saturated block, it was found that the threshold stress across a smooth surface was greater than 6.5 MPa as compared to about 5.5 MPa for the dry block. It was also found that the threshold normal stress was about 5.1 MPa to drive a crack across a smooth interface from Indiana limestone into Nugget sandstone and about 3.9 MPa to go from Nugget sandstone into Indiana limestone. These results are all summarized in Table 2.

Friction experiments. Unbonded interfaces can support shear stresses, due to friction, or normal stresses but not tensile stresses. We therefore decided to investigate the frictional properties of these surfaces in the range of normal stresses near the threshold normal stress for crack growth across the interfaces. At the present time we have only studied friction between like rocks. As described earlier, at each level of normal stress applied the driving force to overcome friction was increased until slippage was initiated at which time the frictional force relaxed (see Fig. 4). The results of the tests are presented in Figs. 8, 9 and 10 in which the shear stress to initiate motion is plotted against the normal stress. Tests were performed on two types of Nugget sandstone, red and yellow, although fracture experiments have been performed only on the red variety. The mechanical properties of these two types is very nearly the same and they come from the same quarry although their appearance is somewhat different.

In Fig. 8 the slopes of the lines indicate that in dry Indiana limestone the frictional coefficient is greater for the roughened interface than for the smooth interface, i.e., about 0.62 and 0.5 respectively. However, no definite change in the threshold stress for crack growth across these interfaces was observed. At the threshold stress, 4.5 MPa (650 psi), the shear stress to initiate motion across the rough surface exceeds that across the smooth surface by about 0.45 MPa (65 psi). The effect of saturating the limestone with water further increases the coefficient of friction to about 0.71. Saturation with water also dereases the tensile strength of the Indiana limestone. Thus the increasing of the coefficient of friction and decreasing of the tensile strength with addition of water are consistent with the observation that the threshold normal stress for crack growth across the interface is decreased by water saturation. However, it is not clear at present why no effect on the threshold in dry limestone is seen by roughening the interface surfaces. At the threshold stress for the dry rock, 4.5 MPa, the macroscope shear frictional stress that the limestone can support before motion occurs is 2.4 MPa (350 psi) for the smooth surface and 2.8 MPa (415 psi) for the rough surface. This stress is about one half the tensile strength. On the roughened surface local stresses on the asperities may greatly exceed either the tensile or compressive stress so that the asperities are broken down and the nature of the rough and smooth surfaces are not too different at the time the crack approaches the interface. Crushed and powdered rock is observed on the interfaces after an experiment is completed. An effect of this type may account for why no discernable difference in threshold stress is seen.

In Figs. 9 and 10 for Nugget sandstone the slopes of the lines for the dry smooth and rough interfaces have about the same slopes (0.55-0.6). The line for the roughened interface is offset above the line for the smooth interface. The smooth and roughened surfaces had threshold stresses of about 5.5 MPa (800 psi) and 3.4 MPa (500 psi) respectively. The increase in capability of transmitting shear frictional stress across the interface is consistent with the

lowering of the threshold stress. The decrease in threshold of 2.1 MPa (300 psi) at first appears not to be consistent with the offset of the curves if crack growth across the interface occurs at the same value of shear stress. At the threshold for the roughened surface, 3.4 MPa (500 psi), the surface can support a macroscopic shear stress of 2.0 MPa (300 psi) before slippage occurs while at the threshold for the smooth surface, 5.5 MPa (800 psi), the surface can support a macroscope shear stress of 3.0 MPa (430 psi). However, these threshold stresses are merely average or representative values (see Fig. 7), as rocks are variable. If σ_{TR} and σ_{TS} are the threshold stresses for the rough and smooth surfaces respectively, then with the present data it would be more correct to say 3.4 MPa $< \sigma_{TR} <$ 4.3 MPa and 4.3 MPa$< \sigma_{TS} <$ 6.06 MPa. In each case the lower number is a normal stress at which cracks repeatedly did not cross that interface and the higher number is a normal stress at which they repeatedly did cross. From Fig. 9 this gives the bounds on the threshold frictional stresses, τ_{TR} and τ_{TS} corresponding to σ_{TR} and σ_{TS} respectively, as 2.0 MPa $< \tau_{TR} <$ 2.6 MPa and 2.2 MPa $< \tau_{TS} <$ 3.2 MPa. In the few experiments performed on saturated Nugget sandstone (red) it was found that the threshold stress for crack growth across the interface was greater than 6.5 MPa. Although no frictional experiments were performed on saturated red Nugget sandstone, the saturated friction curve for the yellow Nugget sandstone, Fig. 10, whose properties are quite similar to those of the red, indicates that for values of the normal stress greater than 6.5 MPa (940 psi) the value of the shear frictional stress is greater than 2.6 MPa (375 psi). These data, within the scatter expected due to inhomogenieties in rocks, are consistent with a threshold shear stress in the neighborhood of 2.6 MPa that an unbonded interface in Nugget sandstone must be able to support in order that a hydraulic crack grow across it.

THEORY

THEORETICAL MODELS

The equations that are used to describe the elastic continuum are:

$$\frac{\partial \sigma_x}{\partial x} + \frac{\partial \tau_{xy}}{\partial y} = 0$$

and (1)

$$\frac{\partial \sigma_y}{\partial y} + \frac{\partial \tau_{xy}}{\partial x} = 0$$

with the Hookean constitutive relations

$$\sigma_x = 2\frac{\partial \mu}{\partial x} + \lambda\left(\frac{\partial \mu}{\partial x} + \frac{\partial v}{\partial y}\right),$$

$$\sigma_y = 2\mu\frac{\partial v}{\partial y} + \lambda\left(\frac{\partial \mu}{\partial x} + \frac{\partial v}{\partial y}\right),$$

and (2)

$$\tau_{xy} = \mu\left(\frac{\partial \mu}{\partial y} + \frac{\partial v}{\partial x}\right).$$

Here σ_x and σ_y are the normal stresses. τ_{xy} is the shear stress in the rectangular coordinate system, μ and v are the displacements in the x and y directions, respectively, and λ and μ are the local Lamé constants for the material.

When discretized using the bilinear forms,[7] these equations are written as matrices that are solved by a matrix-iteration scheme. The iteration scheme is a variation of the incomplete Cholesky-conjugate gradient method by Kershaw.[13]

A porous-flow description is used to calculate the changes in pore pressure. The porous-flow equations are dynamic to allow for time-dependent changes in pore pressure and time-dependent growth of the fracture. The equation used in the two-dimensional model to describe the porous-flow effects is

$$S \frac{\partial h}{\partial t} = \frac{\partial}{\partial x} \left(T_{xx} \frac{\partial h}{\partial x}\right) + \frac{\partial}{\partial y} \left(T_{yy} \frac{\partial h}{\partial y}\right), \qquad (3)$$

where S is the storage coefficient, h is the head, and T_{xx} and T_{yy} are the principal transmissivities (permeability-height term). This equation is differenced using standard, finite--difference techniques and solved in the continuum using a line-iteration scheme. The porous--flow part of the model overlays the elastic continuum to provide a simultaneous description of the flow with the elastic solution. Our techniques for calculating the permeability in the crack have been described previously.[7]

Calculating stress in the crack region is of prime importance in studying crack stability. Classical techniques to calculate the stresses yield singular stresses at the crack tips, that is, the stresses are inversely proportional to $\sqrt{r}$ where r is a radius vector originating at the crack tips. The coefficient of this singular stress is the stress-intensity factor and is identified as K_I for the tensile case. The value K_I is compared to the measured critical value of (K_{IC}) to predict incipient fracture instabiity in a brittle material. We are using a method proposed by Chow and Lau[14] to determine the stress-intensity factor in our calculations. Using this method the shape of the crack determines the stress-intensity factors. With the finite-element model, one uses the position of the nodal points which lie on or close to the crack face.

In this paper we discuss some of the analyses performed with our model. Using these analyses we describe how:

- An interface separating two elastic materials with different modulii affects the stress-intensity factor.
- Natural fractures complicate fracturing near the interface.

PRESSURIZED FRACTURING NEAR A WELL-BONDED INTERFACE

We have applied the models to analyze some simple cases of fracturing near a well-bonded interface. In these calculations we assumed that the permeability in the material was zero; therefore we ignored the pore-pressure effects. The models were applied to calculate the mode I stress-intensity factors as a crack approaches and passes through a bonded interface between two materials.

Calculations were performed so that static relaxation was achieved at several fracture-tip positions near the interface. Using this technique, we determined the mode I stress-intensity factors at each location and then simply connected the points with a smooth curve. Sneddon and Lowergrab[15] indicate that the stress intensity factors define the condition for the onset of fracture propagation. We assume that the Young's modulus on one side of the interface was twice that on the other side. Poisson's ratio was taken as 0.25 for both materials. In these calculations, we solved one set of problems where a fracture was moved from the lower modulii material toward the interfce and into the higher moduli material; we also solved a second set of problems where we reversed the situation.

Figure 11 presents a sample geometry of the type of problems calculated. The mode I stress--intensity factor was calculated and normalized by the factor $P\sqrt{a}$. The factor $P\sqrt{a}$ is the classical Sneddon mode I stress-intensity factor for a pressurized crack in an infinite continuum where P is the pressure in the crack and a is the semimajor axis of the fracture eclipse.

Figure 12 shows the results of the calculation where the fracture tip is moving from a lower modulus material toward the interface and into the higher modulus material (e.g., $E_2 = 2E_1$ in the geometry of Fig. 11). We normalized the coordinates of the fracture-tip position in

Fig. 12 with the crack length and arbitrarily set the origin of the abscissa (x axis) at the material interface. For these calculations we maintained a constant fracture length but positioned the crack at various distances from and through the interface. The material to the right of the x-axis origin had the modulus E_2 while the material to the left had the modulus E_1. These results show that as a fracture approaches a material interface from a lower modulus material toward a higher modulus material, the stress intensity factor decreases. However as the tip penetrates the interface into the higher modulus material, the intensity factor at this tip dramatically increases. Not shown in these plots is the fact that as the fracture penetrates with the right tip the stress-intensity factor at the other tip also decreases.

Figure 13 shows the results of the opposite case where a fracture is moved from a higher modulus material toward an interface and into a lower modulus material (e.g., $E_1 = 2E_2$ in the geometry of Figure 11). The normalized stress-intensity factor is again displayed as a function of normalized fracture-tip distance from the interface. The calculations show that as the crack tip approaches the interface from the higher modulus material, the stress-intensity factor drastically increases. However, as the tip penetrates the interface, the stress-intensity factor at the opposite tip (not shown) increases as the right tip enters, and is moved into the lower modulus material.

These calculations indicate a reduction in the tendency to break as the tip of a pressurized fracture propagates from a lower modulus material toward a well-bonded interface with a higher modulus material. Other authors[16] tend to believe that this condition can make the interface inpenetrable, which may be the case in some instances. However, a series of mineback experiments at the Nevada Test Site has shown that penetration did occur. From these results it is evident that if the critical stress intensity factor were similar for both materials, the fracture tip in the higher modulus material would have a greater tendency to propagate. In addition, as a tip approaches an interface from a higher modulus material toward a lower modulus material, the tip will probably be drawn toward the interface, but the tendency to propagate would be reduced after penetration. Note that these arguments all assume a well-bonded interface in an originally isotropic field.

THE EFFECT OF EXISTING FRACTURES ON A PRESSURIZED FRACTURE NEAR AN INTERFACE

In the previous section, we discussed how the mode I stress-intensity factor changes as a fracture tip approaches a well-bonded interface between two materials. There were indications that the change in material properties on either side of the interface could have an effect on the growth of the fracture in the interfacial region. the experimental evidence[17] from some mineback experiments at the Nevada Test Site shows that a hydraulically driven fracture crosses an interface between two materials where the modulus changed by more than an order of magnitude. Hence, we undertook some preliminary calculations to determine if existing fractures near the interface could enhance fracturing across an interface. In these calculations we simulated the hydraulically pressurized fractures in the material with the smaller Young's modulus.

Poisson's ratio for both materials was the same, and the larger modulus was twice that of the smaller, $E_2 = 2E_1$. We have not performed the calculations for the case when the pressurized crack penetrates the interface, therefore, we are only assessing the effects of existing cracks in the higher modulus material on the stress-intensity factor of the fracture that is approaching the interface. The results of two sets of calculations are presented and compared with the results of previous calculations where there are no pre-existig cracks in the medium, designated herein as Case I. The geometry of the problems with existing cracks is shown in Figure 14. Figure 4a shows the geometry of the problem (Case II) with one existing crack in the higher modulus material with length a. This pre-existing fracture did not intersect the interface. the length of the pressurized crack is 2a. Figure 14b shows the geometry with two pre-existing cracks in the higher modulus material (Case III). Here the pre-existing cracks are symmetrically located on either side of an extended fracturte axis with an equal length of (a) spaced 2a apart. The length of the pressurized fracture is again 2a. Figure 5 shows the stress-intensity factor as a function of normalized distance of the fracture from the interface. This plot compares the stress-intensity factor for the two cases with pre-existing cracks to Case I (no pre-existing fractures in the medium). The pre-existing fractures were assumed to be perfectly slipping (no frictional stress).

We can see from these preliminary calculations that pre-existing fractures can reduce the effects of a materials properties change across an interface on the stress-intensity factor. For the preliminary geometries studied, Case III (two pre-existing fractures in the higher modulus material) showed the largest change from the base case (Case I). This brings up an important point. When we measure the mechanical properties we normally choose an intact sample of the material. However, in many cases the bulk material has a significant amount of fractures greater than some given size. Although effective bulk elastif moduli are imporant parameters, as shown in the above results, they may be extremely difficult to measure.

SUMMARY AND CONCLUSIONS

Experiments have been performed to study the conditions under which a hydraulically driven crack which is initiated in one block of rock will cross an unbonded interface and penetrate an adjacent block of rock. The experiments have shown that in Nugget sandstone and Indiana limestone a threshold normal stress across the interface exists below which the crack will not cross the interface. In the sandstone the threshold stress was found to depend upon the surface finish of the interface while no such dependence was observed for the limestone. Saturation with water increased the threshold stress level for the sandstone and decreased it for the limestone. These results suggest that the frictional shear stress that the interface can support without slippage being initiated may be important in controlling crack growth across it. Experiments were performed to measure the frictional shear stress that these surfaces can support as a function of normal stress. As expected, a rough surface finish could support more shear stress than a smooth surface. However, saturation of the rock with water increased the frictional stress in the limestone and decreased the frictional stress in the sandstone at a given normal stress which is consistent with the observed effects of water on the threshold stress for crack growth across the interface. The friction measurements suggest, at least for the sandstone, that there is a critical threshold shear frictional stress that the interface must be able to support in order to initiate crack growth across that interface. In the sandstone this shear stress is in the vicinity of 2.6 MPa. The fact that cracks can be driven from sandstone into limestone at a lower threshold normal stress across the interface than from limestone into sandstone is probably related to the relative magnitudes of their mechanical properties (e.g., elastic moduli, strength). This phenomenon should be investigated further.

These experiments do indicate that in modeling crack growth near interfaces that the nature of the interface itself must be characterized. Furthermore the presence of water in the rock may produce different effects on crack growth across the interface depending upon the nature of the rock. Due to the variations in mechanical properties and inhomogenieties from rock to rock and among different specimens of the same type of rock, many more experiments are needed to quantify these threshold quantities. Even then, at best, the results will only give ranges of values.

Theoretically, our calculations predict a reduction in the stress intensity factor (decrease in the tendency to break) as a pressurized fracture in a lower modulus material approaches a bonded interface with a higher modulus material. However, on penetration of the interface, we note that the stress intensity factor abruptly increases and finally stabilizes at a larger value than it had in the lower modulus material. Conversely, when the pressurized crack is in a higher modulus material approaching an interface with a lower modulus material, the stress intensity decreases until the crack penetrates the interface. It then arrives at a lower stabilized value than it had in the higher modulus material. This indicates that well bonded interfaces between materials with a modulii contract could in some cases act as a barrier to fracture propagation; however, we have also shown that existing cracks in the interfacial regions would tend to reduce the barrier effect. That is the changes in stress intensity factor due to mechanical modulii differences across an interface are significantly reduced when other cracks exist in the interfacial region.

TABLE 1
MECHANICAL PROPERTIES OF ROCKS

Material	Tensile Strength (MPa)	Compressive Strength (MPa)	Bulk Modulus (GPa)	Poisson Ratio	Initial Density (Mg/m^3)
Nugget sandstone	3.7-7.5* 6.3-8.6**	230.0[18]	11.7[18]	.07[18]	2.55
Indiana limestone (dry)	4.7-5.9[5]	62.0[19]	11.3[19]	.115[19]	2.28
Indiana limestone (saturated)	1.9				2.45

* Perpendicular to bedding
** Parallel to bedding

TABLE 2

MEAN INTERFACE THRESHOLD STRESS

Materials	Stress (MPa)
DRLM to DRLM* (smooth)	4.5
DRLM to DRLM (rough)	4.5
WTLM to WTLM (smooth)	3.4
DRNU to DRNU (smooth)	5.5
DRNU to DRNU (rough)	3.4
DRNU to WTNU (smooth)	6.5
DRLM to DRNU (smooth)	5.1
DRNU to DRLM (smooth)	3.9

*DRLM = dry limestone
WTLM = wet limestone
DRNU = dry sandstone
WTNU = wet sandstone

REFERENCES

1. M. King Hubert, Structural Geology (Hafner Publishing Company, New York, 1972).

2. B. Haimson, Hydraulic Fracturing in Porous and Nonporous Rocks and Its Potential for Determining In-Situ Stresses, PhD thesis, University of Minnesota, (1968).

3. A. A. Daneshy, "True and Apparent Direction of Hydraulic Fractures," SPE Paper 3226, Society of Petroleum Engineers (Dallas 1971).

4. M. E. Hanson, R. J. Shaffer, G. D. Anderson, D. N. Montan, W. Lin, B. Haimson, and M. P. Cleary, LLL Gas Stimulation Program Quarterly Progress Report, October 1977-December 1977, Lawrence Livermore Laboratory Rept. UCRL_50036-77-4 (1978).

5. Jones, A. H., A. S. Abou-Sayed, and L. A. Rogers, "Rock Mechanics Aspects of the MHF Design in Eastern Devonian Shale Gas Reservoirs," Enhanced Oil, Gas Recovery and Improved Drilling Methods Conference, Tulsa, OK, Aug.-Sept. 1977.

6. Daneshy, A. A., "Hydraulic Fracture Propagation in Layered Formations," SPE Paper 6088, AIME, 1976.

7. Hanson, M. E., and R. J. Shaffer, "Some Results from Continuum Mechanics Analysis of the Hydraulic Fracture Process," Lawrence Livermore Laboratory, UCRL-81707, May 1979.

8. J. C. Jaeger and N. G. W. Cook, Fundamentals of Rock Mechanics, (Chapman and Hall, London 1969).

9. A. G. Petschek and M. E. Hanson, "Difference Equations for Two-Dimensional Elastic Flow," J. Comp. Phys., 3, 307 (1968).

10. M. E. Hanson and A. R. Sanford, "Some Characteristics of a Propagating Brittle Tensile Crack," Geophys. J. R. Astr. Soc. 24, 231 (1971).

11. M. E. Hanson, "Some Effects of Macroscopic Flaws on Dynamic Fracture Patterns Near a Pressurized Driven Fracture," Int. J. Rock. Mech. Min. Sci. and Geomech. Abstr. 12, 311 (1975).

12. R. J. Shaffer, L. E. Murr, M. E. Hanson, A. G. Petschek, and W. A. Szilva, Laser-Induced Fractures in Silicon, Flaw Interaction Studies and Fracture in Granular Materials, Air Force Weapons Laboratory, Kirtland Air Force Base Rept. AFWL-TR-74-267 (1976).

13. D. S. Kershaw, The Incomplete Cholesky-Conjugate Gradient Method for the Iterative Solution of Systems of Linear Equations, Lawrence Livermore Laboratory Rept. UCRL_78333, Rev. 1 (1977).

14. C. L. Chow and K. J. Lau, "On the Finite Element Method for Calculating Stress-Intensity Factors with a Modified Elliptical Model," Int. J. Frac. Mech. 12 (1), 59 (1976).

15. I. M. Sneddon and M. Lowengrub, Crack Problems in the Classical Theory of Elasticity (John Wiley, New YOrk 1969).

16. A. S. Abou-Sayed, A. H. Jones, and E. R. Simonson, "On the Stimulation of a Geothermal Reservoir by Downward Hydraulic Fracturing," in Proc. of ASME Energy Technology Conference, Houston, Sept. 1977, Rept. no. 77-PET-81.

17. N. R. Warpinski, D. A. Northrup, and R. A. Solmidt, Direct Observation of Hydraulic Fracture: Behavior Near a Fracture Interface, Sandia Laboratories, Albuquerque, NM, SAND 78-1935 (1978).

18. Schock, R. N., A. E. Abey, B. P. Bonner, A. G. Duba, and H. C. Heard, "Mechanical Properties of Nugget Sandstone," UCRL-51447, Lawrence Livermore Laboratory, August 28, 1973.

19. Heard, H. C., A. E. Abey, and B. P. Bonner, "High Pressure Mechanical Properties of Indiana Limestone," UCID-16501, Lawrence Livermore Laboratory, August 28, 1973.

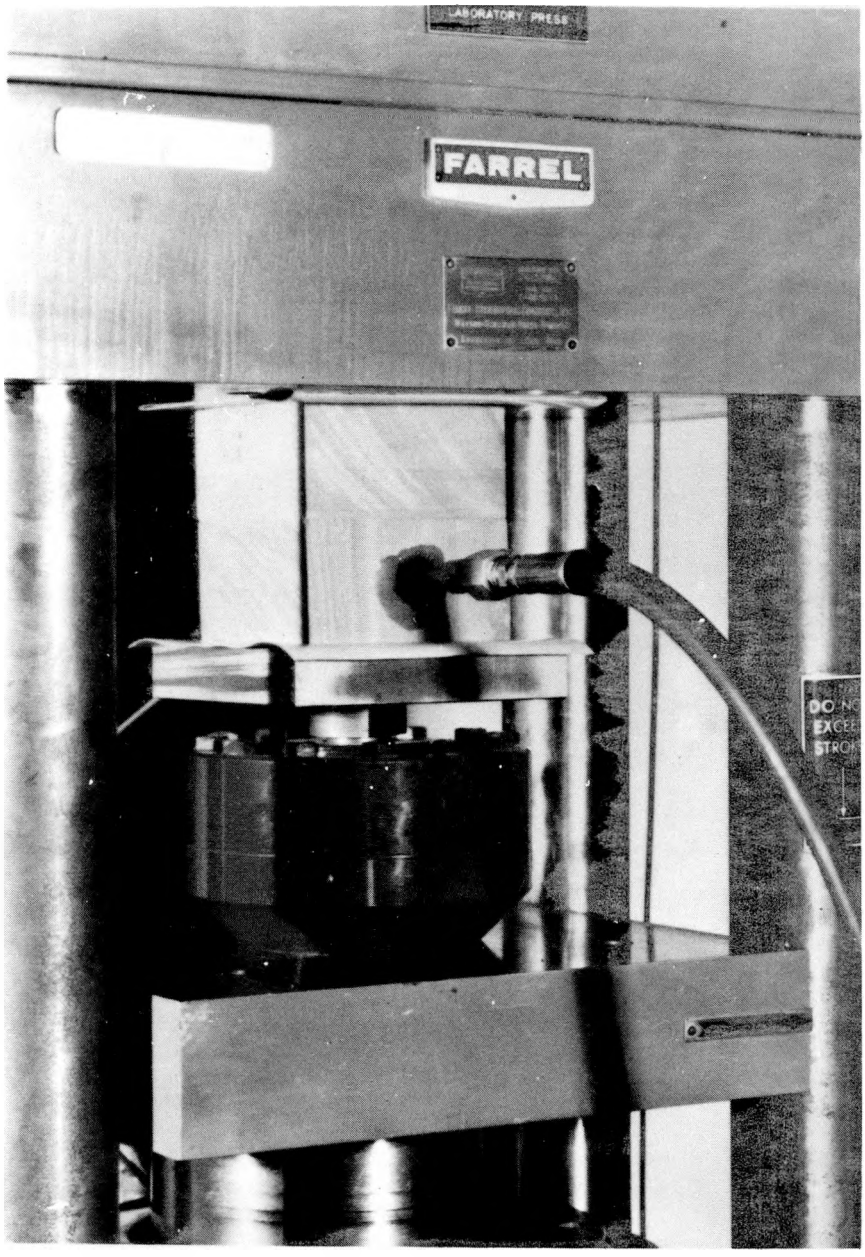


Figure 1 Hydraulic fracture experimental apparatus.

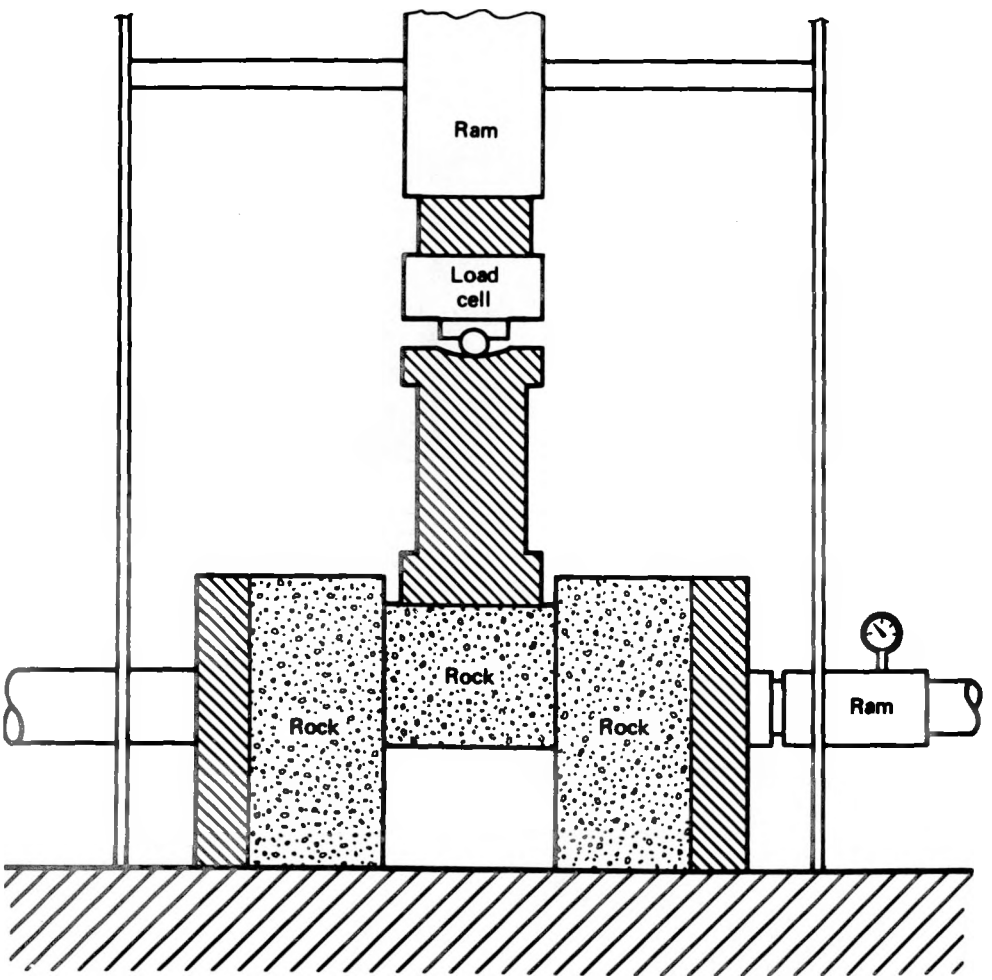


Figure 2. Schematic of friction experiment.

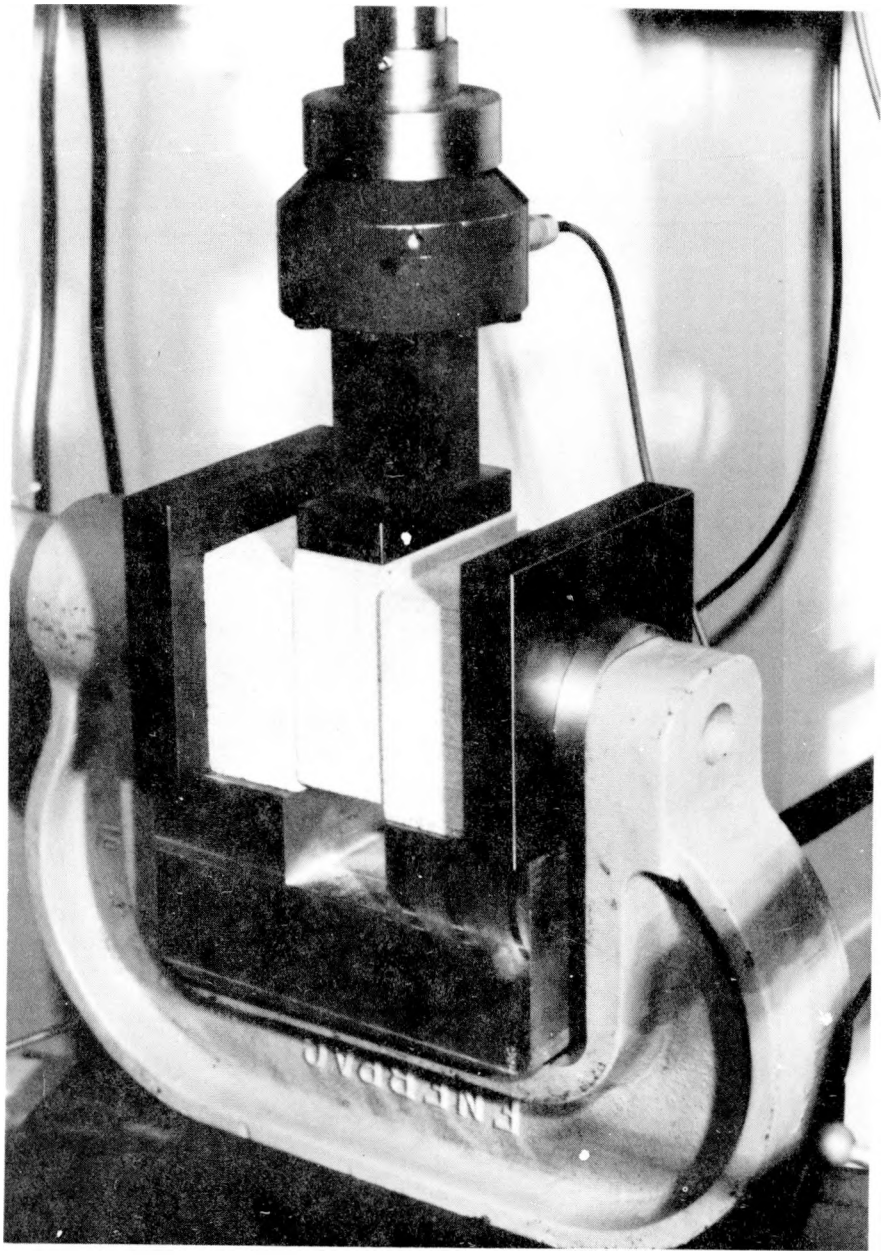


Figure 3. Friction experimental apparatus.

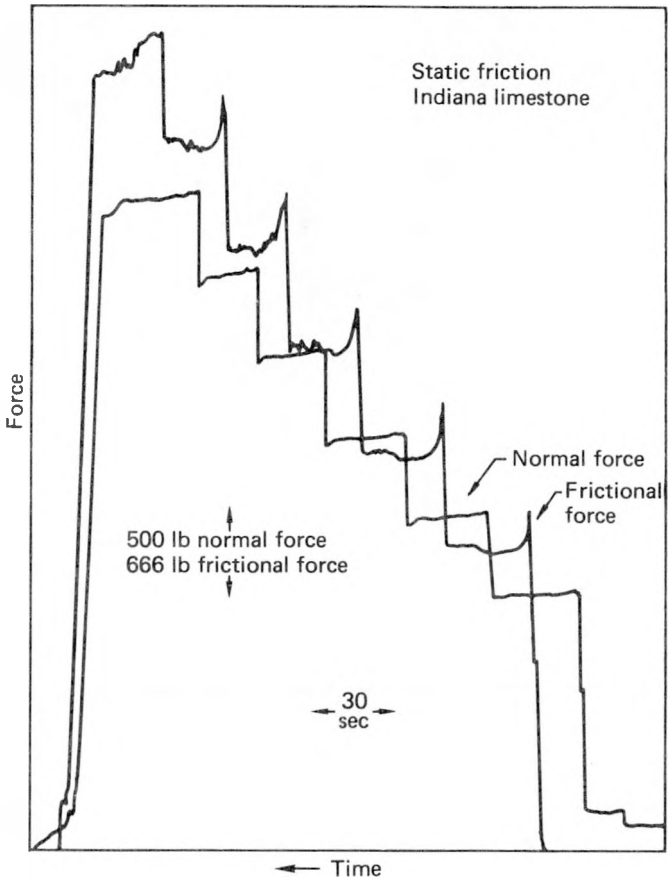


Figure 4. Data record from friction experiment.

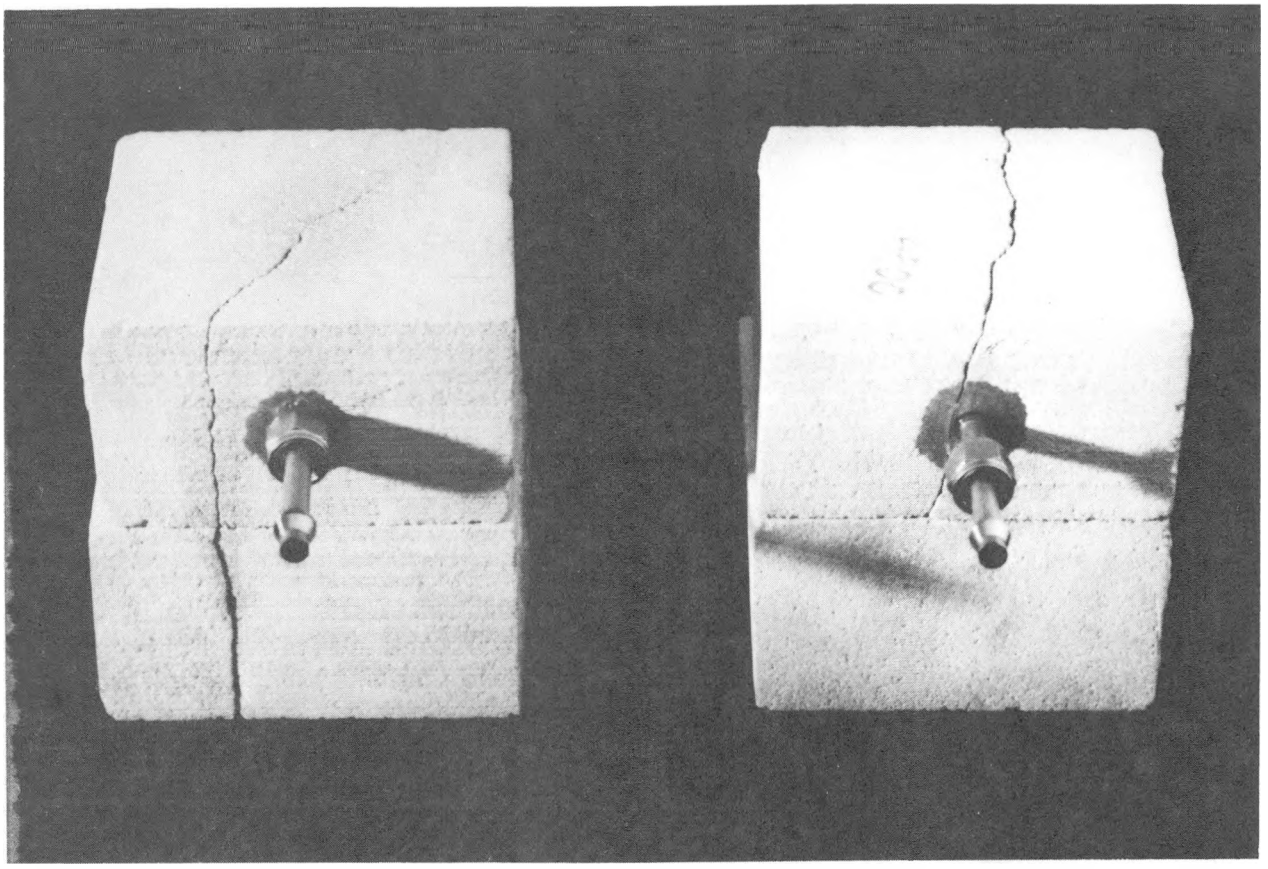


Figure 5. Fractured Indiana limestone blocks.

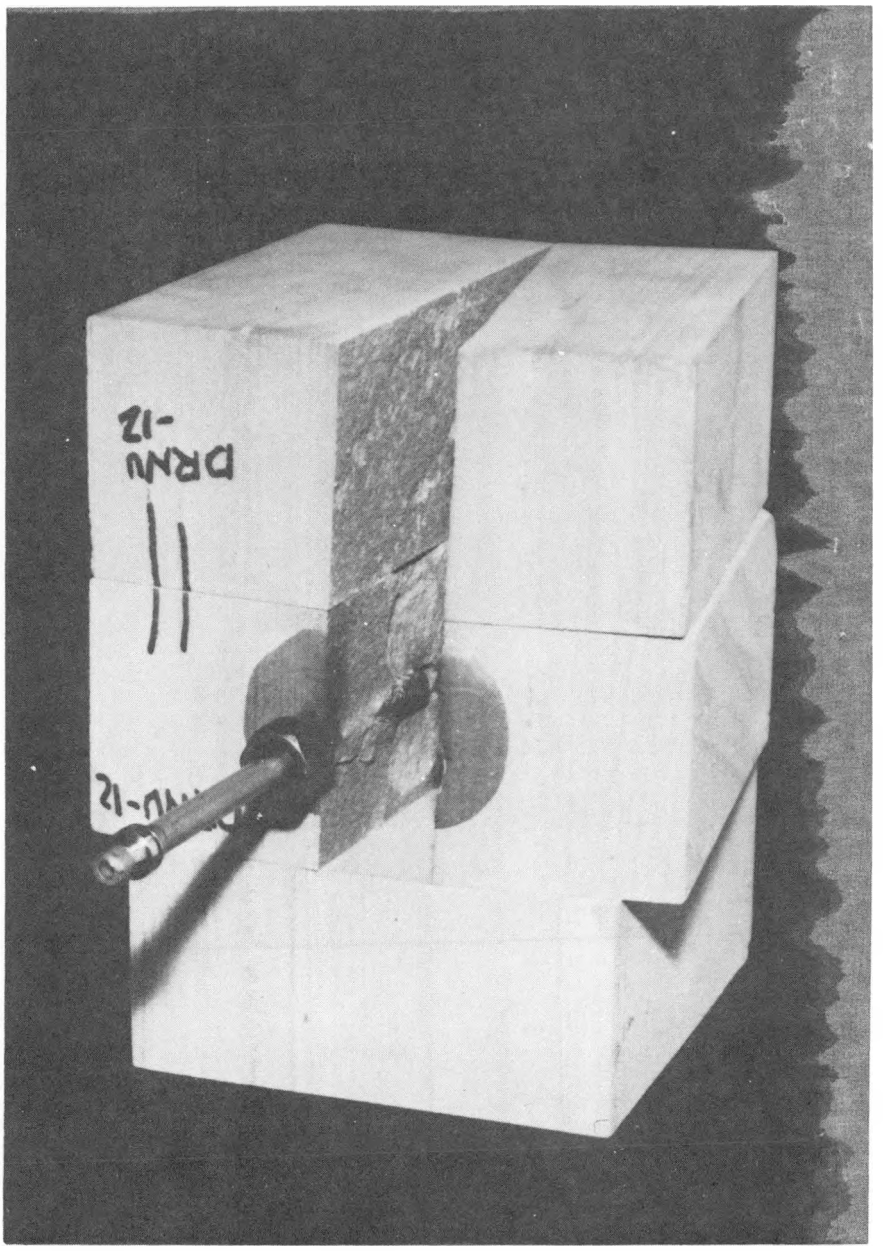


Figure 6. Fractured Nugget sandstone blocks.

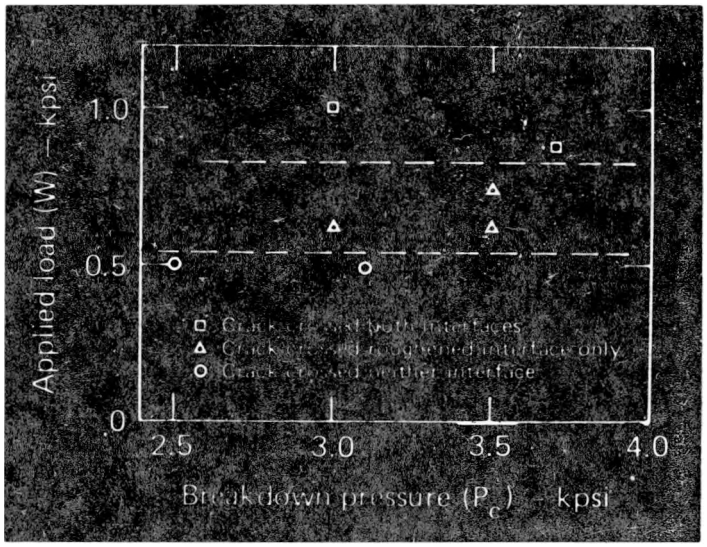


Figure 7. Results from Nugget sandstone fracture experiments.

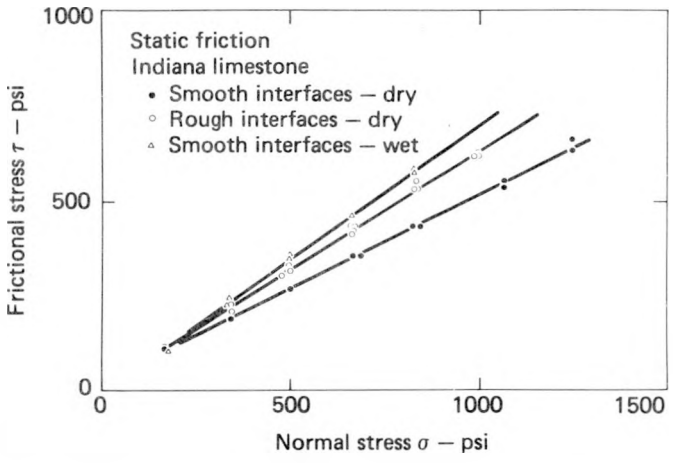


Figure 8. Friction results for Indiana limestone.

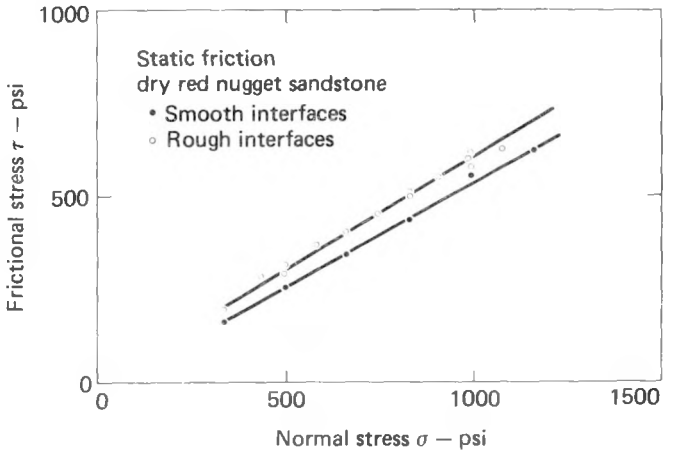


Figure 9. Friction results for red Nugget sandstone.

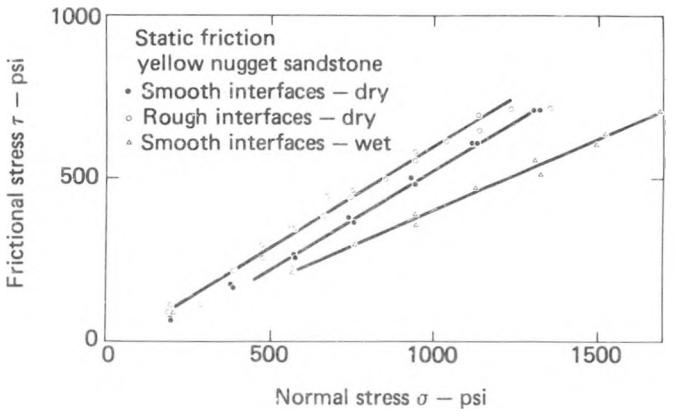


Figure 10. Friction results for yellow Nugget sandstone.

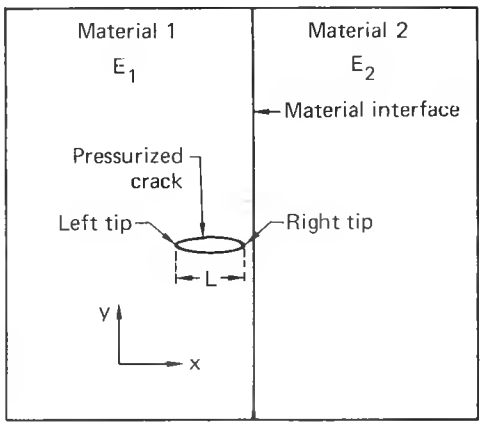


Figure 11. Geometry of a fracture near an interface.

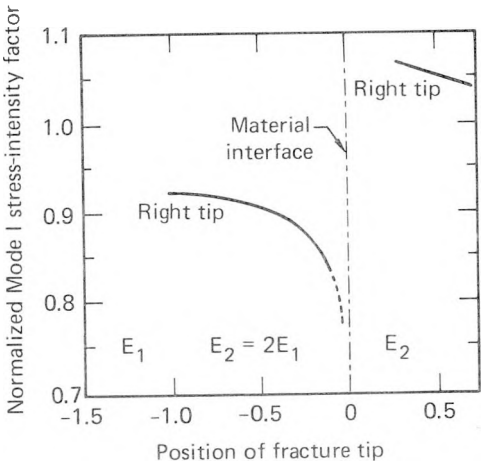


Figure 12. Normalized stress-intensity factor as a function of the position of the crack tip to the interface. The Young's modulus to the right of the interface is twice the modulus to the left, $E_2 = 2E_1$; crack is approaching the interface from the left.

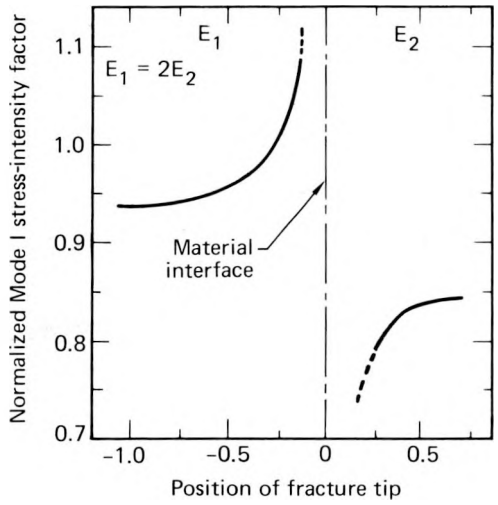


Figure 13. Normalized stress-intensity factor as a function of the position of the crack tip to the interface. The Young's modulus to the left of the interface is twice the modulus to the right, $E_1 = 2E_2$; crack is approaching the interface from the left.

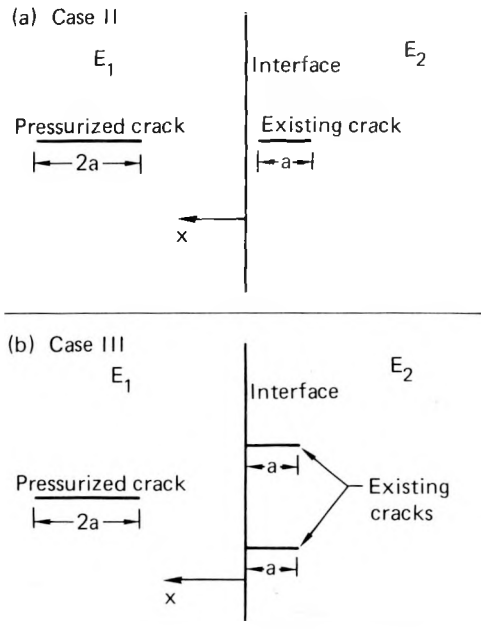


Figure 14. Geometries of the problems for a pressurized fracture near an interface with: a) one fracture across the interface in the higher modulus material (Case II); and b) two fractures across the interface in the higher modulus material (Case III).

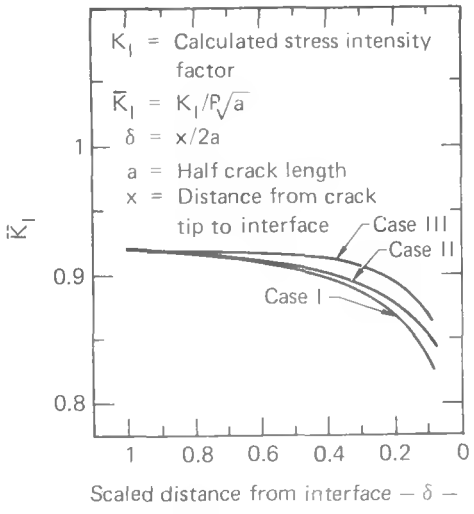
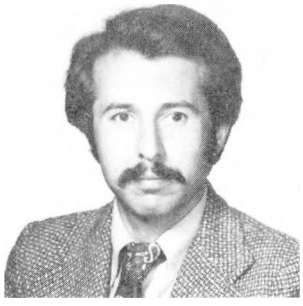


Figure 15. Normalized mode I stress-density factors as a function of scaled distance from the interface for no pre-existing fractures near the interface (Case I), and with pre-existing fractures (Cases II and III).

MODELING OF DEVONIAN SHALE GAS RESERVOIR PERFORMANCE

Fikri Kucuk, Science Applications, Inc., Morgantown, WV

Walter Sawyer, Petroleum Engineering Dept., WVU



ABOUT THE AUTHORS

Fikri Kucuk is a staff scientist with Science Applications, Inc., in Morgantown. He holds a MS degree from the Technical University of Istanbul, a MS and a PhD degree from Stanford University. Kucuk has been involved with numerical modeling, well-test analysis and geothermal reservoir engineering.

Walter K. Sawyer is an Associate Professor of Petroleum Engineering at West Virginia University. He is a graduate of Glenville State College and West Virginia University with degrees in Chemistry (BS) and Mathematics (MS), respectively. Mr. Sawyer has been involved in reservoir simulation work for the nine years at Morgantown Energy and Technology Center of the Department of Energy.

2 MODELING OF DEVONIAN SHALE GAS RESERVOIR PERFORMANCE

ABSTRACT

A recent trend in developing new natural gas reserves has been the intensified efforts to exploit Devonian Shale gas reservoirs in the Appalachian Basin. The Department of Energy (through the Morgantown Energy Technology Center, METC) is engaged in the Eastern Gas Shale Project, which is aimed at accelerating the economical development of this resource.

Most Devonian Shale reservoirs are expected to consist of very tight porous shale formations which may be rather highly fractured in certain tectonic terranes. Under these conditions, the fractures may provide most of the gas permeability, but contribute very little to the overall storage capacity. By comparison, the matrix of the shale may provide most of the storage capacity, but contribute very little to flow because of the low permeability.

Gas transport in Devonian Shale reservoirs, according to the assumption adopted here, occurs only in the permeable fractured medium, into which matrix blocks of contrasting physical properties deliver their gas contents. That is, the matrix acts as a uniformly distributed gas source in a fractured medium. Furthermore, desorption from pore walls will be treated in the modeling as a uniformly distributed source within the matrix blocks.

This paper presents a mathematical model for the purpose of simulating well performance of Devonian Shale gas reservoirs. The applications of the model to Devonian Shale gas reservoir problems (e.g. well test and history matching problems) will have considerable practical interest.

INTRODUCTION

Most Devonian Shale reservoirs are believed to consist of very tight porous shale formations which are often rather highly fractured. Under these conditions, the fractures may provide most of the permeability for gas flow, but contribute very little to the overall storage capacity. By comparison, the matrix of the shale may provide most of the storage capacity of the shale, but contribute little to flow. The gas release and adsorption isotherm data from the Devonian Shale samples indicate that gas resides in the matrix of the shale as a free gas phase and as an adsorbed gas phase.[1] Figure 1 shows methane sorption isotherms at 28°C for the shale samples from the Illinois Basin.[1] In Figure 1, the upper curves measure the total gas content (free + adsorbed gas) as a function of pressure, while the lower curves measure physically adsorbed gas.

The transport of gas through any porous material is largely determined by the pore structure. Since the pore size of the shale matrix is small, gas slippage phenomena cannot be ignored. Moreover, gas desorbs from the pore walls into the shale matrix as pressure drops.

The purpose of this work is to investigate the behavior of gas transport through Devonian Shale gas reservoirs.

DEVELOPMENT OF FLOW MODELS

It is assumed that gas transport in Devonian Shale reservoirs, occurs only in a porous fracture medium into which matrix blocks of contrasting physical properties deliver their gas contents. That is, the matrix acts as a uniformly distributed gas source in a fracture medium.[2] Gas desorption from pore walls will be treated as a uniformly distributed source within the matrix blocks.

The matrix blocks act as a uniformly distributed source. Absence of a fracture network will change the model. The reservoir model without a fracture network will be more simple. The gas transport in such a model will consist of gas flow through pores of the shale with gas desorption from pore walls.

It is believed that Devonian Shale reservoirs usually have fracture network systems. Spacing of fractures is most probably variable from one field to another. In some fields two or more fractures often intersect with a wellbore. It is also believed that most of the fractures are vertical or almost vertical.

A fractured reservoir can be idealized as shown in Figure 2.[3,4] All the fractures can be vertical (see model I in Figure 2), or all vertical and semi-vertical fractures can be replaced by an equivalent orthogonal fracture network (see model II in Figure 2).

The mathematical formulation will be the same for both models. However, the approximation for the matrix block will be a cylindrical element for model I and a spherical element for model II.[22]

The general assumptions for the mathematical model are:

1. Single phase gas flow.
2. The reservoir is horizontal with a homogeneous matrix and fracture systems.
3. The reservoir is at an isothermal condition.
4. The well is centrally located in a finite circular reservoir.
5. Surface diffusion of adsorbed molecules on the walls of the pores will be neglected in the mathematical model. However, those gases which are adsorbed on pore walls pass through more efficiently than those which are not. For example, helium is not easily adsorbed at ordinary and higher temperatures and therefore, does not flow readily through a porous medium. The adsorbed phase must contribute to the overall flow. Thus, neglecting surface diffusion in the model will reduce the flow rate from the matrix.

The gas flow through the fracture system is described by the following equation:

$$\nabla \left[\rho \frac{k_f}{\mu} \nabla p_f \right] + w_m(p_f,t) = \frac{\partial}{\partial t}(\phi_f \rho) \tag{1}$$

Where:

ρ = density, g/cm^3

k_f = fracture permeability, darcy

μ = viscosity, cp

ϕ_f = fracture porosity

p_f = fracture pressure, atm

t = time, sec

w_m = mass flow rate per volume of shale matrix element, g/sec/cm^3

The equation of state for real gas is given by:

$$\rho = \frac{M}{RT} \frac{p_f}{z} \tag{2}$$

Where:

M = molecular weight, g mole

R = Universal gas constant, cm^3 - atm/g mole K

T = Reservoir temperature, K

z = real gas deviation factor

Substitution of Eq. 2 into Eq. 1 yields:

$$\nabla \left[\frac{k_f}{\mu} \frac{p_f}{z} \nabla p_f \right] + \frac{p_f}{z} q_m = \frac{\partial}{\partial t} \left(\phi_f \frac{p_f}{z} \right) \tag{3}$$

Where:

q_m = volumetric flow rate per volume of shale matrix element, cm^3/sec/cm^3

$$= - \frac{A_m}{V_m} \frac{k_m}{\mu} \left(\frac{\partial p_m}{\partial n} \right)_{surface}$$

A_m = surface area of matrix element, cm^2

V_m = volume of element, cm^3

Equation 3 describes gas flow through the fractured shale reservoir with a source term which is the contribution from the shale matrix. Gas transport through the matrix is also described by the diffusivity equation with a source term due to desorption of gas from the pore walls of the matrix. The following equation describes the motion of gas through the matrix.

$$\nabla \left[\rho_m \frac{k_{gm}}{\mu} \nabla p_m \right] + w_d = \frac{\partial}{\partial t} (\phi_m \rho_m) \tag{4}$$

Where:

k_{gm} = permeability to gas, darcy

w_d = desorption rate, $g/sec/cm^3$ shale

p_m = matrix pressure, atm

ϕ_m = matrix porosity

The rate of desorption can be expressed as:

$$w_d = - M \left(\frac{dc_d}{dp_m} \right) \frac{\partial p_m}{\partial t} \tag{5}$$

Where:

c_d = concentration of gas at the surface of pore walls, $mole/cm^3$ shale

$\left(\frac{dc_d}{dp_m} \right)$ = slope of gas desorption isotherm curve, $mole/cm^3$ shale/atm

The gas permeability of a porous medium usually exceeds the liquid permeability of the same medium. The difference in these permeabilities is due to the phenomenon known as gas slippage which is related to the mean free path of the gas molecules relative to pore diameter. Consequently, the gas permeability of a porous medium should be a function of the temperature, pressure, and the nature of the gas. Klinkenberg[5] developed the relationship between gas permeability of a porous medium to a non-reactive liquid,[6,7] viz:

$$k_g = k_\ell \left(1 + \frac{4C\bar{\lambda}}{r} \right) \tag{6}$$

This equation was derived assuming that all the capillaries in the porous medium are of the same diameter, and are oriented at random through the solid material. In Eq. 6, k_g is gas permeability, k_ℓ is liquid permeability in a single phase completely filling the pores of the medium at constant temperature, $\bar{\lambda}$ is the mean free path of the gas molecules, r is the radius of capillaries, and C is a proportionality constant. The mean free path can be expressed as:

$$\bar{\lambda} = \frac{1}{\sqrt{2\pi}\, d^2 n} = \frac{RT}{\sqrt{2\pi}\, \bar{p}_m N d^2} \tag{7}$$

where d is collision diameter, n is concentration of molecules per unit volume, N is Avogadro's Number, $\bar{p}_m$ is mean local pressure, T is temperature, and R is the universal gas constant. The following is obtained by combining Eqs. 6 and 7:

$$k_g = k_\ell \left(1 + \frac{4CRT}{\sqrt{2\pi}\, rNd^2 \bar{p}_m} \right) = k_\ell \left(1 + \frac{b}{\bar{p}_m} \right) \tag{8}$$

where b is the Klinkenberg factor, which is constant for a given gas and a given porous medium at a constant temperature. A graph of k_g vs. $1/\bar{p}_m$ should result in a straight line with an intercept of k_ℓ and a slope of bk_ℓ. Thus, gas permeability is greater at low pressures.

As can be seen from Eq. 8, k_g is a function of mean pore pressure and pore diameter only because all other parameters are constant for a given gas and a given temperature. Since pore diameters are small for Devonian Shales, "b" is expected to be large. Therefore, the Klinkenberg effect or slippage factor cannot be ignored in the Devonian Shale model.

Substitution of Eqs. 2, 5, and 8 into Eq. 4 yields:

$$\nabla\left[\frac{k_\ell}{\mu}\frac{p_m}{z}\left(1+\frac{b}{\overline{p}_m}\right)\nabla p_m\right] = \phi_d\frac{\partial p_m}{\partial t} + \phi_m\frac{\partial}{\partial t}\left(\frac{p_m}{z}\right) \tag{9}$$

Where:

$$\phi_d = \frac{dc_d}{dp}RT, \text{ dimensionless}$$

The source term in Eq. 3 can be determined from the solution of Eq. 9. The solution of Eq. 3 with respect to following initial and boundary conditions then gives the pressure distribution in a Devonian gas reservoir.

Initial Condition:

Initially the reservoir pressure will be assumed to be uniform and equal to p_i. Mathematically this can be stated as follows:

$$p(r,o) = p_i \tag{10}$$

Inner Boundary Condition:

For a general purpose simulation, the flow rate or pressure will be assumed to be a function of time at the inner boundary (wellbore). Mathematically, a variable rate or pressure condition can be expressed as:

$$\text{Variable rate: } \left(r\frac{\partial p(r,t)}{\partial r}\right)_{r=r_w} = \frac{q(t)\mu}{2\pi hk} \tag{11}$$

$$\text{Variable pressure: } p(r_w,t) = p_{wf}(t) \tag{12}$$

Outer Boundary Condition:

The reservoir will be assumed to be bounded with no flow at the outer boundary i.e."

$$\left(r\frac{\partial p(r,t)}{\partial r}\right)_{r=r_e} = 0 \tag{13}$$

ANALYTICAL METHODS

The flow equations presented above are complex and not amenable to exact solution except under special conditions. Analytical solution typically requires very simple and idealized reservoir models and flow conditions (initial and boundary). Nevertheless, analytical solutions may contribute in several ways to the goal of predictive reservoir modeling.

Such solutions produce very useful benchmarks for model testing, refining, and revealing potential problem areas with the more cumbersome numerical solution techniques. However, the accuracy or reliability of any large-scale computer code should never be assumed without extensively testing the ability of that code to reproduce the results of a variety of exact analytical solutions. Thus, before attempting to solve Eqs. 3 and 9 numerically, these equations will be solved analytically,

with the following simplifying assumptions in addition to the initial assumptions which have been made in the development of the flow models:

1. An isotropic finite reservoir of uniform thickness h.
2. All formation properties independent of pressure.
3. No Klinkenberg effect.
4. No desorption within the matrix elements.
5. Matrix elements consist of cylinders with radius a and height h which are equal to the formation thickness.
6. Well produces at a constant pressure.

Under these conditions, the flow equation and initial and boundary conditions for the fracture system becomes:

$$\nabla\left[\frac{p_f}{z\mu}\nabla p_f\right]+\frac{p_f}{zk_f}q_m=\frac{\phi_f}{k_f}\frac{\partial}{\partial t}\left(\frac{p_f}{z}\right) \tag{14}$$

$$p_f(r,o)=p_i\ ,\ r_w\le r\le r_e \tag{14a}$$

$$p_f(r_w,t)=p_{wf}\ ,\ t>0\ ;\ \text{constant flowing pressure at the wellbore} \tag{14b}$$

$$\left(\frac{\partial p_f}{\partial r}\right)_{r=r_e}=0\ ,\ t>0 \tag{14c}$$

The flow equation and initial and boundary conditions for the matrix element become:

$$\nabla\left[\frac{p_m}{z\mu}\nabla p_m\right]=\frac{\phi_m}{k_m}\frac{\partial}{\partial t}\left(\frac{p_m}{z}\right) \tag{15}$$

$$p_m(r,o)=p_i\ ,\ o\le r\le a \tag{15a}$$

$$p_m(o,t)=\text{finite},\ t>0 \tag{15b}$$

$$p_m(a,t)=p_f\ ,\ t>0\ ;\ \text{at the surface of the matrix element} \tag{15c}$$

The solution of Eq. 14 in terms of pseudo-pressure with respect to initial and boundary conditions for a finite reservoir is developed in Appendix A and is given by:

$$\overline{\Delta\psi_f}=\frac{\Delta\psi_{wf}}{s}\frac{U_o(\alpha,r_e,r)}{U_1(\alpha,r_w,r_e)} \tag{16}$$

Where:

ψ_f = fracture pseudo-pressure

s = Laplace space variable

$$\frac{1}{\eta(s)}=\frac{2k_m}{sak_f}\lambda\frac{I_1(\lambda a)}{I_o(\lambda a)}+\frac{1}{\eta_f}$$

$$\lambda^2=s/\eta_m$$

I_1, I_o = Modified Bessel function

$$\alpha^2 = \frac{s}{\eta(s)}$$

$$\Delta\psi_{wf} = \psi_i - \psi_{wf}$$

$$U_o(\alpha, r_e, r) = K_1(\alpha r_e)\, I_o(\alpha r) + I_1(\alpha r_e)\, K_o(\alpha r)$$

$$U_1(\alpha, r_w, r_e) = K_1(\alpha r_e)\, I_o(\alpha r_w) + I_1(\alpha r_e)\, K_o(\alpha r_w)$$

K_1, K_o = Modified Bessel function

This equation gives the Laplace transform of the pseudo-pressure distribution in a finite-dual porosity gas reservoir producing at a constant pressure.

The volumetric flow rate entering the wellbore at a constant pressure is given as:

$$\bar{q}_{sc} = \frac{\gamma \Delta\psi_{wf}}{\sqrt{s\ \eta(s)}} \frac{U_2(\alpha, r_w, r_e)}{U_1(\alpha, r_w, r_e)} \tag{17}$$

Where:

$$\gamma = \pi k_f h\, r_w \frac{T_{sc}}{Tp_{sc}}$$

$$U_2(\alpha, r_w, r_e) = K_1(\alpha r_e)\, I_1(\alpha r_w) - I_1(\alpha r_e)\, K_1(\alpha r_w)$$

The exact inversion of Eq. 17 is complicated. Therefore, the flow rate (q_{sc}) is computed using a numerical Laplace transform inversion technique.

Further, the cumulative production (Q_{sc}) will be determined which is related to q_{sc} by:

$$Q_{sc} = \int_o^t q_{sc}\, dt' \tag{18}$$

The Laplace transform of Q_{sc} is:

$$\bar{Q}_{sc} = \frac{\bar{q}_{sc}}{s} = \frac{\gamma \Delta\psi_{wf}}{s^{3/2}\sqrt{\eta(s)}} \frac{U_2(\alpha, r_w, r_e)}{U_1(\alpha, r_w, r_e)} \tag{19}$$

This equation will also be inverted using the numerical Laplace transform inverter.

Computed values of Q_{sc} and q_{sc} from Eqs. 17 and 19 will be used to check the values of Q_{sc} and q_{sc} from the numerical solution.

NUMERICAL METHODS

Simultaneous solution of the equations presented above is achieved each time-step considering the following three principal aspects of the problem: (1) desorption of gas from pore walls of the shale matrix, (2) Darcy flow through the pores of the matrix into a fracture system considering the "Klinkenberg effect", and (3) Darcy flow through fracture system to a producing well. Figure 3 shows the geometry of a one-dimensional radial model which will be used in simulating single well behavior with radial symmetry.

In the first stage, the production of gas from the wellbore causes a pressure drop in the fracture system. This in turn provides a reduced pressure on the outer surfaces of the shale matrix which causes Darcy flow modified by the Klinkenberg effect within the shale matrix. As this flow occurs, the pressure in the pores of the shale matrix decreases and gas is "fed" into the fracture system. Finally, this reduction in pressure within the pores of the shale matrix causes gas to be desorbed from the walls of the pores which provides "feed gas" to the matrix.

Once gas desorbs from the pore walls it flows through the shale matrix element to its outer surface where it can enter the fracture system via Darcy's law, giving the source term for the reservoir equation:

$$q_m = -\frac{A_m}{V_m}\frac{k_m}{\mu}\left(\frac{\partial p_m}{\partial r}\right)_{r=a} N_m \qquad (20)$$

Here, a, A_m, and V_m are respectively, the radius, surface area, and volume of the matrix element and N_m is the number of elements per reservoir volume unit; i.e.:

$$N_m = \frac{\text{reservoir grid-block grain volume}}{\text{matrix element volume}}$$

For continuity of pressure at the matrix-fracture interface must equal $(p_m)_{r=a}$ must equal p_f. Thus, the reservoir pressure serves as a boundary condition for the shale matrix element.

Using q_m as a source term for the radial diffusivity equation, together with a closed outer boundary and a specified rate or pressure at the wellbore, the reservoir pressure distribution as a function of time may be obtained. Details of the solution procedure are given in Appendix B. Care must be taken to assure that, at the end of each time-step, reservoir pressure, matrix element pressure, desorption rate, and source rate are consistent. The procedure described below was developed for this purpose.

Iterative Solution Procedure

Step 1. Begin new time-step by initializing matrix source rate q_m to zero and solving for reservoir pressure distribution, $p_f^{(m)}$; where m = number of iterations, m = 1, 2, ---.

Step 2. Use reservoir pressure $p_f^{(m)}$, from Step 1 as boundary condition to solve for matrix pressure $p_m^{(m)}$ and source rate q_m; then use q_m to calculate new reservoir pressure, $p_f^{(m+1)}$.

Step 3. Set m=m+1 and calculate average of last two reservoir pressures, i.e.:
$p_{f(avg)}^{(m)} = \frac{1}{2}\left(p_f^{(m)} + p_f^{(m-1)}\right)$

Step 4. Use $p_{f(avg)}^{(m)}$ as boundary condition to solve for new matrix pressure, $p_m^{(m+1)}$.

Step 5. Use $p_m^{(m+1)}$ and N_m to solve for new source rate q_m.

Step 6. Use new source rate to solve for new reservoir pressure, $p_f^{(m+1)}$.

Step 7. If $\left| p_{f(avg)}^{(m)} - p_f^{(m+1)} \right|$ is less than a specified tolerance, accept $p_f^{(m+1)}$ as the new reservoir pressure, and go to Step 1; otherwise, go to Step 3.

Wellbore conditions include the capability to simulate a variable rate or pressure history with skin damage and wellbore storage effects upon shut-in. A back pressure option is provided so that a specified wellhead pressure as a function of time may be used directly as input data.

The model consists of a main program, which has approximately 1000 lines of FORTRAN IV code, together with several subroutines for repetitive procedures such as transmissibility and bottom-hole pressure calculations.

WELLBORE OPTIONS

In addition to the capability to specify any rate or pressure each time-step, the numerical model has the following options and special features:

1. Skin damage. As presented by Craft and Hawkins,[11] the "infinitesimal" skin factor, s, introduced by van Everdingen[13] can be related to a finite damaged zone of radius r_{skin} and permeability k_d as follows:

$$s = \frac{k - k_d}{k_d} \, In\left(\frac{r_{skin}}{r_w}\right) \tag{22}$$

In the finite-difference model it is convenient to take $r_3 = r_{skin}$ as shown in Figure 7. Thus, for any specified skin factor, we can solve Eq. (22) for the correct value of k_d to find:

$$k_d = \frac{k_2}{1 + \frac{s}{In(r_3/r_w)}} \tag{23}$$

Where k_2 is the undamaged permeability of Node 2.

2. Wellbore storage (afterflow). If the wellbore (tubing and annulus) is full of fluid at the time of shut-in, which is nearly always the case for gas wells, the sand-face rate is given by:

$$q_{sc} = \frac{T_{sc} V_w}{p_{sc} T} \frac{d(p/z)}{dt} \tag{24}$$

The finite-difference from Eq. 24 is:

$$q_{sc}^{n+\frac{1}{2}} = \frac{T_{sc} V_w}{p_{sc} T} \frac{1}{\Delta t} \left[(p/z)^{n+1} - (p/z)^n\right] \tag{25}$$

Equation 25 will be used for wellbore storage in the numerical simulator.

3. Back pressure equation. The Cullender-Smith Equation[12] solved for bottom-hole pressure is:

$$p_{bh}^2 = e^S \, p_{wh}^2 + \frac{q_{MCFD}^2 \, G \, T_a z_a \, f \, X}{40000 \, d^5} \left(\frac{e^S - 1}{S}\right) \tag{26}$$

Where:

G = gas gravity

T_a = average wellbore temperature, deg R

z_a = average gas deviation factor

f = friction factor

X = well depth, ft.

d = tubing ID, in.

p_{wh} = wellhead pressure, psia

p_{bh} = bottom-hole pressure, psia

$S = .0375 \, G \, X/T_a z_a$.

Subroutines have been written to calculate both the friction factor and bottom-hole pressure so that any specified back pressure can be used each time-step. These options provide a very powerful tool for studying gas well performance. In fact, together with the capability to vary rate or pressure as a function of time, virtually any gas well test or production performance can be simulated, with or without the effects of gas desorption and the dual porosity system.

RESERVOIR-INPUT PARAMETERS

The Devonian gas reservoir simulator requires input of all information describing the geometry of the flow system, shale and gas properties, adsorption and desorption properties of the shale matrix, the initial condition of the system, and wellbore conditions.

A simulation model may represent the behavior of laboratory equipments, individual wells, or reservoir systems. The simulator enables the engineer to examine and evaluate the physical and economic consequences of various alternative production policies. But a successful output from a simulator is really dependent on the reliability of the input data. Perhaps the most critical data are matrix and fracture permeabilities, fracture spacing and desorption data. Unfortunately, most of the necessary data for Devonian Shale reservoir simulations are not reliable. There are no available data for fracture spacing, geometry of the matrix elements, and desorption characteristic of the shale. In the following paragraphs, some of the data used in the simulator will be discussed.

Gas slippage, or Klinkenberg effects, are pronounced in Devonian Shales. Jones and Owens[16] noted that the conventional extrapolative procedure (in which permeability ploted versus reciprocal arithmetic mean pressure is extrapolated to zero reciprocal pressure) for determing Klinkenberg permeability, k_ℓ might not yield a straight line for very low permeability. Unfortunately, there is no experimental data to validate or refute this statement for the Devonian Shale.

The equation for the Klinkenberg "b" factor used in the simulator is given by:[16]

$$b = 0.86\ k_\ell^{-0.33} \tag{27}$$

This equation is only valid for: $0.0001\ \text{md} < k_g < 1\ \text{md}$

and the shale matrix permeability may go several orders of magnitude below 0.0001 md. Therefore, the "b" factor needs to be determined experimentally for shale samples. There is no systematic measurement of matrix permeability for Devonian Shales. Schettler[17] et al. have presented some diffusion constant measurements at atmospheric pressure and an equation to relate permeability and the diffusion constant for the shale matrix.

Except for some measurements of high pressure adsorption isotherms for shale samples from the Illinois Basin[1] (as shown in Figure 1), and the work of Schettler, at atmospheric pressure on shale samples from Lincoln County, WV, there is practically no data available on the Devonian Shale.

As stated earlier, fracture spacing is an important parameter for which there is no known measurement technique. However, Muskat presented an equation for fracture permeability as:[18,19]

$$k_f = \frac{10^8 W^3}{12\ S},\ \text{darcy} \tag{28}$$

Where: W = fracture width, cm.

S = fracture spacing, cm.

Figure 8 shows fracture spacing versus fracture permeability for various fracture openings as calculated from the above equation. Thus, if provided with good data on fracture permeability (determined from reliable well test data) and fracture openings (measured from core samples), the fracture spacing can be approximated by Eq. 28.

The fracture permeability calculated from Eq. 28 usually yields high values because open tension fractures must be filled by an intruded foreign rock or a recrystallized component of the surrounding rock. In the Devonian Shale, fractures might be filled with either carbonate or pyritic material.[20,21]

As a reservoir is produced, some permeability reduction in the fracture system might be expected because fractures created during stress conditions might become sealed after release of the stress.[21]

As a last resort, the history matching technique with production or pressure data (or both) can be used to determine some of the reservoir parameters from the simulator. However, combinations of at least ten parameters for a typical Devonian Shale reservoir must be used to find a good match between field data and simulated data. Thus, the uniqueness of the matching may not be achieved if many permutations of the parameters are possible.

In summary, much of the general, qualitative and quantitative understanding of the gas transport mechanism and reservoir parameters have to be based on field and laboratory measurements. In order to make an engineering analysis, it is essential to determine and measure all of the necessary basic information about the actual Devonian Shale reservoir. Then a "sound" reservoir model can be built and simulation runs can be made. Otherwise, one may end up with a useless solution which is called "garbage in--garbage out!"

DISCUSSIONS OF RESULTS

Due to its complexity, the validity of the numerical model was impossible to prove using current techniques of analysis for stability and convergence. Therefore, it was necessary to conduct numerical experiments to evaluate the Devonian Shale reservoir simulation techniques described above. Use of finite difference approximations in the solution of Eqs. 3 and 9 introduced time and space truncation errors. If these truncation errors are sufficiently small, the numerical solution will be satisfactory. To evaluate the accuracy of these numerical solutions, the Devonian Shale gas simulator was used to calculate the performances of single and dual porosity models for which analytical solutions exist.

Slider[23] presented an equation for a single porosity gas reservoir producing at a constant pressure as:

$$Q_{MSCF} = \frac{0.111\ \phi h\ r_w^2\ c\ \left(p_i^2 - p_{wf}^2\right)\ Q_{tD}}{z_{avg}\ T_f} \qquad (29)$$

Q_{tD} can be read from the van Everdingen - Hurst[24] table for a given t_D.

Where:

ϕ = porosity

h = formation thickness, ft.

r_w = wellbore radius, ft.

c = compressibility of gas, $psia^{-1}$

p_i = initial reservoir pressure, psia

p_{wf} = flowing wellbore pressure, psia

Q_{tD} = dimensionless cumulative production

z_{avg} = average compressibility factor, calculated at $(p_i + p_{wf})/2$ and T_f

T_f = formation temperature, R

$$t_D = \frac{6.33\ 10^{-3}\ k\ t}{\phi \mu\ c\ r_w^2}$$

t = time, day

k = permeability, md

μ = viscosity, cp

Cumulative production values calculated from the simulator for a single porosity model should be the same as cumulative production calculated from Eq. 29. The differences in cumulative production values calculated from the simulator and Eq. 20 are less than two percent, even though Eq. 29 is not an exact solution of the unsteady-state gas flow.

By eliminating the desorption from the simulator, the model reduces to the dual porosity system described in the Analytical Methods section. The cumulative production results calculated from the analytical solution (Eq. 19) and from the simulator were presented in Figure 9. The numerical results were within two percent of the analytical solution. These comparisons show that the numerical solutions are of satisfactory accuracy for most engineering calculations.

Table 1 presents the reservoir parameters selected as a base case for the sensitivity analysis of Devonian Shale reservoirs. The effects of reservoir parameters on the cumulative production of a Devonian Shale gas well which produces at a constant pressure will be discussed.

The upper curve in Figure 10 represents cumulative production versus time for a dual-porosity model with desorption. The middle curve represents cumulative production versus time for a dual-porosity model without desorption. The lower curve represents cumulative production versus time for a single porosity model. During the early life of the reservoir, the effects of secondary porosity with or without desorption on production are small. But after the initial flow period of a few years, gas flow from the matrix of the shale is very pronounced.

Figure 11 shows the effect of varying the fractured shale reservoir permeability, k_f, on the cumulative production as a function of time. All the reservoir parameters in these three cases are the same except k_f. The flow behavior of this model was dominated by the permeability of the fracture system. Secondary porosity and desorption improve the well performance; in fact the well with a 1000 feet drainage radius acts in an infinite system, even after 25-30 years of production. Long life of an individual well makes Devonian Shales a valuable resource even though production rate is usually low.

Figure 12 shows the shale matrix permeability, k_m, to be another important parameter which effects well productivity. As the matrix permeability decreases, the effect becomes very dominant. The relationship between the cumulative production and the matrix permeability is not linear; i.e., if the permeability is reduced from 0.1×10^{-3} md to 0.1×10^{-7} md the reduction in cumulative production will be 5 percent. However if permeability is reduced from 0.1×10^{-7} md to $0.1\ 10^{-9}$ md the reduction in the cumulative production will be 34 percent.

Figure 13 presents the cumulative production values for different fracture porosities (ϕ_f) as a function of time. The effects of fracture porosity on the cumulative production is almost negligible. The range of fracture porosity that is $\phi_f = 0.05$ to 0.002 is representative for Devonian Shales.

Figure 14 describes the well performance for different values of matrix porosity (ϕ_m). Here the effect of the matrix porosity on the cumulative production is small. However, a maximum matrix porosity of 4 percent may be very low for Devonian Shales because the commercial mercury porosimeter has a lower limit of pore-diameter penetration of about 30° Angstrom[1] (Å). But according to Ref. 1, the pore-diameters for Devonian Shales can be less than about 4 Å.

Figure 15 shows that a three fold increase in matrix size causes about a 10 percent increase in cumulative production. If the matrix permeability is greater than 10^{-6} this effect is almost negligible. But when the matrix permeability decreases, the effect of matrix size will dominate well performance.

Figure 16 shows the cumulative production for various drainage radii as a function of pressure. Here the effect of the outer boundary was felt by the well after about 6 years for r_e=500 feet but the cumulative production continues to increase as a function of time due to production from the matrix element. A Devonian Shale reservoir with a drainage radius of 1000 or 2000 feet acts as an infinite reservoir.

Figure 17 shows production rate versus time as a function of fracture system permeability (k_f). The rate decline is very slow as in the actual curves in Figure 6 of Ref. 25. Figure 17 also shows that the production decline is not an exponential decline as given in Ref. 26.

Figure 18 shows a breakdown of resource recovery at low values of matrix permeability (k_m). As k_m approaches zero, a single porosity system is approached where gas is only produced from fracture systems. As k_m increases, the recovery of original fracture and matrix gas approaches a common value. For the base case value of $k_m(.1 \times 10^{-3})$, the matrix and fracture recovery was 22.1 percent at 27 years, which is very close to the average of r_f and r_m in Figure 18. Note that as matrix permeability increases, the recovery of adsorbed gas increases since a higher k_m results in larger pressure drops in the shale matrix which, in turn, allows more gas to be desorbed. Of particular significance is the fact that for a low, but not unreasonable, matrix permeability of $.1 \times 10^{-8}$md, the total resource recovery, r_t, is only 13.5 percent after 27 years.

CONCLUSIONS

Since the turn of the century, gas has been produced from the more favorable regions of Devonian Shales in the Appalachian Basin. Various techniques have been utilized for the quantitative evaluation of the gas resource in the Appalachian region. This study has indicated that the resource calculations based on limited data are insufficient to be representative of the whole region. Data are insufficient for many of the important reservoir parameters which are the controlling factors of well performance. The following conclusions have been reached in this study:

1. A new reservoir model capable of predicting Devonian Shale reservoir performance, taking into account the shale matrix contribution to the production and desorption from the pore walls, has been proposed; a one-dimensional radial model has been tested by comparison of calculated cumulative production values with results for limiting cases obtained with analytical methods.

2. The sensitivity analysis showed that the early performance of shale reservoirs is dominated by fracture system parameters, while the later performance of the shale reservoir is primarily controlled by shale matrix and desorption parameters.

3. The sensitivity analysis also showed that fracture system permeability, matrix permeability and size, and desorption isotherms are the determining factors of reservoir performance.

4. The model developed here is capable of handling various wellbore conditions including wellbore storage and skin as well as prescribed wellbore or wellhead conditions such as constant back-pressure, variable back-pressure or constant or variable pressure or rate at the wellbore.

5. The tests so far are one-dimensional radial, although no qualitative difference in applying the approach in more space dimensions is expected.

NOMENCLATURE

a	Radius of shale element, cm	r	Radius, cm
c	Concentration, g mole/cm^3	r_w	Well radius, cm
D	Diffusivity, cm^2/sec	r_e	Drainage radius, cm
k_f	Fracture permeability, Darcy	R	Universal gas constant, atm-cm^3/g mole K
k_m	Matrix permeability, Darcy	s	Laplace space time variable
M	Molecular weight, g-mole	T	Temperature, ^oK
q_m	Volumetric flow rate from matrix element, cm^3/sec/cm^3	w_m	Mass flow rate from shale matrix element, g/sec/cm^3
q_{sc}	Production rate, cm^3/sec	t	Time, sec
p_f	Fracture pressure, atm	ϕ_f	Fracture porosity
p_i	Initial reservoir pressure, atm	ϕ_m	Matrix porosity
p_m	Matrix pressure, atm	ρ	Density of gas, g/cm^3
p_{wf}	Flowing well pressure, atm	ψ	Pseudo-pressure, atm^2/cp

μ Viscosity of gas, cp z Compressibility factor

ACKNOWLEDGEMENTS

The authors are grateful to Mr. Walter Rose, Senior Staff Scientist, Science Applications, Inc., for his advice and encouragement during this work. We thank the management of Science Applications, Inc., Morgantown for permission to present this paper.

We also acknowledge the aid and encouragement given by Mr. Charles A. Komar, Assistant Project Manager of the Eastern Gas Shales Project, and Mr. C. David Locke, Chief of Oil, Gas, and In Situ Coal R&D Branch at the DOE Morgantown Energy Technology Center (METC).

REFERENCES

1. Thomas J., Jr., and Frost, R. R.,: "Internal Surface Area and Porosity in Eastern Gas Shales from the Sorption of Nitrogen, Carbon Dioxide, and Methane," in preprints of First Eastern Gas Shales Symposium, Morgantown, WV, Oct. 17-19, 1977.

2. de Swaan, D. A.: "Analytical Solution for Determining Naturally Fractured Reservoir Properties by Well Testing, Soc. Pet. Eng. J. (June 1976), p. 112-117.

3. Warren, J. E. and Root, P. J.: "The Behavior of Naturally Fractured Reservoirs," Soc. Pet. Eng. J. (Sept. 1963), p. 245-255.

4. Kazemi, H.: "Pressure Transient Analysis of Naturally Fractured Reservoirs with Uniform Fracture Distribution," Soc. Pet. Eng. J. (Dec. 1969), p. 451-462.

5. Klinkenberg, L. J.: "The Permeability of Porous Media to Liquids and Gases," Drilling and Production Practice (1941), p. 200-213.

6. Rose, W. D.: "Permeability and Gas-Slippage Phenomena," Trans., AIME (1948), v. 28, p. 127-135.

7. Ramey, H. J., Jr., Brigham, W. E., Chen, H. K., Atkinson, P. G., and Arihara, N: Thermodynamic and Hydrodynamic Properties of Hydrothermal Systems, SGP-TR-6, Stanford University (1974).

8. Al-Hussainy, R., Ramey, H. J., Jr., and Crawford, P. B.: "The Flow of Real Gases Through Porous Media," J. Pet. Tec. (May 1966), p. 624.

9. von Rosenberg, D. U.: Methods for the Numerical Solution of Partial Differential Equations, Elsevier Publishing Co., Inc., New York (1969).

10. van Poolen, H. C., Bixel, H. C., and Jargon, J. R., Reservoir Modeling, The Petroleum Publishing Co., Tulsa, OK.

11. Craft, B. C. and Hawkins, M. F.: Applied Petroleum Reservoir Engineering, Prentice-Hall, Inc., Englewood Cliffs, NJ (1959).

12. Katz, D. L., Cornell, D., Kobayashi, R., Poettmann, F. H., Vary, J. A., Elenbaas, J., and Weinaug, C. F.: Handbook of Natural Gas Engineering, McGraw-Hill Book Co., Inc., New York, NY (1959).

13. van Everdingen, A. F., "The Skin Effect and Its Influence on the Productive Capacity of a Well", Trans., AIME (1953), v. 198, p. 171-176.

14. Breitenbach, E. A., Thurnau, D. H., and van Poolen, H. K.: "Immiscible Fluid Flow Simulator," SPE paper 2019, Presented at the Symposium on Numerical Simulation of Reservoir Performance, SPE-AIME, Dallas, TX, April 22-23, 1968.

15. Staggs, H. M. and Herbech, E. F.: "Reservoir Simulation Models - An Engineering Overview," J. Pet. Tech. (Dec. 1971), p. 1428-1436.

16. Jones, F. O. and Owens, W. W.: "A Laboratory Study of Low Permeability Gas Sands," SPE paper 7551, Presented at the SPE Symposium on Low Permeability Gas Reservoirs, SPE-AIME, Denver, CO, May 20-22, 1979.

17. Schettler, P. D., Jr., Wampler, D. L., Sipling, P. J., and Mitchell, D. J.: "The Relationship of Thermodynamic and Kinetic Parameters to Well Production in Devonian Shale," in Preprints of First Eastern Gas Shales Symposium, Morgantown, WV, Oct. 17-19, 1977, Morgantown Energy Research Center, p. 450-461.

18. Muskat, M.: The Flow of Homogeneous Fluids Through Porous Media, McGraw-Hill Book Co., Inc., New York (1937).

19. Elkins, F. L.: "Fractures in the Devonian Shale and the Spraberry," A letter to J. P. Brashear, Lewin and Associates, Inc., Sept. 8, 1979.

20. Kucuk, F., Alam, J., and Streib, D. L.: "Reservoir Engineering Aspects and Resource Assessment Methodology of Eastern Gas Shales," in Preprints of Second Eastern Gas Shales Symposium, Morgantown, WV, Oct. 16-18, 1977.

21. De Sitter, L. W.: Structural Geology, McGraw-Hill Book Co., Inc., New York (1964), p. 70.

22. Ancell, K. L., Price, H. S., and Ford, W. K.: "An Investigation of the Gas Producing and Storage Mechanism of the Devonian Shale at Cottageville Field," SPE paper 2938, Presented at the SPE Symposium on Low Permeability Gas Reservoirs, SPE-AIME, Denver, CO, May 20-22, 1979.

23. Slider, H. C.: Practical Petroleum Reservoir Engineering Methods, The Petroleum Publishing Co., Tulsa, OK (1976), p. 223-224.

24. van Everdingen, A. F., and Hurst, W.: "The Application of the Laplace Transformation to Flow Problems in Reservoirs," Trans., AIME, v. 186 (1949), p. 305-324.

25. Smith, E. C., Cremean, S. P., and Kozair, G.: "Gas Occurrence in the Devonian Shale," SPE paper 7921, presented at the SPE Symposium on Low Permeability Gas Reservoirs, SPE-AIME, Denver, CO, May 20-22, 1979.

26. Kuuskraa, V. A., Brashear, J. P., Doscher, T. M., and Elkins, L. E.: "Enhanced Recovery of Unconventional Gas Sources," Section on Devonian Shale Gas of the Appalachian Basin, V. III (1978).

APPENDIX A

The flow in the fracture systems is given by Eq. 14, with respect to initial conditions Eq. 14a, and boundary conditions Eq. 14b and 14c. Equations 14 to 14c can be linearized by applying the pseudo-pressure transformation. The pseudo-pressure[8], ψ, is defined as:

$$\psi_f = 2 \int_o^{p_f} \frac{p_f}{z\mu} dp_f \qquad \text{(A-1)}$$

The variable ψ_f has the dimension of pressure-squared per centipoise. Equations 14 to 14c can be rewritten in terms of the pseudo-pressure in radial coordinates as:

$$\frac{1}{r}\frac{\partial}{\partial r}\left(r\frac{\partial \Delta\psi_f}{\partial r}\right) - \frac{2\,k_m}{ak_f}\left(\frac{\partial \Delta\psi_m}{\partial r}\right)_{r=a} = \frac{1}{\eta_f}\frac{\partial \Delta\psi_f}{\partial t} \qquad \text{(A-2)}$$

$$\Delta\psi_f\,(r,o) = 0 \;;\; r_w \leq r \leq r_e \qquad \text{(A-3)}$$

$$\Delta\psi_f\,(r_w,t) = \Delta\psi_{wf} \;;\; t>0 \qquad \text{(A-4)}$$

$$\left(\frac{\partial \Delta\psi_f}{\partial r}\right)_{r=re} = 0 \;;\; t>0 \qquad \text{(A-5)}$$

Where:

$$\Delta\psi_f = \psi_i - \psi_{wf} \;;\; \eta_f = \frac{k_f}{\phi_f \mu_i c_i}$$

To solve equation A-2, with subject to initial conditions Eq. A-3, and boundary conditions Eq. A-4 and A-5, Eq. A-1, A-4 and A-5 are transformed in Laplace space as:

$$\frac{1}{r}\frac{\partial}{\partial r}\left(r\frac{\partial \Delta\bar{\psi}_f}{\partial r}\right) - \frac{k_m}{ak_f}\left(\frac{\partial \Delta\bar{\psi}_m}{\partial r}\right)_{r=a} = \frac{s}{\eta_f}\Delta\bar{\psi}_f \tag{A-6}$$

$$\Delta\bar{\psi}_f(r) = \frac{1}{s}\Delta\bar{\psi}_{wf} \tag{A-7}$$

$$\left(\frac{\partial \Delta\bar{\psi}_f}{\partial r}\right)_{r=\bar{r}_e} = 0 \tag{A-8}$$

To solve Eq. A-6, $\left(\frac{\partial \Delta\psi_m}{\partial r}\right)_{r=a}$ must be determined and therefore the flow equation for the matrix element must be solved.

The flow in the matrix element is given by Eq. 15, with initial and boundary conditions given by Eqs. 15a, 15b, and 15c. Equation 15 can be linearized by applying psuedo-pressure[8] in radial coordinates as:

$$\frac{1}{r}\frac{\partial}{\partial r}\left(r\frac{\partial \Delta\psi_m}{\partial r}\right) = \frac{1}{\eta_m}\frac{\partial \Delta\psi_m}{\partial t} \tag{A-8}$$

Eq. A-8 will be solved for a cylindrical matrix element with subject to the following initial and boundary conditions:

$$\Delta\psi_m(r,o) = 0 \; ; \; o \leq r \leq a \tag{A-9}$$

$$\Delta\psi_m(o,t) = \text{finite} \; ; \; t > 0 \tag{A-10}$$

$$\Delta\psi_m(a,t) = \Delta\psi_f \text{ , at the surface of the matrix element; } t>o \tag{A-11}$$

Where:

$$\Delta\psi_m = \psi_i - \psi_m$$

$$\eta_m = \frac{k_m}{\phi_m c_i \mu_i}$$

$$\psi_m = \int_o^{p_m} \frac{p_m}{z\mu}\, dp_m$$

The general solution of Eq. A-8 subject to Eqs. A-10 to A-11 in Laplace space is given by:

$$\Delta\bar{\psi}_m = \Delta\bar{\psi}_f \, I_o(\lambda r) \, / \, I_o(\lambda a) \tag{A-12}$$

Where:

$$\lambda^2 = \frac{s}{\eta_m}$$

Taking the derivative of Eq. A-12 with respect to r, and setting r equal to a yields:

$$\left(\frac{\partial \Delta\bar{\psi}_m}{\partial r}\right)_{r=a} = \lambda \Delta\bar{\psi}_f \, I_1(\lambda a) \, / \, I_o(\lambda a) \tag{A-13}$$

Substitution of Eq. A-13 into Eq. A-6 yields:

$$\frac{1}{r}\frac{\partial}{\partial r}\left(r\frac{\partial \Delta\psi_f}{\partial r}\right) - \frac{s}{\eta(s)}\Delta\bar{\psi}_f = 0 \qquad \text{(A-14)}$$

Where:

$$\frac{1}{\eta(s)} = \frac{2\,k_m}{sak_f}\lambda\frac{I_1(\lambda a)}{I_o(\lambda a)} + \frac{1}{\eta_f}$$

The solution of this equation with respect to boundary conditions Eqs. A-7 and A-8 gives Eq. 16 in the main text.

APPENDIX B

NUMERICAL PROCEDURES

The flow equations for fracture systems and matrix elements are given by Eqs. 3 and 9 in the main text. These two equations must be coupled with the source term into the fracture system. The source term is given by:

$$q_m = -\frac{A_m}{V_m}\frac{k_m}{\mu}\left(\frac{\partial p_m}{\partial r}\right)_{r=a} N_m \qquad \text{(B-1)}$$

Simultaneous solution of Eqs. 3 and 9 coupled with Eq. B-1 and the fact that p_f is a boundary condition for the matrix element, describes gas transport through the Devonian Shales.

In discussing finite-difference techniques for solving Eqs. 3 and 9, subscripts "f" and "m" will be dropped for simplicity and readibility.

Solutions of Flow Equation for the Fracture System

Equation 3 may be efficiently solved numerically using the following stepwise procedure.

Step 1: Define a block-centered grid with radii defined as illustrated in Figure 4.

Step 2: Write the finite-difference approximation of Eq. 3 for node i over a time interval Δt as:

$$\frac{T_{sc}}{p_{sc}T}\frac{\left[\frac{1}{\bar{r}_i}\left(\frac{pk}{\mu z}\frac{\partial p}{\partial \ln r}\right)_{i+\frac{1}{2}} - \left(\frac{pk}{\mu z}\frac{\partial p}{\partial \ln r}\right)_{i-\frac{1}{2}}\right]}{(r_{i+1} - r_i)} + (q_{sc})_i = \frac{T_{sc}}{p_{sc}T}\frac{\phi_i}{\Delta t}\left[(p/z)_i^{n+1} - (p/z)_i^n\right] \qquad \text{(B-2)}$$

Superscript "n" denotes time and q_{sc} is the source rate in SCF/day/cu.ft.

Step 3: Expending the flow terms in Eq. B-2 at the grid block boundaries, using the relationship for radial flow through beds in series, and multiplying Eq. B-2 by the grid block volume the implicit-difference form becomes:

$$TR_{i-\frac{1}{2}}^{n+1}\left(p_{i-1}^{n+1} - p_i^{n+1}\right) + TR_{i+\frac{1}{2}}^{n+1}\left(p_{i+1}^{n+1} - p_i^{n+1}\right) + \left(q_{sc}\right)_i = \Gamma_i\left[(p/z)_i^{n+1} - (p/z)_i^n\right] \qquad \text{(B-2)}$$

Where:

$$TR^{n+1}_{i-\frac{1}{2}} = \pi h \left(\frac{T_{sc}}{p_{sc} T}\right) TM_{i-\frac{1}{2}} \left(p^{n+1}_{i-1} + p^{n+1}_{i}\right)$$

= interblock transmissibility

$$\Gamma_i = \frac{T_{sc}}{p_{sc} T} \frac{(V_p)_i}{\Delta t}$$

V_p = pore volume

$$TM_{i-\frac{1}{2}} = \frac{k_{i-1}\, k_i}{k_i\, (\mu z)_{i-1}\, ln(r_i/\bar{r}_{i-1}) + k_{i-1}\, (\mu z)_i\, ln(\bar{r}_i/r_i)} .$$

$(q_{sc})_i$ = SCF/day

The grid block volume used in Eq. B-2 is defined as:

$$V_i = 2\pi k \bar{r}_i \left(r_{i+1} - r_i\right) \tag{B-4}$$

Step 4: Expand the p/z term on the RHS of Eq. B-2 to get:

$$(p/z)^{n+1}_i - (p/z)^n_i = p^n_i \left(\frac{1}{z^{n+1}_i} - \frac{1}{z^n_i}\right) + \frac{1}{z^{n+1}_i} \left(p^{n+1}_i - p^n_i\right) \tag{B-5}$$

Step 5: Define an iteration scheme for solving Eq. B-3 with the RHS expanded as in Eq. B-5. Begin with old time level values for $TR_{i-\frac{1}{2}}$ and z^{n+1}_i in Eq. B-5; then iterate until no further change in pressure is observed; i.e., if "*" denotes the latest calculated values for p and z then Eq. B-2 can be written as:

$$TR^*_{i-\frac{1}{2}} \left(p^{n+1}_{i-1} - p^{n+1}_i\right) + TR^*_{i+\frac{1}{2}} \left(p^{n+1}_{i+1} - p^{n+1}_i\right) + \left(q_{sc}\right)_i = \tag{B-6}$$

$$\Gamma_i \left[p^n_i \left(\frac{1}{z^*_i} - \frac{1}{z^n_i}\right) + \frac{1}{z^*_i} \left(p^{n+1}_i - p^n_i\right)\right].$$

Equation B-6 can be written as a tri-diagonal system:

$$a_i\, p^{n+1}_{i-1} + b_i\, p^{n+1}_i + c_i\, p^{n+1}_{i+1} = d_i \tag{B-7}$$

Where:

$$a_i = TR^*_{i-\frac{1}{2}}$$

$$b_i = TR^*_{i-\frac{1}{2}} - TR^*_{i+\frac{1}{2}} - \Gamma_i / z^*_i$$

$$c_i = TR^*_{i+\frac{1}{2}}$$

$$d_i = -\left(q_{sc}\right)_i - \Gamma_i \left(p^n_i / z^n_i\right)$$

The Thomas Algorithm[9] may be used to solve the system of equations given in Eq. B-7 for new reservoir pressures. TR*'s and z*'s are then recalculated and the process is repeated until the maximum change in pressure at any node is less than some specified tolerance. Note that at convergence, z_i^* will be essentially equal to z_i^{n+1}.

This iterative procedure is described by van Poolen[10] and has been found to work very well. Usually it will converge in two or three iterations and seldom requires more than six iterations, even for very large changes in wellbore conditions.

Boundary Conditions: The external reservoir radius is closed which is easily accomplished in the Thomas Algorithm by setting:

$$c_N = TR_{N+\frac{1}{2}} = 0 \tag{B-8}$$

where N is the outermost node.

The internal reservoir radius will be less than the wellbore radius and will also be closed by setting:

$$a_1 = TR_{1+\frac{1}{2}} = 0. \tag{B-9}$$

Thus node 1 will actually be "within the wellbore" as shown in Figure 5. This permits easily specifying either a constant rate or a constant pressure over any time-step.

Solution of the Flow Equation for the Matrix Element

Solution of Eq. 9 may be accomplished using the same basic procedure described above. Subscript "j" will be used to distinguish the matrix equations from the reservoir finite-difference equations.

The Klinkenberg term can be handled by using the relationship:

$$(k_m)_j = k_\ell \ (1 + b/p_j^n) \tag{B-10}$$

An additional term due to the desorption in the matrix flow equation is present. The finite difference-scheme for Eq. 9 is as follows:

$$TR_{j-\frac{1}{2}}^{n+1}\left(p_{j-1}^{n+1} - p_j^{n+1}\right) + TR_{j+\frac{1}{2}}^{n+1}\left(p_{j+1}^{n+1} - p_j^{n+1}\right) = \tag{B-11}$$

$$\Gamma_j \ p_j^n\left[\left(\frac{1}{z_j^*} - \frac{1}{z_j^n}\right) + \frac{1}{z_j^*}\left(p_j^{n+1} - p_j^n\right)\right] +$$

$$\frac{V_j}{\Delta t}\left(\frac{dc}{dp}\right)_{p_j}{}^{**}\left(p_j^{n+1} - p_j^n\right)$$

where: ** denotes the average of p_j^* and p_j^n .

A tri-diagonal system is again present as:

$$a_j \ p_{j-1}^{n+1} + b_j \ p_j^{n+1} + c_j \ p_{j+1}^{n+1} = d_j \tag{B-12}$$

where:

$$a_j = TR_{j-\frac{1}{2}}^*$$

$$b_j = -TR_{j-\frac{1}{2}}^* - TR_{j+\frac{1}{2}}^* - \frac{\Gamma_j}{z_j^*} - \frac{V_j}{\Delta t}\left(\frac{dc}{dp}\right)_{p_j}{}^{**}$$

$$c_j = TR_{j+\frac{1}{2}}^*$$

$$d_j = -\left[\frac{j}{z_j^n} + \frac{V_j}{\Delta t}\left(\frac{dc}{dp}\right)_{p_j^{**}}\right] p_j^n$$

The Thomas Algorithm and the iterative procedure described in the previous section may again be used to solve Eq. B-12.

Boundary Conditions for the Matrix Element

The pressure in the outermost node will be held constant (over a time-step) at the prevailing fracture pressure of the reservoir node in which the matrix element lies as in Figure 6.

Source Term for Reservoir Equation

In order to evaluate the source terms $(q_{sc})_i$ in Eq. B-3 we observe that the flow rate out of the matrix elements within reservoir block i due to holding p_j constant at $p_{f,i}$ is:

$$\left(q_{sc}\right)_i = TR_{j-\frac{1}{2}}\left(p_{m,j-1} - p_{f,i}\right)\left(N_m\right)_i \qquad \text{(B-13)}$$

Where: $p_{f,i}$ and $p_{m,j}$ denote the fracture and the matrix pressure respectively, $TR_{j-\frac{1}{2}}$ = transmissibility between the two outer matrix nodes:

$$\left(N_m\right)_i = \frac{\left(r_{i+1}^2 - r_i^2\right)\left(1 - \phi_i\right)}{a^2} \qquad \text{(B-14)}$$

In developing the code it was found that the use of Eq. 13 sometimes gave inconsistent results with a = 10 cm due to the very small distances and very small pressure drops involved. Thus, an alternative method is used which determines q_{sc} from material balance considerations as shown below:

$$\left(q_{sc}\right)_i = \left\{\begin{bmatrix}\text{decrease in gas}\\ \text{content over}\\ \text{time-step}\end{bmatrix}_i + \begin{bmatrix}\text{amount of gas}\\ \text{desorbed over}\\ \text{time step}\end{bmatrix}\right\}\frac{1}{\Delta t} \qquad \text{(B-15)}$$

It was determined by comparison with both analytical and numerical models that the pressure distribution within the matrix element was correct.

TABLE 1 – MODEL INPUT DATA FOR THE BASE CASE

Wellbore radius	0.292 ft
Drainage radius	1000 ft
Reservoir Temperature	110°F
Initial Reservoir Pressure	500 psia
Wellbore Flowing Pressure	60 psia
Specific Gravity of Gas	0.60
Shale Bulk Density	2.60 g/cm^3
Gas Viscosity	0.0118 cp
Formation Thickness	622 ft
Formation Depth	3,720 ft
Fracture Porosity	0.005
Fracture Permeability	0.10 md
Shale Matrix Porosity	0.025
Shale Matrix Permeability	0.0001 md
Shale Matrix Element Radius	20 cm
Klinkenberg Factor	$b = .86\ km^{-.33}$
Total Simulation Time	27 years

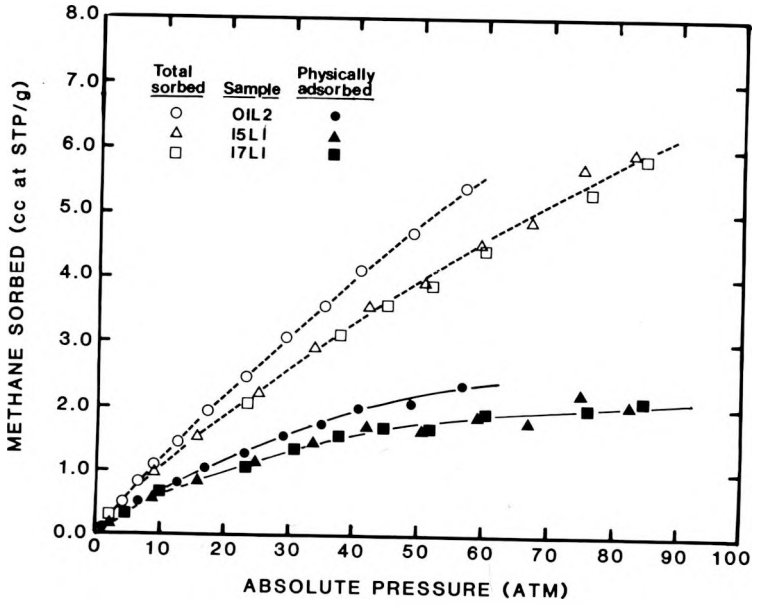


Fig. 1 - Methane Sorption Isotherms at 28°C

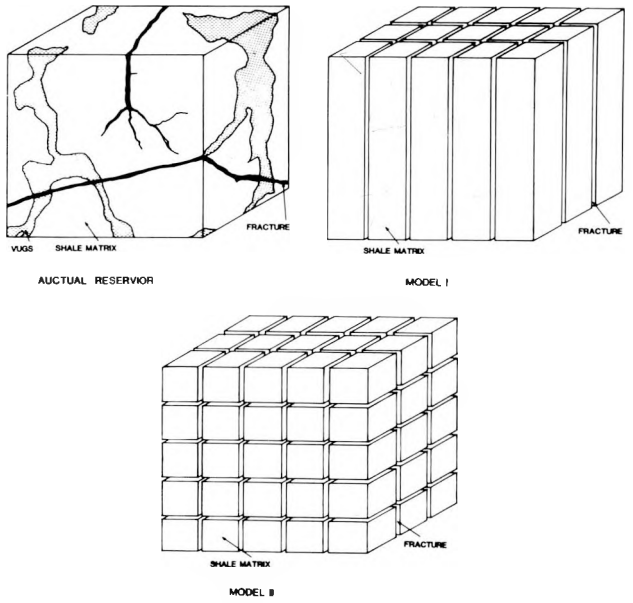


Fig. 2 - Fractured Devonian Shale Reservoir Systems

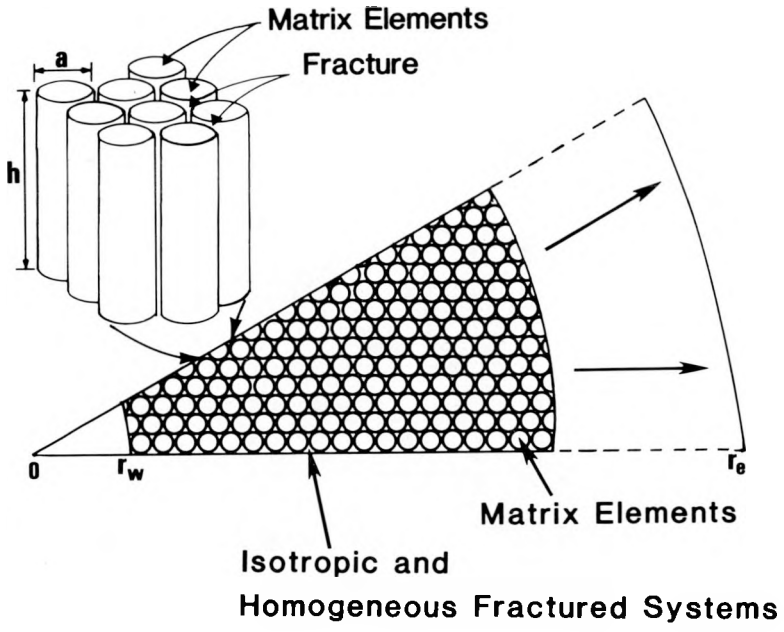


Fig. 3 - Radial One-Dimensional Devonian Shale Reservoir Model

$$\bar{r}_i = \frac{1}{2}(r_{i+1} + r_i)$$

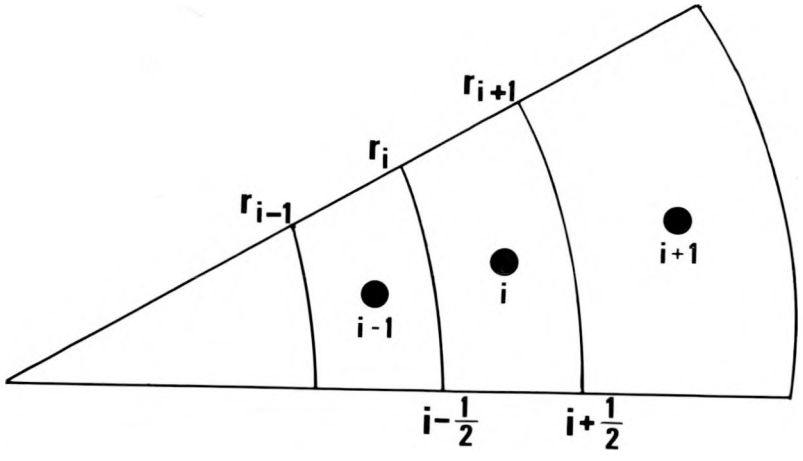


Fig. 4 - Reservoir Finite-Difference Grid System

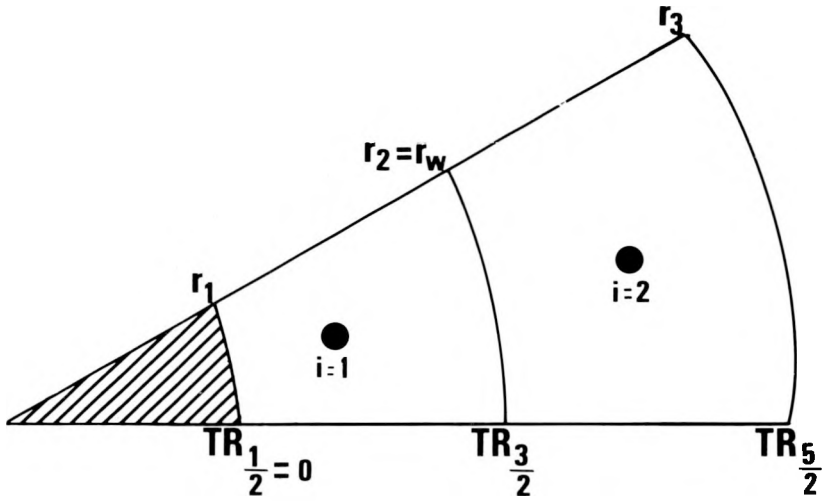


Fig. 5 - Block-Centered Finite-Difference Scheme at the Wellbore

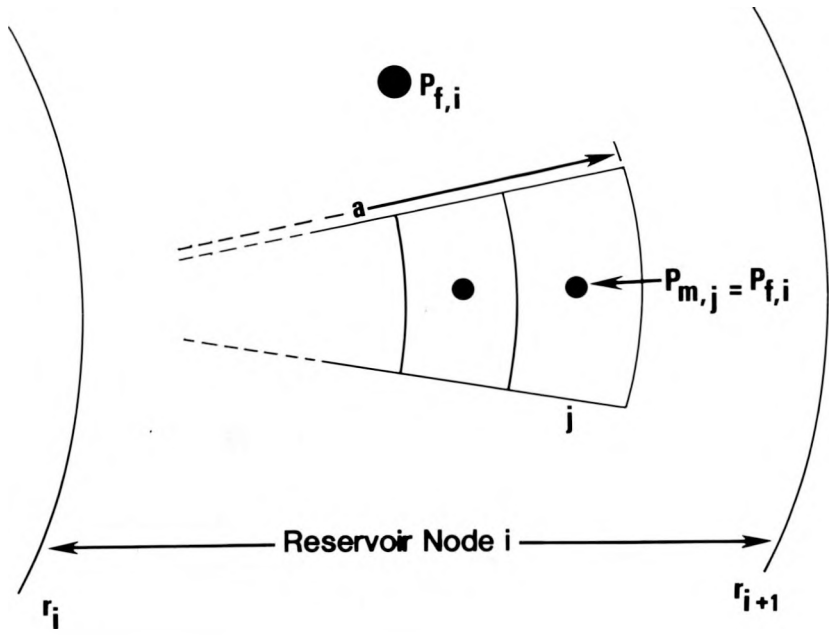


Fig. 6 - Matrix Element Finite-Difference Scheme

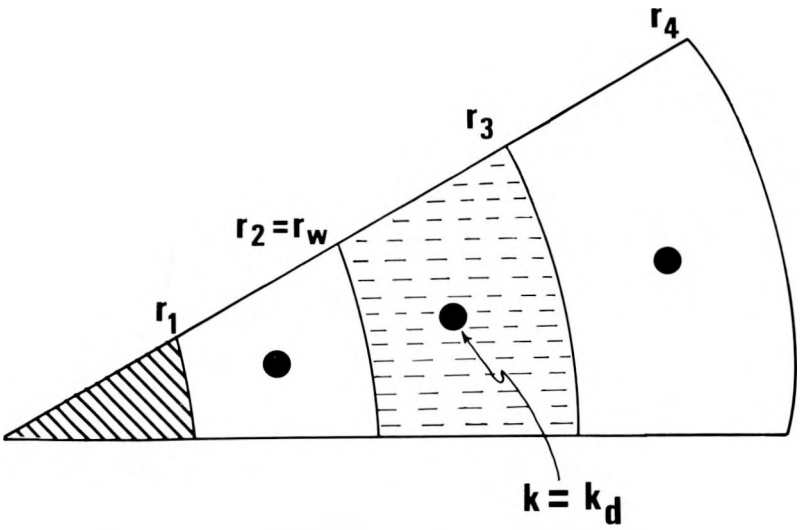


Fig. 7 - Damaged Zone in Finite-Difference Scheme

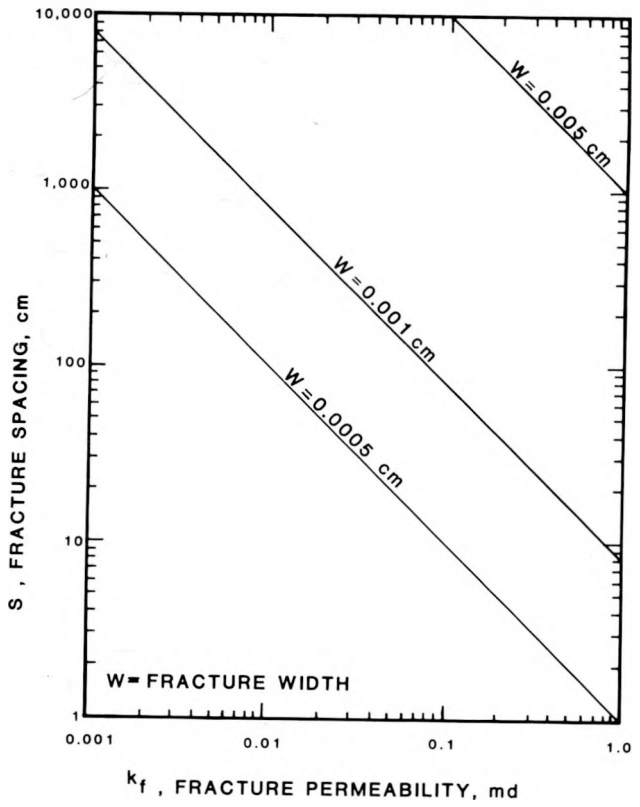


Fig. 8 - Fracture Permeability versus Fracture Spacing for Various Fracture Width

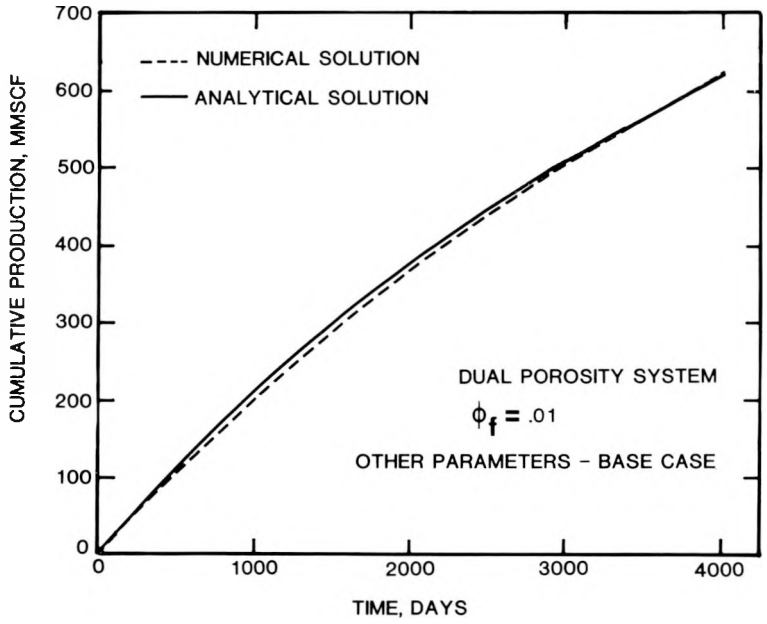


Fig. 9 - Comparison of Numerical and Analytical Solutions

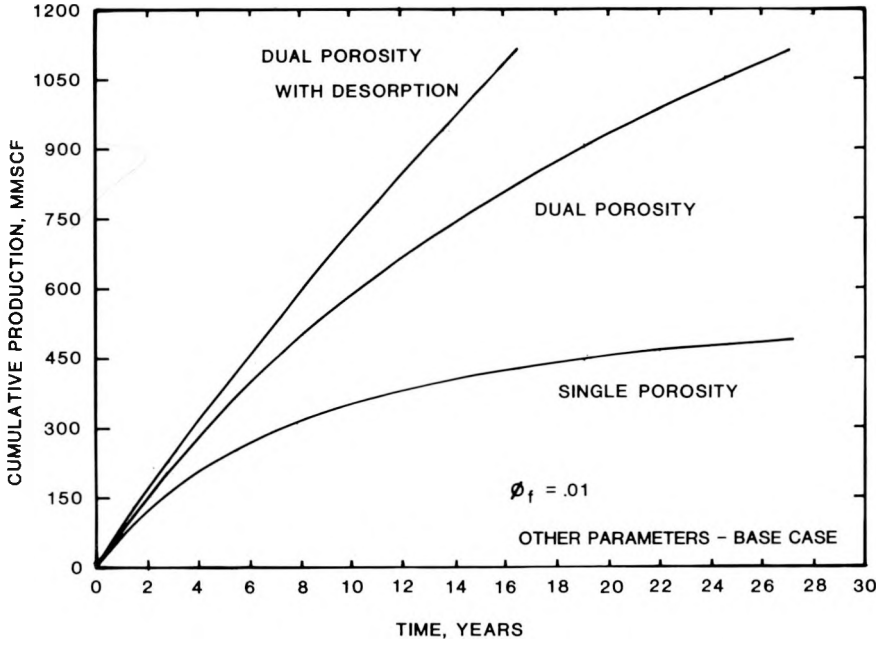


Fig. 10 - Productivity Improvement with Dual Porosity and Desorption

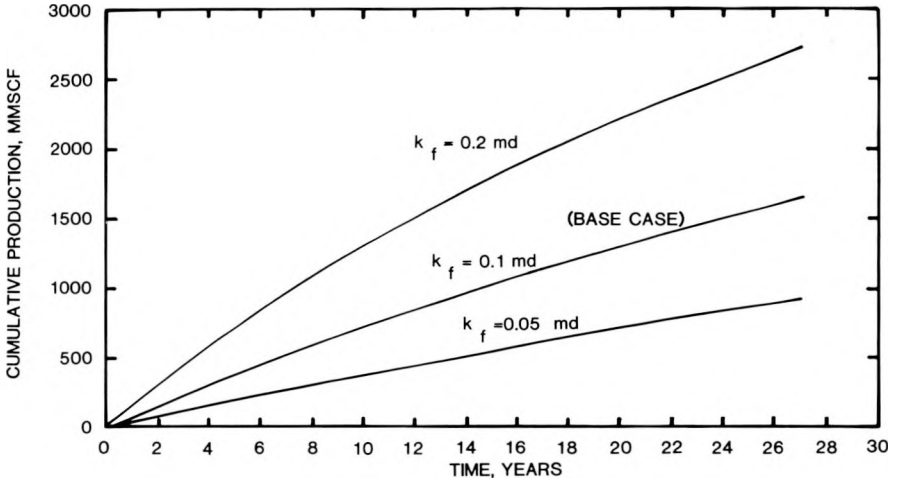


Fig. 11 - Cumulative Production as a Function of Time for Various Fracture Permeability

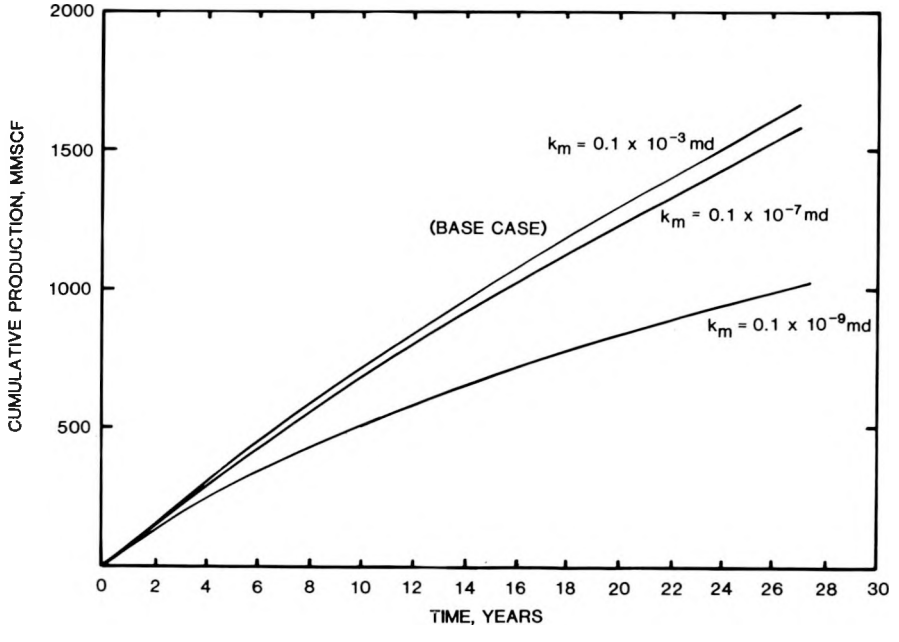


Fig. 12 - Cumulative Production as a Function of Time for Various Matrix Permeability

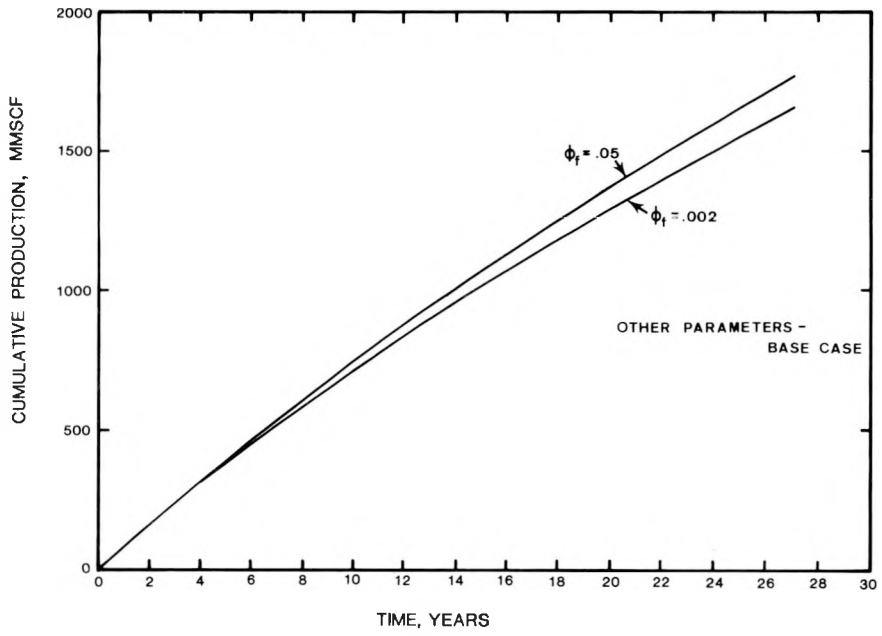


Fig. 13 - Effects of Fracture Porosity on Cumulative Production

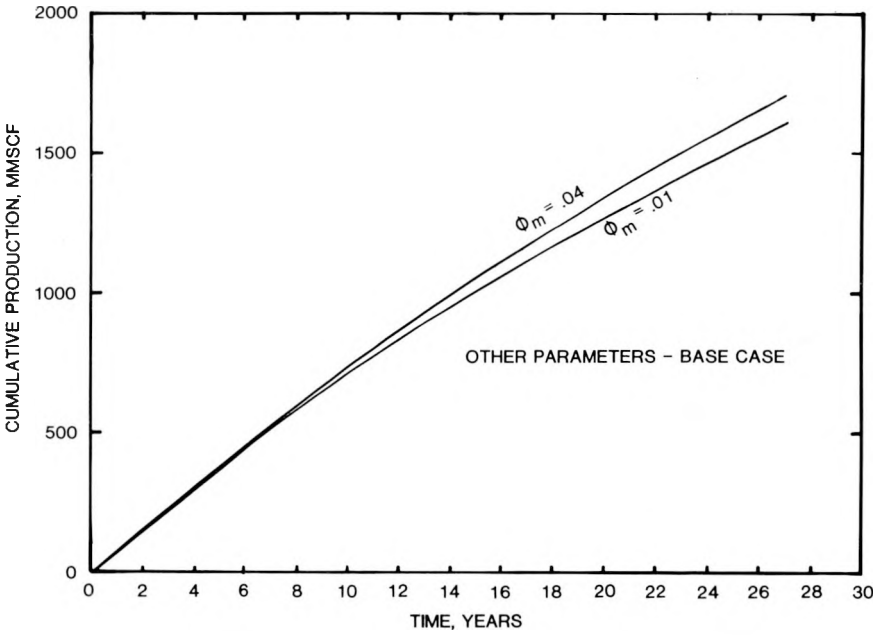


Fig. 14 - Effects of Matrix Porosity on Cumulative Production

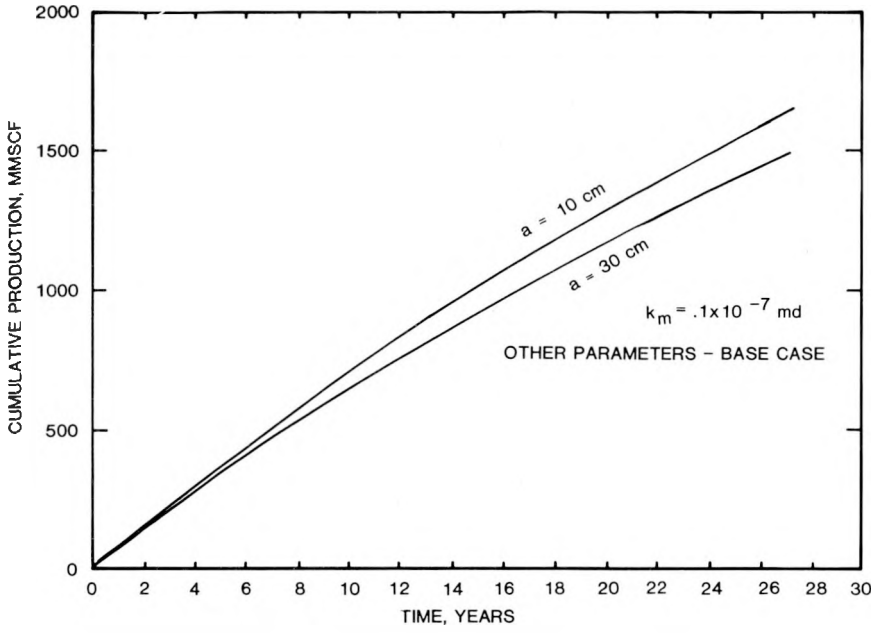


Fig. 15 - Comparison of Cumulative Production for Different Matrix Element Sizes

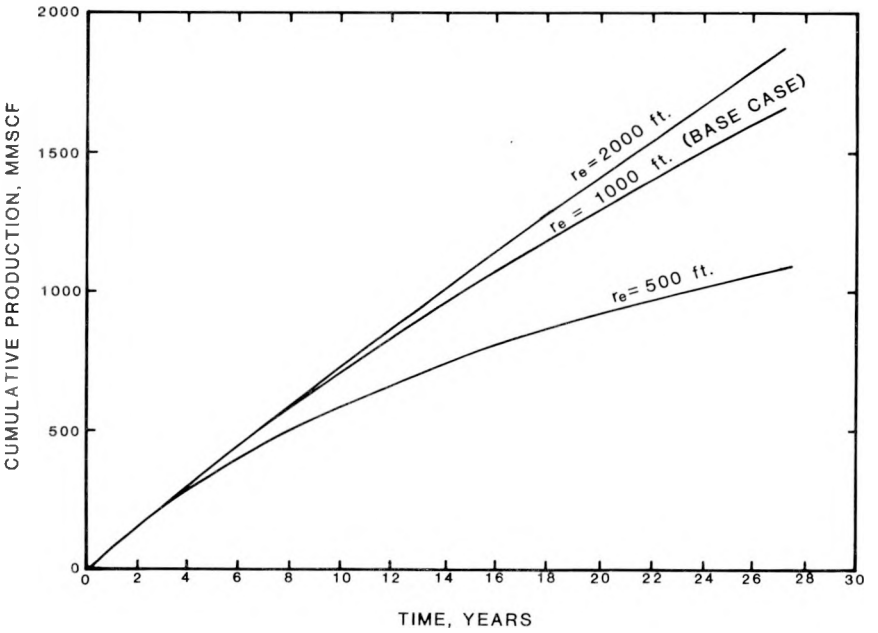


Fig. 16 - Cummulative Production for Different Drainage Radii

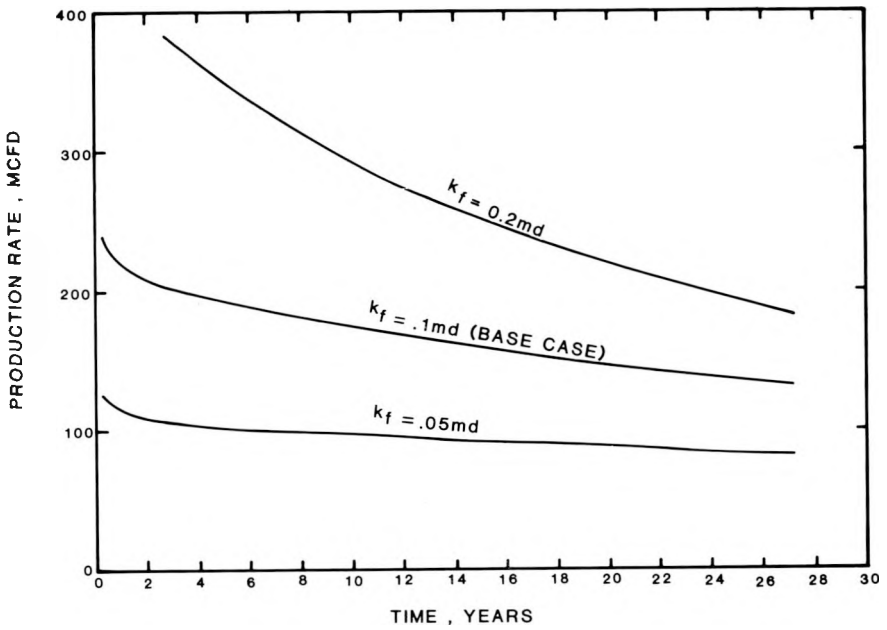


Fig. 17 - Production Rate for Different Fracture Permeability as a Function of Time

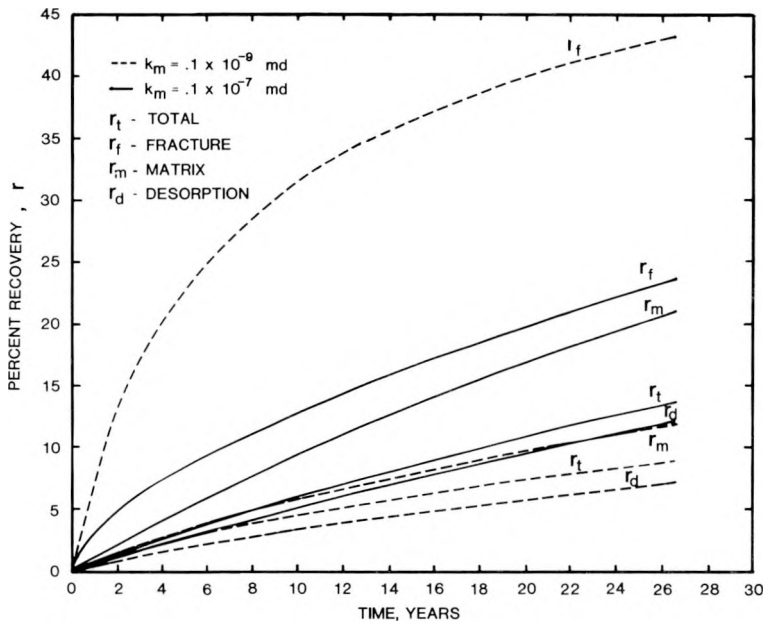


Fig. 18 - Breakdown of Recovery at Low Matrix Permeability

LINEAMENTS AND GROUND-WATER CHEMISTRY AS EXPLORATION TOOLS FOR DEVONIAN SHALE GAS IN THE MIDWAY-EXTRA FIELD OF WEST VIRGINIA

by

Robert R. Beebe
and
Dr. Henry W. Rauch



(Rauch)

ABOUT THE AUTHORS

Mr. Beebe received his B.S. degree in Geology from Northeastern University in 1976. He has attended West Virginia University during 1977-1979, and will be receiving an M.S. degree in Geology in 1979. He is presently employed by Exxon Corporation in Corpus Christi, Texas.

Dr. Rauch received his B.A. degree in Chemistry-Geology from Alfred University in 1965. He also received his Ph.D. degree in Geochemistry from The Pennsylvania State University in 1972. Since 1970 he has been employed by West Virginia University, Department of Geology and Geography, and is an Associate Professor of Geology. His primary research interests are in hydrogeology and geochemistry. Current research mainly involves hydrogeologic and geochemical exploration techniques for natural gas; the effects of coal mining on ground water; and lineament analysis in ground-water exploration.

2 LINEAMENTS AND GROUND-WATER CHEMISTRY AS EXPLORATION TOOLS FOR DEVONIAN SHALE GAS IN THE MIDWAY-EXTRA FIELD OF WEST VIRGINIA

ABSTRACT

A hydrogeologic study was done in the Midway-Extra gas field where gas wells tap Devonian shales in northern Putnam County, West Virginia. Lineaments were mapped and shallow ground water was surveyed for physical and chemical parameters, to determine if lineaments or ground water may be useful for shale gas exploration. Landsat lineaments, defined from satellite imagery, have no effect on water well yield and are associated with low gas well yields. Short photolineaments, defined from low-altitude stereo photography, are excellent sites for high-yielding water wells and good sites for high-yielding gas wells. These lineaments appear to represent permeable zones about 400 feet wide at shallow depth, and perhaps 0.5 miles wide in the Devonian shales. Photolineaments oriented N60°W-N30°E are especially well associated with high-yielding gas wells. Photolineaments bearing 60°-90° from the general structural trends are strongly related to high-producing gas wells in both the Midway-Extra and Cottageville [1] study areas. Final open flow is in general greater for gas wells near high-producing water wells, but the trend is not statistically significant. Final open flow is especially great for gas wells near water wells or springs having high bicarbonate or nitrate concentrations. High bicarbonate content is in part likely to be caused by oxidation of methane gas in shallow ground water. Photolineaments and ground-water chemistry may well prove to be valuable exploration tools for Devonian shale gas in other areas.

INTRODUCTION

A hydrogeologic investigation was undertaken in the Midway-Extra gas field of Putnam County, West Virginia, to determine if lineaments and shallow ground-water chemistry are associated with gas well productivity in Devonian shale. This study follows a similar earlier study in the Cottageville gas field of Jackson County, West Virginia.[1] The primary purpose of this study was to determine if the same statistical trends for gas well yield exist for both the Midway-Extra and Cottageville gas fields; any such trends could then aid in developing new inexpensive exploration techniques for Devonian shale gas.

Figure 1 depicts the study area in northern Putnam County. This region is about 100 square miles in area, with about one-third of it being occupied by the Midway-Extra gas field. A portion of this gas field located southwest of the Kanawha River was not included in this study. Also the circled gas wells of Figure 1, located near Eleanor, were excluded from the study since they are not within the Midway-Extra field. Open flow data are available for most of the 101 remaining gas wells in Figure 1; these wells produce mainly from Devonian shales.

Two types of lineaments were mapped for this study - Landsat lineaments and short photolineaments. On Figure 1, lines at least 1 1/2 miles long represent Landsat lineaments mapped from satellite imagery. Shorter lines are photolineaments, mapped from low-altitude black-and-white photographs in stereo coverage; these lineaments are defined by straight valleys or stream segments at least one-quarter mile long. Photolineaments were classified according to three degrees of certainty - certain (class 1), somewhat certain(class 2), and uncertain(class 3); class 1 photolineaments are indicated by the boldest lines on Figure 1. All lineaments were identified and plotted before gas well locations and yields were determined from Schaefer[2], in order to avoid subjective bias in testing for lineament-yield associations.

Seventy-four water wells and six springs were studied for characterizing shallow ground water (Figure 1). Physical well parameters such as well yield, well depth, and original depth to water were obtained from well owners and drillers. Water chemical tests were performed for 32 water wells and springs, and 20 of these are located within the Midway-Extra gas field. Temperature and specific conductance were measured in the field, and two water samples were taken from each well and spring. One set of samples was field tested with acid and later analyzed in the laboratory for iron, calcium, and magnesium concentrations. Water samples of the second set were kept cool until they could be analyzed for pH, bicarbonate, nitrate, sulfate, chloride, and sodium in the laboratory. All analyses were done within 48 hours of sampling.

LINEAMENT ASSOCIATIONS

First water well yield and then gas well yield were tested for possible associations with lineament proximity. Water well yield, estimated in gallons per minute, was tested for associations with Landsat lineament proximity. By the one-tailed Mann Whitney U test,[3] yield is not significantly different for water wells located closer than versus those farther than a critical distance from the nearest Landsat lineament, for tests involving 500, 1000, and 2000 feet as critical distances. Landsat lineaments are therefore not associated with water well yield in either the Cottageville field of Jackson

County[1] or in the Midway-Extra field.

Water well yield was next tested against photolineament proximity. Wells within 200 feet of a photolineament center line have significantly greater yield (about four times greater) than more distant wells at the 0.01 alpha probability level by the Mann Whitney U (one tailed) test; the alpha probability indicated the probability that no significant difference exists between two groups of tested data. Water wells within 150 feet yield about four times greater than wells 150-200 feet of a photolineament center line, but this difference is not statistically significant at the 0.05 alpha probability level. These results are in general similar to those for the Cottageville area[1] and other clastic rock terrains studied elsewhere in West Virginia. Near Cottageville, water well yield is significantly greater for wells located within 100-200 foot wide photolineament zones centered along plotted photolineament center lines; in the Midway-Extra area, influencial photolineament zones are 300-400 feet in width. Short photolineaments apparently represent underlying zones of increased fracture permeability, at least with respect to shallow ground water. A resistivity survey run across one photolineament in the study area indicated a resistivity anomaly resembling the effect of a fracture zone at least 60 feet in width.

Gas well yield was next tested for possible trends with lineaments. Both initial open flow (measured before well stimulation by fracturing) and final open flow (measured after well stimulation) were tested. These data were obtained from Schaefer.[2] Figure 2 shows contoured initial open flow for all shale gas wells in the study area. Initial open flow is probably the better indicator of natural gas reservoir permeability. Figure 3 depicts contoured final open flow for all shale gas wells. Final open flow is probably the better measure of relative well productivity and rock fracture influences on well yield.

Figures 2 and 3 show locations of plotted Landsat lineaments with respect to the major gas producing areas. Such lineaments, represented in general by valleys, appear to bound the high gas production zones to the north and south; Landsat lineaments are poor locations for shale gas wells. Landsat lineaments are similarly associated with low shale gas yields in the Cottageville area.[1,4,5] Perhaps deeply-penetrating fractures have bled off the shale gas under the Landsat lineaments.

Photolineament proximity was next tested for possible associations with gas well yield. Although both initial and final open flow are generally greater for wells located within 0.4 kilometers of a photolineament, these trends are not statistically significant at the 0.05 alpha probability level by the Mann Whitney U test. Scattergram plots of gas well yield versus photolineament proximity suggest that about 0.8 kilometers or 0.5 miles is the optimum width for photolineament zones associated with high-yielding gas wells.

Photolineament orientation was then tested for possible associations with gas well yield. When yield was plotted versus the orientation of the nearest photolineament to a well, definite trends were apparent. As is evident from Figure 4, the percentage of high-yielding gas wells is greatest for wells near photolineaments oriented N60°W-N30°E, for both initial and final open flows. Well yield is significantly greater for gas wells near N60°W-N30°E photolineaments than for gas wells near photolineaments having other orientations; by the Mann Whitney U test, this trend is significant at the 0.05 and 0.10 alpha probability levels, for initial open flow(IOF) and final open flow(FOF) respectively. Also, FOF is significantly greater (at a 0.05 alpha probability) for wells near N60°W-N0°E photolineaments than for wells near photolineaments having other orientations. High gas well yield is significantly associated with photolineaments oriented 60°-90° from the general structural trend of shale gas fields in both the Cottageville and Midway-Extra areas; this suggests that such photolineaments represent fracture zones that are especially permeable to gas flow in these areas.

In order to test the usefulness of N60°W-N30°E bearing photolineaments in exploration for Devonian shale gas, a density map was prepared for these lineaments and compared to the gas yield trends of Figures 2 and 3. The density map of Figure 5 was prepared by use of an orthogonal grid of lines defining square sections one mile long on a side. This grid was oriented parallel to the north-south and east-west directions. The density of N60°W-N30°E photolineaments was determined for each square-mile section, by measuring the cumulative length of these lineaments and plotting this number at the center of each section. Figure 5 represents hand-contoured density in miles per square mile, based on 100 square-mile sections.

The photolineament density map of Figure 5 was superimposed on the gas yield maps of Figures 2 and 3, to determine if significant overlaps occur between high photolineament density and high gas yield areas. A second orthogonal grid defining square sections 2000 feet long on a side was superimposed on the overlays of Figure 5 on Figures 2 and 3; grid line intersections were then counted as points

occurring in one of four type areas - high photolineament density and high gas yield; high photolineament density and low gas yield; low photolineament density and high gas yield; and low photolineament density and low gas yield. The 221 grid points were categorized, totaled for each area type, and plotted in 2X2 contigency tables. Chi-square contingency tests with the Yates correction were then performed to determine if any significant associations exist between N60°W-N30°E photolineament density and gas yield, for both IOF and FOF and for various definitions of high versus low density and gas yield. The only data tested were for grid points located within an area containing the plotted gas wells of the Midway-Extra field in Figure 1.

Table 1 shows the results of comparisons between IOF and the density of N60°W-N30°E photolineaments. Chi-square test results indicate that photolineament density is significantly associated with IOF. High lineament density areas have a significantly large proportion of high-yielding wells (over 100 MCF/day IOF), compared with low lineament density areas. Locating gas wells in high-density areas for N60°W-N30°E photolineaments would yield a 45 percent success rate for densities exceeding 1.5 mi/mi^2, and a 71 percent success rate for densities exceeding 2.0 mi/mi^2, if success is defined by yields exceeding 100 MCF/day for IOF.

Table 2 gives the results of statistical comparisons between FOF and the density of N60°W-N30°E photolineaments. Again all tests show statistically significant associations between lineament density and FOF. Locating gas wells in areas with lineament densities exceeding 1.5 mi/mi^2 would respectively yield 89, 58, and 11 percent success rates with regard to 100, 500, and 1000 MCF/day for FOF. Similar results are evident in Table 2 for wells in areas with lineament densities exceeding 2.0 mi/mi^2, but such areas are smaller and would place greater restrictions on gas exploration.

The photolineaments of Figure 1 were next examined for possible differences among class 1, 2, and 3 photolineaments with respect to gas yield associations, to determine if additional gas exploration trends could be discovered based on photolineament class. Gas wells near class 1(most certain) photolineaments have higher yields for both IOF and FOF than wells near class 2 or class 3 photolineaments, but these trends are not strong enough to be statistically significant at the 0.05 alpha probability level by the Mann Whitney U test. Class 1 photolineaments were next tested alone for possible well yield associations with lineament proximity. Gas wells within 0.4 kilometers of the nearest class 1 photolineament have higher IOF and FOF yields than more distant wells; for FOF data, this trend is statistically significant by the Mann Whitney U test at the 0.05 alpha probability level, with yields being three to four times greater for wells within 0.4 kilometers of a class 1 photolineament. However since about 86 percent of the mapped class 1 photolineaments are oriented N60°W-N30°E, it is possible that this trend for class 1 photolineament proximity is caused mainly by factors relating to photolineament orientation.

Class 1 photolineament density was calculated, hand contoured in a manner similar to Figure 5, and statistically tested against gas well yield using 2X2 contingency table tests similar to Tables 1 and 2. Only trends for FOF data proved to be significant at the 0.05 alpha probability level. FOF gas yield is significantly greater for wells located in areas having at least 1.0 mi/mi^2 densities of class 1 photolineaments; if gas wells were located at random using an orthogonal grid, 64 percent would have FOF yields exceeding 100 MCF/day, and 39 percent would have FOF yields exceeding 500 MCF/day. Although these success rates are remarkable, results for N60°W-N30°E photolineament density are better (from the first two tests of Table 2).

GROUND-WATER ASSOCIATIONS

Water wells and springs were next tested for possible associations with gas well yield. A comparison was made of water well yield with gas well yields for the closest gas well to each water well, within the study area portion of the Midway-Extra gas field. Both initial and final open flow are higher on average for gas wells near high-producing water wells, but this trend is not statistically significant at a 0.05 alpha probability by the Mann Whitney U test. Photolineament associations with both high water well and high gas well yields could possibly explain this trend.

Ground-water chemistry was next tested for possible associations with gas well yield. Trends of chemical parameters with gas well yield were explored for the 19 water wells and one spring within the Midway-Extra field. Of all the chemical parameters tested for well and spring waters, only bicarbonate and nitrate concentrations exhibit significant associations with FOF gas well yield. Wells or springs located within areas having gas wells exceeding 100 MCF/day FOF (from Figure 3) have significantly higher bicarbonate and nitrate concentrations compared to ground-water supplies elsewhere in the Midway-Extra field, at the 0.05 alpha probability level by the Mann Whitney U test. Figure 6 illustrates the trends for bicarbonate and nitrate versus FOF gas yield. Similar plots and tests

were not done with regard to greater-than versus less-than 500 MCF/day FOF, since only two water wells occur on or within the 500 MCF/day contour of Figure 3. Also, tests of IOF data did not indicate any statistically significant associations between gas well yield and bicarbonate or nitrate concentration.

The statistical associations of bicarbonate and nitrate contents with FOF gas yield in the Midway-Extra gas field are similar to bicarbonate and nitrate associations with IOF gas yield in the Cottageville gas field.[1] FOF data were not tested in the Cottageville study. These similarities between two Devonian shale gas fields strongly suggest that bicarbonate and nitrate are not coincidentally associated with gas well yield. Optimum ground-water concentrations of bicarbonate and nitrate are at least 470 mg/l and 1.75 mg/l respectively, for gas exploration in the Midway-Extra area. When results from the Midway-Extra study and Cottageville study[1] are combined, optimum gas exploration concentrations appear to be at least 475 mg/l and 3 mg/l for bicarbonate and nitrate respectively. In the cottageville area, five out of seven gas wells should exceed 100 MCF/day IOF where ground water exceeds 475 mg/l bicarbonate, and two out of three gas wells should exceed 100 MCF/day iof where ground water exceeds 3 mg/l nitrate.

Shallow ground-water chemistry could well serve as the basis for a new gas exploration technique in Devonian shale and other rock terrains, if similar chemical associations are found in future studies elsewhere. Gas exploration would also be more reliable if plausible explanations with supporting evidence were available for the observed chemistry-gas yield trends. Since the Cottageville study was published,[1] new evidence strongly suggests a particular origin for the high bicarbonate concentrations in shallow ground water over high-producing gas zones. It is likely that a significant portion of ground-water bicarbonate over major gas-producing reservoirs is derived from the oxidation of methane gas. Such gas could have slowly migrated upward along rock fractures to shallow aquifers. Oxidation of methane could then have occurred with either sulfate or dissolved oxygen as the oxidizing agent. Evidence for this theoty is derived from a study of six water wells known to be contaminated with natural gas in Monongalia County, West Virginia. These wells exhibit abnormally high bicarbonate and abnormally low sulfate and hardness concentrations compared to nearby wells lacking gas contamination. No explanations are proposed at present for the association of ground-water nitrate with gas well yield.

CONCLUSIONS

Several conclusions are apparent from this study of lineaments and shallow ground water in the Midway-Extra gas field, especially in relation to a similar earlier study in the Cottageville gas field. Landsat lineaments (defined from satellite imagery) have no effect on water well yield but are poor places to locate high-yielding shale gas wells in the Midway-Extra and Cottageville areas. Short photolineaments (defined from low-latitude photographs) mark excellent sites for high-yielding water wells in both areas, but photolineaments have a more pronounced effect on water well yield in the Midway-Extra area, where they denote zones of increased near-surface permeability about 400 feet wide.

Gas wells located within 0.4 kilometers of a photolineament in the Midway-Extra area have higher yields. Final open flow (after well stimulation) is especially higher for wells near class 1 (most certain) photolineaments. When broken down by orientation, photolineaments bearing N60°W-N30°E are especially associated with high-producing gas wells in the Midway-Extra area. In both the Cottageville and Midway-Extra gas fields, photolineaments oriented 60°-90° from general structural trends are especially associated with high-yielding gas wells; this suggests that such photolineaments represent permeable fracture zones of similar orientation in Devonian shale reservoirs.

Final open gas flow is related to shallow ground water in the Midway-Extra area. Gas wells usually have high final open flows near high-yielding water wells, which might be explained by permeable rock fractures associated with photolineaments near the high-yielding wells. Final open flows are higher for gas wells near water wells or springs with high bicarbonate or high nitrate concentrations, in both the Midway-Extra and Cottageville study areas. Optimum ground-water concentrations for gas exploration in both areas appear to be at least 475 mg/l for bicarbonate and at least 3 mg/l for nitrate. One likely theory concerning bicarbonate is that methane gas is migrating upward along rock fractures to shallow aquifers, where it is being oxidized to bicarbonate.

NOMENCLATURE

MCF/day = thousands of cubic feet per day (gas flow)
IOF = initial open flow, in MCF/day
FOF = final open flow, in MCF/day

mi/mi^2 = total photolineament length in miles, per square mile of area
mg/l = milligrams per liter concentration units
N = north
W = west
E = east

ACKNOWLEDGEMENTS

The authors wish to thank the U.S. Department of Energy and the Morgantown Energy Technology Center for financial support of this study. Appreciation is also extended to Dr. Robert Shumaker for his support, to Mr. William Schaefer for gas yield data, and to the many individuals who provided useful well and spring data.

REFERENCES

1. Jones, D. S., and Rauch, H. W.: "Lineaments and Ground-Water Quality as Exploration Tools for Ground Water and Gas in the Cottageville Area of Western West Virginia", in Preprints for the Second Eastern Gas Shales Symposium; Morgantown, West Virginia; October 1978; Morgantown Energy Technology Center, pp. 196-205.

2. Schaefer, W. W.: "Geology and Producing Characteristics of Certain Brown Shales in the Midway-Extra Field, Putnam County, West Virginia", an unpublished M.S. thesis; West Virginia University, Morgantown, West Virginia, 1979.

3. Siegel, S. M.: "Nonparametric Statistics for Behavioral Sciences" McGraw-Hill, New York, 1956.

4. Werner, E.: "Interrelationships of Photolineaments, Geologic Structures, and Fracture Production of Natural Gas in the Appalachian Plateau of West Virginia", in Proceedings of the Seventh Appalachian Petroleum Geology Symposium; Morgantown, West Virginia; March, 1976; Morgantown Energy Technology Center.

5. Werner, E.: "Application of Remote Sensing Studies to the Interpretation of Fracture Systems and Structural Styles in the Plateau Regions of Eastern Kentucky, Southwestern Virginia, and Southwestern West Virginia for Applications to Fossil Fuel Extraction Processes", a final project report on open file at the Morgantown Energy Technology Center; December, 1977.

TABLE 1

INITIAL OPEN FLOW GAS WELL YIELD VERSUS
DENSITY OF N60°W-N30°E BEARING PHOTOLINEAMENTS

Photolineament Density

1.50 mi/mi^2

Gas Well Yield	Low	High
Low	191	11
100 MCF/day		
High	10	9

Chi Square = 32.2

Probability of Error = 0.001

Success Rate = 45%

2.00 mi/mi^2

Gas Well Yield	Low	High
Low	199	2
100 MCF/day		
High	10	5

Chi Square = 28.7

Probability of Error = 0.001

Success Rate = 71%

TABLE 2

FINAL OPEN FLOW GAS WELL YIELD VERSUS
DENSITY OF N60°W-N30°E BEARING PHOTOLINEAMENTS

Photolineament Density

1.50 mi/mi^2

Gas Well Yield	Low	High
Low 100 MCF/day	96	2
High	106	17

Chi Square = 9.0

Probability of Error = 0.01

Success Rate = 89%

1.50 mi/mi^2

Gas Well Yield	Low	High
Low 500 MCF/day	186	8
High	16	11

Chi Square = 35.9

Probability of Error = 0.001

Success Rate = 58%

1.50 mi/mi^2

Gas Well Yield	Low	High
Low 1,000 MCF/day	200	17
High	2	2

Chi Square = 4.3

Probability of Error = 0.05

Success Rate = 11%

2.00 mi/mi^2

Gas Well Yield	Low	High
Low 100 MCF/day	98	0
High	116	7

Chi Square = 4.7

Probability of Error = 0.05

Success Rate = 100%

2.00 mi/mi^2

Gas Well Yield	Low	High
Low 500 MCF/day	186	3
High	28	4

Chi Square = 7.4

Probability of Error = 0.01

Success Rate = 57%

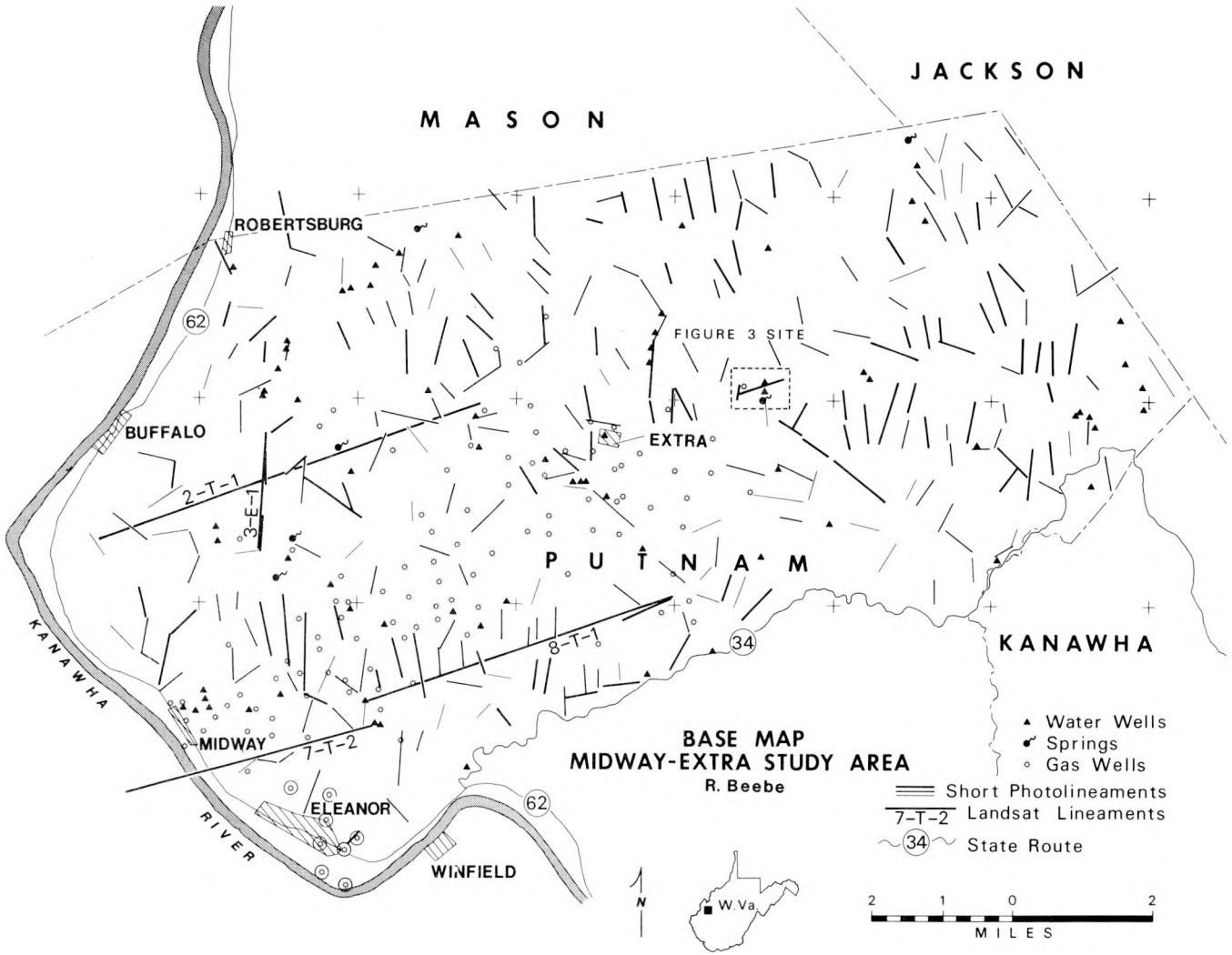


Figure 1. Map of the Midway-Extra Study Area, Showing Lineaments, Devonian Shale Gas Wells, and Surveyed Water Wells and Springs. Circled shale gas wells near Eleanor are not within the Midway-Extra gas field.

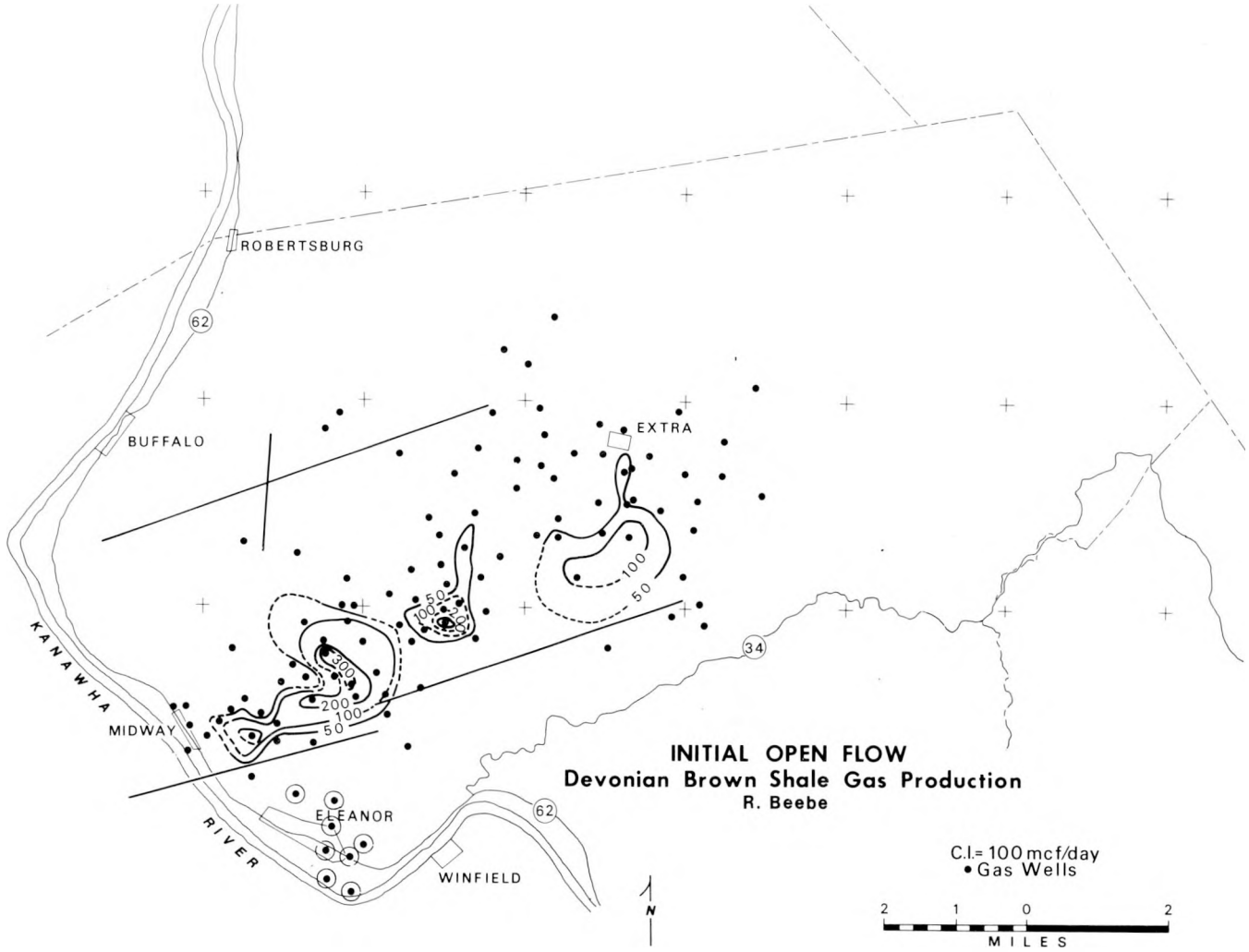


Figure 2. Contour Map of Initial Open Flow (Before Stimulation) for Shale Gas Wells of the Study Area.

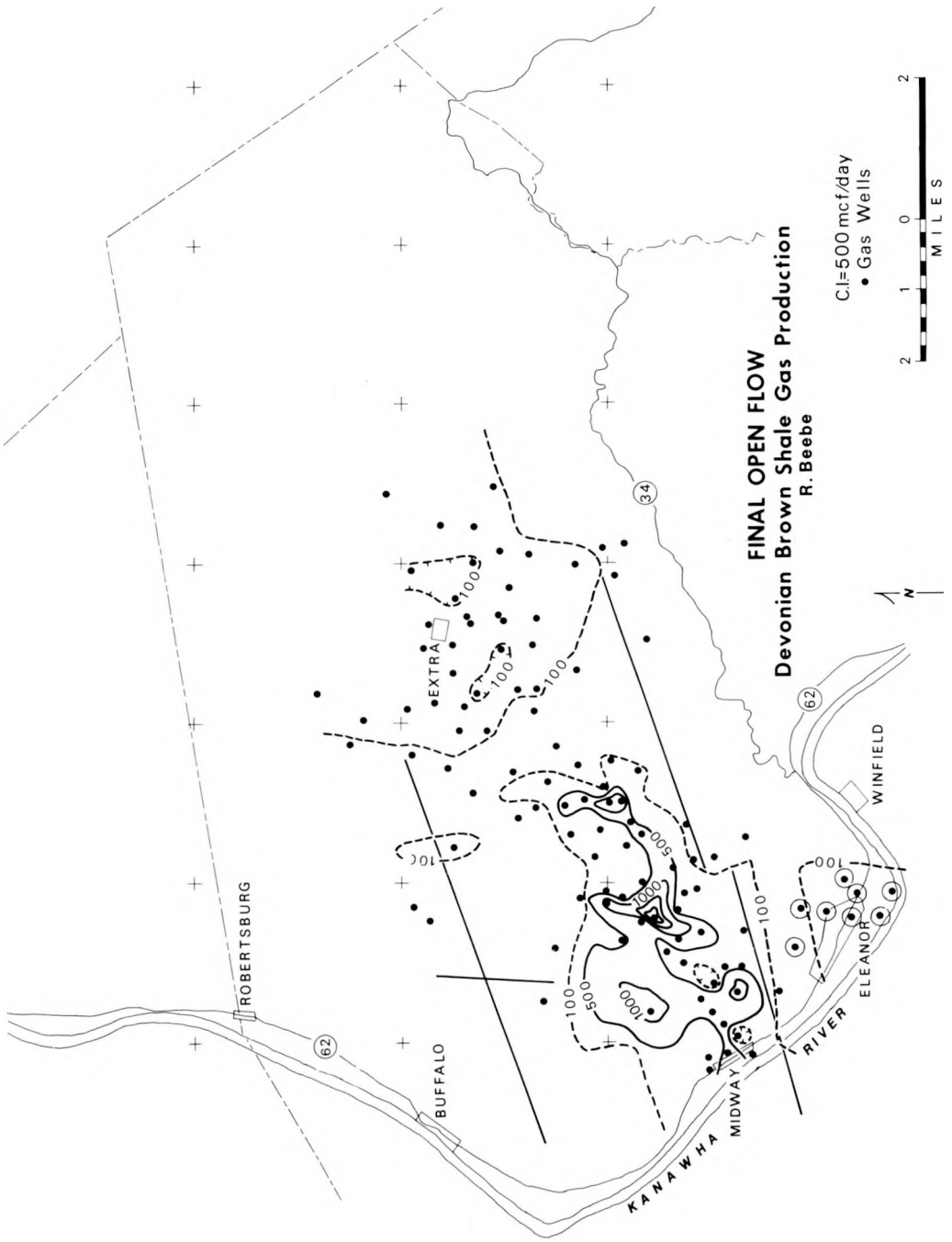


Figure 3. Contour Map of Final Open Flow (After Stimulation) for Shale Gas Wells of the Study Area

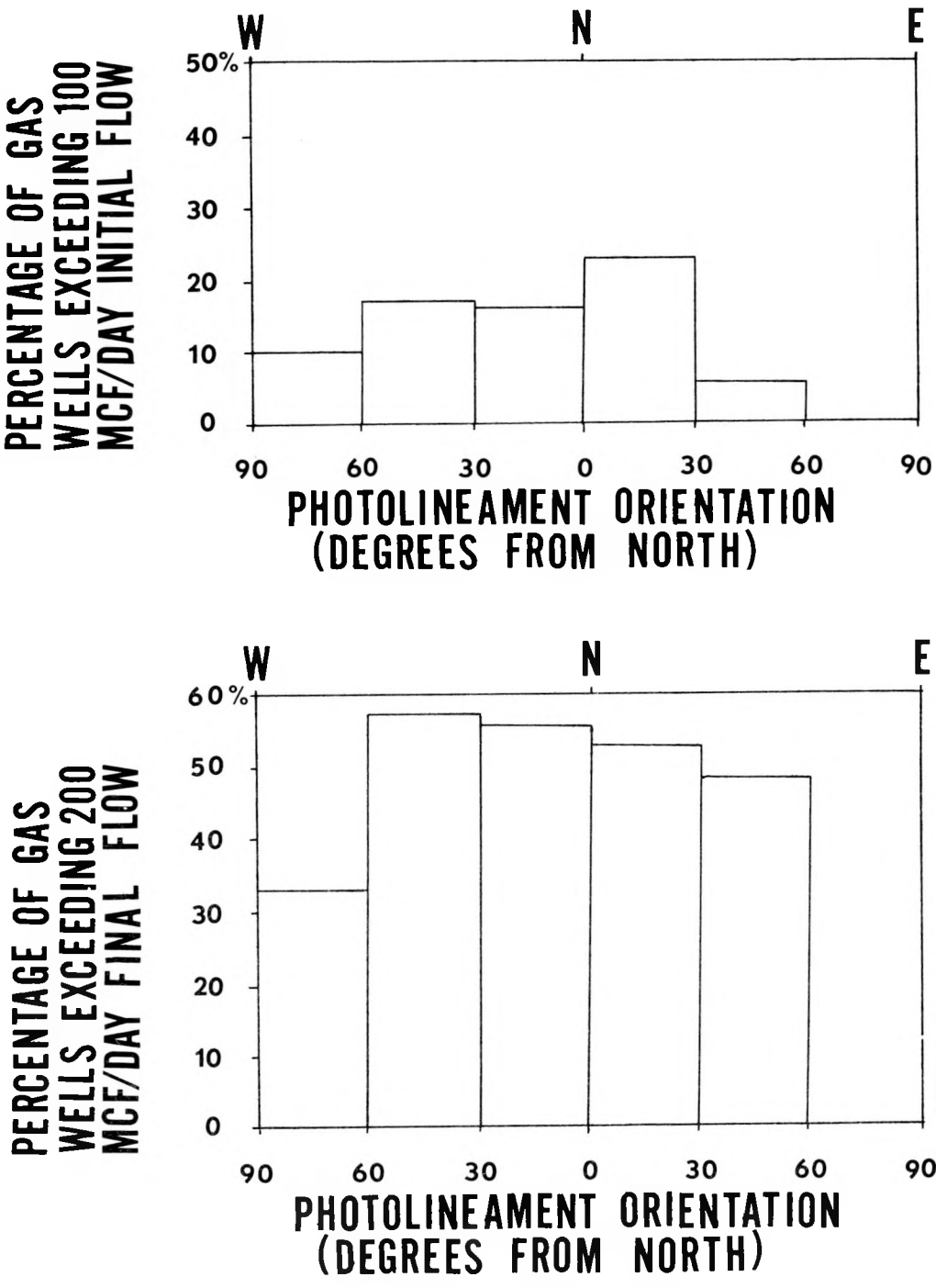


Figure 4. Gas Well Yield Versus Orientation of Nearest Photolineament to a Gas Well for the Study Area.

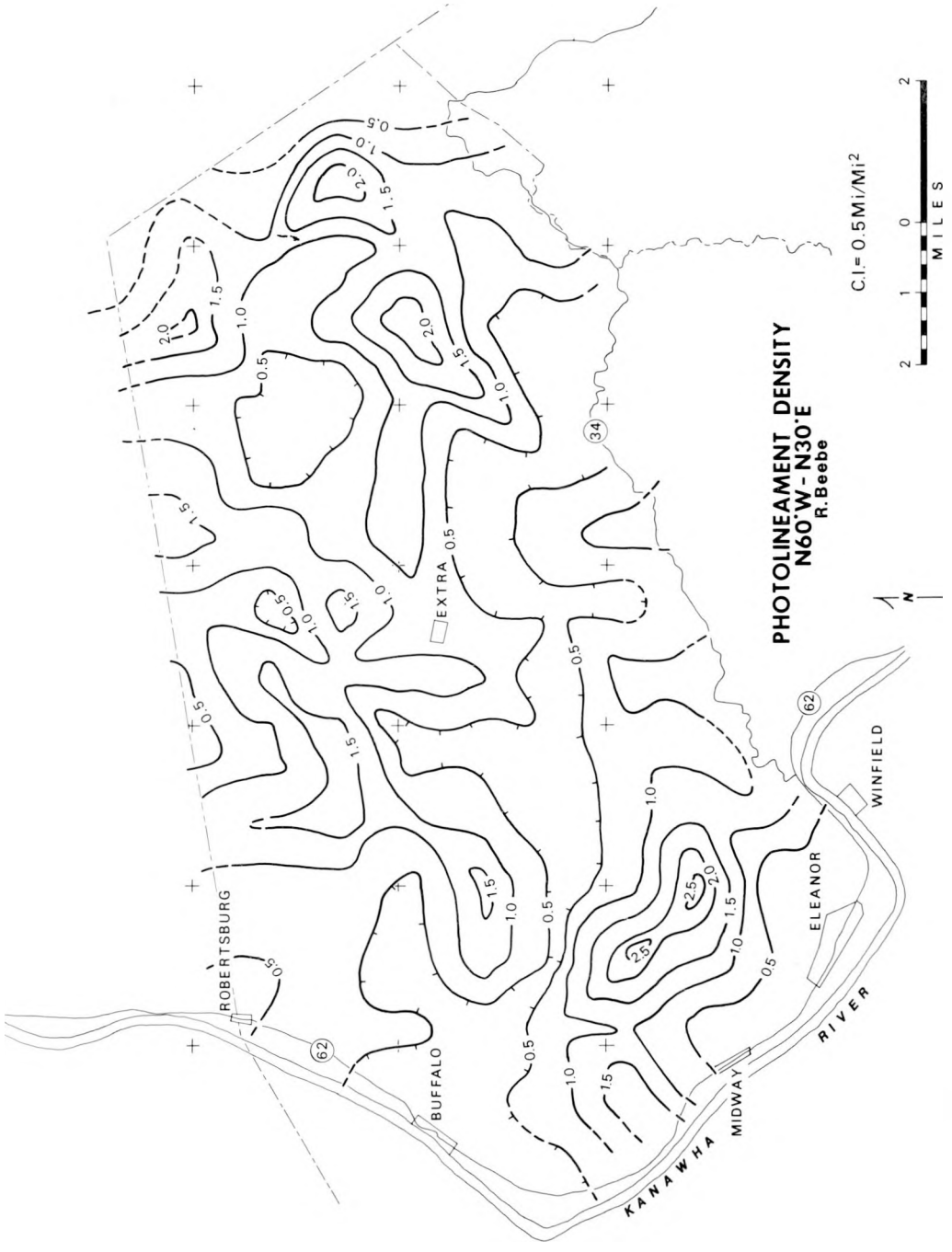


Figure 5. Density Map for Photolineaments Oriented N60°W-N30°E in the Study Area. Density is reported in miles of lineament length per square mile of area.

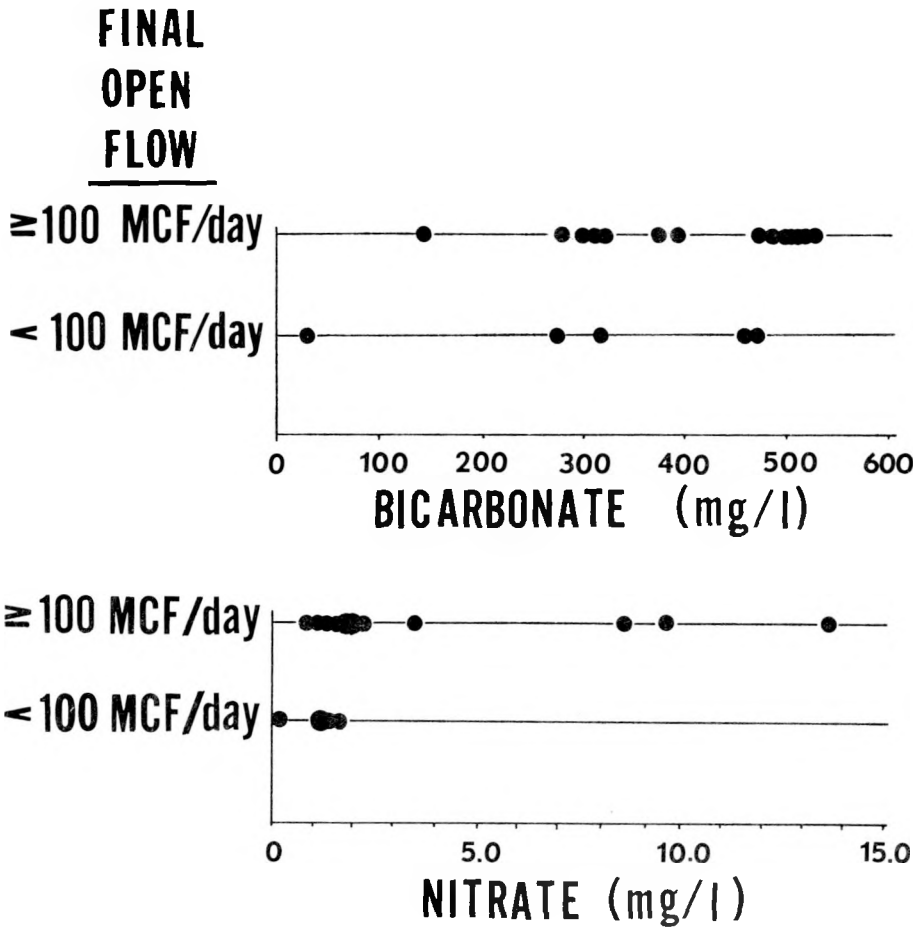


Figure 6. Plot of Bicarbonate and Nitrate Concentrations for Water Wells and Springs Versus Contoured Final Open Flow of Gas Wells. Small dots represent one water well or spring, and large dots indicate two wells.

INTERPRETATION AND STATISTICAL ANALYSIS OF KENTUCKY - WEST VIRGINIA OPEN FLOW DATA, INCORPORATING GEOCHEMICAL INFORMATION

P. W. Seabaugh and R. E. Zielinski
Mound Facility*

C. A. Komar
Morgantown Energy Technology Center

ABSTRACT

Cluster and regression analyses have been used to screen for predictive models and to test whether open flow data can provide insight to aid in the assessment of near optimum design for gas production from Devonian Shale. The analysis shows that data from a Kentucky - West Virginia Frac Study should be partitioned. The vertical stress variable (X_6) was found to be the key variable; it is directly related to depth. Maximum flow occurs when $3400 < X_6 < 4100$ and minimums flow occurs when either $X_6 < 3400$ or $X_6 > 4100$. This zonation characteristic of the high flow values implies that the location of the prolific reservoir is the key to successful well production. This reservoir effect is consistent with our recent geochemical data and an extension of the geochemical cross section can be made. The optimization aspect was addressed using nonlinear (quadratic) models. Useable, optimal parameters, valid on a regional basis can be generated. This study serves to illustrate that priority should be given to effort to accurately establish a geochemical cross section of the Basin if the development of the Devonian Shale is to be optimized.

Note: Paper not available at time of publication.

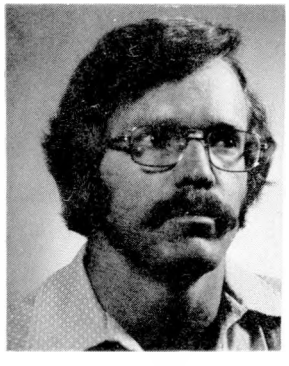
*Mound Facility is operated by the Monsanto Research Corporation for the U.S. Department of Energy under Contract No. DE-AC04-76-DP00053.

IN SITU TESTING OF WELL-SHOOTING CONCEPTS

BY

Richard A. Schmidt, Norman R. Warpinski,
and David A. Northrop

Geotechnical Research Division
Sandia Laboratories
Albuquerque, NM 87185



About the Author

R. A. Schmidt received his B.S., M.S., and Ph.D. in Applied Mechanics from Lehigh University in 1969, 1970, and 1972. His specialty is fracture mechanics and since joining Sandia Laboratories in 1972 his research has focused on applying fracture mechanics principles to rock. This has involved laboratory investigations of fracture toughness as well as more applied studies of hydraulic fracturing and dynamic fracturing. He is active in the International Society for Rock Mechanics, the American Society for Testing and Materials, and the annual U. S. Rock Mechanics Symposium.

N. R. Warpinski received all his degrees in Mechanical Engineering: B.S. from Illinois Institute of Technology in 1971 and M.S. and Ph.D. from the University of Illinois in 1973 and 1976. His specialty is fluid mechanics and he has been involved with many aspects of hydraulic fracturing activities since joining Sandia Laboratories in March 1977.

D. A. Northrop received his B.S. M.S. and Ph.D. in Chemistry with emphasis in geochemistry from the University of Chicago in 1960, 1961, and 1964. He has been at Sandia Laboratories since graduation and initially was active in materials research and development, particularly in the ceramic, thermoelectric, and carbon/carbon composite areas. He was promoted to Division Supervisor in 1971. He initiated and directed Sandia's program in instrumentation development for in situ coal gasification and now heads Sandia's program in Enhanced Gas Recovery.

ABSTRACT

Explosive charges are sometimes detonated in wellbores in efforts to stimulate production of gas or oil; often these efforts meet with little or no success. In this paper, attention is given to the physical phenomena which control the dynamic response of rock to deeply-buried charges. The description of the mechanical behavior of rock focuses on the creation of an impermeable "cage" of residual stresses that develops around the charge, impedes fracturing induced by explosive gases, and can actually reduce the flow of fluids into the wellbore. The general description of the pertinent physical processes is applicable to most, if not all, rock types as well as to both spherical and cylindrical charges.

The implications that this behavior has on conventional well shooting with explosives are described and several alternatives to current techniques are discussed. These alternatives involve tailored-pulse loading concepts and include the use of decoupled explosives, explosive gases, and propellants.

A series of experiments are described in which a propellant concept called Gas Frac was tested at the Nevada Test Site. The tests were performed in boreholes drilled from a tunnel complex which provides in situ conditions and, with mineback, provides direct observations of results. Another series of in situ experiments are presently being conducted at NTS to evaluate several other tailored-pulse loading concepts. The test plans are outlined and a coordinated modeling effort is also described.

INTRODUCTION

Oil and gas wells have been stimulated with high-energy explosives since the late 1800's. It appears, however, that the term "well shooting" originated many years before this in days when a water well was sometimes rejuvenated by pointing a rifle down the well and pulling the trigger. This method of "shooting" a well is even used today and presumably the concussion helps to break out encrustation. Well shooting as discussed herein refers to any rapid release of energy from a chemical reaction in a wellbore for the purpose of stimulating production, presumably by fracturing the reservoir rock. This includes explosives (solid, liquid, and gas) and propellants that deflagrate rather than explode. In a broad sense, well shooting has been applied in several geotechnical fields: e.g., preparation of oil shale beds for true in situ processing, preparation of underground mineral deposits for solution mining, etc.

With regard to oil and gas wells, well shooting techniques are applied to introduce random multiple fracturing rather than a single large fracture as is created by hydraulic fracturing. Multiple fracturing is desired for eliminating "skin damage" caused during drilling and for effectively connecting the wellbore to an existing fracture system as might occur in, say, a gas-bearing Devonian shale. Connecting a well to a fracture network is often not possible by hydraulic fracturing since there is little or no control over fracture orientation and the hydrofrac will often run parallel to existing fractures.

The term well shooting has many unfavorable connotations and conjures up many thoughts in the mind of the petroleum engineer. Problems of wellbore damage, safety hazards, and unpredictable results have reduced the relative number of wells stimulated by high strength explosives. The lack of predictability and the lack of definitive guidance in well shooting is pointed out in a statement from Blasters' Handbook:[1]

> "Detailed instructions for shooting wells cannot be given since there are too many complicating factors. It is always advisable to have the work carried out by an experienced person, and even then there can be no assurance that the results will be satisfactory."

There seems to have been little attempt to perform definitive studies of the physical phenomena involved with wellbore detonations so as to improve the fracturing techniques. On the other hand, a number of related studies have recently been performed primarily to understand the containment aspects of underground nuclear detonations.[2,3] These studies, as well as others performed that deal with well shooting for in situ oil shale processing,[4] have repeatedly demonstrated that contained explosions can cause deleterious effects in a wellbore and indicate alternatives that may improve our dynamic fracturing techniques.

The following section deals with the general behavior of deeply-buried charges as it is now understood. This understanding is a result of several investigations and has developed over some period of time. The phenomena are described in general, first briefly and then in more detail.

GENERAL BEHAVIOR OF DEEPLY-BURIED CHARGE

One important aspect common to most well shooting configurations is the fact that there is no free surface near enough to the charge to affect the behavior. The phenomena associated with deeply-buried charges, as they are called, differ significantly from those of blasts that occur near a free surface as in excavations, quarries, and road cuts.

Briefly, the high pressures of a detonation in a wellbore are known to be sufficient to cause the nearby rock to yield and compact (plastic flow). When the stress wave passes, the rock unloads elastically leaving an increased borehole diameter and a residual stress field which is compressive near the wellbore. The creation of this residual stress field is closely analogous to the process of autofrettage or the "gun barrel problem" in which pressure vessels are often over-pressurized sufficiently to yield the inside wall and develop residual compressive stresses that help prevent crack growth during service. The zone of highly compacted rock with its associated residual compressive stresses is sometimes referred to as a stress cage and the phenomenon is sometimes called the bladder effect. Fracturing caused by high pressure gas may also be inhibited in this situation since fines are created during the compaction process that can plug newly formed cracks and prevent gas penetration. Some or all of these effects may actually cause decreased permeability near the wellbore and are probably responsible for many well-shooting failures.

More specifically, when an explosive charge is detonated in a cylindrical wellbore, a compressive stress wave is immediately transmitted into the surrounding rock medium and the material in the near vicinity of the wellbore moves radially outward (Fig. 1). For typical explosives, detonation pressures are from 10 to 50 times greater than the yield stress of most rock. As a result, stress levels realized in the rock near the wellbore are sufficient to cause irreversible or plastic deformation. Material in this near-field region will thus tend to remain at its deformed location after the transient effects of the detonation have subsided. At greater radial distances, the amplitude of the propagating stress wave will have been mitigated by geometrical divergence effects and by material-related dissipative mechanisms. When sufficient attentuation has occurred, the material response to the dynamic stress will be elastic, rather than plastic; this implies that material in the far-field, which also experiences an initial outward motion, will tend to return to its original position. Full return of the far-field material is not possible, however, because of the presence of the permanently deformed material in the near field. In effect, then, the near-field and far-field materials push against each other, creating a region of residual stress around the cavity produced by the detonation. In the circumferential direction the result is increased compression near the cavity and reduced compression (or possibly tension) farther away with a return to the in situ stress state at great distance. The time required to establish the residual stress field is on the order of a few milliseconds for typical borehole diameters (10's of centimeters) and charge lengths (several meters). This time period is short compared with that required for the explosive gases to move from the borehole into the formation, or even up the wellbore if it is not stemmed.

During the initial traversal of the detonation-induced stress wave in the rock, a number of fractures, primarily radial fractures, will be formed because transient tensile stresses develop behind the compression pulse. These fractures will be formed prior to the development of the residual stress field and, as a result, may be closed again. In the absence of a residual stress region, the explosive gases could move into the fractures, and extend them into the formation. The residual stress field, the highly compacted material, and the fines available to plug cracks, however, produce a type of bladder which will tend to contain the gases within the borehole. Hence, the development of an extensive gas-induced fracture system will be impeded.

The conditions which limit the initial creation of a fracture system will also be present to restrict fluid flow from the reservoir into the wellbore after the shot. Thus, the enhanced production desired, whether it be gas, oil, or water, may not be realized. In addition, this general behavior of a deeply-buried charge is rather universal since it has been demonstrated to occur for detonations ranging from a one pound charge of TNT to a nuclear detonation of several kilotons.

The existence of residual stress regions around boreholes that have been subjected to explosive detonations is a well documented phenomenon. Most of these observations have been made with regard to field experiments at the Nevada Test Site[3] as well as laboratory experiments[5] and computer code calculations[3] for the prupose of understanding containment of underground nuclear blasts. Details of this supporting evidence have been described elsewhere[2] and won't be repeated here. However, to elucidate the description of this general behavior, the results of a code calculation are displayed in Fig. 2. These calculations were performed in conjunction with a containment experiment called

Puff 'n Tuff[3] conducted at NTS. Radial and tangential stresses are shown as occur 3.5 msec after detonation of a 116 kg spherical charge of TNT in ash-fall tuff. The compressive pulse seen in the figure at 7.5 m is the initial attenuated wave still propagating outward, but the large compressive stresses near the cavity are stable and are considered permanent residual stresses.

ALTERNATIVES TO CONVENTIONAL WELL SHOOTING

With the basic knowledge that the bladder effect impedes fracture growth near an explosively loaded cavity, one might wonder how conventional well shooting would ever enhance production. Experience has shown, however, that improved production is sometimes realized. There are several reasons for such results, including the possibility that explosive stimulation may at times be capable of removing skin damage, and that leakage paths may be formed that connect the cavity to the region outside the stress cage. Situations can also occur in which the stress cage will break up and slough into the wellbore. These possibilities are not necessarily predictable or applicable in all formations. It would, of course, be desirable if reliable procedures could be developed to replace conventional well shooting.

Several viable alternatives to explosive well shooting have been considered and tested in recent years that show promise of substantial improvement.[6-9] An approach that has received considerable attention is to tailor the pressure-time behavior of the explosive or a suitable propellant so as to keep the maximum pressure below the yield stress of the rock and thereby avoid forming the stress cage. Several of these concepts rely on the use of propellants which deflagrate rather than detonate. Unlike explosives, the burn front in these materials travels slower than the sound speed, and the burning rate can be varied over a wide range. Pressure-time behavior of propellants differ from explosives in that peak pressures are lower, and burn times are longer. Total energy available, however, is similar in both materials (typically 1000 cal/g).

One of the first tailored-pulse concepts investigated was Dynafrac,[6] which achieves lower amplitude stress waves in the rock by means of a decoupled explosive. A conventional explosive is used, but the charge diameter is some eight times less than the wellbore diameter. The charge is surrounded by water and the peak pressure after detonation is thus mitigated to a value below the yield stress before the wave reaches the rock. The total explosive energy, however, is limited by the small diameter of the charge.

The Augmented Dynafrac[6] concept uses the same decoupled explosive in conjunction with a small propellant charge. The decoupled explosive is designed to initiate multiple cracks and the propellant is then burned to drive water into these cracks to extend them. The propellant is essentially a rocket motor that burns for several seconds. Some field testing has been performed using this device but results are inconclusive.

Kinefrac[7] is a small diameter (4cm) pressure-insensitive propellant charge that is designed both to initiate and propagate multiple cracks. A typical rise time is 3 ms with a burn time of 0.5 s. This device is also designed to push water into the cracks ahead of the gas generated by the propellant reaction products. Kinefrac has been used in the field as a cleaning tool and as a fracture initiating device to reduce the breakdown pressure for hydraulic fracturing. The number and size of the fractures created by this tool are largely unknown.

The Controlled Explosive Rock Breaker (CERB),[8] on the other hand, employs an explosive fuel-air mixture to produce high pressure, high temperature gases to fracture rock. This device has been used primarily for excavation, tunneling, and demolition where the lower peak pressure helps to reduce the quantity of fines typically produced and reduces the ground shock which minimizes the disturbance to surrounding structures. Its use as a stimulation device has not been adequately investigated.

Gas Frac[9] is similar to Kinefrac and consists of a gas producing propellant with a suitable rise time to initiate and propagate multiple cracks. The main differences are that Gas Frac uses a charge diameter that fills the wellbore and the gas products themselves are pushed into the fractures rather than water. A series of Gas Frac experiments was conducted in a tunnel complex at the Nevada Test Site that allowed for direct observation of created fractures through the use of mineback. These experiments were significant in that the ability of a propellant to create multiple fractures in a wellbore was demonstrated. A brief description of that test series follows. Another in situ test series at NTS has been initiated that involves Dynafrac, Augmented Dynafrac, Kinefrac, and Gas Frac. These test plans and associated modeling efforts will be outlined in a later section.

GAS FRAC[9]

The concept of Gas Frac is to tailor the pressure-time behavior of the deflagration of a suitable propellant to create multiple fractures and avoid limitations inherent in both hydraulic fracturing and explosive fracturing. Hydraulic fractures, which are propagated at pressures that are slightly higher than the minimum in situ stress and pumping times that are on the order of hundreds of seconds, typically produce only a single fracture whose orientation is perpendicular to the minimum principal stress. Higher borehole pressures are needed to drive cracks in less favorable directions, but pressures must not be allowed to exceed the flow stress to avoid rock crushing and the formation of a stress cage.

Gas Frac, then, is designed to impart a controlled pressure about one order of magnitude above the in situ stresses but below the flow stress of the rock. This pressure load is applied over an interval on the order of milliseconds to create and extend multiple fractures radially from the borehole. The initial loading rate should be large enough to initiate multiple fractures although some rock may already contain an adequate distribution of flaws. The number of fractures created is probably rate dependent being influenced by the velocity of sound in the rock, the size of the borehole, the in situ stresses, and the number of available flaw sites for crack nucleation. The propellant must continue to burn for a sufficient period to allow the hot, high-pressure gases to enter the created fractures and extend them. Under these conditions of elevated temperature, pressure and gas velocity it is also expected that the fractures will be somewhat self-propping, but propping agents could be added, although this would reduce the volume of propellant that can be employed.

Three different propellants were tested at the Nevada Test Site in boreholes drilled from an existing tunnel complex so that mineback of the tests would provide direct observational evidence to characterize the results. These tests were conducted in a water-saturated ash-fall tuff medium having the material properties listed in Table I. In each test, canisters containing 20 lb of propellant, ignitors, and a fluid-coupled-plate pressure transducer (Fig. 3) were stemmed into an 8 in. diameter horizontal borehole, 20 ft. deep, with a high strength grout (Fig. 4). The propellants utilized were JPN, a relatively slow burning rocket propellant, M26, used in large-bore gun ammunition having an intermediate burn rate, and M5, used in small arms ammunition with a fast burn rate.

The results of the three tests showed phenomenologically different behavior. JPN, the slow propellant (burn time = 0.9 sec), had a pressure loading rate of 0.09 psi/μsec and a peak pressure of 6250 psi. Mineback of this test showed that this relatively low loading rate and low peak pressure resulted in a single fracture that was similar in appearance to hydraulic fractures typically observed in this formation.[10] M26, the intermediate propellant (burn time = 9.4 msec) had a loading rate of about 20 psi/μsec and a peak pressure of 13,800 psi (Fig. 5). This was sufficient to initiate and extend 12 separate fractures in random radial directions. Lengths of these fractures varied from 6 in. to 8 ft. There was no apparent crushing of the rock near the wellbore. The fast propellant (burn time $\lesssim$ 1 msec) had a pressure loading rate greater than 1500 psi/μsec and a peak pressure greater than 20,000 psi. These values were so large that considerable crushing of the rock near the wellbore was observed and only one fracture was extended a significant distance from the wellbore. Several incipient cracks ($<$ 4 in.) that barely extended out of the crushed zone were also observed. The crushed cavity region was similar in appearance to typical high explosive shots conducted in tuff.

Analysis of the intermediate propellant test shows that a lower bound crack length of 1.6 ft. is calculated by assuming a loaded borehole with no gas entering the fractures. On the other hand, if it is assumed that gas enters the fracture and the crack propagates at its maximum velocity for as long as the pressure is higher than the fracturing pressure in this medium, an upper bound crack length of 30 ft. is obtained. The observed crack lengths in general fall between these two bounds. This implies that the fractures are, in fact, extended due to gas penetration, but that substantial pressure losses occur that prevent the final crack lengths from achieving their theoretical maximum. Realistic calculations for these final crack lengths will require knowledge of the complex gas dynamics in the cracks.

Gas Frac was shown to be a viable technique for creating multiple, randomly oriented fractures in a borehole. This field test demonstrated that a propellant can be suitably designed to provide (1) a large enough loading rate to initiate multiple fractures, (2) high enough pressures to extend fractures radially, but not so high as to exceed the flow stress of the rock, and (3) sufficient gas generation to allow several fractures to be pressurized and propagated.

MULTI-FRAC TEST SERIES

Another series of five in situ experiments are presently being conducted at the Nevada Test Site in a similar ash-fall tuff formation as for the Gas Frac test series. The purpose of these tests is: 1) to evaluate the characteristics of five tailored-pulse fracturing concepts mentioned previously -- Dynafrac, Augmented Dynafrac, Kinefrac, multiple firings of Kinefrac, and Gas Frac and 2) to provide inputs for modeling efforts which are necessary if such concepts are to be applied effectively to particular reservoirs, such as the Devonian shales, with substantially different properties from ash-fall tuff.

The previous tests with Gas Frac demonstrated the feasibility and usefulness of performing dynamic borehole tests in situ with mineback, but were not instrumented except for a pressure transducer to measure dynamic cavity pressures. These new tests will involve several pressure transducers as well as stress gages and accelerometers grouted in the rock to measure formation response. These measurements will be especially valuable for modeling efforts. In addition, caliper logs will be performed before and after each shot to determine if any permanent borehole enlargement occurred, which would give indications of the existence of a stress cage. A permeability measurement will be made to give an indication of the conductivity of a particular fracture network. Televiewer logs are also planned.

In a previous Gas Frac test, shot debris such as cabling and connectors were found in several cracks some distance from the borehole. Thus, a few light-weight bauxite beads of various sizes will be introduced into each hole of this test series in hopes that the location of these markers along with accelerometer records will help define dynamic crack widths.

The setup for all five tests will be similar and a schematic of the Augmented Dynafrac shot is depicted in Fig. 6. The shots will be performed in horizontal boreholes that are 6 in. diameter and 40 ft. deep. There will be a 10 or 20 ft. open-hole test section, depending on the test, with the remainder being grouted casing. All tests except Gas Frac will be shot in water.

The modeling and analysis efforts that are being conducted in conjunction with these tests are being performed cooperatively by Sandia Laboratories, Los Alamos Scientific Laboratory, Stanford Research Institute, and Science Applications Incorporated. These efforts have two primary goals: 1) to provide design criteria for the optimization of stimulation efforts for a particular, site-specific well and 2) to provide a predictive capability for determining, a priori, the number, length, and conductivity of fractures created by any particular pulse in any given well. Achieving the second goal automatically includes the first, but developing a design optimization scheme may not require the complete solution necessary in a predictive capability.

The modeling efforts have had substantial impact on the test plans for the Multi-Frac Test Series. This cooperative effort is intended to maximize the usefulness of the test results for the analytical efforts. This approach is necessary to provide the understanding of what effect each of the five tailored-pulse concepts would have if used in a Devonian gas well.

SUMMARY

Recent experimental and analytical studies of the behavior of deeply-buried charges have shown conclusively that the high pressures of the explosive detonation plastically deform the rock and leave a residual stress field which is compressive near the wellbore. The so called stress cage of highly compacted rock with its associated residual compressive stress inhibits fracture growth. Alternatives to the use of high strength explosives for well shooting include the use of decoupled explosives, explosive gases, and propellants. A propellant concept known as Gas Frac was tested in situ in a tunnel complex at the Nevada Test Site which provided for direct observation of results by mineback. Gas Frac was demonstrated as capable of producing multiple cracks that connect to the borehole without forming a stress cage. Another test series was described in which five tailored-pulse concepts will be evaluated in a similar manner. Modeling and analysis efforts are expected to provide the link between these results in ash-fall tuff to expected results in Devonian shale.

ACKNOWLEDGEMENT

The author wishes to give special thanks to Rodney R. Boade for his many helpful discussions and assistance in preparing this manuscript. Appreciation is also extended to C. A. Komar and R. L. Wise at the Morgantown Energy Technology Center for their support of the Multi-Frac Test Series. This work was supported by the United States Department of Energy (DOE) under contract DE-AC04-76DP 00789.

REFERENCES

1. Blasters' Handbook, E. I. DuPont de Nemours and Company, Inc., Explosives Department, Wilmington, Delaware (1977).

2. Schmidt, R. A., Boade, R. R., and Bass, R. C., "A New Perspective on Well Shooting - The Behavior of Contained Explosions and Deflagrations," Proceedings of 1979 Society of Petroleum Engineers Annual Technical Conference and hxhibition, SPE 8346 (1979).

3. Smith, C. W., Bass, R. C., and Tyler, L. D., "Puff 'n Tuff, A Residual Stress - Gas Fracturing Experiment," Proceedings of 19th U. S. Symposium on Rock Mechanics, Stateline, Nevada (1978).

4. Boade, R. R., Stevens, A. L., Harak, A. E., and Long, A., "Bed Preparation Concepts for True In Situ Oil Shale Processing: An Evaluation of Current Technology," Proceedings of the 1979 Society of Petroleum Engineers Annual Technical Conference and Exhibition, SPE 8447 (1979).

5. Florence, A. L., and Gates, R. W., "Explosive Cavity Residual Stress Experiment," 76-3702-2, Stanford Research Institute, Menlo Park, CA (1976).

6. Moore, E. T., Mumma, D. M., and Seifert, K. D., "Dynafrac - Application of a Novel Rock Fracturing Method to Oil and Gas Recovery," Physics International Final Report 827, April 1977.

7. Fitzgerald, R., and Anderson, R., "Kine-Frac: A New Approach to Well Stimulation," ASME Paper 78-PET-25, ASME Energy Technology Conference and Exhibition, Houston, TX, November 5-19, 1978.

8. Bligh, T. P., "Principles of Breaking Rock Using High Pressure Gases," Advances in Rock Mechanics, Proceedings of the Third Congress of the International Society for Rock Mechanics, Denver, CO, 1974, Vol. II, Part B, p. 1421.

9. Warpinski, N. R., Schmidt, R. A., Cooper, P. W., Walling, H. C., and Northrop, D. A., "High-Energy Gas Frac: Multiple Fracturing in a Wellbore," Proceedings of 20th U. S. Symposium on Rock Mechanics, Austin, TX (1979).

10. Northrop, D. A., Warpinski, N. R., Schmidt, R. A., and Smith, C. W., "Stimulation and Mineback Experiment Project - The Direct Observation of Hydraulic and Explosive Fracturing Tests," Proceedings of the Fourth Annual DOE Symposium on Enhanced Oil and Gas Recovery, Tulsa, OK, August 1978, p. E-4.

Table 1

ASH FALL TUFF PROPERTIES

Density	1.8 gm/cc
Porosity	40 %
Permeability	0.01 md
Elastic Modulus	0.6×10^6 psi
Poisson's Ratio	0.2
Compressional Wave Velocity	7000 ft/sec
Shear Wave Velocity	4000 ft/sec
Tensile Strength	400 psi
Compressive Strength (Unconfined)	5000 psi
Fracture Toughness	450 psi$\sqrt{in}$
Calculated Terminal Crack Velocity	1500 ft/sec

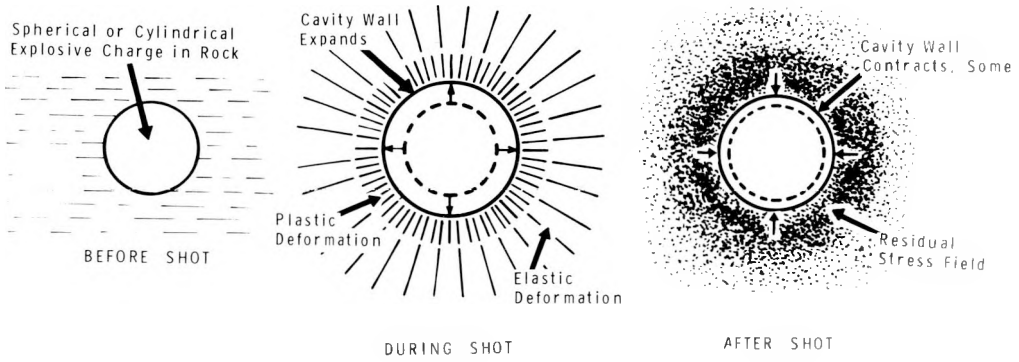


Figure 1. General phenomenology of rock behavior for a deeply-buried charge whether cylindrical or spherical.

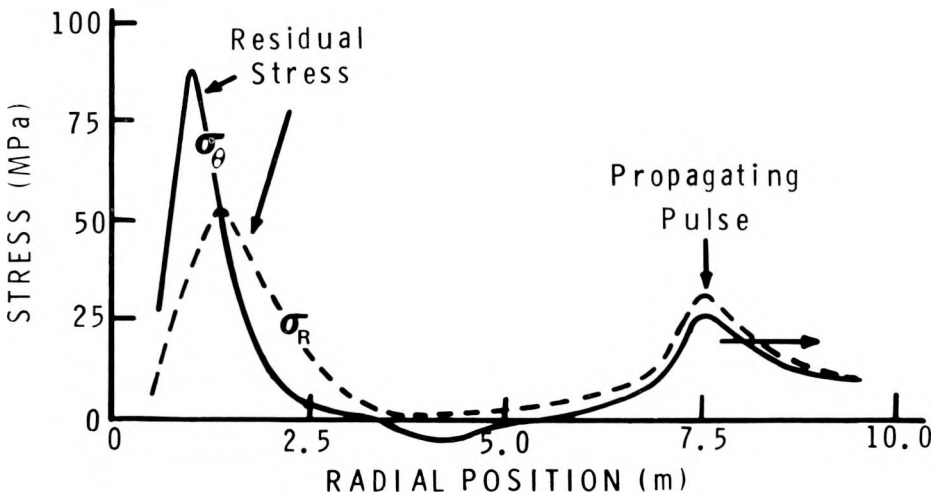


Figure 2. Profiles of radial and tangential stress as determined with CSQ after a spherical detonation of 116 kg of TNT in ash-fall tuff.

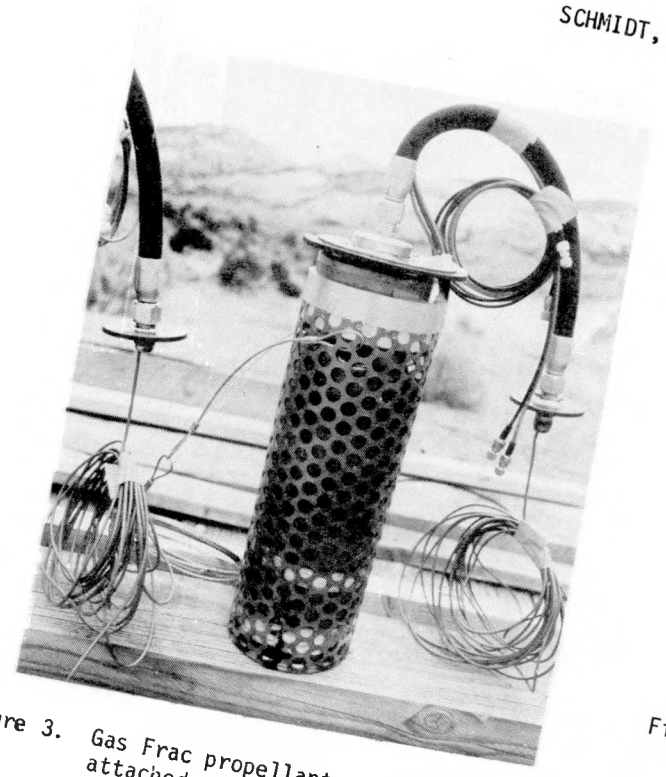


Figure 3. Gas Frac propellant canister with attached pressure transducer.

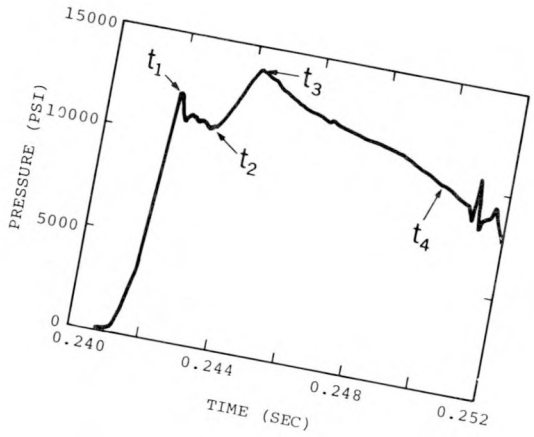


Figure 5. Gas Frac pressure-time record from within the cavity

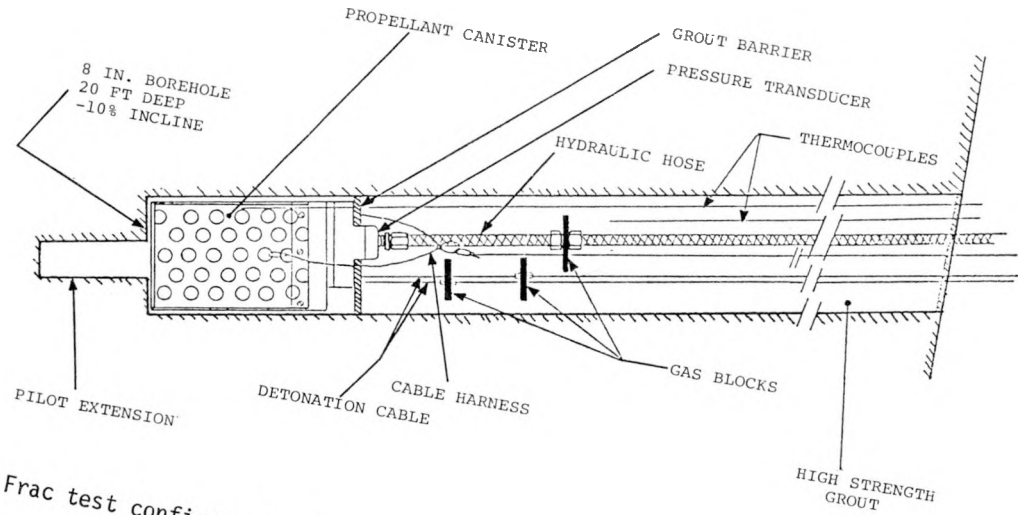


Figure 4. Gas Frac test configuration in borehole.

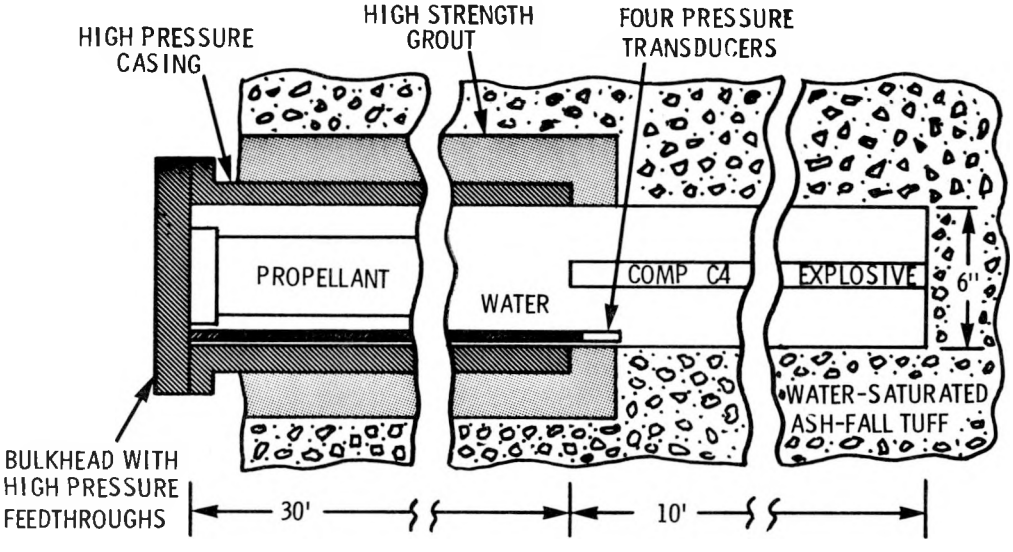


Figure 6. Test setup for Augmented Dynafrac which is similar to the other four experiments in the Multi-Frac test series.

PRINCIPAL CONSIDERATIONS GOVERNING HYDRAULIC FRACTURE PROPAGATION IN EASTERN GAS SHALES

S.H. Advani
The Ohio State University

C.A. Komar
Morgantown Energy Technology Center

ABSTRACT

The role of in situ stresses, pore pressure, and shale material and geometric properties is identified in terms of fracture treatment selection. Factors governing hydraulic fracture initiation and propagation (vertical and lateral) are discussed by means of structural, fracture mechanics, and fluid response models. These models illustrate the effects of multi-layering, variable in situ stress, and fracturing fluid properties on the induced vertical fractures. Supporting rationale for foam fracture and dendritic fracture experiments is also presented.

Numerical results revealing the fracture response at a bi-material interface, fracture widths, fluid leak-offs, and predicted fracture lengths are given and compared with existing model results. In addition, the mechanisms governing crack stability and branching are reviewed.

Note: Paper not available at time of publication

CROSS-STRIKE STRUCTURAL DISCONTINUITIES: THEIR USE IN AN EXPLORATION RATIONALE FOR EASTERN PLATEAU PROVINCE, APPALACHIAN BASIN

by

Russell L. Wheeler

U.S. Geological Survey
Box 25046, MS 966
Denver Federal Center
Denver, Colorado 80225

ABOUT THE AUTHOR

Wheeler received his B.S. and Ph.D. degrees in geology from Yale and Princeton Universities, in 1966 and 1973 respectively, specializing in structural analysis of metamorphic rocks. From 1971 to 1979 he taught structural geology, tectonics, and statistical applications at West Virginia University as Assistant and Associate Professor. His work on structural analysis of the eastern Plateau and western Valley and Ridge provinces of the central Appalachians continued during a part-time appointment with the U.S. Geological Survey (1975-1977) and leaves of absence funded by that appointment (1977) and Eastern Gas Shales Project (1978).

In June 1979 he joined the U.S. Geological Survey in Denver, Colorado, to attempt to detect seismogenic structures in the Eastern United States and to play in the mountains.

2 CROSS-STRIKE STRUCTURAL DISCONTINUITIES

ABSTRACT

Cross-strike structural discontinuities (CSD's) are zones of structural disruption several kilometers wide in the Appalachian and other overthrust belts. CSD's are not faults or fault zones. They typically contain about 1000 km^3 (240 mi^3) of unusually fractured rock. For example, in eastern West Virginia, one CSD (Parsons lineament) trends west-northwest at least from the Appalachian to the Intra-Plateau structural fronts of the eastern Plateau province, with no evidence of basement involvement. Where the Parsons lineament crosses the Deer Park and Elkins Valley anticlines, exposed Upper Devonian siltstones have about twice their normal joint intensity (surface area of systematic joints per unit volume of rock). Another CSD (Petersburg lineament) trends west-southwest from the western Valley and Ridge province and crosses the Appalachian structural front. The Petersburg lineament alines with a probable basement flexure under the western and central Plateau province and has twice normal joint intensity in exposed Lower Pennsylvanian sandstones at the front. The two CSD's appear to intersect in southern Tucker and northern Randolph Counties, W. Va.

CSD's and intersections of CSD's, particularly where either underlies intersections of short, airphoto lineaments, may comprise highly permeable, fractured, gas-filled reservoirs. Where the seal is preserved, CSD's can provide a guide for extending exploration into the little-tested eastern Plateau province of West Virginia and adjacent States, where organic-rich Devonian shales are thick and thermally mature.

INTRODUCTION

Purpose

This paper has three purposes: (1) To present an exploration rationale for the Devonian clastic sequence on the basis of a particular kind of large structural lineament; (2) to apply that rationale to an area in the little-explored and largely or wholly untested eastern Plateau province of West Virginia, where the Devonian rocks are detached (involved in thin-skinned or overthrust tectonics); and (3) to suggest a method whereby other exploration rationales can be generated.

Most of this paper is based on work already published or otherwise available to contractors and others interested in the Eastern Gas Shales Project (EGSP). For that reason and because of time constraints, I will refer to and cite that work or compilations of it but will not repeat or summarize its evidence here. Many of the ideas presented here are based on results of detailed mapping and analyses of fracture systems exposed near Parsons and Petersburg and in Pendleton County, W. Va. (Figure 1).

Readers should bear in mind that the exploration rationale presented here has not yet been tested, either against production data or with the drill. Such testing against extant well data, particularly records of shows, is planned for the near future.

Setting

Although many of the ideas presented in this paper apply throughout the Appalachian Basin, they deal mostly with part of eastern West Virginia (Figure 1). As one follows eastward the dark Middle and Upper Devonian shales that form both the source and the main fractured reservoir of interest to EGSP, those shales thicken, become more deeply buried and poorer in organics, and are coarser grained upward in the section. Between the Intra-Plateau structural front and the Appalachian structural front (Figure 1), the reservoir rocks approach the surface and are locally exposed in cores of anticlines. East of the Allegheny (topographic) Front, they are mostly exposed or eroded but are preserved locally. East of the Burning Springs and Mann Mountain anticlines (Figure 1), the reservoir rocks are detached[1,2] and their fracture characteristics are probably determined largely by that detachment, rather than, or in addition to, basement structure.

EXPLORATION RATIONALE

According to the ideas of this report, exploration should be concentrated where two features known to produce locally intense fracture systems coincide: cross-strike structural discontinuities and short airphoto lineaments. Most of the material presented in this section is condensed, with few additions and changes, from previous reports[3,4,5,6] and other work cited therein.

Cross-strike structural discontinuities (CSD's)

CSD's are alinements of disruptions of strike-parallel structural, geophysical, geomorphic, or other geological patterns in overthrust belts. Most studied CSD's are 1 to 12-km (0.6 to 7.5-mi) wide and lie about 60° from regional strike. CSD's occur in the Appalachians, Ireland, southern Chile, probably the eastern Rockies, and perhaps the Jura. CSD's are defined by one or more of the following: alined bends and ends of map-scale folds and longitudinal faults; alined and sometimes flat-ended gravity and magnetic anomalies; diverse geomorphic anomalies, including water and wind gaps; and changes in sedimentation patterns and stratigraphic thicknesses. Seismic activity, mineralization, thermal springs, and anomalous water-well yields and chemistries can occur along them. They are not simply faults or fault zones, although faults of various orientations, sizes, types, and times of movement occur in or parallel to some CSD's. They are not "lineaments" in the overly restricted sense in which many EGSP workers use that term (imagery lineaments), although most CSD's have satellite or airphoto lineaments in, parallel to, or near them; however, CSD's include zones of anomalously close fracturing (mostly jointing) wherever examined at ground level. By assumption, this unusually jointed rock extends to depths sufficient to provide permeable fractured reservoirs.

There are few depth estimates for CSD's. In West Virginia, interpretation and modelling of residuals from terrain-corrected Bouguer gravity data and balanced cross sections constructed from surface mapping, well logs, and seismic sections show changes in map-scale structure across CSD's down to Middle Ordovician and Middle Cambrian shales that lie as deep as 2.7 km (9,000 feet) below ground level[4,7,8,9]. In Pennsylvania, Alabama, and Ireland, magnetic anomalies, faults of long-term activity and changing senses of slip, some economic mineralization, and some volcanic centers are evidence for basement faults underlying CSD's[5]. The few known depth estimates for CSD's have a median of about 4 km (2.5 mi), based mostly on depth to the deepest known detachment fault in a particular area. Together with medians of estimated minimum lengths and estimated widths, the depths suggest that a typical CSD contains about 1,000 km^3 (240 mi^3) of unusually fractured rock.

Wherever data are sufficient to allow a test for basement involvement, CSD's have been interpreted to overlie basement faults that are also at high angles to regional strike. Thus, that characteristic is probably true of CSD's generally; however, in eastern West Virginia (Figure 1), I know of no characteristics of CSD's that cannot be explained by processes and structures known to occur within the detached (overthrust) prism of sedimentary rocks. Thus, when the exploration rationale described herein was first suggested[3,6] I conservatively restricted its application to the area east of the subsurface line at which the deepest detachment cuts up into the Middle Devonian dark shales. That line of restriction runs along the Mann Mountain anticline[2] (Figure 1), and along or just west of the Burning Springs anticline[1], and omits the area of present production from the shales.

The likelihood that CSD's generally occur over basement faults releases that restriction, because basement faults occur west of detachments in the shales (W. J. Perry, Jr., oral and written communications, 1978 and 1979). CSD's can be regarded, at least tentatively, as fractured gas reservoirs as far west as one can trace their structural, geophysical, geomorphic, or other signatures.

Short airphoto lineaments

Lineaments one to several kilometers long seen on airphotos have been assumed to be, and often are shown to be, expressions of small zones of unusually fractured rock in the Appalachian Basin. Wheeler[4] summarized evidence of several EGSP workers, and others working at West Virginia University and elsewhere, that such short airphoto lineaments and their intersections overlie fracture systems that may extend down to gas-filled reservoirs whose seals are intact, but that lineaments visible on

LANDSAT images may have broken such seals. D. W. O'Leary (written communication, 1979) has pointed out that short airphoto lineaments may comprise some LANDSAT photolineaments. It is not clear whether the two types of image record fracture systems differing in kind or only in degree.

Rationale: CSD's and airphoto lineaments

Given the considerations above, I suggest the following exploration rationale, modified from that of Wheeler[4]. Step 1, below, is based on geochemical work of Claypool and others [10] and Maynard [11,12,13] (and J. B. Maynard, oral communications, 1978 and 1979).

1. Seek areas or stratigraphic intervals that are thermally mature and have abundant organic carbon derived from nonmarine sources.

2. Within those areas, such as eastern West Virginia, drill on intersections of short airphoto lineaments in CSD's. Within the kilometers-wide CSD's, avoid lineaments that are visible only on LANDSAT photos.

APPLICATION

Parsons and Petersburg lineaments

The Parsons and Petersburg lineaments are two CSD's in eastern West Virginia (Figure 1). The most complete study of a CSD that I am aware of to date is that made of the Petersburg lineament where it is superbly exposed in the western Valley and Ridge province[9]. Specific locations and descriptions of the two CSD's are given by Wheeler[4] and in other work cited by Wheeler and others[5]. Wheeler[4] (p. 23-31 and Figures 9-11) discussed possible subsurface map-scale structures in the two CSD's near their probable intersection in southeastern Tucker County and adjacent parts of Grant, Pendleton, and Randolph Counties, W. Va. Other reports [14-17] and unpublished data permit the following additional generalizations.

Intensity of systematic joints is defined as the surface area of systematic joints per unit volume of rock and is calculated from perpendicular spacings of adjacent joints in individual sets [14-17]. The two CSD's have roughly twice normal joint intensity in the eastern Plateau province. It is not yet known whether that high intensity is caused by larger joints, more abundant joints, or both. The first would be more favorable than the second for a fracture-permeable reservoir such as the dark shales, because fractures contribute more to the permeability of the shales than to the porosity, and a few large fractures will increase long-distance permeability more than will many small ones.

Considerable variation in joint intensity exists within the CSD's. Patches and elongate zones of high intensity are interspersed with areas of normal or even below normal intensity. Thus, a CSD should not be tested by only a single well. It would be useful if the patches and elongate zones of high joint intensity could be shown to lie along aircraft or satellite photolineaments, or to overlie rock masses that have low seismic velocities or high electrical resistivities. Those phenomena might be developed into tools for locating small, intensely fractured rock volumes at depth, after an enclosing or overlying CSD had been found using faster methods.

The CSD's, and perhaps their zones of high joint intensity, are wider in the relatively soft dark Devonian shales than in the overlying stiffer sandstones and limestones of Late Devonian to Pennsylvanian age. Thus, the exact locations of CSD boundaries at the surface, in those stiffer units, is not important; however, widths of CSD's can vary greatly, even along the length of a single CSD[5].

Continuing research at West Virginia University attempts to further characterize the fracture systems of CSD's and the dark Devonian shales. J. M. Dixon is determining whether the high joint intensity inside the Parsons lineament is attributable to increased joint size, increased joint abundance, or both. She is also investigating changes in joint intensity and in the width of the high-intensity

zone with changing lithology and stratigraphic level within the Petersburg lineament. T. H. Wilson is examining the effect of the Parsons lineament and map-scale structures in the Oriskany Sandstone on joint intensity in the overlying dark Middle Devonian shales. Both studies are attempts to identify a hypothesized extension of the Parsons lineament west of the Intra-Plateau structural front (Figure 1); Sites [9,18] gives evidence for such an extension of the Petersburg lineament.

Assumptions

Several untested assumptions of this paper's exploration rationale and its application are:

1. That the fracture systems generated in and under CSD's and short airphoto lineaments are not rendered impermeable by gouge, slickensides, or mineralization. H. King (oral and written communications, 1979) found asphaltic material in heavily mineralized joints in Devonian siltstones exposed near the Parsons lineament. He reported that the asphaltic material postdates at least some crystals of the joint fillings. He did not observe the asphaltic material in the last-formed of four joint sets present in the exposure. His observations could be interpreted to suggest that mineralization did render some joint sets impermeable before the joint systems had completely formed. On the other hand, those siltstones are stratigraphically and structurally above the dark Devonian shales, so that King's observations could also be interpreted to suggest that assumption (2) below (intact seal) is valid.

2. That the fracture systems formed in the dark Devonian shales by CSD's and short airphoto lineaments have retained an intact overlying seal and have not degassed. The seals might consist of overlying, poorly fractured shale, of gouge or slickensides produced by overlying detachment faults, or of tightly mineralized (filled) joints, for example.

3. That lineaments visible only on LANDSAT photos have broken the seals. (Note that failure of this assumption will not invalidate the rationale.)

4. That the fracture systems in and under CSD's penetrate down into the dark Devonian shales. The shales are folded up closer to ground level east of the Intra-Plateau structural front than they are west of it, and they lie closest to the surface in the vicinity of Parsons (T. H. Wilson, oral and written communications, 1979).

OTHER EXPLORATION RATIONALES

Method

An approach similar to that used to generate this exploration rationale can be used to produce others in a systematic way. At least 16 factors can produce concentrations of natural fractures in the dark and light shales and siltstones of the Devonian clastic sequence (Table 1; see discussion below). Of those factors, 14 are partly or wholly structural and two are entirely stratigraphic. Another fourteen occur partly or wholly in detached rocks and only two entirely in undetached rocks below or west of the overthrusts. Where the shales are detached, it may be that no one of the appropriate factors produces enough porosity or permeability to be attractive at the greater drilling depths characteristic of the eastern Plateau province, but exploration might profitably focus where two or more factors occur together. This multi-factor approach has two advantages. It increases the chance of finding economically attractive amounts of fracture porosity and permeability, and it decreases the rock volume to consider in an exploration program.

A systematic development of that approach may be particularly useful where the shales are detached. Although thermal maturity increases eastward, so does drilling depth, with the local exceptions of shallower drilling depths in the anticlines of the eastern Plateau province and in some synclines in the western Valley and Ridge province. Those generally greater depths make it possible that a factor that is apparently undesirable in the area of present production, such as lineaments visible

on LANDSAT photos, will be desirable farther east because the thicker seal may be unbroken; for that reason, LANDSAT photolineaments appear in Table 1. Further, because structural and stratigraphic factors are more varied and interact in more complex ways as one goes eastward into the area of detached shale, different combinations of factors are likely to apply in different areas and, perhaps, even in different parts of the same structure. As an extreme and unlikely example, factors 1, 5-13, and 15 could all occur in different parts of a single detached anticline. The number of possible combinations of two of those factors is 55.

Some structures can decrease fracture permeability and thus should be avoided. Slickensides are relatively impermeable, and existing gouge zones are weak and can cause hydrofractures to follow them rather than opening up new fractures that cross the gouge. Finally, note that the list of factors in Table 1 is almost surely incomplete.

Factors

Wheeler[6] discusses and cites sources for factors 1-11 and 13 and 14 of Table 1; a summary of that material is presented herein. Extension faults and extension fractures open when stiff beds are extended, when and where folding in detached rocks causes limb dips to exceed about 45°. Fracture facies are stratigraphic intervals that are lithologically predisposed to fracture intensely over a specific, but usually large, geographic area. Westward fracture propagation refers to extension of fracture systems produced by detachment, into undetached or incipiently detached rocks. Differential horizontal shortening between two stratigraphic levels is a specific type of westward fracture propagation. As overthrust blocks move, their soles can acquire abundant normal faults and other fractures. As a detachment fault ramps up westward to a shallower stratigraphic and structural level, the footwall beneath the ramp is stressed and may fracture. Upward propagation of fractures is self-explanatory. CSD's may have their fracture systems sealed by slickensides or fault gouge produced by overlying thrusts. Crestal fractures form where and when stiff beds are stretched over crests of growing anticlines and, to a lesser degree, under troughs of growing synclines. Noses of plunging anticlines are observed to be unusually jointed, presumably because beds there are flexed or stretched, or both, in more than one direction. The 38th Parallel lineament trends northeastward across West Virginia as a zone about 80 km (50 mi) wide. It contains unusually abundant photolineaments of many sizes and, thus, probably has fracture characteristics different from those of rocks north and south of the lineament. The lineament follows approximately along Arkle's[19] hinge line, which is the boundary between older (southern) and younger (northern) coal basins. Sites[9] suggested that the hinge line is the westward continuation of the Petersburg lineament. He has agreed that, of the three structures, the hinge line may be the most fundamental (oral and written communications, 1978 and 1979). Lundegard and others[20] identified turbidite siltstone bundles, found in the Upper Devonian Brallier Formation, as potentially attractive fractured reservoirs where interlayered with organic-rich shales. In eastern West Virginia, the Brallier Formation is entirely detached[1,2]. Finally, Advani and others[21], Kulander and others[22], and Kulander and Dean[23] suggested the presence of unusually intense fracturing above border faults of the Rome trough.

Procedure

A useful procedure would be to make a 16 x 16 chart of each factor combined with each other factor. Eliminate doublet combinations that are geologically unlikely. Factor 2 (fracture facies) is likely to be present everywhere there are dark shales to act as a gas source, and so can be dropped once the dark shales are known to be present in an area of interest. Remaining doublets can be crossed with the factors again to produce triplets. One expects many doublets but very few triplets. Quadruplets may be desirable for areas of great drilling depth. Specific localities and depths where favorable doublets, triplets, or quadruplets are likely to occur may then be predicted.

CONCLUSIONS

1. In broad regions selected geochemically, exploration could focus on intersections of short airphoto lineaments in cross-strike structural discontinuities. In this rationale, LANDSAT photolineaments would be avoided unless there is reason to expect the reservoir seal to be intact.

2. In the eastern Plateau province of West Virginia, geological and geophysical data needed to apply the rationale of conclusion 1 are best developed and interpreted in and near Tucker and Randolph Counties, where the Parsons and Petersburg lineaments intersect and are mapped.

3. Other exploration rationales can be developed by a systematic evaluation of combinations of structural processes and stratigraphic phenomena known to increase fracturing in detached shales.

ACKNOWLEDGMENTS

The manuscript was improved by the suggestions of D. W. O'Leary, J. P. Ohl, P. C. Thenhaus, and L. M. Carter. It is based on work done while I was on the faculty of West Virginia University, supported partly by the donors of the Petroleum Research Fund (PRF) of the American Chemical Society, and by Contract No. EY-77-C-21-8087, Task Order No. 25, from the Eastern Gas Shales Project (EGSP) of the Morgantown Energy Technology Center, U.S. Department of Energy. Most of that work was done by undergraduate and graduate students at WVU and by workers elsewhere. Citations appear in Wheeler[4] and Wheeler and others[5]. Most students were supported by the West Virginia Geological and Economic Survey, EGSP, PRF, Amoco Oil Company, and Sigma Xi. Many ideas are based on unpublished data, opinions, and preliminary results of work in progress. I thank all who have shared such material with me. Any errors of speculation, interpretation, or fact are mine.

REFERENCES CITED

1. Cardwell, D. H., Erwin, R. B., and Woodward, H. P., compilers, 1968, Geologic map of West Virginia: Morgantown, W. Va., West Virginia Geological and Economic Survey. Scale 1:250,000.

2. Perry, W. J., Jr., 1978, Mann Mountain anticline--probable western limit of detachment in south-central West Virginia: Geological Society of America Abstracts with Programs, v. 10, no. 4, p. 194.

3. Wheeler, R. L., 1978, Cross-strike structural discontinuities: possible exploration tool in detached forelands: Geological Society of America Abstracts with Programs, v. 10, no. 4, p. 201.

4. Wheeler, R. L., 1978, Fracture intensity predictions for eastern gas shales: Eastern Gas Shales Project open-file report 137, 78 p.; available from U.S. Department of Energy, Morgantown Energy Technology Center, Morgantown, W. Va.

5. Wheeler, R. L., Winslow, M., Horne, R. R., Dean, S., Kulander, B., Drahovzal, J. A., Gold, D. P., Gilbert, O. E., Jr., Werner, E., Sites, R., and Perry, W. J., Jr., 1979, Cross-strike structural discontinuities in thrust belts, mostly Appalachian: Southeastern Geology, v. 20, p. 193-204.

6. Wheeler, R. L., 1980, Cross-strike structural discontinuities: possible exploration tool for natural gas in detached Appalachian foreland, in Dean, C. S., and Wheeler, R. L., eds., Western limits of detachment and related structures in the Appalachian foreland: Morgantown, W. Va., Morgantown Engergy Technology Center, U.S. Department of Energy (in press).

7. Kulander, B. R., and Dean, S. L., 1978, Gravity, magnetics, and structure of the Allegheny Plateau/Western Valley and Ridge in West Virginia and adjacent states: Morgantown, W. Va., West Virginia Geological and Economic Survey, Report of Investigation RI-27, 91 p.

8. Perry, W. J., Jr., 1971, The structural development of the Nittany anticlinorium in Pendleton County, West Virginia: Yale University, Ph. D. dissertation, 227 p.; available from Ann Arbor, Mich., University Microfilms; also in West Virginia Geological and Economic Survey open-file report.

9. Sites, R. S., 1978, Structural analysis of the Petersburg lineament, central Appalachians: West Virginia University, Ph. D. dessertation, 274 p.; available from Ann Arbor, Mich., University Microfilms.

10. Claypool, G. E., Threlkeld, C. N., and Bostick, N. H., 1978, Natural gas occurrence related to regional thermal rank of organic matter (maturity) in Devonian rocks of the Appalachian Basin: Eastern Gas Shales Symposium, 2d, Morgantown, W. Va., October 16-18, 1978, Preprints, v. 1, p. 54-65 METC/SP-78/6 v. I; available from National Technical Information Service, Springfield, Va. 22161.

11. Maynard, J. B., 1976, Organic geochemistry applied to the geology of shales, in Shumaker, R. C., and Overbey, W. K., Jr., eds., Devonian shale-- production and potential: Appalachian Petroleum Geology Symposium, 7th, Morgantown,W. Va., Proceedings, MERC/SP-76/2, p. 96-99; available only from National Technical Information Service, Springfield, Va. 22161.

12. Maynard, J. B., 1978, Carbon isotopes in the Devonian shale sequence: utility as provenance indicators: Eastern Gas Shales Symposium, 2d, Morgantown, W. Va., October 16-18, 1978, Preprints, v. 1, p. 396-403, METC/SP-78/6 v. I; available from National Technical Information Service, Springfield, Va. 22161.

13. Maynard, J. B., 1978, Quarterly report, Cincinnati Group, April 25, 1978 (Contract E(40-1) 5210): Eastern Gas Shales Project open-file report 071-78-Q2, 28 p.; available from U.S. Department of Energy, Morgantown Energy Technology Center, Morgantown, W. Va.

14. Dixon, J. M., 1979, A method to identify zones of intense jointing with application to the Parsons lineament, West Virginia: Geological Society of America Abstracts with Programs, v. 11, no. 4, p. 177.

15. LaCaze, J. A., Jr., 1978, Structural analysis of the Petersburg lineament in the eastern Appalachian Plateau province, Tucker County, West Virginia: West Virginia University, M.S. thesis, 69 p.

16. LaCaze, J. A., Jr., and Wheeler, R. L., 1979, Structural expression of the Petersburg lineament in easternmost Plateau province, Dolly Sods Wilderness Area, West Virginia: Geological Society of America Abstracts with Programs, v. 11, no. 4, p. 186.

17. Wheeler, R. L., 1979, A numerical estimate of joint intensity, confidence limits on it, and applications to large structural lineaments: Geological Society of America Abstracts with Programs, v. 11, no. 1, p. 58-59.

18. Sites, R. S., 1979, Structural analysis of the Petersburg lineament, central Appalachians: Geological Society of America Abstracts with Programs, v. 11, no. 4, p. 212.

19. Arkle, T., Jr., 1972, Appalachian structures and the deposition of strata of the late Paleozoic in West Virginia, in Lessing, P., and others, eds., Appalachian structures: origin, evolution, and possible potential for new exploration frontiers - A seminar: Morgantown, W. Va., West Virginia University and West Virginia Geological and Economic Survey, p. 227-255.

20. Lundegard, P. D., Samuels, N. D., and Pryor, W. A., 1978, The Brallier Formation - Upper Devonian turbidite slope facies of the central and southern Appalachians: Eastern Gas Shales Symposium, 2d, Morgantown, W. Va., October 16-18, 1978, Preprints, v. 1, METC/SP-78/6 v. I, p. 4-23; available from National Technical Information Service, Springfield, Va. 22161.

21. Advani, S. H., GangaRao, H. V. S., Chang, H. Y., Dean, C. S., and Overbey, W. K., Jr., 1978, Stress trajectory simulations across the Appalachian Plateau province in West Virginia, in Schott, G. L., Overbey, W. K., Jr., Hunt, A. E., and Komar, C. A., eds.: Eastern Gas Shales Symposium, 1st, Morgantown, W. Va., October 17-19, 1977, Proceedings, MERC/SP-77/5, p. 442-448; available from National Technical Information Service, Springfield, Va. 22161.

22. Kulander, B. R., Dean, S. L., and Williams, R. E., 1978, Rome trough structure in Kanawha County, West Virginia, in Schott, G. L., Overbey, W. K., Jr., Hunt, A. E., and Komar, C. A., eds.: Eastern Gas Shales Symposium, 1st, Morgantown, W. Va., October 17-19, 1977, Proceedings, MERC/SP-77/5, p. 484-495; available only from National Technical Information Service, Springfield, Va. 22161.

23. Kulander, B. R., and Dean, S. L., 1978, Fracture domain correlation with Rome trough structure, geophysical anomalies and regional stress configuration, south-central West Virginia: Geological Society of American Abstracts with Programs, v. 10, no. 4, p. 173.

24. Gwinn, V. E., 1964, Thin-skinned tectonics in the Plateau and northwestern Valley and Ridge provinces of the central Appalachians: Geological Society of America Bulletin, v. 75, p. 863-900.

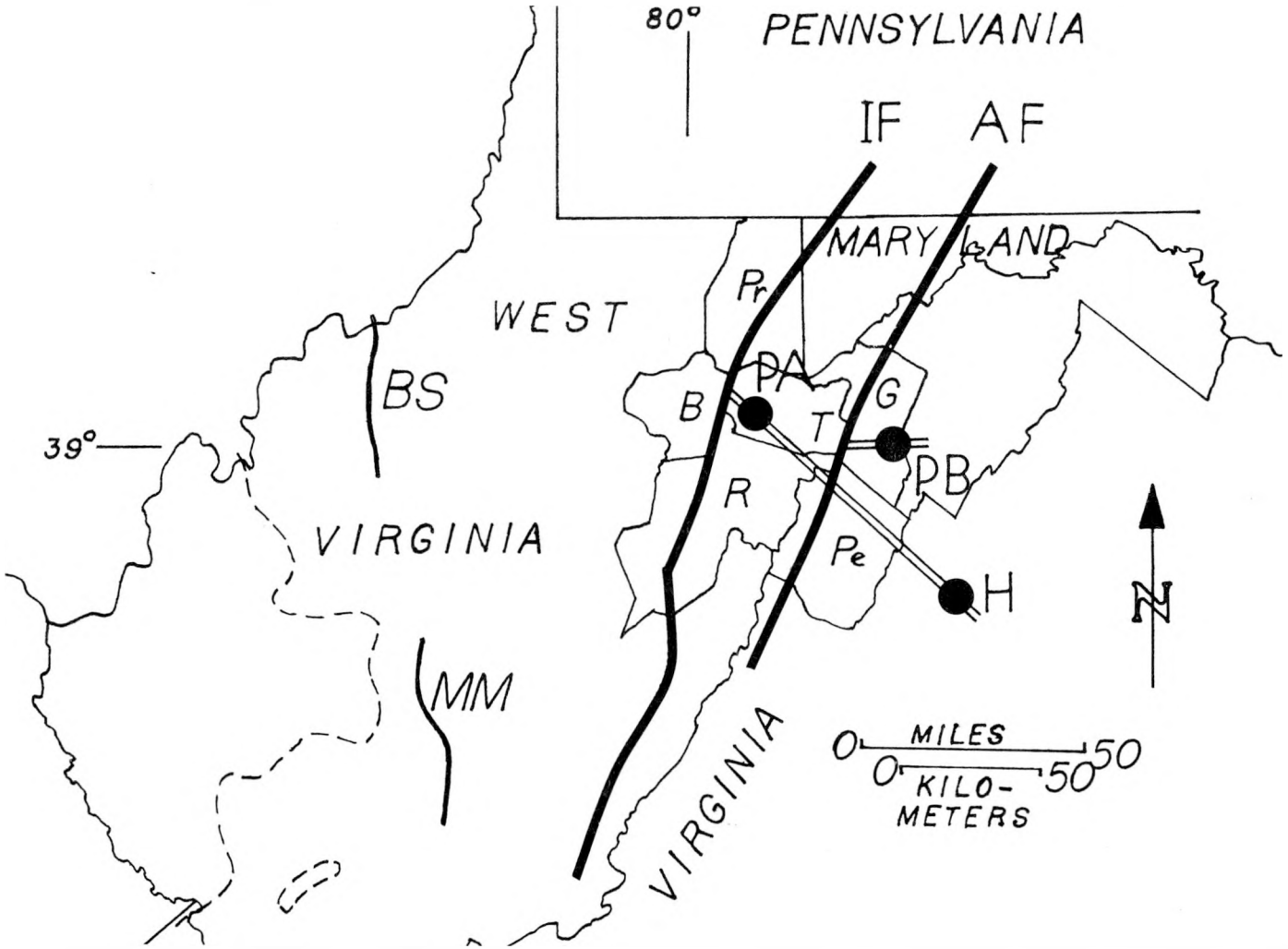


Fig. 1 - Index map of West Virginia. Solid circles are towns: Parsons (PA), and Petersburg (PB), W. Va., and Harrisonburg, Va. (H). Double lines are approximate locations and mapped extents of Parsons and Petersburg lineaments. Hypothesized westward projection of Petersburg lineament intersects Parsons lineament in or near southern Tucker County. Light-weight solid lines are State and county borders: Preston (Pr), Barbour (B), Tucker (T), Grant (G), Randolph (R), and Pendleton (Pe) Counties. Medium-weight solid lines are axial traces of Burning Springs (BS) and Mann Mountain (MM) anticlines. Heavy-weight solid lines are Allegheny Front (AF) and Intra-Plateau structural front (IF) of Gwinn[24]. AF is topographic divide separating Plateau province on the west from Valley and Ridge province on the east and closely coincides with Appalachian structural front. IF is outcrop of western limbs of high folds of eastern Plateau province that expose Devonian rocks. Dashed lines are approximate edges of gas production from Devonian shales.

TABLE 1

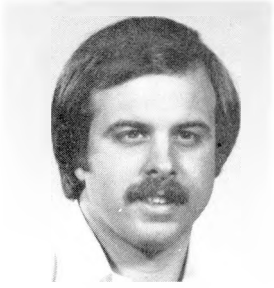
Structural and stratigraphic factors tending to increase fracturing. (n.a., not applicable; ?, unknown, or insufficient data to generalize.)

FACTOR	ORIGINS		LOCATIONS IN EASTERN WV	
	Structural	Stratigraphic	Detached rocks	Undetached rocks
1. Extension faults and fractures	x	?	x	n.a.
2. Fracture facies	n.a.	x	x	x
3. Westward fracture propagation	x	n.a.	n.a.	x
4. Differential horizontal shortening	x	x	n.a.	x
5. Fractured soles of thrust blocks	x	x	x	n.a.
6. Footwall fractures	x	?	x	x
7. Upward propagation of fractures	x	n.a.	x	x
8. CSD's	x	n.a.	x	?
9. Thrust-sealed CSD's	x	x	x	?
10. Crestal fractures	x	x	x	n.a.
11. Short airphoto lineaments	x	n.a.	x	?
12. LANDSAT photolineaments	x	n.a.	x	?
13. Noses of plunging anticlines	x	x	x	n.a.
14. 38th Parallel lineament	x	n.a.	x	x
15. Turbidite siltstones	n.a.	x	x	n.a.
16. Rome trough faults	x	n.a.	?	x

COTTAGEVILLE GAS FIELD CORRELATION ANALYSES FOR RESERVOIR MODELING

by
Thomas E. Springer
E. B. Nuckols

Los Alamos Scientific Laboratory
Los Alamos, New Mexico 87545



E. B. Nuckols



Thomas E. Springer

ABOUT THE AUTHORS

Tom Springer received his B.A. degree in physics from the College of Wooster in 1954 and his M.S. and Ph.D. degrees in physics from Yale University in 1955 and 1959. A native of West Virginia, in late 1958 he joined the Los Alamos Scientific Laboratory in New Mexico where he worked on controls and simulation of nuclear rockets for about 15 years. In the last few years as associate leader in the Electronics Controls and Systems Analysis Group, he has been involved with simulation on both hybrid and digital computers; has done some economic analysis of gas-water reservoirs for the U.S.G.S.; and, more recently, has been involved with data analysis and modeling of gas shale reservoirs.

E. B. Nuckols received his B.S. degree in geology in 1970 from Virginia Polytechnic Institute and State University. From 1970 to 1975 he was a staff geologist with the Virginia Division of Mineral Resources in Charlottesville, Virginia where he worked in the Piedmont, Blue Ridge, and Valley and Ridge provinces of Virginia. In 1975 he joined the staff of Consolidated Gas Supply Corporation in Clarksburg, West Virginia as an exploration geologist. In early 1977 he left Consolidated Gas to pursue graduate studies at West Virginia University where he was a Research Associate under a Department of Energy contract. Also in 1977 he joined the staff of TRW Energy Systems as a systems engineer involved in various Department of Energy contracts. In early 1979 he joined the In-Situ Sciences Group at the Los Alamos Scientific Laboratory where he is currently in charge of all enhanced gas recovery programs.

2 COTTAGEVILLE GAS FIELD CORRELATION FOR RESEVOIR MODELING

ABSTRACT

At the Los Alamos Scientific Laboratory we are currently developing a model for the fractured Devonian gas shale reservoir in Cottageville, West Virginia. This involves integrating all the available geological, geophysical, and gas production data into a self-consistent model that will account for the observed flows and pressures. The purpose is to further the understanding of possible production mechanisms in a highly fractured reservoir and to develop tools and methodology to apply to other reservoirs.

We are using a single-phase Darcy-flow simulator and a data base management code that provides capabilities for selecting, ranking, rotating, mapping, meshing, and plotting various attributes of wells in the field.

We have been determining how to use the known data in the model by various correlation processes. Subsea depths of stratigraphic zones near the producing horizon, obtained from 99 wells in the field, have been interpolated onto a 250-m-interval grid pattern from which isopach and structure maps have been computer generated. The producing horizon's structural elevations and thickness and their first and second derivatives were computed at each well location and correlated with well flow data as represented by initial or final open flow, integrated production, and the shape of decline curves. When considering the set of all wells, we found very little correlation of structure or isopach surfaces and derivatives with production or final open flow. Producing wells occur in a narrower structural range than do the nonproducing wells. Some correlation, but with weak confidence, was observed when only wells of a particular type of decline curve were compared.

INTRODUCTION

Reservoir modeling can serve as a focal point to relate various pieces of information about a physical reservoir to a self-consistent picture of what may be occurring. It can, when the basic flow and source mechanisms are well understood, be used to estimate reserves, to determine further development of the reservoir, to analyze enhanced recovery methods, and so forth. When the basic nature of the reservoir is not understood, modeling can provide insight into the nature of the flow and source mechanisms. Thus we are attempting to model a naturally fractured gas shale reservoir, the Cottageville field, where there exist approximately a hundred wells in less than a hundred square kilometers. The available well data (flow, pressure, and various subsea horizon depths) come in general from drillers' logs rather than from the result of a planned, controlled experiment. Nevertheless, it is a source of data that may bear interesting insight.[1,2]

Modeling is a process of interrelating observed data through certain hypothesized mechanisms. The type of data we had available consisted of well locations, completion dates, initial rock pressures, initial and stimulated open flows, subsea depths of various stratigraphic horizons, yearly production, and occasionally line pressures and a few cases of long-term shut-in pressure.

To form a model of the Cottageville field we have had to gather a number of tools, usually computer programs, to manage, correlate, display, fit, and prepare data to be used in the model. While the final modeling work has not been completed, preliminary correlational analyses of the data have been effected to determine how to formulate a model. This paper will describe the tools developed, the results of initial study of the data, and plans for the model as a result of this study.

SOURCE OF DATA

Raw geological, geophysical and production data for this study were obtained from Consolidated Gas Supply Corporation, Columbia Gas Transmission Corporation, and Cities Service Company. Annual gas production data were obtained from the before-mentioned companies while stratigraphic and structural data were obtained from one of the authors' previous work in the Cottageville field. It is noteworthy to explain that reservoir pressure data were not realistically obtained from down-hole pressure bomb testing but were gathered at the well head assembly. In the same note, stratigraphic and structural data were, for the most part, not obtained from geophysical log suites but from drillers' logs. Because drillers' logs were not normally developed by technical personnel, subsurface geological units must be deduced from their scant description of rock units. Therefore, errors in

subsurface correlations can occur frequently. This can easily be observed in the computer contouring of structural and stratigraphic maps where erroneous interpretation of data causes unusually sharp deflections and large curvatures in the contour patterns. This problem can be overcome by careful examination of the data base or by comparison of spurious well data with other nearby well data.

COMPUTER TOOLS

In the process of developing a reservoir model, we have acquired, modified, or developed a number of computer programs. A data-base management code, called ACOT, contains data on 248 wells in the Cottageville area. Less than 100 of these are associated with production from the Devonian shale. Table I shows 16 pieces of information stored on each well. If the well had production, the year, production per year, and sometimes average reservoir pressure and average line pressure per year are stored. ACOT is operated by a user in an interactive mode from a computer terminal. It has a list of some 20 tasks it can perform. The descriptive items in Table I are called attributes of the well. Other special attributes of the wells may be computed by a task, such as the average production for the first n years or the total production from a well. Another task can select a set of wells some of whose attributes lie in a certain range, such as all wells inside a certain area whose rock pressure was between 600 and 700 psig. One can rank these selected wells by any attribute, e.g. ordered by low to high values of final open flow. One can rotate the coordinate system, print, map, plot, and generate data files for other programs.

In order to generate surface contour plots, we acquired the National Center for Atmospheric Research (NCAR) graphics package[3], which was superior to existing contouring packages at our facility. All of the contour plots in this paper were generated from the NCAR package, which labels specified contours, has different patterned lines, and smooths the curves. A new version is forthcoming that will eliminate some of the crowded lines and labels seen in Fig. 1. In order to define the surface to be contoured, points interpolated onto a rectangular mesh were required. For this we used a method of bivariate interpolation and smooth surface fitting for irregularly distributed data points developed by H. Akima[4]. This algorithm locally fits the surface by a polynomial using suitably selected close data points. Characteristics of the algorithm are that the surface goes through all data points and is continuous between data points. One can specify the number of data points to be used in the interpolation: we typically used 4 and found little difference when 10 points were used. As with any interpolation method, care must be used in interpreting the extrapolated contours far from any wells. This is illustrated in Fig. 1, where accumulated production is contoured. Since no data exist in the lower right corner, extrapolation of increasing production is occurring. We used a square mesh spacing of 250 m for contouring.

A two-dimensional single phase, anisotropic Darcy flow simulator has been developed from the METC SIMPAC general-purpose diffusion code[5]. A 10.75-km by 6-km section of the Cottageville field, rotated to N 45° E, was split into 43 by 25 grid blocks 0.25 km square. At most one producing well occurs in one grid block. Total production from the wells in this area account for 10.5 BCF of 10.6 BCF from all wells in the data base. The flow simulator has been modified and will continue to be modified to fit indicated requirements as the modeling progresses. For a single simulator run, the geometry, the two principal permeabilities, and the porosity in each grid block and the initial and boundary conditions must be specified. In the end, one would hope to select these in a manner that will assure in some sense a minimum deviation between the measured and the computed production through time at each well and between measured and computed pressures. In whatever manner the reservoir model is constructed, there will be a few parameters to be determined by some minimum deviation of measured and computed variables. The reservoir simulator has been combined with a modified Levenberg-Marquardt algorithm[6] to minimize a set of functions of n parameters in a least-squared sense. This allows, for example, the reservoir to be divided into several regions of different, but uniform, permeability and allows the algorithm to determine the permeability in each region. Alternatively, the permeability might be made a function of the local structure of the producing horizon. It is important to keep the number of parameters to be fitted to a minimum, both to reduce computation time and to retain an understanding of the physical significance of the computation.

CORRELATIONAL ANALYSES OF COTTAGEVILLE DATA

Figure 2 shows the general Cottageville area with the sections selected for correlation study and for flow modeling shown in shading. Figure 3 is a structure map of the bottom of the Lower Huron (Zone II) Shale Member of the Ohio Shale. Most production appears to come from the lowest 100 ft. of this 250 ft. section[1]. Structure depths for 6 of the 99 wells in this region were eliminated because they deviated significantly enough to produce sharp mountains or valleys in the computer contouring and were not supported by any neighboring well showing similar structure. Similarly, Fig. 4 is an isopach map of Zone II. Figures 1 and 5 show contours of constant accumulated production and of final open flow. Is there any relation between the structure or isopach maps and the observed production?

Since we were motivated to generate reservoir parameters at least partially from data other than production or flow data, we tried to correlate quantitatively production and open flow data with structure and isopachs and with their slopes and curvature (second derivative) parallel and normal to the map orientation.

First and second derivatives with respect to the two map directions were determined from structure and isopach values interpolated onto a 3 by 3 array of points of 0.25 km spacing, centered at each well location. The four corner points were needed to compute the mixed second derivative. Figures 6 and 7 are contour maps of the first derivative of structure normal to the general fracture trend (y-direction) and of the second derivative of structure along the fracture trend (x-direction). When dealing with the set of all wells, we found very little correlation of structure or isopach surfaces and derivatives with production or final open flow. Figure 8 is a scatter plot of accumulated production vs structure. We can see that the producing wells occur in a narrower range of structural elevation than do the nonproducing wells in a vertical line on the left. Little can be said about relating the magnitude of production to structure. The same was apparent for the derivatives and the isopachs.

We then broke the decline curves into four classes called single exponential declines, break in declines, fluctuating declines, and short declines (i.e., less than 10 years). The first three types are illustrated in Figs. 9-11. The selection was a qualitative judgment. Three wells that were difficult to place in either the single exponential or the break in decline category were not used.

Table II shows the correlation coefficient, which indicates the degree of a linear relationship between the flow parameters and the geological parameters for the four decline curve categories. The flow parameters are final open flow and accumulated production. The geological parameters are structure and isopach values and first derivatives F_x,F_y and second derivatives F_{xx}, F_{yy}, and F_{xy}. Figures 12-14 show plots of a few geological parameters vs flow parameters for wells having a particular type of decline curve. Since the sample size is small (7 to 12 wells per category), one must not put a high degree of confidence in the correlations. The strongest correlation of R = 0.90 occurs when relating structure to production for the wells with fluctuating declines. Here the production increases almost linearly from approximately 100 to 750 MMCF between the structural range -3300 ft to -3100 ft. The other two plots show that a single well can influence the correlation and that we could not draw any strong inferences from these results. From the possible correlations observed within the sets of similar decline curves, we have concluded that the set of wells of similar decline type may indicate a region of the reservoir which may be treated uniformly. That the set of wells producing over 100 MMCF occur in a different region from the set of nonproducing wells can be seen in Figs. 15 and 16. Figures 17-20 show the locations of wells with different type decline curves. Maps such as these are useful in blocking the reservoir model into different regions. For example, the single exponential decline wells may indicate a major fracture region, the decline with break wells may indicate a pocketed region of more tightly connected fractures.

Since structure and isopach data did not correlate strongly with accumulated production and final open flows, we are not using structure data directly in the flow model. The stronger correlations observed among the set of wells of similar type of decline curves suggests partitioning the reservoir into a few different regions of constant flow parameters selected by the decline curve characteristic. The Levenberg-Marquardt algorithm[6] will be used to adjust the parameters of each region.

We also examined the relationship between final open flow and accumulated production. There is considerable scatter in the data shown in Fig. 21, but a linear trend is observed. The dotted line is a least squares fit forced through the origin and weighted inversely proportional to the square

root of final open flow. With that weighting, the slope of the line is the sum of the accumulated production divided by the sum of the final open flows. There are 13 wells for which we have no production data because they were operated by small operators. If these wells come from the same statistical population as the wells in Fig. 21, total production for the field would increase from 10.6 to 12.3 BCF.

Gas-storage mechanisms are important to a model. Our initial analyses of the data before using the Darcy flow simulator have been time independent. Thus, structural parameters were related to accumulated production. We also plotted, in Fig. 22, average initial rock pressure (divided by compressibility) as a function of accumulated production to give insight into gas-storage mechanisms. The P/Z values for each year are plotted where half the production for that year is included. The points are averages for the years 1948 to 1951 and then for the 1974 to 1976 period. The pressures were converted to absolute pressures. Compressibilities Z ranged from 0.88 to 0.96. Note the P/Z values (i.e., free gas density) drops linearly for the first four points. Then there is no new data until 10.4 BCF of gas have been removed. The vertical bars indicate the standard deviation of the sample of initial rock pressures for wells completed in a single year. The drop in average pressure with total production indicates the field is interconnected; the spread in pressures indicates that equilibrium has not been reached in times of the order of a year. The sharp break in average pressure that must occur between the 1951 point and the 1974-76 point probably indicates that the 1951 value is low for a field average and that the new well pressures are correlated more with pressures near neighboring wells than with a reservoir average pressure.

A fracture porosity model and a matrix or dual porosity model have been discussed by Kuuskraa, et al.[8], Schettler[9], and Elkins[10]; reviewed by Smith, et al.[11]; and compared in a reservoir model by Ancell, et al.[12]. Unfortunately for our purposes, both models require rate-dependent processes to interpret P/Z vs accumulated production. The fracture porosity model assumes all the gas is stored as free gas in an extensive fracture volume network. The matrix or dual-porosity model assumes the gas is adsorbed in a micropore matrix and diffuses into a macrofracture system that also contains free gas. Both diffusion and restrictive flow in a fracture system are rate-limited processes, while adsorption of gas onto active sites of a surface is not of itself a rate-limited or time-dependent process. From the initial slope of P/Z, if the gas were in a free state being drained from a volume (the macrofracture system), it would intercept the abscissa at 4.6 BCF. For the reservoir size we have selected for modeling of 10.75 km by 6 km by 100 ft, this gives an average initial gas porosity of 0.001 for the field. From this plot one cannot distinguish gas in the fracture space and gas that diffuses from the fracture walls in times less than one year. Using Schettler's estimate of 40 cm^3 STP gas diffusing in 10 years per cm^2 fracture surface area[9], we estimated the equivalent free volume full-width of the fracture would be 0.27 cm to hold gas that might be initially released by diffusion. The actual fracture width could be several orders of magnitude less and still provide reasonable permeability in the fracture network. The average fracture spacing using the previous numbers would be the equivalent fracture width divided by the initial gas porosity or 2.7 m.

The final slope of P/Z is difficult to estimate. Using one-half the slope of the 1951 point to the 1974-76 point, the final slope is about 0.1 of the initial slope. A projection of this slope to a reservoir pressure of 50 psia yields an eventual accumulated production of 23.3 BCF. The additional gas is assumed to come from desorption or diffusion from the walls of the macrofracture system. There are two extremes for representing this additional gas in a model. One is diffusion without adsorption in which two additional blocks as suggested by Elkins[10] are connected in a third dimension to each of the grid blocks in the two-dimensional array representing the macrofracture system. The volumes and transmissibilities of the additional grid blocks are adjusted to best represent linear diffusion. The additional gas observed from the shift in P/Z slope comes from the volumes in the additional grid blocks.

The other extreme is a pure adsorption process that might be assumed to occur on the walls of the fracture system. For free methane or ethane in contact with an adsorbing surface at constant temperature, the quantity adsorbed will increase linearly with pressure for low pressures. With increasing pressure, the active sites become filled, saturation equilibrium is reached, and no more adsorption occurs if we are well below the condensation point. Adsorption isotherm data are sometimes fitted to a parabola, however to preserve the asymptotic behavior, we chose the Langmuir isotherm form used by Antill, et al.[13] on activated charcoal and also discussed by Schettler[9] as a special mono-layer case of the BET (Brunauer-Emmett-Teller) equation.

$$g = \frac{aPg_{sat}}{aP+g_{sat}} \qquad (1)$$

where g is the adsorbed gas per unit surface area, g_{sat} is the saturated value in equilibrium with the surface, a is a constant, and P is the surrounding gas pressure. Some of the Frost and Thomas adsorption data[14] for certain Devonian shale core samples have reached saturation equilibrium before the maximum tested pressure of 100 atm (1470 psia). Other samples had not reached saturation.

The general shape of P/Z vs accumulated pressure in Fig. 22 can be accounted for, after due consideration of transient effects in the macrofracture network, by either diffusion or adsorption or, as is more likely the case, a mixture of both. Pure diffusion will produce additional gas into the fracture network over an extended time period following a drop in pressure in the fracture network. Pure adsorption will produce additional gas instantaneously into the fracture network as the pressure is dropped. In this case, all time-dependent effects in the reservoir must be contained in effective permeabilities and porosities of the fracture network.

We have concluded that the initial modeling should map out the macrofracture system by matching the initial rock pressures as wells were put on line in the 1948 to 1951 time period. We will try to obtain additional monthly production data in this time period. Adsorption isotherms will be used to modify the equation of state or the gas volume factor and gas compressibility in the Darcy flow simulator. It is felt that the initially released gas from the fracture volume and from short-term diffusion can be represented by a single, two-dimensional array of grid blocks containing adsorption for the 1948-1951 period. Using reservoir parameters that best matched initial rock pressures and flow in this time period, we will then see if additional grid blocks representing diffusion are necessary to reproduce the observed production for the next 25 years.

CONCLUSION

A number of computer tools were developed with which to pre-analyze geological and production data in the Cottageville field and to prepare input to a reservoir model. These data base management, interpolation, and contouring programs may be applied to other reservoirs.

Correlation of structural elevation and thickness to production data was found in general to be poor. Some low confidence correlations were found among wells having similar type of decline curves. From correlation of accumulated production to final open flow, it was estimated that an additional 1.7 BCF might have been produced from missing production data. Using maps of wells with different production characteristics, the reservoir can be divided into a few regions, each having uniform flow parameters. Examination of average initial rock pressure per year by plotting P/Z vs accumulated production indicated the order of five times as much gas present as might be accounted for in a conventional gas reservoir. Adsorption isotherms will be added to the Darcy flow simulator and the macrofracture network will be fitted by matching initial rock pressures and production in the initial drilling period 1948-1951. Additional diffusion grid blocks may be added if needed to match the remaining 25 year period.

REFERENCES

1) Nuckols, E. B. III, "Exploration Parameters Derived from Historical Devonian Shale Production in Western West Virginia," Second Eastern Shale Gas Symposium, October 1978, METC/SP-78/6 Vol. I, pp 169-185; and
Nuckols, E. B.: "The Cottageville (Mount Alto) Gas Field, Jackson County, West Virginia: A Case Study of Devonian Shale Gas Production," METC Report, to be published.

2) Shumaker, R. C., Kirk, K. G., Nuckols, E. B. III, and Long, B. R., "Analysis of Structural Geological Parameters that Influence Gas Production from the Devonian Shale of the Appalachian Basin," First Eastern Gas Shales Symposium, October 1977, MERC/SP-77/5, pp. 496-523.

3) Wright, T.: NCAR Graphics Software, NCAR Technical Note, National Center for Atmospheric Research, Boulder, Colorado, October 1978.

4) Akima, H.: "A Method of Bivariate Interpolation and Smooth Surface Fitting for Irregularly Distributed Data Points," ACM Trans. on Mathematical Software 4, 2, June 1978, pp. 148-159.

5) Sawyer, W. K. and Locke, C. D.: "General Purpose Diffusivity Model for Fluid Flow and Heat Conduction in Porous Media," MERC/SP-76/1, Morgantown, West Virginia, April 1976.

6) Brown, K. M. and Dennis, J. E.: "Derivative Free Analogues of the Levenberg-Marquardt and Gauss Algorithms for Non-linear Least Squares Approximations," Numerische Mathematik, Vol. 18, 1972, pp. 289-297.

7) Davis, J. C.: "Elementary Statistics," in Statistics and Data Analysis in Geology, John Wiley & Sons, Inc., New York, 1973, pp. 62-83.

8) Kuuskraa, V. A., Brashear, J. P., Doscher, T. M., and Elkins, Lloyd: "Enhanced Recovery of Unconventional Gas Sources," Lewin Associates Report, 1978.

9) Schettler, P. D.: "Study of Hydrocarbon-Shale Interaction," Progress Reports OPO-5197-1 to 11 for U.S.E.R.D.A, Juniata College, Huntingdon, PA, 1977.

10) Elkins, Lincoln: Letter to Doscher, T., Jan. 22, 1979.

11) Smith, E. C., Cremian, S. P., and Kozair, G.: "Gas Occurrence in the Devonian Shale," SPE Paper 7921, 1979 SPE Symposium on Low-Permeability Gas Reservoirs, Denver, May 1979.

12) Ancell, K. L., Price, H. S., and Ford, W. K.: "An Investigation of the Gas Producing and Storage Mechanisms of the Devonian Shale at Cottageville," SPE Paper 7938, 1979 SPE Symposium on Low-Permeability Gas Reservoirs, Denver, May 1979.

13) Antill, J., Bradley, D., Flowers, R., and Hodges, N.: "The Purification of Helium in High Temperature Reactors," from Progress in Nuclear Energy, Series IV, Vol. 4., Pergamon Press, 1961, pp. 74-85.

14) Frost, R. and Thomas, J.: "Use of Internal Surface Area and High-Pressure Methane Sorption Data to Estimate Capacity for Gas Production from the New Albany Shale Group," Second Eastern Gas Shales Symposium, October 1978, METC/SP-78/6 Vol. I, pp. 138-148.

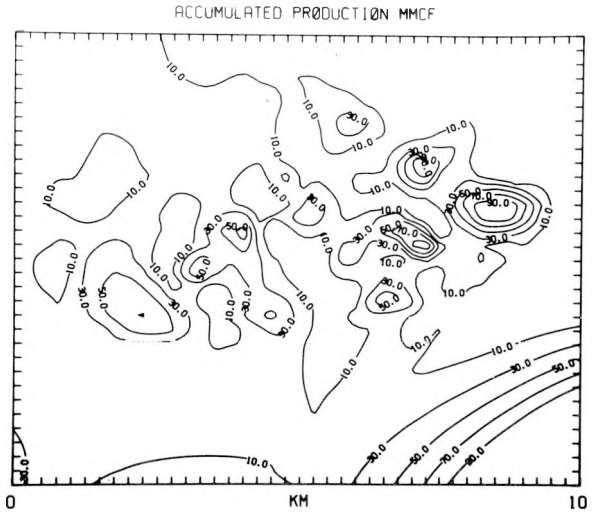


Fig. 1 - Computer-generated iso-production contours with 20 MMCF intervals. Note extrapolation at lower right.

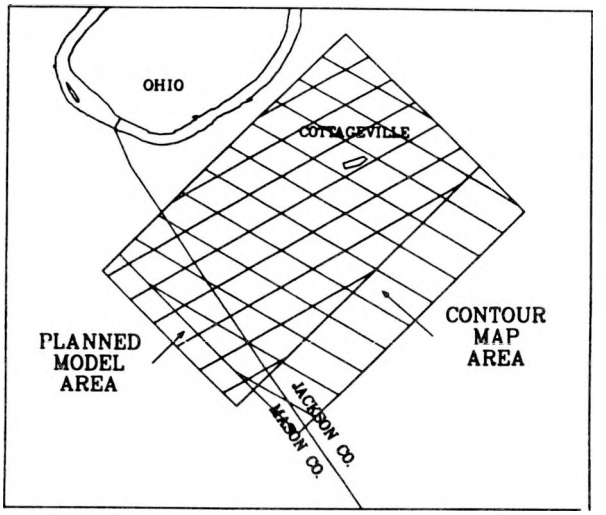


Fig. 2 - General Cottageville area with contouring and planned flow modeling areas depicted.

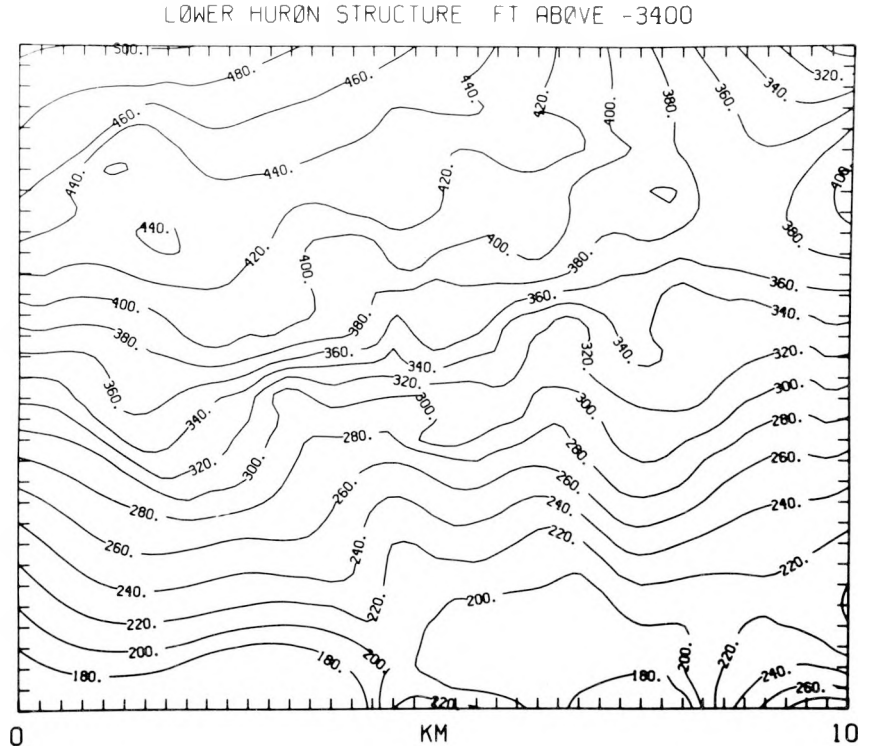


Fig. 3. - Computer generated structure map of the bottom of the Lower Huron (Zone II) Shale with 20-ft contour intervals. The 10 x 8 km area is shown in Fig. 2.

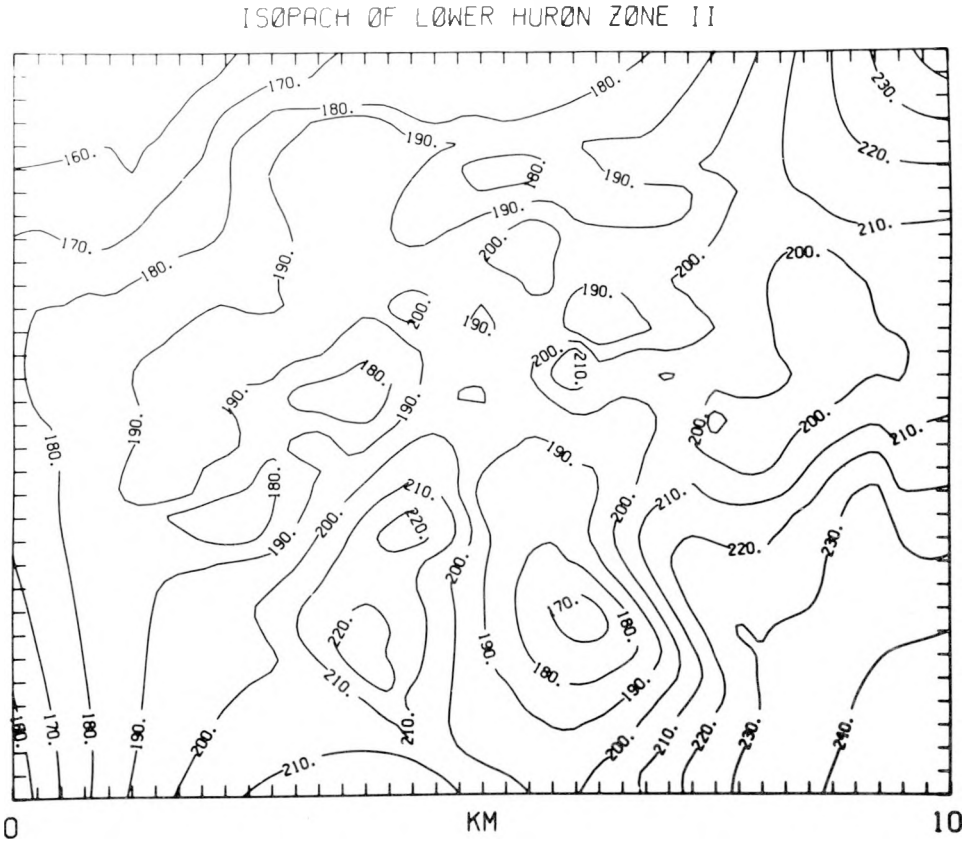


Fig. 4 - Isopach lines of 10 ft interval for the Lower Huron (Zone II) horizon.

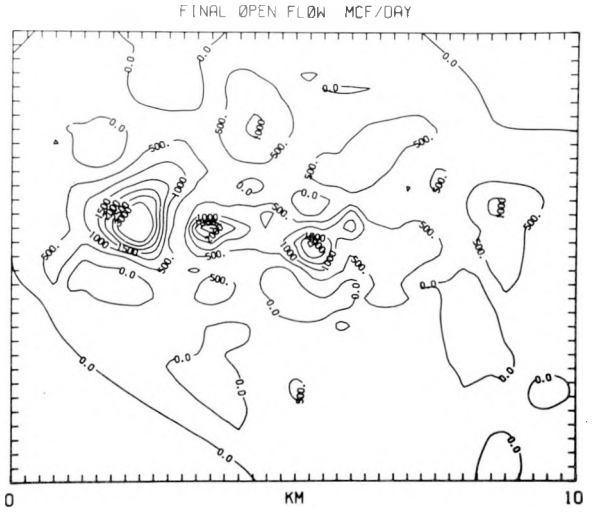


Fig. 5 - Iso-flow lines of 500 MCF/DAY for the same area as Figs. 3 and 4.

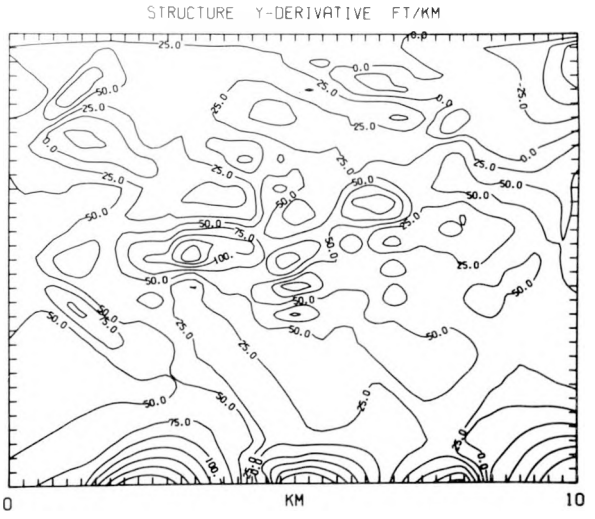


Fig. 6 - Contours of constant derivative of structure in the y-direction normal to fracture trend) with 25 ft/km intervals.

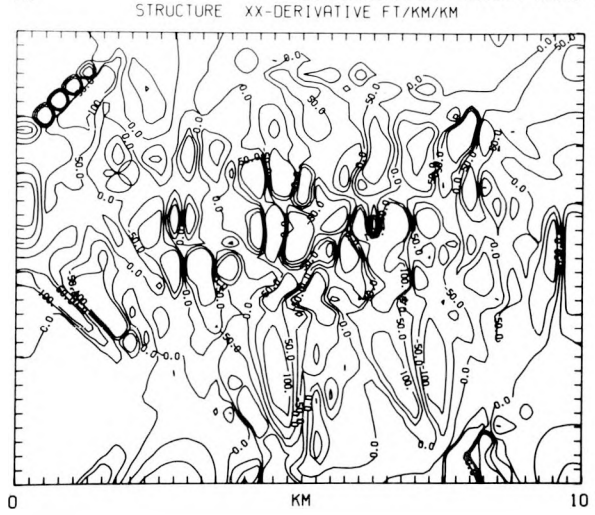


Fig. 7 - Contours of constant second derivative of structure in the x direction (parallel to fracture trend).

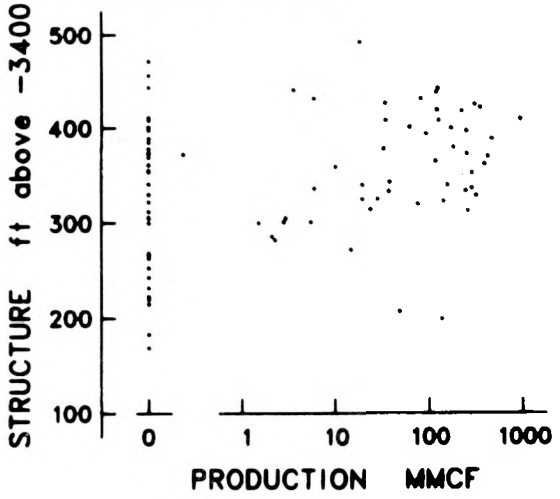
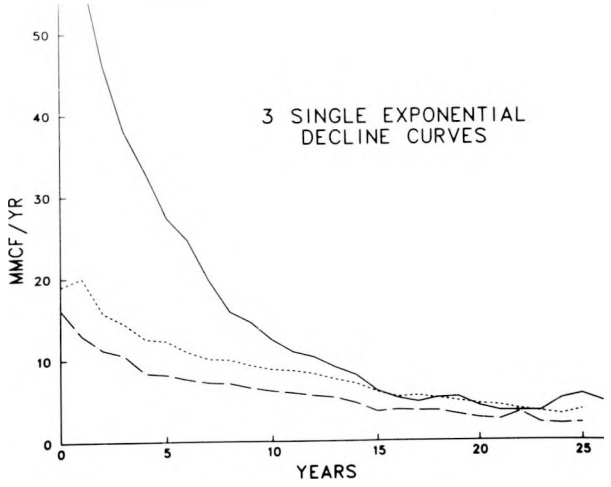
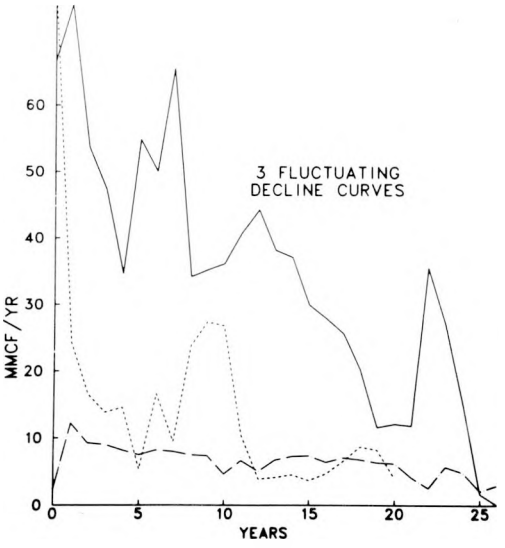
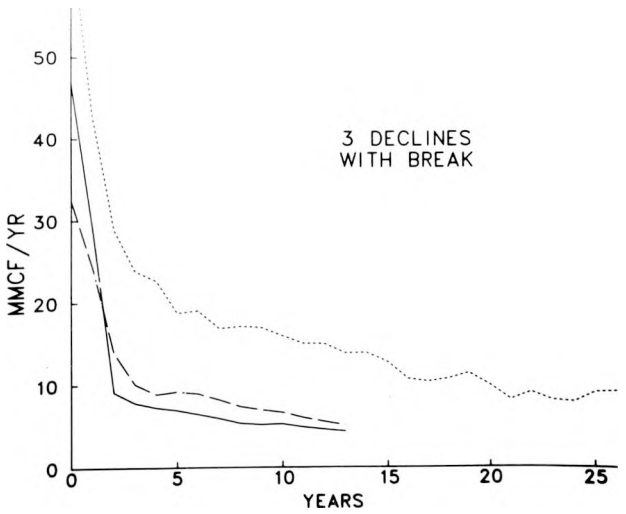


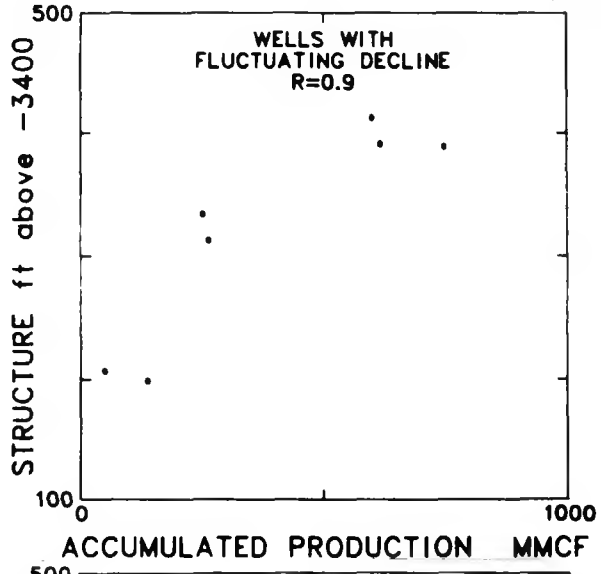
Fig. 8 - Scatter plot of structural elevation vs accumulated production for all wells.

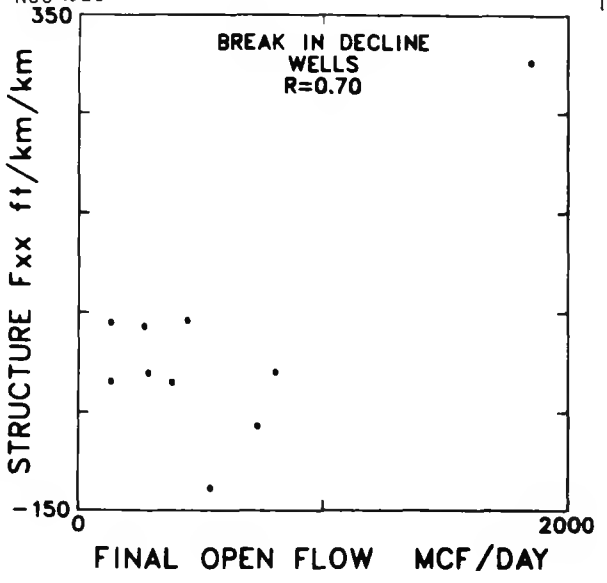


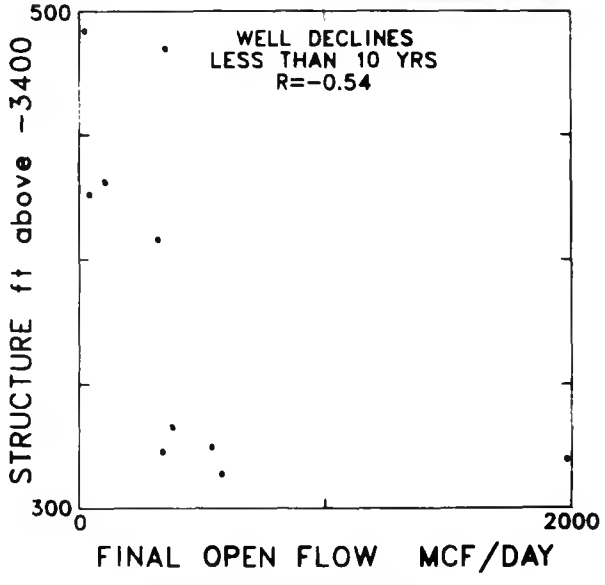




Figs. 9-11 - Some examples of specific decline curves in three of the four categories.







Figs. 12-14 - Scatter plots for 3 of the 92 correlations indicated in Table II.

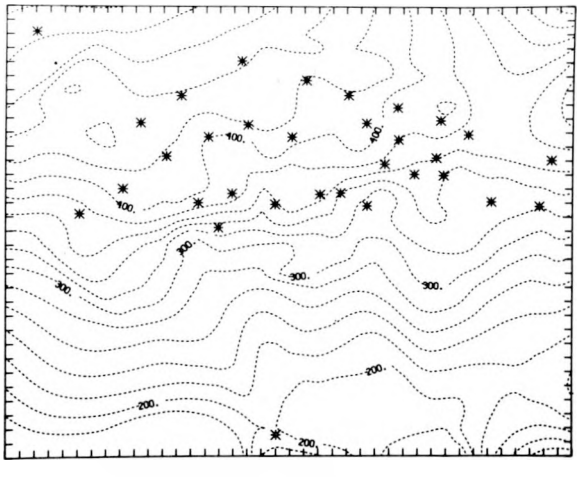


Fig. 15 - Location of wells producing over 100 MMCF on same map as Fig. 3.

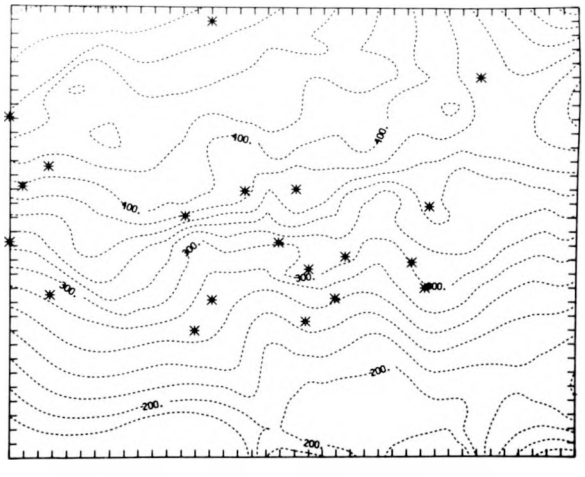
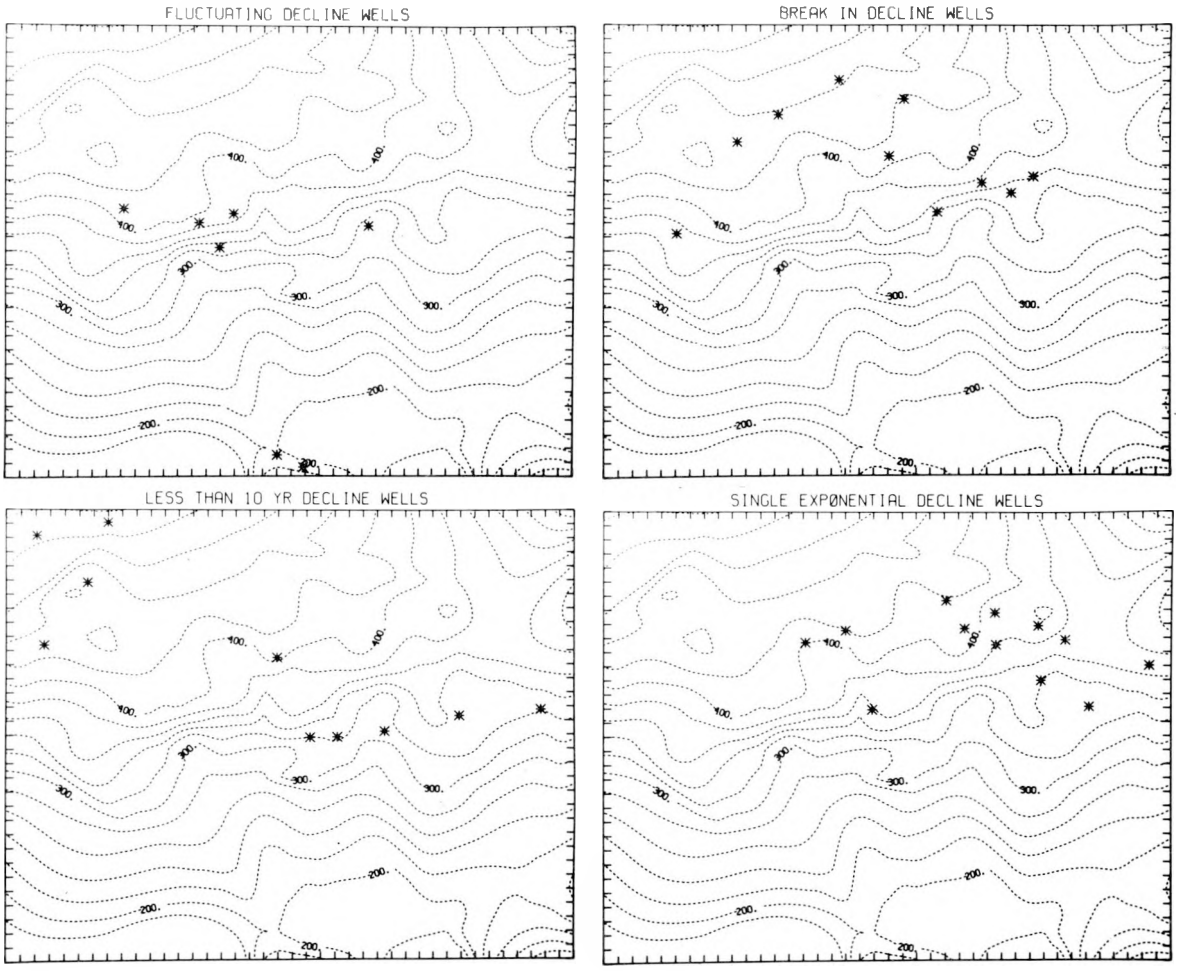


Fig. 16 - Location of nonproducing wells on same map as Fig. 3.



Figs. 17-20 - Location of wells in each of the decline curve categories.

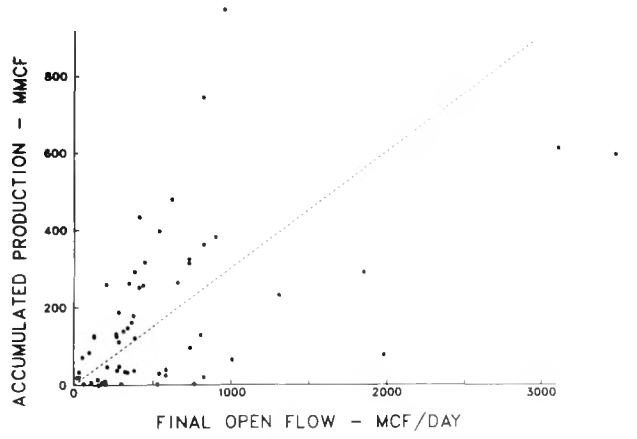


Fig. 21 - Plot showing the relation of final open flow to accumulated production for wells in the Cottageville Field.

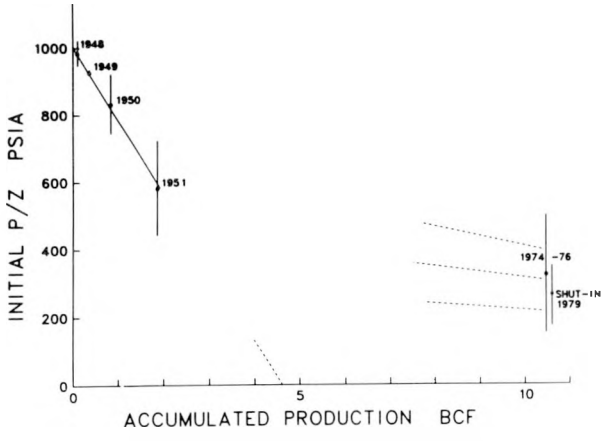


Fig. 22 - Plot of P/Z vs accumulated production from average initial rock pressures per year. Bars indicate standard deviation of sample.

TABLE I: LIST OF WELL ATTRIBUTES

1 = PERMIT NO.
2 = COUNTY, CO. NO., COMPANY
3 = EAST COORDINATE (KM)
4 = NORTH COORDINATE (KM)
5 = NATURAL OPEN FLOW
6 = FINAL OPEN FLOW
7 = DATE OF COMPLETION
8 = ROCK PRESSURE
9 = POINTER
10 = BEREA TOP
11 = LOWER HURON BOTTOM
12 = ONONDAGA TOP
13 = TOTAL SHALE THICKNESS
14 = ZONE III THICKNESS
15 = ZONE II THICKNESS
16 = TOTAL LOWER HURON THICKNESS

TABLE II:

DECLINE CURVE	NO. OF WELLS	SURFACE F OR DERIVATIVES	CORRELATION COEFFICIENT		
			STRUCTURE TO F.O. FLOW	STRUCTURE TO ACC. PROD.	ISOPACH TO ACC. PROD.
FLUCTUATING DECLINES	7	F	0.72	0.90	-0.57
		F_x	0.63	0.19	0.53
Ave. Prod. 380 MMCF		F_y	0.41	0.59	0.79
Ave. FOF 1298 MCF/DAY		F_{xx}	0.06	-0.30	-0.46
		F_{yy}	-0.50	-0.78	-0.17
		F_{xy}	0.41	0.17	-0.53
BREAK IN DECLINE	10	F	-0.52	-0.59	0.36
		F_x	-0.43	0.00	-0.20
Ave. Prod. 224 MMCF		F_y	0.53	0.19	-0.18
Ave. FOF 556 MCF/DAY		F_{xx}	0.70	-0.07	-0.27
		F_{yy}	0.66	0.45	-0.23
		F_{xy}	0.36	0.32	-0.12
SHORT DECLINES	10	F	-0.54	0.29	-0.40
(10 yr)		F_x	-0.03	-0.06	0.05
		F_y	0.22	0.03	0.52
Ave. Prod. 75 MMCF		F_{xx}	0.25	0.36	0.08
Ave. FOF 465 MCF/DAY		F_{yy}	0.36	0.34	-0.21
		F_{xy}	0.20	-0.12	0.02
SINGLE EXPONENTIAL DECLINES	12	F	0.05	0.20	-0.10
		F_x	0.43	0.01	-0.03
Ave. Prod. 345 MMCF		F_y	0.08	-0.25	-0.53
Ave. FOF 532 MCF/DAY		F_{xx}	-0.50	-0.38	0.17
		F_{yy}	-0.14	-0.20	-0.35
		F_{xy}	0.15	-0.10	-0.32

LITHOLOGY STUDIES OF UPPER DEVONIAN WELL CUTTINGS IN THE EASTERN KENTUCKY GAS FIELD

by

J. Negus-de Wys
West Virginia University
Department of Geology and Geography
425 White Hall
Morgantown, West Virginia 26506



ABOUT THE AUTHOR

Ms. Negus-de Wys received her BA with honors in geology from Miami University, Oxford, Ohio. She attended graduate school at the University of Wisconsin, Ohio State University, and U.C.L.A., in Los Angeles, and Law School at Texas Tech University. She is completing her doctorate in Geology at West Virginia University and expects to receive the degree in December, 1979.

Ms. Negus-de Wys taught Geology at Case Western Reserve University; was Curator of the Geology Museum in Madison, Wisconsin; worked with Shell Oil in Midland, Texas, and Mene Grande Corporation in Venezuela; was Research Associate in the Ohio State Research Foundation Mapping and Charting Laboratories (Radar Interpretation); was Senior Scientist and Surveyor Experimenter at Cal-Tech Jet Propulsion Laboratory (Magnet Experiment); was Assistant to Director of Research at the University of Utah Research Institute. Ms. Negus-de Wys has, in addition, worked in top level business management for six years in Jackson, Wyoming. She is included in 1978 Who's Who in the West.

In August of 1977, Ms. Negus-de Wys joined the staff on the Devonian Shale Program as Research Associate in the Geology Department at West Virginia University. Her Ph.D. dissertation is STUDY OF THE EASTERN KENTUCKY GAS FIELD(S): GEOLOGICAL PARAMETERS AND POSSIBLE RELATIONSHIPS TO GAS OCCURRENCE AND PRODUCTION.

2 LITHOLOGY STUDIES OF UPPER DEVONIAN WELL CUTTINGS IN THE EASTERN KENTUCKY GAS FIELD

ABSTRACT

Well cuttings from 14 wells in the Eastern Kentucky Gas Field are studied under reflected light. A comparison of lithology changes across the field and between stratigraphic units is presented.

Fracture indicators are contoured and related to density of high producing wells and other lithologic characteristics. Statistical methods show highly significant correlation between fracture counts and high producing well contours. A table of correlation coefficients is presented for lithologic data and production.

The value of such a field study approach, in more detail, is emphasized for future exploration and evaluation in the production of gas from Upper Devonian Shales in this area.

INTRODUCTION

This study of well cuttings from fourteen wells in the Eastern Kentucky Gas Field is part of a more comprehensive study comparing final open flow values from approximately 4750 wells with geological parameters including structural position on the top of the Ohio Shale, the Ohio Shale thickness, stratigraphy, geochemistry, and fracture data.

Historically, studies of the Eastern Kentucky Gas Field and cross sections through the area have been achieved by using wireline logs, usually formation density logs, in which natural resistivity could be related to the stratigraphic units. Drillers' logs have been used to supplement the existing information, as well as cores from Martin and Perry Counties and more recently one is available from Johnson County. (Provo, 1977; Schwietering, 1977; Wilson, 1977; Negus-de Wys and Shumaker, 1978). The lithology of the main part of the field, however, has remained an interpretation mainly from the wireline logs. Coleman Hunter (1935) studied 700 thin sections from 86 wells, but only general averages by county are reported in his writ.ngs on the study. The 700 thin sections are presently under restudy by the present author.

Recently Swager (1978) related radioactivity, biostratigraphy and lithology of the Ohio Shale sequence along the outcrop belt west of the Eastern Kentucky Field and in the Pine Mountain thrust area. Most of his sites were examined by the present author.

The purpose of this study is to look at lithologic changes across the field and relate such changes to other geological aspects as well as final open flow data, in order to better understand the occurrence and production of gas in the Upper Devonian rocks in the field.

The setting of the Eastern Kentucky Gas Field is shown in Figure 1 (after Negus-de Wys and Shumaker, 1978). The Cincinnati arch is situated to the northwest, the Pine Mountain Thrust to the southeast. The Rome Trough extends in an east-northeasterly direction across the northern section of the field with the asymmetrical graben deepening to the east.

Another basement feature, the Floyd County Channel, extends northward through the center of the field (Figure 2, after Ammerman and Keller, 1978) and is interpreted by some as an aborted graben joining the Rome Trough. The Perry County Uplift and Pike County Uplift are situated west and east, respectively, of the Floyd County Channel.

The Paint Creek Uplift with a north-south trend extends into the center of high production from the north and probably was developing through Mississippian and Pennsylvanian time (McFarlan, 1943).

The stratigraphic sequence involved in the study is Berea-Bedford through Lower Huron. (See Figure 3). The Berea-Bedford is treated as a single unit because of the difficulty in ascertaining the separate units in the southwestern area where both units are shaley. Incomplete samples hampered interpretation of the Berea in the eastern part of the field.

DATA

The locations of the fourteen study wells are shown in Figure 4. Well cuttings in the central portion of the field were extremely difficult to locate. Frequently wells penetrate high pressure zones which blow the cuttings out of the well (Hager, 1978). Other stored well cuttings were lost in warehouse flooding. Most cuttings are from cable tool drilling; one is from rotary drilling.

Well cuttings were examined wet using a binocular microscope with 10 x and 30 x magnification. The Mudrock terminology of Folk (1974) was used. See Figure 5. Early in the study it became apparent that the Ohio Shale sequence was predominantly very silty silt-shale in some wells, although this sequence has usually been referred to as "brown shales."

In constructing cross sections it was deemed advisable to relate logs to the base of the Huron because of difficulties in correlation, higher in the stratigraphic sequence.

Cross sections A-A', B-B', C-C', and D-D' are shown in Figures 6, 7, 8, and 9. Section A-A' (Figure 6), from southwest to northeast, shows the thickening section to the east. The Berea is 100% shale in the southwest grading into a siltstone with some sand grains in the east and northeast. Some dolomitic cementation is observed in the siltstone. Williamson (1974) interpreted the Berea in West Virginia as a channel sand adjacent to Eastern Kentucky oriented approximately north-south, with proximal bar and distal bar facies farther east. In the Eastern Kentucky Field the Berea is of nearly uniform thickness over the entire area, but does show changing lithology. It resembles more a beach sand in the changing lithology and even thickness.

The Cleveland is a black to dark brown, at times greasy looking, highly organic siltstone in the southwest. It grades into a browner silt-shale and then to brown mud-shale in the east and intertongues increasingly with gray clay-shale and mud-shale in the eastern part of the field.

The Three Lick is designated as the upper banded shale by Swager (1978) at the outcrop. This banding of green and gray and brown shale is also apparent in the well cuttings. In some wells, siltier zones are apparent.

The Upper Huron is usually a brown, highly organic mud-shale, and is the lower black shale unit of Swager. The Middle Huron is less organic, siltier, and frequently shows interbedding of gray or green with black shale. The Lower Huron is very highly organic, black to dark brown mud-shale and may show some interbedding. It breaks into blocky rather than plately fragments. In the outcrop it also appeared blockier and less fissile than the Cleveland or other Huron units.

For comparison with the lithological cross sections, similar sections using logs may be compared (Figures 10, 11, and 12) as well as the structural-stratigraphic sections (Figures 13, 14, 15, and 16). These are not identical cross sections, since logs are not available on most of the wells from which well cuttings were used.

In cross section A-A' (Figure 6) the center well appears to be lacking part of the Lower Huron and shows a milky white chert and limestone unit. This is probably Huntersville Chert (Hager, 1978). The chert continues for approximately 75+ feet with a tan-gray sandy, fossiliferous limestone and dark brown sucrose dolomite. Stylolites occur in the limestone. The Boyle cherty limestone observed in some outcrops below the Ohio shale appears similar to the cherty well cuttings. The relationship of the Boyle and Huntersville would appear to be a pertinent problem. This center well shows indications of fracture at 29 different horizons. A normal fault with about 100 feet displacement may cut the well in the Huron, eliminating the lowest part of the Huron and bringing the Huntersville Chert in higher in the section. Such a fault on the side of the Floyd County Channel would not be unreasonable.

Cross section B-B' (Figure 7) north-south through the center of the field shows the thickening of the section to the south. Redbeds occur in the northern two wells, but not in the southern where the sections show more silt. The southern sections also may represent faulted sections. Protosalvinia occurs near the top of the southernmost section (not found in such a horizon in other wells) and repetition appears in the Knott County well suggesting thrust faulting. This is not unreasonable as the Pine Mountain Thrust area is approached.

Fracture indicators include: slickensides, open fractures, filled fractures, fracture sides, and spar. Stylolites occur in the limestone unit in the bottom of the central well with the Huntersville Chert.

Frequency of fractures was contoured (Figure 17) with results showing strong similarities to contours of densities of high producing wells (Figures 18 and 19, after Griffith, 1976).

Figure 20 shows histograms of observed fractures versus lithotypes, stratigraphic units, structure on top of Ohio Shale, and thickness of total shale. The highest degree of correlation is seen in mud-shale lithology, the Middle Huron unit, -1000 to -1250' (below sea level) on Ohio Shale structure, and a thickness of 500 to 600 feet.

Maps of relative percentage of gray, brown, and green shale in the total Ohio Shale sequence studied (Cleveland-Huron) are shown in Figures 21, 22, and 23. The isopach of black shale is shown in Figure 24 in which a striking resemblance is seen to the trends of the density of high producing wells $\leq$ .5 MMcf/day/25 sq. miles. This is also similar to the configuration shown by Harris, deWitt, and Colton, (1978). For comparison with the black shale isopach, the total shale isopach is shown in Figure 25.

Percent shale of total Ohio sequence is shown in Figure 26, which may be compared to percent of silt and sand in Figure 27. Higher silt/sand areas occur in the northeastern section of the field and a patch southwest of field center. If the silt/sand percentage is contrasted, Figure 28 results, showing finer grained clastics to the southwest and coarser material to the northeast. Percent carbonate is shown in Figure 29. It shows a marked similarity to structure on top of the Coniferous (McFarlan, 1943). Percent redbeds of total sequence are shown in Figure 31. An area trending northeast-southwest shows occurrence of redbeds with the highest values to the northeast. This suggests a positive area during late Upper Devonian or preferential currents depositing detrital fragments from higher on the delta.

The results of very scanty data on the Berea-Bedford show the unit to be 100% shale in the southwest, and if the trend is extrapolated, the 50:50 shale:sandstone contour would run through the heart of the gas field. The thickness remains fairly constant over the field. The 1946 isopach map of the Berea-Bedford by Pepper, Demarest, Merrels, and deWitt show the sand in a highly complicated patchy thinning and thickening in the Floyd County area. The 0 isopach would represent 100% shaley facies. The thins are suggestive of small scale doming and basins on the nose of the Paint Creek Uplift. (Figure 32).

STATISTICAL RELATIONSHIPS

Using a stepwise regression procedure for dependent variables D1 (density of high producing wells $\geq$.5MMcf/day/25 sq. miles) and D2 ($\geq$1MMcf/day/25 sq. miles) and independent variables: fractures, structure, shale thickness, percent ss/siltstone in total sequence, carbonate %, green shale %, redbeds, black shale thickness, brown shale %, and gray shale %, the following relationships were observed:

1. D1 was best explained by fractures: R^2 = 83%
   Adding redbed occurrence: R^2 = 92%
   No other variables met the 0.5000 significance level for entry into the model.

2. D2 was best explained by fractures: R^2 = 64%
   Adding Brown shale % of total sequence; R^2 = 92%
   Adding structural position: R^2 = 96%
   No other variables met the 5% significance level for entry into the model.

3. A Table of Correlation Coefficients is shown in Figure 33. Significant relationships are boxed.

PALEOENVIRONMENT

Various deep and shallow water environments have been suggested for the Ohio Black and Brown Shales. After studying outcrop sections and well cuttings, the present author suggests the following criteria could collectively indicate shallow water, but which singly would not necessarily rule out deeper water:

1. occurrence of vitrinite
2. dolomite occurrence suggesting supratidal replacement (present day analogue: Coast of Georgia)
3. Lingula and Orbiculoidea
4. Soil horizon top of the Boyle at outcrop
5. Possible channel in shale at outcrop in Estill County, Kentucky
6. Algae (Protosalvinia)
7. Redbeds

8. anhydrite
9. thinning toward basin edge.

CONCLUSIONS

1. The samples studied indicate a shaley Berea-Bedford unit in the southwest of the field with increasing silt and some sand to the east. The thickness appears fairly uniform.

2. The Ohio Shale shows a high shale content in the southwest with increasing silt and sand to the northeast with one high area to the southwest of the field center. The clastic grain size increases to the northeast.

3. A higher carbonate zone trends northeast-southwest with an enlarged high to the southwest. Redbed occurrence follows the same trend. This may represent a higher area during upper Ohio Shale deposition time, or a preferential current area bringing in detrital redbed fragments. This area also correlates with the thickest area of the Corniferous.

4. Fractures appear to be most strongly related to:

   a) mudshale lithology,
   b) Middle Huron stratigraphic unit,
   c) 500-600 foot thickness of total shale, and
   d) -1000 to -1250 (below S.L.) structural elevation of top of Ohio Shale.

   Figure 34 shows the outline of the resulting area which may be compared with contours of high density of high producing wells.

5. The higher fractured well in Floyd County may penetrate a normal fault of approximately 100 feet on the west side of the Floyd County Channel. The Ohio Shale is approximately 100-150 feet short. The Huntersville Chert appears to underlie the section.

6. The Knott County well may have penetrated a shallow thrust fault.

7. Positive identification of all Ohio shale units in cuttings is not feasible without other information. More studies of lithology, biostratigraphy, and radioactivity are needed in subsurface (similar to Swager's outcrop studies) to better understand the stratigraphy of the Eastern Kentucky field.

ACKNOWLEDGMENTS

The author wishes to express appreciation to Ernie Jenkins and Bob Hager of Kentucky-West Virginia Gas Company for supplying well cuttings and other information for this study, to Dr. R. C. Shumaker and Dr. Milton Heald for direction of the study, and to Jean Cheng for statistical and computer operations.

The study was performed under DOE Contract number DE-AC21-76MC05194 (formerly EY-76-C-05-5194).

REFERENCES

Ammerman, M. L. and G. R. Keller, 1979, Delineation of Rome Trough in eastern Kentucky by gravity and deep drilling data: AAPG Bulletin, v. 63, no. 3 (March), p. 341-353.

Folk, R. L., 1974, Petrology of sedimentary rocks: Hemphill Publishing Co., Austin, Tex. 78712, p. 147.

Griffiths, J., 1976, private communication.

Hager, R., 1978, private communication, Kentucky-West Virginia Gas Co., Prestonsburg, Ky.

Harris, L. D., Wallace de Witt, Jr., and G. W. Colton, 1978, What are possible stratigraphic controls on gas fields in eastern black shale?: The Oil and Gas Journal, April 3, p. 162-165.

Hunter, C. D., 1935, Natural gas in eastern Kentucky: Geology of Natural Gas, AAPG, Henry A. Ley, ed.

McFarlan, A. C., 1943, Geology of Kentucky: University of Kentucky, Lexington, Ky.

Negus-de Wys, J., and R. C. Shumaker, 1978, Study of the geology and gas occurrence in the Eastern Kentucky Gas Field: Eastern Devonian Gas Shales Symposium, Lakeview Country Club, Morgantown, W. Va.

Pepper, J. F., D. F. Demarest, C. W. Merrels, 2nd, and W. de Witt, Jr., 1946, Isopach map of Berea-Bedford: Oil and Gas Investigations Preliminary Map 69, U.S.G.S.

Provo, Linda, 1977, Stratigraphy and sedimentology of radioactive Devonian-Mississippian shales of the central Appalachian Basin: Ph.D. Dissertation, University of Cincinnati, Cincinnati, Ohio.

Schwietering, J. F., 1970, Devonian shales of Ohio and their eastern equivalents: Ph.D. Dissertation, Ohio State University, Columbus, Ohio.

Shumaker, R. C., 1977, Unpublished map of basement structure in eastern Kentucky.

Swager, D. R., 1978, Stratigraphy of the Upper Devonian-Lower Mississippian shale sequence in the eastern Kentucky outcrop belts: M.S. Thesis, University of Kentucky, Lexington, Ky.

Williamson, N. L., 1974, Depositional environments of the Pocono group in southern West Virginia: Ph.D. Dissertation, West Virginia University, Morgantown, W. Va., p. 127.

Wilson, E., 1977, 1979, private communications.

STATISTICAL ANLYSIS SYSTEM

CORRELATION COEFFICIENTS / PROB |R| UNDER HO:RHO=0 / NUMBER OF OBSERVATIONS

	D1	D2	F	STRU	THICK	SS,SLT	CO_3	GREEN	SH	R	BLK	BR	GRN
D 1	1.00000 0.0000 7	0.94827 0.0039 6	0.91249 0.0041 7	-0.37394 0.4088 6	-0.03624 0.9385 7	-0.09827 0.8340 7	0.09754 0.8148 7	0.09554 0.8385 7	0.09467 0.8400 7	0.19476 0.6756 7	0.47123 0.2858 7	-0.28196 0.5401 7	0.02922 0.9504 7
D 2		1.00000 0.0000 6	0.79768 0.0573 6	-0.12742 0.8094 6	0.21759 0.6788 6	-0.19347 0.7134 6	0.00000 1.0000 6	0.32981 0.5232 6	0.18328 0.7282 6	0.10227 0.8471 6	0.50728 0.3044 6	-0.51729 0.2933 6	-0.08869 0.8673 6
F			1.00000 0.0000 7	-0.62078 0.1364 7	0.01577 0.9731 7	-0.02853 0.9516 7	0.17582 0.7061 7	-0.04941 0.9162 7	0.03118 0.9471 7	0.48867 0.2659 7	0.27429 0.5517 7	-0.04281 0.9274 7	0.04818 0.9183 7
STRU				1.00000 0.0000 7	0.01637 0.9722 7	-0.02186 0.9629 7	-0.08652 0.8537 7	0.03065 0.9480 7	0.01057 0.9821 7	-0.41219 0.3581 7	-0.20766 0.6550 7	-0.19755 0.6711 7	-0.23692 0.6090 7
THICK					1.00000 0.0000 7	-0.08801 0.8512 7	-0.07028 0.8810 7	0.80387 0.0293 7	0.08133 0.8624 7	0.36356 0.4228 7	0.00703 0.9881 7	-0.60940 0.1463 7	-0.28995 0.5282 7
SS,SLT						1.00000 0.0000 7	0.97501 0.0002 7	-0.26922 0.5593 7	-0.99982 0.0001 7	0.02919 0.9505 7	-0.72244 0.0667 7	-0.15200 0.7449 7	0.79581 0.0324 7
CO_3							1.00000 0.0000 7	-0.28395 0.5371 7	-0.97481 0.0002 7	0.15248 0.7441 7	-0.68439 0.0899 7	-0.16235 0.7280 7	0.75147 0.0515 7
GREEN								1.00000 0.0000 7	0.23832 0.5759 7	-0.07048 0.8809 7	0.45626 0.3035 7	0.82426 0.0226 7	-0.24988 0.5889 7
SH									1.00000 0.0000 7	-0.01870 0.9683 7	0.71640 0.0701 7	0.16776 0.7192 7	0.79714 0.0318 7
R										1.00000 0.0000 7	-0.37903 0.4009 7	0.26670 0.5632 7	-0.36631 0.4190 7
BLK											1.00000 0.0000 7	-0.28238 0.5395 7	-0.26567 0.5647 7
BR												1.00000 0.0000 7	-0.15812 0.7349 7
GRN													1.00000 0.0000 7

D 1 DENSITY of HIGH PRODUCING WELLS .5 MMcf/DAY/25 sq. mi.
D 2 DENSITY of HIGH PRODUCING WELLS 1 MMcf/DAY/25 sq.mi.
F FRACTURES
STRU STRUCTURE on OHIO SHALE
THICK THICKNESS of TOTAL SHALE SEQUENCE
SS,SLT PERCENTAGE of SANDSTONE and SILT of TOTAL SEQUENCE
CO_3 PERCENTAGE of CARBONATE of TOTAL SEQUENCE
GREEN PERCENTAGE of GREEN SHALE of TOTAL SEQUENCE
SH PERCENTAGE of SHALE of TOTAL SEQUENCE
R PERCENTAGE of REDBEDS of TOTAL SEQUENCE
BLK THICKNESS of BLACK SHALE in TOTAL SEQUENCE
BR PERCENTAGE of BROWN SHALE of TOTAL SEQUENCE
GRN PERCENTAGE of GREEN SHALE of TOTAL SEQUENCE

5% SIGNIFICANCE LEVEL

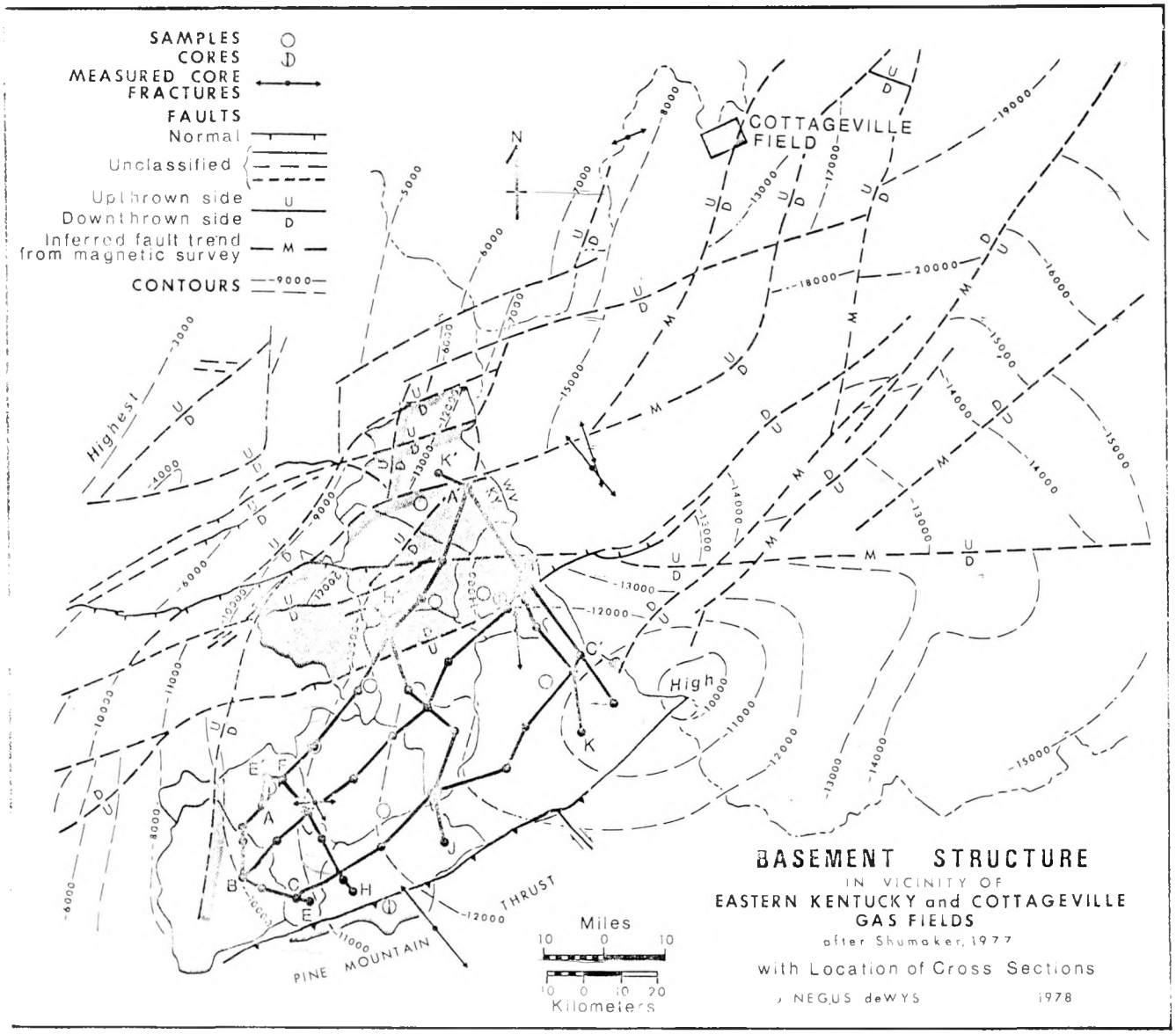


Figure 1 Structural setting of the Eastern Kentucky Gas Field showing the Rome Trough cutting across the northern part of the field and the Floyd County Channel extending from the south into the center of the field. (Same as Figure 1 in geochemical studies paper, Negus-de Wys and Renton.)

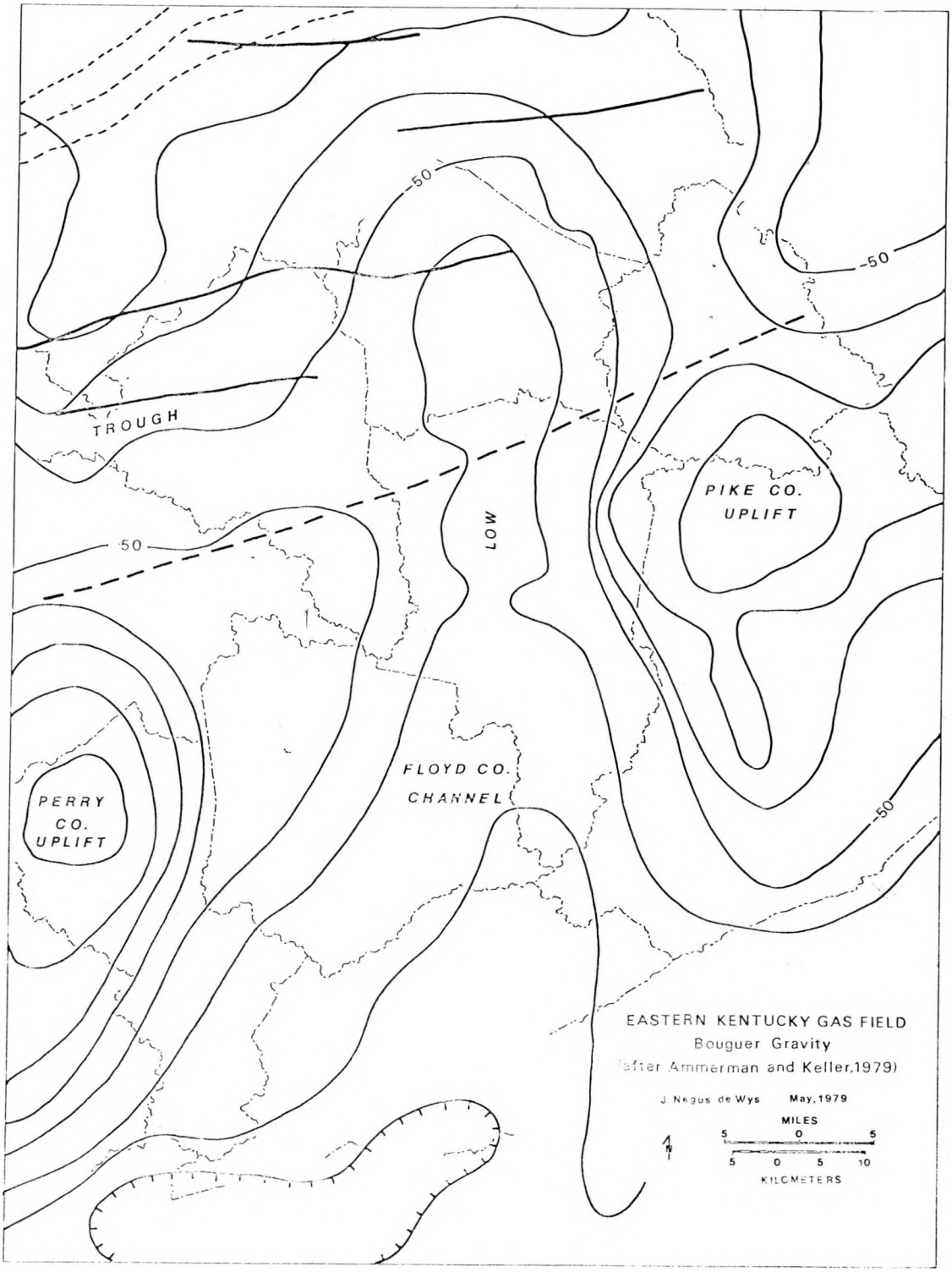


Figure 2 Basement Structure from Bouguer Gravity Map (Same as Figure 3 in Negus-de Wys and Renton.)

STRATIGRAPHIC SEQUENCE	
BEREA/BEDFORD	Berea Sandstone and Bedford Shale, undivided
CLEVELAND	Cleveland Member of Ohio Shale of Ohio
THREE LICK	Three Lick Bed of Provo, Kepferle, and Potter, 1977
UPPER HURON	Upper Part of Huron Member of Ohio Shale of Ohio
MIDDLE HURON	Middle Part of Huron Member of Ohio Shale of Ohio
LOWER HURON	Lower Part of Huron Member of Ohio Shale of Ohio

Figure 3 Stratigraphic units included in study (same as Figure 4 in Negus-de Wys and Renton.)

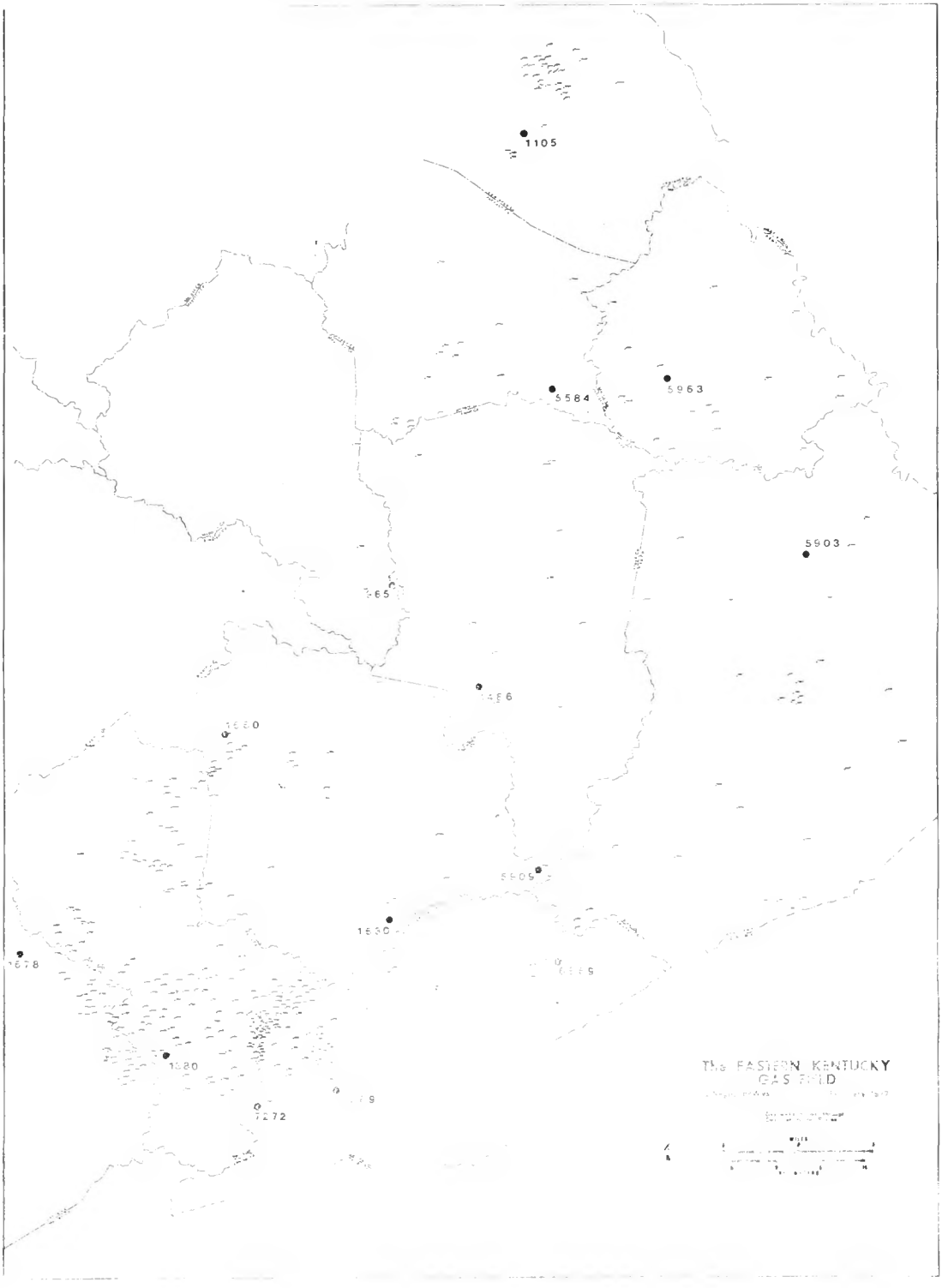


Figure 4 Well locations (large dots) of wells from which cuttings were studied. (Same as Figure 14 in Negus-de Wys and Renton.)

PETROLOGY OF MUDROCKS (Folk, 1974)

Mudrock (word coined by Ingram) is a general term used herein to cover those terriginous rocks that contain more than 50 per cent silt and/or clay. The most obvious division of mudrocks is on the basis of texture and structure:

Grain size of mud fraction	Soft	Indurated, non-fissile	Indurated, fissile
Over 2/3 silt	silt	siltstone	silt-shale
subequal silt and clay	mud	mudstone	mud-shale
over 2/3 clay	clay	claystone	clay-shale

Figure 5 Mudrock Terminology from Folk.

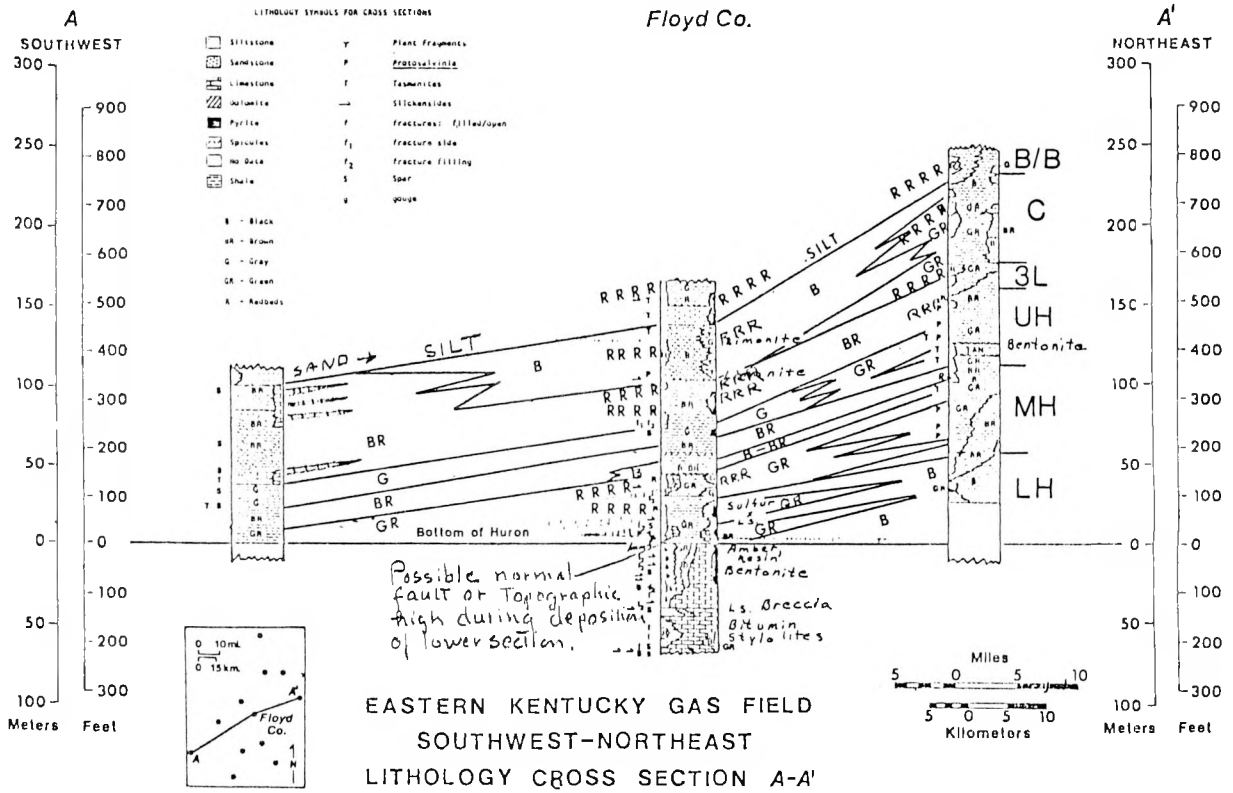


Figure 6 Lithological Cross-section A-A', southwest to northeast.

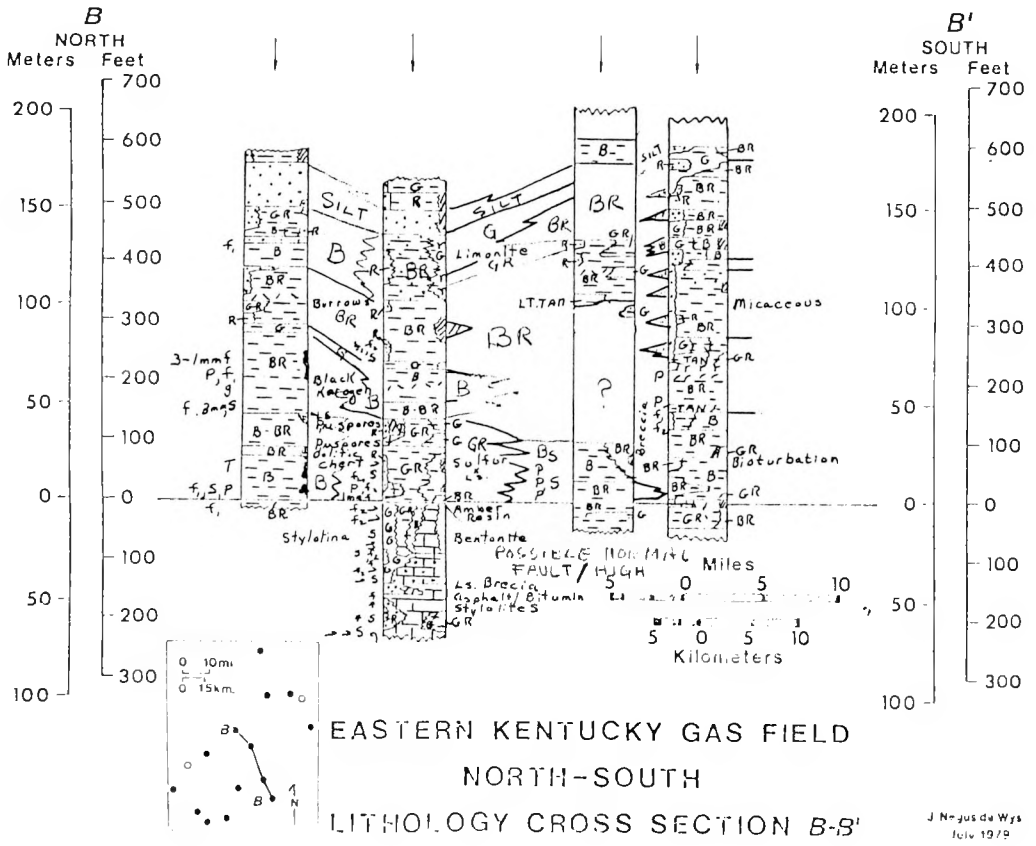


Figure 7 Lithological Cross-section B-B', northwest-southeast.

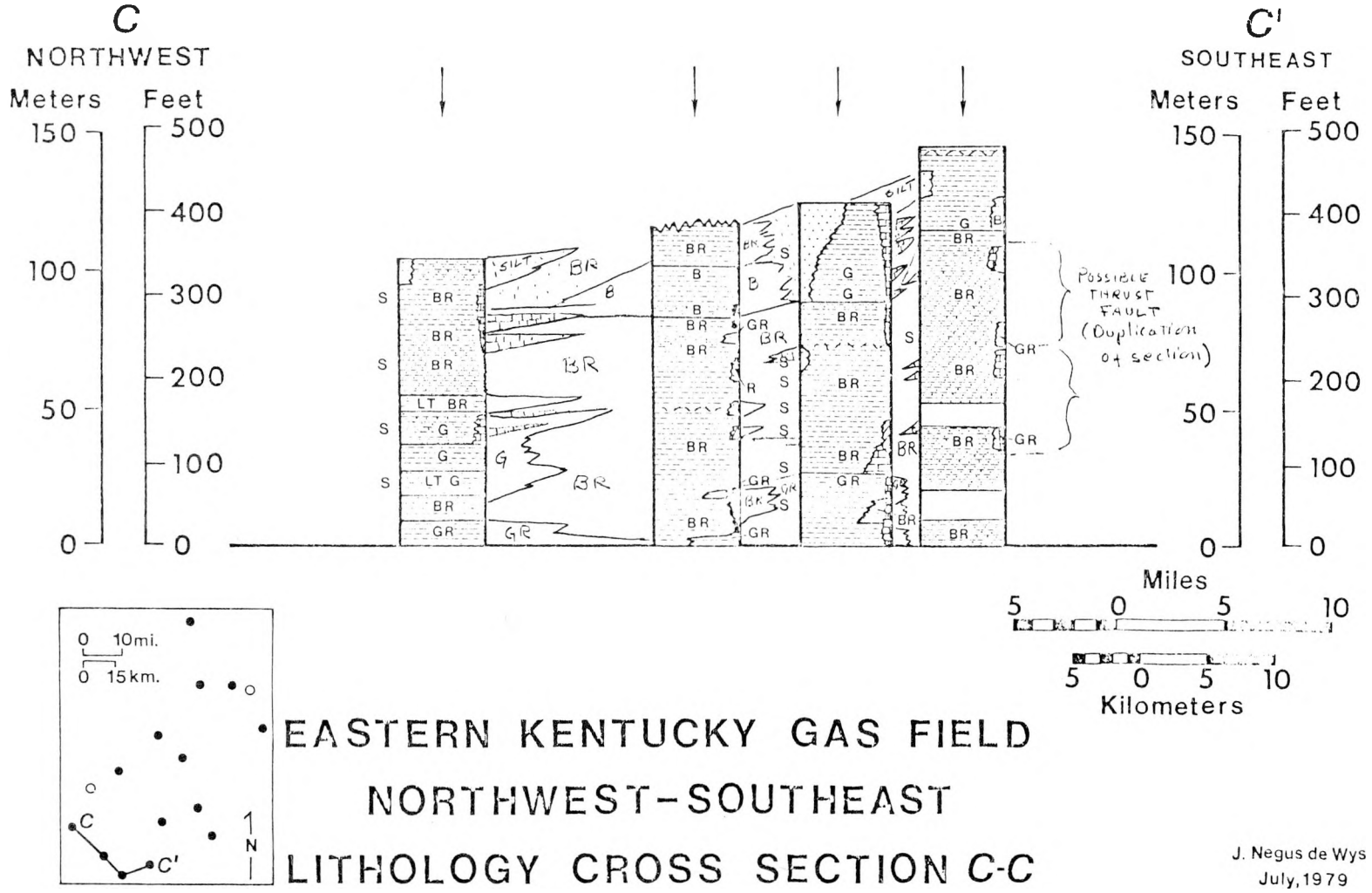


Figure 8 Lithological Cross-section C-C', southwestern section of the field, northwest-southeast.

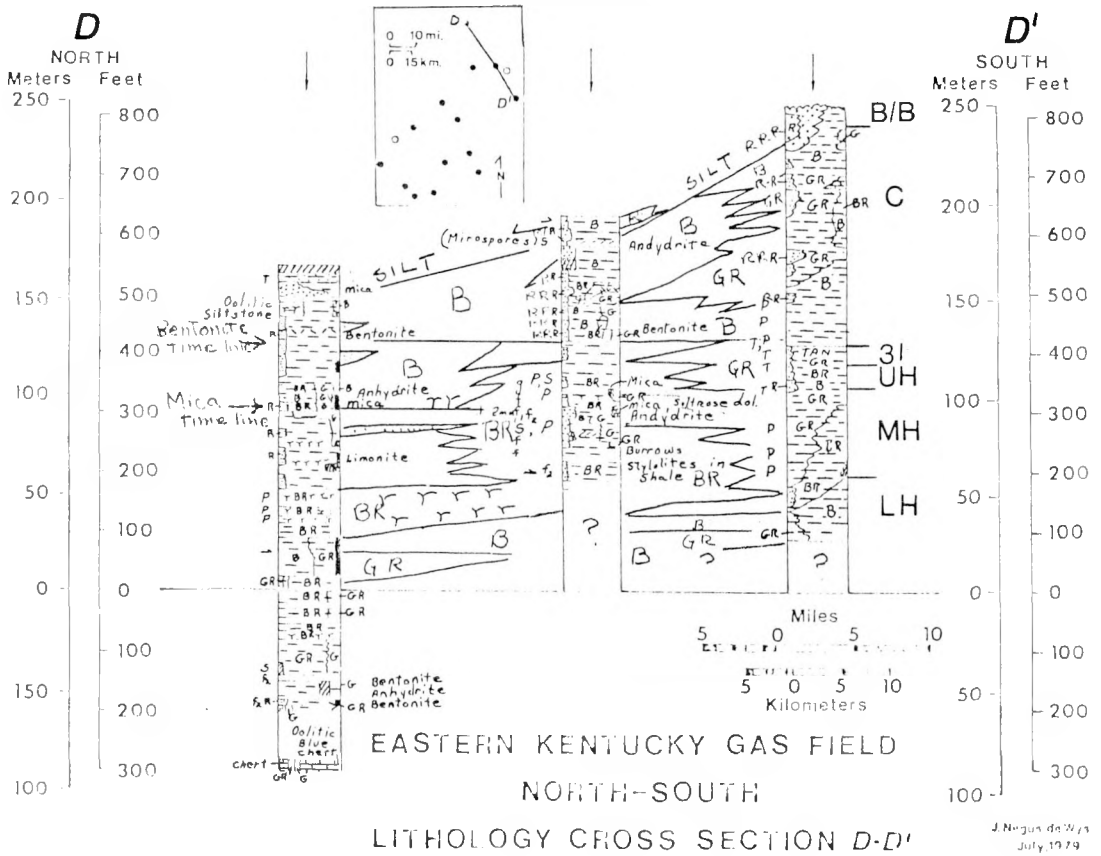


Figure 9 Lithological Cross-section D-D', northeastern section of the field, northwest-southeast.

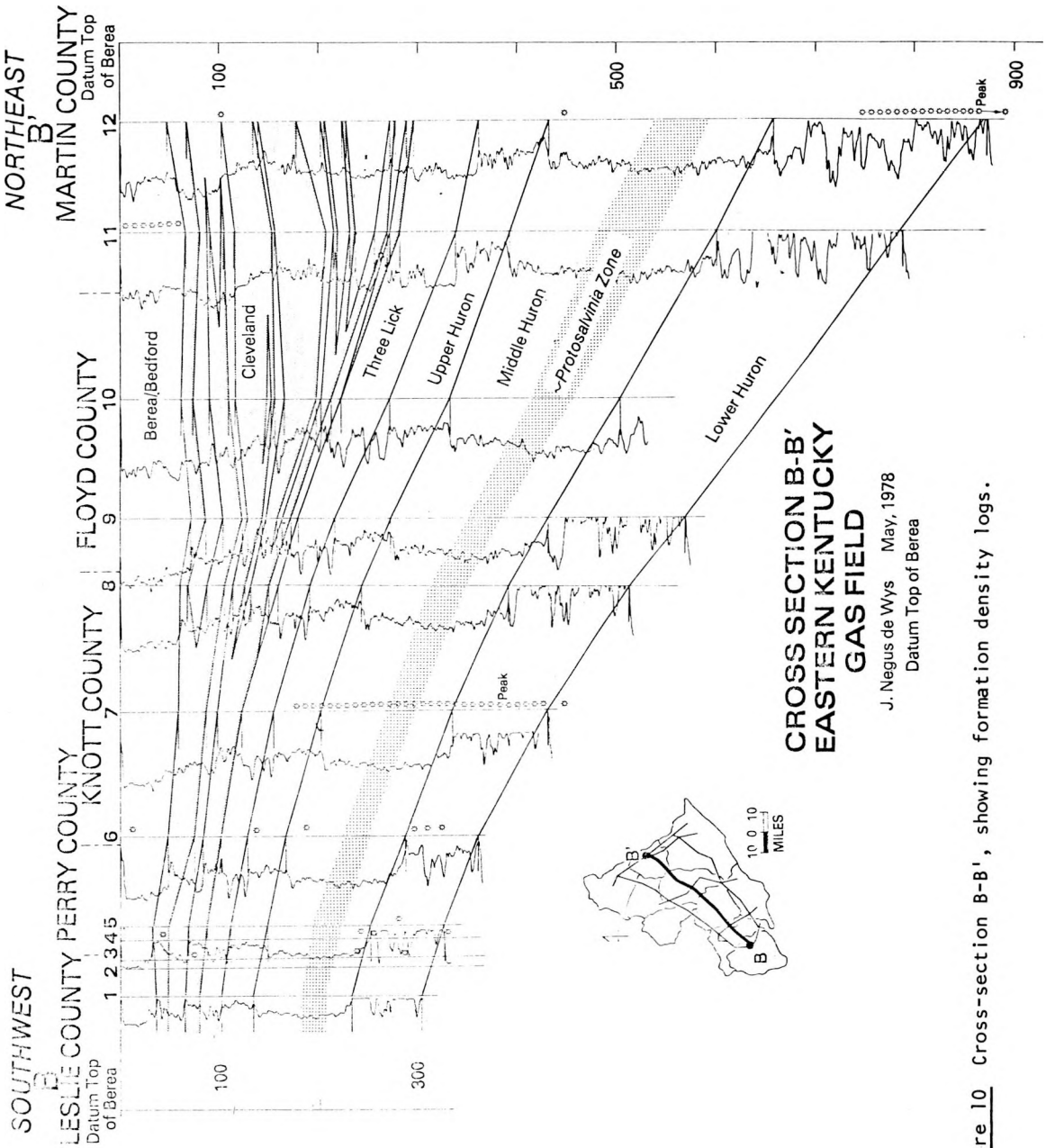


Figure 10 Cross-section B-B', showing formation density logs.

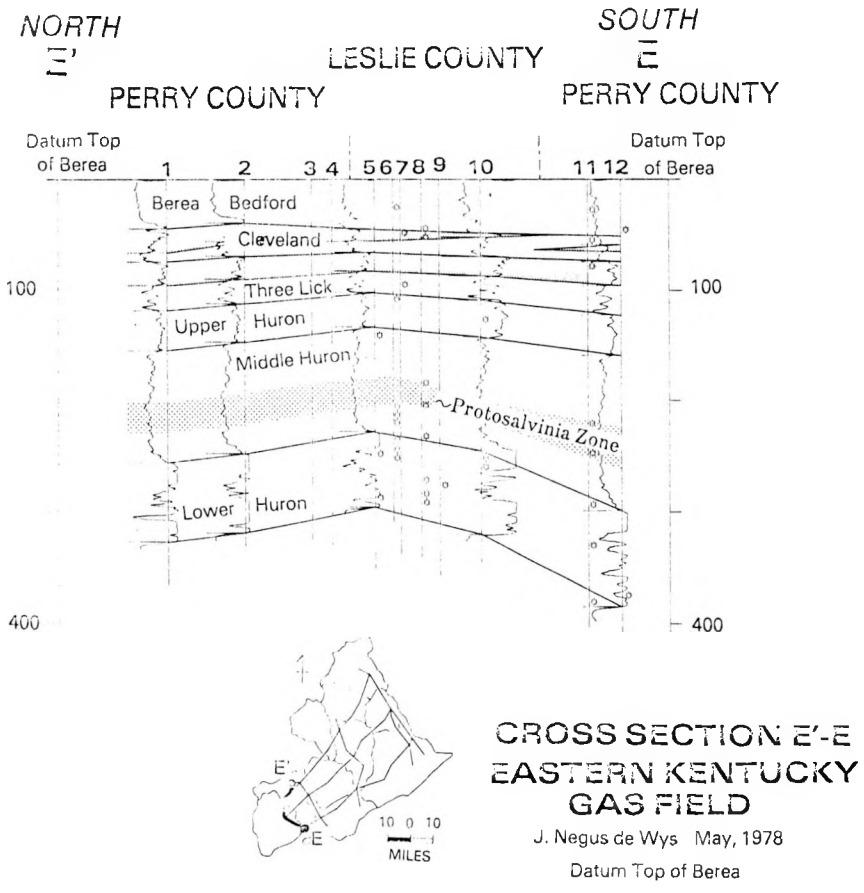


Figure 11 Cross-section E'-E, showing formation density logs.

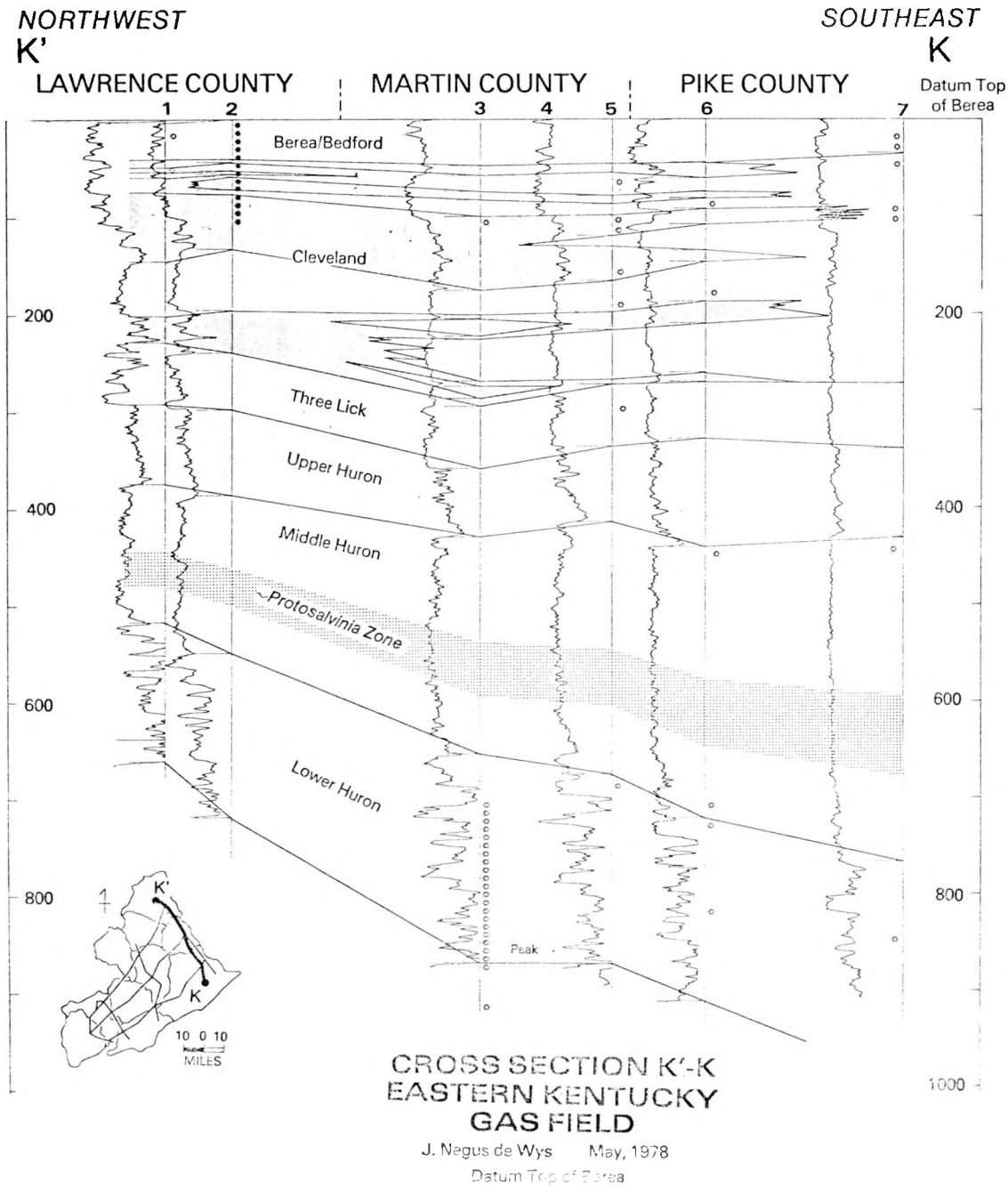


Figure 12 Cross-section K'-K, showing formation density logs.

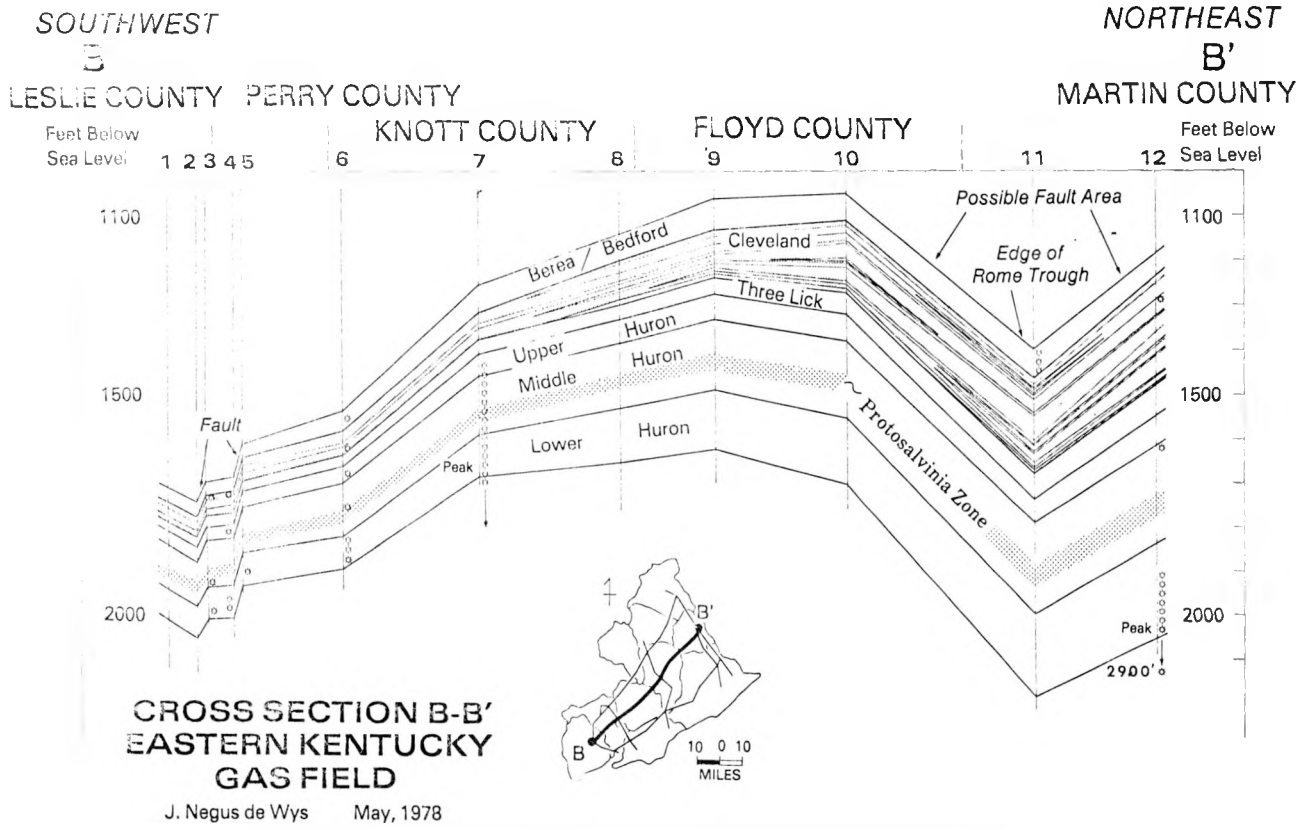


Figure 13 Structural-stratigraphic cross-section B-B' through the center of the field, southwest-northeast. (Same as Figure 6 in Negus-de Wys and Renton.)

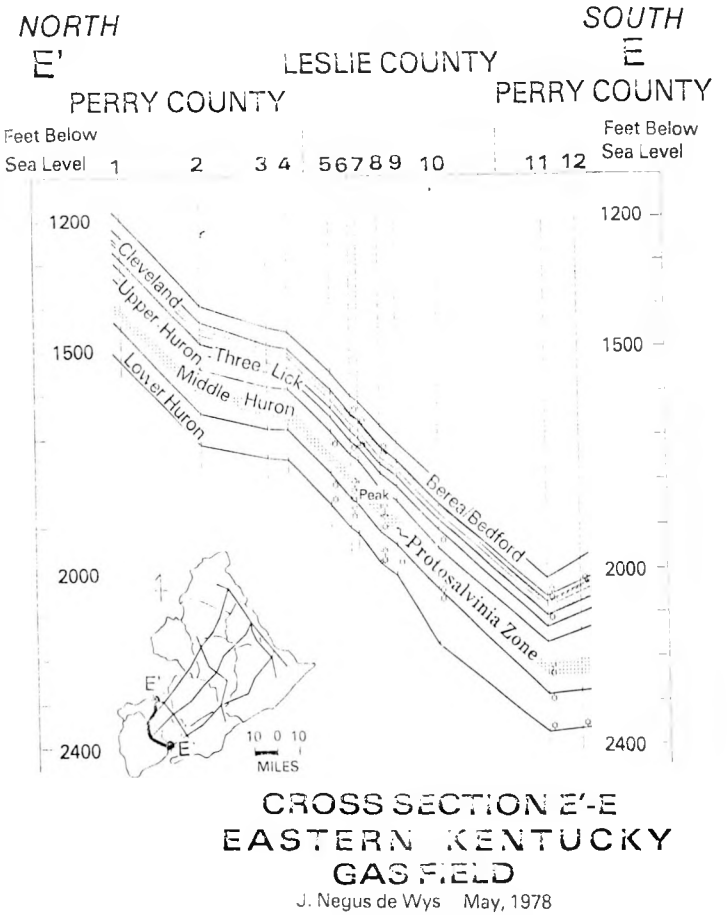


Figure 14 Structural-stratigraphic cross-section E'-E through the southwest end of the field, north to south. (Same as Figure 7 in Negus-de Wys and Renton.)

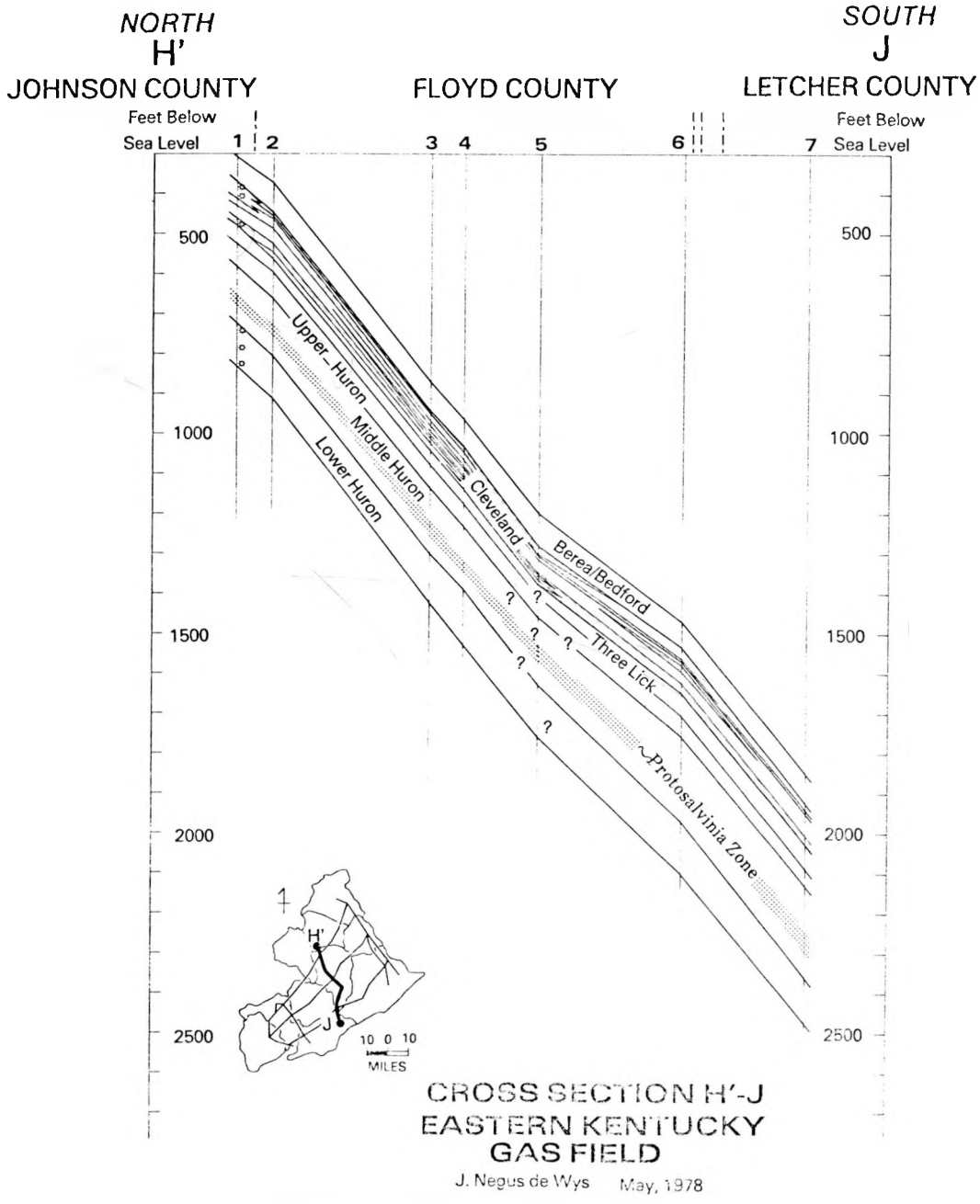


Figure 15 Structural-stratigraphic section H'-J through the center of the field, northwest to southeast.

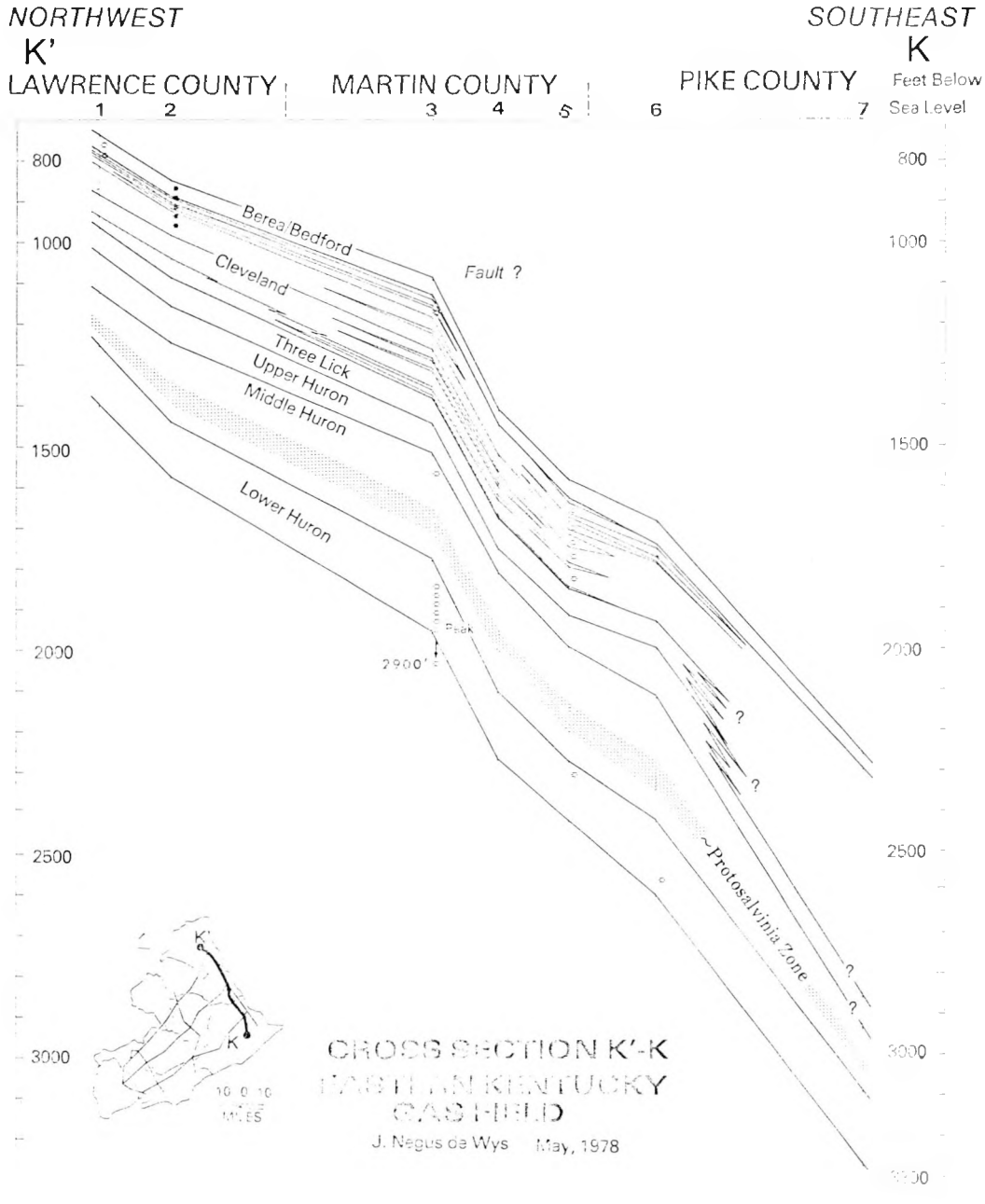


Figure 16 Structural-stratigraphic section K'-K through the northeastern part of the field, north to south. (Same as Figure 8 in Negus-de Wys and Renton.)

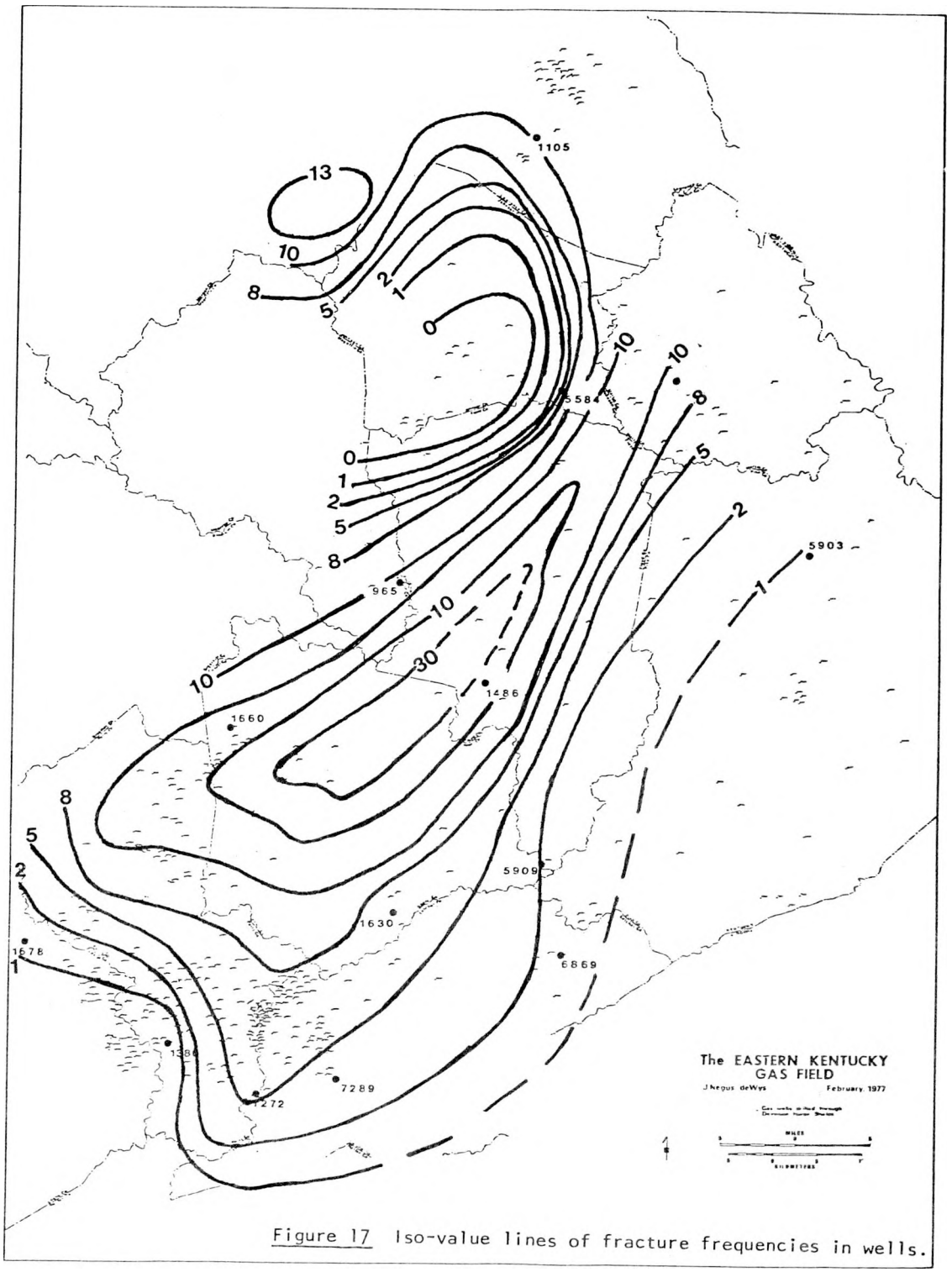


Figure 17 Iso-value lines of fracture frequencies in wells.

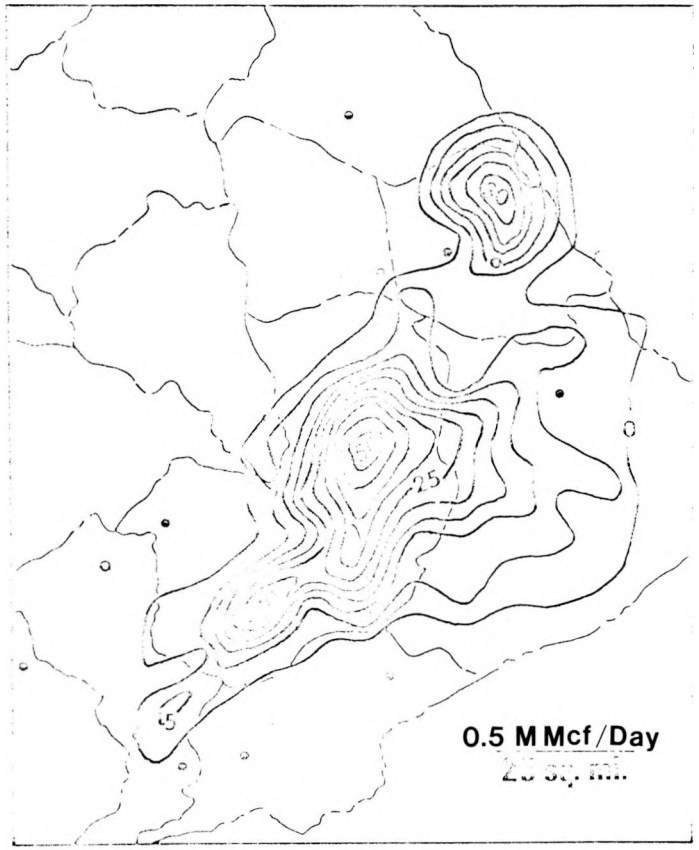


Figure 18A Iso-value lines of density of wells with final open flow >.5 MMcf/day/25 square miles (after Griffith, 1977).

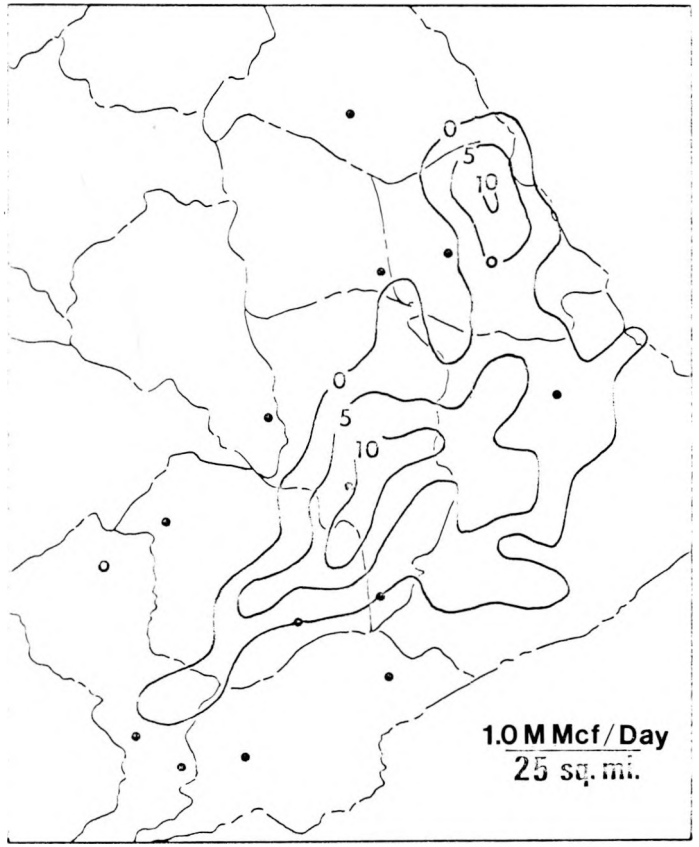


Figure 18B Iso-value lines of density of wells with final open flow >1 MMcf/day/25 square miles (after Griffith, 1977).

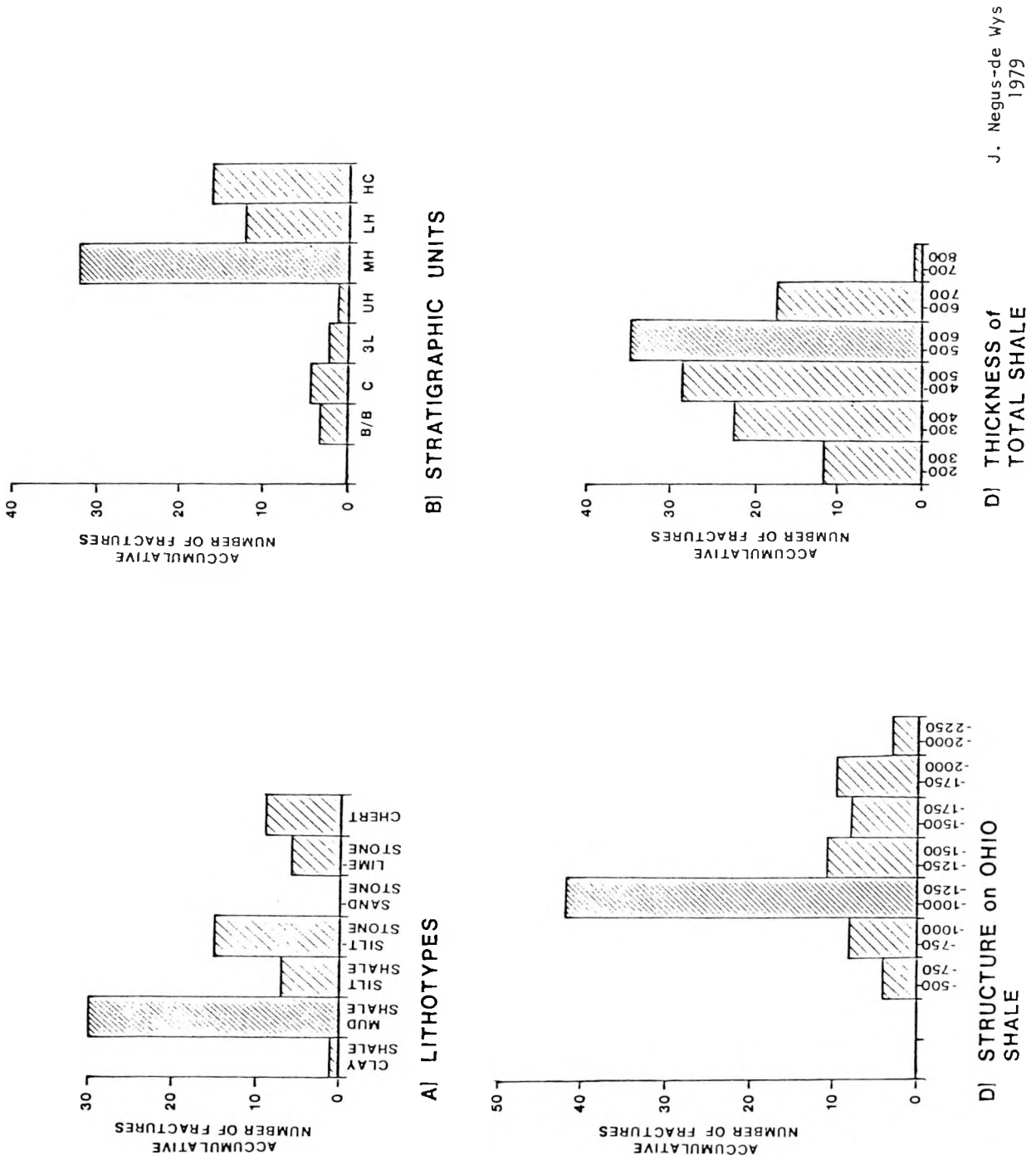


Figure 19 Histograms of Observed Fractures vs A) Lithotypes B) Stratigraphic Unit C) Structure on Ohio Shale, and D) Thickness of Total Shale.

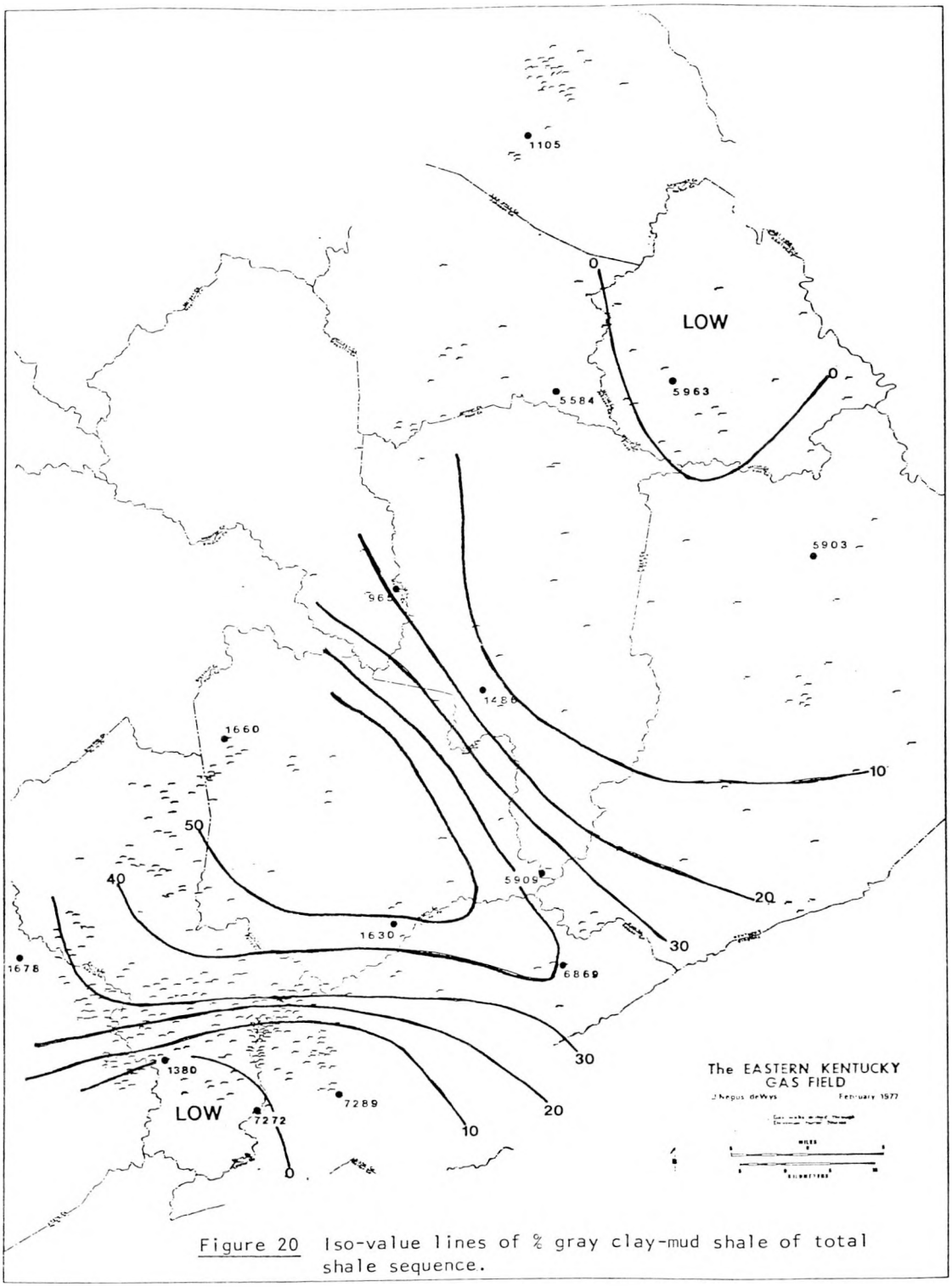


Figure 20 Iso-value lines of % gray clay-mud shale of total shale sequence.

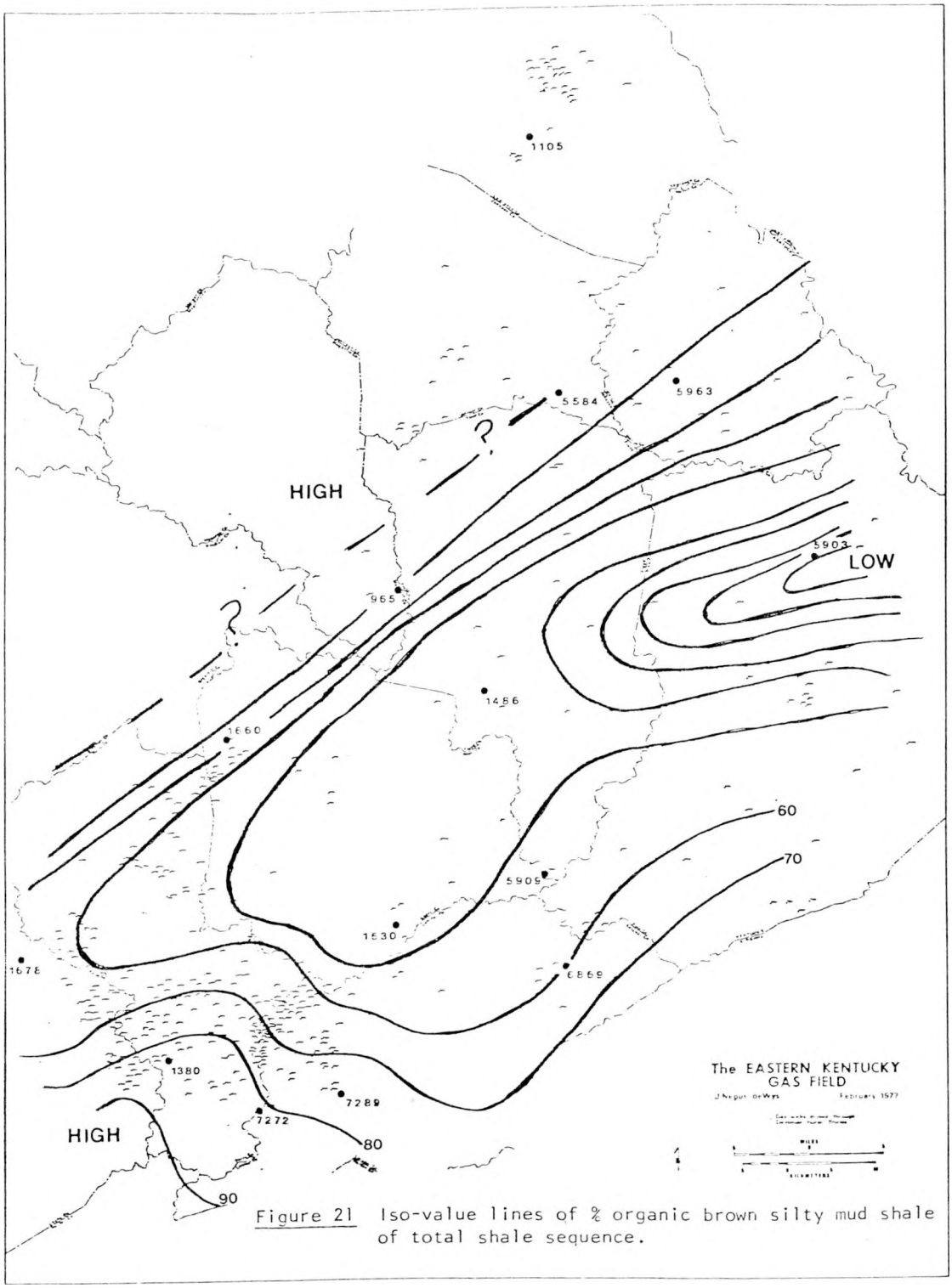


Figure 21 Iso-value lines of % organic brown silty mud shale of total shale sequence.

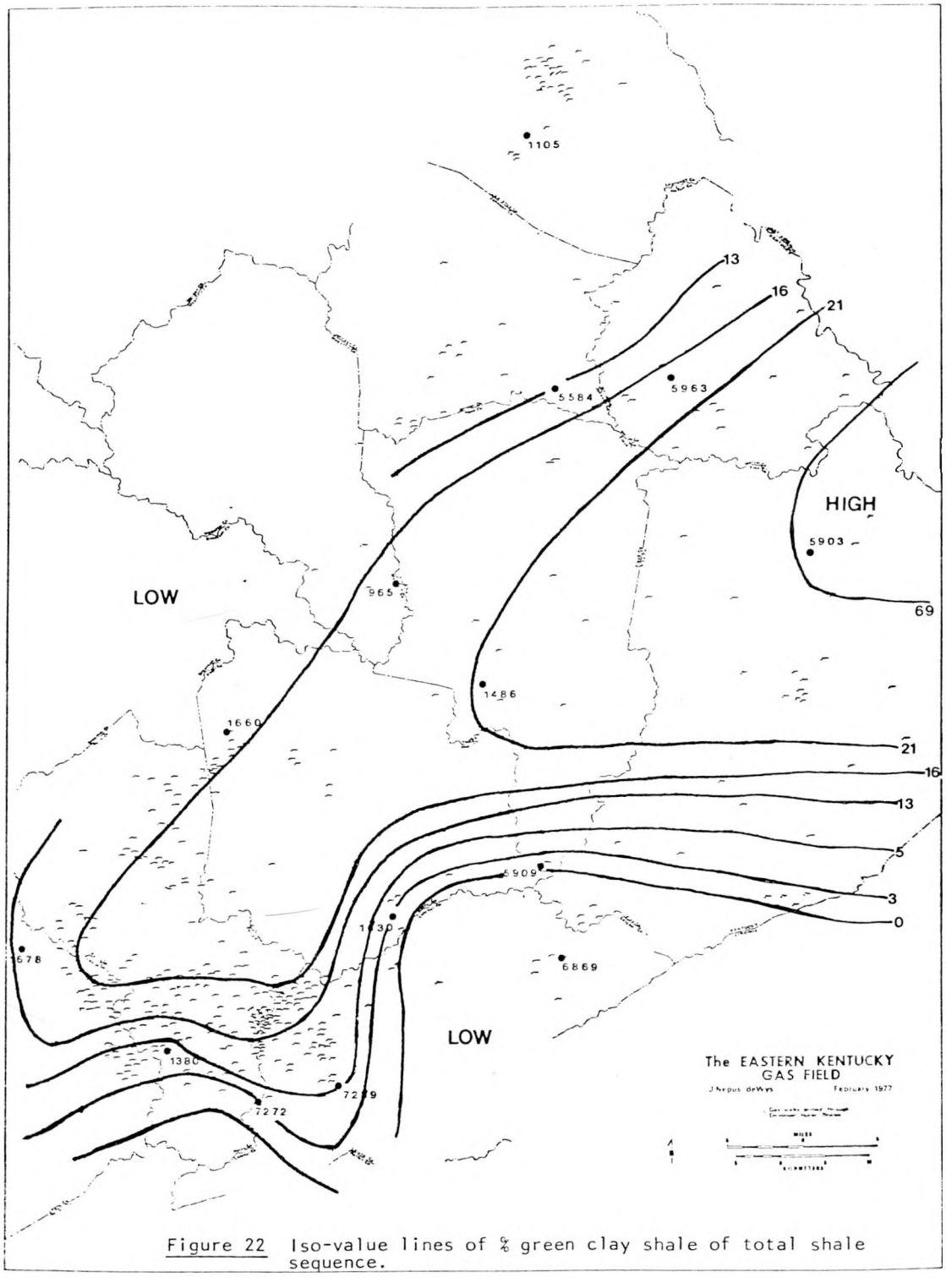


Figure 22 Iso-value lines of % green clay shale of total shale sequence.

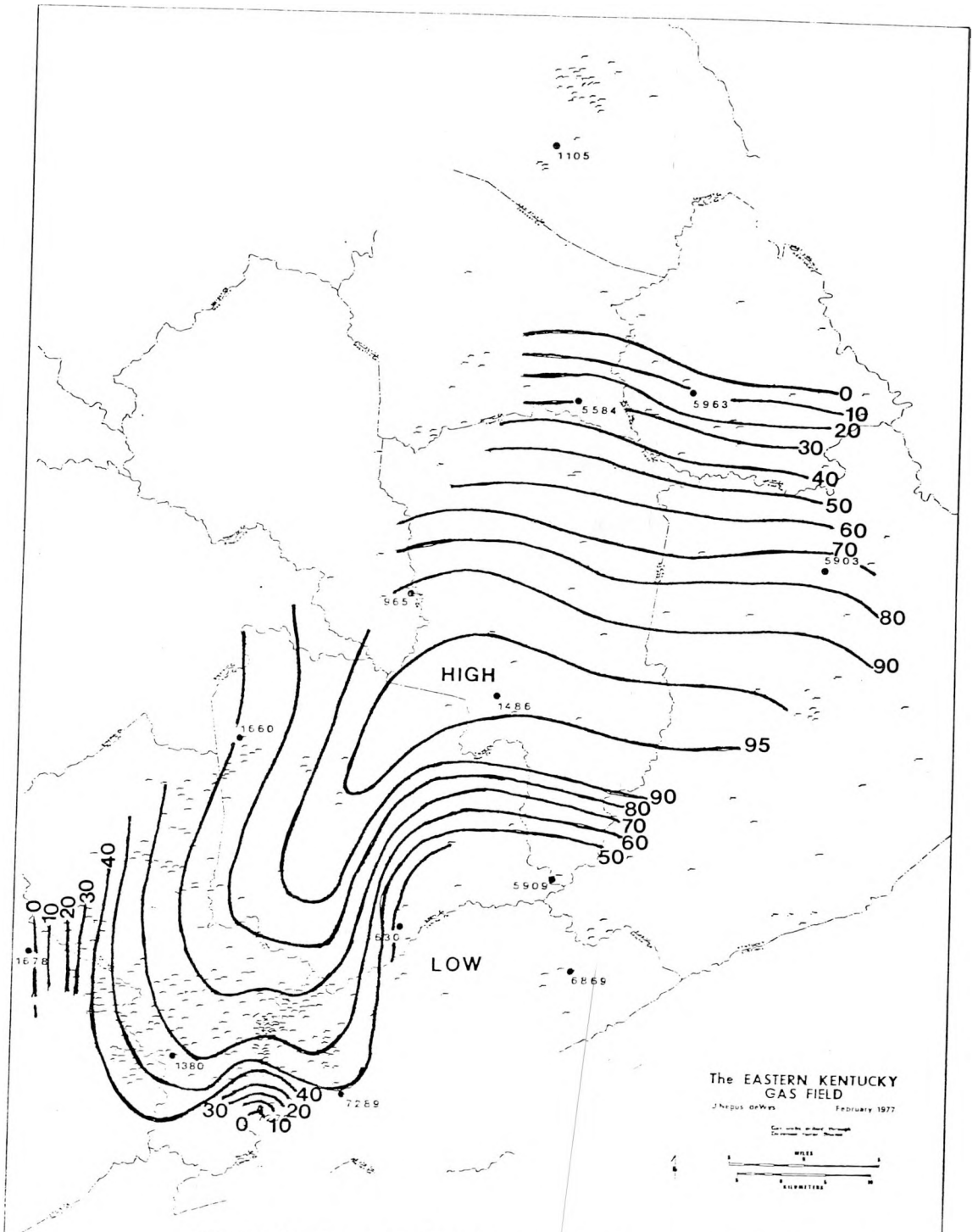


Figure 23 Isopach of highly organic black mud shale (in feet).

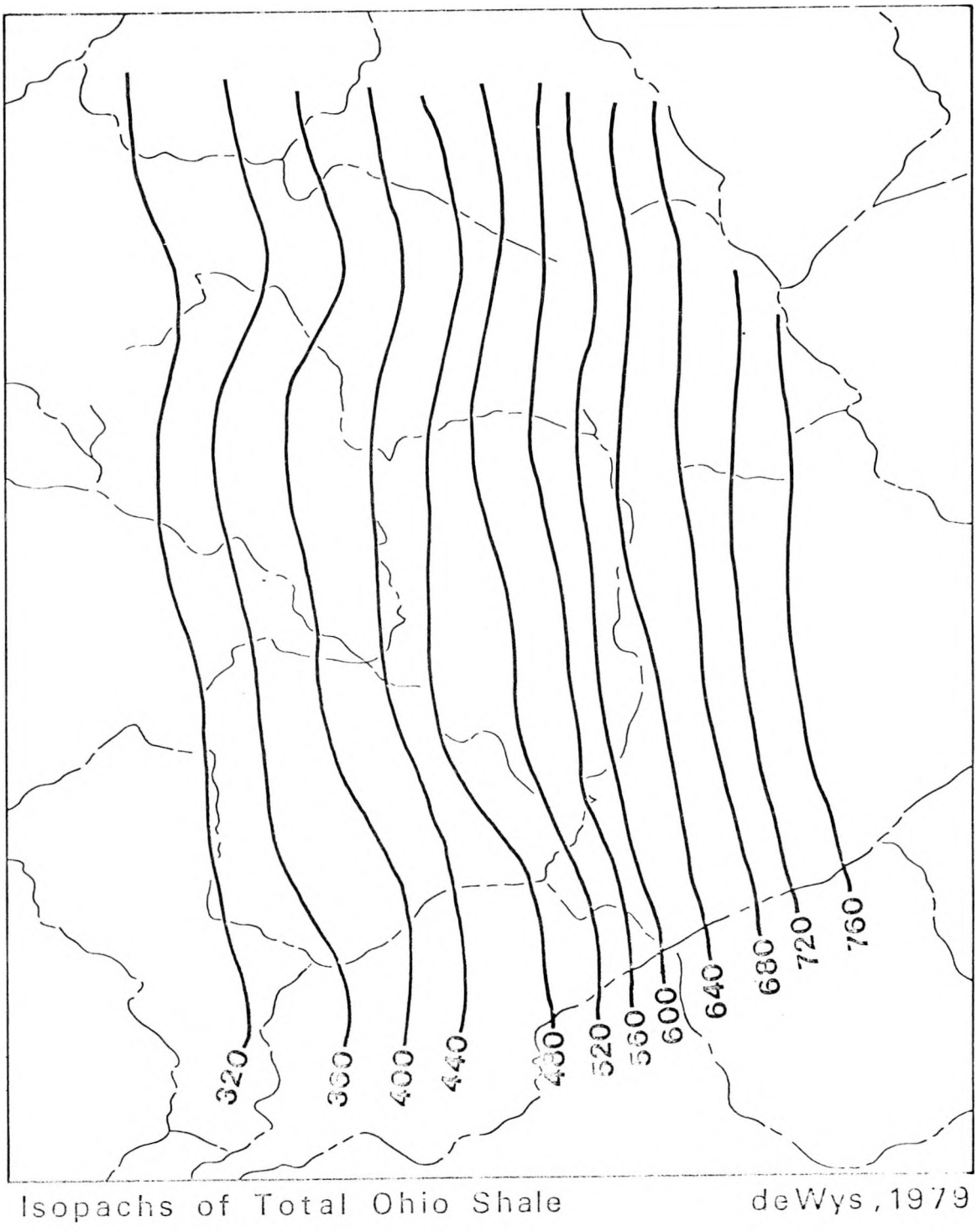


Figure 24 Ohio Shale Isopach Map (after Provo, 1977).

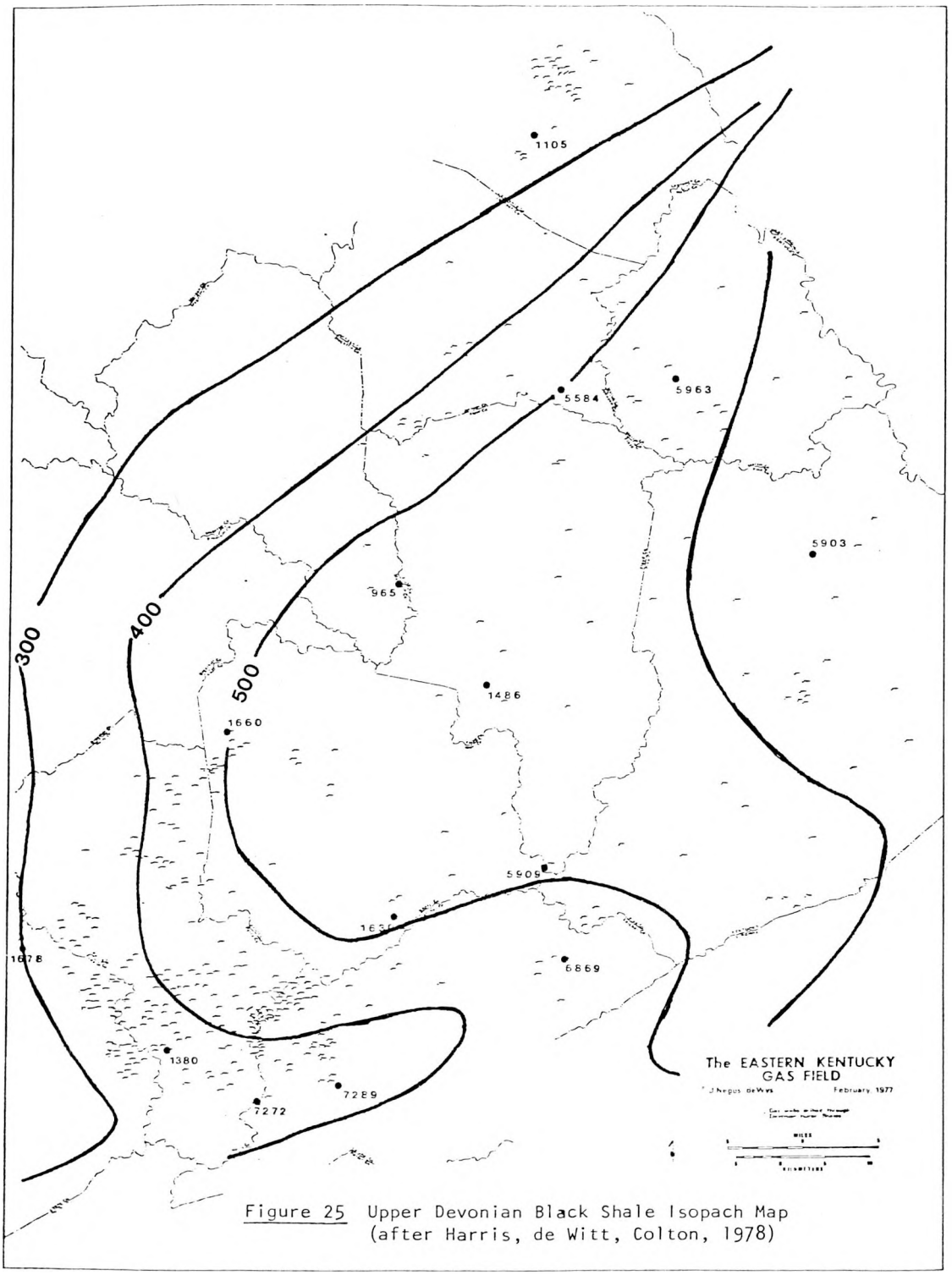


Figure 25 Upper Devonian Black Shale Isopach Map
(after Harris, de Witt, Colton, 1978)

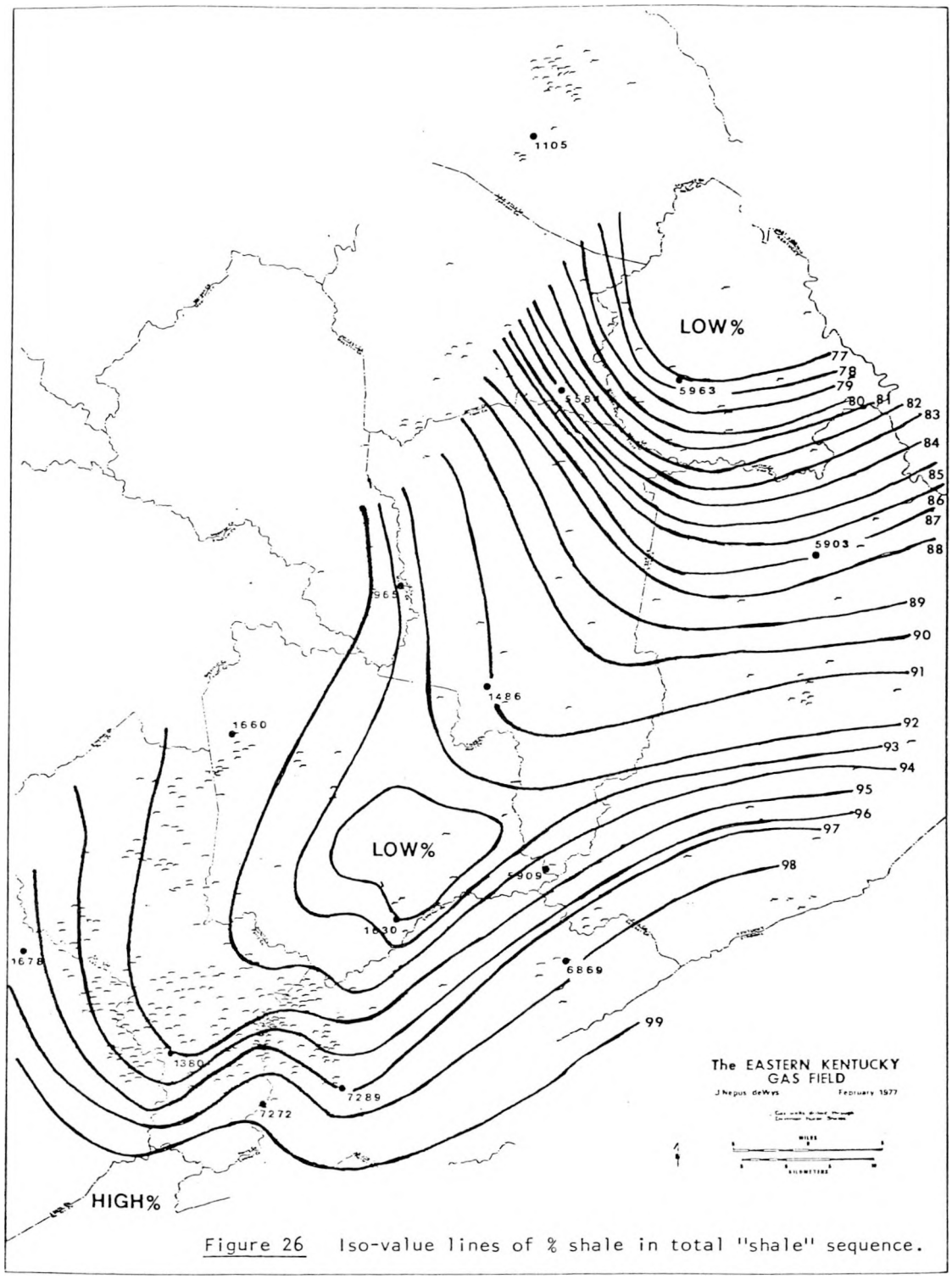


Figure 26 Iso-value lines of % shale in total "shale" sequence.

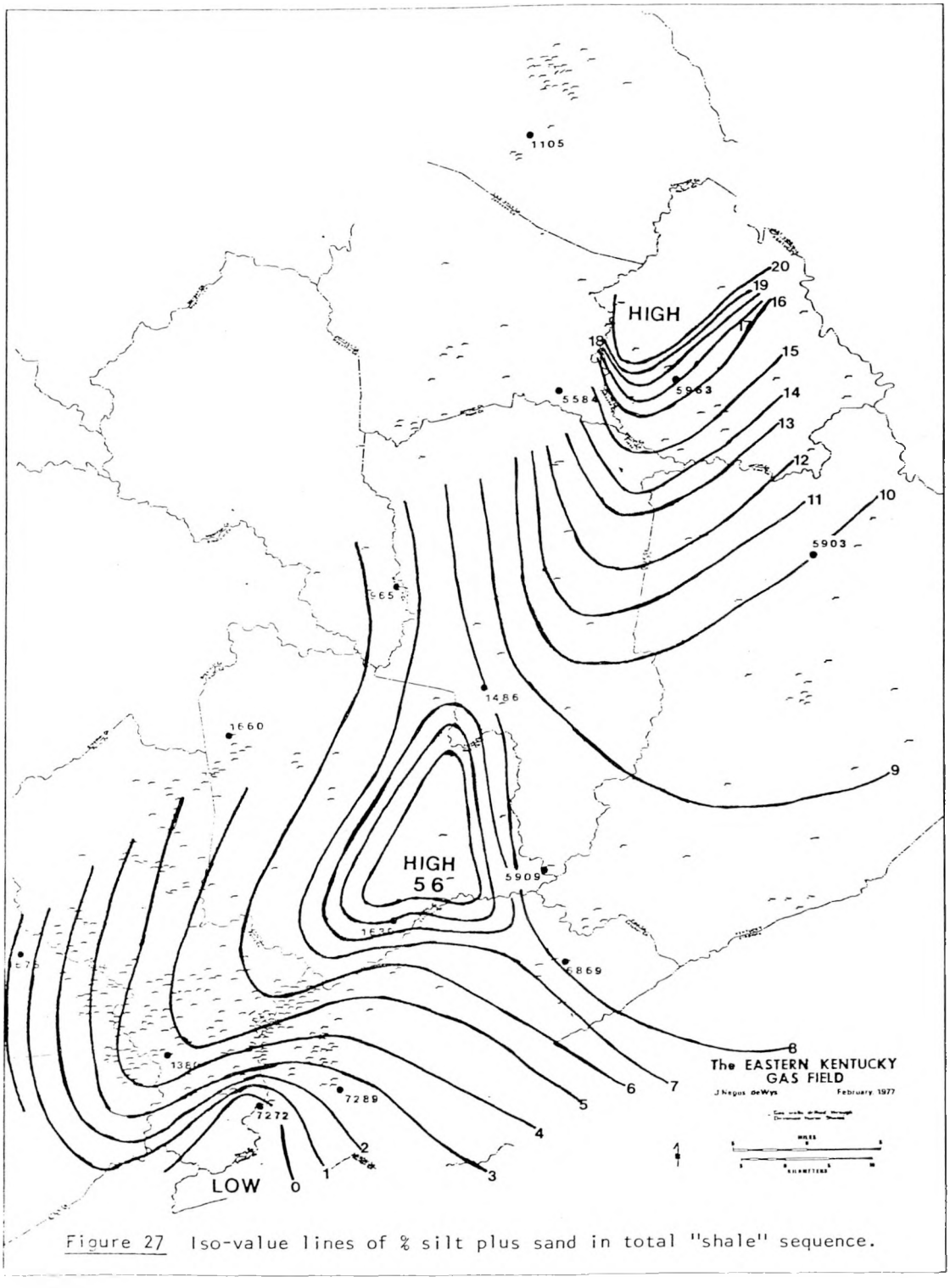


Figure 27 Iso-value lines of % silt plus sand in total "shale" sequence.

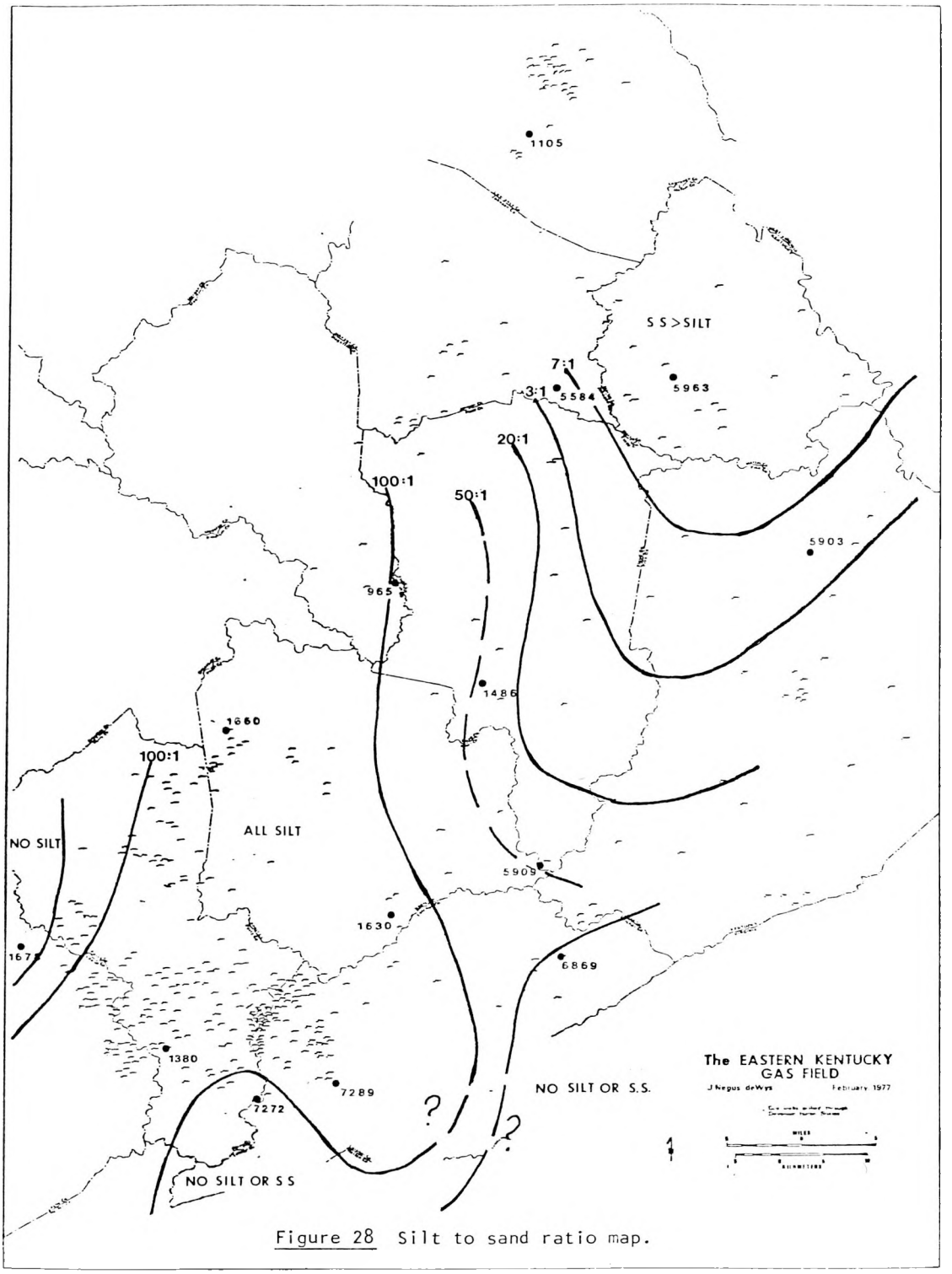


Figure 28 Silt to sand ratio map.

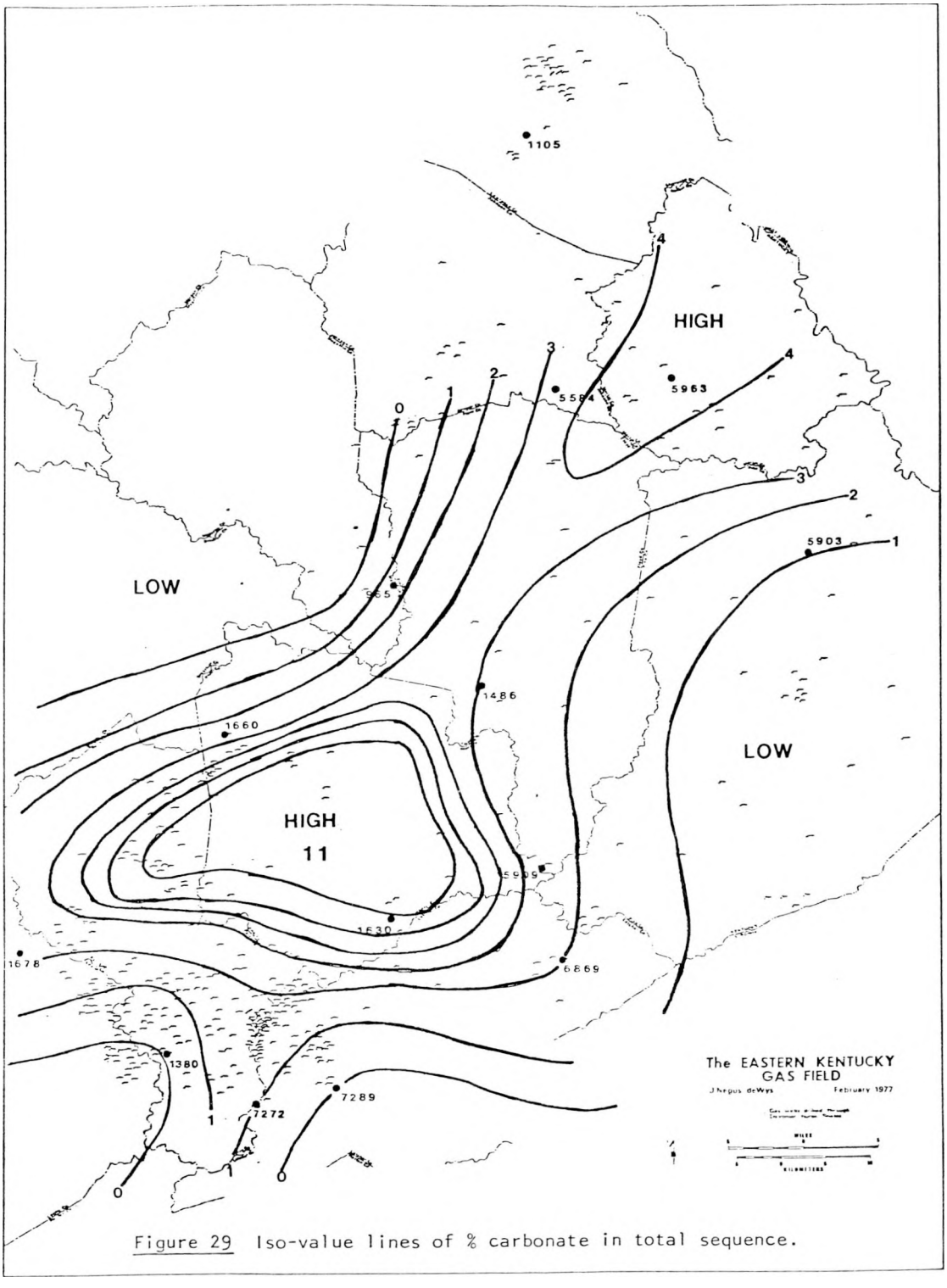


Figure 29 Iso-value lines of % carbonate in total sequence.

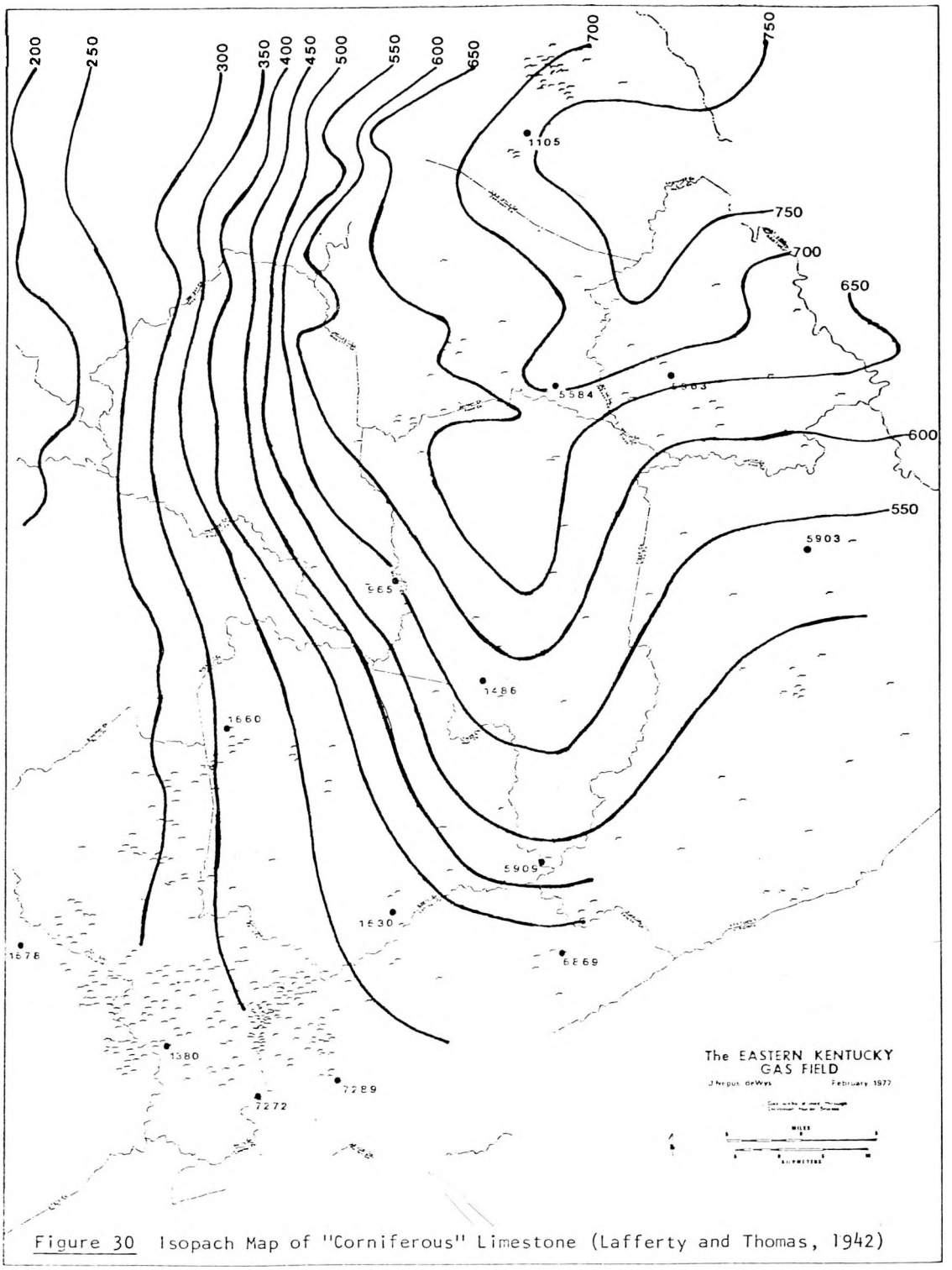


Figure 30 Isopach Map of "Corniferous" Limestone (Lafferty and Thomas, 1942)

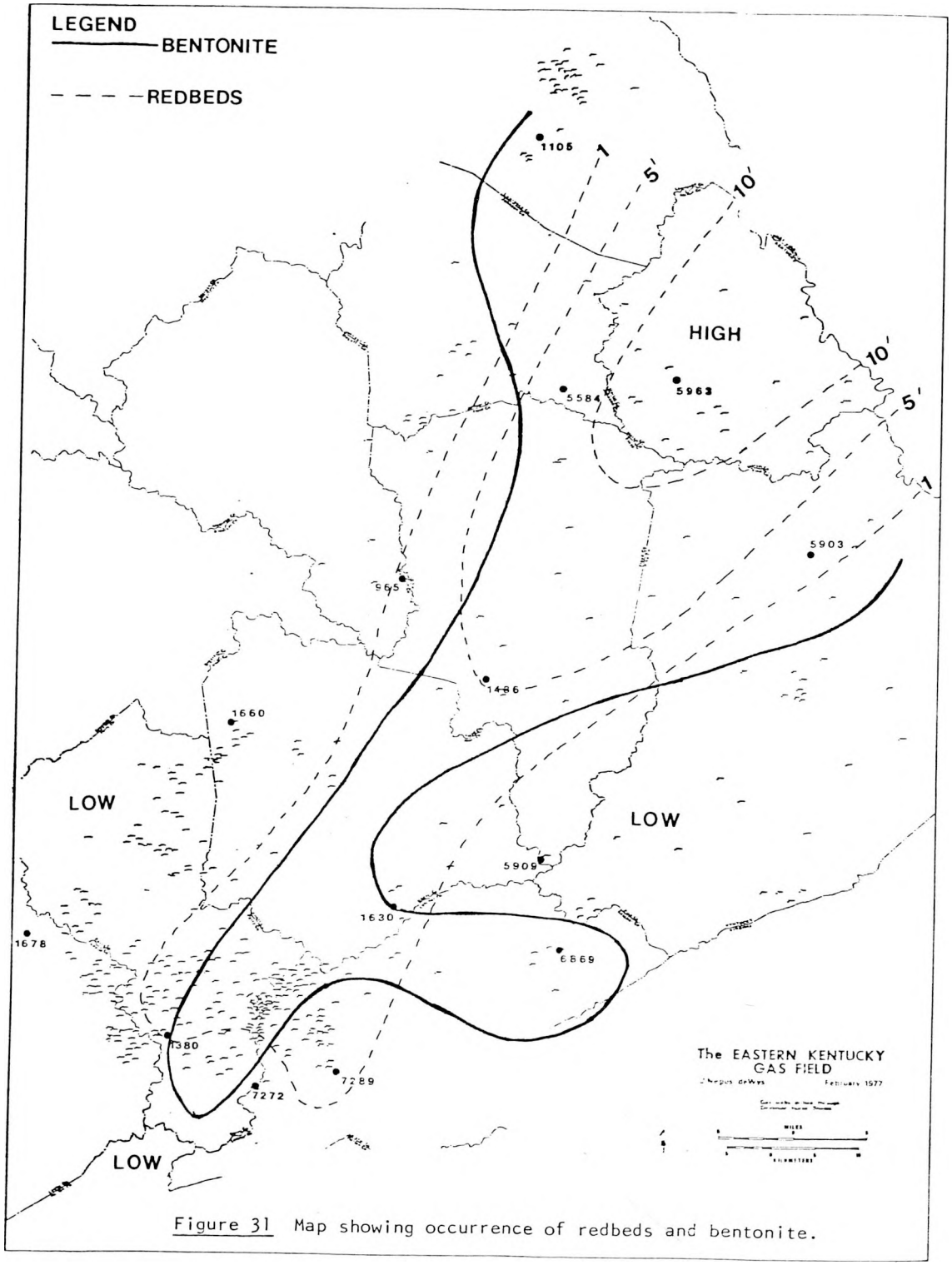


Figure 31 Map showing occurrence of redbeds and bentonite.

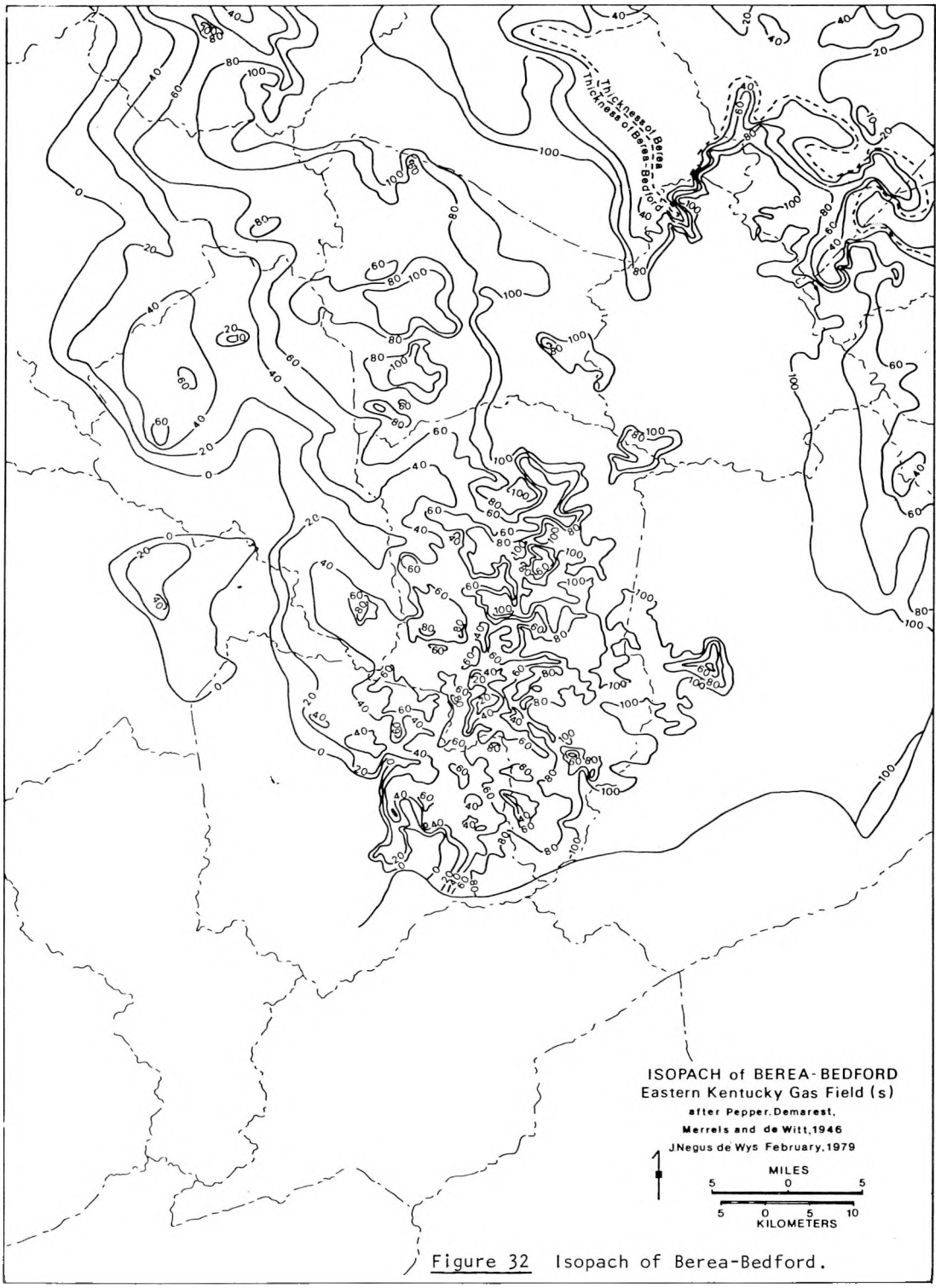


Figure 32 Isopach of Berea-Bedford.

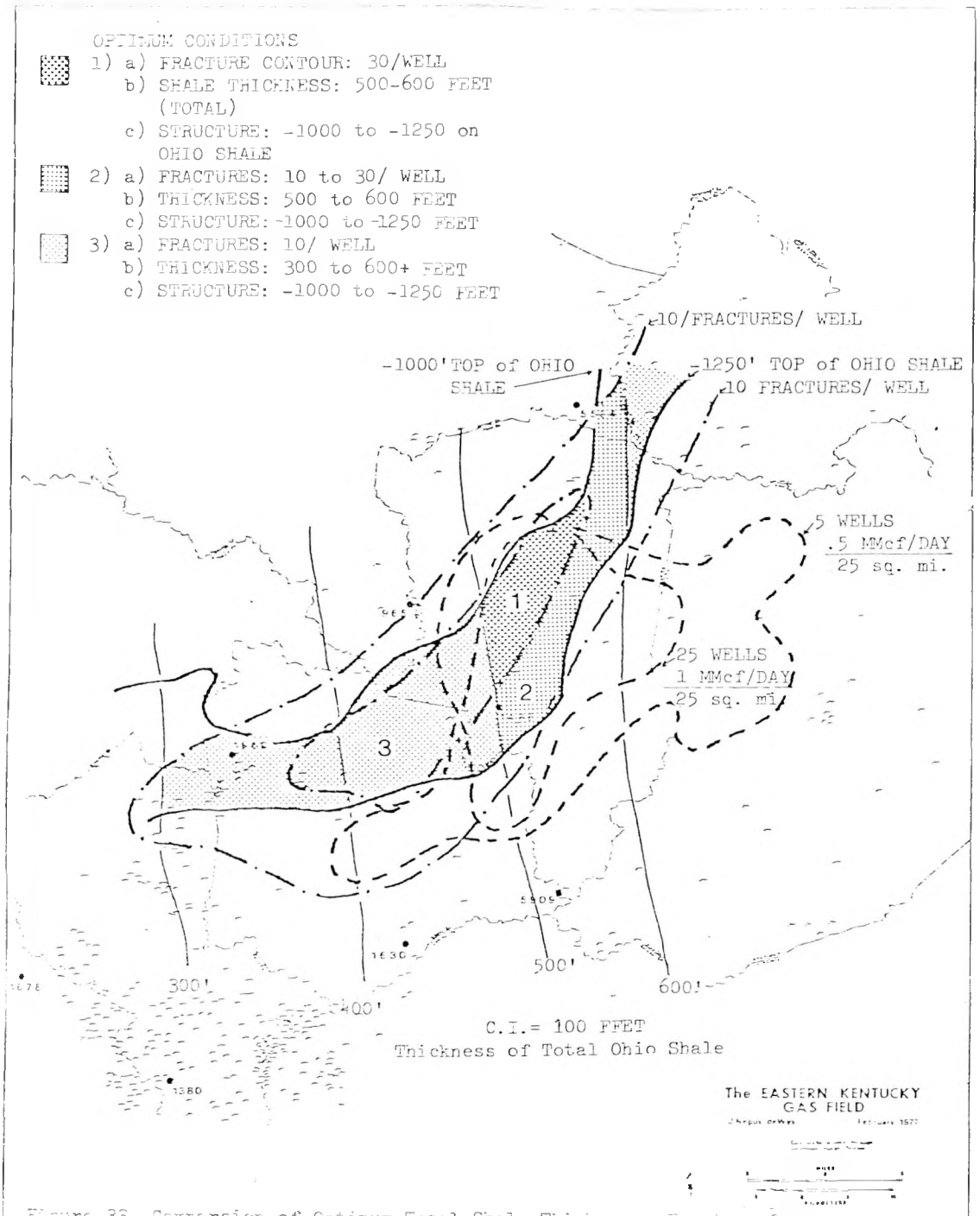


Figure 33. Comparsion of Optimum Total Shale Thickness, Fracture Occurence, Structural Position on Top of Ohio Shale with Density of Wells > 1MMcf/Day /25 sq. mi. (Differences noted in non-producing matching lobes of high wells density contour)

UNCONVENTIONAL EVALUATION OF THE COTTAGEVILLE DEVONIAN SHALE FIELD JACKSON & MASON COUNTIES, WEST VIRGINIA

W. M. Hennington

Manager Exploration, Eastern Division

Mitchell Energy Corporation



ABOUT THE AUTHOR

W. M. (Mack) Hennington graduated from the University of Tulsa Engineering School with a B.G. degree in 1951.

He has served in numerous exploration and exploitation positions at various management levels and personally conducted many practical research investigations throughout the U.S. during nineteen years with Amerada Petroleum Corporation, four years with Columbia Gas System and five years with Mitchell Energy Corporation.

Studies concerning the reconstruction of depositional relationship, compaction fractures and the potential of the shale have been a small but significant part of the search for hydrocarbons for over twenty years.

2 UNCONVENTIONAL EVALUATION OF THE COTTAGEVILLE DEVONIAN SHALE FIELD

ABSTRACT

Recent compilation and publication of data by the U.S. Department of Energy and West Virginia University on the Devonian shale production in the Cottageville Field of West Virginia, has made this a good shale study area.

A preliminary study utilizing the new unconventional exploration technique has been made based on the available data. The technique is an attempt to reconstruct depositional structural conditions which are thought to control development of the natural compaction fracture reservoir.

The depositional highs should have the coarser, less compactible material deposited, while the depositional lows should have the finer more compactible materials deposited. Minimum compaction on the depositional highs and maximum compaction in the depositional lows should result in maximum compaction fractures on the flanks of the depositional highs.

Production from the shale occurs on present day structural noses with about 250 feet of regional dip across the field. There does not appear to be any direct relationship of good producers to present day shale structure.

Most of the producers, approximately 77%, fall within a 50' depositional structure interval and 100% of the producers with initial flows of over 500,000 cfgpd fall within a 50' interval. About 11% of the Cottageville Field wells had initial flows of over 500,000 cfgpd. This indicates the possibility of being more selective in making locations and substantially increasing the chances of making a good well.

The high natural open flows and largest accumulated production seem to be associated with the flanks of the depositional structure.

The preliminary study indicates the utilization of the unconventional technique can substantially improve Devonian shale natural fracture reservoir prediction, improve definition of productive limits and demonstrate the possibility of selectively drilling tests with current economic potential.

INTRODUCTION

This study is based strictly on published reports and public information which was collected for these reports. A preliminary study from the published data was encouraging and additional information was acquired for this expanded study of the Cottageville Field.

The purpose of this paper is to show that favorable Devonian shale fracture reservoirs can be predicted, projected and possibly developed on a systematic, economic system. The use of the New Unconventional Exploration Technique in the Cottageville Field area allows prediction of favorable fracture reservoir development, better definition of productive limits and demonstrates the possibility of selectively drilling tests with current economic potential.

Additional basic information for further study, development and evaluation of the technique is needed for complete utilization and is the objective of additional studies in the Cottageville Field and other Research Projects.

The Regional Location plat, FIGURE 1, shows the approximate outline of the study area and its relationship to the Gallia County, Ohio Devonian - Ohio Shale Project which is approximately fifteen miles west of the Cottageville Field.

METHOD OF STUDY

Data was accumulated from various data sources and publications, tabulated, plotted and remapped utilizing the new Unconventional Exploration technique. A brief discussion of the unconventional exploration technique, the maps and figures will be presented.

PRODUCTION STATISTICS
COTTAGEVILLE FIELD
JACKSON & MASON COUNTIES, WEST VIRGINIA

48 YEARS OF DEVONIAN SHALE PRODUCTION

Discovered: October 9, 1929 by Cities Service (3)
Estimated Total Field Production (2) 15,800,000,000 cfg

Estimated Size (est from 2)	6,840 Acres
Estimated Number Wells with Production (2)	90 Wells
Average Number Acres/Well	76 A/W
Wells By: Consolidated 43; Columbia 17; Cities Service 16	
Approximate Shale interval (2)	2500' to 4000'
1975 Cost/Well $65,000: With $1.00/MCF = 4 year payout (2)	

FLOW	
Highest natural flow (3)	3,480,000 cfg
Average natural flow, 81 wells (3)	188,200 cfg
Number wells with natural flow over 500,000 cfg	10 = 11% +
Average flow after stimulation, 90 wells (3)	355,000 cfg
PRESSURE	
Highest initial pressure (3)	1,000 psi
Average Pressure (3)	639.6 psi
Current Pressure (2)	190-350 psi
PRODUCTION	
Cumulative production, 77 wells (2)	10,080,000,000 cfg
Largest Production/Well (3)	952,500,000 cfg +
Average Production/Well (2)	137,700,000 cfg
About half of the wells are still producing	

The Cottageville Field Devonian - Ohio Shale section was divided into multiple zones for analysis utilizing E. B. Nuckol's subdivisions (4). These zones were based on correlatable radioactive intervals, FIGURE 2. Zone I is near the base of the shale, Zone II is the intermediate interval about 400 feet above Zone I. Zone III is the uppermost radioactive interval just below the middle of the Devonian - Ohio Shale.

Zone I at the base of the Devonian - Ohio Shale was penetrated by 14.8% of the field tests and had 7.5% of the shows reported with 7.1% of the wells having possible production from the interval.

Zone II was penetrated by 99% of the field tests and had 42.1% of the reported shows with 51.6% of the wells having possible production from the interval.

Zone III, near the middle of the shale, was penetrated by 100% of the field tests and had 18% of the reported shows with 33.5% of the wells having possible production from the interval.

The shale interval above Zone III, approximately the top half of the shale, had 20.9% of the shows of which 14.4% do not appear to have been tested.

A total of 32.4% of the reported shows were not in the radioactive intervals.

The Zone above Zone III, termed III-A, had 25 wells with reported shows that were not tested, FIGURE 3. ZONE II-A had 11 shows reported that do not appear to have been tested.

The Well Locations for this study were based on the D.O.E. base map. The type of well and the permit number is indicated for reference. For this study the gas well symbol was used for any well which reported a gas flow from the Devonian - Ohio Shale after stimulation. If a hole was drilled through the shale to a deeper horizon without shale evaluation it is indicated as a control point.

The Unconventional Exploration Technique to be utilized in this study utilizes the depositional theory that coarser, less compactible sediment is deposited on the crest of depositional highs and finer more compactible material is deposited on depositional flanks and in depositional lows. When the sediment compacts there is differential compaction resulting in natural fractures on the flanks of depositional highs.

Present day structure is related to depositional structure. This relationship is approximated by relating production to a series of structural profiles which show apparent dip of an adjustment plane. True dip of the plane can be calculated from any two intersecting profiles and the adjustment applied to the structure map.

After the approximate depositional structure has been computed the other maps can be interrelated. Certainly there are other factors that contribute to sediment variations and natural fracture development, however they are believed to be a minor influence in the Cottageville Field.

STRUCTURE

Maximum structural configuration was accomplish by first contouring the Berea Structure which has a maximum number of control points. The maximum control surface was projected to the Lower Huron horizon.

The Base of the Lower Huron datums (Zone II) were posted from tabulated data and contoured, FIGURE 4. The structure of this horizon within the shale shows 589' of structural relief but does not appear to control Devonian - Ohio Shale Production. Above average producers have a 250' structural range.

The Plot of Structure vs Production, FIGURE 5, shows that there is no apparent direct relationship between present day structure and the productive wells.

DEPOSITIONAL RELATIONSHIP

The arbitrary relationship between present day structure and the productive areas was approximated for adjustment. The Depositional Relationship, FIGURE 6, approximately established with a Strike of N 24.4° E and a dip estimated at 55.8 feet per mile.

The approximate Depositional Structure, FIGURE 7, was calculated and resulted in a series of closures. The Depositional Structure has a 224 foot variation in the study area. Natural compaction fractures are believed to be developed on the flanks of Depositional Structures.

The Cottageville Field wells with initial flows have a Depositional Structure range of 100', FIGURE 8. A 60' Depositional Structure range contains 86.7% of the wells which had initial flows reported. A 50' Depositional Structure range contains 77.3% of the wells reporting initial flows.

Wells with final flows of over 50,000 cfgpd have a Depositional Structure range of 110', FIGURE 9. A 60' Depositional Structure range contains 84.6% of the wells with final flows of over 50,000 cfgpd. A 50' interval conatins 71.9% of these wells.

All wells with Above Average Final Flows are within a 100' Depositional Structure Range, FIGURE 10. The 60' Depositional Structure range includes 88.5% of the producers. The 50' Depositional Structure range includes 77.1% of the above average wells.

The Potential Depositional Structure map, FIGURE 11, shows the most potential interval for natural compaction fracture development. It also shows how the Unconventional Exploration Technique can be used in selecting development locations, extensions and wildcat prospects.

PRODUCTION

Natural Open Flows range from 3,480,000 cfg to zero. The Natural Open Flow was contoured relative to the Depositional Structure, FIGURE 12. For the sake of contouring, the abnormal open flows

were not contoured. A variable contour interval was used: 0-50-100-250-500-1000 MCF/D (4). The high open flows seem to be associated with the flanks of the Depositional Structure with a decrease both on the highs and in the lows.

Final Open Flows, FIGURE 13, range from 3,480,000 cfg to a trace. Most of the wells were stimulated by gelled ammonium nitrate. The wells with large initial potentials (Approximately 16%) were not treated. The areas with the largest Final Open Flow gauges appear to be located on the flanks of the Depositional Highs and decrease both on the highs and into the lows. A variable contour interval was used: 0-50-100-250-500-1000 MCF/D (4).

The Total Accumulated Production Map, FIGURE 14, was made from collected data. Accumulated production varies from almost zero to a maximum of 909,000,000 cfg per well. The accumulated production shows the largest producers to be located on the flanks of the Depositional Structure. The Production patterns are similar to the Initial Flow patterns. A variable contour interval was used: 0-50-100-250-500-1000 MMCF/D.

CONCLUSIONS

Gas has been produced in the Cottageville Field for almost 50 years, and still has productive potential. There is little or no direct relationship of the producing field limits to present day shale structure, however, Depositional Structural approximations appear to have a direct relationship to depositional compaction fracture reservoir development and the better producers.

There are additional significant studies that could be made from the published data.

This study was based upon available data and is subject to refinement by utilization of additional data. It serves to prove that the Unconventional Exploration Technique works. The study demonstrates that fractured shale reservoirs can be predicted, projected and possibly developed on a systematic economic basis. Since the interpretations are based on structure, the more accurate the structure, the more accurate the approximation of depositional structure. Some fracture intervals may be unpredictable such as those that might result from submarine currents. Regional influences, rate of depositional slope and sediment source are also items for consideration and study.

ACKNOWLEDGEMENTS

The author wishes to thank Mitchell Energy Corporation for permission to participate in the Eastern Gas Shale Program and to prepare this paper for presentation. A special note of appreciation is extended to the Morgantown U.S. D.O.E. staff and the W. V. U. authors who prepared and presented the publications which made this paper possible. Personal communications with E. B. Nuckols and Columbia Gas Research staff members was very helpful. The assistance of Mitchell Energy's staff in preparation of the paper was greatly appreciated.

REFERENCES

1. Larese, R. E. & Heald M. T., 1977, "Petrography of Selected Devonian Shale Core Samples From the CGTC 20403 & CGSC 11940 Wells Lincoln & Jackson Counties, West Virginia." MERC/CR - 77/6, ERDA, Morgantown, W. Va.

2. Marten, P. & Nuckols, E. B., 1976, "Geology & Oil & Gas Occurrence in the Devonian Shales: Northern West Virginia, in Devonian Shale Production & Potential" Proceedings of the 7th Appalachian Petroleum Geology Symposium, MERC SP - 76/2, ERDA, Morgantown, W. Va. P. 20-40.

3. Nuckols III, E. B., 1977 "Production Characteristics of Devonian Organic Shales in the Cottageville Field Near Ripley, W. Va." First Eastern Gas Shale Symposium, October 1977 Morgantown, W. Va. EGS - 33 pages 503-523.

4. Nuckols III, E. B., 1978 "Exploration Parameters Derived from Historical Devonian Shale Production in Western West Virginia" Second Eastern Gas Shales Symposium, October 1978, METC/SP - 78/16, Vol. 1, EGS - 75, pages 169-185.

5. Patchen, D. G. & Larese, R. E., 1976, "Stratigraphy & Petrology of the Devonian Brown Shale in West Virginia in Devonian Shale Production & Potential," MERC/SP - 76/2, ERDA Morgantown Energy Research Center, Morgantown W. Va.

6. Tegland, E. R., 1977, "Update Concerning the Three - Dimensional Seismic Investigations in the Cottageville Field," pages 2-16, (EGS-2) First Eastern Gas Shales Symposium, Preprints.

7. De Wys, J. N. & Shumaker, R. C. 1978, "Pilot Study of Gas Production Analysis Methods Applied to Cottageville Field," MERC/CR - 78/6.

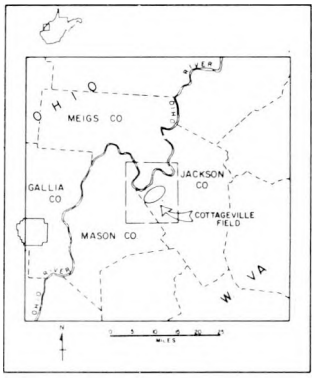


FIGURE 1

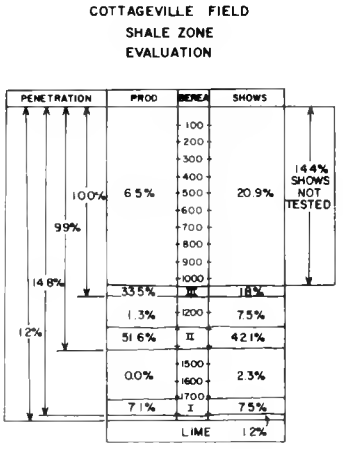


FIGURE 2

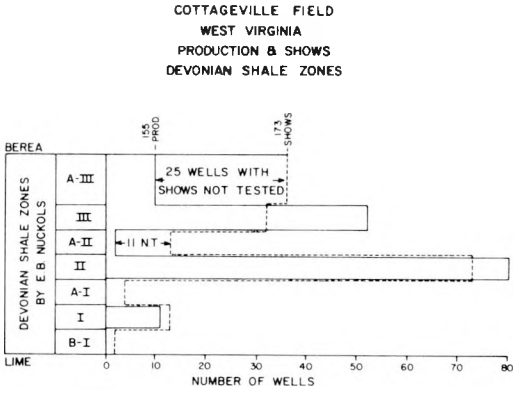


FIGURE 3

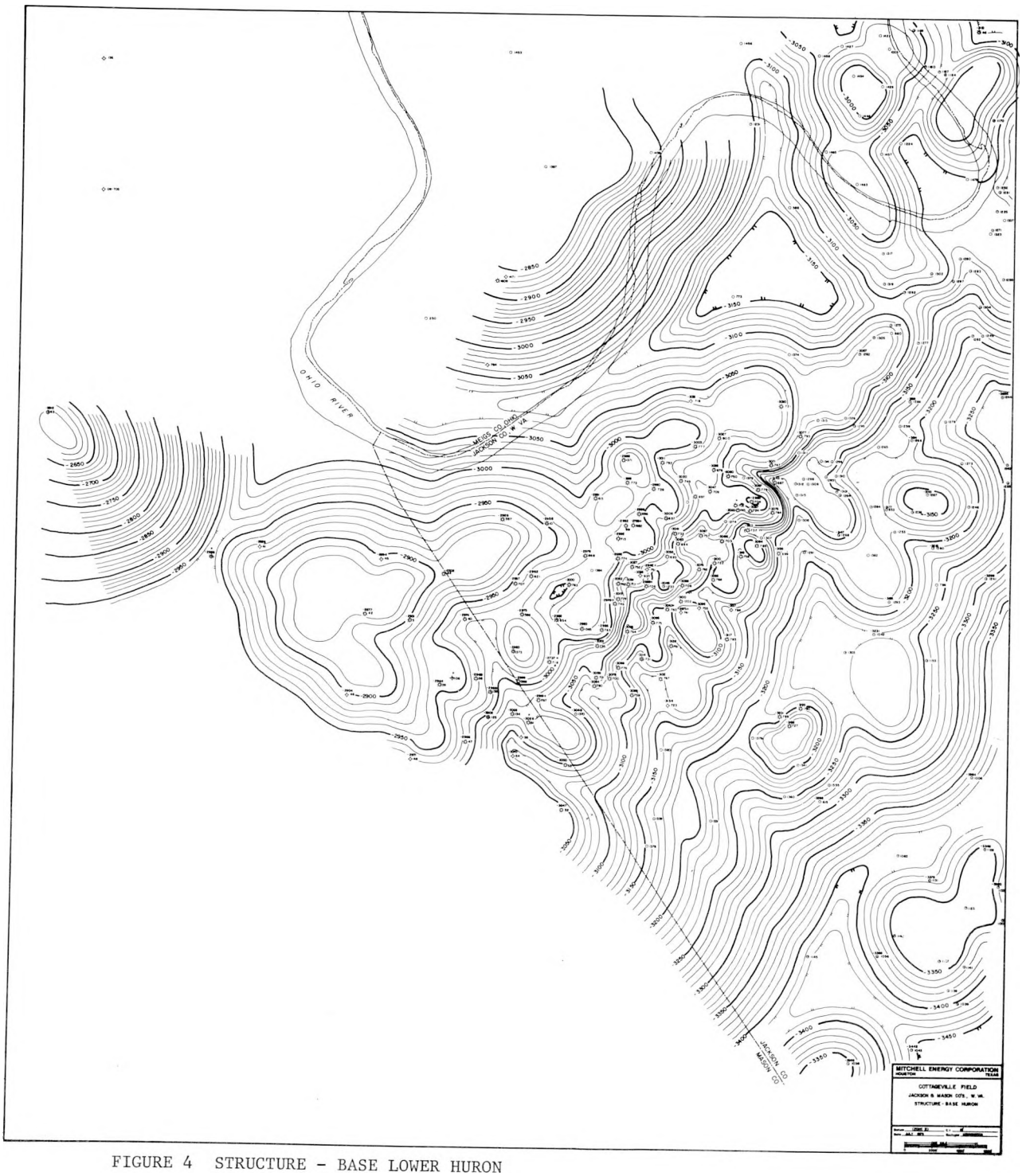


FIGURE 4 STRUCTURE - BASE LOWER HURON

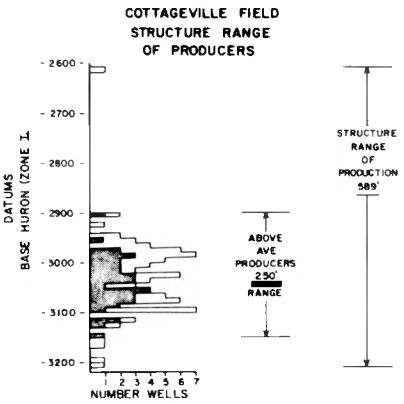


FIGURE 5

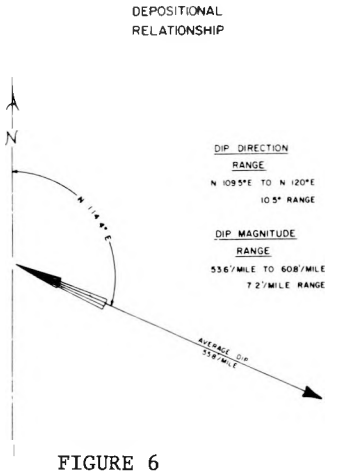


FIGURE 6

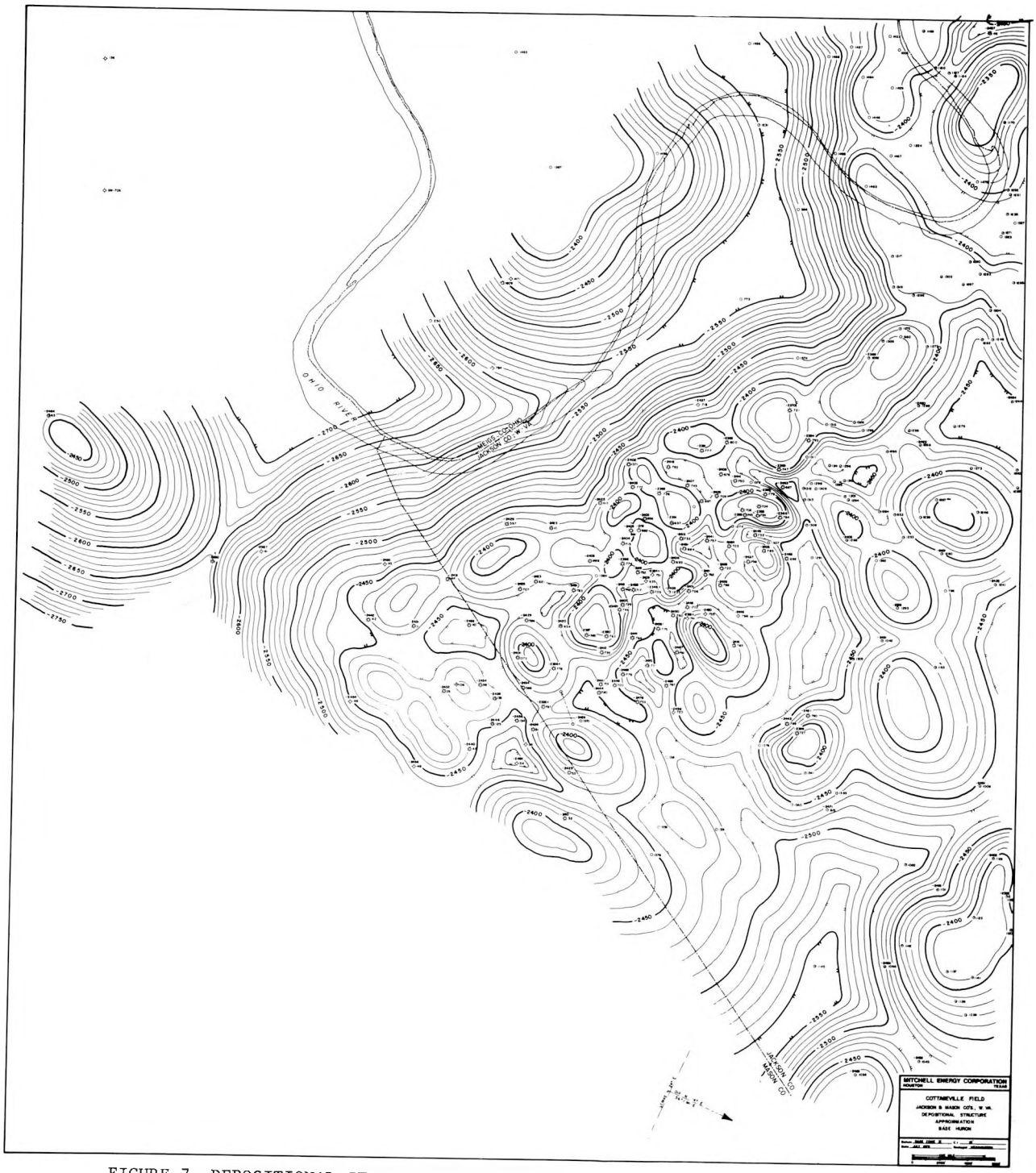


FIGURE 7 DEPOSITIONAL STRUCTURE APPROXIMATEION

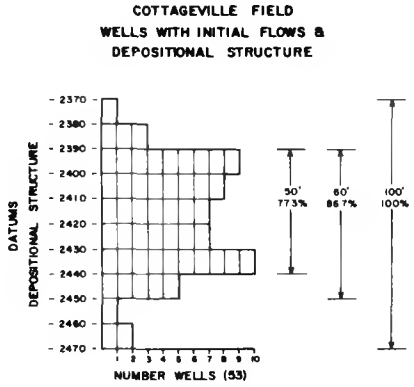


FIGURE 8

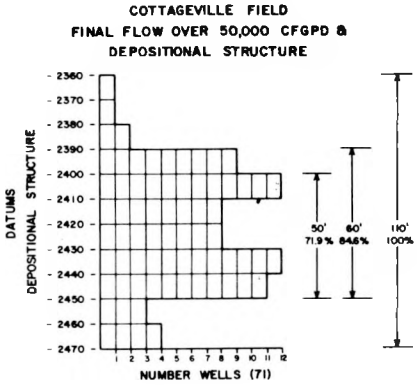


FIGURE 9

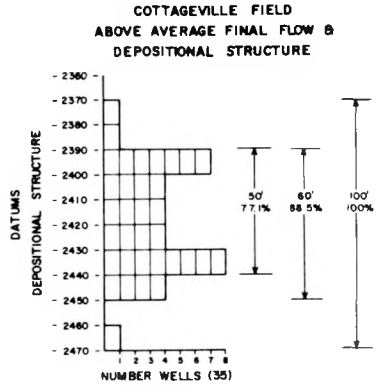


FIGURE 10



FIGURE 11 POTENTIAL DEPOSITIONAL INDICATIONS

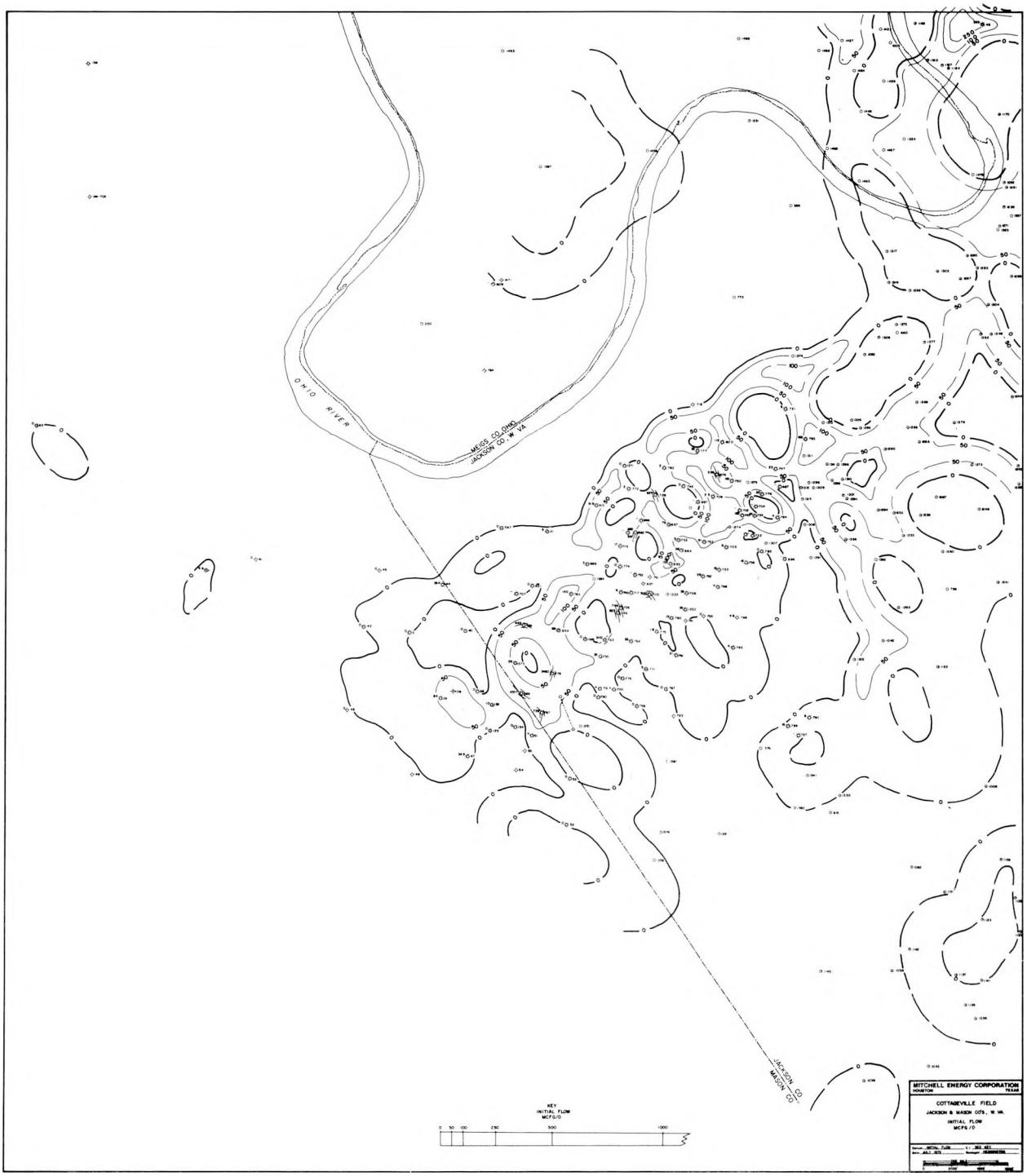


FIGURE 12 INITIAL OPEN FLOW

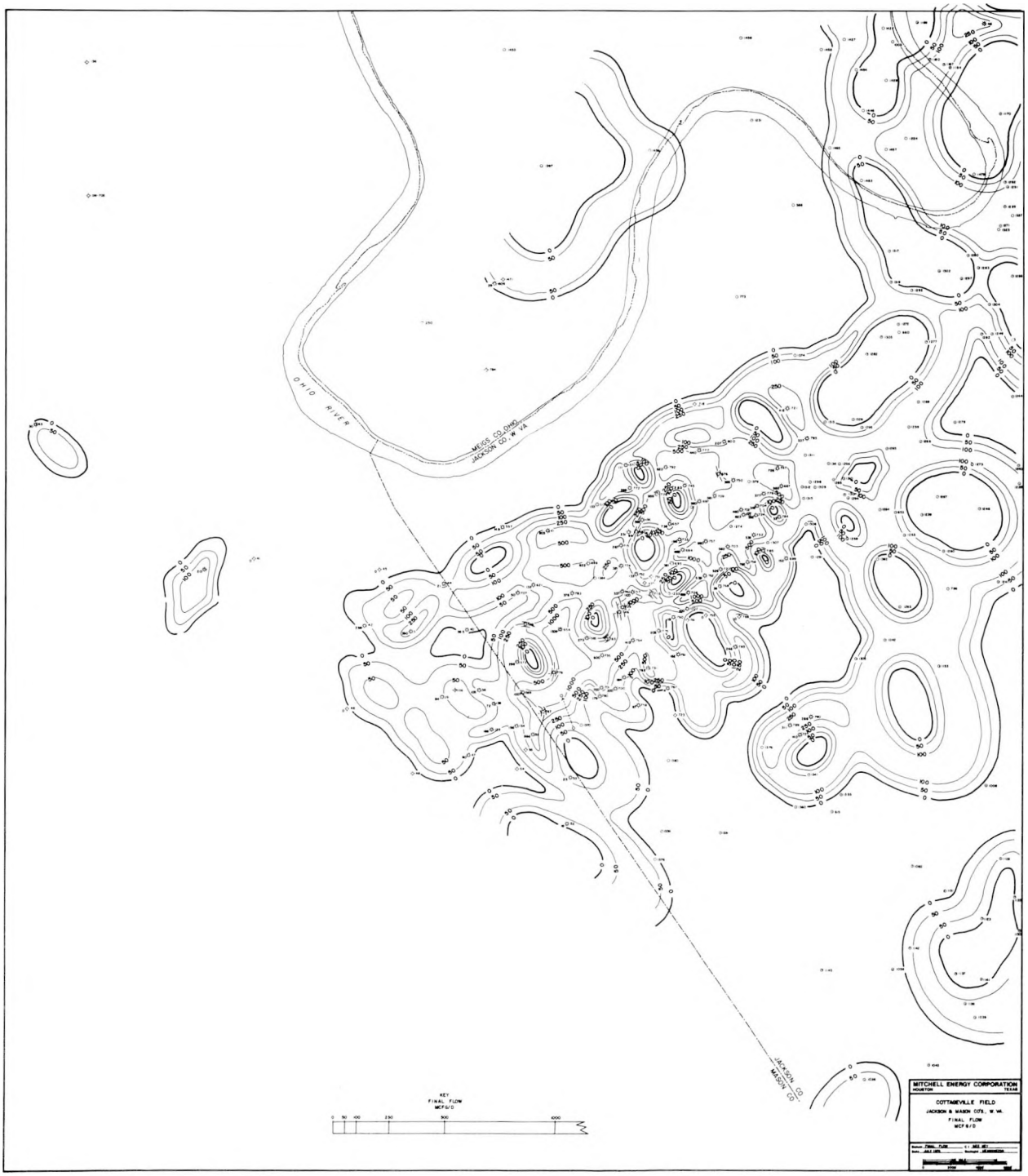


FIGURE 13 FINAL OPEN FLOW

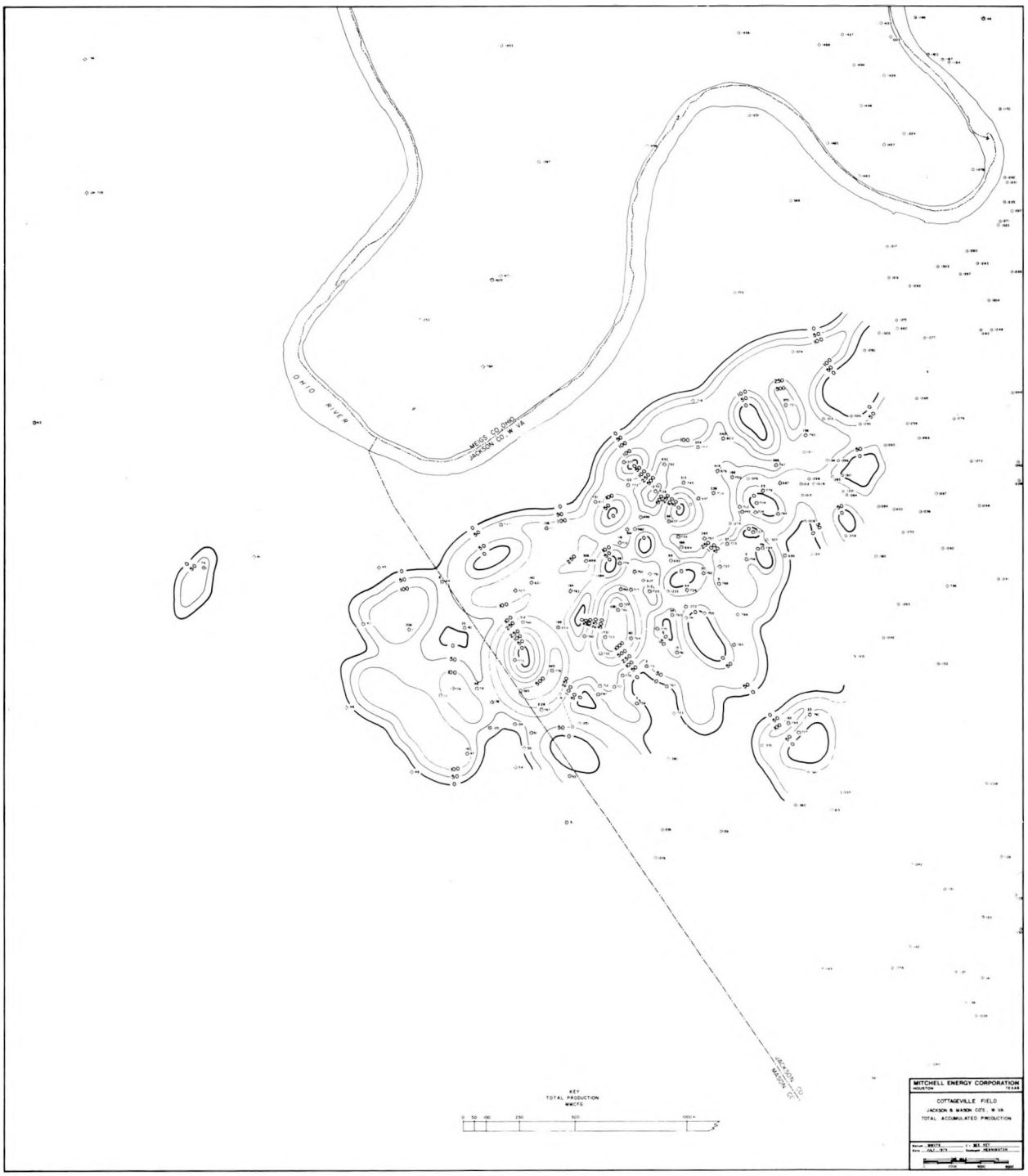


FIGURE 14 TOTAL ACCUMULATED PRODUCTION

PROJECTION OF FAVORABLE GAS-PRODUCING AREAS FROM PALEOENVIRONMENTAL AREAS

R.E. Zielinski, J.A. Dixon

R.D. McIver

Mound Facility

Geochem Research

ABSTRACT

Paleoenvironmental biofacies analysis of recent wells in dark Devonian shales in the Appalachian Basin has shown that these facies can be projected to areas with no control points. In particular, the facies distribution in Perry County, Kentucky, were found to be precisely those that were predicted earlier from biofacies and organic geochemical data from the VA-1 well in Wise County, Virginia, and the KY-2 well in Martin County, Kentucky. This demonstrates the importance of these data in assessing the volume of gas in the shale throughout the basin as well as in selecting future test sites.

The recent biofacies and geochemical work together with a review of the tectonics of the basin have contributed to an evolving interpretation of the geologic control of the biofacies.

While a marine environment persisted throughout the Upper Devonian over the Appalachian and Illinois Basins (and probably the Michigan Basin), dynamic emergent areas controlled an intermittent introduction of large amounts of organic matter. Large amounts of non-marine organic matter were periodically transported into the basin from dynamic source provenance to the Southeast; massive "blooms" of Tasmanites intermittently spread both east and west from the edges of the emerging Cincinnati Arch. At times one or the other of these organic types swept entirely across the basins; at other times a more normal open marine biota fluorished and was deposited, probably under the influence of connections to the open seas to the south and northwest, the north being closed by the collision and suturing of continental plates and the east by the growing Appalachian Mountains.

Note: Paper not available at time of publication.

THE CHARACTERIZATION OF THE PRODUCTION MECHANISM IN THE DEVONIAN SHALE AND ITS SENSITIVITY TO CHANGES IN VARIOUS RESERVOIR PARAMETERS

W. K. Ford

Senior Engineer

INTERCOMP Resource Development and Engineering, Inc. Houston, TX

Mr. Ford received his B.S. and M.S. degrees in Petroleum Engineering from Mississippi State University.

He spent five years with Chevron Oil Company in various production and reservoir engineering assignments in Mississippi and Louisiana. From September, 1974 to April, 1977, he was a member of Chevron's specialized well log analysis group in Houston developing and applying computer techniques to analyze well logs. In April of 1977, he was transferred with Chevron into a reservoir simulation group responsible for the reservoir management of certain Saudi Arabian fields operated by the Arabian American Oil Company.

In November, 1977, he joined the consulting firm of H. J. Gruy and Associates in Houston as a Senior Reservoir Engineer where he conducted numerous property evaluation studies including log analysis, reserve estimates, and production forecasting.

In June of 1978, he joined INTERCOMP Resource Development and Engineering, Inc., in Houston as a Senior Engineer and was appointed Project Manager of the INTERCOMP's study of the Eastern gas shale.

ABSTRACT

As part of the U.S. Department of Energy's Eastern Gas Shales Project, we undertook the task of making a comprehensive analysis of the production of natural gas from the Devonian shales of Eastern United States. This paper presents results of a part of that study.

Two basic reservoir simulation models were formulated for our analysis. Only the results from one of the models are being reported in this paper, that being a single well radial gas model of a well located in Lincoln County, West Virginia. The model was used to study whether the gas in the Devonian shale was more likely present in a dual-porosity system or single-porosity system. The sensitivity of the production characteristics to changes in various reservoir parameters and the validity of conventional pressure analysis techniques were also studied.

The results indicate that it is virtually impossible to discern between the two systems because, within the range of measured parameters, either system will adequately describe the production history being studied. The production characteristics are most sensitive to reservoir permeability and induced fracture half-length. The study also showed that most conventional pressure analysis techniques are valid in the Devonian shale environment.

INTRODUCTION

The United States Department of Energy is supporting cooperative research for enhanced gas recovery in a major effort to help reverse our country's decline in natural gas reserves. A potential major source of natural gas is the Devonian shales of the Appalachian Region, estimated to contain in the hundreds of trillion cubic feet of natural gas. As part of DOE's Eastern Gas Shales Project, we undertook the task of making a comprehensive analysis of the production of natural gas from the Devonian Shales. This paper presents the results of some of the work done in that effort.

One objective of this study was to identify through the validation of a numerical model the physical processes considered to be the most important in the production of gas from shale. There are two widely held theories on the occurrence of natural gas in the Devonian shales. One theory, referred to as the single porosity theory, is that gas entrapment occurs in natural fractures and a macroporous system as free gas and is produced from that system according to Darcy's Law. The second, referred to as a dual-porosity system, assumes that entrapment occurs not only by containment in fractures and macropores but also by an adsorbed layer on the internal surfaces of the shale matrix itself. The adsorbed gas phase diffuses to the fracture system and is then produced by Darcy Law flow as the pressure at the wellbore is reduced.

A single-well, radial gas model incorporating the adsorbed gas concept with conventional Darcy flow in porous media was used in an attempt to identify the presence of such a dual porosity system. Pressure test and production data from a well in Lincoln County, West Virginia was used as a validation test of the model.

MODEL DESCRIPTION

The program numerically solves the non-linear partial differential equation which describes transient gas flow in cylindrical coordinates. An r-z-θ (radial-vertical-angular) coordinate system is employed. Figure 1 illustrates the geometry.

Reservoir heterogeneities are represented by variable-thickness layers with horizontal and vertical permeabilities and porosities which can vary arbitrarily with layer radius, or angular segment as specified by input data. Simultaneously with solution of the equation describing flow in the reservoir, the models solves equations accounting for skin of each layer and afterflow into the wellbore. The calculations account for transient effects of turbulence throughout the reservoir and not just in grid blocks near the wellbore. Also included in the program are equations describing the gas diffusion process in the shale matrix and the linkage of this mechanism to the Darcy flow taking place in the fracture or macroporous system.

If the user specifies well rate, constant or variable, then the model calculates bottomhole and wellhead flowing pressures. Alternately, flowing bottomhole pressure can be specified and the model then calculates production from each layer, well total rate, cu ·lative production and flowing wellhead pressure.

Production rate from each layer during flow and wellhead shut-in is printed every time step. These results show any recirculation through the wellbore after wellhead shut-in.

A direct method of solution is used so that the user need not select iteration parameters. The difference equations are implicit so that the model is unconditionally stable.

Completion interval, skin factor and rate specification, (i.e., fixed rate or bottomhole pressure) can vary with time.

A generalized grid system used in a radial model is shown in Figure 1. A fracture (shaded area) is modelled as a narrow segment that extends radially a specified number of grid blocks and vertically a specified number of layers. Reservoir and fracture properties are assigned to each grid block. PVT relationships and well data are input along with any variation of permeability and porosity. Assuming symmetry of the reservoir around the well, it is necessary to simulate only one reservoir quadrant as shown in Figure 2. Production from the quadrant is then simulated as one-fourth total well production, resulting in a significant savings in computer time.

COLUMBIA GAS TRANSMISSION CORP.'S WELL NO. 20403

Selected for study was Columbia Gas Transmission Corporation's Well No. 20403, which was drilled in February, 1976, in Lincoln County, West Virginia, as one of three wells in a project Columbia Gas had undertaken to investigate the technical and economic effectiveness of massive hydraulic fracturing (MHF) techniques for enhanced gas recovery from the Devonian shales.

The Devonian shale in this well is subdivided into several productive zones separated by non-productive less organic intervals. For our study, only the Lower Brown/Lower Gray shales, hereafter referred to as Zone 1, and the Middle Brown shale, hereafter referred to as Zone 2, were considered. These zones are shown on the log section presented in Figure 3. Well No. 20403 was initially tested in Zone 1 before any fracture treatment was conducted. The results were inadequate for analysis. Additional tests were attempted after massive hydraulic fracturing Zone 1 but results, again, were questionable. There was, therefore, no usable test data obtained on Zone 1 (Lower Brown/Lower Gray).

In October, Zone 1 was isolated in the wellbore and Zone 2 (Middle Brown shale) was perforated from 3409 feet to 3651 feet. Since the open flow potential of this zone before fracturing (95 MCFD) was suspiciously close to that of Zone 1 after fracturing (110 MCFD), an interference test was conducted. The test indicated there was communication between the zones and it was evident that the MHF treatment on Zone 1 propagated vertically into the untreated Zone 2. Nevertheless, a flow test of 168 hours was conducted in this interval. Flow rates during the test did not stabilize until about 60 hours into the test. This, along with the uncertainty of which zone the production was coming from, makes any analytical analysis questionable.

A pre-frac buildup of 354 hours was then conducted from October 26 to November 10. A downhole shut-off tool was used to shut the well in, thus minimizing the wellbore storage effects. The initial bottomhole pressure extrapolated from this buildup was 269 psig.[1]

On November 15, 1976, Zone 2 was fractured (MHF) with 320,000 gallons of foam and 439,000 pounds of sand. The well was cleaned-up for an unknown length of time after which it was shut-in until February 8, 1977, when a 187 hour post-frac flow test was conducted at a nearly constant rate averaging 23.6 MCFD. Again due to indicated communication, the interval from which the production was coming is uncertain.

Following the post-frac flow test, the well was again shut-in with a downhole shut-off tool and a 384.8 hour pressure buildup test was run.

NUMERICAL MODEL AND RESULTS

In an effort to identify the physical processes contributing to the production of Devonain shale gas wells, we employed the three-dimensional radial gas simulator to history match the pre-frac drawdown and buildup tests and the post-frac drawdown and buildup tests conducted on Zone 2, the Middle Brown shale interval of Columbia Gas No. 20403. Because of the established communication between zones we assumed in formulating the model that production was coming from both Zone 1 and Zone 2 over a total interval of 622 feet. The intervals correspond to those used by H. K. van Poollen and Associates in their conventional analysis of the data.[1]

From a review of core data from the Devonian shales, average porosity is about 3-4 percent, and water saturation is 65-75 percent. The core analysis on Columbia Well No. 20403 resulted in anomalously low values of porosity (less than 1%) and water saturation (0.0). An effective gas porosity of 1.0 to 1.5 percent was used as a beginning value in history matching. An initial value of permeability of 0.15 millidarcies was used based on a review of the conventional analysis of the test data. The adsorption data used in this study was that reported by Thomas and Frost[2] on a shale well in Illinois. The data is presented in Figure 4. This was the only shale adsorption data available in the pressure range of the test.

The grid system used in modelling the test data was a configuration of the generalized model illustrated in Figures 1 and 2. Since it was fairly certain that gas produced during the pressure tests was from both zones even though only Zone 2 was open to the wellbore, a two layer model configuration was used. It consisted of eight radial blocks and 5 angular segments. Only the top layer was open to production and vertical flow was allowed only in the fracture. For purposes of modelling, a drainage boundary was chosen such that there would be no significant pressure reduction in the outer most grid cells. The fracture was modelled by an angular segment of .01 degree scaled internally by the simulator to represent a constant-width fractur of .05 inches. Permeability within the fracture was set at 250,000 millidarcies based on a 20-40 mesh sand proppant. An initial bottomhole presure of 284 psia[1] was used in the model. Wellbore storage effects were neglected since a downhole shut-off tool was used during the tests.

An attempt to history match simulated data with the measured test data was made by varying permeability, porosity, fracture length, drainage radius, and the adsorption diffusion constant. The best fit was obtained with the following parameters:

	Pre-Fracture Test	Post Fracture Test
Interval Thickness, h, ft.	622	622
Effective Gas Porosity, Ø	.015	.015
Permeability, k, md.	.05	.1
Fracture Half-Length, x_f, ft.	24	54
Drainage Radius, ft.	1200	1200
Adsorption Diffusion Constant cm/sec^2	10^{-11}	10^{-11}

Only the top 205 feet of the total 622 foot interval was open to the wellbore. Figures 5 through 7 present the results of our best match of the pre-frac and post-frac drawdown and buildup. During simulation of the pre-fracture drawdown, simulation pressures were set equal to measured pressures and the quality of match judged on resultant computed flow rates compared to measured flow rates. Since only one quadrant of the total well drainage volume was modelled, the flow rates plotted are one-fourth the total well rate.

The quality of the history matches of the test data are probably within the boundaries of the measured data. Two possible sources of error in the measured data that may have affected the pressure match are:

(1) The flow rates during pre-frac drawdown were continually decreasing and probably difficult to measure accurately.

(2) There appears to be an anomaly in the measured pressures during the post-frac drawdown when the pressure bombs were changed.

The primary objective of this study was to identify the physical processes considered to be the most important in the production of gas from shale. Or even more concisely, does adsorption/desorption play a major role in gas production. After obtaining the above history matches, a study was made to see what effect removing the adsorption mechansim would have on the history match and could a match be obtained without desorption/adsorption. Figures 8 through 10 present the results of the pre-frac and post-frac tests using the same parameters as were used for Figures 5 through 7 except adsorption was omitted.

Although omitting the desorption/adsorption contribution did generally adversely affect the pressure matches, it did not produce a drastic change and could probably be compensated for by varying some other parameter. This illustrates the difficulties encountered in conclusively identifying a dual

porosity system in the Devonian shale. As indicated above the solution is not unique. Within the range of acceptable values of reservoir parameters, a satisfactory match can be made with either a single porosity system (no adsorption) or a dual porosity system (with adsorption).

Although test data for this well was history matched relatively well, the true test of the model is in accurately predicting future production. Figure 11 presents a comparison of an eight month prediction and actual production data for the well using the adsorption model. The simulated production matches the actual data very well after about 130-140 days. Prior to that time, the well is believed to be cleaning up resulting in a poor match between actual data and simulated data, which do not include the effects of well cleanup.

SENSITIVITY ANALYSIS

The history matched adsorption model discussed above was used to investigate the sensitivity of Devonian shale production characteristics to changes in various reservoir and induced fracture properties including: porosity and permeability, interval thickness, drainage radius, adsorption diffusion constant, adsorption data, induced fracture half-length, induced fracture permeability, matrix turbulence, and fracture turbulence. The analysis was carried out by varying the parameters being studied from those of post-fracture history matched model of the 20403 well. The base parameters were:

Effective Gas Porosity, $\emptyset$	= .015
Permeability, k	= 0.1 md
Interval Thickness, h	
Layer 1	= 205 ft
Layer 2	= 417 ft
Drainage Radius, r_e	= 1200 ft
Adsorption Diffusion Constant, D	= 10^{-11} cm^2/sec
Fracture Half-Length, x_f	= 54 ft
Fracture Permeability, k_f	= 250,000 md
Matrix Turbulence, β_m	= 0.0 ft^{-1}
Fracture Turbulence, β_f	= 0.0 ft^{-1}

The base adsorbed gas volume was that derived from the data of Thomas and Frost.

The sensitivity analysis indicated that reservoir permeability and fracture half-length were two parameters having the greatest effect on production characteristics. Figures 12 and 13 are plots of rate divided by four and cumulative production versus time in days, respectively, for values of reservoir permeability from 0.05 md to 5 md. Figures 14 and 15 are similar plots presenting the effects on production of varying the fracture half-length from zero to 1200 feet.

The remaining parameters all had lesser effects on the production characteristics and therefore the results have not been included in this paper. Worth noting, however, are the results of the drainage radius sensitivity which indicates that even after twenty-five years of production the volume outside a drainage radius of 1800 feet is hardly affected. This has also been noted in other work on the Devonian shales. Also from the sensitivity analysis are indications that the adsorption diffusion constant increases in importance as the drainage radius is reduced (and the drainage volume is more significantly depleted over the 25 year prediction).

VALIDITY OF CONVENTIONAL PRESSURE ANALYSIS TECHNIQUES

One of the primary tools for evaluating a reservoir is that of running well pressure tests. In the Devonian shale (as well as other tight gas sands) the procedure is complicated by the inherent nature of the reservoir, that is, very low permeability that requires long test times and also the fact that the wells usually have to be fractured before they will produce. Another uncertainty present in the Devonian shale formation is the effect of the adsorbed gas mechanism on the conventional analysis techniques. Because of this uncertainty, an investigation was made into the applicability of conventional analysis techniques in the Devonian shale.

The applicability of conventional pressure analysis techniques in the Devonian shale reservoirs was studied using the single well radial flow model discussed earlier in this paper. For simplicity, only one layer was used in the model. The model was used to generate a 90 day drawdown followed by

a 30 day buildup. This data was then analyzed by conventional transient pressure methods and the results compared to the parameters input into the model. The basic data input into the model were:

Effective Gas Porosity, Ø	= .015
Permeability, k	= .1 md
Interval Thickness, h	= 205 ft
Drainage Radius, r_e	= 1200 ft
Fracture Half-Length, t_f	= 28 ft
Initial Pressure	= 265 psia

A constant flow rate of 20 MCFD was used to generate the drawdown data. A semilog plot of the drawdown and Horner plot of the buildup are presented in Figure 16 and Figure 17, respectively. Conventional analysis techniques gave the following:

	Drawdown	Buildup
Slope of semi-log straight line, 10^4 psi^2/cp/cycle	89	88
kh, md-ft	20.8	21.0
k, md (h=205')	.101	.102
S, skin factor	-4.1	-4.2
x_f, fracture half-length, ft		27

When the above analytical results are compared to the input parameters, it is apparent that conventional techniques do apply in the Devonian shale enviroment for the estimation of basic parameters (k, S, x_f).

As a further test of the analytical techniques in an adsorption/desorption environment, the model was used to generate an extended drawdown, or reservoir limit test. A drawdown test of 600 days at a constant rate of 10 MCFD was simulated to insure that the pseudo-steady state flow regime was reached. Both adsorption and no adsorption cases were run and the data in the pseudo-steady state region analyzed with conventional techniques to obtain drainage volume. The results are presented in Figures 18 and 19. A comparison of results is presented below.

	Drainage Volume, ØhA
Model	13.9×10^6 ft^3
Conventional Reservoir Analysis	
Without Adsorption	15.4×10^6 ft^3
With Adsorption	23.1×10^6 ft^3

The estimated drainage volume by conventional techniques for the no adsorption case (15.4×10^6 ft^3) is in relatively good agreement with actual volume of the model (13.9×10^6 ft^3). However, the drainage volume estimated from the adsorption case (23.1×10^6 ft^3) is too great, although not nearly by the amount of the calculated adsorbed gas volume in place (approximate 140×10^6 ft^3). It should be noted also that the pressure versus time plot (Figure 19) for the adsorption case appears to continue to decrease in slope even after 600 days. This study indicates that a reservoir limit test gives erroneously high values of drainage volume. The results were expected due to the free gas in the void volume being supplemented by the contribution of the gas from the adsorbed phase. This error should not be of too great a concern since the time requirement for a reservoir limit test in this environment makes it somewhat impractical.

CONCLUDING REMARKS

Our study has demonstrated the difficulty of isolating the production and storage mechanism of the Devonian shale. From the results we, unfortunately, cannot discern between the single and dual porosity systems. Although it probably exists as evidenced by laboratory measurements and outgassing

studies, the dual porosity system appears to be important only in that it extends the life of a well beyond that of a well with only a free gas phase. Sensitivity studies indicate that the production rate is very dependent on the effective reservoir permeability and that the rate can be significantly increased by an induced fracture of relative long half-length. The sensitivity analysis also indicated that the adsorption diffusion constant becomes increasingly important as the system is depleted. This suggests that one area of needed research might be in determining a method of altering the diffusion constant.

This study raised the level of confidence in using conventional techniques to analyze pressure data from Devonian shale reservoir. It showed that most conventional techniques are applicable in the shales with the exception of those yielding drainage volume.

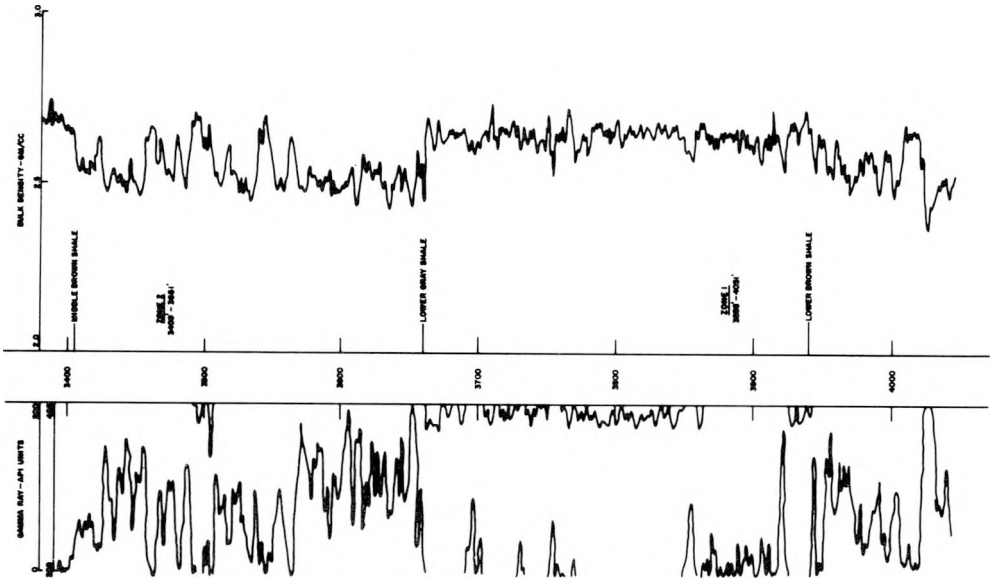
ACKNOWLEDGEMENTS

The author wishes to thank Ken Ancell, Harvey Price, and Walter Dowdle for their suggestions and comments during the course of this study and in preparation of this paper.

REFERENCES

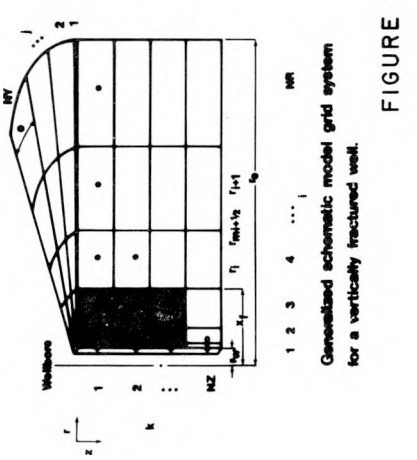
1. "Analysis of Columbia Gas Transmission Corporation's Well No. 20403, Lincoln County, West Virginia", (Preliminary Report), H. K. van Poollen and Associates, Inc., Colorado, April, 1977.

2. Thomas, Josephus, Jr., and Frost, Robert R., "Internal Surface Area and Porosity in Eastern Gas Shales from the Sorption of Nitrogen, Carbon Dioxide and Methane - A Status Report", Illinois State Geological Survey, Urbana, Illinois.



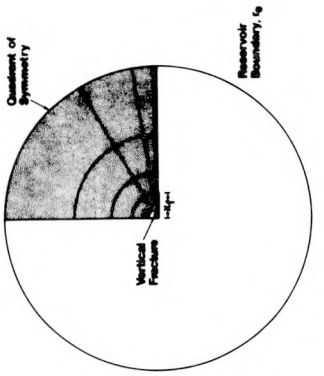
LOG SECTION COLUMBIA GAS WELL NO. 20403

FIGURE 3



Generalized schematic model grid system for a vertically fractured well.

FIGURE 1



Schematic grid system for vertically fractured well examples.

FIGURE 2

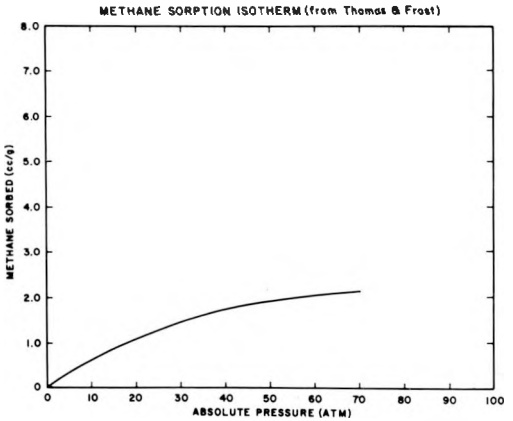


FIGURE 4

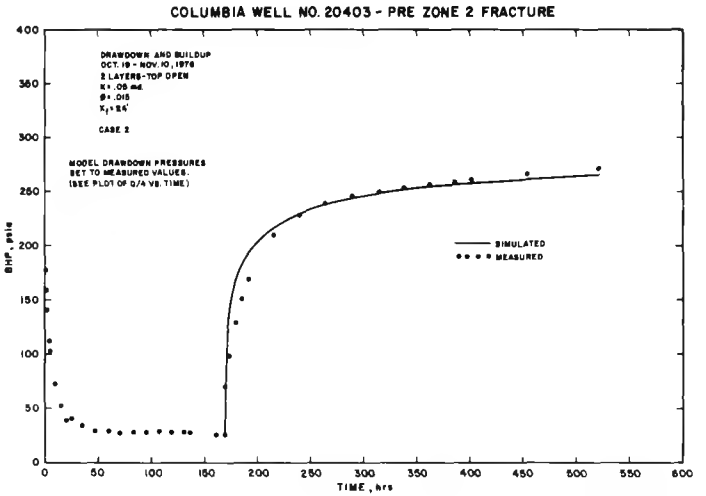


FIGURE 5

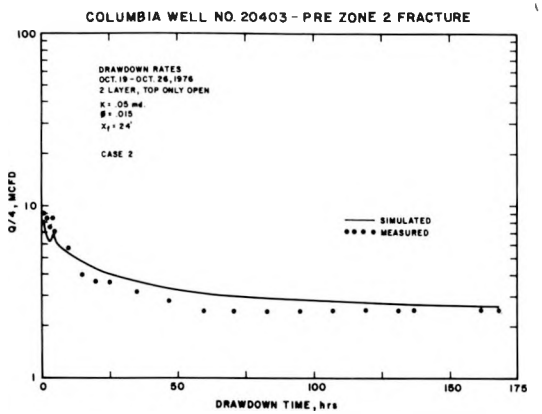


FIGURE 6

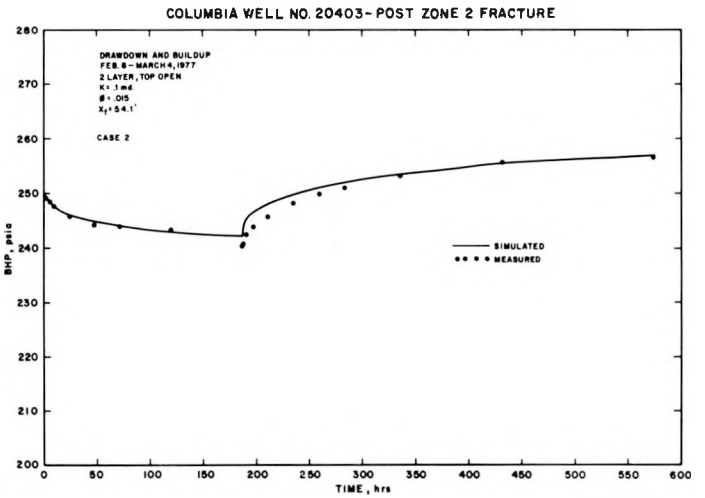


FIGURE 7

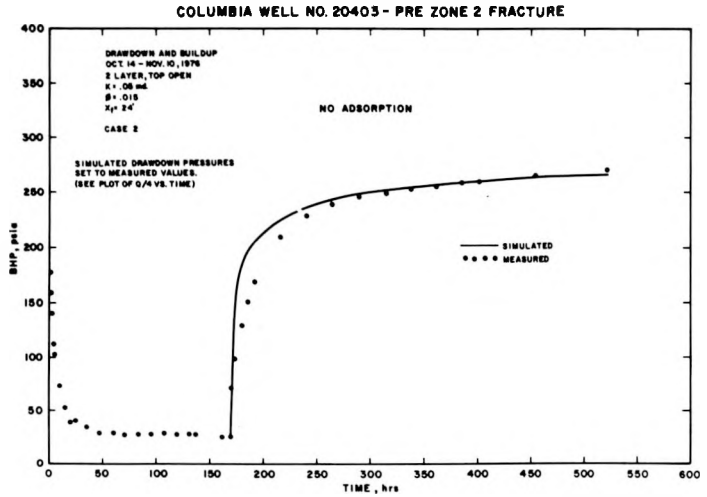


FIGURE 8

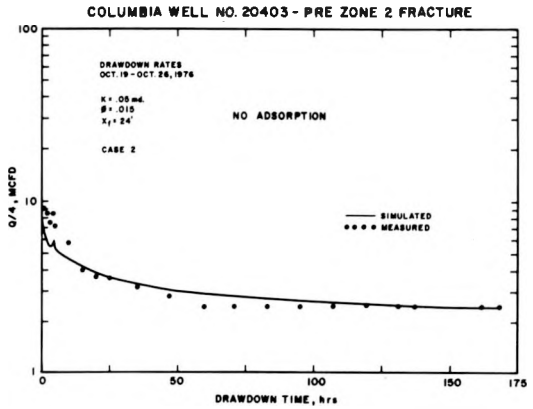


FIGURE 9

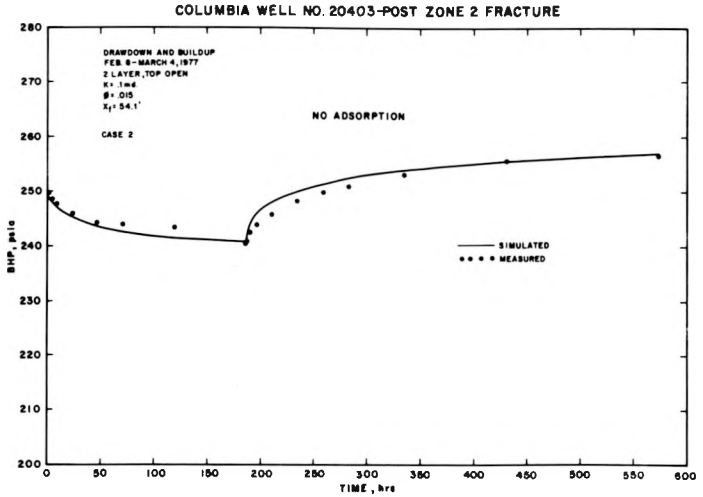


FIGURE 10

COLUMBIA GAS WELL NO.20403
ACTUAL VS. SIMULATED PRODUCTION RATES
MAY—NOVEMBER,1978

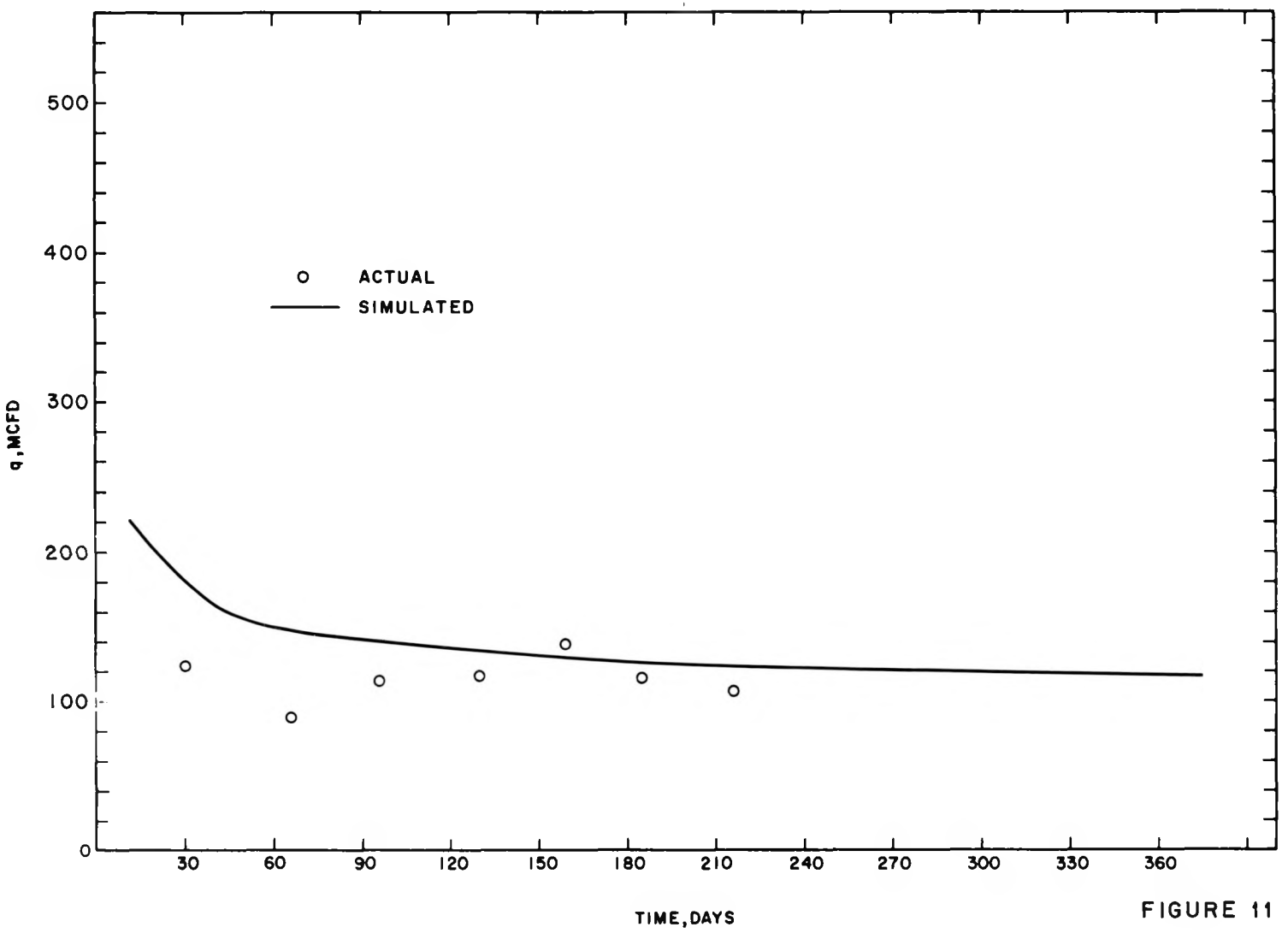


FIGURE 11

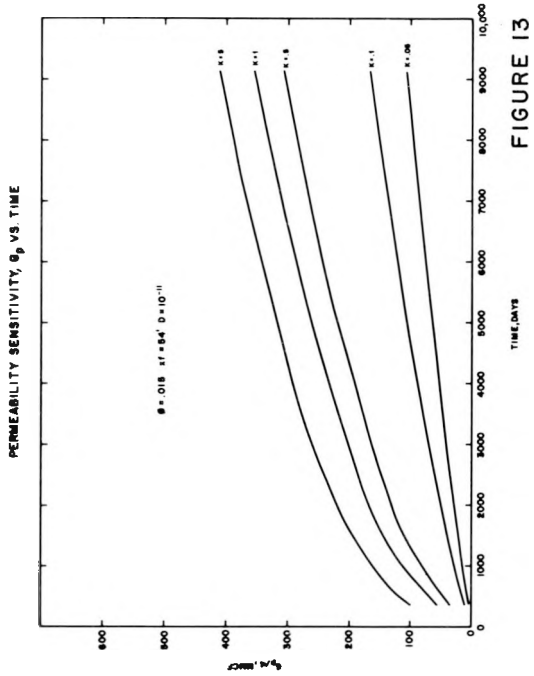


FIGURE 13

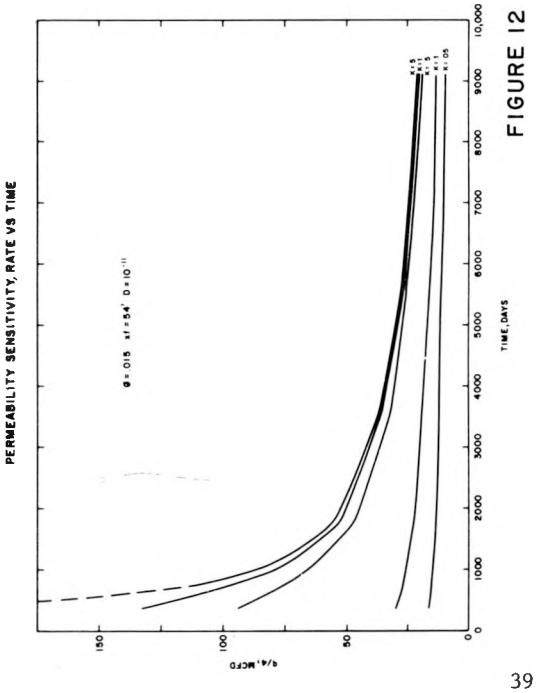


FIGURE 12

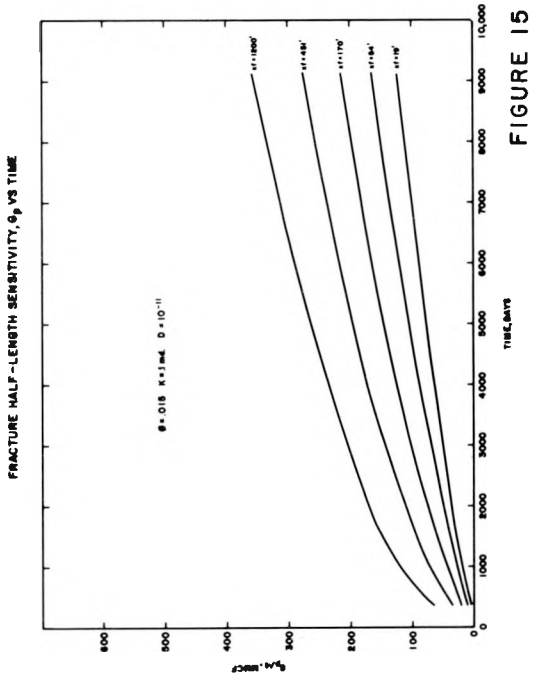


FIGURE 15

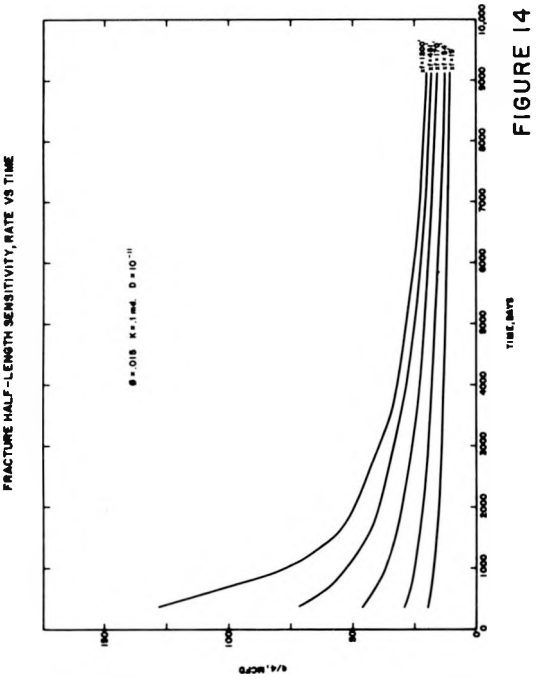


FIGURE 14

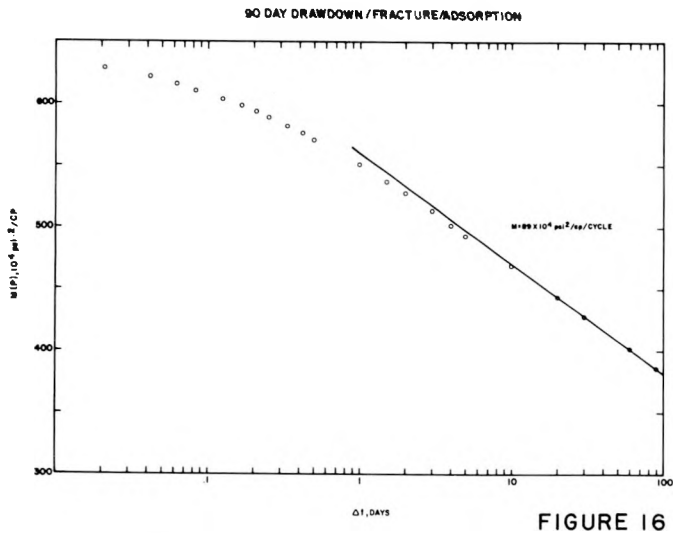


FIGURE 16

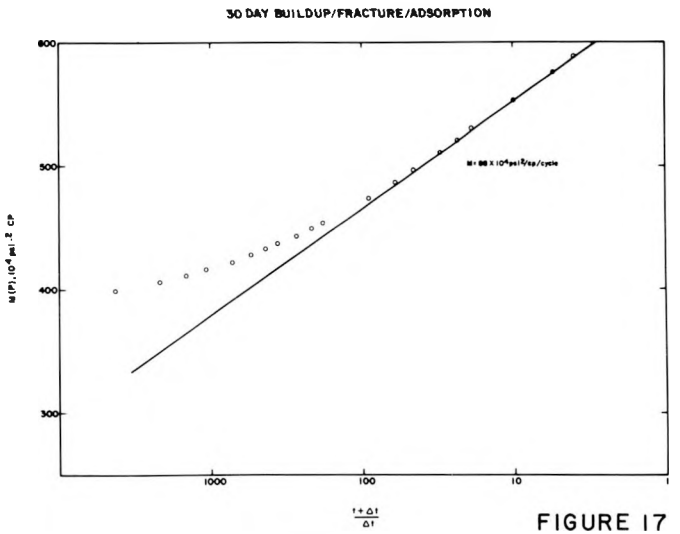


FIGURE 17

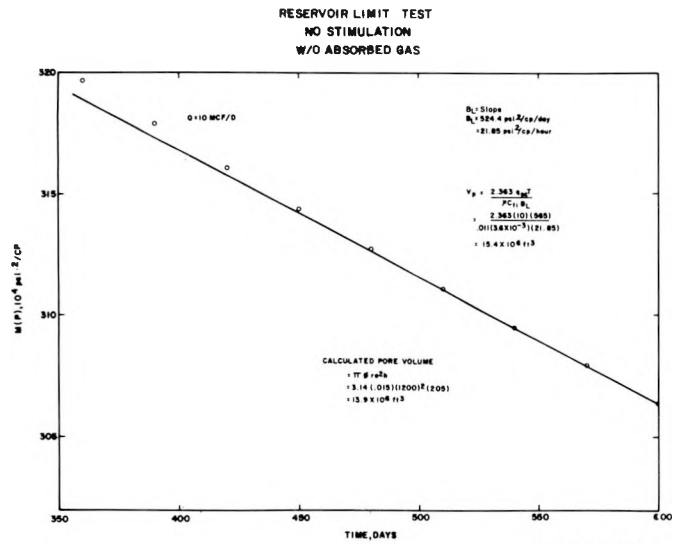


FIGURE 18

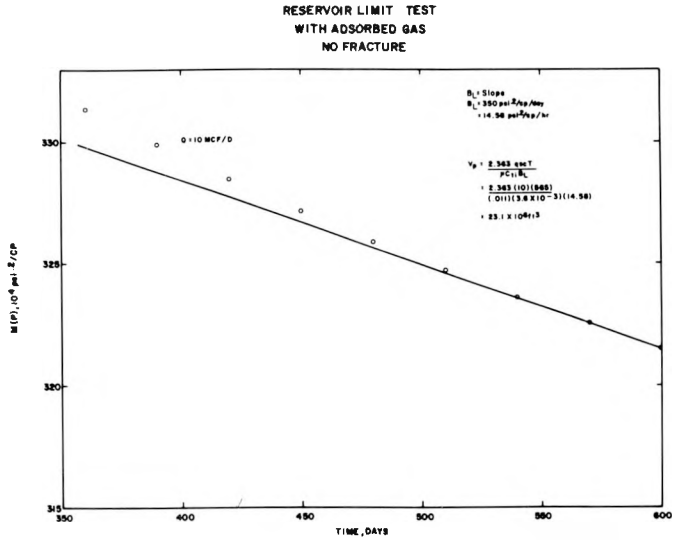


FIGURE 19

THE INTERACTION OF PROPPANTS WITH CRACK FORMATION AND PROPAGATION IN HYDRAULIC FRACTURING

Stuart L. Mchugh, Paul E. Senseny,

Douglas D. Keough and Alexander L. Florence

ABSTRACT

Well productivity can often be increased by repeated hydraulic fracturing. Repeated flow cycling has also been shown to increase productivity, in some cases significantly above what can be obtained with a single cycle. The increased productivity from repeated flow cycling suggests that a predictive capability for treating specific wells could be developed if the controlling parameters and their interactions in the flow/cycle treatment process were better understood. Although the primary role of the proppant in hydraulic fracturing is to maintain fracture opening, the proppants may have other effects such as altering the pressure distribution along the fracture (e.g., by blocking the tip) and hence significantly affecting the fracture mechanics.

Although proppant transport by fluids has been studied intensively, the coupled interaction problem of fracture propagation, fluid flow, and proppant transport has not been previously investigated. In SRI International's program to analyze the coupled interactions of proppants and fracture mechanics, proppant distributions are being determined for the coupled problem of fluid-proppant-fracture interaction, and the effects of the proppant distributions on fracture production are being evaluated for the flow/cycle treatment.

Scaled experiments in several media (PMMA and rock simulant) will check the correlation of fluid penetration and fracture propagation rate with a calculational model for the fluid-fracture interactions. The scaled experiments will also constrain the relationship between the proppant distributions and the fluid-fracture interactions. The computational model will be verified by comparing calculations of the proppant distributions in the scaled experiments, for which viscous or gravitational effects are dominant, with the scaled experiments.

NOTE: Paper not available at time of publication.

PAST AND CURRENT DEVLEOPMENTS FOR DRILLING NEW ALBANY SHALE GAS WELLS IN WESTERN KENTUCKY

Julian Duffy* and Howard Schwalb*

ABSTRACT

Gas from the New Albany Shale was produced in western Kentucky prior to 1890. Old fields have been abandoned with little record of production history. Current exploration for gas in the New Albany Shale began in 1976. Three fields have been discovered, and development has been progressing steadily spurred on by the increase in gas price. Drilling and completion techniques have varied. Sale of natural gas has been limited to availability of local markets, and proximity to existing natural gas pipelines. Leasing of exploration acreage is continuing and plans for future drilling to develop the New Albany Shale as a reservoir and source for natural gas appear to be excellent in western Kentucky.

INTRODUCTION

Historically, the New Albany Shale is probably the earliest natural gas producing zone in western Kentucky. Production of gas was reported prior to 1900 from the Doe Run and Old Rock Haven fields near Brandenburg in Meade County, Kentucky. Although some of the gas was used locally, most was piped to Louisville by the Louisville Gas and Electric Company. With the depletion of the indigenous gas from the New Albany Shale in the Brandenburg area, the Louisville Gas and Electric Company converted the fields to gas storage. Currently, this company is charging the New Albany Shale with pipeline gas in the Doe Run field and then recycling the gas to its customers. Several high-volume gas wells (2 MMCF) have recently been drilled in this storage field which indicates the excellent reservoir and storage characteristics of the New Albany Shale in this area.

Prior to the current drilling activity for New Albany Shale gas, there were several wells completed in western Kentucky either as shut-in gas wells or commercial producers in the shale. About 1931, gas was produced from the shale in the Shrewsberry field in Grayson County and a shut-in gas well was drilled in the Post field in the same county. Another shut-in gas well was drilled in Breckinridge County in Carter Coordinate section 3-0-38, but no further development was conducted near this well.

With the increased price recently allowed for natural gas, the drilling and development of new fields is actively taking place in western Kentucky after a long period of dormancy.

---

* Kentucky Geological Survey

2 PAST AND CURRENT DEVELOPMENTS FOR DRILLING NEW ALBANY SHALE GAS IN WESTERN DENTUCKY

NEW FIELD DEVELOPMENTS

CLARK

In the Clark field in Christian County, Carter Coordinate section 10-G-25, New Albany Shale gas was discovered as deeper pay production in January 1977, with the drilling of the Orbit Gas Company No. 1 King-Badgett well. Since the initial discovery, five additional wells have been drilled. Three of these wells have been shut-in, one has been added to the line, and the fifth is awaiting completion. Additional expansion of the field is planned for the coming year. The two producing wells are delivering gas against an approximate line pressure of 210 pounds without the aid of compressors. The drilling depth to the New Albany Shale in this field is 2,100 feet and the thickness of the shale averages 165 feet.

CLAYMOUR

The Claymour field in Todd County, Carter Coordinate section 23-E-29, was discovered in May 1979 by the drilling of the Huff Drilling Company No. 1 Richard Mallory well. Since the drilling of the first, five additional wells have been drilled. The distance between the outside wells is about six miles. Only one of the Claymour field wells has been completed at this time; the remaining are awaiting treatment. Average drilling depth for the field is 1,470 feet and the thickness of the shale averages 80 feet. The drilling of ten additional wells has been planned for this field in late 1979 and 1980. The operator of this field plans to install a compressor to expedite delivery of the gas to the pipeline.

CADIZ EAST

The Cadiz East field in Trigg County, Carter Coordinate section 19-E-21, was discovered in November 1976 with the completion of the Vincent and Reynolds No. 1 Ira Humphries well. The discovery well was drilled to the Ordovician Knox Dolomite and plugged back to the New Albany Shale at a depth of 1,139 feet. A second well, Hoffman No. 1 Eddie Majors, was drilled in October 1977 and is currently carried as a shut-in gas well. Although further activity has not been evident in the Cadiz East area it still retains a high potential. Gas from the discovery well, being delivered to the pipeline without the aid of a compressor, is sold to the town of Cadiz. The thickness of the shale in this well is 180 feet and the entire shale section was shot with 274 quarts of nitroglycerine to increase its flow capacity. After cleanout, the well gauged an open flow of 380 MCF with a bottom-hole pressure of 594 pounds. The well is reported to be delivering 30 MCF per day against a line pressure of 100 pounds.

DRILLING AND COMPLETION

The current drilling of the New Albany Shale is being done with both cable tool and rotary equipment. In many instances, both types of equipment are used on the same well. One operator is using a rotary rig to drill to the New Albany Shale, at which point casing is cemented in the well bore. A cable tool rig is then brought in to drill the shale pay section. In another instance the exact opposite is taking place; the cable tool equipment starts the hole and the rotary equipment completes the drilling. Some of the drilling is with air rotary equipment, which is used with the hope of keeping the shale dry during drilling operations. Surface casing is set through the shallow water zones, and often no additional water is encountered. Wells drilled with rotary mud or wells where formation water has wet the shale give no indication of their productive capability while being drilled. If samples are examined at the time the shale section is penetrated, some bleeding of gas from the cuttings may be seen. When the shale is drilled dry, and casing is set on top of the formation, the wells will gas to the surface after cleanout. In most cases wells are completed with similar production potential despite the type of dirlling technique used. In order to obtain commercial production from the wells, the shale must be stimulated with some type of treatments.

Although there are a variety of treatments available, the most widely used is a judymite shot, which is used in preference to nitroglycerine because of the lower temperatures involved. Hydraulic fracture treatment was used on one well in the Clark field with unsuccessful results.

MARKETING AND SALES

There is a ready market available for natural gas in western Kentucky and with several pipelines near producing areas there should be no major problems with marketing shale gas. With the expected

longevity of the New Albany wells (operator estimates vary from 10 to 30 years production) the dependability of the gas for market should be a major selling factor. The selling price of the New Albany Shale gas is reported to be around $2.00 per MCF with some adjustment for BTU value. Analysis of gas from two wells indicate that the BTU value is between 921 and 981 per cubic foot.

After stimulation, wells yield volumes of gas ranging form 50 MCF to 300 MCF open flow. The deliverability from these wells depends on the line pressure of the pipeline. The shale gas is not known to contain any harmful compounds and without scrubbing is introduced directly into the pipeline.

LEASING AND DEVELOPMENT

The progress of the New Albany Shale gas "Miniboom" is proceeding at an encouraging pace and should continue to expand in the immediate future in western Kentucky. New wildcat areas are reported under consideration by several companies, and wells drilled expressly for gas from the shale are expected to increase. Although the development of current New Albany Shale gas fields is continuing, room for more extensive exploration for this energy source is still available.

REFERENCES

Freeman, L. B., 1951, Regional Aspects of Silurian and Devonian Stratigraphy in Kentucky: Ky. Geol. Survey, Ser. 9, Bull. 6, 575 p.

Jillson, W. R., 1931, Natural Gas in Western Kentucky: Dy. Geol. Survey, Ser. 6, V. 38, 190 p.

Schwalb, H. R. Wilson, E. N., and Sutton, D. G., 1972, Oil and Gas Map of Kentucky, Sheet 2, West-Central Part: Ky. Geol. Survey, Ser. 10, Scale 1:250,000.

Schwalb, H. R., and Norris, Ronald, 1979, Structure Map on the Base of the New Albany Shale, Western Kentucky Unpublished.

Schwalb, H. R., and Potter, Paul E., 1978, Structure and Isopach Map of the New Albany-Chattanooga-Ohio Shale (Devonian and Mississippian) in Kentucky, Western Sheet: Ky. Geol. Survey, Ser. 10, Scale 1:250,000.

THE PARSONS CROSS STRIKE STRUCTURAL DISCONTINUITY AS AN EXPLORATION AREA FOR FRACTURED GAS RESERVOIRS

by

Jeanette M. Dixon and Thomas H. Wilson
Research Associates, Devonian Shale Program

West Virginia University
Department of Geology and Geography
425 White Hall
Morgantown, West Virginia 26506





ABOUT THE AUTHORS

Miss Dixon received her B.A. from Baylor University and her M.S. from the University of Akron. Presently, she is completing requirements for her doctorate in geology at West Virginia University. She has been engaged in various structural and fracture research projects since 1975.

Mr. Wilson received a B.A. (1974) and a M.S. (1977) in Physics at West Virginia University. He is currently employed in the Department of Geology and Geography at West Virginia University as a research associate engaged in surface and subsurface structural and geophysical studies for the Department of Energy's Eastern Gas Shales Project while working toward a Ph.D. in Geology.

2 THE PARSONS CROSS STRIKE STRUCTURAL DISCONTINUITY AS AN EXPLORATION AREA FOR FRACTURED GAS RESERVOIRS

ABSTRACT

The Parsons cross-strike structural discontinuity of the Plateau, and Valley and Ridge provinces in the Central Appalachians is defined as a cross-strike alignment of noses, bends and saddles of major folds. Structural shortening in the lineament is generally taken up by smaller folds and more abundant thrust faults. In the Plateau, Upper Devonian shale, mudstone and siltstone, and Lower and Middle Pennsylvanian sandstone are more intensely jointed. In the Middle Mountain syncline of the Valley and Ridge Province, the Middle Devonian shales exposed within the structural lineament are characterized by larger and more numerous deformation domains. These deformation domains are areas of disrupted bedding associated with faulting and folding of the shales and the underlying Lower Devonian Oriskany Sandstone. These deformation domains also define areas of more intensely jointed shale so that information about Devonian Oriskany structure can be used to predict the locations of intensely fractured gas producing Devonian shales. Future exploration for fractured gas reservoirs can then be optimized by concentrating surface and subsurface studies along cross-strike structural discontinuities, and determining their westward extent into the Appalachian Plateau.

INTRODUCTION

Much of the current research in the D.O.E.'s Eastern Gas Shales Project is directed toward predicting the locations of fractured reservoirs in the gas producing Devonian shales. The Middle Devonian shales that outcrop in the Valley and Ridge Province are the mechanical equivalent of the Upper Devonian Brown shale beneath the Allegheny Plateau Province. The current work in the Middle Mountain syncline and on the Allegheny Plateau is aimed at determining the effects of cross-strike structural discontinuities (in this case the Parsons structural lineament) on the organic-rich Middle Devonian shales exposed in this area, and to suggest an exploration rationale for locating fractured gas reservoirs associated with structural discontinuities in the Allegheny Plateau.

Previous studies have indicated that the Parsons structural lineament (cross-strike structural discontinuity) is a zone of anomously intense jointing (Wheeler and Holland, 1978; Henderson, 1973; Mullennex, 1975; Trumbo, 1976). Increased jointing and deformation has often been cited as a reason for some gas production in fractured reservoirs. Thus, the Parsons structural lineament has been suggested as a possible area for gas exploration (Wheeler, 1978a, 1978b; Wheeler and others, 1974). In order to recommend specific areas for drilling, detailed mapping, and joint intensity included in detailed mapping studies have been conducted along parts of the Parsons structural lineament (Figure 1).

The Parsons structural lineament is a northwest trending zone up to 10 km wide, of cross-strike alignment of noses, bends and saddles of major folds in the Valley and Ridge and Plateau provinces (Gwinn, 1964; Wheeler and others, 1974). It extends at least 55 km in length. More recently, the lineament is also defined as an area of anomously intense jointing (Wheeler and Holland, 1978; Dixon, 1979a, 1979b).

JOINT INTENSITY

A method to identify and quantify zones of intense jointing has been described by Dixon (1979a, 1979b), by Wheeler and Dixon (in review), and by Wheeler (1979). It was determined that joint orientation and spacing were the only necessary measurements needed to determine joint intensity or joint surface area per unit volume of rock. For a specific exposure, a measurement of intensity was made by using the sum of inverses of average spacings for each systematic joint set (Vialon and others, 1976; Dixon, 1979a, 1979b; and Wheeler, 1979). In the first part of this study, joints were measured in the Upper Devonian Chemung siltstone, mudstone, and shale exposed in western Tucker County. A SYMAP (computer generated contour map) map shows areas of more intense jointing within the lineament (Figure 2). Of the three dominant joint sets measured (N 35-55° W, N 25-45° E, and N 80° E - N 80° W) the northeast set contributes most to the increase in joint intensity by a marked increase in abundance and closer spacing of that set. Average spacings of all joints measured in the Chemung is approximately 25 cm.

Northwest, along the trend of the lineament in southeast Taylor County, the Parsons structural lineament is manifest in Lower and Middle Pennsylvanian sandstone as two narrow zones of intense jointing; the lineament is disrupted or terminates in northeast Taylor County (Figure 1). Joint intensity inside the lineament in the Plateau is approximately twice as great as outside the lineament. Four dominant sets were measured in the sandstone: (1) N 10-40° E, (2) N 45-55° W, (3) N 65-85° W, and (4) N 70-90° E. Spacings commonly range from 2 to 10 meters. Neither the Tucker County nor the Taylor County segments of the lineament shows any apparent correlation between the trend of the

lineament and the trends of the joint sets.

A joint intensity study of Middle Devonian shales exposed in the Middle Mountain syncline (Figure 1) similarly shows that the intensity of systematic jointing is greater within the Parsons structural lineament (see Deformation Domains).

DEFORMATION DOMAINS

During the mapping and structural analysis of the Middle Mountain syncline in the Valley and Ridge (Figure 1), methods were developed which permit the interpretation of bedding orientation contours in terms of fold geometry and internal structure (Wilson, 1979a, 1979b). The resulting maps are particularly useful as a tool in mapping the poorly exposed, mechanically less competent, organic-rich Middle Devonian shales exposed in this syncline.

Bedding orientation contours are constructed from detailed measurements of bedding strike and dip. The map area is divided into a regularly spaced square grid. The contoured values of strike or dip are the mean of the measurements contained in each square division of the map area. The center of each square grid represents a control point. The standard deviations of the samples within each cell were also contoured. Areas of high standard deviation in bedding dip defined the extent of fault related deformation within the shale mass. These areas have been defined as deformation domains (Wilson, 1979b).

Structural shortening within the Parsons structural lineament in the Middle Mountain syncline is generally taken up by smaller folds and more abundant thrust faults than outside the lineament. The increase in minor folding and particularly the increased number of thrust faults in the Middle Devonian shale result in an increase in the size and number of deformation domains. A joint intensity study (Wilson, 1979b) has shown that the intensity of systematic jointing is greater within deformation domains. Thus the Parsons structural lineament in the Middle Mountain syncline is a zone of greater fracture intensity because it is also a zone of more intensely faulted and folded shales. A thrust fault is more likely to flatten out as it propagates into a weak layer, although high angle faulting is possible (Rodgers and Rizer, 1979a, 1979b). As the fault propagates into the weak layer, secondary structures and fractures will remain in the region initially near the fault tip after the fault tip has propagated out of that region (Rodgers, oral communication, 1979). Relic secondary faults observed in the Upper Devonian Lower Huron Shale Member of the Ohio Shale Formation were used to identify the interval of detachment in the Pine Mountain thrust sheet (Wilson and others, 1979, these Preprints). An increased intensity of jointing was also observed in the interval of detachment (Wilson and others, 1979, these Preprints). Secondary faulting will also deform the area in advance of the leading edge of a thrust fault (Anderson, 1951; Hafner, 1951; Chinnery, 1966; Rodgers and Rizer, 1979b). Northwest trending slickenlines observed in the Brown Shales of the Nicholas Combs #7239 core (Kulander and others, 1977) and slickenlines observed in the Martin County core were explained in this way (Wilson and others, 1979, these Preprints) and were suggested to represent the porous fracture facies discussed by Shumaker (1978).

Bedding-transverse thrust faults cut across the Devonian Oriskany Sandstone on the northwest limb of the Elkhorn Mountain anticline (adjacent to the southeast of the Middle Mountain syncline) and probably represents secondary splay thrusts off a major splay that rises from a decollement in the Ordovician Reedsville Formation and above which the Elkhorn Mountain anticline is formed. The deformation domains on both limbs of the Middle Mountain syncline are interpreted as a direct result of the thrust faults and associated folding in the underlying Devonian Oriskany Sandstone.

RECOMMENDATIONS FOR FUTURE EXPLORATION EFFORTS

The association of deformation domains with mapped faults and more intensely jointed shales suggests that the deformation domain is a small analogue of the fracture facies. Although the presence of shear surfaces may act to decrease the porosity of these shales (Bagnell and Ryan, 1976), the presence of more intense jointing in these shales may increase the porosity and permeability producing a fractured gas reservoir.

Brown Shale gas production is in part related to the quantity of open fractures that intersect the well bore (Shumaker, 1978; Schaefer, 1979). In the Midway-Extra Field, Putnam County, West Virginia, the "highest production potential and thus, the most intense fracturing is located on the west flank of the Midway anticline, just east of the syncline" (Schaefer, 1979). The Midway anticline is associated with basement faulting along the Rome Trough (Shumaker, 1978). Originally vertical faults are known to flatten up section producing reverse movement above the downthrown blocks (Sanford, 1959).

Although the presence of faulting is not indicated, the increased fracturing on the west limb of the Midway anticline may be the result of similar but smaller horizontally directed stresses arising from vertical basement movements.

Shallowest drilling depths to the base of the Devonian shales within the Parsons structural lineament occur near central western Tucker County, West Virginia, (Figure 3) along the southwest plunging nose of the Deer Park anticline. Structure contours on the Onondaga Limestone (Cardwell, 1973) show that the plunging nose of the Deer Park anticline is faulted by a strike-trending, detachment-related, normal fault with the upthrown block to the southeast. The presence of increased joint intensity in faulted volumes of rock make this area an excellent test site in the effort to extend shale gas production into the eastern Plateau.

CONCLUSIONS

1. Rocks in the Parsons structural lineament are more intensely jointed than rocks outside. This increase in intensity is manifest in rocks from the Middle Devonian of the Valley and Ridge to the Middle Pennsylvanian in the Plateau.

2. Joint intensity inside the lineament in the Plateau is approximately twice as great as outside the lineament.

3. Contour maps of standard deviations in bedding dip are of considerable value in mapping structures in poorly exposed, mechanically incompetent shales and in defining deformation domains.

4. The relationship between joint intensity and deformation domains to structural lineaments like the Parsons lineament may represent an important factor to consider in developing an exploration rationale to locate fractured gas reservoirs.

ACKNOWLEDGMENTS

The authors would like to thank the Morgantown Energy Technology Center and the Department of Energy (Contract number DE-AC21-76MC05194, formerly EY-76-C-05-5194) for funding the research, Drs. R. C. Shumaker and R. L. Wheeler for their suggestions and assistance, and P. E. Haring for drafting.

REFERENCES

Anderson, E. M., 1951, The dynamics of faulting: Oliver and Boyd, Ltd.

Bagnall, W. D., and Ryan, M., 1976, The geology and production characteristics of the Devonian shale in southwestern West Virginia, in Shumaker, R. C., and Overbey, W. K., Jr., eds., 1976, Devonian Shale Production and Potential: Seventh Appalachian Petroleum Geology Symposium Proc.: U. S. Energy Research and Development Administration, Morgantown Energy Research Center, MERC/SP-76/2, p. 41-53; Springfield, Va., National Tech. Inf. Service.

Cardwell, D. H., 1973, Deep well and structural geologic map of West Virginia: Morgantown, W. Va., West Virginia Geol. and Econ. Survey.

Chinnery, M. A., 1966, Secondary faulting: Canadian Journal of Earth Science, v. 3, p. 163-190.

Dixon, J. M., 1979a, A method to identify zones of intense jointing with applications to the Parsons lineament: Morgantown Energy Technology Center Open-File Report, Morgantown, W. Va., 46 p.

_____, 1979b, A method to identify zones of intense jointing with application to the Parsons lineament, West Virginia (abs): Geol. Soc. Amer. Abs. with Programs, v. 7, p. 1286.

Gwinn, V. E., 1964, Thin-skinned tectonics in the Plateau and northwestern Valley and Ridge Provinces of the Central Appalachians: Geol. Soc. Amer. Bull., v. 75, p. 863-900.

Hafner, W., 1951, Stress distributions and faulting: Geol. Soc. Amer. Bull., v. 62, p. 373-398.

Henderson, C. H., ms, 1973, Minor structures of the High Plateau, northeastern Tucker County, West Virginia: M.S. thesis, West Virginia University.

Kulander, B. R., Dean, S. L., Barton, C. C., 1977, Fractographic logging for determination of pre-core and core-induced fractures . . .Nicholas Combs No. 7239 Well, Hazard, Kentucky: U.S. Energy Research and Development Administration, Morgantown Energy Research Center, MERC/CR-77/3.

Mullennex, R. H., ms, 1975, Surface expression of the Parsons lineament, southwestern Tucker County, West Virginia: M.S. thesis, West Virginia University.

Rodgers, D. A., Rizer, S. D., 1979a, Deformation and secondary faulting near the leading edge of a thrust fault (abs): Thrust and Nappes Symposium, Imperial College, London, Abstracts, p. 6.

Rodgers, D. A., Rizer, W. D., 1979b, Deformation and secondary faulting near the leading edge of a thrust fault (preprint): Thrust and Nappes Tectonics Symposium, Imperial College, London, Proceedings.

Sanford, A. R., 1959, Analytical and experimental study of simple geologic structures: Geol. Soc. Amer. Bull., v. 70, p. 19-52.

Schaefer, W. W., ms, 1979, Geology and producing characteristics of certain Devonian Brown shales in the Midway-Extra field, Putnam County, West Virginia: M.S. thesis, West Virginia University, 67 p.

Shumaker, R. C., 1978, Porous fracture facies in the Devonian shales of West Virginia and eastern Kentucky: Second Eastern Gas Shales Symposium, Morgantown Energy Technology Center, Morgantown, West Virginia, v. 1, METC/SP-78/6, p. 360-369.

Trumbo, C. B., ms, 1976, The Parsons lineament, Tucker County, West Virginia: M.S. thesis, West Virginia University.

Vialon, P., Ruland, M., and Grolier, J., 1976, Elements de tectonique analytique: Paris, Masson, 118 p.

Wheeler, R. L., ms, 1978a, Fracture intensity predictions for eastern gas shales: Morgantown Energy Technology Center Open-File Report 137, Morgantown, W. Va., 81 p.

_____, 1978b, Cross-strike structural discontinuities: possible exploration tool in detached forelands (abs): Geol. soc. Amer. Abs. with Programs, v. 10, p. 201.

_____, 1979, A numerical estimate of joint intensity, confidence limits on it, and applications to large structural lineaments (abs): Geol. Soc. Amer. Abs. with Programs, Northeastern Section of the Geol. Soc. of Amer. 14th Annual Meeting, v. 11, no. 1, p. 58-59.

Wheeler, R. L., and Dixon, J. M., ms, Intensity of systematic joints (in review).

Wheeler, R. L., and Holland, S. M., 1978, Style elements of systematic joints: effects of structural position on an anticline (abs): in Abs. of the 3rd Int'l Conf. on Basement Tectonics, Durango, Co., Fort Lewis College, p. 51.

Wheeler, R. L., Mullennex, R. H., Henderson, C. D., and Wilson, T. H., 1974, Cross-strike structural discontinuities: possible exploration tool in detached forelands (abs): Geol. Soc. Amer. Abs. with Programs, v. 10, p. 201.

Wilson, T. H., 1979a, Bedding orientation contours of Middle Devonian shales in the Middle Mountain syncline, Valley and Ridge Province, West Virginia (abs): Geol. Soc. Amer. Abs. with Programs, Northeastern Section of the Geol. Soc. of Amer., 14th Annual Meeting, v. 11, no. 1, p. 60.

Wilson, T. H., 1979b, Bedding orientation contours of Middle Devonian shales exposed in the Middle Mountain syncline, Valley and Ridge Province, West Virginia: Morgantown Energy Technology Center Open-File Report, Morgantown, W. Va., 39 p.

Wilson, T. H., Dixon, J. M., Shumaker, R. C., Wheeler, R. L., 1979, Fracture patterns observed in cores from the Appalachian Basin: in Preprints of the 3rd Annual Eastern Gas Shales Symposium, Morgantown, W. Va.

THE PARSONS CROSS STRIKE STRUCTURAL DISCONTINUITY
AS AN EXPLORATION AREA FOR FRACTURED GAS RESERVOIRS

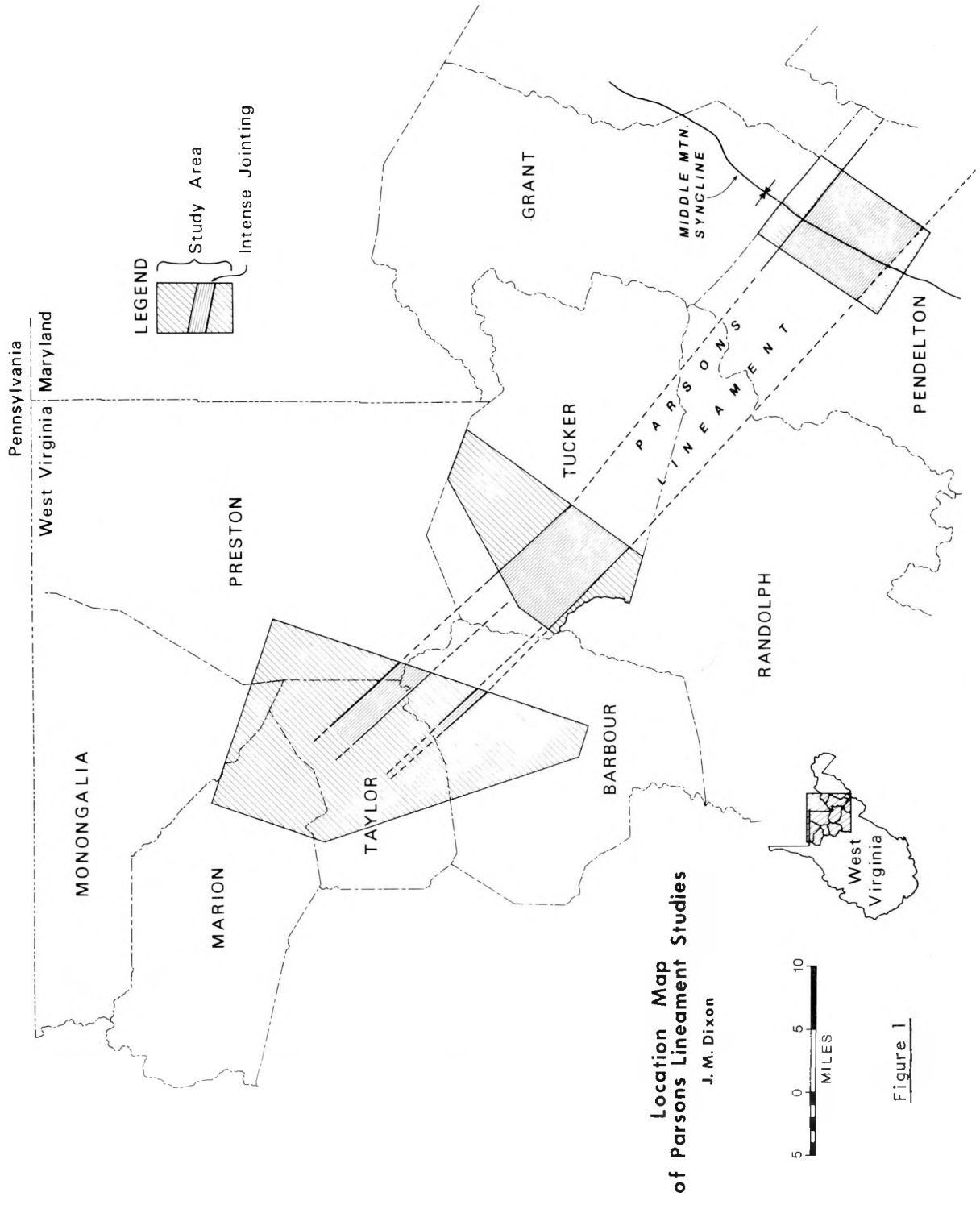


Figure 1

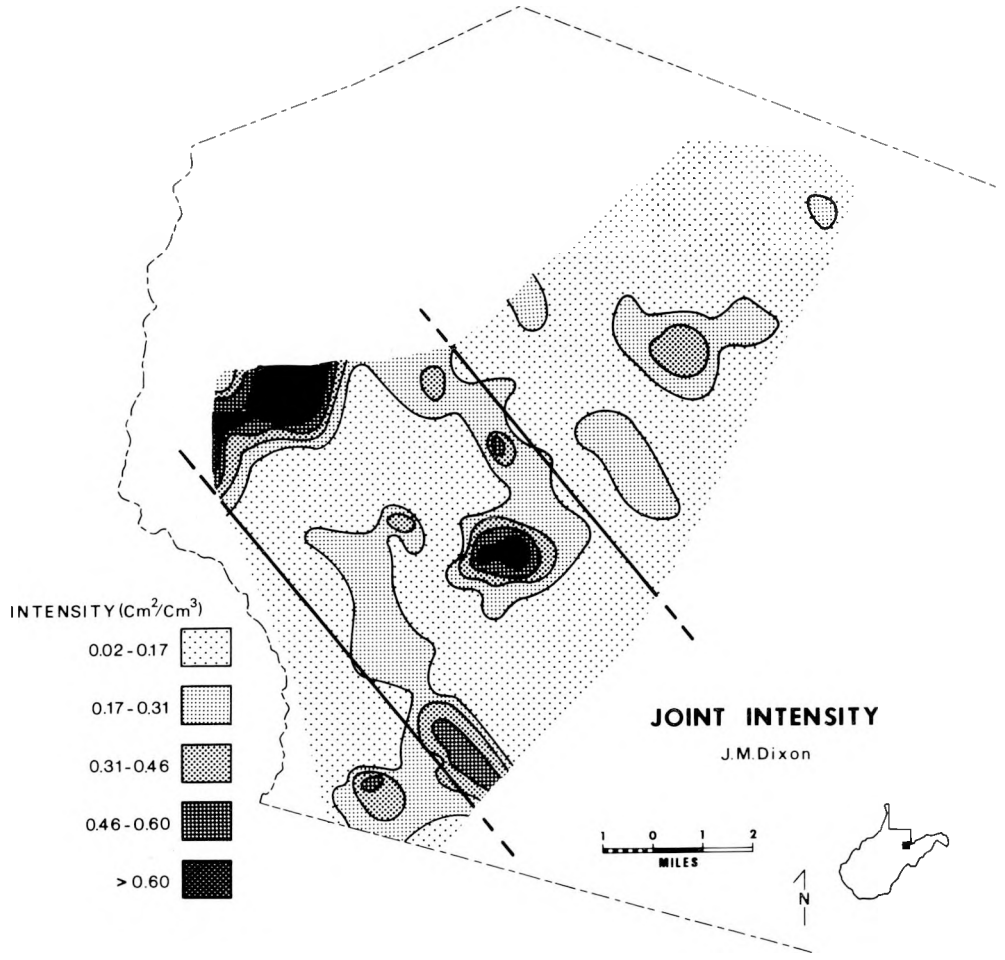


Figure 2 Parsons structural lineament, Tucker County, West Virginia, located between solid lines.

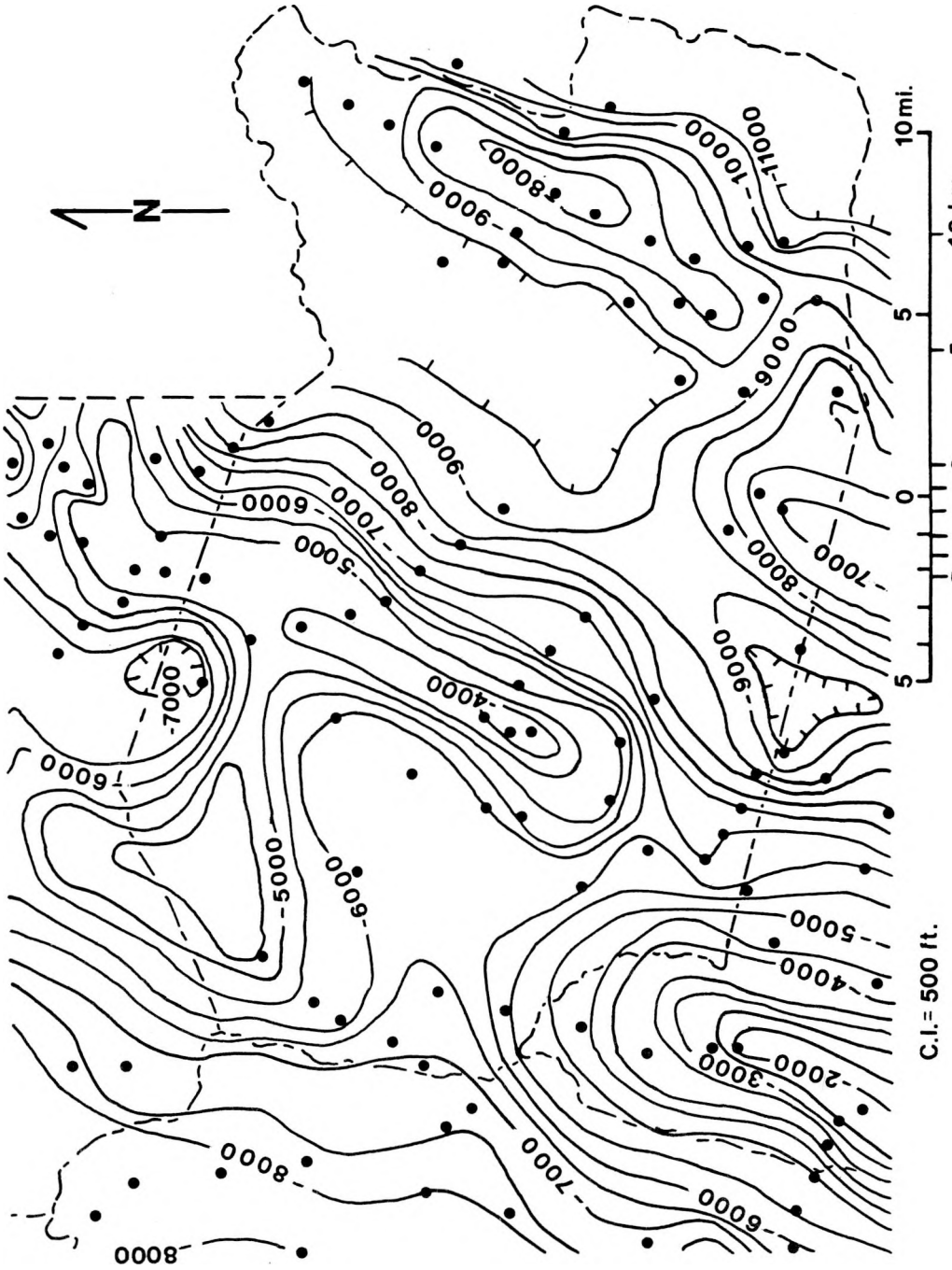


Figure 3 Isopach of drilling depth to the base of the Devonian shales - T. H. Wilson, 1979

THE EFFECT OF EXPLOSIVE GASES ON THE FRACTURE PROCESS IN GEOLOGIC SOLIDS

Dr. Stuart McHugh
Geophysicist

Douglas D. Keough
Senior Physicist

Poulter Laboratory
SRI International
Menlo Park, CA 94025

ABOUT THE AUTHORS

Stuart McHugh received a Ph.D. in Geophysics (1977) from Stanford University. As an undergraduate he worked as an exploration geologist and geophysicist for mining and oil companies. As a graduate student, he worked as a geophysicist for the National Center for Earthquake Research, U.S. Geological Survey. His Ph.D thesis was on "Short Period Tilt Events and Episodic Slip on the San Andreas Fault." He is currently employed as a geophysicist at SRI International and is involved in programs on the dynamic failure of brittle materials. These programs include brittle fracture in oil shale, pulse-tailoring in eastern gas shales, and the phenomenology of explosive gas penetration into fractures.

Douglas Keough is a senior physicist in SRI International's Poulter Laboratory. He received a Bachelor's degree from the University of New Hampshire and did graduate work at Temple University. At SRI he has headed the electronic instrumentation section and has directed research and development efforts in the physics of shock wave phenomena.

2 THE EFFECT OF EXPLOSIVE GASES ON THE FRACTURE PROCESS IN GEOLOGIC SOLIDS

ABSTRACT

In investigations of explosively produced fracture, it is often assumed that the primary mechanism for crack extension is the action of the shock wave propagating through the material. However, recent work suggests that the explosive gases may penetrate fractures and thus contribute directly to the fracture process in a way that is separate from the effect of the shock wave.

To investigate the likelihood that the explosive gases penetrate the fractures and contribute to fracture extension, we performed some simple calculations to estimate the gas pressures in an expanding crack and to examine the effect the pressures may have on the stress intensity at the crack tip. In general, these calculations suggest that even relatively small pressures in a crack can cause crack propagation and that such pressures can, in principle, be achieved within a crack being opened by tensile stresses from the shock wave. These calculations were checked by two simple laboratory experiments using a 1/8-inch-diameter PETN charge in a 1/2-inch-diameter by 6-inch long borehole, either lined (to contain the gases) or unlined (to allow gas penetration) in a 12-inch-diameter by 12-inch-long transparent plastic cylinder. A comparison of the calculations with these experiments and an examination of the experimental results suggests that gas penetration is an important mechanism for crack extension.

I. INTRODUCTION

The use of explosives to fracture and rubblize geologic materials is a well established technique and is extensively used in the recovery of a variety of natural resources. Because of the potentially large reserves of natural gas trapped in impermeable rock in the eastern United States and kerogen trapped in oil shale in the western United States, the Department of Energy and Sandia and Los Alamos Scientific Laboratories are sponsoring research programs on methods for recovering the gas and kerogen. Some of the programs involve enhanced well stimulation by explosive loading or rubblization of the rock by explosives for later processing. In these programs it is often desirable to evaluate in advance the effect of a particular explosive configuration on the surrounding material; consequently, theoretical and computational models have been developed to describe the explosive and the dynamic fracture process. Most research on explosive fracturing techniques and the associated fracture process has concentrated on the role of the stresses produced by the explosive.[1]

The role of the explosive gases has generally been neglected in this research. However, it has been estimated that only 5% to 15% of the energy produced by the explosive is contained in the shock wave.[2] Much of the remaining energy is contained in the explosive gases. Consequently, it is important that the effects of the explosive gases be investigated to evaluate their role in the fracture process.

The purpose of this paper is to examine the effect of the explosive gases produced in borehole shooting, apart from the explosively produced shock wave, on the fracture process. The basis interactions between the explosive gases and the fractures are defined and briefly reviewed, then one interaction, dynamic crack pressurization, is evaluated in more detail for its importance in the fracture process.

SUMMARY OF GAS-FRACTURE INTERACTIONS

For purposes of this discussion, we assumed that the shock wave has produced fractures around the explosive cavity and that the fractures are then available for interaction with the explosive gases. The time scale for this interaction may be of the same order as the time required to produce the cracks (i.e., dynamic effects should be considered) up to times much greater (i.e., static effects should be considered).

These assumptions suggest that the interaction of the explosive gases with fractures can be separated into the following categories:

Case I - No Gas Penetration into Fractures. The gases are entirely contained with the explosive cavity, and they are limited to exerting a pressure on the cavity boundary.

Case II - Gas Penetration into Fractures.

- (a) The pressure in the fracture is never large enough to contribute to the crack growth.
- (b) The fracture extends initially because of the explosively produced stresses, halts its growth when the stresses have decayed, then extends again under the action of the infiltrating gases.
- (c) The fracture extends due to a combination of effects from the shock wave and the internal gas pressure.

When there is no gas penetration into the fractures, Case I, or the gas pressure is not large enough to affect crack growth, Case II(a), and the effects of the shock wave are ignored, the static stability criterion for the cracks involves the number of cracks and their length and the gas pressure in the borehole. For these conditions, Ouchterlony[3] determined that the critical gas pressure required to cause the extension increases with the number of cracks (if their lengths are identical) and increases with crack length (if the number of cracks is constant, note that this relationship is opposite to the behavior expected when the cracks are pressurized). Johansson and Persson[4] reported good agreement between calculations and observations when they calculated maximum cracks lengths in bench blasting using the assumption that there was no significant gas penetration into fractures. The assumption of no gas penetration is appropriate (1) if the fractures are closed by compaction of the material around the borehole or clogged by debris or (2) if the crack extends much faster than significant pressures are attained in the crack.

However, if gas penetration does occur, it can significantly affect the fracture pattern. Case II(b) is equivalent to the static, or quasi-static, fracture pressurization investigated by Ouchterlony,[3] Bowie,[5] Kutter,[6] Westmann,[7] and Theocaris and Ioakimides.[8] The results of these static analyses show that (1) the critical pressure for crack extension increases with increasing number of cracks, (2) short cracks do not influence the crack tip stresses of long cracks when the crack length ratio is greater than about two, (3) uniform extension of cracks is virtually impossible, and (4) in short cracks the stress intensity for total gas penetration is twice that for no gas penetration, an effect that increases with crack length. Kutter and Fairhurst[9] and Porter and Fairhurst[10] experimentally determined that (1) for static pressurization, the least critical pressure was the pressure required to extend two diametrically opposed radial cracks and (2) in a system of radial cracks, the longest crack would extend first.

If the time required for the gas pressure in the fracture to become effective is comparable to the time required to form or extend the cracks, then it is likely that the preceding static or quasi-static analyses are not applicable to the problem of determining the effect of the gases on the fracture pattern. Lownds[11] theoretically examined the performance of various explosives in field tests and, in part of the analysis, assumed that the crack length could be determined from the sound velocity of the gas. Dally et al.[12] experimentally examined the effect of venting and containing explosive charges in a thick plastic sheet and concluded that containment increases the final crack lengths by a factor of five compared with venting. Coursen[13] and Warpinski et al.[14] report (1) the results of field tests in which either explosives or propellants were detonated to form fractures, and (2) analyses of cavity volume and the final crack lengths in which it is assumed that gas pressurization of the fractures is the primary mechanism for crack extension. The results of these investigations suggest that explosive gases may penetrate cracks and cause significant crack extension beyond what is expected from the shock wave acting alone.

EFFECT OF DYNAMIC CRACK PRESSURIZATION

The previous investigations suggest that one effect of gas pressurization, either in the borehole or in the fractures, is the extension of preexisting cracks. The consequences of static pressurization have been well-treated as described previously, but currently no explicit model accounts for the dynamic interaction of the shock wave and the gas pressure in fractures. Furthermore, dynamic gas pressurization will probably occur when propellants or intermediate burn-rate explosives are used to fracture rock.[12-14] Consequently, to describe and evaluate the effects of the shock wave and gas pressure on fracturing in field tests or experiments, we must make some simplifying assumptions. The following analysis treats the effect of dynamic gas pressurization on fractures and is performed only for laboratory springing experiments so that the results may be applied to the actual experiments described at the end of this section.

It will be assumed that the effects of the shock wave and gas pressure can be treated independently and that only their effects on crack length are of interest. If it is further assumed that the fractures caused by the shock wave are produced by the tensile stresses, a dynamic tensile fracture model such as NAG-FRAG[1] can be used to estimate the extent of radial fracturing for various explosive pulse widths applied to the borehole. The NAG-FRAG calculations of the effect of the tensile stresses simulated the laboratory springing experiments (described in Reference 1) and suggest that radial fracturing will extend to at least 15 cm for a 1 μsec pulse width, 2 cm for a 5 μsec pulse width, and about 1/2 cm for a 10 μsec pulse width. These results for tensile fracturing will be compared with the effect of dynamic gas penetration in the springing experiment described below.

To determine the effect of the dynamic interaction of the explosive gases with the fractures and the effect of the interaction on fracture length, we will use the following procedure. It will be assumed that a perfect gas can be used to represent with PETN explosive gases in the springing experiments.

Then the maximum gas velocity, V, for one-dimensional flow is:

$$V = \left[\frac{2\gamma}{\gamma-1} \frac{P}{\rho} \right]^{1/2} \quad (1)$$

where γ is the ratio of specific heats, P is the pressure, and ρ is the density. For PETN (γ = 1.3)[15] the maximum gas velocities are in the range of 1.5 x 10^5 cm/sec to 3 x 10^5 cm/sec for typical pressures and densities.[16] This range is greater than, or comparable to, typical crack velocities, suggesting that the explosives gases will penetrate fractures extending because of the tensile stresses and that significant gas pressures may occur within the crack and contribute to crack extension. To determine crack lengths resulting from either a constant or linearly decreasing internal gas distribution within a fracture we assumed that the explosive products are a perfect gas expanding isentropically from the borehole into the crack; then

$$P_i V_i^{\gamma} = P_f V_f^{\gamma} \quad (2)$$

In equation (2), the subscript i represents the initial value and f the final value of pressure P and volume V. If P_o is the equilibrium borehole and crack pressure and V_c is the volume of an individual penny-shaped crack of constant width, then

$$P_i V_i^{\gamma} = P_o (V_c + V_1)^{\gamma} \quad (3)$$

and

$$V_c = 1/2\ \pi C^2 W \quad (4)$$

where C is the crack radius and W is the crack width. For a constant internal gas pressure,[16]

$$K_I = \frac{2}{\sqrt{\pi}} P_o \sqrt{C} \quad (6)$$

and for a linear pressure distribution,[16]

$$K_I = \frac{2\sqrt{c}}{\sqrt{\pi}} P_o\ (1 - \pi/4) \quad (6)$$

where K_I is the stress intensity. Substituting equations (4), (5), and (6) into equation (3) yields the following:

$$C^{2-\frac{1}{2\gamma}} + \frac{2V_i}{\pi W} C^{-\frac{1}{2\gamma}} - \frac{2V_i}{\pi W} \left(\frac{2\ P_i}{\sqrt{\pi}\ K_{1c}} \right)^{1/\gamma} = 0 \quad (7)$$

$$C^{2-\frac{1}{2\gamma}} + \frac{2V_i}{\pi W} C^{-\frac{1}{2\gamma}} - \frac{2V_i}{\pi W} \left(\frac{0.44\ P_i}{\sqrt{\pi}\ K_{1c}} \right)^{1/\gamma} = 0 \quad (8)$$

where K_{1c} is the fracture toughness of the material. Equation (7) applies to a constant internal pressure and equation (8) to a linear pressure distribution in the crack. It is also assumed in this derivation that the equilibrium crack length occurs when $K_1 = K_{1c}$.

Because these calculations are intended to model laboratory-scale spring experiments,[1] we assumed that the initial pressure (P_i) is between 1 kbar and 5 kbar, K_{1c} = 100 bars $\sqrt{cm}$, $V_i \sim 8$ cm^3, w = 0.01 cm, γ = 1.3, and the number of cracks is between one and ten. Thus, the corresponding range in crack lengths is between 0.1 m and 3.0 m.[16] This range of crack lengths is roughly 100 times greater than what would occur if the tensile stresses acted alone (i.e., 0.005m - 0.015m) and suggests that even relatively moderate gas pressures may be quite effective for extending cracks, even when the effects of many cracks and a pressure gradient are included.

To check these simple calculations and evaluate the effect of dynamic gas pressurization on fracture length, we performed two experiments in 12-inch-diameter by 12-inch Lucite blocks constructed from 4-inch thick sheets (Figure 1). A 6-inch-long by 1/8-inch-diameter charge of PETN + 15% ZnS, 0.7 gm/cm^3, was centered in a 1/2-inch-diameter borehole in the Lucite. In one experiment, a 15-mil-thick stainless steel sheath was used to line the borehole to prevent the gases from penetrating the fractures. In the other experiment, the explosive cavity was unlined so that the gases could penetrate

the cracks. A 1000 psi overburden pressure was applied to both blocks. Borehole pressure gages (described in Reference 1) were used to monitor the pressure but were too noisy to be analyzed. The peak pressure at the Lucite-borehole boundary was estimated to be between 1 and 2 kbars from calculations using the PETN equation of state and the PUFF[1] wave propagation code for a one-dimensional cylindrical geometry. After the explosive was detonated, the confining pressure was relieved and the Lucite blocks were sectioned, polished, and photographed.

Figures 2 and 3 show the resulting fracture patterns when a borehole liner is used, and Figure 4 shows the results when the borehole is unlined. The center portion of the Lucite block was unaffected by the explosive gases, in the lined shot, and consequently it can be assumed that the 0.5 to 2.0 cm long, half-penny shaped radial cracks (Figure 2) were produced by the circumferential tensile stresses only. The simulation of this experment using the PUFF code suggests that the input pressure duration was 5 to 10 μs, and these measured crack lengths are in agreement with the lengths expected for this pulse width.

The explosive gases escaped through the plug at the base of the sheath however and entered the cracks in the lower portion of the Lucite block in the lined shot (Figure 3). These cracks, which were greatly extended by the gases, were confined to the lower portion of the block by the interface between the lower and middle 4-inch thick sheets.

The effect of the escaping explosive gases is more dramatically illustrated in the unlined shot (Figure 4). The residue of the explosive gases can be seen throughout these cracks, including the crack tips. Some of the cracks in Figure 3, and most of the cracks in Figure 4 intersected the boundaries of the block, and consequently the minimum crack lengths for the gas penetration cases are 10 to 15 cm, or approximately a factor of 5 to 10 longer than the cracks when no gas penetration occurred.

The effect of the gases on fracture lengths is difficult to quantify because of the presence of the Lucite block boundaries and uncertainties in the stress distributions. However, it does appear from these experiments that the gas penetration into the fractures increased the crack length by at least a factor of five to ten, although the presence of the block boundaries and the confining pressure makes it impossible to compare the value with the factor of 100 predicted by the simple theory discussed earlier. Nevertheless, the effect of gas penetration on fracture length is quite significant and should be considered in any description of the fracture process when explosive gases are present.

SUMMARY

These experiments and calculations suggest that the effect of explosive gases from borehole shooting on fracture extension should be considered in any description or evaluation of the fracture process.

In future work it will be necessary to determine the relevant parameters describing dynamic gas penetration of fractures (e.g., temperature and gas pressure), the effect of these parameters and their interactions on crack length, and to develop a model for dynamic gas penetration on the fracture pattern.

REFERENCES

1. S. L. McHugh, W. J. Murri, L. Seaman, D. R. Curran, D. D. Keough, "Fracture of Devonian Shale by Tailored Pulse Loading," SRI Final Report, Project PYU 6700, to Department of Energy, Morgantown Energy Technology Center, Morgantown, WV (December 1978).

2. U. Langefors and B. Kihlstrom, "The Modern Technique of Rock Blasting," 3rd ed. (Halstead Press, John Wiley & Sons, 1978).

3. F. Ouchterlony, "Fracture Mechanics Applied to Rock Blasting," Proc. 3rd Cong. Intl. Soc. Rock Mech., Denver, CO. (1974), pp. 1377-1383.

4. C. H. Johansson and P. A. Personn, "Fragmentation Systems," Proc. 3rd Cong. Intl. Soc. Rock Mech., Denver, CO. (1974), pp 1557-1566.

5. O. L. Bowie, "Analysis of an Infinite Plate Containing Radial Cracks Originating at the Boundary of An Internal Circular Hole," J. Math. & Phys., 35, 60-71 (1956).

6. Herbert Kutter, "Stress Analysis of a Pressurized Circular Hole with Radial Cracks in an Infinite Elastic Plate," Int. J. Fract. Mech., 6, 233-247 (1970).

7. R. A. Westmann, "Pressurized Star Crack, " J. Math. & Phys., 43, 191-198 (1964).

8. P. S. Theocaris and N. J. Ioakimidis, "A Star-Shaped Array of Curvilinear Cracks in an Infinite Isotropic Elastic Medium," J. Appl. Mech., 44, 619-624 (1977).

9. Herbert K. Kutter and C. Fairhurst, "The Roles of Stress Wave and Gas Pressure in Presplitting," in Status of Practical Rock Mechanics, Proc. 9th Symp. on Rock Mech. (AIME, Golden, CO, 1968), Ch. 14, pp. 265-284.

10. D. D. Porter and C. Fairhurst, "A Study of Crack Propagation Produced by the Sustained Borehole Pressure in Blasting," Dynamic Rock Mechanics, Proc. 12th Symp. on Rock. Mech. (AIME, Rolla, MO, 1971), Ch. 25, pp. 497-515.

11. C. M. Lownds, "Prediction of the Performance of Explosives in Bench Blasting," J. South African Institute of Mining and Metallurgy, 165-180 (1975).

12. J. W. Dally, W. L. Fluorney, and D. C. Holloway, "Influence of Containment of the Borehole Pressures on Explosively Induced Fracture," Int. J. Rock Mech. Min. Sci. & Geomech. Abstr., 12, 5-12 (1975).

13. D. Linn Coursen, "Cavities and Gas Penetration from Blasts in Stressed Rock with Flooded Joints," draft of paper presented at 6th Intn'l. Colloquium on Gas Dynamics, Explosives, and Reactive Systems, Sweden, Stockholm (August 1977).

14. N. R. Warpinski, R. A. Schmidt, and P. W. Cooper, "High Energy Gas Frac: Multiple Fracture in a Wellbore," 20th U.S. Symp. Rock Mech., Austin, TX (1979), p. 143-152.

15. P. J. Cagliostro, "Experiments on the Response of Hexagonal Subassembly Ducts to Radial Loads," SRI Second Interim Report to Argonne National Laboratory, SRI Project PYD 1960, (August 1975).

16. Stuart L. McHugh and Douglas D. Keough, "The Effect of Explosive Gases on the Fracture Process in a Geologic Solid," Poulter Laboratory Technical Report (in preparation).



Figure 1: Lucite block, unlined borehole. Leads from borehole pressure gages shown at top of block

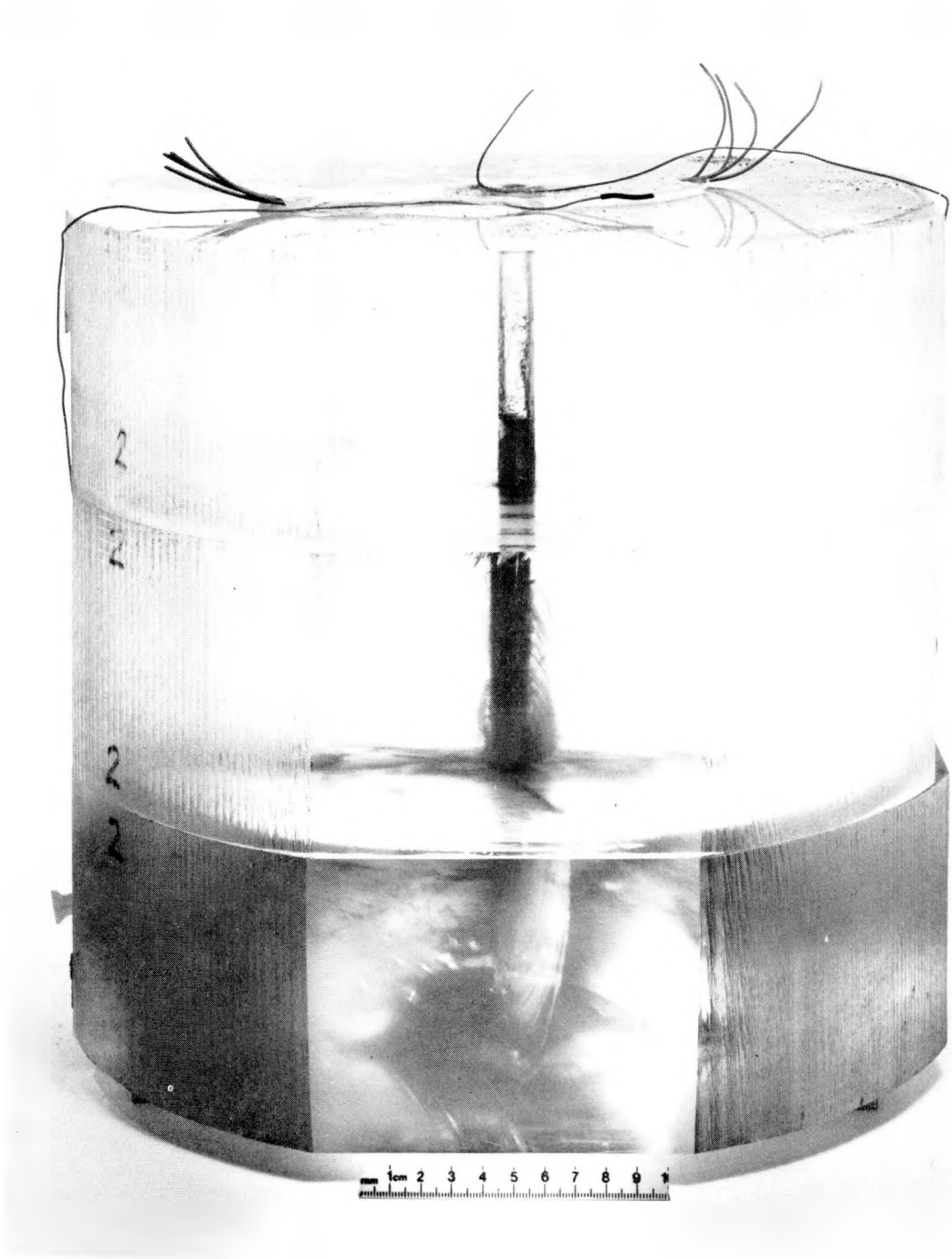


Figure 2: Lucite block with lined borehole, after detonation of PETN. Note that 1) there is no damage in the upper portion of the block where the detonator was placed, 2) there are only small cracks in the central portion, and 3) the explosive gases escaped from the sheath and entered cracks in the lower portion of the block.



Figure 3: Closeup of central portion of Lucite block with lined borehole, after detonation of PETN showing the small fractures around the sheath and the larger fractures that the explosive gases created.

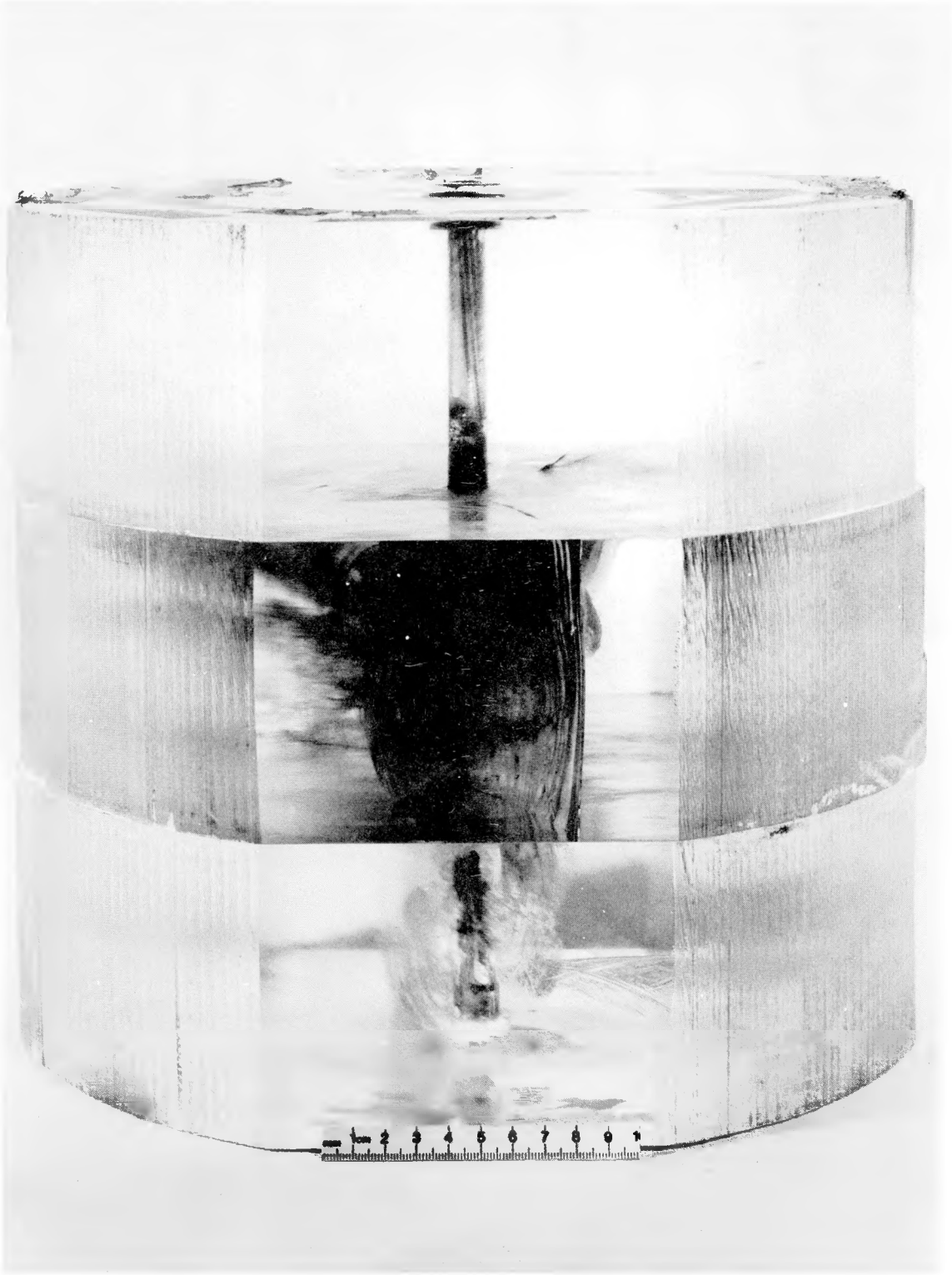


Figure 4: Lucite block, with unlined borehole, after detonation of the PETN. The fractures are stained by the explosive gases.

CROSS-POLARIZATION CARBON-13 NMR OF KEROGENS FROM DEVONIAN SHALE AND COAL

Stephen K. Beer[1] and Larry C. Headley[2]

Physicist[1] and Chief[2]

Biomedical and Environmental Research Branch

Morgantown Energy Technology Center, WV



ABOUT THE AUTHOR

Mr. Beer received his B. S. degree in physics from the University of Pittsburgh in 1971 and his M. S. in nuclear physics from West Virginia University in 1976. Since 1976, he has been employed at the Morgantown Energy Technology Center, Morgantown, West Virginia, where, among other projects, he has worked with hot gas cleanup and performed pulsed nuclear magnetic resonance studies for the Eastern Gas Shales Project.

CROSS-POLARIZATION CARBON -13 NMR OF KEROGENS FROM DEVONIAN SHALE AND COAL

ABSTRACT

The carbon-13 cross polarization (CP) technique has been applied to Hazard, KY and Cottageville, WV Devonian gas shale kerogens and Arkwright, WV bituminous and Rosebud, Montana subbituminous coal kerogens. CP spectral features and estimated aromatic fractions were compared with C/O and H/C atomic ratios determined from elemental analyses.

CP lineshapes were generally similar in most samples although there may be some variance in the downfield part of the aliphatic region. Definition of the aromatic and aliphatic lines was generally good with the exception of the Hazard sample.

Possibly because of residual mineral matter or changes in the organic content during the kerogen extraction process, we did not find either carbon contents or C/O ratios to be good predictors of spectral features in kerogens despite the effects C-O and C=O bonds are expected to have on the aliphatic line. In particular, both the carbon content and C/O ratio in the coal kerogens are low compared to those in a wide variety of bituminous coals, although this is not obvious from the CP spectr

The coal kerogens, like bituminous coals, were found to be highly aromatic substances, while the shale kerogens were more aliphatic. The aromatic fraction is seen to decrease in a roughly linear fashion as the H/C atomic ratio increases.

INTRODUCTION

In recent years, pulsed nuclear magnetic resonance techniques have been extensively used in the investigation of solid, untreated materials being considered as alternative energy sources. Since practically all the energy reserves of such materials are contained in the kerogen or organic content (as opposed to mineral content), it is desirable for the spectroscopist to discriminate between the organic and inorganic content as much as possible. In theory the use of carbon-13 cross-polarization (CP) NMR should facilitate this discrimination for the following reasons:[4]

A. Inorganic carbons tend to be separated by larger distances from protons than organic carbons. By virtue of the dipolar interaction which transfers magnetization from protons to carbons, carbons further from protons will not polarize as readily, and will not contribute significantly to the signal if the mixing time is sufficiently short.

B. Some inorganic protons have long spin-lattice relaxation times compared to organic protons. Signals from carbons associated with these protons will be attenuated at sufficiently short pulse repetition times.

It has been pointed out, however,[9] that some mineral carbonates can contribute to the CP signal. More accurate CP characterization might be expected from kerogen extracts, which in theory have had the mineral matter removed with minimal changes in the organic residue. In this work, bituminous and subbituminous coal kerogens are compared with a number of eastern Devonian gas shale kerogens and with previous work on kerogens and raw samples.

EXPERIMENTAL

The kerogen extracts of one Hazard, Kentucky and four Cottageville, West Virginia Devonian shales were obtained by treating the raw shales with HCl and HF and centrifuging to remove mineral matter. In addition, all but two of these (Cottageville No. 8 and Hazard No. 24) were treated with $FeCl_3$ to oxidize and remove any remaining pyrite. The coal kerogens (Rosebud, Montana subbituminous, and Arkwright, West Virginia bituminous) were extracted by the Illinois State Geological Survey.

Elemental analyses were done with a Carlo Erba elemental analyzer. CO_2, H_2O, and N_2 were produced from catalytic combustion of the kerogens and passed through a gas chromatograph to obtain estimates of the C, H, O, and N contents. (References to brand names here and below are provided to facilitate understanding and in no way imply endorsement by DOE.)

CP signals for averaging and Fourier transformation were obtained with the CP sequence developed by Pines, Gibby, and Waugh[1], using a Bruker SXP 90 MHz spectrometer coupled with a B-C 104 transient recorder and Nicolet BNC-12 computer with 16K data memory. Proton irradiation was provided by a B-HP 300 power amplifier driven by a B-SV3 B 90 MHz RF oscillator and carbon irradiation was provided by the "main" spectrometer circuitry normally used in conventional pulsed NMR. This was sufficient to provide a proton H_1 of $\sim$9 gauss (90° pulse width = 6.5 microseconds) and a carbon H_1 of $\sim$36 gauss in the dual-coil probe head. The 21 kilogauss field was stabilized to within one ppm using the deuterium signal from a doped D_2O sample.

For all samples run, the proton flip angle was 90°, contact time .99ms, proton decoupling time (following contact) 4ms, and the repetition time one second, with a single thermal contact during each sequence. In view of the proton T_1 of $\leq$ 100 ms[3] of the kerogen samples and the room temperature $T_{1\rho}$ of 5-10ms for whole coals[4], we expect minimal CP intensity distortions from proton relaxation effects. The contact time of .99ms should be adequate to polarize protonated carbons and carbons surrounded by protonated carbons, although possible intensity shortfalls caused by proton-proton isolation and more isolated carbons[4] have not yet been investigated in these samples.

Spin temperature alternation was employed to minimize DC offset in the accumulated signals as well as spurious signals and intensity distortions from spin locking of the initial C-13 magnetization produced by quadrature phase transients in the C-13 pulse[2]. Spin locking in particular is of concern since it can produce signals from isolated (including inorganic) carbons.

Frequency dependent phase shifts, which can lead to baseline distortions when phase corrections are attempted in the FT spectra, were minimized by beginning data acquisition immediately after the end of the C-13 pulse and by bypassing the four-pole Butterworth filter normally used in the system. No frequency-dependent phase corrections were performed on the FT spectra.

The pulse feed-through occurring at the beginning of the time-domain signals was minimized by increasing the receiver bandwidth to about three times the sweep width (at some cost to signal-to-noise) and adjusting the detector phase. A sweep width of 100 KHz and a receiver bandwidth of 300 KHz were sufficient to limit feed-through to the first two dwell times (10 microseconds), reducing the amplitude and frequency of the baseline roll enough for accurate numerical integration of the spectral intensities.

For all samples run, the C-13 RF freqnency was 22.650 MHz, or about 18 KHz above the aromatic line, while protons were irradiated approximately on resonance. Spectrometer tuning and Hartmann-Hahn matching were done on adamantane at the same frequencies. The relatively large C-13 resonance offset was chosen to minimize the foldback of the FT spectrum on itself[5], a problem (particularly with our single phase detection) which causes baseline distortions dependent on the detector phase and compensatory phase correction. No corrections were made for possible intensity distortions due to deviations from Hartmann-Hahn matching[6] or possible effects arising from the off-axis character of the effective C-13 field. These were assumed not to change significantly in the immediate vicinity (± 150 ppm) of the C-13 signal.

RESULTS AND DISCUSSION

A. Deconvolution Technique

The coal and shale kerogens were deconvoluted as shown in Figure 1. The estimated aromatic lineshape is approximately a linearly decreasing function on the upfield side and is consistent with both theory and with the lineshape derived by VanderHart and Retcofsky[4], who likewise deconvoluted by taking linear combinations of spectra with appreciably different aromatic fractions (f_A). We note here that despite the availability of a number of spectra with different aromatic fractions, the aliphatic linewidths were frequently different enough (by as much as 15 percent) to prevent "good" deconvolutions, and that Fig. 1 is an optimum case. The aromatic, rather than the aliphatic lineshape, was then used in estimating the aromatic fractions. By assuming the invariance of the aromatic lineshape from sample to sample, we minimize the dependence of the calculated f_A values on varying aliphatic lineshapes.

B. Results

Estimated carbon aromatic fractions (f_A) are listed in Table 1 and compared with C/O, H/O, weight percent O and C, and proton-spin lattice relaxation times T_1 ($\frac{1}{\epsilon}$).

The coal kerogens appear to be significantly more aromatic ($f_A \sim .73$) than any of the shale kerogens. The ~60 percent carbon contents of the coal kerogens are significantly lower than the ~70 percent to 90 percent observed in moisture and ash-free (maf) analyses of whole bituminous coals from Canada and Japan[7] and from the Pittsburgh and Pocahontas seams[4]. This, together with the observed C/O atomic ratios for both coal kerogens (4.1 and 5.1) might lead one to expect downfield tailing from the aliphatic line and poor definition of the aromatic line, provided there are large numbers of C-O and C=O bonds able to give a CP contribution[4]. However, the "well-defined" aromatic lines in the Rosebud and Arkwright kerogens are more characteristic of whole coals in the 80-90 percent carbon range[4]. We must note that the high oxygen content of these coal kerogens is puzzling and suggests that sizable amounts of mineral matter were not removed during the extraction process, or that the organics themselves underwent some chemical changes during extraction. A further point which may or may not be related to this is the close similarity of the f_A values (Table 1) and lineshapes, although C-19854 whole coal is subbituminous, and C-19824, bituminous.

The aromatic and aliphatic lineshapes are about the same among the Cottageville kerogens (Fig. 2), with the f_A values ranging from 0.38 to 0.55. The Hazard spectrum is appreciably different from the other spectra in this work in that there is very little drop in intensity between the two peaks (Fig. 3). As mentioned above, this is consistent with a significant number of C-O and C=O bonds. It is of interest that Cottageville No. 49 kerogen, which has about the same C/O atomic ratio (~ 14), has a well-defined aromatic peak more characteristic of the other Cottageville kerogens, whose C/O ratios are as much as twice as large. It would appear from this and the above remarks about the coal kerogens that the correlation of C/O with C-O and C=O and/or CP spectra can be poor when dealing with kerogen extracts as opposed to untreated samples.

There is a tendency of f_A to decrease in a roughly linear fashion with increasing H/C ratio (Fig. 4). This is consistent with a similar trend observed in Ref. 4 and is expected because of the larger number of C-H bonds occuring with increasing H/C[8]. A least squares fit (Fig. 4) to both shale and coal kerogens (excluding Hazard No. 24, where separation was questionable) gives the relation

$$f_A = 1.097 - .580\ H/C \qquad (1)$$

and for comparison fitting the Cottageville samples only (not shown) yields

$$f_A = 1.201 - .677\ H/C \qquad (2)$$

We compare these to the aromaticity equation of Brown and Ladner[8] in a slightly rearranged form

$$f_A = 1 - (H^*_\alpha/x + H^*_o/y)\ (H/C) \qquad (3)$$

where H^*_α is the fraction of total protons on benzylic carbons, H^*_o is the fraction of total protons on other nonaromatic carbons, and x and y are respectively the H/C ratios for benzylic and other nonaromatic carbons. If as generally believed, CH_2 groups are the predominant component of the aliphatic structures in substance derived from coal, x and y are approximately 2. If this assumption is extended to the shale kerogens, equating H/C coefficients in (1)(2)and(3) implies $H^*_\alpha + H^*_o = 1.16$ and 1.34 for coal plus shale and shale kerogens respectively, a contradiction in terms since $H^*_\alpha + H^*_o$ cannot be greater than unity. A number of things can account for this, including overestimation of the f_A values and/or effective H/C. The latter can be overestimated if there are significant numbers of hydrogens not associated with carbons (as in unremoved mineral matter) or possibly reaction products from the extraction process. We cannot say at present whether this is more important than upward bias in the f_A values resulting from our spectral deconvolutions and/or experimental procedure. A third possibility, an H/C ratio much greater than 2 for aliphatic groupings in shale kerogens, is not considered to be a predominant factor in view of the chain structure of the aliphatic components. The fact that f_A is forced to be greater than unity for H/C = 0 in the least squares fits (particularly for the shales alone) is more suggestive of upward bias in H/C and/or f_A.

If both coal kerogens and shale kerogens are considered, f_A to increase with carbon contents from ~ 57 percent to 78 percent (Fig. 5). This differs from the trend for f_A to increase with carbon contents from ~ 70 percent to 95 percent in untreated coals and coal vitrains [4,7], al-

though the small overlap between these two ranges prevents a meaningful comparison. It would appear from this that f_A correlates more closely with H/C than with carbon content.

No significant trends were observed when proton spin-lattice relaxation times were compared with f_A and carbon content. Plots of these were omitted from the present work.

ACKNOWLEDGEMENTS

The authors gratefully acknowledge E. Childers, S. Lamey, and A. Hiser for providing the shale kerogens and elemental analyses, and E. Fisher S. Lamey, and T. Keech for their helpful discussions.

REFERENCES

1. Pines, A., M. G. Gibby, and J. S. Waugh. J. Chem. Phys. 59:569 (1973).

2. Stajskal, E.O., J. Schaefer. J. Mag. Res. 18:560 (1975).

3. Unpublished work done at Morgantown Energy Technology Center.

4. VanderHart, D. L., H.L. Retcofsky. "Analysis of the Aromatic Content of Whole Coals by High-Power Proton Decoupled C-13 NMR," Preprints of the 1976 Coal Chemistry Workshop at Standard Research Institute, Howard M. Peters and David S. Ross, ed. pp. 202-218.

5. Stejshal, E.O., J. Schaefer, J. Mag. Res. 14:160 (1974).

6. Stejskal, E. O., J. Schaefer, and J.S. Waugh. J. Mag. Res. 28:105 (1977).

7. Yokono, Tetsuro and Sanada Yuzo. Fuel 57:334 (1978).

8. Brown, J.K., W.R. Ladner, Fuel 39:87 (1960).

9. Resing, Henry A., Alan N. Garroway, and Robert N. Hazlett. Fuel 57;450 (1978).

TABLE 1

ANALYSIS OF KEROGEN SAMPLES

Sample	f_A	Weight % C	H/C Atomic Ratio	C/O Atomic Ratio	Proton T_1 $(\frac{1}{e})$(ms)
Arkwright C-19824	.72	60.5	.62	5.1	∿ 100
Rosebud C-19854	.73	56.7	.65	4.1	80
Hazard No. 24	.60(?)	65.2	1.03	13	10.5
Cottageville No. 8	.51	66.8	1.04	18	22
Cottageville No. 43	.38	76.3	1.21	28	66
Cottageville No. 49	.50	64.7	1.02	14	25
Cottageville No. 86	.55	77.6	.96	28	12.2

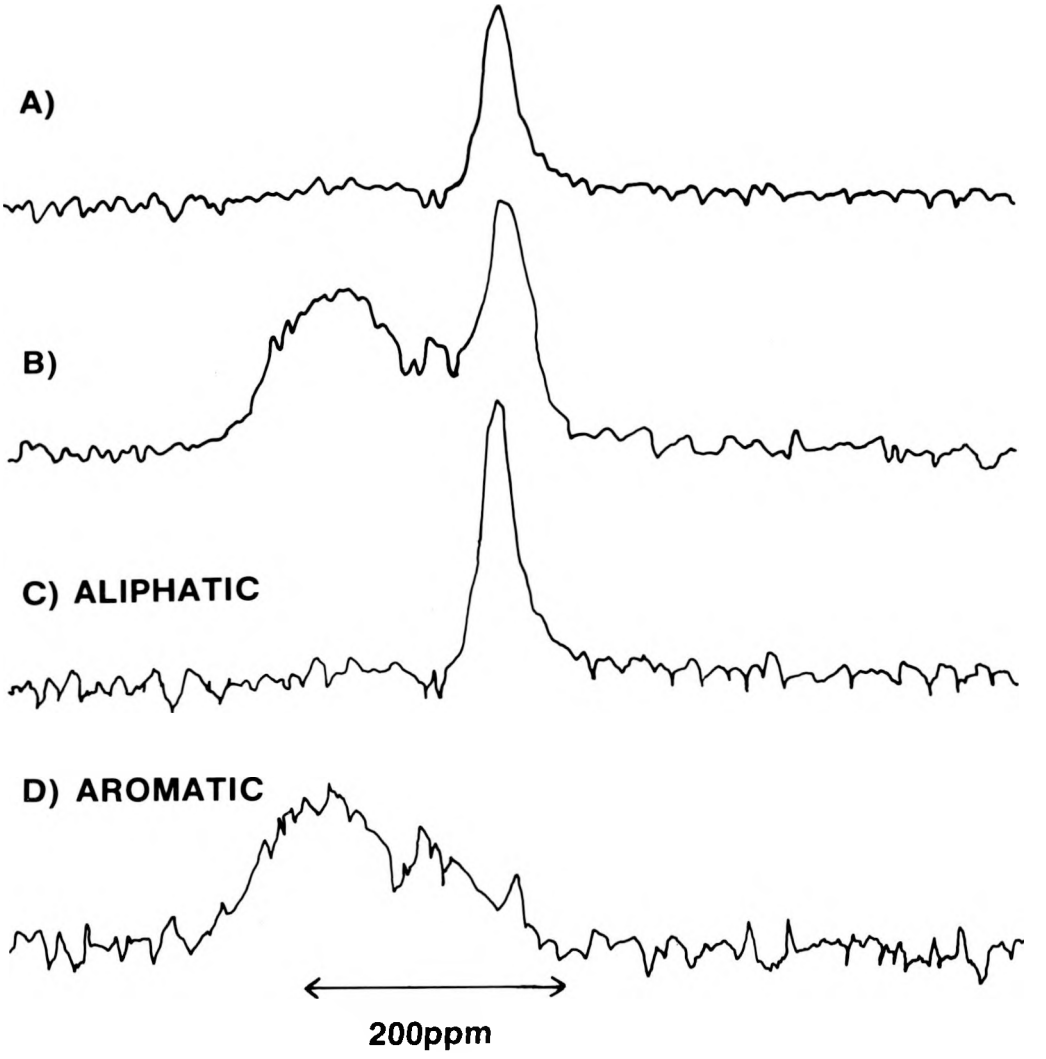


FIGURE 1. - CP spectra of Cottageville, W.V. Devonian gas shale kerogen No. 43(a) and Arkwright, W.V. bituminous coal kerogen C-19824(b). The deconvoluted aromatic and aliphatic lineshapes were obtained by appropriate linear combinations of (a) and (b).

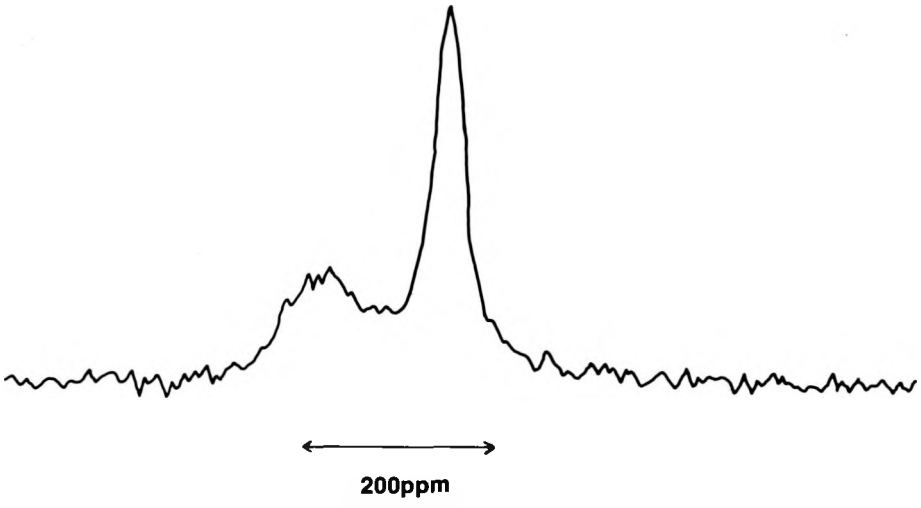


FIGURE 2. - CP spectrum of Cottageville No. 49 gas shale kerogen. (7200 scans at 25°C, repetition time one second, sample size 190 mg.)

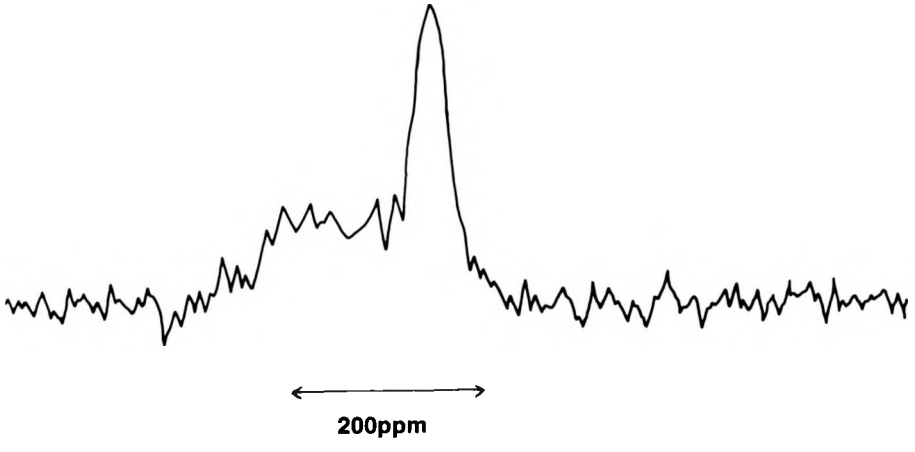


FIGURE 3. - CP spectrum of Hazard, KY gas shale No. 24 kerogen. (7200 scans at 25°C, repetition time one second, sample size 84 mg.)

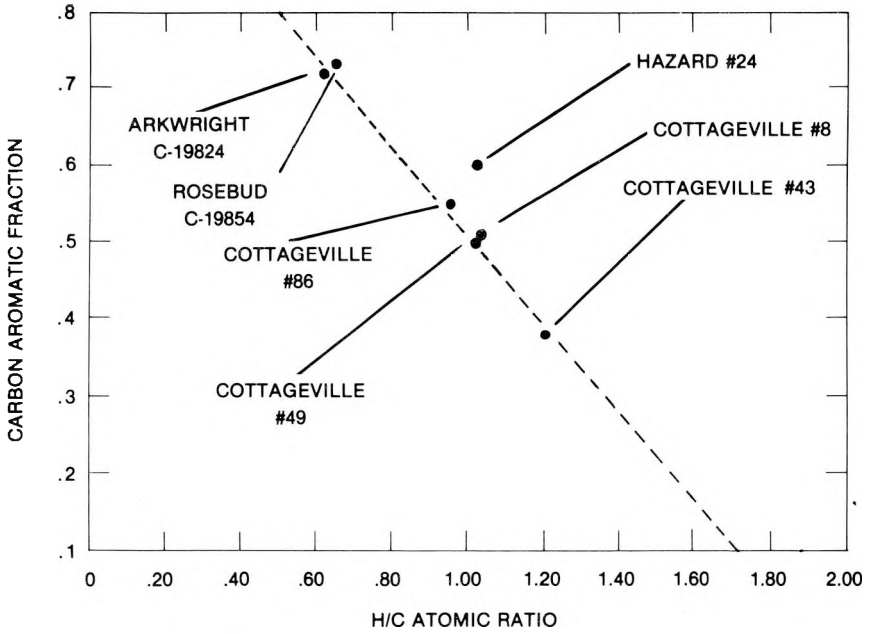


FIGURE 4. - Carbon aromatic fraction vs H/C atomic ratio. Least squares fit is given by $f_A = 1.079 - .546$ (H/C). Hazard #24 was omitted when fitting because of its f_A deviation and questionable aromatic-aliphatic separation.

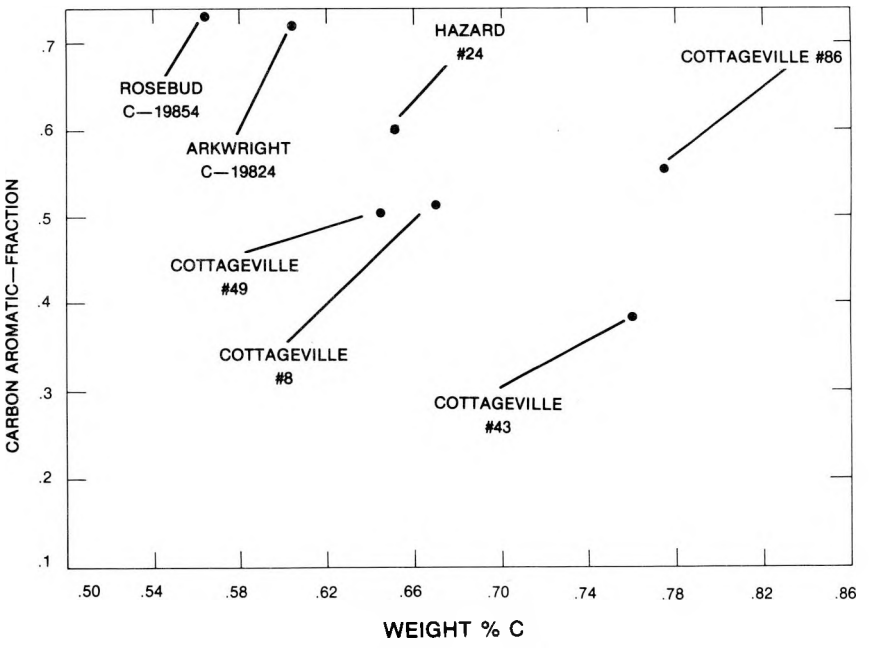


FIGURE 5. - Carbon aromatic fraction vs weight percent carbon.

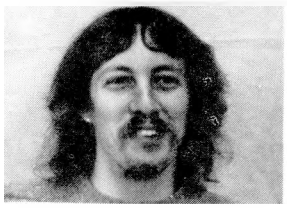
COMPOSITIONAL VARIATIONS IN A FABRIC-ELEMENT BASED LITHOLOGIC TYPE CLASSIFICATION FOR DEVONIAN SHALES

by

David S. Klanderman

Michael Ed. Hohn

West Virginia Geological and Economic Survey
P.O. Box 879, Morgantown, WV 26505





ABOUT THE AUTHORS

David Klanderman received his BS degree in geology from Northern Arizona University, and an MS degree in geology from Oregon State University. He has worked for Amax Exploration Inc., Exxon, and the Oregon Department of Geology and Mineral Industries. At present, he is a research associate (sedimentary petrology) with the West Virginia Geological Survey/Eastern Gas Shales Project and is working on a doctorate at West Virginia University.

Michael Ed. Hohn received a BS degree in geology from the State University of New York at Binghamton, and an AM and Ph.D. degrees in geology from Indiana University. He worked for two years in the School of Chemistry, University of Bristol, researching the use of multivariate statistics in organic geochemistry. He is presently a geostatistician with the Eastern Gas Shales Project at the West Virginia Geological and Economic Survey.

2 COMPOSITIONAL VARIATIONS IN A FABRIC-ELEMENT BASED LITHOLOGIC TYPE CLASSIFICATION FOR DEVONIAN SHALES

ABSTRACT

The use of fabric elements to classify specific shale lithotypes permits rapid qualitative evaluation of productive potential and interpretation of general depositional enviroments without recourse to detailed chemical and mineralogical characterization.

In order to evaluate the usefulness of subjective lithotype classification, 169 samples from the Lincoln 1637 cored well, classified into four shale lithotypes were examined through parametric and nonparametric statistical tests performed on petrophysical and compositional data derived from these same samples. The lithotypes consisted of: 1) sharply-banded shale, 2) thinly-laminated shale, 3) lenticularly-laminated shale, and 4) non-banded shale. Analytical parameters considered were: bulk density, matrix density, porosity, log density, sonic travel time, resistivity, gamma-ray-log response, silt (by thin-section point counts), quartz, illite, pyrite, and 14 angstrom clays quantified relatively by X-ray diffraction, total sulfur by rapid LECO method, and organic matter by loss-on-ignition between 100° and 550°C. The data were tested for normality by means of a one-sample Kolmogorov-Smirnov test and then for significant differences between lithotypes by means of both the Analysis of Variance and the nonparametric analogue, the Kruskal-Wallis test.

The test results show that significant differences do exist between the specific lithotypes, and therefore, that classification by fabric elements does reflect real differences in rock properties. Fabric element classification must precede more destructive physical and analytical tests so that this valuable information is not lost and so that later test results can be related back to specific rock types.

INTRODUCTION

A major difficulty in the classification of fine-grained sedimentary rocks arises from the fact that the major compositional constituents are generally too small to be studied using standard light microscopy. Although thin section point counts are important in determining compositions of coarser grained clastic rocks, resolution limitations of polarizing microscopes severely limit the importance of such techniques on rocks composed of material finer than silt (1/256 mm). Past classifications of fine-grained clastic rocks have generally relied on the mineralogical or geochemical composition of the whole rock or of the silt-sized fraction (Keller and Ting, 1950; Payton and Thomas, 1959; Krumbein and Sloss, 1963; Davis, 1970; Lewan, 1978).

Nuhfer and Vinopal (1979) employ a classification based on rock fabric observed from thin sections and x-radiographs of slabbed samples. One can observe systematic differences in mean geochemical and mineralogical composition and physical characteristics among the lithologic types, suggesting that the empirical classification of Nuhfer and Vinopal (1979) and Nuhfer, Vinopal, and Klanderman (1979) can provide information about physical, chemical and biological processes in effect during Devonian shale deposition. The purpose of this paper is to test the statistical significance of the observed differences.

In the past three years, a number of cores from the Devonian Shales have become available as a result of drilling operations initiated by the Department of Energy's Eastern Gas Shales Project. One such core, Lincoln 1637 (Columbia Gas Transmission Co. Well #20403) (Figure 1), is the object of this study. The cored interval extends from the base of the Mississippian Berea Sandstone through the entire Devonian shale sequence present in western West Virginia. Our investigation took two directions: first, testing the normality of residuals after fitting a parametric, linear model for each variable about group means, and second, comparing the results of the analysis of variance (ANOVA) with the nonparametric analogue, the Kruskal-Wallis test.

ANALYTICAL METHODS

One hundred sixty-nine samples of Devonian shale from the Lincoln 1637 core were classified according to lithologic type by Nuhfer, Vinopal, and Hohn (1978). Classification was based on the study of negative prints made from standard 45 x 28 mm petrographic thin sections and from x-radiographs made from slabs (2 mm thick) cut from core samples prior to thin section and x-ray diffraction sample preparation. Only those samples classified as sharply-banded, thinly-laminated, lenticularly-laminated, and nonbanded shales were utilized in this study. Those samples classified as siltstone and concretions were disregarded because they are easily distinguishable by standard petrographic techniques. For a complete description of the lithologic types, see Nuhfer and Vinopal, elsewhere in this volume.

Thin section point counts were used to estimate the amount of silt-sized quartz and feldspar. Pyrite total quartz, illite and 14 Å clay (mostly chlorite) were determined by x-ray diffraction. Total sulfur values were determined by LECO analyses of ground samples. Organic content of ground samples was estimated by loss on ignition between 100°C and 550°C.

Three density measurements were made on each sample; 1) bulk density, measured by immersion of krylon-coated whole-rock samples in kerosene, 2) matrix density, measured by the vacuum-crucible method for ground whole-rock samples (Nuhfer, 1979), and 3) log density, measured from bulk density logs at log corrected sample depths. Sonic, gamma ray, and resistivity values were likewise measured directly from well logs. Porosity values were calculated from previously-measured bulk and matrix density values.

STATISTICAL TESTS

A linear model was fit to the 169 samples for each variable, yielding F-ratios testing significance of differences among the four shale type group means, and also yielding residuals of the samples from their respective group means. The same data were employed in Kruskal-Wallis tests for each variable, allowing comparison of results of a parametric test assuming normality and a nonparametric test. A one-sample Kolmogorov-Smirnov test on the residuals for each variable was also conducted under the null hypothesis that no difference exists between the observed distribution and a normal distribution.

RESULTS

The Kolmogorov-Smirnov tests show that eight of the 14 variables satisfy the assumption of normality for the parametric analysis of variance (Table 1). The remaining variables, those displaying measurably nonnormally-distributed residuals, should be tested for significant differences by means of the nonparametric Kruskal-Wallis test. In this study, however, both the analysis of variance and the Kruskal-Wallis tests produced results at such high significance levels for all variables (Table 2), that observed nonnormality apparently does not adversely affect the parametric test. We conclude that real differences do exist among the lithologic types and that the empirical classification by fabric elements does stand up to objective scrutiny.

Visual inspection of summary statistics (Table 3) shows that for each variable, one or two means may vary noticeably from the other lithologic group means. For instance, three of the groups have mean values for thin section silt within the range of 0.30 to 0.34, but the mean value for the thinly-laminated samples is relatively large (0.36). This comparison of mean values - summarized in Table 4 - shows that the thinly-laminated samples possess very high or low values for 10 of the variables. The loss on ignition and sulfur variables are probably related to a high organic content of the sediments during deposition, with subsequent preservation. Accordingly, these samples show low matrix and well log densities.

Most of the variables exhibit a pattern of only one extreme group mean, but the clays show a pattern of two low mean values corresponding to the sharply-banded and thinly-laminated samples, and two high means corresponding to the lenticularly-laminated and nonbanded samples. This observation relates to the stratigraphic distribution of the lithologic types (Figure 2). Note that the quartz measured by x-ray diffraction is highest in the sharply-banded shales which occur in association with siltstone in the upper part of the cored interval. That the highest mean for the silt corresponds to the thinly-laminated samples suggests that point counts of silt give spurious results, perhaps because silt is easier to identify as such in the thinly-laminated samples. The association of siltstone with the sharply-banded shale supports the conclusion that point counts of silt ought to be interpreted with care.

Of the four lithologic types, the lenticularly-laminated type is the most difficult to distinguish from the others. This lithology shares with the nonbanded shale a high clay content, and differs from it only in a somewhat higher porosity (Table 3).

Table 3 also shows the heterogeneity of variance about the group means for a given variable. We did not test for homogeneity of variance because of the sensitivity of appropriate tests to nonnormality. In addition, the similarity of results between ANOVA and the Kruskal-Wallis test demonstrates that heterogeneity of variance does not seriously disturb the parametric test.

DISCUSSION

Although samples were classified by lithologic type independently of stratigraphic position, the shale types do show stratigraphic control (Figure 2); each stratigraphic unit is composed predominantly of one lithologic type. The undifferentiated shale at the top of the sequence and the upper and middle Huron Members of the Ohio Shale are composed almost entirely of siltstone and sharply-banded shale (siltstones were omitted from this study because they are easily studied by conventional petrographic techniques). The lower Huron member and the Rhinestreet Member of the West Falls Formation contain primarily thinly-laminated and nonbanded shales while lenticularly-laminated and nonbanded shales dominate in the Java Formation and upper part of the West Falls Formation. Subsequent petrographic characterization of other cores from western West Virginia has shown that a more diverse admixture of shale types exists within the Huron Member than that present in the Lincoln 1637 core. Cores from Jackson County contain very little thinly-laminated shale, but much more lenticularly-laminated and nonbanded shale than the Lincoln County core. These geographic variations in the proportions of lithologic types in a given interval suggest that the different shale types correspond to differences in depositional processes and biotic activity through the Appalachian Basin.

The shale types may be useful in predicting compositional and physical properties of samples from other cores. As more cores are retrieved, the effort should be made to gather textural information on samples prior to conducting more sample-destructive analyses.

CONCLUSIONS

Several shale lithologic types occur in the Devonian sequence in the Lincoln 1637 core and can be identified through visual inspection of thin sections and x-radiographs. Because these lithologic types also differ statistically in 14 mineralogical, geochemical, and physical properties, they can also be used to predict relative compositional and physical differences between samples of unknown lithologic type.

Parametric and nonparametric analyses of variance give very similar results, suggesting that the parametric test is not sensitive to the degree of nonnormality found in the data analyzed in the present work.

ACKNOWLEDGEMENTS

This study was funded under U.S.D.O.E. Contract No. EY-76-C-05-5199 and is published with the permission of the Director and State Geologist, West Virginia Geological and Economic Survey. The authors wish to thank Jeff Clagett and Bob Vinopal for their critical review of the paper and their many helpful suggestions.

REFERENCES

1. Davis, J.C., 1970, Petrology of Cretaceous Mowry Shale of Wyoming: Am. Assoc. Petrol. Geol. Bull. 54, 487-502.

2. Keller, W.D., and C.P. Ting, 1950, The petrology of a specimen of the Perry Farm Shale: Jour. Sed. Petrology 20, 123-132.

3. Krumbein, W.C., and L.L. Sloss, 1963, Stratigraphy and Sedimentation: W.H. Freeman and Company, San Francisco, 660 p.

4. Lewan, M.D., 1978, Laboratory classification of very fine grained sedimentary rocks: Geology 6, 745-748.

5. Nuhfer, E.B., R.J. Vinopal, and M.E. Hohn, 1978, Report of petrologic characterization of Lincoln 1637 (Columbia Gas Transmission Co. Well #20403): U.S. Dept. Energy open-file report-METC, 212p.

6. Nuhfer, E.B., 1979, Determination of density and porosity in Procedures for petrophysical, mineralogical, and geochemical characterization of fine-grained clastic rocks and sediments, Nuhfer, E.B., R.J. Vinopal, and R.R. Romanosky, eds: U.S. Dept. Energy open-file report-METC, 39 p.

7. Nuhfer, E.B., and R.J. Vinopal, 1979, A fabric-element based classification for low-porosity-shale gas reservoirs: Preprints - third Eastern Gas Shales Symposium - METC/ERDA.

8. Nuhfer, E.B., R.J. Vinopal, and D.S. Klanderman, in press, X-radiograph atlas of lithotypes and other structures in the Devonian shale sequence of West Virginia and Virginia: U.S. Dept. of Energy open-file report-METC.

9. Payton, E.E., and L.A. Thomas, 1959, The petrology of some Pennsylvanian black "shales": Jour. Sed. Petrology 29, 172-177.

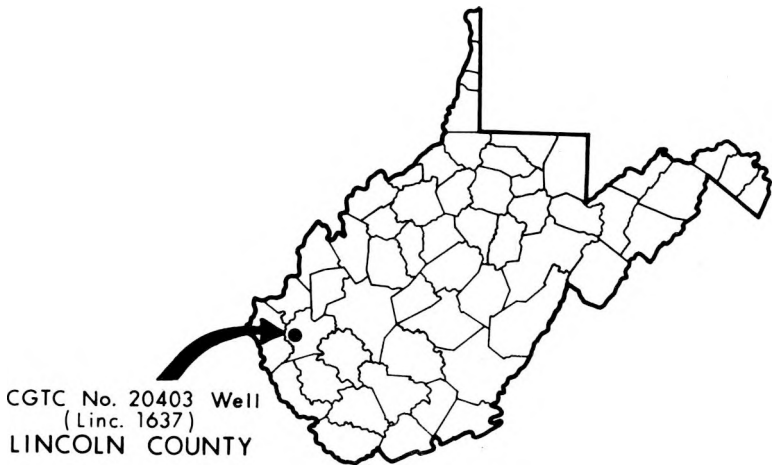


Figure 1. Index map of West Virginia showing location of cored well (CGTC #20403) utilized in this study.

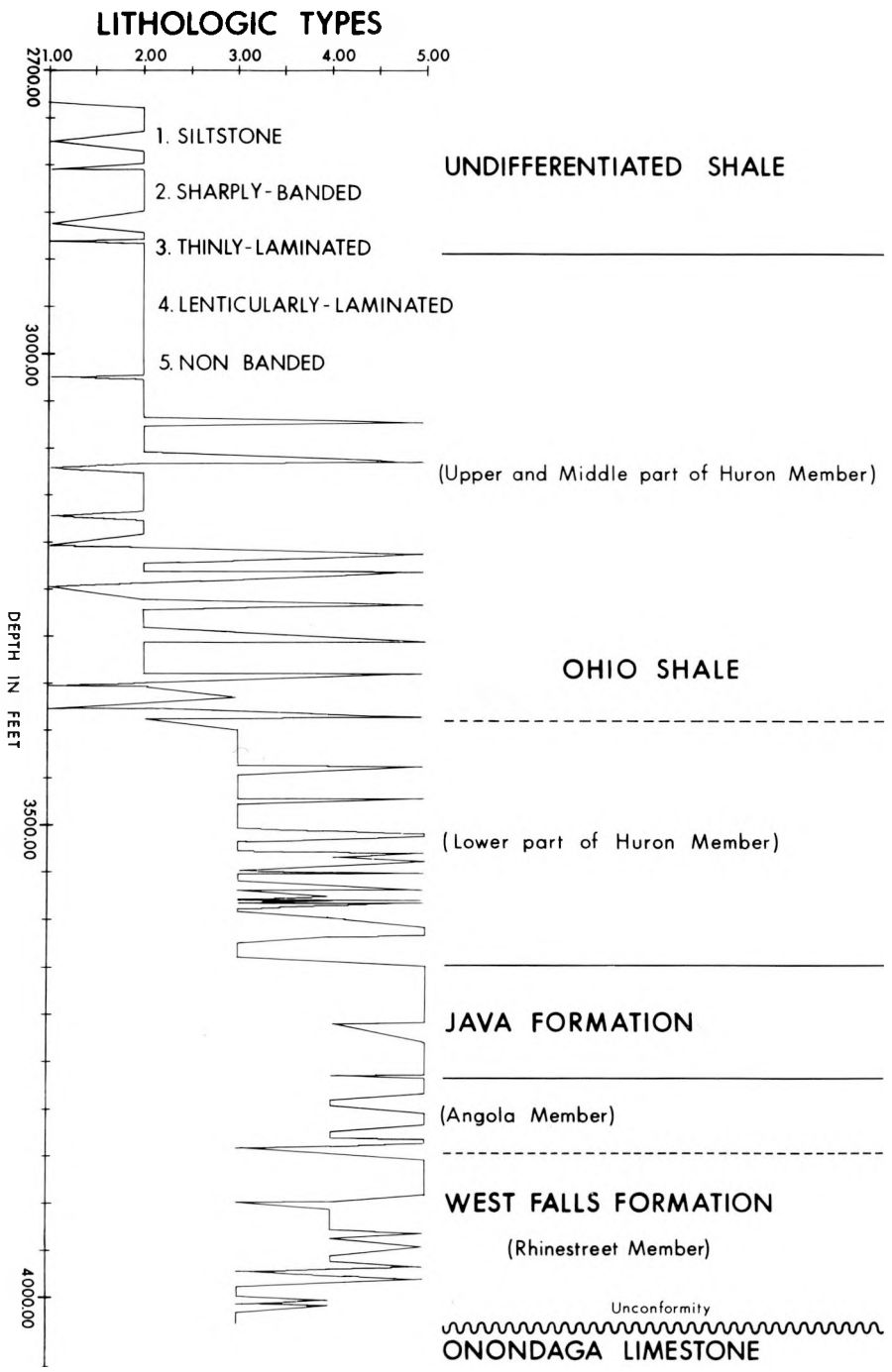


Figure 2. Distribution of shale lithotypes in the Lincoln 1637 core.

Table 1. Kolmogorov-Smirnov normality test on residuals of 14 variables.

Variable	N	D: Normal	P>D	Parametric tests applicable
14 Å clay	169	1.3573	0.05	no
Illite	169	0.4630	1.00	yes
thin section silt	169	0.6219	0.92	yes
Pyrite	169	0.8441	0.48	yes
LOI 100°C	169	1.2172	0.10	yes
Sulfur	169	1.2946	0.07	yes
Bulk density	169	1.3163	0.06	yes
Sonic	169	1.1216	0.16	yes
Resistivity	169	2.7194	0.00	no
Matrix density	169	1.4451	0.03	no
Log density	169	2.2888	0.00	no
Porosity	169	0.5398	1.00	yes
Gamma ray	169	2.0427	0.00	no
X-ray quartz	169	1.4240	0.03	no

Table 2. Significance test results of 14 variables measured on four shale lithologic types.

Variable	N	Degrees of freedom	KRUSKAL-WALLIS (non-parametric) K-W H	P>H	ANALYSIS of VARIANCE (parametric) F Value	PR>F
14 Å clay	169	3	21.25	.0001	6.20	.0006
Illite	169	3	21.90	.0001	8.00	.0001
Thin section silt	169	3	23.33	.0001	8.25	.0001
Pyrite	169	3	30.55	.0001	11.50	.0001
Losig 100	169	3	70.49	.0001	62.46	.0001
Sulfur	169	3	37.24	.0001	11.31	.0001
Bulk density	169	3	81.46	.0001	72.14	.0001
Sonic	169	3	71.39	.0001	37.58	.0001
Resistivity	169	3	41.41	.0001	16.56	.0001
Matrix density	169	3	68.51	.0001	59.56	.0001
Log density	169	3	67.86	.0001	13.94	.0001
Porosity	169	3	28.46	.0001	10.34	.0001
Gamma ray	169	3	56.10	.0001	22.43	.0001
X-ray quartz	169	3	36.65	.0001	17.59	.0001

Table 3. Means and standard deviations of lithologic types for 14 compositional and physical variables.

Variable	sharply-banded $\bar{x}$	sharply-banded σ	thinly-laminated $\bar{x}$	thinly-laminated σ	lenticularly-laminated $\bar{x}$	lenticularly-laminated σ	non-banded $\bar{x}$	non-banded σ
14 Å clay	0.0074	0.0047	0.0060	0.0027	0.0088	0.0034	0.0096	0.0042
Illite	0.4890	0.1071	0.4709	0.0841	0.5540	0.0735	0.5497	0.0771
Thin section silt	0.3388	0.0573	0.3643	0.0573	0.3045	0.0484	0.3161	0.0417
Pyrite	0.042	0.0283	0.0639	0.0293	0.0524	0.0362	0.0276	0.0254
LOI 100°C	3.3123	1.3164	7.1622	2.4990	4.1600	2.0699	2.4596	0.8637
Sulfur	1.9645	1.2723	2.5054	0.6484	1.7245	1.3314	1.1549	0.9398
Bulk density	2.6895	0.0444	2.5343	0.0703	2.6120	0.0873	2.6713	0.0275
Sonic	77.4377	3.5793	87.0541	5.0824	84.1000	5.3306	81.8298	5.0230
Resistivity	37.9231	11.0712	87.3243	71.3014	34.8500	45.3330	30.3830	29.6227
Matrix density	2.7266	0.0473	2.5814	0.0767	2.6890	0.0912	2.7364	0.0366
Log density	2.6568	0.0452	2.5370	0.0598	2.6450	0.2274	2.6011	0.0656
Porosity	1.4325	1.0893	2.0230	1.3081	2.8720	1.0973	2.4051	1.2596
Gamma	194.5538	15.7312	279.3243	57.5442	240.5000	95.1578	228.6170	50.6126
X-ray quartz	0.2340	0.1391	0.1458	0.0574	0.1091	0.0415	0.1211	0.0448

Table 4. Summary of relative values of means in Table 3; "L" represents those means that appear markedly low from others for each variable, and "H" represents relatively high mean values. No statistical significance is claimed for this summary.

	lithologic type			
Variable	sharply-banded	thinly-laminated	lenticularly-laminated	non-banded
14 Å clay	L	L	H	H
Illite	L	L	H	H
Thin section silt		H		
Pyrite				L
LOI 100°C		H		
Sulfur		H		
Bulk density		L		
Sonic	L			
Resistivity		H		
Matrix density		L		
Log density		L		
Porosity	L		H	
Gamma ray	L	H		
X-ray quartz	H			

REGIONAL SURVEY OF SURFACE JOINTS IN EASTERN KENTUCKY

by

Brian R. Long
Research Associate, Devonian Shale Program
West Virginia University
Department of Geology and Geography
425 White Hall
Morgantown, West Virginia 26506

ABOUT THE AUTHOR

Mr. Long received his A.B. from Alfred University, Alfred, New York, in 1971. He received his M.S. degree from West Virginia University, Morgantown, West Virginia, in 1979, and is presently employed by the Department of Natural Resources' Reclamation Office, Charleston, West Virginia.

2 REGIONAL SURVEY OF SURFACE JOINTS IN EASTERN KENTUCKY

ABSTRACT

A regional survey of eastern Kentucky surface joints was completed. Maps of joint strikes plotted a. rose diagrams show coal has the most consistent regional orientation of joints of all lithologies studied. Coal face cleats and coal structure form lines swing in the foreland of the Pine Mountain thrust fault. The face cleat swing could be due to the thrust, but may instead be a separate system related to basement shape or an edge effect created by the Russell Fork tear fault. The apparent independence of coal cleat strikes from the Pine Mountain thrust may be a result of isolation of coal from fault stress by movement along the fault plane or by the coal having too low a rank for fracturing when faulting occurred.

Outcropping Devonian shales show consistent joint strikes of N25E, N45E and N65W. First-formed and second-formed joints strike northeast and northwest, respectively. The N45E joint strikes occur predominantly along the eastern flanks of the Cincinnati Arch and Nashville Dome. The N25E joint strikes are concentrated in the Cumberland saddle between the Cincinnati Arch and Nashville Dome.

INTRODUCTION-LOCATION

It is generally believed that fractures in the Devonian shale provide the permeability needed for significant commercial gas production. It follows that if the nature, orientation and intensity of jointing in the Devonian shale can be determined, then the extent and location of potentially productive permeable zones can be predicted and better estimates of ultimate gas production realized. Jointing of the Devonian shales in gas producing areas may be reflected in surface joints through regional joint strike, size and spacing trends. A survey of surface joints was completed in order to establish these trends within the largest Devonian shale gas field in the world, the Big Sandy Field.

The study area is located in the unglaciated Appalachian Plateau of eastern Kentucky (Figure 1). Joints from 130 quadrangles east of a north-south line drawn between Maysville and Middlesboro, Kentucky and from quadrangles in the Devonian shale outcrop belt on the east side of the Cincinnati Arch were documented.

Rocks of Pennsylvania, Mississippian and Devonian age are exposed in the study area. Pennsylvanian strata are composed of deltaic sequences of sandstone, shale and coal. The Mississippian contains sandstones with some shales and older massive limestone formations. The Devonian comprises black shales underlain in some areas by a thin limestone.

METHOD

A random sampling system was used by considering the boundaries of 7½ minute quadrangles as a grid and obtaining one or more stations within each quadrangle. At each sampling station the strike and dip of joints, lithology (shales separated by color only), bed thickness, horizontal and vertical joint extent and joint spacing were noted.

The sequence of jointing was determined through abutting relationships. Kulander and others (1977) have shown that tension joints which form first provide a free surface which, unless cemented closed, cannot be crossed by later formed tension joints. Therefore, first-formed joints are abutted by second-formed joints, usually at or near a 90 degree angle. The first- and second-formed joint sets are generally the best formed joints at any given outcrop.

RESULTS

In addition to dewatering and devolatilization, tectonic stress plays an important part in coal cleat formation (Ting, 1977). Cleats generally have a directional relationship relative to coal form line structure and basement structure trends in West Virginia (Kulander and Dean, 1979) and eastern Kentucky. In eastern Kentucky, coal face cleat strikes rotate in the foreland of the Pine Mountain thrust (Figure 2). The thrust appears to have caused the cleat rotation; however, with the limited data available several alternative possibilities are feasible.

If coal fracturing occurred at the same time and as a direct result of the Pine Mountain thrust movement, then the coal cleats should have extension and release orientations relative to thrust movement. The thrust movement is presumed to be northwestward, so the tensional joint trend should be northwestward. These extension-release orientations would be expected to form a second cleat set

with any previously formed sets. These trends are not present. The coals do show one simple face-butt cleat set but it has a regional rotation.

Assuming coal cleats formed prior to the Pine Mountain thrust, a second fracture system related to the thrust should be present on the foreland, but it is not. The simplicity of cleat sets and their rotation in the foreland suggest that the cleat formation may be post thrust in response to basement deformation shape. Basement shape is poorly defined in the Pine Mountain foreland, however, the coal form line map (Figure 3) shows a general contour swing in this area. Coal face cleats show a consistent orthogonal relationship to coal form lines through West Virginia and rotate with them in front of Pine Mountain.

A second explanation for the absence of a fracture system related to the Pine Mountain thrust is linked to the time of coal lithification. Coal lithification may not have progressed far enough by the time of the thrust movement to allow significant fracturing. Lignite will fracture with wide spacing compared to normal coal fracturing; these fractures may have formed, but could have been obscured by later fractures operating under a different stress field.

A third explanation for coal cleat rotation in the foreland may relate to the Russell Fork fault. The junction of the Russell Fork and Pine Mountain faults (Figure 1) appears to be the hub around which coal face cleats rotate (Figure 2). This junction was probably an area of considerable stress between the Pine Mountain thrust sheet and sheets adjacent to it. Coal cleat rotation may be the foreland effect of two sheets moving at different speeds and having a definite point of stress at their extreme edges.

Plotting of joint strikes as rose diagrams by station and lithology on the map reveal consistent coal face cleat orientations over relatively large areas (Figure 2). Shale and sandstone joints are not consistently oriented and their first- and second- formed joint strikes were plotted separately to determine their degree of correlation with coal cleat strikes. Plotting of the angles formed between coal cleats and first- and second-formed joints as histograms found several relationships. Black shales show 46 percent of the angles are within 10 degrees of coal cleats and 37 percent lie between 20-30 degrees of coal cleats. This fairly good correlation may reflect the close proximity of coal and black shale often seen in the stratigraphic sequence. Gray shales show 41 percent of the angles are within 15 degrees of coal cleats and 44 percent are between 25-40 degress. The lack of close proximity of gray shales to coal and their increased silt content (with resulting change in strength characteristics) may account for these angular relationships. Sandstone showed no significant angular relationship to coal cleats. This indicates sandstone jointing in the deltaic Pennsylvanian sequence is too complex for regional interpretation.

DEVONIAN SHALE

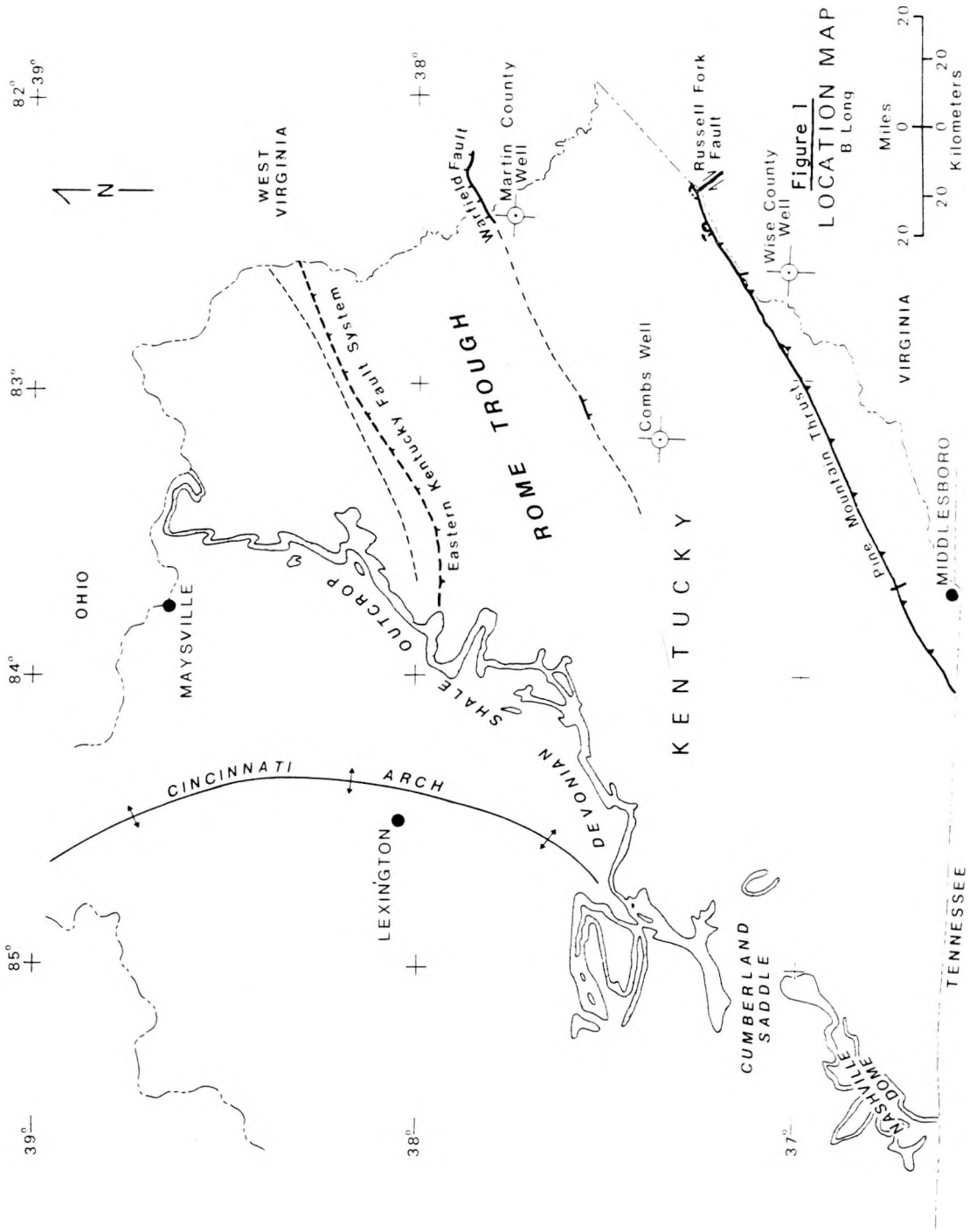
Devonian shales along the eastern flank of the Cincinnati Arch and Nashville Dome (Figure 1) show consistent joint strikes of N25E, N45E and N65W. First-formed and second-formed joints strike northeast and northwest, respectively. The N45E joint strikes occur predominantly along the eastern flanks of the Cincinnati Arch and Nashville Dome. This strike set is roughly parallel to the N40E striking outcrop belt and may have formed as a tension feature related to the regional dip of the Cincinnati Arch and Nashville Dome. The N25E joint strike set is concentrated in the Cumberland saddle area (Figure 1) and is clearly a rotation from the previously discussed strike set. The Cumberland saddle is an area of Cambrian age basement faulting which probably rotated the regional stress fields of the Cincinnati Arch and Nashville Dome.

REFERENCES

Kulander, B. R., and Dean, S. L., 1979, ms, Rome trough relationship to fracture domains, regional stress history and decollement structures: (in review for Proc. of the Southeast Section Geol. Soc. of America Symposium on Western Limits of Detachment and Related Structures in the Appalachian Foreland).

Kulander, B. R., Dean, S. L., and Barton, C. C., 1977, Fractographic logging for determination of pre-core and core induced fractures - Nicholas Combs No. 7239 Well, Hazard, Kentucky: MERC-77/3, Distribution Category VC-02, Energy Research Center, Morgantown, W. Va., p. 20 and 33.

Ting, F. T. C., 1977, Origin and spacing of cleats in coal beds: Journal of Pressure Vessel Technology, v. 99, p. 624-626.


82°
39°
83°
84°
85°
39°
38°
37°
N
WEST VIRGINIA
OHIO
MAYSVILLE
LEXINGTON
CINCINNATI ARCH
OUTCROP SHALE
DEVONIAN
Eastern Kentucky Fault System
ROME TROUGH
Warfield Fault
Martin County Well
Combs Well
Russell Fork Fault
Wise County Well
Pine Mountain Thrust
KENTUCKY
VIRGINIA
MIDDLESBORO
CUMBERLAND SADDLE
TENNESSEE
WASHBOWELL
Figure 1
LOCATION MAP
B Long
Miles
Kilometers
20
0
20
20
0
20

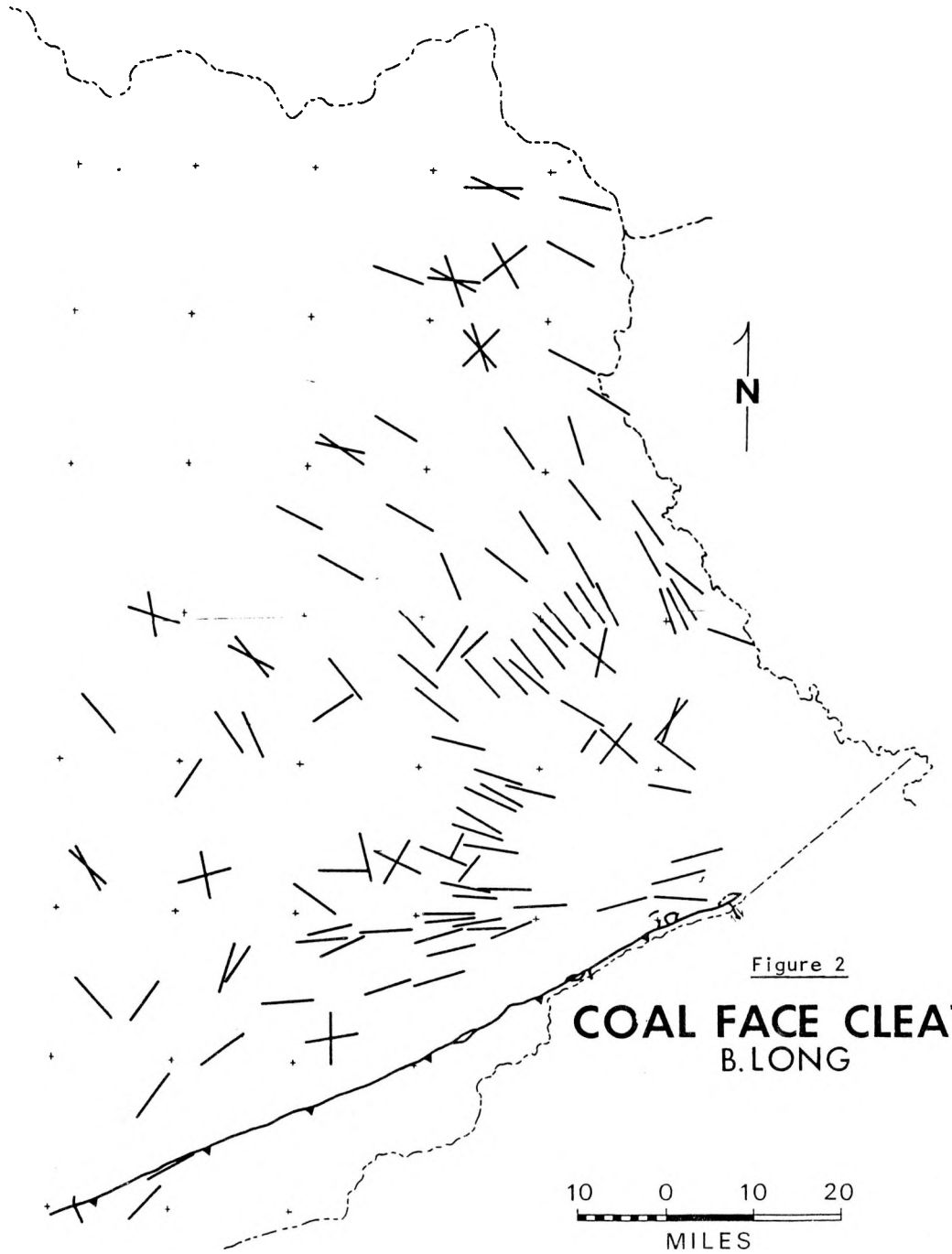


Figure 2

COAL FACE CLEATS
B. LONG

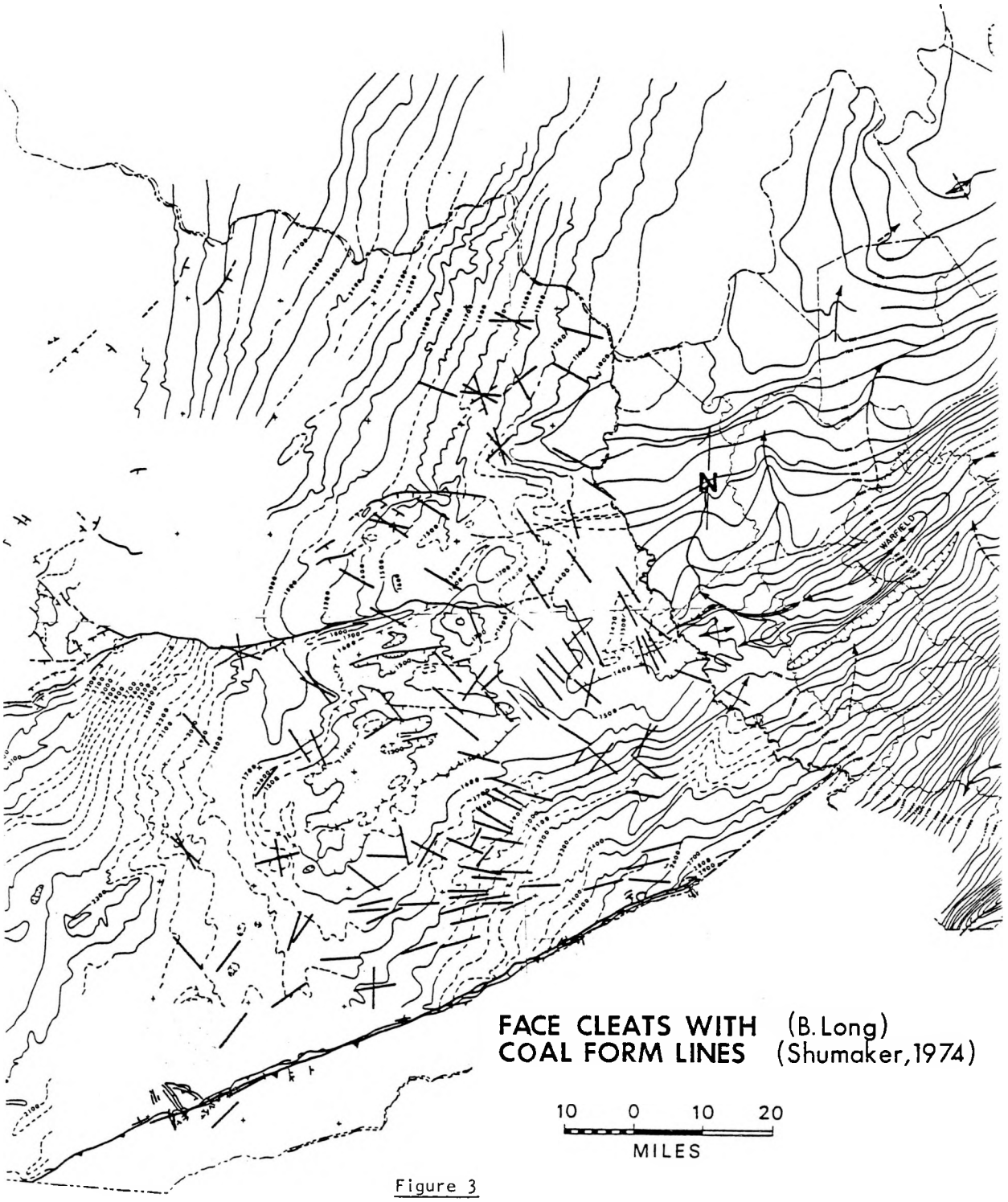

N
WARFIELD
FACE CLEATS WITH (B. Long)
COAL FORM LINES (Shumaker, 1974)
10 0 10 20
MILES

Figure 3

PARAMETERS OF GEOLOGIC STRUCTURE WHICH AFFECT DEVONIAN GAS SHALE PRODUCTION IN WEST VIRGINIA AND EASTERN KENTUCKY - A PROGRESS REPORT 1978-1979

by

R. C. Shumaker, Project Director
Devonian Shale Program

co-authored by

R. R. Beebe, J. Negus-de Wys, J. M. Dixon, M. A. Evans, K. G. Kirk,
K. D. Lee, B. R. Long, H. W. Rauch, J. E. Ruotsala, W. W. Schaefer,
R. L. Wheeler, R. T. Williams, T. H. Wilson

West Virginia University
Department of Geology and Geography
425 White Hall
Morgantown, West Virginia 26506

ABOUT THE AUTHORS

Dr. Shumaker is director of the West Virginia University - Department of Energy contract investigating the structural parameters that influence Devonian shale gas production. Drs. Wheeler, Williams, and Rauch direct the surface structure studies, geophysical, and ground water studies of this program respectively. Dr. Wheeler is presently with the U. S. Geological Survey, Denver, Colorado. All principal investigators were enrolled in the graduate studies program at West Virginia University during the 1978-79 academic year.

PRINCIPAL INVESTIGATORS

Robert R. Beebe, B.S. Northeastern University 1976, Boston, Massachusetts
- Hydrology (completed 2 years, M.S. candidate) presently with Exxon, Corpus Christi, Texas

Jane Negus-de Wys, A.B. Miami University 1946, Oxford, Ohio
- Production (2nd of 3 years, Ph.D. candidate)

Jeanette M. Dixon, A.B. Baylor University 1970, Waco, Texas; M.S. University of Akron 1976, Ohio
- Surface Structure (2nd of 3 years, Ph.D. candidate)

Mark A. Evans, B.S. West Virginia University 1978, Morgantown, West Virginia
- Subsurface Fractures (1st of 2 years, M.S. candidate)

Keith G. Kirk, B.S. Penn State University 1973; M.S. West Virginia University 1976
- Geophysics (completed 3 years, Ph.D. candidate) presently with U.S.G.S., Denver, Colorado

Kevin D. Lee, B.S. West Virginia University 1978
- Regional Structure (1st of 2 years, M.S. candidate)

Brian R. Long, A.B. Alfred University 1971, Alfred, NY; M.S. West Virginia University 1979
- Fractures - Eastern Kentucky (completed 2 years, M.S.) presently with W. Va. Department of Natural Resources, Charleston, W. Va.

2 PARAMETERS OF GEOLOGIC STRUCTURE WHICH AFFECT DEVONIAN GAS SHALE PRODUCTION IN WEST VIRGINIA AND EASTERN KENTUCKY - A PROGRESS REPORT 1978-1979

James E. Ruotsala, B.S. Michigan Tech 1973; M.S. Michigan Tech 1975, Houghton, Michigan
- Geophysics (1st year of 3 years, Ph.D. candidate)

William W. Schaefer, B.S. Campbell College 1971, Buies Creek, North Carolina; M.S. West Virginia University 1979
- Production, consulting geologist

Thomas H. Wilson, A.B. West Virginia University 1974; M.S. West Virginia University 1977
- Surface Structure (2nd of 3 years, Ph.D. candidate)

ABSTRACT

Major accomplishments during 1978-1979 include:

1. Production studies: A recognition that the best production (fracture porosity) occurs in synclines, off structure, in two West Virginia fields. Two exploration rationales developed from this study. Continued accumulation of basic geologic, geochemical, and production data for the large Eastern Kentucky Shale Gas Field is in preparation for an integrated analysis.

   Studies using XRF and XRD on well cuttings from 14 wells in eastern Kentucky yielded elemental data for 12 elements and mineralogical data for 16 minerals. A high correlation was found between contoured averages of seven elements and density contours of high producing wells (final open flow).

2. Surface structure: A technique was developed to estimate the fracture intensity in areas of limited rock exposure, and a study continues of Devonian shale deformation along a cross-strike structural discontinuity that intersects an Appalachian Valley and Ridge fold.

3. Fracture studies: Surface fractures of eastern Kentucky showed diverse trends dependent on lithology. Predicting the trends of subsurface fractured reservoirs from surface fracture trends is hazardous in areas of detached deformation. Natural fractures and induced fractures were logged and summarized for Devonian shale oriented cores taken in Mason County and Monongalia County, West Virginia. Gas shows in these two wells relate to partially mineralized fractures. Some 13 Appalachian Basin cores are described.

4. Hydrology: The comparison of shallow ground water productivity and quality with production from shale gas wells within the Midway-Extra field was completed, and there is a correlation of gas production with one low-altitude photo lineament trend.

5. Geophysics: Several seismic and resistivity techniques were tested to evaluate what method can best detect shallow fractures. These techniques are being applied to the Cottageville, West Virginia, field area to determine if shallow geophysical techniques are useful in determining fracture production trends.

INTRODUCTION

Most of the research tasks in our program, outlined below, reached or exceeded a two year level of effort this October, so that we are now beginning to reap benefits from our research efforts concerning the origin of fracture porosity in the Devonian shale of the study area (Figure 1). By the time of this third annual meeting of the Eastern Gas Shales Project and the publication of the Preprint volume, we will have completed five separate studies which relate fracture porosity and structural parameters; these include: two production studies which document the effect of geologic structure on production in specific West Virginia shale gas fields, the Cottageville and Midway-Extra fields, a third study which documents surface fractures in eastern Kentucky, a hydrologic study which compares shallow water well productivity and quality with shale gas production from the Midway-Extra field, and finally we completed a study on fracture porosity related to tectonic thinning and shale flowage as studied in selected folds of the Appalachian Plateau and Valley and Ridge physiographic-structural Provinces.

In the first part of this report we introduce the objectives and organization of our contract for those unfamiliar with its background. We then briefly summarize progress made toward attaining these objectives. However, we have expanded this discussion and emphasized significant results of completed studies wherever an important subject is not covered by companion papers published in this Preprint volume. These companion papers which discuss the results of studies progressing under this

contract include:

1.) Cross-strike Structural Discontinuities: Exploration Rationale for Eastern Plateau Province - Russell L. Wheeler

2.) Tectonic Thinning by Extension Faulting and Shale Flowage, and Implications for Fractured Gas Reservoirs - Philip S. Berger and Russell L. Wheeler

3.) Lithology Studies of Upper Devonian Well Cuttings in the Eastern Kentucky Gas Field - Jane Negus-de Wys

4.) Inorganic Geochemical Studies of Eastern Kentucky Gas Field(s) and Comparison with Gas Production - Jane Negus-de Wys and John J. Renton

5.) Regional Survey of Surface Joints in Eastern Kentucky - Brian R. Long

6.) Lineaments and Water Wells as Exploration Tools in the Midway-Extra Gas Field - Robert R. Beebe and Henry W. Rauch

7.) The Parsons Cross Strike Structural Discontinuity as an Exploration Area for Fractured Gas Reservoirs - Jeanette M. Dixon and Thomas H. Wilson

One important subject not covered in a companion paper includes work which the senior author considers to be a major breakthrough in understanding the origin of the fracture porosity in commercial shale gas wells that are located near the periphery of commercial production in West Virginia (Figure 1). This understanding is most significant to the Eastern Gas Shale Program; so we will place our emphasis in this text on a description of the examples and the data on which we base our conclusions. We believe that the results of our work on fracture porosity in shale also have application to other tight reservoirs, particularly in exploration for fractured tight reservoirs of the mid-continent region, an area where basement tectonics dominates. The senior author emphasizes this model developed through an integrated approach where the efforts of the following people have been essential: Mr. E. B. Nuckols III's effort in collecting the data at the Cottageville field (1976[1] and 1978),[2] Mr. William W. Schaefer's investigation and report on the Midway-Extra field (1979),[3] Mrs. Jane Negus-de Wys' analysis of production data from the Cottageville field (de Wys and Shumaker, (1978)[4] and Mr. Glenn R. Sundheimer's excellent seismic interpretation of the Cottageville field area (1978).[5] This integration of work and the extrapolation of ideas is the responsibility of the senior author.

OBJECTIVES

The general objective of our research funded under United States Department of Energy Contract number DE-AC21-76MC05194 (formerly EY-76-C-05-5194) is to study the structural parameters of the Devonian shales that affect gas production in eastern Kentucky and West Virginia (Figure 1).

To that end our program is specifically designed to:

1. Collect, compile, and analyze geologic data to construct regional structure maps of eastern Kentucky and West Virginia.

2. Determine if structural types and styles affect production and influence production characteristics.

3. Determine if shallow seismic surveys can detect near-surface faults and fracture zones, and if such structures can be detected, to further determine how fractures relate to both production from the shale and to lineations observed on remotely sensed data.

4. Determine if a relationship exists between ground water movement and shale gas productivity.

Through the integration of our work with others, it is our ultimate goal to discover if relationships exist between Devonian shale gas production and geologic structure. If such a relationship is established, we will attempt to develop a method or methods for selecting favorable sites to drill shale wells that have a greater potential for gas production than the norm for that region.

PARAMETERS OF GEOLOGIC STRUCTURE WHICH AFFECT DEVONIAN GAS SHALE PRODUCTION IN WEST VIRGINIA AND EASTERN KENTUCKY - A PROGRESS REPORT 1978-1979

4

ORGANIZATION

In order to attain the stated objectives we have designed several tasks which have been organized into five study groups. Four of these groups: regional structure studies, fracture studies, structural type studies, and production studies, are carried under the U.S.D.O.E.'s Resource Inventory Tasks. One group, geophysical studies, is carried under Shale Characterization Tasks.

In essence, the first two tasks, that is the regional structure and fracture studies, are designed to provide a regional structure base for the study area. The structural type studies seek to document, by analytical field work, details of structures which are either similar to structures producing gas or which are similar to those which we feel could be prospective. The production studies will seek out and study gas fields where detailed well production records are available that permit thorough analysis and documentation of the geologic parameters that influence gas production from the shale. The geophysical studies are charged with the task of developing inexpensive geophysical techniques that can locate shallow fracture zones of high permeability.

PROGRESS AND PLANS 1978-1979

Regional Structure Studies

The emphasis of our effort here has shifted from compilation of areal structure maps to the construction of detailed structure maps for specific areas. A shift in emphasis was made because results of our production studies show that the shale gas production is related to structures that have very low structural relief at the Devonian level, and that such prospective structures frequently can be located only through the construction maps with a contour interval of ten or twenty feet. We are applying this technique to areas adjacent to the Cottageville and Midway-Extra fields in West Virginia, and we are accumulating data for analysis and characterization of the largest shale gas field, the Big Sandy Gas Field, of eastern Kentucky. The object of these investigations is to test our ideas concerning the relationships between production and geologic structure, characterize relationships in other productive areas of the basin, and to define prospective shale gas trends so that industry will be challenged to use our work or ideas in field well step outs and wildcat exploration.

Production Studies

Detailed investigation of the Midway-Extra field of Putnam County, West Virginia, by William W. Schaefer (1979)[3] established a direct relationship between production from the lower Huron Devonian shale and the structural trend of that field. Schaefer was able to confirm that initial and final open flows from wells at Midway-Extra are greatest along the northwestern limb of the Midway anticline, that is, in the adjacent syncline, off structure. He also found a lesser increase on the southeastern limb. The striking similarity of high flow rates with structural position along the fold is forcefully brought out by comparing Figures 2 and 3 taken directly from Schaefer's text (1979)[3]. Furthermore, he showed that the thickening of the lower Huron shale, the primary reservoir, into the adjacent syncline (Figure 4) suggests growth of the structure during sedimentation. He interpreted this to mean that basement deformation is important in the formation of the Midway anticline. From these data (Figures 2, 3, 4, and 5) at the Midway-Extra field one cannot be absolutely certain if it is the over-thickened lower Huron-organic shale or if it is fractures associated with the folding which contributes most to the noted increase of off-structure flow rates. One also might argue that even if fractures are present, they are not necessarily structural in origin. They could be caused by other lithologic factors or even as a result of differential compaction between thin shale on and thick shale off structure. Regardless of the cause, an empirical exploration rationale was proposed based on Schaefer's study (1979).[3] Direct evidence for the exact underlying cause as well as the precise siting of wells expecting commercial production was still elusive even though Schaefer had made a major guiding breakthrough.

If, however, we combine what we learned at the Midway-Extra field with what we know of the Cottageville field, then additional insight is gained into the specific cause for shale gas production for that portion of West Virginia (Figure 1). At first glance, the similarity between Cottageville (Martin and Nuckols, 1976;[1] Nuckols, 1978;[2] and de Wys and Shumaker, 1978)[4] and the Midway-Extra field is not striking. Structurally, the Cottageville field appears to lie along a very low relief flexure on a southeast dipping regional slope. The cause for the flexure was inferred to be a basement fault (Martin and Nuckols, 1976[1] and Shumaker, unpublished maps).[7] Detailed interpretation of seismic data collected by Geophysical Services, Incorporated, by Glenn Sundheimer (1978[5]

and 1979)[6] confirmed this interpretation, and his work further established that a basement fault directly underlies the trend of the most productive wells along the south flank of the Cottageville field (compare Figures 6 and 7). Please note the southeast regional dip, and also note that Sundheimer mapped a subdued flexure and syncline just updip from the fault (Figure 6), that is, northwest of the fault. These structures are similar to, although not identical to ones mapped by E. B. Nuckols III (Manuscript in preparation), from detailed subsurface geologic data. Nuckols has found that sedimentary patterns of the organic shales are complex around this structure. His unpublished maps also show that the best production does not uniquely follow the thickest lower Huron organic shale section. The best production lines up with the fault as mapped by Sundheimer. If one eliminates the regional dip from Sundheimer's isotime structure map (Figure 6), then the Cottageville field becomes a low fold with flanking synclines. It is only now that the Cottageville field appears similar to the Midway-Extra field, but Cottageville has far less relief. Keeping this in mind, compare the position of the fault, the fold crestal trace, and the trace of the flanking northern syncline with the production trends at Cottageville as mapped by de Wys and Shumaker (Figures 8, 9, and 10). There is a marked similarity of the final open flow map of the Midway-Extra field with production maps at Cottageville. This similarity is noted by lower productivity along the structural crest of both structures. In the case of Cottageville there is a near coincidence of productive trends shown on the summary trend map (Figure 11) above and parallel to the fault. The trends are not nearly as numerous for the northern syncline (Figures 6 and 11) which, incidentally, may be the southwest terminus of another buried fault. In the case of Cottageville, the comparison between structure and production seems far more conclusive than at Midway-Extra simply because of the greater quality and quantity of data. At Cottageville it is clear that better wells occur off-structure and that the best wells generally occur directly above the basement fault. De Wys and Shumaker (1978)[4] contoured the production data at Cottageville (Figures 7 thru 10) with a mechanical style, attempting to avoid bias in their contouring. Had they contoured the production data as Schaefer did, and if they had both Schaefer's results and Glenn Sundheimer's map, then the Cottageville production maps would be different, and the identity of structure with production trends would be more striking.

Using re-interpreted Cottageville as background, we can now go back to Midway-Extra and re-interpret the northwestern flank of the anticline suggesting that it is faulted at depth. The justification for this interpretation is that the high productivity wells at Cottageville are located along and above a fault.

Thus far we have pointed out the similarity between the fields, but there still is uniqueness to each field. This uniqueness is seen at Cottageville as we reimpose regional dip toward the southeast on that structure. We now have a logical reason for why the best producing wells occur near the western terminus of the fault and near the western terminus of the east plunging syncline on the north flank of the field. We interpret these areas as the updip end of fracture porosity associated with the structure. It is reasoned that the fracture porosity acts like a stratigraphic or diagenetic trap encased within the lower Huron shale (Shumaker 1978).[8] Shale gas has migrated up-plunge, westward, to the end of the fracture porosity. Furthermore this area appears to be along a change in the regional dip, a line of change or flexure from the broad flat Parkersburg syncline to the steeper slope leading toward the Cincinnati Arch. The significance of this observation remains unaccessed until we have more regional data, but it may be a key to why the Cottageville field produces compared with Devonian shale above other basement faults.

If we carefully study the Midway-Extra field we note a uniqueness there; the high flow wells align into minor north trending patterns (Figure 3) parallel to minor structural trends and an intersecting structural trend at the northeastern end of that field (Figure 2). We reason that these better wells occur at the intersection of the two fault trends. This, again, is a logical extension of the interpretation given above. We hypothesize that, if one fault yields good porosity, then the intersection of two should yield more porosity and therefore excellent production. This observation leads to a second substantive rationale for exploration; drill on the intersection of fault trends - on the low side.

There are a multitude of methods to develop fractures and thereby potential fracture permeability, that is, by: basement structure, detached structure, compaction, sedimentary diagenesis, overburden removal, etc., it is the senior author's conclusion that basement growth structure is the most effective means of producing commercially effective porosity within this area of West Virginia. The importance of this understanding and the application of these exploration guidelines to southwestern West Virginia are heightened by a similar observation made by Don Neal (manuscript in preparation) of the West Virginia Geological and Economic Survey concerning the coincidence of higher initial flow from gas wells located on the flanks of geologic structures. This conclusion is based on his work in

the adjacent area of West Virginia to the south. It therefore seems likely that these rationales can be extended southward into adjacent counties of southern West Virginia.

As to why the fractures select the lower Huron shale section as the host unit, one can only speculate. The physical response of the lower Huron to deformation must be related to its lithology, but the exact nature and origin of the stress field creating the fractures still remains uncertain. Vertical basement tectonics seems to be an important source of that stress within the area described, but one cannot eliminate the importance of a horizontally directed stress field modifying and intensifying the local stress field (Advani 1978[9] and Shumaker 1978).[8]

A word of caution regarding the model and rationales described in this paper. The model was developed as a result of our characterization of structural parameters that affect shale production in southwestern West Virginia, and therefore it should not be applied indiscriminately or universally as a unique solution to other areas. It clearly is not a unique solution for fracture porosity. Certainly there are numerous ways to produce open fractures and therefore potentially productive shale gas areas in the multitude of tectonic environments and structural styles within the Appalachians. Our interpretations do not deny the existence or the influence of other fracture types on production even within these southwestern West Virginia shale gas fields, for we know that other genetic fracture types, which may be significant to production, are present within the Devonian shale (Shumaker 1978).[8]

The model described above obviously has its greatest application to southern West Virginia, but we believe it also has application to the mid-continent area. This area is largely undeformed. The prevailing structure is systematic, largely orthogonal, joints; but where the flat lying sediments are deformed, it is generally by basement deformation and often recurrent basement deformation (Shumaker 1979).[10] We suggest for your consideration that a reason for lack of shale production within this immense mid-continent area may relate to the position of most wells on structural prospects. They clearly are not drilled on the flanks of structures, down-dip from the crest, unless there is a stratigraphic reason. We may have a reason for such exploration: structurally controlled fracture facies.

The Eastern Kentucky Gas Field is the third field selected for detailed analysis. We are presently in the midst of our work. Well cuttings (500+) from 14 wells in the Eastern Kentucky Gas Field have been examined and described. Cross sections are being constructed to study details of lithological changes in the Berea-Huron stratigraphic sequence. Results to date are presented in a separate paper in these meetings (de Wys, these Preprints).

Graphs, computer maps, and statistical analyses are in progress on a geochemical study of well cuttings from 14 wells in the Eastern Kentucky Gas Field (same wells as lithology studies with one exception). Fourteen elemental oxides (except Sulphur) and sixteen minerals are under examination. Certain maps show a high degree of correlation to density contours of high producing wells (based on 5000 wells). Results to date are presented in a separate paper in these meetings (de Wys, these Preprints).
Final stages of the study of the Eastern Kentucky Gas Field are commencing. Final open flow data are being compared to structural depths, shale thickness, lithological changes, evidence of fracture occurrence, high organic content, and geochemistry. Results of this phase of the field study will be presented at a later date.

A paper on the paleogeographic development of the field as relative to plate tectonics is presented in the AAPG section of these meetings (de Wys, these Preprints).

Structural Type Studies

Analysis of the Parsons and Petersburg cross-strike structural lineaments (Figure 1) in the high plateau country of West Virginia have been conducted to determine: (1) joint intensity within and adjacent to the lineaments, (2) the nature of joint intensity with depth, and (3) the westward extent of the two lineaments. Rock is found to be more intensely jointed within the Parsons lineament in the Upper Devonian Chemung siltstones, mudstones, and shales of Tucker County, West Virginia, (Dixon, 1979a,[11] 1979b;[12] Dixon and Wilson, these Preprints).[13] The lineament extends northwest and terminates in Taylor County. It is expressed in Lower and Middle Pennsylvanian sandstones as two zones of intense jointing (Dixon and Wilson, these Preprints). The Petersburg lineament was studied along the Allegheny Front to determine the effect of joint intensity with depth. Joints in Devonian shales, siltstones, and sandstones and Lower Mississippian sandstones were measured. The width of the zone of intense jointing does not vary with depth. However, intensity is significantly

greater in the Middle Devonian black shales than in other lithologies (Figure 12). The Petersburg lineament extends west-southwest to the Randolph-Upshur County line where it is disrupted or terminates. This lineament is manifest in Lower and Middle Pennsylvanian sandstones with intensities similar to those in Parsons lineament.

A three phase study of surface structures in Middle and Upper Devonian shales in Middle Mountain syncline (Figure 1) of the Valley and Ridge province, Pendleton County, West Virginia, has been completed. The study included the following: 1) detailed mapping of the Middle Mountain syncline, 2) an analysis of bedding orientation contours of the syncline (Wilson, 1979a[14] and 1979b),[15] and 3) a study of the orientations and spacings of systematic joints in the shales of the syncline. The studies were designed to characterize the Parsons cross-strike structural discontinuity (PCSD) in terms of faulting, folding and jointing in the exposed Devonian shale sequence. The PCSD is found to coincide with a zone in which structural shortening is taken up by smaller folds and more abundant thrust faults. In consequence, the shales within this zone are also more intensely jointed. The details of parts of this study are discussed in Dixon and Wilson, 1979, presented in this Preprints volume.[13]

Fracture Studies

A regional survey of eastern Kentucky surface joints was completed to determine if surface fracture trends or domains, areas of similar trending joints, relate to high producing trends or high producing areas within the eastern Kentucky shale gas fields. Maps of joint strikes plotted as rose diagrams show that coal has the most consistent regional orientations of joints in the lithologies studied. Joints in black shale, brown shale, gray shale, and sandstone have varying angular relationships to regional coal cleat strikes. This dissimilarity between trends associated with each surface lithology makes prediction of subsurface fracture trends in the Devonian shale reservoir hazardous. Coal face cleats and coal structure form-lines change trend to become sub-parallel to the trace of the Pine Mountain thrust fault (Figure 13). Regardless of its origin, this gradual change in trend of face cleat trends is coincident with the most productive area in the eastern Kentucky shale gas field. The precise significance of this coincidence has not been determined as shale gas production extends into the areas of usual face cleat trend, that is, perpendicular to Appalachian fold axes. (Results of this study are also given in a companion paper (see Long these Preprints).

Outcropping Devonian shales along the east flank of the Cincinnati Arch show consistent joint strikes of N25E, N45E and N65W. First-formed and second-formed joints strike northeast and northwest, respectively. This is opposed to the coal cleat trend over the eastern Kentucky gas field where face cleats (first-formed) strike northwest and change to become nearly E-W in the Pine Mountain thrust area.

Thirteen oriented Devonian shale cores from the Appalachian Plateau of West Virginia, Kentucky, Ohio, Virginia, and Pennsylvania have been examined for fractures (Figure 1). The orientation, type of mineralization (if any), and presence of fractographic features, i.e., plume, hackle, and arrest lines, were recorded for each fracture. Fractures were differentiated into three types: natural, core induced and slickenside. Frequency and orientation for each type of fracture have been plotted against core depth to determine the existence of possible fracture facies and decollement zones as well as changes in current in-situ stress and paleo stress as a function of depth or lithology. Regional subsurface fracture patterns are plotted and are being examined for comparison with the regional structure. Open file reports are available for two of the cores studied, Mason County #3 D/K core, West Virginia, and Monongalia County MERC #1 core, West Virginia. Reports on the other cores examined will be available in early 1980.

Ground Water

A hydrogeologic characterization study was done in the Midway-Extra Devonian shale gas field (Figure 1) of northern Putnam County, West Virginia. Lineaments were mapped and water wells were surveyed for physical and chemical parameters to compare with initial yield of nearby shale gas wells.

Northwest trending short straight photolineaments are significantly associated with water-well yield. Water wells located within 200 feet of a lineament's center line have significantly higher yields. Gas wells located near short photolineaments of the same trend had significantly higher initial open flows (both before and after stimulation) than wells located near other photolineaments. Gas wells also had significantly higher initial open flows when located in areas where photolineament density is high. Gas wells located near the most certain photolineaments had higher initial open flows than wells near less certain photolineaments. Landsat lineaments appear to be poor locations for gas

wells, and they do not overlap the high gas-producing areas.

Certain water-well parameters are also associated with initial gas well yield. Water wells located within high initial gas flow areas (over 100 MCF/day after stimulation) have significantly higher bicarbonate and nitrate concentrations than wells in low producing gas areas.

The results of our analyses here at Midway-Extra are similar to those found at Cottageville (Jones and Rauch, 1978)[16] except that at Cottageville the trend of gas associated short lineaments is west-northwest. More detailed results of this study are reported in a companion paper of this Preprint (see Beebe and Rauch).

Geophysical Studies

The main thrust of the geophysical effort at West Virginia University is the characterization of some of the acoustic properties of both the fractured and unfractured zones. The hope, of course, i to determine which properties may serve as reliable exploration criteria.

Refraction seismic surveying will be used for shallow studies of lateral velocity changes. The nature of both the method and our equipment limits the depth of investigation to ±800 feet. Since w will record waveforms (as well as travel times) attenuation anomalies may be observed.

High resolution reflection seismic surveying will provide data on small scale structures, attenuatio anomalies, and acoustic velocity at depths greater than is possible with our refraction method. Our high resolution reflection seismic method uses an explosive source in a 7 foot deep shot hole. The geophones are in 4 foot deep holes. Since attenuation of high frequency acoustic energy is most severe in the weathered, near surface material, this procedure results in band width wider than that of more conventional techniques; and shot and geophone ground coupling are improved. Surface waves are eliminated from the records by burial of the geophones and high pass input filters. Burying the geophones also attenuates noise from other sources (e.g., wind, traffic, etc.). Signal to noise ratio is thus improved. Our signal band appears to be ±300 hz to ±1 khz resulting in vertical resolution of a few feet.

Results from a test site in Wetzel County and a high frequency line from Cottageville should be available by the date of this meeting (Figure 1, Test Site II).

REFERENCES

1. Martin, P., and Nuckols, E. B., III, 1976, Geology and oil and gas occurrence in the Devonian shales, northern West Virginia, in Shumaker, R. C., and Overbey, W. K., eds., Devonian shale production and potential: USERDA - Morgantown Energy Research Center Special Report, MERC/SP-76/2, p. 20-40.

2. Nuckols, E. B., III, 1978, Exploration parameters derived from historical Devonian shale production in western West Virginia: Preprints 2nd Eastern Gas Shales Symposium, U. S. Department of Energy, METC/SP-78, v. 6, no. 1, p. 169-185.

3. Schaefer, William W., 1979, Geology and producing characteristics of certain Devonian brown shales in the Midway-Extra field, Putnam County, West Virginia: M.S. thesis, West Virginia University, 67 p.

4. de Wys, J. Negus, and Shumaker, R. C., 1978, Pilot study of gas production analysis methods applied to Cottageville field, Devonian Shale Program: Department of Geology and Geography, West Virginia University, under Contract EY-76-C-05-5194, U. S. Department of Energy, Morgantown Energy Research Center.

5. Sundheimer, Glenn R., 1978, Seismic analysis in the Cottageville field: Preprints 2nd Eastern Gas Shales Symposium, DOE/METC/SP-78/6, v. 1, p. 192-193.

6. Sundheimer, Glenn R., unpublished isotime structural map: top of the basement (Cottageville field, West Virginia).

7. Shumaker, Robert C., unpublished maps: structure on top of the basement, West Virginia and eastern Kentucky.

8. Shumaker, Robert C., 1978, Porous fracture facies in the Devonian shales of eastern Kentucky and West Virginia: Preprints 2nd Eastern Gas Shales Symposium, U. S. Department of Energy, METC/SP-78, v. 6, no. 1, p. 360-369.

9. Advani, S. H., Gangaroa, H. V. S., Chang, H. Y., Dean, C. S., and Overbey, W. K., 1977, Stress trajectory simulations across the Appalachian Plateau Province in West Virginia, in Schott, G. L., Overbey, W. K., Hunt, A. E., and Komar, C. A., eds., 1st Eastern Gas Shales Symposium, U. S. Department of Energy, Morgantown Energy Research Center, MERC/SP-77/5, p. 442-448.

10. Shumaker, Robert C., 1979, Paleozoic disruptive deformation in North American continent and its relationship to the formation and development of interior basins and deformation within the Orogenic core: oral presentation Eastern Section of Amer. Asso. of Pet. Geol., Oct. 1-4, 1979, Lakeview Country Club, Morgantown, WV.

11. Dixon, J. M., 1979a, A method to identify zones of intense jointing with application to the Parsons lineament, West Virginia: Morgantown Energy Technology Center Open-File Report, Morgantown, WV, 46 p.

12. Dixon, J. M., 1979b, A method to identify zones of intense jointing with application to the Parsons lineament, West Virginia (abs): Geol. Soc. Amer. Abs. with Programs, v. 7, p. 1286.

13. Dixon, J. M., and Wilson, T. H., 1979, The Parsons cross-strike structural discontinuity as an exploration area for fractured gas reservoirs: Preprints 3rd Eastern Gas Shales Symposium, Oct. 1-4, 1979, Lakeview Country Club, Morgantown, WV.

14. Wilson, T. H., 1979a, Bedding orientation contours of Middle Devonian shales in the Middle Mountain syncline, Valley and Ridge Province, West Virginia (abs): Geol. Soc. Amer. Abs. with Programs, Northeastern Sec. of the Geol. Soc. of Amer., 14th Annual Meeting, v. 11, no. 1, p. 60.

15. Wilson, T. H., 1979b, Bedding orientation contours of Middle Devonian shales exposed in the Middle Mountain syncline, Valley and Rodge Province, West Virginia: Morgantown Energy Technology Center Open-File Report, Morgantown, WV, 39 p.

16, Jones, D. S., and Rauch, H. W., 1978, Lineaments and ground water quality as exploration tools for ground water in the Cottageville area of western West Virginia: 2nd Eastern Gas Shales Symposium, U. S. Department of Energy, METC/SP-78, v. 6, no. 1, p. 196-206.

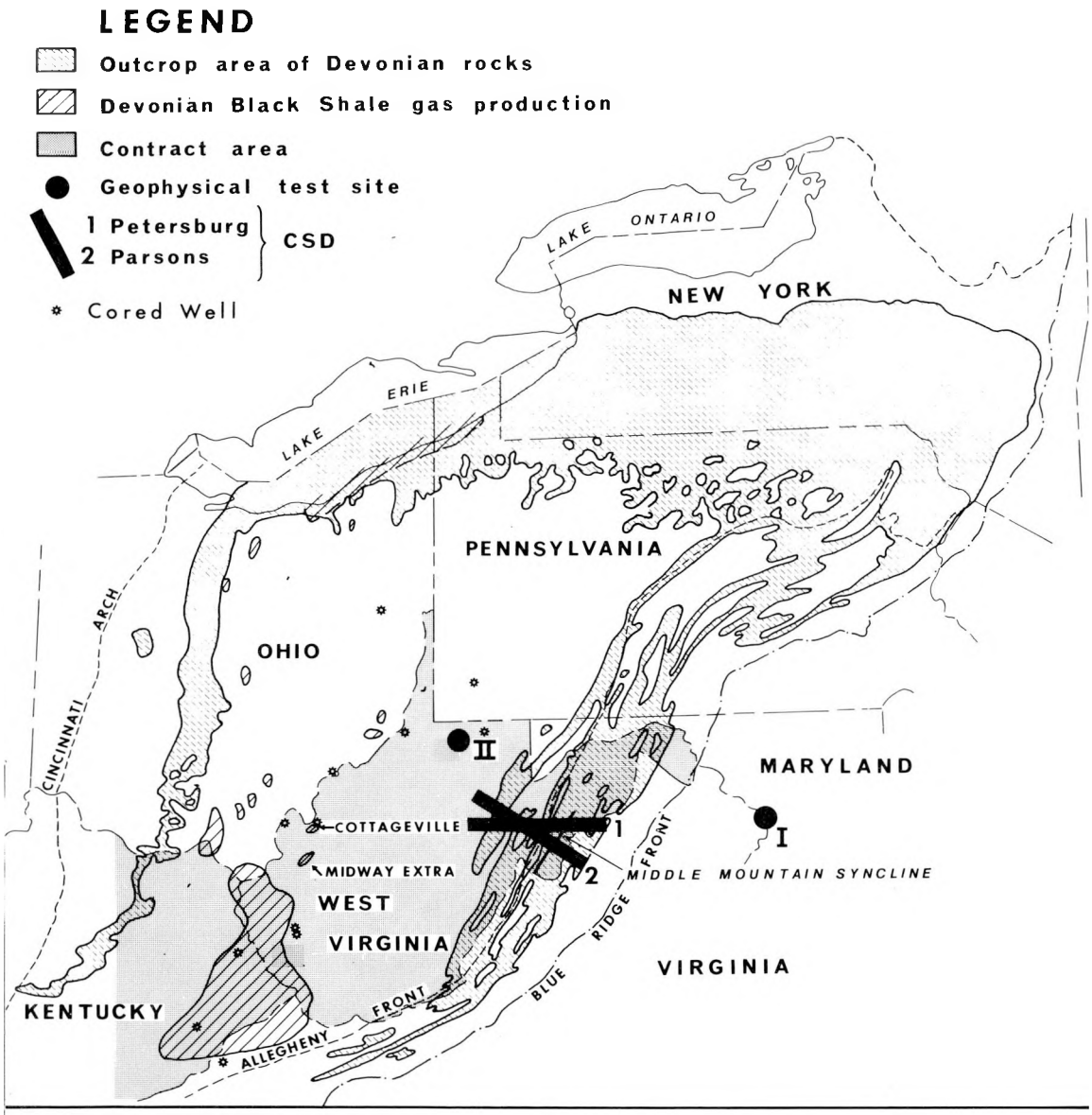


Figure 1 Index Map - Structural Parameters that Affect Devonian Shale Gas Production

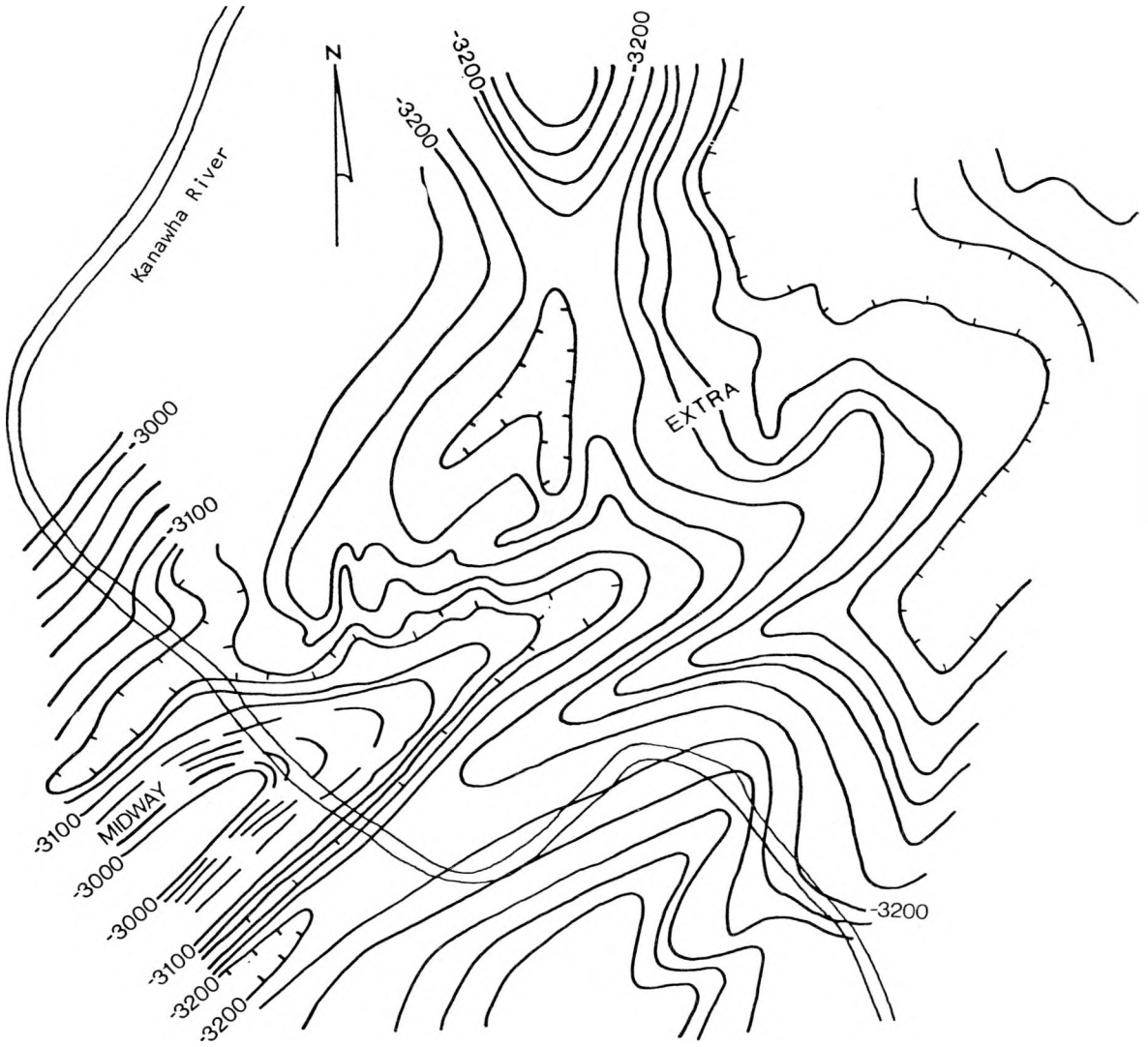


FIGURE 2
STRUCTURE-BASE OF BROWN SHALE (L.HURON)

Midway-Extra Field
Putnam County, W. Va.

MIDWAY-EXTRA FIELD

Putnam County, W. Va.


N
Kanawha River
MIDWAY
EXTRA
100
100
100

MIDWAY-EXTRA FIELD
Putnam County, W. Va.

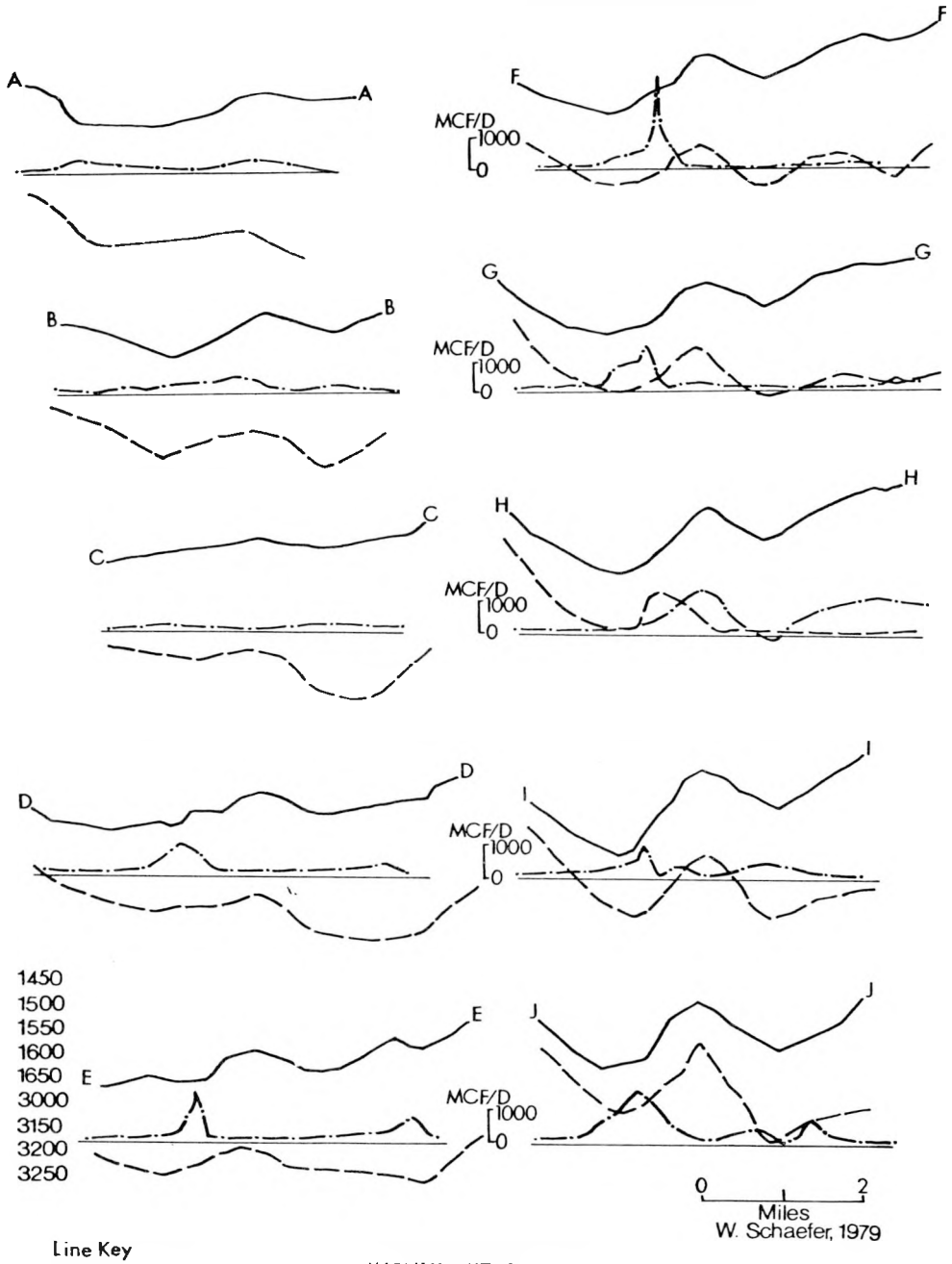


Figure 4

LOWER HURON ISOPACH MAP

W. Schaefer 1979

STRUCTURE AND ISOPOTENTIAL CROSS SECTIONS



Line Key
Berea ——
Brown Shale — — —
Prod .—.—.

MIDWAY-EXTRA FIELD

Putnam County, W. Va.

Figure 5

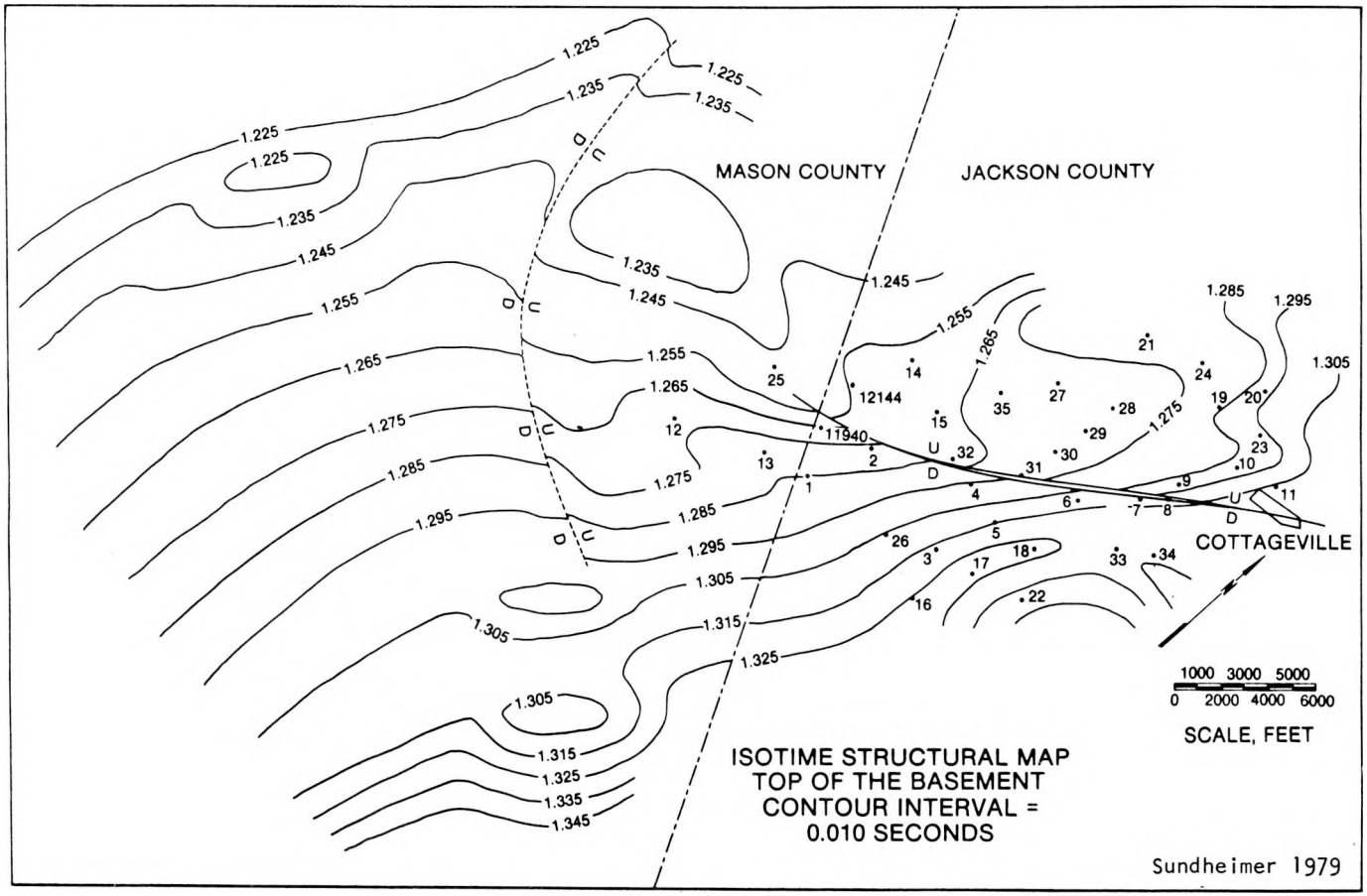

MASON COUNTY
JACKSON COUNTY
COTTAGEVILLE
1.225
1.235
1.245
1.255
1.265
1.275
1.285
1.295
1.305
1.315
1.325
1.335
1.345
D
U
12144
11940
1000 3000 5000
0 2000 4000 6000
SCALE, FEET
ISOTIME STRUCTURAL MAP
TOP OF THE BASEMENT
CONTOUR INTERVAL =
0.010 SECONDS
Sundheimer 1979

Figure 6

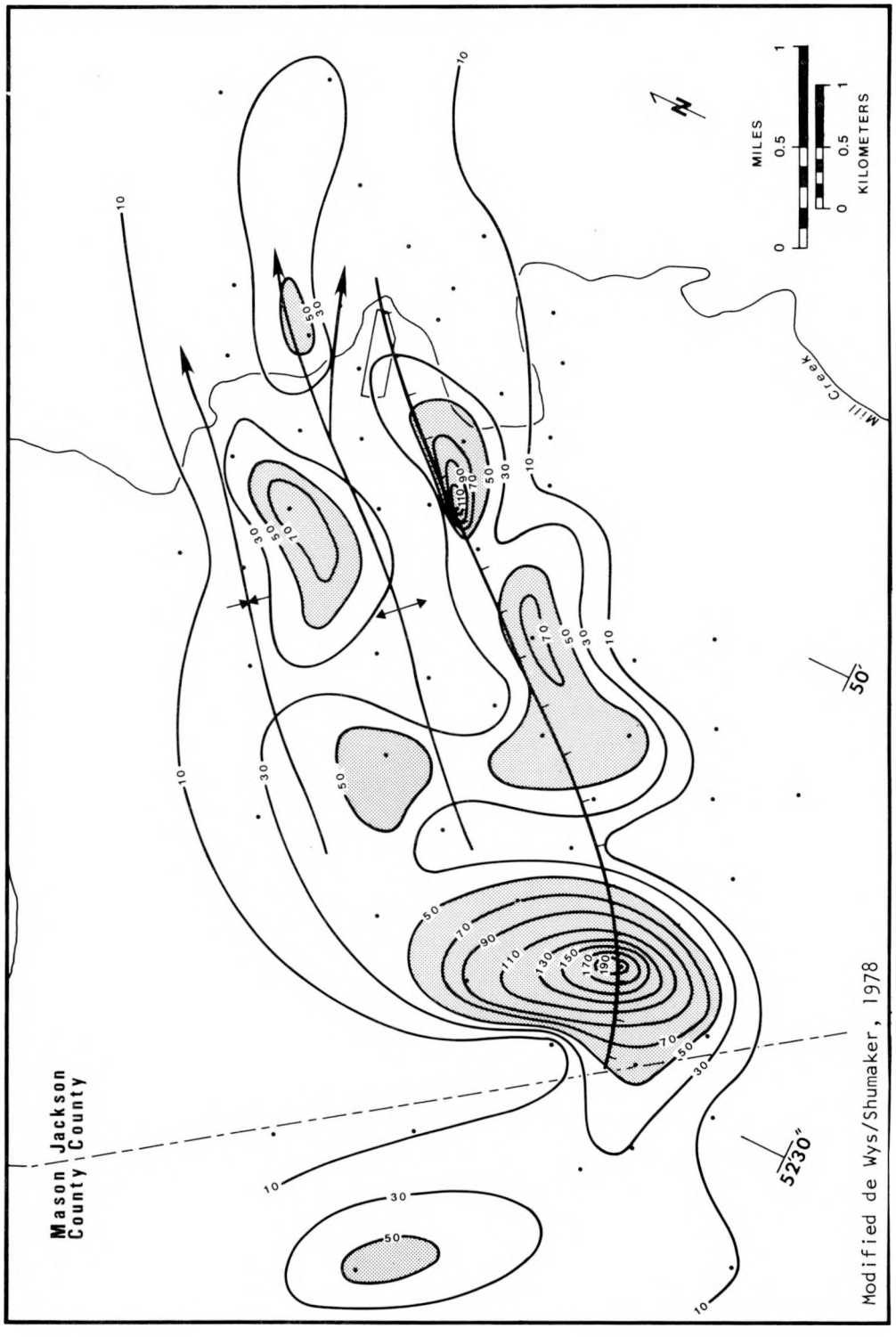


Figure 7 Isocontours of Highest Annual Production (1st or 2nd year production). Contour Interval = 20MMcf/yr.

Fault and Fold Axes from Seismic - Sundheimer, 1978 (personal communication)

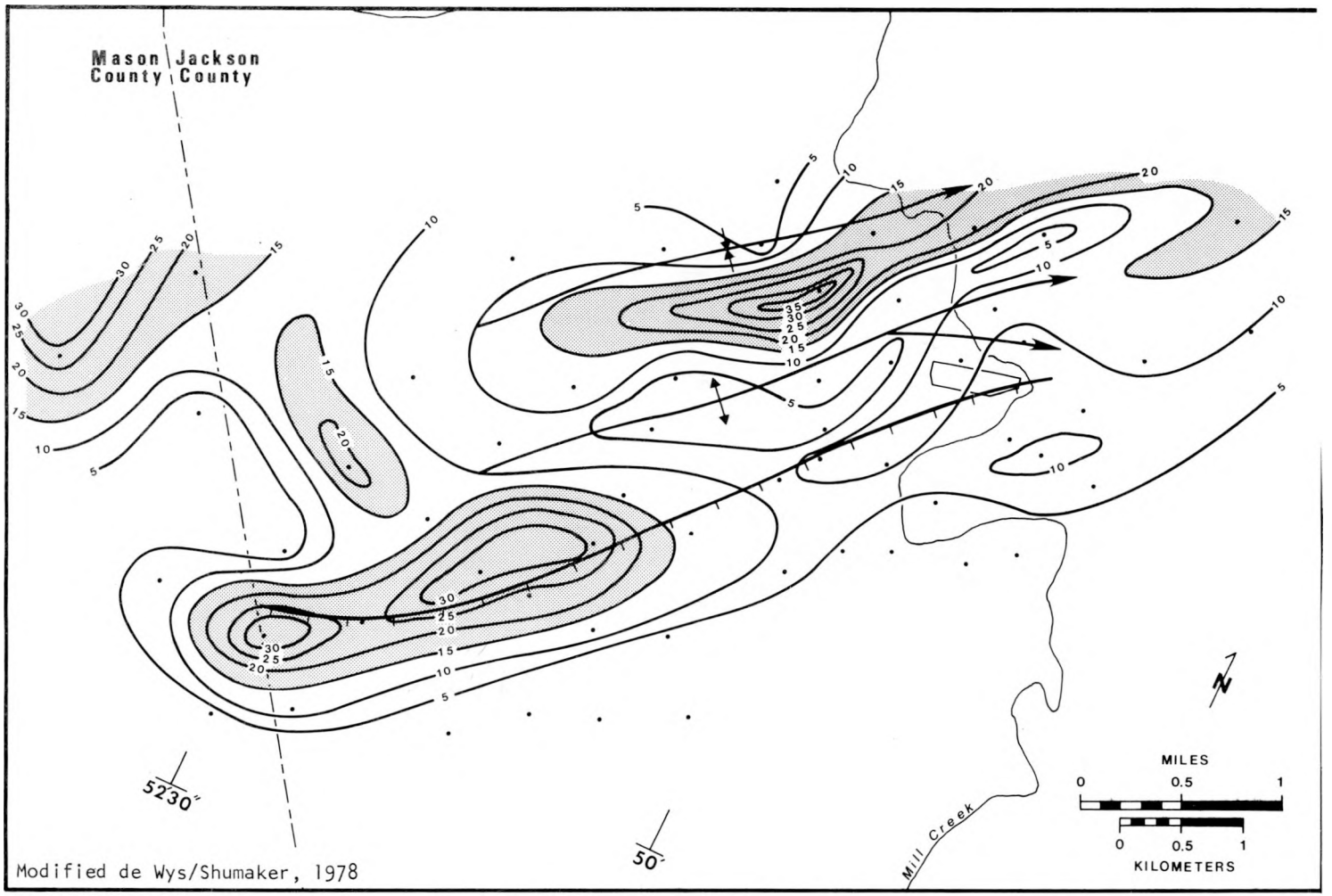


Figure 8 Isocontours of Mean Annual Gas Production. Contour Interval = 5MMcf

Fault and Fold Axes from Seismic - Sundheimer, 1978 (personal communication)

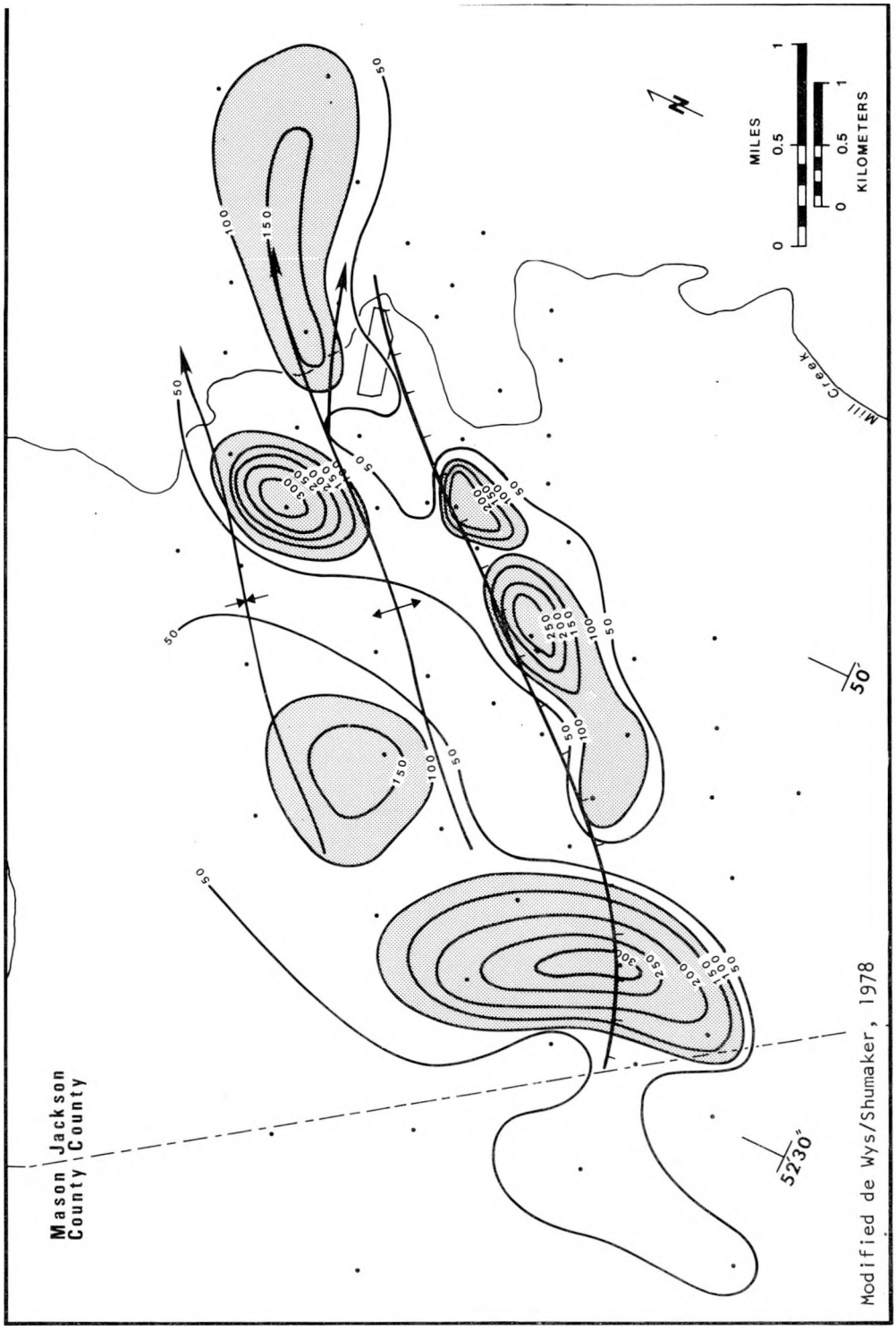


Figure 9 Isocontours of First Five Years Accumulated Gas Production. Contour Interval = 50MMcf/yr.

Fault and Fold Axes from Seismic - Sundheimer, 1978 (personal communication)

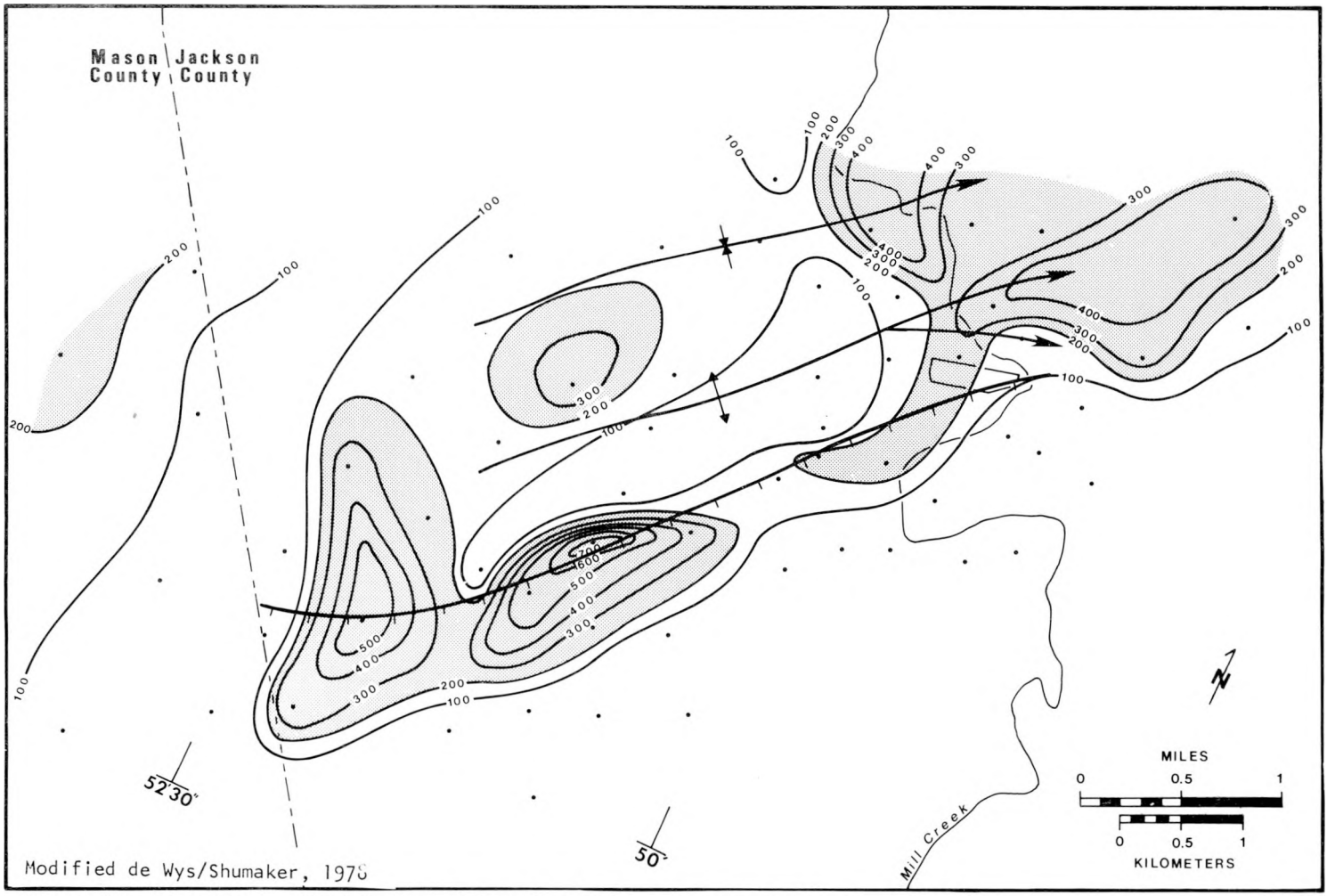


Figure 10 Isocontours of Total Accumulated Production. Contour Interval = 100MMcf

Fault and Fold Axes from Seismic - Sundheimer, 1978 (personal communication)

PARAMETERS OF GEOLOGIC STRUCTURE WHICH AFFECT DEVONIAN GAS SHALE PRODUCTION
IN WEST VIRGINIA AND EASTERN KENTUCKY - A PROGRESS REPORT

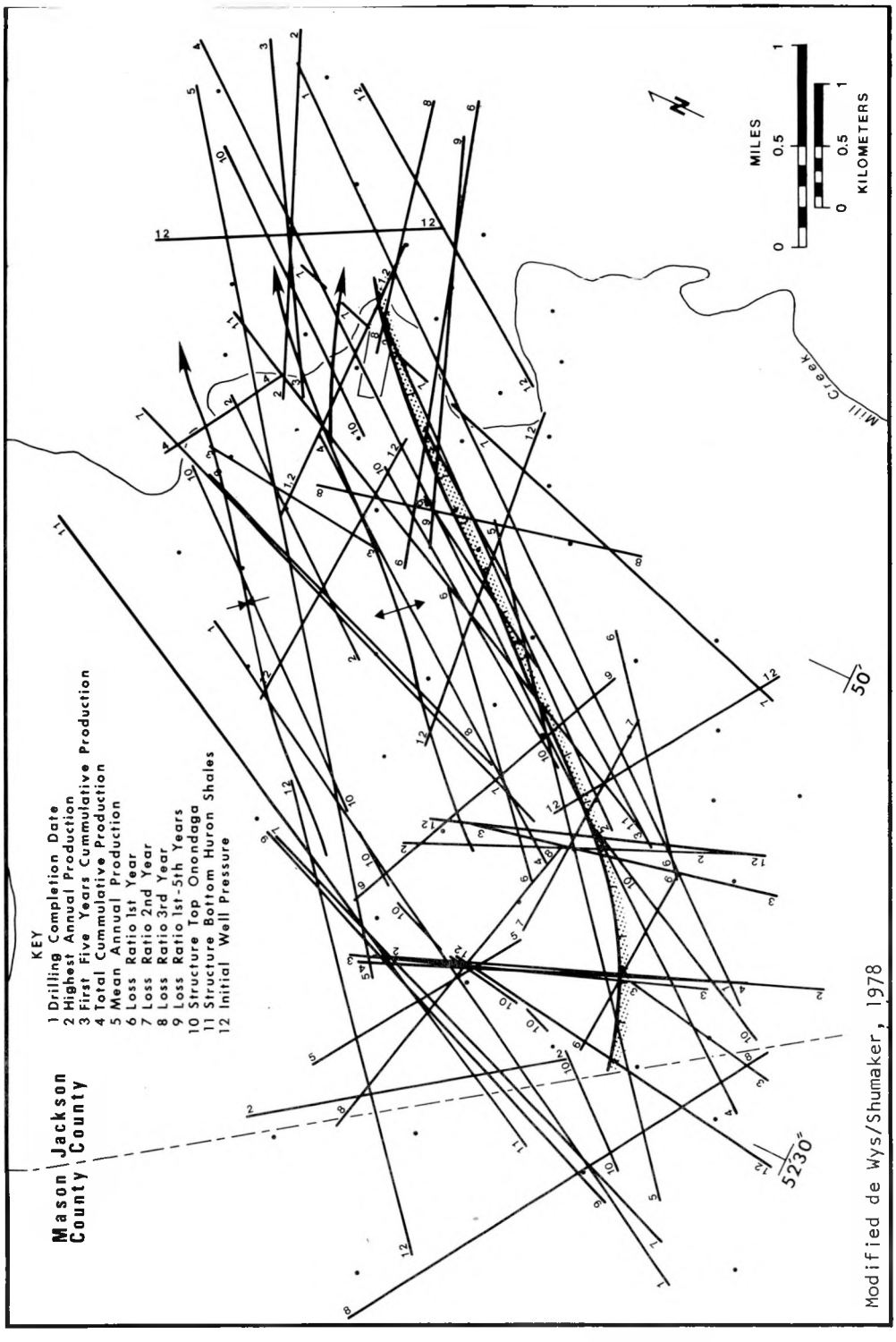
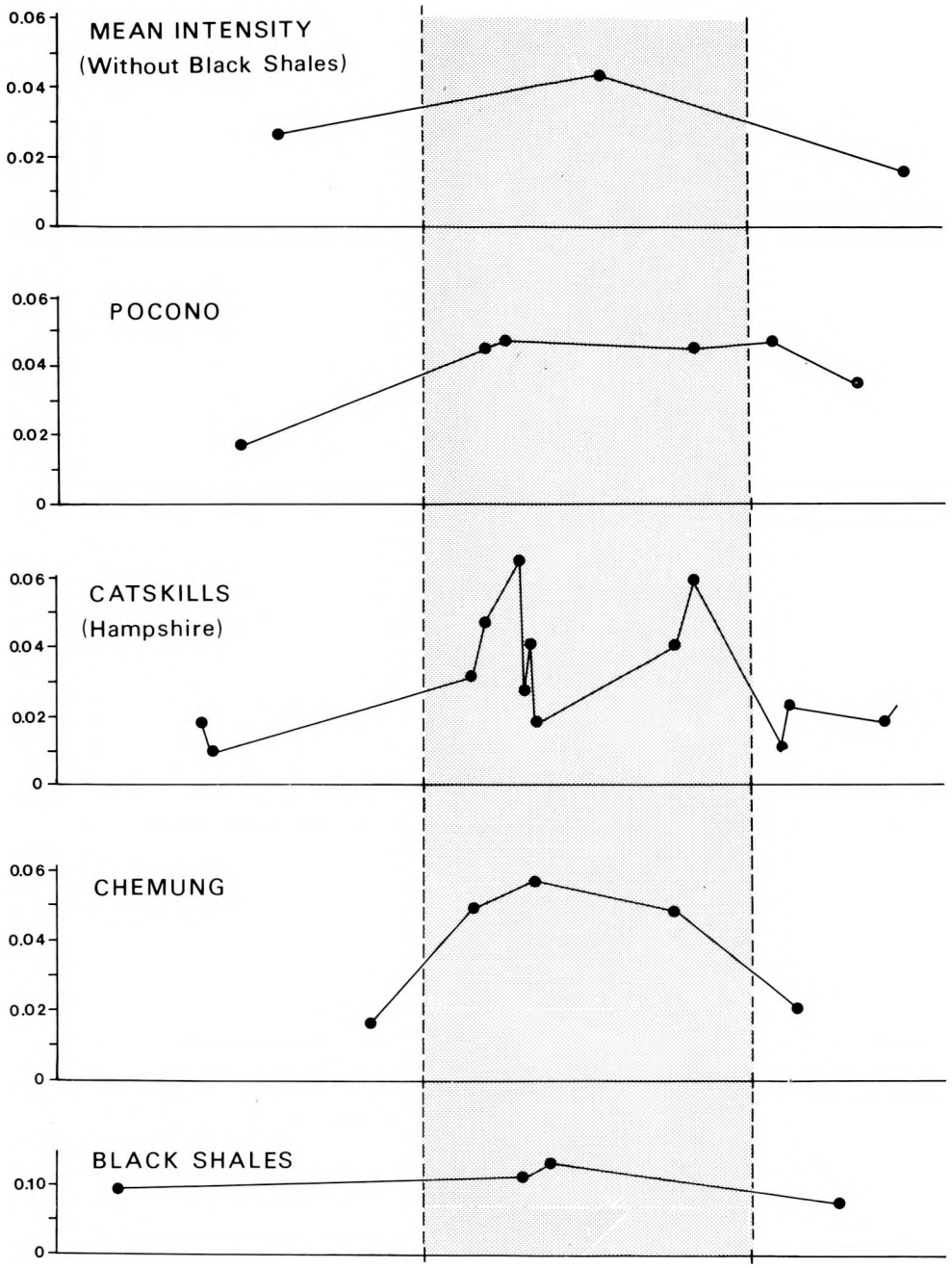


Figure 11 Axial Trends of Contours from Production Maps.

Shading on down side of fault.



Joint Intensity of Petersburg Lineament
along Allegheny Front

Figure 12

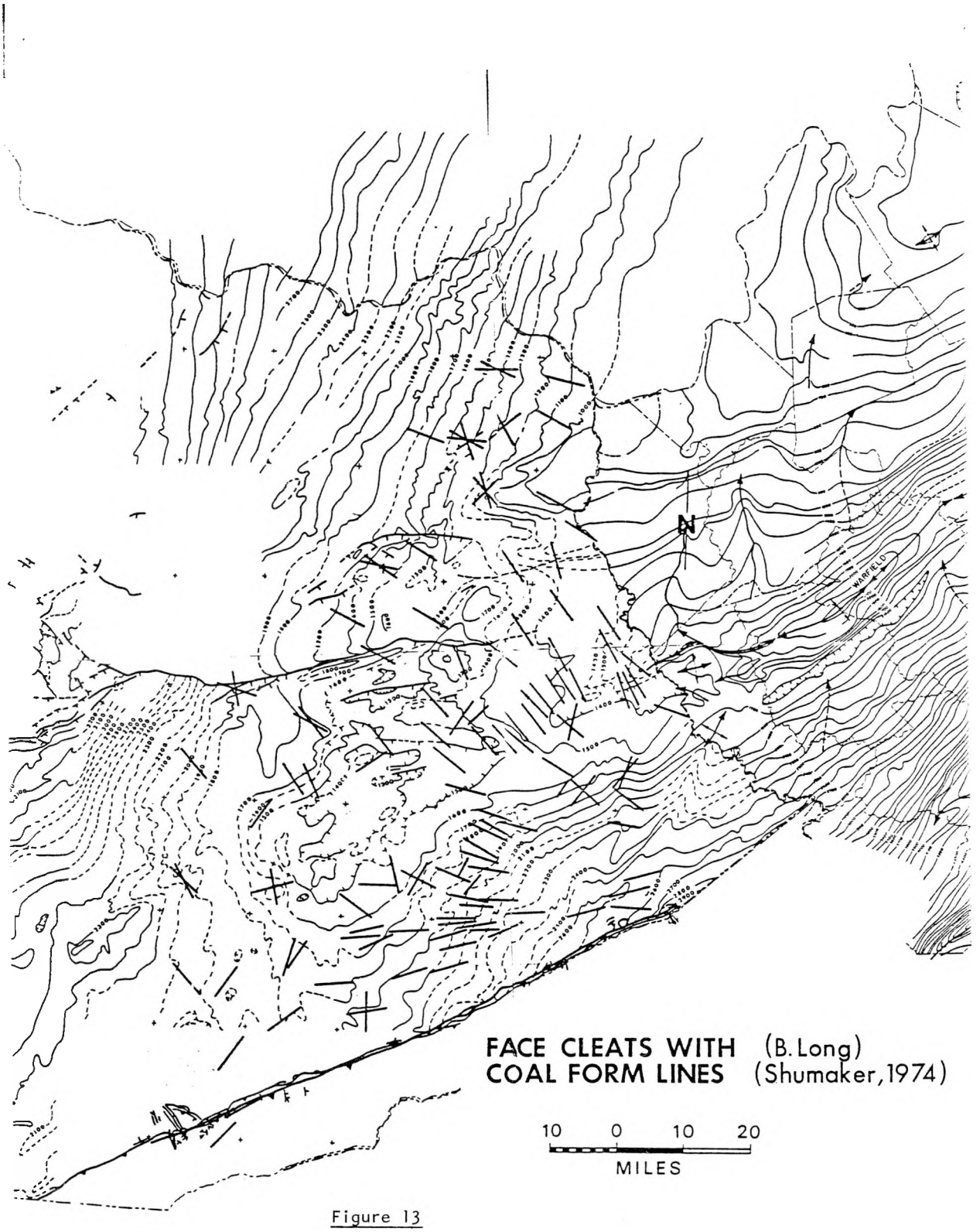

N
WARFIELD
FACE CLEATS WITH (B. Long)
COAL FORM LINES (Shumaker, 1974)
10 0 10 20
MILES

Figure 13

EFFECTS OF AQUEOUS CARBON DIOXIDE ON DEVONIAN SHALES

James F. Miller, J. Parke Boyer, Susan J. Kent, M. Jack Snyder, and
BATTELLE

John C. Sharer
Gas Research Institute

ABSTRACT

The quality and extent of the gas in the thick hydrocarbon-bearing Devonian shales which underlie most of the Eastern U.S. is being investigated by a number of concerns. Although the gas resource locked in these shales has been variously estimated to be up to three times the current proven gas reserves in this country, the economic feasibility of producing large quantities from this source remains in question due to the fine-grained nature and low permeability of these shales. Because of the nature of these formations, classical hydraulic fracturing to stimulate these sources may result in extensive formation damage. In addition, many of the fractures in these formations appear to have been sealed by deposited salts and carbonates. Because of these factors, enhanced or improved fracturing and stimulation methods are needed.

This paper presents progress made to date in a program aimed at the development of information, techniques, and procedures for improved gas or hydraulic fracturing of the tight Devonian shale formations with minimum formation damage.

Results are presented which show that the shale is attacked by aqueous CO_2, supercritical CO_2 fluid, and water at typical downhole temperatures and pressures at, or below, lithostatic or fracing pressures, producing fractures, solubilization of a shale material and some increase in permeability to gas flow.

INTRODUCTION

The thick hydrocarbon-bearing Upper Devonian Shales, commonly referred to as simply Devonian shale, which underlie many of the mideastern states has become a primary target for development based on estimates that the gas locked in these shales exceed by several times our current proven reserves. Unfortunately, these shales, formed from muds deposited approximately 350 million years ago are extremely fine grained with very low permeabilities making it difficult to economically produce large quantities of gas from them. The problem is that the system of natural open fractures in the Devonian shale is not particularly extensive nor well interconnected as evidenced by comparison of the low gas flow rates to the gas content present based on the analysis of cored specimens.

Based on other work being conducted at Battelle on behalf of the Eastern Gas Shale Program and the work of other participants in this program, these shales can be characterized as a fairly simple and uniform assemblage of quartz (30 to 40 percent), illite and chlorite (40 to 60 percent), and minor amounts of feldspars, carbonates, and pyrites. The feature that is of the most importance to this work is the presence of joints, pores, delaminations and old fractures that are filled with carbonate materials -- principally siderite, dolomite, and calcite. These latter materials were deposited in the open structure of the shales during the many wetting and drying cycles experienced by these formations and resulted in a fairly complete closing of a majority of the existing microcracks in the material.

From these observations of the fabric of the shales it was postulated that if these microcracks can be opened they can serve to interconnect the gas-filled fracture network and porosity systems. In 1978 researchers at Battelle conducted a limited number of experiments to confirm this postulate and identified a chemical treatment designed to dissolve the carbonates. These experiments resulted in significant increases in permeability, surface area, and porosity of the shale. Based on this concept and the preliminary experimental data, this program was initiated at Battelle on behalf of the Gas Research Institute.

This paper is a progress report on the research program which presents some of the preliminary findings.

OBJECTIVE AND SCOPE

The objective of this program is the development of information, techniques, and procedures for improved gas or hydraulic fracturing of tight formations with minimum formation damage. The work specifically is concerned with examination of the feasibility and effectiveness of utilizing CO_2 fluid and aqueous CO_2 to dissolve the carbonate material present in the shale microstructure as a means of providing additional permeation paths for the gas present in the shale to reach the well hole. The program is a laboratory study to develop the basic information that will be required to support a full scale field test at some later point.

In the course of the planned laboratory research three types of studies will be undertaken:

1. A laboratory investigation of the chemical effects of CO_2 treatments to determine what reactions are involved, what phases are dissolved, which components of shale respond to the treatments, and the optimum conditions for enhanced fracturing
2. A laboratory investigation of the chemomechanical effects of identified optimum treatments on the hardness, toughness, and fracture behavior of the shale
3. A scale model laboratory investigation of the behavior of shale when subjected to stresses and conditions that simulate those which might be utilized in the field for enhanced fracturing.

The work to date has been primarily in the first area and this paper will be concerned largely with that investigation.

SPECIMEN SELECTION AND CHARACTERIZATION

Utilizing the extensive data available from the large number of shale core samples collected and analyzed for Morgantown Energy Technical Center as a part of their Eastern Gas Shale Program a cross section of samples was identified that represent the range of shale and gas characteristics encountered. These initial samples were taken from well EGSP VW No. 5 drilled in Mason County, West Virginia, in January, 1978. The samples selected for use in the initial investigations are listed in Table 1.

These specimens for use in the first two types of laboratory studies are 0.25-inch thick by 1-inch diameter discs. This configuration was selected to permit the use of the specimens in the permeability test apparatus and the physical property test rig. The specimen preparation procedure is to cut 0.25-inch thick slices from the core sample perpendicular to the well bore axis. A diamond core drill is then used to remove 1-inch diameter specimens from this slice. The cutting is done dry at very low speeds to minimize specimen damage.

In addition to the characterization parameters listed in Table 1 these specimens are being characterized on the basis of chemical analysis, X-ray diffraction, mineralogical analysis, permeability, surface area, and physical properties. Based on our initial investigations it has become evident that although these characterizations are important a reliable and functional technique suitable for pre- and post-treatment characterization must be developed.

At present the most useful technique appears to be simply permeability measurements. These measurements are made with helium gas at a 1 atmosphere pressure differential normal to the bedding planes. Helium gas was selected because the permeability of the shales is normally so low (<0.01 microdarcys) that a gas with small molecular size must be utilized. In previous work at Battelle methane permeabilities have been determined on as-received shales and were found to be lower than our detection limits. Comparative helium and methane permeabilities will be determined on treated specimens in the future.

At this point one of the principal problems with characterizations is that with some specimens the treatments are so effective that there is insufficient specimen integrity to permit post-treatment analysis. Analyses by radiography, resistivity, and ultrasonic pulse velocity measurements are now being investigated. It appears, however, that surface area or porosity determinations may be the most useful because the specimen must be crushed prior to making these measurements. The drawback is, of course, that pretreatment analysis is not possible for each specimen since these are destructive tests.

LABORATORY CHEMICAL TREATMENTS OF SHALE

The laboratory chemical treatment experiments involve the exposure of shale specimens to the experimental fluids in a laboratory autoclave. The shale specimens are treated under a range of conditions that might be employed in actual hydraulic or gas fracture stimulation of wells in the eastern gas shale region. The pressure treatment vessel has provisions for measuring and controlling the temperature and pressure and for slowly moving the specimens (1 rpm) in the fluid. The gas or fluid content of the vessel can be sampled, if desired.

The matrix of treatment conditions that is being investigated in this apparatus includes pressures from 1800 psi to 50 psi to represent conditions from the well bore to some distance into the formation. The treatment times are being varied from 5 minutes to 8 days. It is recognized that the long times may be economically unrealistic and the majority of our work will be with times less than

24 hours. The long times are important to provide a more complete understanding of the reactions and reaction rates involved. The temperatures of the experiments are being held at the level representative of downhole conditions. The other variable in the current matrix is, of course, the shale chemistry and later work will consider the use of CO_2 in conjunction with fracturing fluids other than water. To date only aqueous CO_2, water, and supercritical CO_2 fluid have been used; emphasis probably will remain on investigation of the use of these fluids for technical as well as economic reasons.

Table 2 shows a descriptive analysis of the results of several of the first runs that were made. The principal conclusions from these results are that supercritical CO_2 fluid appears to offer no advantage over aqueous CO_2 and that the reactions involved are more complex than simple dissolution of carbonates as evidenced by the weight gains found for specimens which were fractured. The photograph of a typical group of treated samples which is shown in Figure 1 illustrates what is meant by major specimen deterioration.

The aqueous solution from the third treatment (34836-11) was analyzed and the results are shown in Table 3. This analysis indicates that calcite was probably the principal phase attacked, although other alkali and alkaline earth phases and siderite and/or pyrite also were dissolved in the aqueous CO_2. In contrast, results of analysis of dissolved solids from similar treatment of shale with water, which are given in the second column of Table 3 show that the water dissolves primarily alkali metal compounds, but relatively little of alkaline earth or iron-containing compounds. The recovered dissolved solids from the aqueous CO_2 treatment corresponded to 1.1 percent by weight of the shale treated, whereas that from the water treatment was equivalent to just 0.32 percent.

Descriptive results of several short-term treatments of specimens from Ohio well EGSP O-3 which are given in Table 4 show that shale from some locations is broken down by both carbonated and pure water very rapidly, whereas other specimens from the same well may be attacked at a much lower rate. Further investigation of short-term treatment times and the phenomenon involved in rapid breakdown of the shale are planned.

Effect on Shale Permeability

The effectiveness of these treatments with respect to permeability are shown in Table 5. Most of the untreated shales show no measurable permeability. The exception is the No. 6 sample from R146-3201. However, this permeability is so high that it is believed that this specimen contains a significant crack. It is certainly not representative of typical specimens. The treated specimens show that the treatments, both with aqueous CO_2 and with water, have resulted in increase in permeability. Specimen R146-3331-1 did not show any permeability after treatment inspite of the weight loss seen and shown in Table 2. An adequate explanation for this result is not yet available. The ability to predict which specimens are going to respond to treatment is, of course, fundamental to developing an assessment of the usefulness of these procedures for stimulation and as the data base develops it is anticipated that these predictions can be made.

Ultrasonic Velocity Evaluation

Measurements of the velocity of propagation of ultrasonic radiation through the shale were made as a potential means of detecting effects of the treatments. The results of the initial measurements which are given in Table 6 show little, or no, difference in propagation velocity in the radial direction before and after treatment. However, in the majority of the specimens ultrasonic velocity is significantly reduced in the axial direction following treatment. This decrease in propagration velocity is interpreted to indicate the creation of some voids in the shale.

CHEMOMECHANICAL EFFECTS

The work in this area will involve principally the development of an understanding of what the fracturing treatments do to the physical fabric of the shale and to subsequent fracture mechanics of the material. This work is important in assessing whether these treatments will make these formations more responsive to conventional hydraulic fracturing, both from an energy required point and whether the basic mode of fracture is altered. Some initial determinations of strength have been made and are shown in Table 7. These results are consistent with results reported by other researchers on the Eastern Gas Shale Program.

An apparatus to load the specimens to a known level while it is subjected to the chemical treatment environment has been designed. This apparatus is designed to permit observation of the specimen an optical microscope while it is being stress loaded in the treatment environment.

LABORATORY SCALE FRACTURING

Utilizing the best conditions identified in the previously discussed studies, core samples will be treated under conditions designed to simulate gas and CO_2-promoted hydraulic fracturing in the field. The hydraulic fluid will be injected under pressure into a borehole in the core sample. An inert gas will be used as the fluid to provide a simulated lithostatic pressure around the shale in the pressure vessel.

The effectiveness and nature of this simulated hydraulic treatment will be evaluated by examination of fractured or sliced cross sections of the core. An attempt will be made to obtain a bulk permeability measurement on the core on the basis of the rate at which the pressure of the envelope gas falls off when the borehole is opened to atmosphere.

Work on this task will be initiated in the very near future.

CONCLUSIONS

The shale is attacked by aqueous CO_2, supercritical CO_2 fluid, and water at downhole temperatures and pressures at, or below, static pressures that might be used for fluid fracing of the shale formations, producing fractures and some increase in permeability to gas flow.

Water dissolves primarily alkali constituents from the shale, whereas aqueous CO_2 dissolves primarily alkaline-earth and iron-containing constituents and is indicated to solubilize a greater proportion of the shale.

Effects of treatments with the fluids can be detected by permeability, ultrasonic velocity transmission, and mass measurements and visually.

ACKNOWLEDGMENTS

The authors acknowledge Gas Research Institute support of this research, the provision of shale samples by the Eastern Gas Shales Program, DOE, and wish to thank GRI for permission to publish this paper.

TABLE 1

Samples from Well R-146.

DEPTH	COLOR	OPEN POROSITY	TOTAL HYDROGEN	HYDROGEN SHALE	N	O	CO_2	BULK DENSITY	TRUE DENSITY	SURFACE AREA	TEMP, F
3064	N4	12.45	0.15	0.00	78.50	21.40	0.13	2.675	3.055	2.57	98
3084	N2	11.27	13.32	0.12	70.10	16.00	0.59	2.638	2.973	--	99
3152	N3	6.88	57.19	1.49	40.30	0.49	2.04	2.551	2.870	4.05	100
3201	N3	0.83	3.07	0.02	78.80	18.04	0.08	2.673	2.659	5.690	101
3272	N3	0.49	25.22	0.41	63.70	10.60	0.58	2.695	2.708	1.12	103
3311	N3	3.33	56.48	1.21	40.90	2.17	0.48	2.560	2.648	3.450	103
3331	N3	8.40	66.60	1.50	31.80	1.00	0.59	2.688	2.934	7.470	104
3351	5YR2/1	3.37	44.87	0.88	46.60	8.24	0.36	2.446	2.531	4.630	104
3369	5YR2/1	0.84	47.68	0.83	46.40	4.85	1.10	2.518	2.539	4.280	105

TABLE 2

Descriptive results of initial treatment experiments.

TREATMENT NO.	TREATMENT CONDITIONS	RESULTS		
		SPECIMEN	WEIGHT CHANGE, %	DESCRIPTION OF FINAL SPECIMEN CONDITION
34836-7	Aqueous CO_2	R-146-3152a	-0.2	Visible fractures in cleavage planes
	CO_2/H_2O = 2.15 by wt	-3152b	--	Ditto
	~2 days	-3331	-0.4	No visible fractures
	1800 to 990 psi	-3084	-1.0	Minor fractures in cleavage planes
	38 C	-3272	-0.8	Major fractures parallel and perpendicular to cleavage
		-3064	--	Complete specimen deterioration
34836-9	Supercritical CO_2	R-146-3152-2a	-0.33	Attack on specimens was similar to that
	~2 days	-3331-2	-0.44	with aqueous CO_2, but less severe
	1800 to 1460 psi	-3084-2	-0.41	
	38 C	-3272-2	-0.35	
		-3152-2b	-0.58	
		-3064-2	-0.40	

TABLE 2 (Continued)

TREATMENT NO.	TREATMENT CONDITIONS	RESULTS		
		SPECIMEN	WEIGHT CHANGE, %	DESCRIPTION OF FINAL SPECIMEN CONDITION
34836-17	Deionized water ~8 days 2000 to 1000 psi N_2	R-146-3201B	-0.7	Cleavage fractures
		-3201A	-0.8	Fractures
		-3311A	-0.5	No visible fractures
		-3311B	-0.36	Ditto
		-3351A	-0.08	Ditto
		-3351B	-0.06	Ditto
34836-14	Aqueous CO_2 CO_2/H_2O = 2.15 by wt ~5 days 1765 to 1240 psi 40 C	R-146-3311	-0.8	Cleavage fracture at one edge
		-3201	--	Extensive cleavage fractures
		-3351	-0.06	No visible fractures
34836-15	Aqueous CO_2 CO_2/H_2O = 2.15 by wt ~3 days 2000 to 1320 psi	R-146-3311 (3 specimens)	--	Cleavage fractures -- all specimens
		-3201 (2 specimens)	--	Cleavage fractures -- all specimens
		-3351 (1 specimen)	--	No visible fractures

TABLE 3

Chemical analysis[a] of dissolved solids.

ELEMENT	DISSOLVED IN AQUEOUS CO_2 (TREATMENT 34836-11) WT %	DISSOLVED IN DEIONIZED WATER (TREATMENT 34836-17) WT %
Ca	Major	2-4
Na	5-10	Major
K	1-3	2-4
Mg	0.5-2	0.1
Sr	0.1	0.03
Ba	0.01	0.1
B	0.1	0.3
Cu	<0.01	<0.01
Ni	6-10[b]	0.1
Si	2-4	3-5
Fe	1-3	0.2
Al	0.5	0.3
Mn	0.2	<0.01
Co	0.02	<0.01
Cr	0.02	0.03
Ti	0.02	<0.01
Mo	--	

(a) Optical emission spectrographic analysis; other elements were sought, but were not found.

(b) Shown to be from pressure vessel.

TABLE 4

Descriptive results of short-term treatment experiments.

TREATMENT NO.	TREATMENT CONDITIONS	RESULTS: SPECIMEN	RESULTS: WEIGHT CHANGE, %	RESULTS: DESCRIPTION OF FINAL SPECIMEN CONDITION
34836-19	Aqueous CO_2 [a] pH = 3.9 ~15 min Ambient air pressure 34 C	0-3-712 (6 specimens)	--	Extensive fracture deterioration of all specimens
34836-20	Deionized water ~1 hr Ambient air pressure 40 C	0-3-712 (3 specimens)	--	Extensive fracture deterioration of all specimens
34836-21	Aqueous CO_2 ~1.5 hr 1700 psi CO_2 38 C	0-3-790-11 -7 -4 -6	-0.27 -0.25 -0.28 -0.13	Cleavage fracture No visible fractures Ditto Ditto

(a) The water previously was carbonated at 1700 psi CO_2, then pressure was released; pH of the aqueous solution was measured following the treatment.

TABLE 5

Permeability of treated and untreated shales.

SPECIMEN NO.	PERMEABILITY, MICRODARCY: BEFORE TREATMENT	PERMEABILITY, MICRODARCY: AFTER TREATMENT	TREATMENT
R-146-3152-B-2	--	1.25	Supercritical CO_2, 34836-9
-3152-A-A	--	4.99	Ditto
-3272-2	--	2.49	Ditto
-3084-1	--	9.98	Aqueous CO_2, 34836-7
-3152-A-1	--	12.5	Ditto
-3331-1	--	0[a]	Ditto
R-146-3201-6	28.7	279	Deionized water, 34836-17
-3201-8	0[a]	713	Ditto
-3311-5	0	23.9	Ditto
-3311-8	0	7.48	Ditto
-3351-4	0	5.74	Ditto
-3351-7	0	6.74	Ditto

TABLE 6

Results of ultrasonic velocity tests on shale specimens before and after treatment.

(Treatment 34836-15, aqueous CO_2)

	TRAVEL TIME (MICROSECONDS)				
	RADIAL DIRECTION		AXIAL DIRECTION		
SAMPLE NUMBER	BEFORE	AFTER	BEFORE	AFTER	COMMENTS
R-146-3311-4	6.0	6.0	2.75	5.8	
R-146-3311-3	5.9	5.95	2.95	6.05	
R-146-3311-2	5.85	5.85	2.55	5.5	
R-146-3311-1	6.0	6.0	4.10	6.45	
R-146-3201-3	6.3	6.0	3.8	8.5	Split in half after treatment
R-146-3201-1	6.65	Broken	3.8	Broken	Fell in pieces after treatment
R-146-3341-3	6.3	6.05	3.1	2.7	
R-146-3351-2	6.35	6.2	2.75	2.6	

TABLE 7

Compressive strength of Devonian shale.

SAMPLE NUMBER	σ MAXIMUM, PSI PERPENDICULAR TO PLANES	σ MAXIMUM, PSI PARALLEL TO PLANES
R-146-3112-1	1815	--
R-146-3112-2	2345	--
R-146-3112-3	2195	--
R-146-3112-4	1350	--
R-146-3112-5	--	435
R-146-3112-6	--	575

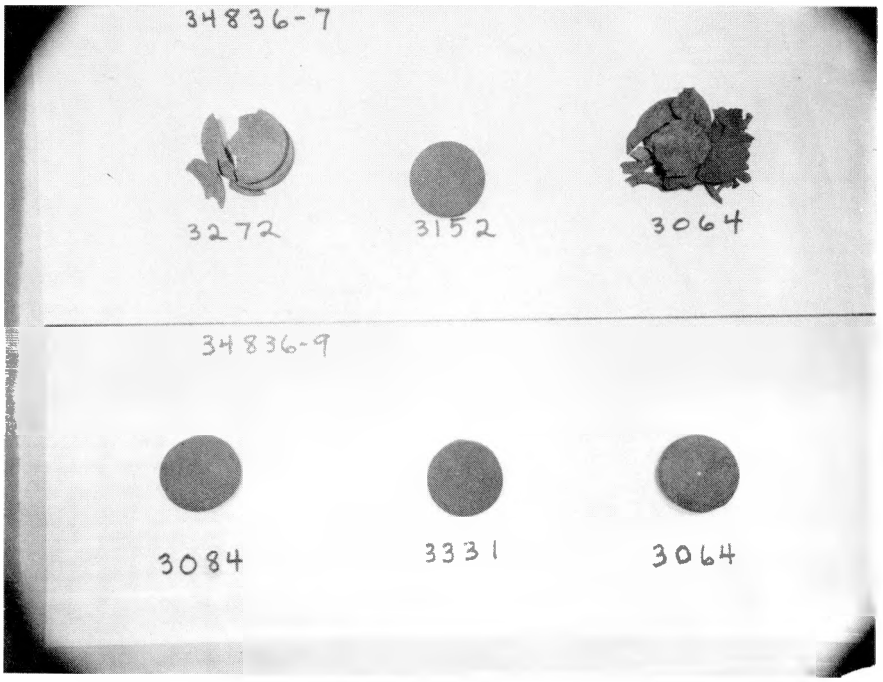


Fig. 1 - Shale specimens from Well R - 146 after treatment.

A FABRIC-ELEMENT BASED CLASSIFICATION FOR LOW-POROSITY-SHALE GAS RESERVOIRS

by

Edward B. Nuhfer,* and Robert J. Vinopal

West Virginia Geological Survey
P.O. Box 879
Morgantown, West Virginia 26505

ABOUT THE AUTHORS



Nuhfer



Vinopal

Edward Nuhfer received his B.S. and M.S. degrees in geology from West Virginia University and is completeing PhD requirements at the University of New Mexico. He taught for two years at Marietta College and is presently teaching at the University of Wisconsin. His principal research interests and publications are in geochemistry and petrology of recent muds, determinative mineralogy, analytical geochemistry, well log evaluation, and economic geology. Professional experience includes two years as a petroleum geologist with Chevron Oil Company and four years as an economic geologist and sedimentary petrologist with the West Virginia Geological and Economic Survey.

Robert Vinopal received his B.S. and M.S. degrees in geology from Kent State University and is working on a doctorate at West Virginia University. Research interests include petrology of clastic rocks and coal. He was employed for one year as a petroleum geologist for Earth Resources Consultants and is presently a sedimentary petrologist with the Eastern Gas Shales Project at the West Virginia Geological and Economic Survey.

*Present address-Geosciences Department, University of Wisconsin, Plattsville, WI 53818

2 A FABRIC-ELEMENT BASED CLASSIFICATION FOR LOW-POROSITY-SHALE GAS RESERVOIRS

ABSTRACT

Several hundred shale samples have been characterized by us with respect to mineralogical composition, chemical composition and petrophysical properties. However, no compositional-based study reveals the fabric or manner in which the components are put together to form the resultant rock. Classification by fabric elements, based on X-radiography and direct prints from thin sections, is practical and appears useful for interpretation of both depositional environments and reservoir properties of shale.

Six lithotypes based on fabric elements are defined in Devonian shale of West Virginia: 1) sharply-banded shale; 2) thinly-laminated shale; 3) lenticularly-laminated shale; 4) non-banded shale; 5) siltstones; and 6) concretions. A traditional series exists from thinly-laminated through lenticularly-laminated to non-banded. Thinly-laminated and organic-rich lenticularly-laminated shales appear the most favorable types for gas productivity because the laminated fabric permits the best lateral continuity of the low porosity (about 2 percent) present. The higher organic content of these lithotypes also probably acts as sites for significant sorption of gas, which is slowly released during production.

No microfracture system appears to exist, and macroscopic fractures do not necessarily coincide with productive zones. Wells without natural fractures prove productive after stimulation, which suggests that outgassing of a favorable rock type is responsible for the bulk of productive gas in Devonian shale wells. Natural fracture porosity, while important in extending effective volume tapped by a given well, represents only a minor portion of reservoir storage volume.

Thinly-laminated shales are interpreted as being generally representative of shallow-marine deposits (dominantly shelf deposits) accumulating under anoxic conditions. Non-banded and lenticularly-laminated shales are deeper water accumulations deposited further from shore. Sharply-banded shales and some siltstones generally represent pulses of more rapid sedimentation in the prodelta environment. A single sample in itself is not diagnostic of depositional environment, but relative abundance of specific lithotypes in a given vertical section is useful for general environmental reconstruction. Better definition of the diagnostic worth of shale fabric-element lithotypes awaits results of more detailed fabric-element studies of modern fine grained clastics and marine muds.

INTRODUCTION

The lower part of the Huron Member of the Ohio Shale is the main gas-producing interval in the Middle to Upper Devonian strata of southwestern West Virginia. Production from individual wells occurs at modest rates of around 50 to 100 Mcfpd, but, more importantly, production is of long duration, usually in excess of 20 years. The success ratios for Devonian shale gas wells in the 27 named fields in southwestern West Virginia is over 90 percent (Patchen, 1977, p. 13-14). The association of gas productivity with a particular stratigraphic unit infers that certain properties inherent in this rock, be they compositional, textural, or structural, are favorable to containing gas and transmitting it to the wellbore. The 1300' core from a Lincoln County well (Figure 1) penetrated shales from undifferentiated Upper Devonian gray shales which overlie the Huron Member down through the dark shales of the Rhinestreet Member of the West Falls Formation. The core thus offered a splendid opportunity to contrast petrographic and petrophysical properties of productive versus non-productive shale types.

A number of workers have stated that fractures are of major importance in influencing gas productivity from these shales (see, for example, Brown, 1976; Bagnall and Ryan, 1976; Patchen, 1977). Fractures act as an extension of effective borehole radius, but gas contained in the limited void space of the fracture must be recharged from the rock matrix as gas is produced from the well. Their importance with respect to reservoir capacity must be estimated from the frequency and sizes of the fractures seen in the core. In the studied well, total fracture porosity is apparently equivalent to less than 5 percent of matrix porosity (Nuhfer, Vinopal, and Hohn, 1978). This observation is in accord with the contention of Schettler (1978) that gas in fractures encountered in the wellbore in these shales is depleted in a very short time, perhaps within a few hours. Thus, most of the cumulative gas production over the life of the well comes from outgassing from a favorable rock type. The fractures serve to enhance the permeability of the rock, but do not contribute significantly to gas storage volume.

Differences of mean porosity are insignificant between the four shale lithotypes. Hence, porosity appears of no importance in explaining the productive character of the lower Huron.

DESCRIPTION OF LITHOTYPES

Petrologic study and the classification of fine-grained rocks have emphasized composition (Payton and Thomas, 1959; Keller and Ting, 1950; Bates and Strahl, 1957; Davis, 1970; Picard, 1971; and Lewan, 1978 are examples) rather than definition of fabric elements. A number of workers have examined the microstructure of shales by scanning electron microscopy (see, for example, Heling, 1970; O'Brien, 1970; Gipson, 1965). Examination of such ultrastructure is tedious and therefore of little use for general classification of rock types. Harvey and others (1977), however, have made use of larger-scale fabric elements in characterization of shale. In the strata observed in this well, fabric elements which are deduced from simple imaging techniques appear to reveal more contrasts between shale samples than does any single mineralogical, petrophysical, or geochemical parameter. Initial classification by fabric elements requires no expensive, time-consuming compositional studies nor any elaborate terminology for description.

Five lithotypes (exclusive of concretions) are defined: 1) Siltstone (Figure 2); 2) Sharply-banded shale (Figure 3); 3) Thinly-laminated shale (Figure 4); 4) Lenticularly-laminated shale (Figure 5) and 5) Non-banded shale (Figure 6). Divisions between thinly-laminated, lenticularly laminated, and non-banded shales are gradational (Figure 7). The distribution of these lithotypes within the Lincoln County well is shown in Figure 8.

The siltstones are typically cross-bedded and are tightly cemented by carbonate minerals. Calcite is the dominant carbonate cement and is sometimes seen as poikilotopic patches where a single crystal has grown to fill a number of pore spaces. Fold (1974) has described formation of large calcite crystals as possible products of phreatic meteoric diagenetic environment. The rather complete cementation in the siltstones gives most a lower mean porosity than any of the shale types.

Often associated with the siltstones are shales of the sharply-banded lithotype. Their fabric is characterized by alternating light and dark bands each of which is usually greater than 1 cm thick. The bedding planes defining the contacts between bands are usually sharply defined. Pyritic materials are usually arranged as linear fabric elements. The most common forms of pyrite in this shale type are spherical bodies which consist of framboids, spherical aggregates of framboids which are perhaps pyritized pellets, and pyritized algal spores.

The thinly-laminated lithotype is usually found in the lower part of the Huorn Member and lower part of the Rhinestreet Member. It is characterized by laminae usually less than 2 mm in thickness which arise from alternate layering of light and dark shales, silt, and/or pyritic matter. Thinly-laminated shale generally contains the highest organic content of the lithotypes. This is reflected in the responses of geophysical logs as higher resistivity, sonic travel time, and gamma ray counts and lower bulk density relative to the other shales and siltstones found in the well. Silt sizes found in the thinly-laminated lithotype in the lower part of the Huron are generally coarser than those found in the other shale types. Silt occurs as dispersed grains, as well defined laminae and as linear wisps which are often only a single grain in thickness. In thin section, many of the thicker silt laminae are observed to be cemented by calcite and dolomite.

Lenticularly-laminated shales are associated with the non-banded shales. The laminae are discontinuous alignments of lenticles. Silt grain-sizes are noticeably smaller in lenticularly-laminated shales than in thinly laminated or sharply banded shale types. Burrows are common and pyritic matter occurs as nodular or wiry forms which are not often oriented along bedding planes to produce the linear fabric element commonly seen in sharply-banded shales. Organic content of some lenticularly-laminated shales approaches that of thinly laminated shale.

Non-banded shales represent the most random arrangement of fabric elements. Bands or laminae are either originally absent or are so disrupted by bioturbation that only mottling is apparent. The color of the rock is usually light gray or greenish gray. Sizes of silt particles in non-banded shales are generally smaller than in any other lithotype, although silt-rich non-banded shales possibly produced from bioturbation of coarse muds exist. Much quartz is clay-sized. Pyritic matter and silt are uniformly disseminated through the rock and do not concentrate to produce a linear fabric.

The accumulation of the Rhinestreet Member on top of the unconformity surface at the Onondaga Limestone in the Lincoln County well (see Duffield, 1978), leaves little doubt that the thinly-laminated lithotype can accumulate in a shallow marine environment. The abrupt transition from the light gray non-banded and lenticularly-laminated shales of the Java Formation to the dark thinly-laminated shales of the lower part of the Huron (Figure 7) suggests a distinct change in environment of deposition in Lincoln County.

Nearby low-relief land masses to the west, and high-relief ones to the south and east are plausible sources for the sediments of the Rhinestreet, found in Lincoln County, but western land masses were submerged when deposition of the lower Huron commenced (Schwietering, 1979, personal comm.). No evidence of an unconformity between the Java (distal turbidite environment) and Huron in Lincoln County has been documented, and consequently deposition of the basal Huron is interpreted to have commenced in waters deeper than those present at time of deposition of the basal Rhinestreet.

Models of black shale deposition invoke thermoclines (Brongersma-Sanders, 1971), haloclines (Mannheim, 1961), algal flotants (Merrill, 1975), or a combination of these conditions (see Heckel, 1977) to permit the formation of anoxic conditions required to permit accumulation and preservation of organic matter. The tropical climate and restricted marine basin at time of deposition makes plausible both the formation of thermally stratified waters in the upper regions and sinking of waters made increasingly saline by evaporation. The preservation of organic matter in these Devonian shales could plausibly be explained by the above models. However, the grain sizes of silt found in the lower Huron are too large and too poorly sorted to be accounted for by simple constant settling from suspensions in quiet waters. This statement is supported by the senior author's work with sediment traps in lakes located in both humid and arid regions, where quartz is ubiquitous in suspended sediments, but most of the grain sizes of quartz lie in the very fine silts through clay size ranges. Only in periods of storms and floods generated at spring thaw are the sizes of the suspended quartz-silt observed to approach sizes seen in the lower part of the Huron. Storms merely cause resuspension of bottom matter and erosion from nearby shorelines, and are not likely in themselves to be mechanisms for explaining accumulations of over two-hundred feet of comparatively uniform fine-grained, thinly-laminated rocks. Only transport by currents and a relatively extensive and a temporally durable sediment source is likely to explain this accumulation. Data from McIver and Zielinski (1978) and Zielinski, Nance, Seabaugh, and Larson (1978) based on organic geochemistry and palynology indicate increasing amounts of terrestrially derived organic matter southward from Lincoln County, and increasing marine influence to the north and east. Thus streams from a low-relief land mass to the south and southeast could be designated as the sediment source of the thinly-laminated shales of the lower Huron in Lincoln County. Frequent (annual ?) floods could have provided a current mechanism for moving the fine-grained organic-rich detrital sediment into the shallow basin to settle to a bottom made anoxic either by water stratification or by the sheer volume of organic matter being contributed from both the source area and from algal productivity in the upper water column. The laminae are interpreted as being produced by sedimentation from current-generated suspension clouds (see Reineck and Singh, 1975, p. 220-221) in the upper water column and by subtidal currents which probably gently reworked the bottom sediments to produce some laminae of silt wisps and lenses. Further laminae were created by formation of early diagenetic pyrite at or very near to the sediment-water interface. Lack of scour features, non-disruption of linear fabric of pyrite, absence of rip-up clasts, scarcity of burrowing organisms and high content of organic matter indicate general persistence of low-energy anoxic bottom conditions. These conditions were infrequently disturbed in Lincoln County but more frequently in Jackson County by turbidites as evidence by relative abundance of non-banded shales, lenticularly-laminated light shales and siltstone beds found within the lower Huron shales. In Jackson County, thinly-laminated shales comprise only a minority of the lower Huron, but lenticularly-laminated shales and non-banded shales increase in abundance.

Non-banded and lenticularly-laminated shales generally contain much finer silt sizes, less organic matter, and more abundant bioturbation features than thinly-laminated shale. Together, these characteristics indicate an oxygenated environment in more open marine waters which were deeper than the shelf waters where the thinly laminated shales accumulated. The Java Formation and Angola Member, where the non-banded and lenticularly-laminated shales are dominant (Figure 7), are correlative with the thick siltstones and shale of the Brallier Formation to the east which are interpreted as turbidites deposited by westward-flowing paleocurrents (McIver, 1961). The lenticularly-laminated lithotype is very similar in appearance to the "vague turbidite" described by Bauma (1968) from the deeper areas of the Guld of Mexico. Thus, interpretation of these lithotypes as products of generally deeper water sedimentation of very fine materials carried as distal turbidites appears not unreasonable.

SUMMARY AND CONCLUSIONS

A shale classification based on fabric elements is useful for the investigation of reservoir properties and for the interpretation of depositional environments. Fabric elements rank at least of equal importance with composition for characterization of shale. Four lithotypes have been identified.

1. thinly-laminated shale,

2. sharply-banded shale,

3. lenticularly-laminated shale, and

4. non-banded shale. The order here, from 1 to 4, generally follows decreasing organic content, decreasing grain size of quartz, decreasing pyritic content, and decreasing lateral fabric continuity.

Gas production from the lower portion of the Huron Member and the Rhinestreet Member in southwestern West Virginia is explained by the dominance there of the organic-rich laminated shale lithotypes which promotes lateral continuity of the meager porosity present. The associated high organic content probably increases the methane-sorption capacity of the shales so that this lithotype can store more gas per given volume of rock than would be indicated from porosity measurements alone (Schettler, 1978).

Porosity varies little between the four shale lithotypes and does not appear to be an important factor in determining productivity. Porosity occurs in voids associated with pyritic crystals and framboids, in defects within the illite-rich matrix, with lesser amounts in uncemented silt laminae and nearly insignificant amounts as cracks in organic matter. Fracture porosity is minor in volume in comparison to matrix porosity. No microfracture system as postulated by others was documented after study of over 400 X-radiographs and thin sections.

REFERENCES CITED

1. Bagnall, W.D., and Ryan, W.M., 1976, The geology, reserves, and production characteristics of the Devonian Shale in Southwestern West Virginia: in Devonian Shale Production and Potential: N.T.I.S., MERC/SP-76/2, p. 41-53.

2. Bates, T.F. and Strahl, E.O., 1957, Mineralogy, petrography, and radioactivity of representative samples of Chattanooga shale: Geol. Soc. America Bull., v. 68, p. 1305-1314.

3. Bouma, A.H., 1968, Distribution of minor structures in Gulf of Mexico sediments: Trans. Gulf Coast Assoc. Geological Soc., v. 28, p. 26-33.

4. Brongersma-Sanders, M., 1971, Origin of major cyclicity of evaporites and bituminous rocks; an actualistic model: Marine Geology, v. 11, p. 123-144.

5. Brown, P.J., 1976, Energy from shale - a little used natural resource: in Natural Gas from Unconventional Geologic Sources: Board on Mineral Resources; Commission on Natural Resources, National Acad. Sci., p. 86-99.

6. Davis, J.C., 1970, Petrology of Cretaceous Mowry Shale of Wyoming: AAPG Bull., v. 54, p. 487-502.

7. Duffield, S.L., 1978, Devonian conodont biostratigraphy in a Lincoln County, West Virginia, core: M.S. thesis, W.V. University, 61 p.

8. Folk, R.L., 1974, The natural history of crystalline calcium carbonate: effect of magnesium content and salinity: Jour. Sed. Petrology, v. 44, p. 40-53.

9. Gipson, M., Jr., 1965, Application of the electron microscope to the study of particle orientation and fisility in shale: Jour. Sed. Petrology, v. 35, p. 408-414.

10. Harvey, R.D., and others, 1977, Petrology of New Albany Shale Group (Upper Devonian and Kinderhookian) in the Illinois Basin, a preliminary report: Proceedings First Eastern Gas Shales Symposium: N.T.I.S., MERC/SP-77/5, p. 328-354.

11. Heckel, P.H., 1977, Origin of phosphatic black shale facies in Pennsylvanian cyclothems of midcontinent North America: AAPG Bull., v. 61, p. 1045-1068.

12. Heling, D., 1970, Micro-fabrics of shales and their rearrangement by compaction: Sedimentology, v. 15, p. 247-260.

13. Keller, W.D., and Ting, C.P., 1950, The petrology of a specimen of the Perry Farm shale: Jour. Sed. Petrology, v. 20, p. 123-132.

14. Lewan, M.D., 1978, Laboratory classification of very fine grained sedimentary rocks: Geology, v. 6, p. 745-748.

15. Mannheim, F.T., 1961, A geochemical profile in the Baltic Sea: Geochim. et Cosmochim. Acta, v. 25, p. 52-70.

16. McIver, N.L., 1961, Upper Devonian marine sedimentation in the central Appalachians: Ph.D. thesis, Johns Hopkins Univ., 530 p.

17. McIver, R.D., and Zielinski, R.E., 1978, Geochemical evaluation of the eastern gas shales - part 1: Monsanto Research Corp., Mound Facility, Miamisburg, Ohio, MLM-2563.

18. Merrill, G.K., 1975, Pennsylvanian conodont biostratigraphy and paleoecology of northwestern Illinois: Geol. Soc. America Microform Pub. 3.

19. Nuhfer, E.B., Vinopal, R.J., and Hohn, M.E., 1978, Report of petrologic characterization of Lincoln 1637 (Columbia Gas Transmission Co. Well #20403): U.S. Dept, Energy open-file report - METC, 212 p.

20. O'Brien, N.R., 1970, The fabric of shale - an electron-microscope study: Sedimentology: v. 15, 1970, p. 229-246.

21. Patchen, D.G., 1977, Subsurface stratigraphy and gas production of the Devonian shales in West Virginia: U.S. Dept. Energy, N.T.I.S. MERC/CR-77/5, 35 p.

22. Payton, C.E., and Thomas, L.A., 1959, The petrology of some Pennsylvanian black "shales": Jour. Sed. Petrology, v. 29, p. 172-177.

23. Picard, M.D., 1971, Classification of fine-grained sedimentary rocks: Jour. Sed. Petrology, v. 41, p. 179-195.

24. Reineck, H.E., and Singh, I.B., 1975, Depositional Sedimentary environments: New York: Springer Verlag, 439 p.

25. Schettler, P.D., Jr., 1978, The implication of specific degasibility for models of gas production from shale: U.S. Dept. Energy, Preprints for Second Eastern Gas Shales Symp., VI; N.T.I.S., METC/SP-7816, vol. 1, p. 370-373.

26. Zielinski, R.E., Nance, S.W., Seabaugh, P.W., and Larson, R.J., 1978, Characterization and resource assessment of the Devonian shales in the Appalachian and Illinois basins: U.S. Dept. Energy, Preprints for Second Eastern Gas Shales Symp., V. II; N.T.I.S., METC/SP-78/6, vol. II, p. 15-31.

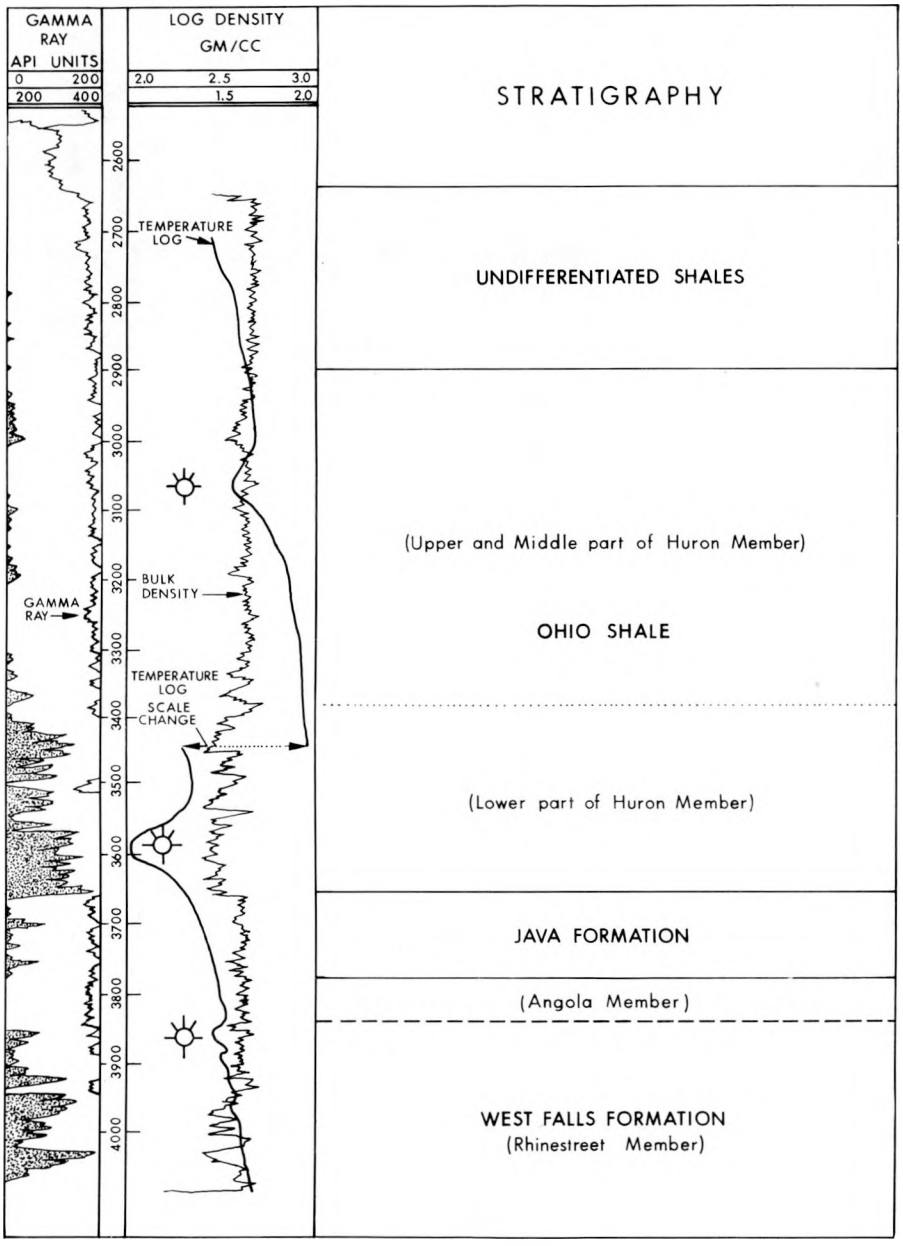


Figure 1. Stratigraphic division of Columbia Gas Transmission Co. well #20403 (Linc-1637). This well supplies the only complete cored profile of the Devonian Shale section present in western West Virginia.

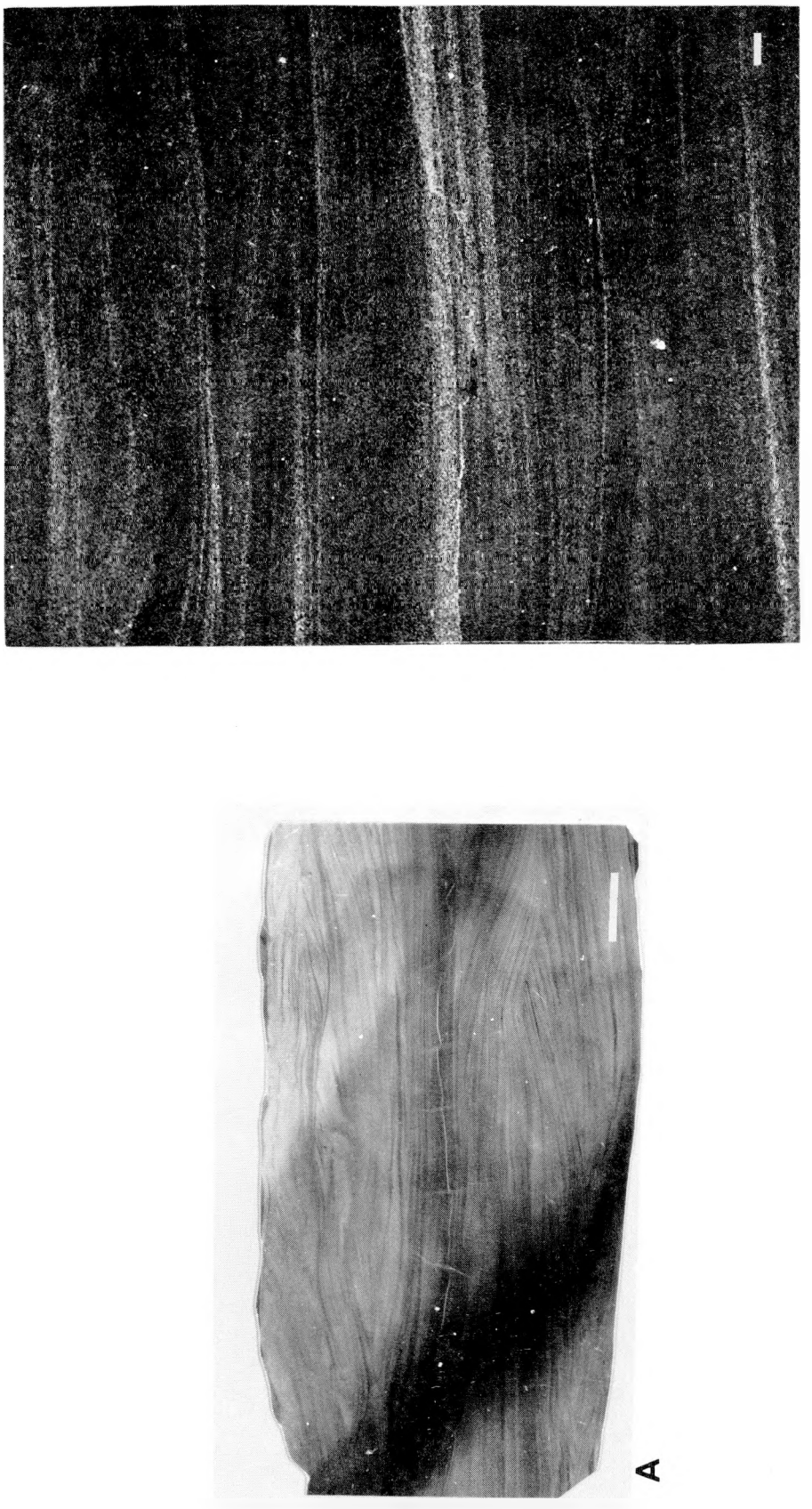


Figure 2. Siltstone from undifferentiated shales above the Hurcn Member. A) Radiograph positive print. B) Negative print image of thin section. Scale bar in A is 1 cm, in B, 1 mm. All fractures are induced.

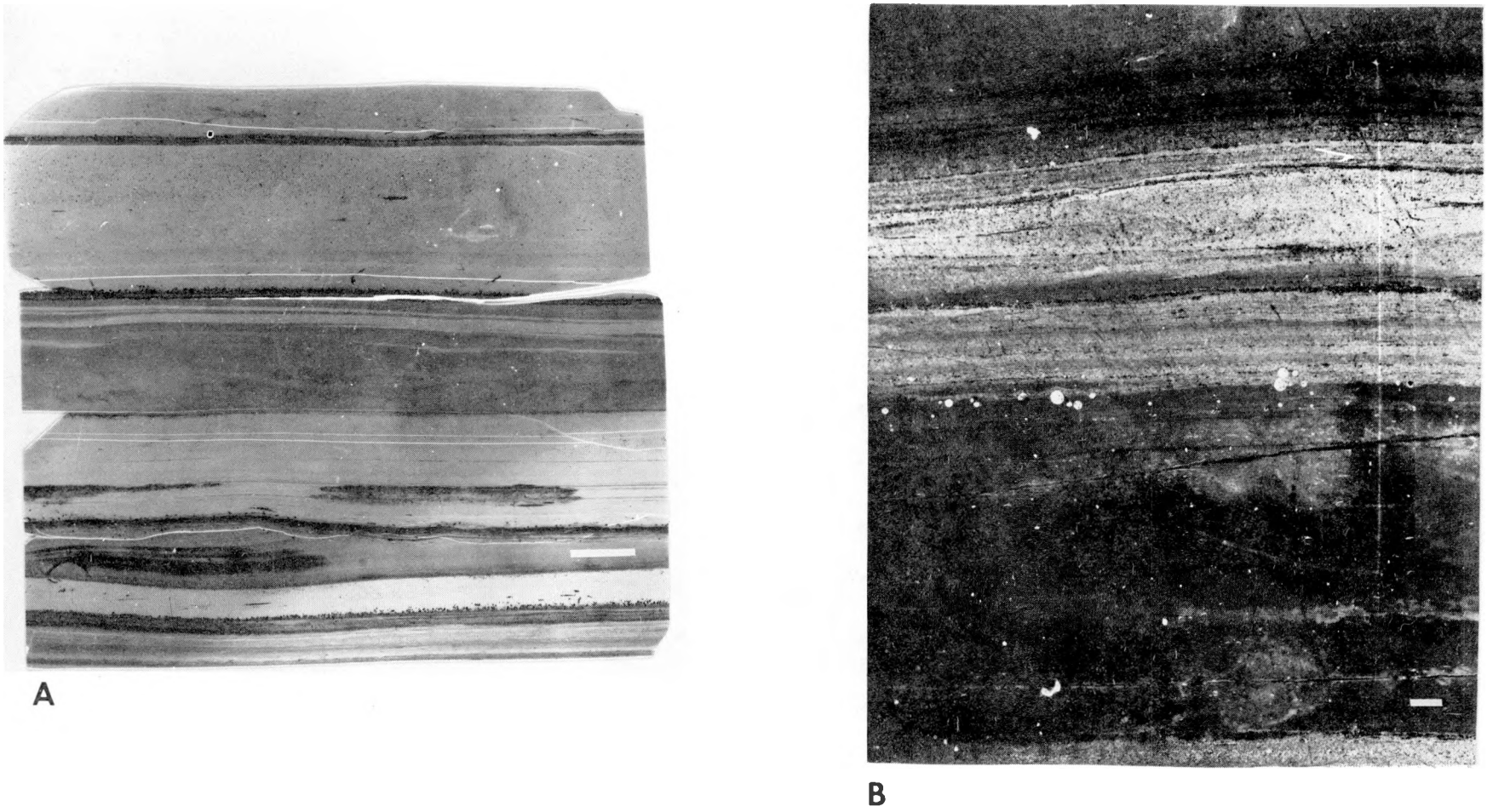


Figure 3. Sharply-banded shale from upper-middle portion of Huron Member. A) Radiograph positive print. Organic rich bands are darker due to greater pyrite content. B) Negative print image of thin section. Light spheroids are large pyrite framboids. Scale bar in A is 1 cm, in B ,1 mm.

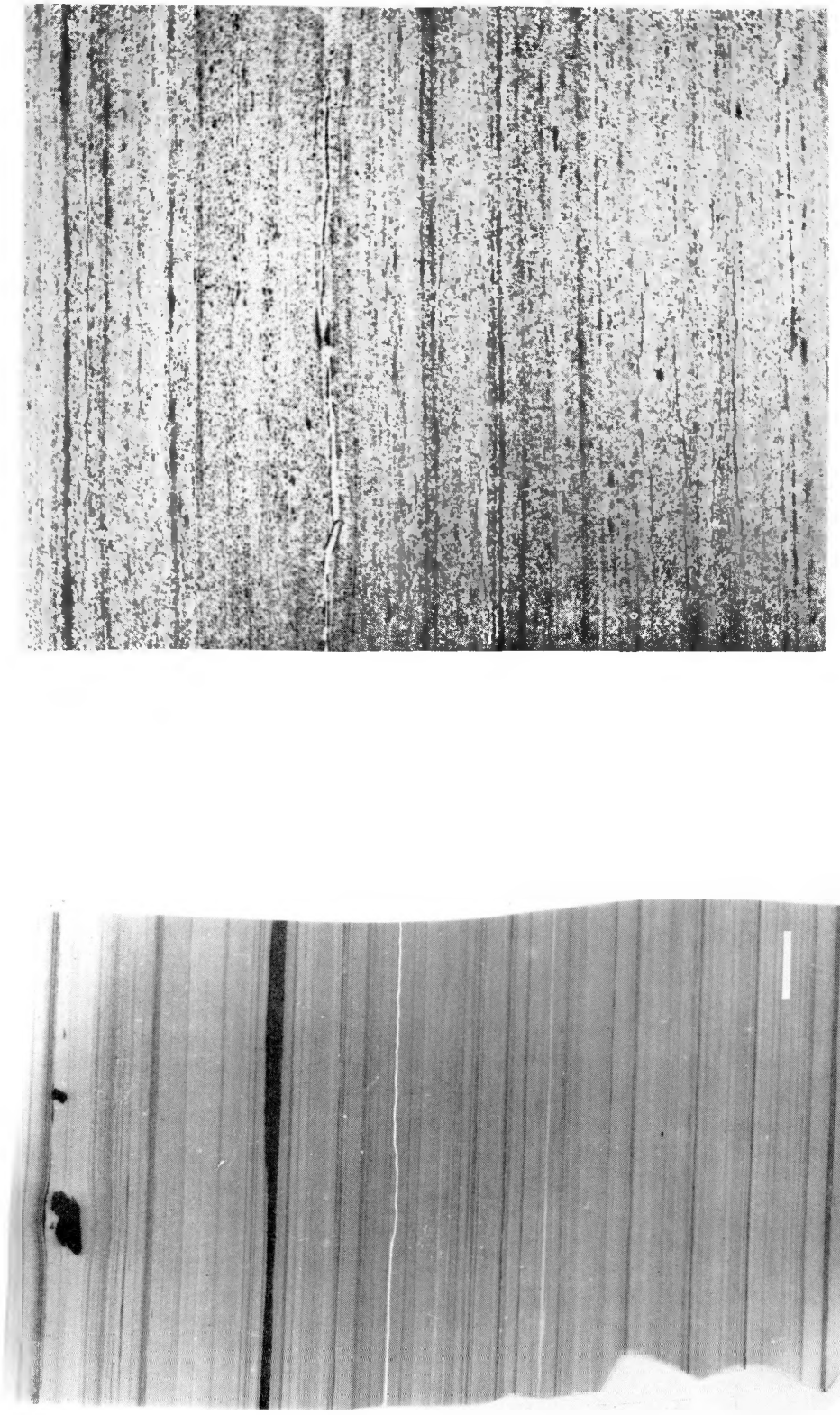


Figure 4. Thinly-laminated shale from Rhinestreet Member of the West Falls Fm. A) Radiograph positive print. Pyrite rich laminae have darker tones. B) Negative print image of thin section. Dark tones are silt. Scale bar in A is 1 cm, in B, 1 mm.

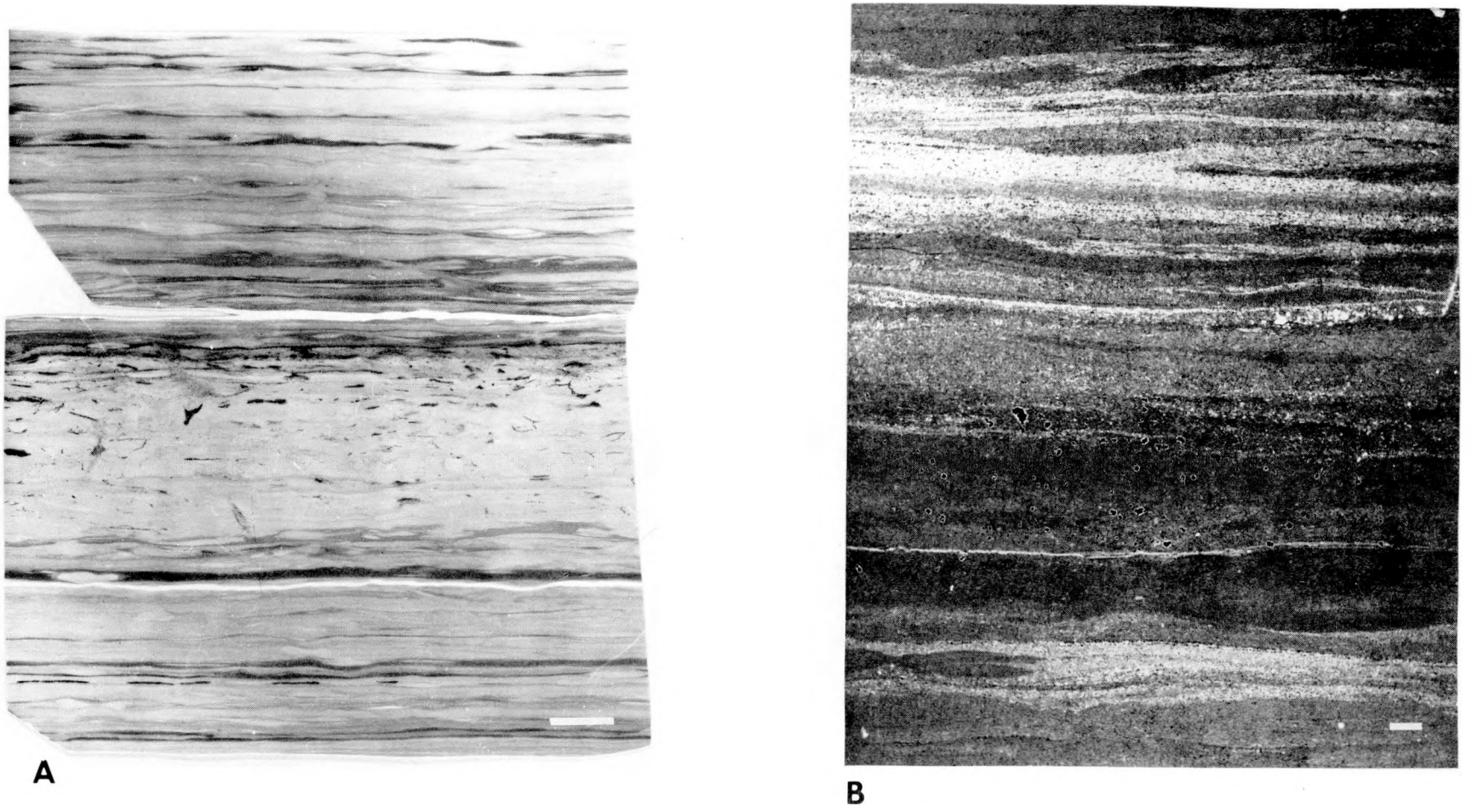


Figure 5. Lenticularly-laminated shale from Angola Shale Member of West Falls Formation. A) Radiograph positive print showing evidence of burrowing, but linear fabric is apparent. B) Negative print image of thin section. Pyrite rich zones have lightest tone. Scale bar in A is 1 cm, in B,1 mm. Fractures are induced.

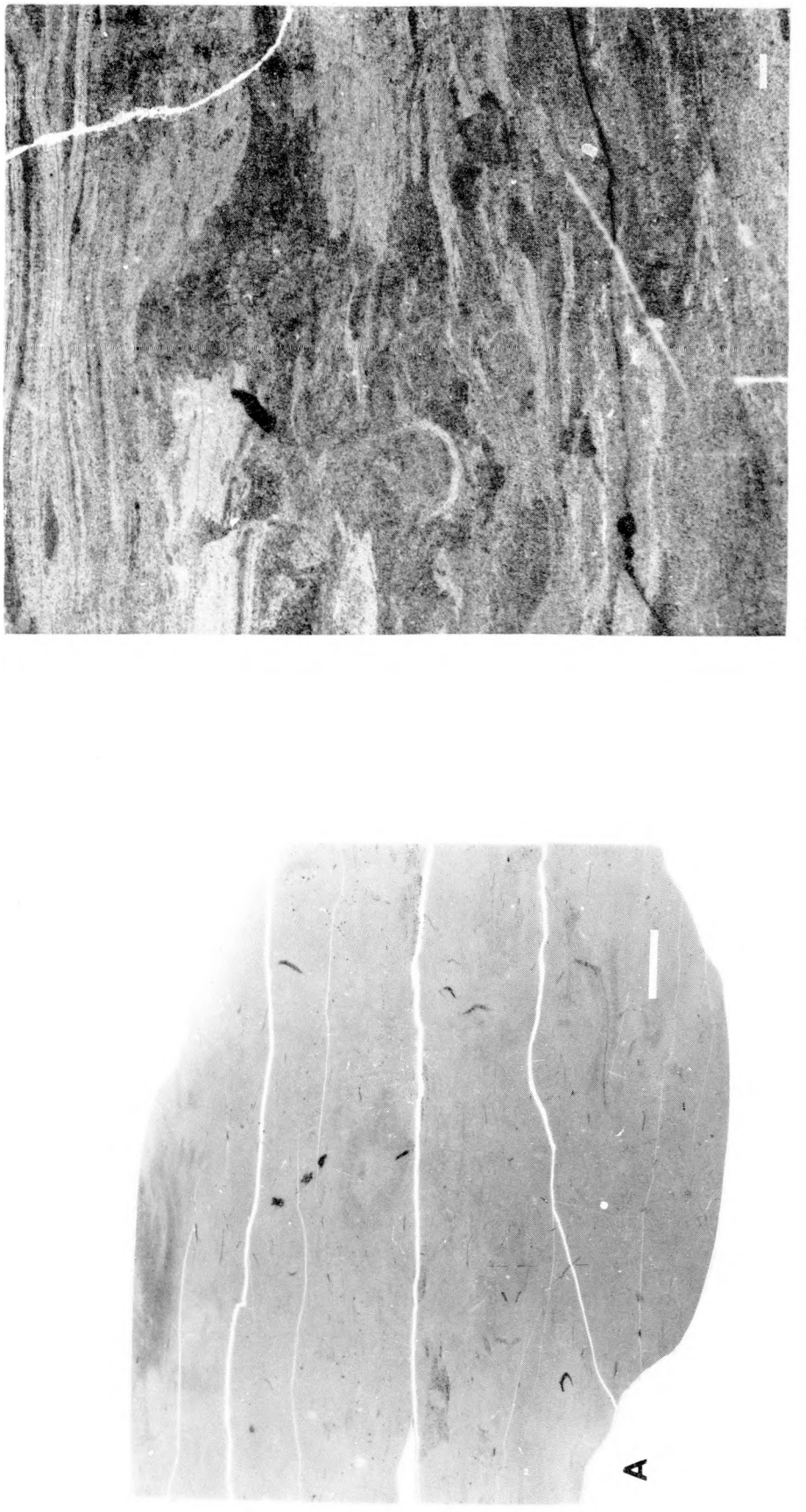


Figure 6. Non-banded shale from lower portion of Huron Member. A) Radiograph positive print showing extensive bioturbation. B) Negative print image of thin section showing lack of linear fabric. Scale in A is 1 cm, in B,1 mm.

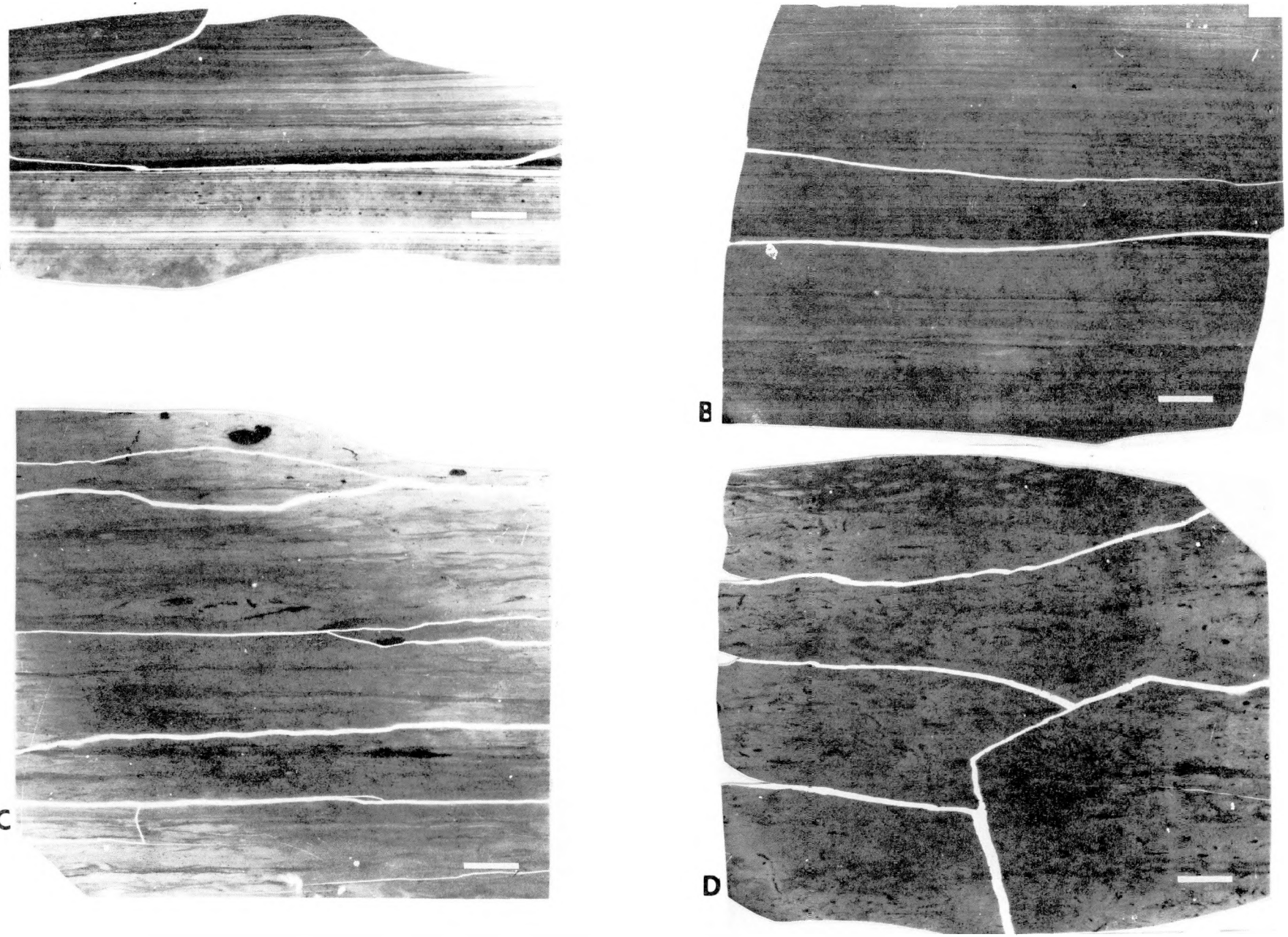


Figure 7. Transition series from highly ordered linear fabric to random fabric as shown in radiograph positive prints. A) Thinly-laminated shale. B) Thinly-laminated shale with some burrowing. C) Lenticularly-laminated shale. D) Non banded shale. Scale bar is 1 cm.

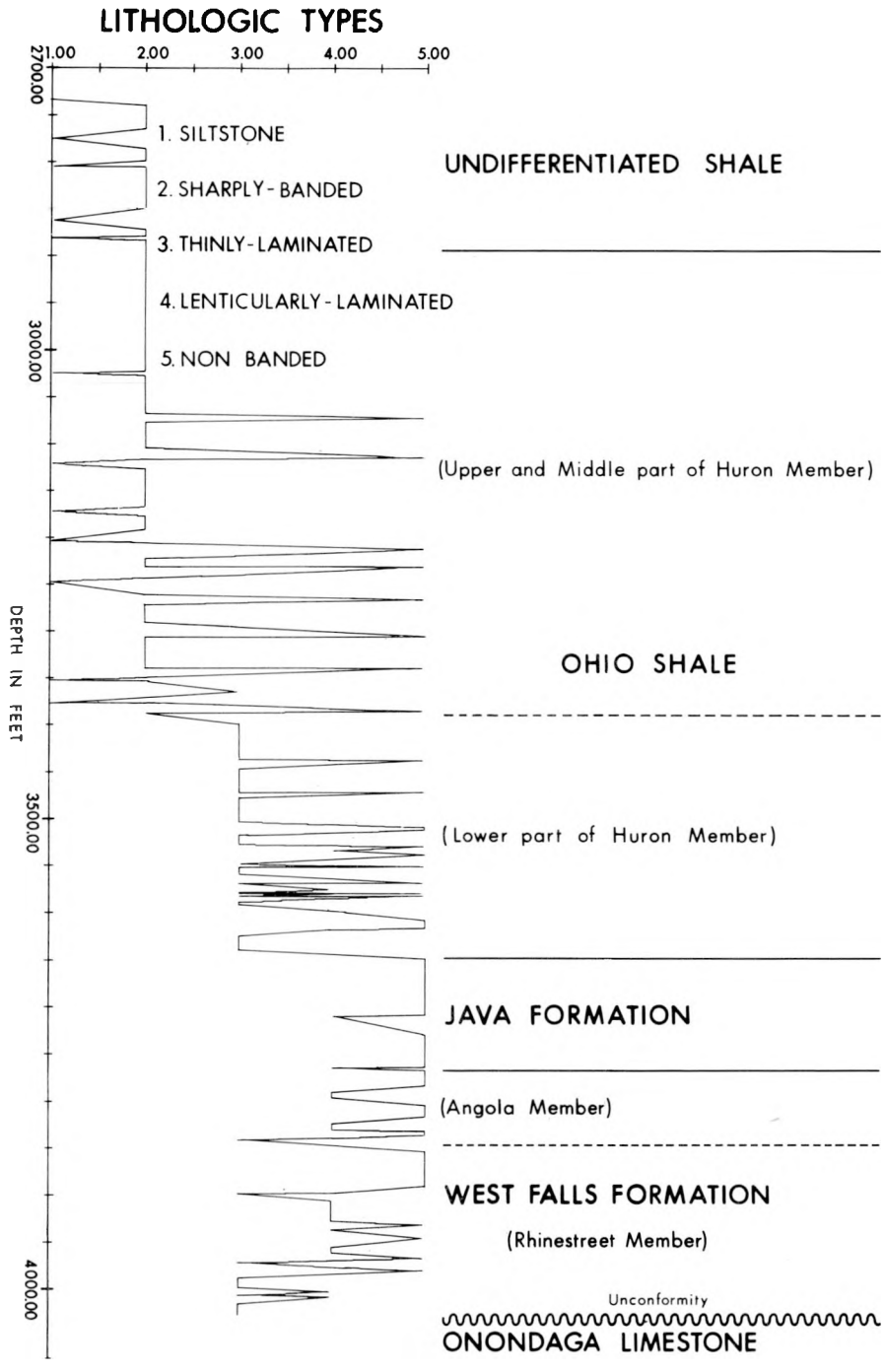


Figure 8. Distribution of shale lithotypes in CGTC #20403 (Linc-1637).

THE ELUCIDATION OF GEOMATRICES BY LASER PYROLYSIS/GAS CHROMATOGRAPHY AND PYROLYSIS/MASS SPECTROMETRY.

by

N. E. Vanderborgh

and

C. E. R. Jones

Los Alamos Scientific Laboratory
Los Alamos, New Mexico 87545



ABOUT THE AUTHORS

Nicholas E. Vanderborgh received his AB degree in Chemistry from Hope College in 1960 and his MS and Ph.D. degrees from Southern Illinois University in 1962 and 1964. He then joined the Chemistry Department of the University of New Mexico, teaching and doing research. He joined the staff of the Los Alamos Scientific Laboratory in 1975 and is presently alternate leader of the *In Situ* Sciences Group. His research interests center on new measurements for rock characterization and for the elucidation of *in situ* flows through sediments.

Charles Edward Roland Jones was born in London, England and educated at Norwood College. He recently completed his doctorate at Ecole Polytechnique (Paris). During much of Jones' professional career, he was employed at Vinyl Products, Ltd. where he pioneered a variety of pyrolysis techniques for the elucidation of macromolecules, especially synthetic polymers. He has served as the Chairman of the Chromatographic Discussion Group and is currently an editor of the Journal of Analytical and Applied Pyrolysis. Presently, he is an independent consultant and serves the Los Alamos Scientific Laboratory, among others.

2

THE ELUCIDATION OF GEOMATRICES BY LASER PYROLYSIS/GAS CHROMATOGRAPHY AND PYROLYSIS/MASS SPECTROMETRY

ABSTRACT

Present methods for the examination of organics entrained in geological matrices are tedious even if not fallible. Thermal degradative techniques combined with the separatory power of a gas chromatographic column or a quadrupole mass spectrometer operating low voltage electron impact mode afford rapid access to detailed profiles of such materials. The virtue of these parallel approaches are compared and contrasted in application to the elucidation of Devonian Shale and other geological material.

INTRODUCTION

Although there has been novel advance (1, 2, 3) in the methodology of latent fossil fuel resource investigations, perhaps the full potential of the methods of analytical pyrolysis or controlled thermal degradation in conjunction with other instrumental techniques has yet to be fully realized. Geological samples are complex mixtures of interrelated organic and mineral components. Maturation processes in these sediments are only partially understood (4, 5, 6). Organic rich debris, mainly condensed isoprenes, lignin and cellulose, are deposited under reductive conditions and maintained at elevated temperature and pressure. Initially, due partly to biological action, the debris are converted to complex organic material and methane is released. With continued high pressure, the material forms condensed carbonaceous macromolecules and additionally more methane. Continued evolution of lower molecular species generates a mobile material that can migrate from the source rock. Estimation of production potential of a particular formation requires a measurement of both the total quantity of carbonaceous material per volume of rock and a measurement of the nature of that material.

Standard procedures for these tasks are suggested in the typical separation scheme for organic sediments shown in Fig. 1. Initial sampling requires homogenization of a selected rock sample, then extensive mechanical grinding, then extraction in organic solvents. Frequently, the organic fraction is entirely insoluble. The mineral portion of the matrix is then dissolved in concentrated aqueous acids. There exists a certain potential for alteration of the sample during these several attritions. Although a number of workers claim little evidence for such chemical modifications, it would seem that such a rapid disturbance of an equilibrium gently established over an eon of time could accord change to the organic system.

It is also necessary to acquire meaningfully detailed profiles of geologically likely zones at a rate concomitant with that with which samples are actually produced. Consequently, improved organic geochemical techniques must consider analyses time as an important component. Sample integrity will be preserved if analyses are completed immediately after removal and rapid results could factor meaningfully into production techniques. It is thus apparent that field processing of drilling chips as they are brought to the surface could not only expedite exploration but could make substantive contribution to the economics of the exercise.

These rapid conditions are approached by modern analytical pyrolysis systems. We describe two techniques and contrast these complimentary fast heating methods for rock characterization.

EXPERIMENTAL SECTION

The equipment used for the measurements described below was of two basic types:

(1) Laser pyrolysis in combination with gas chromatography/mass spectrometry (Laser/GC-MS). (7)

(2) Curie-point pyrolysis in combination with mass spectrometry (Py/MS). (8)

Each will be described sequentially.

The laser pyrolysis system is shown schematically in Fig. 2. The sample, either small chips or compacted powders, is inserted into a cylindrical quartz chamber. Carrier gas is then fed through the pyrolysis chamber and into a chromatographic column. After the flow conditions have stabilized, the pulsed Nd laser is fired, through a focusing lens, into the sample. Pyrolysis products are transferred directly onto the column and eluted. Carrier gas is stripped by a molecular jet separator and enriched products are introduced into the ion source of a mass spectrometer. There a 70 eV electron beam is used to degrade the sample into characteristic molecular fragments. Data are obtained of normal fragmentation patterns from each characteristic peak. The system is insensitive to changes in carrier gas velocity and sample overloading. Data speed requirements are no more demanding than other high performance GC/MS systems because data is produced at rates set by column performance.

The Py/MS instrumentation is shown schematically in Fig. 3. This system requires that the sample is finely divided. This powder is then suspended in a volatile organic solvent and the suspension coated on a Curie-point wire. Then the sample-coated wire is inserted into the high vacuum of a mass spectrometer and positioned within an RF coil. The coil is energized and the wire is heated. Volatile fragments are driven off into a low voltage (14 eV) ion source. These charged fragments are then accelerated through a quadrupole filter and analyzed. Although the pyrolysis event is fast indeed (1-3 ms), products must have sufficient volatility so that they persist in the vacuum system and analyses are completed in much longer times. For instance, in the data presented here, RF energy was used to pyrolyze for 1.0 s at 510°C. (Sample sizes were of the order 20-25 μg). Data were recorded after 250 repetitive mass scans at a rate of 10 scans/sec. This system requires an expansion volume and a differential pumping to introduce sample into the filter at a continuous rate.

These complimentary techniques are contrasted in Table 1. In each case, the intent is to heat a rock sample rapidly enough to minimize secondary reactions. Considerable differences exist for sample procedures. Py/MS techniques require homogenization and grinding of selected rock sections and then that sample is dispersed in an organic solvent. The sample is then suspended on the Curie-point filament. Pyrolysis utilizes the entire suspensed sample although less volatile fragments may remain behind on the filament or precipitate on the walls of the vacuum chamber. Laser/GC-MS is a far more rigorous procedure. Most geomatrices absorb Nd-laser photons (1.06 μm), so the problem of nonabsorbing samples is of little concern. The laser "drills" a small section in a larger sample. This sampling procedure permits the direct interrogation of rock chips and other material. For samples chosen to be representative of specific zones, it is possible to grind and blend and then pelletize these materials to a uniform density and convenient shape, usually a cylinder.

Typically pyrolysis are done under inert conditions. Py/MS is performed in a vacuum while Laser/GC-MS can be accomplished under a variety of inert (including vacuum) and reactive conditions. In these experiments, the Laser/GC-MS experiments were accomplished in the flowing carrier gas stream, He. (7)

THE NATURE OF CARBONACEOUS SEDIMENTS

There is considerable literature on the pyrolysis of carbonaceous sediments. (1, 2) Clearly these insoluble, condensed materials are challenging. Although *in situ* measurements may reveal labile, low molecular weight compounds in sediments, typically, unless special techniques are used, by the time measurements are made, such species are lost. The geomatrices consist of cross-linked, three dimensional condensed polymeric material. Thermal treatment, like *in situ* maturation, leads to bond cleavages between the carbon-rich, semiaromatic polymeric backbone and pendant groups. Typically, these cleavages involve the formation of free radicals. Unpaired electrons are formed both on the parent species and on the newly separated pendant. The cleaved section then couples with other radical species to form lower (than the parent) molecular weight products. Should geomatrices be suitable, two adjacent free radicals in the backbone can couple to form more condensed residue. This sort of scheme has been identified in the coal literature, for instance, where it is well known that coal, when heated, forms "volatiles" and "char," both products from the same starting material. (9)
It is important to recognize that such phenomena are general during carbonaceous pyrolysis. It is also important to recognize that only the volatile materials are detected. The residual compounds are aromatic in nature, carbon-rich graphitic compounds of vanishingly small volatility, char.

This sort of behavior is paralleled in polymer pyrolysis. For instance, vinyl chloride polymers give only a small pyrolysis yield of the monomer. Rather, when pyrolyzed, product HCl and condensed "char" are formed. This result is quite different from systems with aromatic pendant groups like polystyrene, that degrade preferentially to yield monomeric species, like styrene. (10)

The implications are that during rapid pyrolysis the only discernible products will be those cleaved from the parent species. That such radical species can couple to form stable compounds is unquestioned and such coupling may be an important step in petroleum genesis.

PYROLYSIS MECHANISMS

Rapid heating of these sediments is essential. If slow heating techniques are used, solid condensation reactions can concurrently produce different types of materials that will, in turn, produce other fragment types. Py/MS, in a vacuum, is fairly well understood although free radical coupling is not impossible. Although the average chamber pressure may be low enough to lower collision rates, pressures are high enough in the vicinity of the filament to promote coupling and other interactions involving energy exchange between the primary molecular fragments.

Laser pyrolysis is complicated because of plasma interactions. (7) Initially, during the early part of the laser pulse, elements on the surface are ionized by the intense photon flux. Ions and electrons are pumped into a dense, hot gas. This plasma then grows between the laser source and the sample. Since photon absorbtivities for free electrons are far more probable than for atoms, the electrons continue to absorb energy and rapidly re-radiate this energy to the sample. The sample, then, during the later part of the pulse is subjected to a black-body radiative flux that heats the surface. The plasma state is kinetically isothermal during the pulse life since unbound electrons have sufficient velocity to rapidly distribute energy. Shortly after the termination of the pulse, electrons re-enter atomic manifolds; once this happens, heat transfer becomes less efficient and a high temperature "equilibrium" distribution of matter is frozen from the plasma. In carbon rich systems, a significant species in this distribution is the acetylene radical, C_2H^+. There is ample evidence that this species plays a major role in the formation of pyrolysis products.

As has been shown previously, laser pyrolysis results in a series of product types. The plasma quenches to an ensemble of low molecular weight gases, including acetylene. Then higher molecular weight fragments, pyrolysis fragments and condensed fragments results. Such results are shown in Fig. 2 and Table 2 obtained with a sample of Gilsonite removed from the Independence Vein. It is thought that Gilsonite is composed of a complex mixture of asphaltenes . (11) Fig. 2 shows a tracing of the total ion current following the laser pulse. As each peak is eluted into the mass spectrometer, the data system is activated and an electron-impact mass spectra is recorded. Table 2 lists the relevant data as well as suspected identification of major peaks.

The first peaks are low molecular weight gases. As expected, acetylene (plasma) results in an intense peak. The fourth peak is pro ylene, the first of a series of terminal acetylenic compounds. For instance, acetylene derivatives of methyl (propyne), ethyl, isopropyl, N-propyl, etc. are apparent. Lastly, higher molecular weight fragments such as $C_7H_{12}O_2$, possibly molecular fragments from cleavage across the substituted back of the pyrrole ring, appear. Interestingly, there is little evidence of nitrogen containing products compounds. Neither do we observe any compounds of molecular weight in excess of, approximately, 150.

From this behavior, we conclude that free radical products are tagged with acetylenic fragments. The sediment is rapidly heated, forming, in part, and intense, carbon-rich plasma. This plasma radiates an intense thermal flux on the surface. At the termination of the event, the collapsing plasma, rich in the acetylene radical, merges into the hot surface and into short-lived radical species. Due to the triple bond, the acetylene moiety is an effective quenching agent. Consequently, stable, terminal acetylene species are formed, typified by $HCC-CH_3$, from methyl radicals. Interestingly, we observe little ethane, a compound that should form from dimerization of two methyl radicals. This compound cannot result when the acetylene species is present in high enough concentration that the radical-radical coupling reactions are dominated by acetylene.

The fact that these data show few nitrogeneous compounds is interesting and still only partially understood. This fact suggests that the nitrogen is left behind in the char, an observation that might have application in high temperature fossil fuel processing or might evolve as HCN.

Py/MS data were determined for a series of carbonaceous shales dating from the Devonian period. These samples were removed from a section of core cut from Hazard, Kentucky (USA) - Well #7239. (12) Core sections were examined and geometric samples of 15 cm were ground and carefully homogenized. Standard geochemical measurements were made on those samples; results are given in Table 3. Results show these samples contain both mineral carbon and organic carbon. The color of these samples was from white-grey to dark brown. The color is, perhaps, a measure of pyrite concentration. Some of the samples, like that from 742.2 m, have very low quantitie of organic carbon (0.3%) while the sample removed at 792.5 m has 25 times as much. These sediments are known to be matured and produce only small quantities of low molecular weight gases when heated.

The Py/MS sampling technique offers methodology to deal with such materials. First, the sample size can be readily adjusted for optimum product delivery rates to the quadrupole filter. This is done by first using a trial suspension loading and then increasing or decreasing the sample size depending upon initial results. In that way, larger samples for low carbon content rocks are used than for rocks that have a high carbon content. Low electron impact conditions are used. The intent is to gently charge the various fragments so that the possibility of additionally fragmenting pyrolysis products is minimized. This is essential since all products are analyzed concurrently.

A typical tracing from the Py/MS instrumentation is shown in Fig. 5. This result is the analog output of the data system that displays peak heights for each amu channel from 10 through 160. (No peaks

were apparent at higher amu values). Suspensions were made in methanol. Although the solvent was evaporated, residual methanol may appear at amu = 32. These data were run, once the proper sample loading was determined, in duplicate. Peak intensities depend on sample quantities. Moreover, the filament-sample interface complicates heat transfer. However, the ratios of particular components are a measure of replication. We chose to measure the ratio of the alkene/alkanes for C_3 through C_7. Data are presented in Table 4 showing the two sets for each of the six shale samples. As can be seen, the replication of these product ratios is adequate and suggests that sampling from such a liquid suspension does sufficiently homogenize the sample to obtain representative results.

Py/MS data in Fig. 5 show a variety of possible product types. It follows that unambiguous identities can be assigned to certain masses but tentative identification can only be made in those other cases where a number of possibilities exist. The significance of the chemistry of a particular situation must assist in limiting choices only to sensible possibles. By intelligent appraisal one can arrive at a completely meaningful interpretation.

The present series of samples derived from this Devonian Shale core show a rather uniform picture of the organic constituents. There is also clear definition of the way that the distribution of these organic presences change over the depth of the core section examined. Table 6 summarizes results of aliphatic and aromatic hydrocarbon presences along with some important derivatives. These data are plotted in Fig. 6 to correlate the distribution of "organics" with depth and indeed presents a supportingly homogeneous picture. These results are in complete contrast to those emanating from classical geochemical methods which are to be seen in Table 3 and imply a far more hetereogeneous situation. (12) The C, H, and N analyses (Table 3) tend to support the pyrolysis mass spectral data. The interplay between the relative yields of aliphatics and aromatics/heterocyclics is immediately apparent and could well be due to some directive element within the matrix that increases the tendency for cross linking and hence of formation and evolution of aliphatic species in the cases of samples B, C, D, and E. Although the two outlying samples are low in carbon, these two samples show the same general maturation extent with subtle differences mentioned above.

Laser/GC-MS on these similar samples showed a series of low molecular weight compounds predominantly due to quenching of the high temperature plasma. The most intense high-molecular weight compound was CS_2. This stable compound should indeed form from pyrolysis of carbon rich pyrite systems. Most probably the acetylene radicals are efficiently quenched by the dominant sulfur in the pyrolysis environment.

CONCLUSIONS

There is every indication that both these approaches to problems inherent in the elucidation of a carbonaceous geomatrices have merit. Data suggest a subtle equilibrium between various carbon types and may point to the necessity for direct *in situ* sampling, and, possibly, analyses. High energy laser pyrolysis in conjunction with GC-MS reveals interesting free radical reactions that could be feasibly promoted in a system under controlled conditions. Py/MS can be viewed more as indicative of the direct excision of organics from a geomatric by simple, perhaps serial, low-energy bond ruptures occurring under nearly ideal conditions. Here we probably approach the isolation of primary events.

Considerably more work is necessary before it would be wise to speculate upon the full significances of these results. It may be claimed, however, that we stand on the threshold of a new understanding of the interrelated processes of maturation and, perhaps, with that understanding a new appreciation of the energy potential of abundant fossil fuel resources.

ACKNOWLEDGEMENTS

This work was supported by the U.S. Department of Energy as part of the Eastern Gas Shales Project. The authors thank S. Lamey (METC) for supplying both analytical samples and results for these studies as well as the FOM Institute (Amsterdam) for their assistance with the Py/MS practical work.

REFERENCES

1. A. Giraud, "Application of Pyrolysis and Gas Chromatography to Geochemical Characterization of Kerogen in Sedimentary Rock," Amer. Assoc. Petr. Geol. Bull., 54, 439 (1970).

2. C. Barker, "Pyrolysis Techniques for Source Rock Evaluation," Amer. Assoc. of Petr. Geol. Bull., 58, 2349 (1974).

3. G. E. Claypool and P. R. Reed, "Thermal-Analysis Technique for Source-Rock Evaluation: Quantitative Estimate of Organic Richness and Effects of Lithologic Variation," Amer. Assoc. of Petr. Geol. Bull., 60, 608 (1976).

4. A. Hood, C. C. M. Gutjahr, and R. L. Heacock, "Organic Metamorphism and the Generation of Petroleum," Amer. Assoc. of Petro. Geol. Bull., 59, 986 (1975).

5. T. Gold, "Terrestrial Sources of Carbon and Earthquake Outgassing," J. Petr. Geol., 1, 3 (1979).

6. B. Tissot, B. Durand, J. Espitalie, and A. Combaz, "Influence of Nature and Diagenesis of Organic Matter in Formation of Petroleum," Amer. Assoc. Petr. Geol. Bull., 58, 499 (1974).

7. N. E. Vanderborgh and R. L. Hanson, "Characterization of Coals Using Laser Pyrolysis-Gas Chromatography," Analytical Methods for Coal and Coal Products, vol. 3, ed. by C. Karr, Jr., Academic Press, NY.

8. H. L. C. Meuzelaar, A. Tom, H. v. d. Brink, P. G. Kistemaker, W. Eshuis, and H. H. Tuithof, "The Scope of Automated Pyrolysis Mass Spectrometry," Analytical Pyrolysis, ed. by C. E. R. Jones and C. A. Cramers, Elsevier, Amsterdam, 1977, p. 412.

9. H. C. Howard, "Pyrolytic Reactions of Coal," Chemistry of Coal Utilization, ed. by H. H. Lowry, Supplementary Volume, John Wiley & Sons (1963).

10. N. E. Vanderborgh, "Laser Induced Pyrolysis Techniques," Analytical Pyrolysis, ed. by C. E. R. Jones and C. A. Cramers, Elsevier, 1977, p. 235.

11. E. W. Baker, "Porphyrins," Chapter 19 in Organic Geochemistry, Methods and Results, ed. by G. Eglinton and M. T. J. Murphy, Spring, Verlag, 1969.

12. S. Lamey and E. Childers, "Organic Composition of Devonian Shale from Perry County, Kentucky," US Department of Energy, Morgantown Energy Technology Center, Dec. 1977. METC/TPR-77/3.

LEGENDS TO FIGURES

Fig. 1: Typical procedure for organic separation prior to analysis for chemical characterization.

Fig. 2: Schematic of Laser/Gas Chromatographic-Mass Spectrometric Instrumentation. Sample is housed in pyrolysis chamber and products are flushed into gc-ms system.

Fig. 3: Schematic of Pyrolysis/Mass Spectrometer Instrumentation. Sample, coated on Curie-point wire, is inserted into vacuum system and pyrolyzed into expansion volume.

Fig. 4: Pyrogram from Gilsonite (Independence) sample. Tracing of total ion current during column elution. Column, 2m Tenax, 1/8 in. SS; Carrier gas, He; flow. 15 cm^3/min; temperature program, 100-225° 10°C/minute; laser, Nd (1.06μ), 2.5J, 0.001 s.

Fig. 5: Py/MS result from Devonian Shale sample. Pyrolysis, 1 sec at 510°C; Data acquisition, 250 scans; sample, Core 7239 Hazard, Kentucky, removed at depth of 792.5 m.

Fig. 6: Variation of selected parameters with depth of Devonian Shale core. Data shows uncorrected channel counts (% of total) for several species as a function of depth.

TABLE 1

COMPARISON OF PYROLYSIS CONDITIONS BETWEEN Py/MS AND LASER/GC-MS

	Py/MS	Laser/GC-MS
Heating Method	Magnetic wire in RF Field	Photon absorption and plasma
Heating Geometry	Back sample surface	Front surface
Sample Properties	Powder dispersed in organic solvent	Compacted powders; rock chips; whole rocks
Heating Rate	10^5 K/s	10^7 K/s
Cooling Rate	-10^4 K/s	-10^6 K/s
Pyrolysis Conditions	Vacuum	Variable pressure and reactant conditions
Time	1-100 ms	0.1-1 ms
Limitations	Volatile samples Catalytic influences Metal surfaces Back-heating blow off	Transparent materials Variable energy input Plasma complications Photolysis
Separation of products	Quadruple	Chromatographic column
Separator	Differential pressure	Molecular jet
Ionization	14 eV[+]	70 eV[+]

[+]These experiments

TABLE II

LASER gc/ms DATA ON GILSONITE

GILSONITE/INDEPENDENCE VEIN

Peak #	Intensity	Re t	Base	Abund.	1	2	3	4	Peak Ident.
1	1330	1.4	28	313	28.0	16.2	15.2	14.2	CH_4/CO
2	8566	1.6	26.1	3167	26.1	28.1	25.1	44.1	C_2H_2/CO_2
3	6481	2.9	41.1	1636	41.1	39.2	42.2	40.1	$CH_3-CH=CH_2$
4	12251	3.6	40.1	208	40.1	39.1	38.1	28.1	Mixture
5	1199	3.9	40.1	188	40.1	39.1	28.0	44.0	$C_2H \cdot CH_3$
7	2749	5.6	41.1	596	41.1	39.1	56.0	55.0	$CH_3CH_2CH=CH_2$
8	3487	5.9	54.0	539	54.0	39.2	53.0	50.0	$C_2H \cdot C_2H_5$
9	1267	6.3	52.1	160	52.1	51.1	28.0	50.1	$C_2H \cdot CH_2OH$
10	2778	6.9	50.0	931	50.0	49.1	44.0	28.1	$C_2H \cdot C_2H$
11	1629	8.2	55.1	184	55.1	42.2	39.1	28.0	$C_2H \cdot CH(CH_3)_2$
12	2034	8.6	67.1	183	67.1	55.1	53.0	39.2	1 - pentene
13	2431	9.2	66.0	247	66.0	67.1	39.1	65.1	$C_2H \cdot CH_2CH_2CH_3$
14	1862	10.9	41.1	165	41.1	56.0	39.2	28.1	$C_2H \cdot CH_2COOH$
15	2237	11.4	79.0	294	79.0	80.0	77.0	67.1	$C_2H \cdot nC_4H_9$
16	2855	12.1	78.1	548	78.1	77.0	50.1	51.1	$C_2 \cdot CH_2CHCHCH_3$
21	3212	14.0	91.1	552	91.1	92.1	44.1	39.1	$C_2H \cdot C_5H_9$
22	1669	15.3	44.1	178	44.1	91.1	55.1	41.1	$C_2H \cdot C_5H_{10}$
23	2280	15.6	91.1	297	91.1	44.1	28.0	106.1	C_8H_{10}
28	2076	17.5	44.1	254	44.1	117.0	118.0	28.6	R-COOH
30	2420	19.6	44.1	360	44.1	28.1	115.0	130.1	R-COOH
31	2397	20.4	44.1	407	44.1	128.1	38.0	55.1	$C_7H_{12}O_2$

TABLE III

STANDARD ANALYSES OF POWDERED SAMPLES OF DEVONIAN SHALE

Hazard, Kentucky (USA) Well 7239

Sample	Color	Average Depth	%C	%H	%N	$\%CO_2$*	$\%C_{org}$*	%S*	$\%S_{pyr}$*
A	White-Grey	742.2m	0.45	0.43	0.29	0.40	0.34	3.12	2.95
B	Light Brown	749.9m	5.78	0.76	0.23	0.60	5.61	3.00	2.75
C	Brown	761.8m	3.67	0.61	0.22	0.80	3.45	3.20	3.03
D	Dark Brown	765.0m	4.62	0.66	0.22	1.31	4.26	3.04	2.95
E	Dark Brown	792.5m	7.78	0.90	0.30	0.94	7.52	4.38	4.11
F	Grey	813.1m	0.61	9.39	0.10	1.35	0.24	1.31	1.16

*Analysis data supplied by Morgantown Energy Technology Center. (12)

TABLE IV

TYPICAL REPEATABILITY OF Py/MS ON POWDERED ROCK SAMPLES

	Ratio of Peak Intensities (alkene/alkane)				
Sample	C_3	C_4	C_5	C_6	C_7
A	1.71	1.92	2.03	1.67	4.00
	1.65	1.37	1.62	1.45	4.64
B	1.39	0.86	1.01	1.03	2.00
	1.37	0.89	1.12	1.16	3.00
C	1.30	1.01	1.06	1.02	2.67
	1.19	1.03	1.03	1.19	2.42
D	1.39	1.10	1.04	1.12	2.21
	1.42	1.08	1.15	1.08	1.64
E	1.37	0.82	0.95	0.90	1.56
	1.35	0.87	9.98	1.01	1.71
F	1.21	1.06	2.23	1.84	4.20
	1.89	1.47	2.07	1.77	4.14

TABLE V

MAJOR FRAGMENTS FROM LOW VOLTAGE Py/MS
(Data are Percentage of Total Ion Current)

Depth (meters)		742.2	749.9	761.8	765.0	792.5	813.6
COMPOUND	MASS						
NH_3	17	2.88	1.86	2.25	2.00	1.49	1.89
H_2O	18	7.14	5.52	6.21	5.23	4.11	8.26
$HC{\equiv}CH$	26	0.51	0.48	0.40	0.46	0.33	0.66
CH_3OH	32	0.42	0.42	0.51	0.76	0.78	1.07
H_2S	34	0.58	1.33	1.10	1.16	1.84	0.89
C_2H_5OH	46	0.19	0.17	9.20	0.28	0.22	0.32
CH_3SH	48	0.07	0.08	0.10	0.10	0.13	0.05
SO_2	64	0.5]	0.36	0.40	0.30	0.58	0.71
PYRROLE	67	0.64	0.85	0.78	0.82	0.89	0.61
C_5(ALi)	70-72	8.51	8.64	8.82	8.23	8.64	9.18
CS_2	76	0.06	0.08	0.10	0.10	0.17	0.07
BENZENE	78	0.67	0.38	0.35	0.31	0.26	0.81
PYRIDINE	79	0.32	0.43	0.39	0.41	0.41	0.32
MeSSH	80	0.61	0.82	0.81	0.82	0.89	0.62
C_4H_5N	81	1.15	1.66	1.65	1.65	1.80	1.11
C_6(ALi)	84-86	5.19	6.32	6.35	6.16	6.46	5.39
TOLUENE	92	0.43	0.73	0.61	0.59	0.58	0.44
PICOLINE	93	0.37	0.51	0.47	0.51	0.55	0.36
PHENOL	94	1.10	1.25	1.22	1.27	1.27	1.10
FURFURAL	96	1.98	2.62	2.68	3.08	2.82	1.96
THIOPHENE	97	2.30	2.58	2.68	2.59	2.70	2.20
C_7(ALi)	98-100	8.28	5.31	5.63	5.43	4.64	6.96
STYRENE	104	0.54	0.23	0.23	0.26	0.22	0.42
XYLENES	106	0.37	1.00	0.86	0.87	0.90	0.39
C_8(ALi)	112-114	5.21	2.94	3.30	3.08	2.66	0.89
C_9(ALi)	126-128	1.52	1.12	1.18	1.12	1.21	0.89

THE ELUCIDATION OF GEOMATRICES BY LASER PYROLYSIS/GAS CHROMATOGRAPHY AND PYROLYSIS/MASS SPECTROMETRY

10

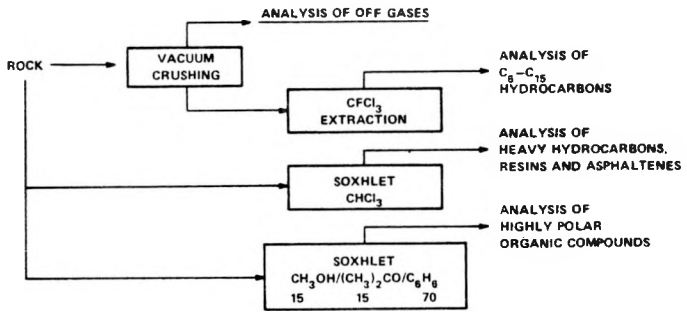


Fig 1

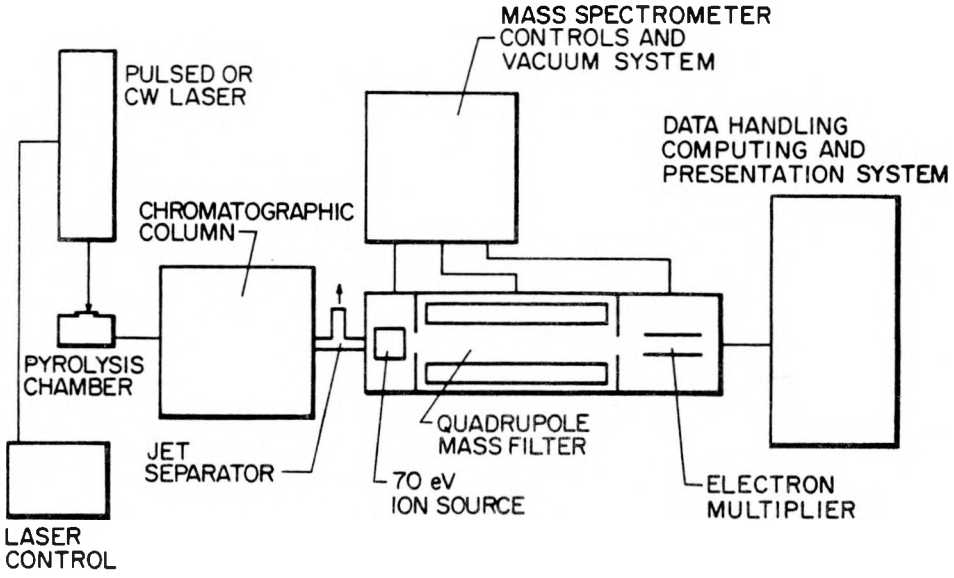


Fig 2

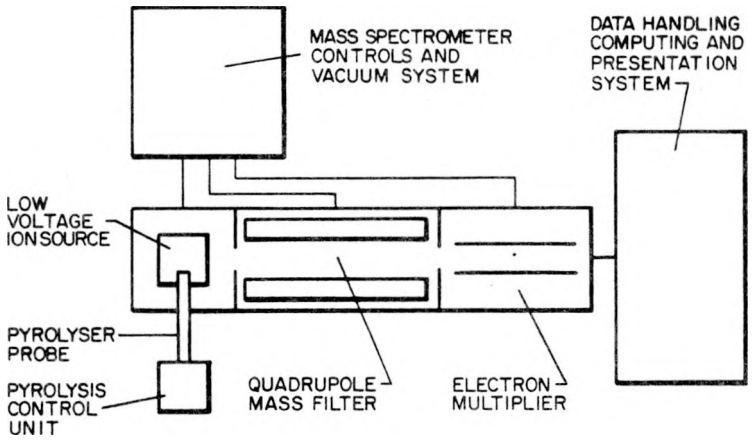


Fig 3

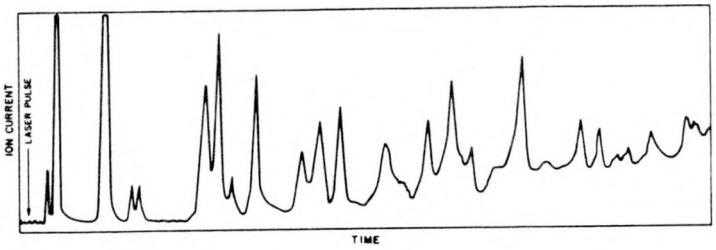


Fig 4

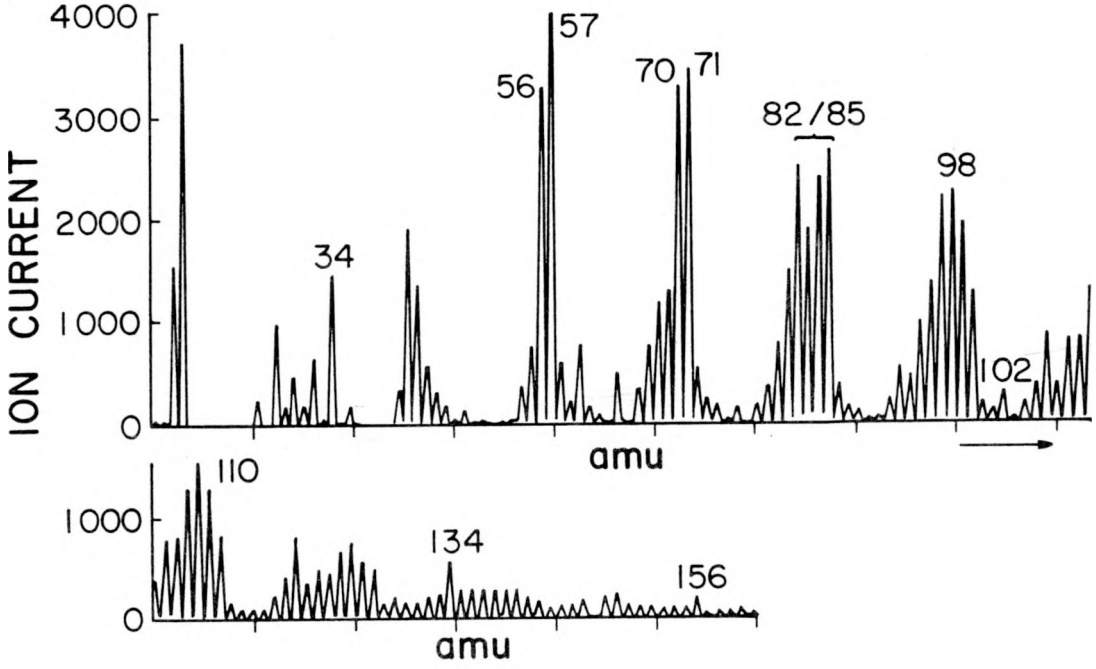


Fig 5

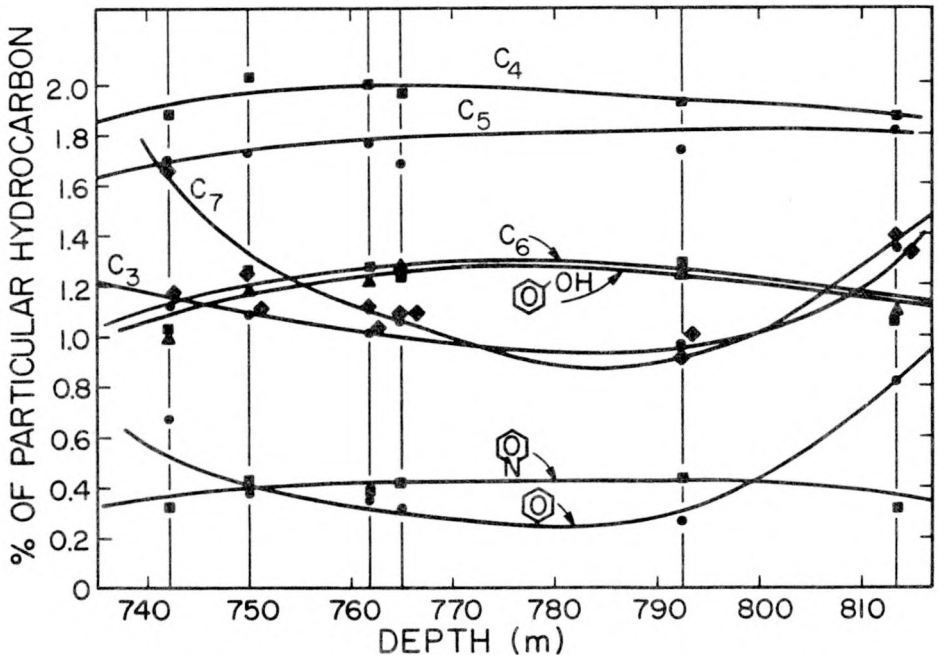


Fig 6

DISTRIBUTION AND GEOCHEMICAL CHARACTERIZATION OF THE HANNIBAL MEMBER OF THE NEW ALBANY SHALE IN INDIANA

Lechler, P. J., Hasenmueller, N. R., Bassett,

J. L., and Leininger, R. K.

Indiana Geological Survey
Bloomington, Indiana

ABSTRACT

The Hannibal Member, the uppermost unit of the New Albany Shale (Mississippian-Devonian) in the subsurface of the Illinois Basin in Indiana, has been correlated with the Jacobs Chapel, Henryville, Underwood, and Falling Run Beds (in descending order) of the southeastern Indiana outcrop area. The stratigraphic completeness of the Hannibal Member and its outcrop equivalents is geographically variable. The Hannibal is overlain by the Rockford Limestone (Lower and Middle Mississippian) or by the New Providence Shale (Middle Mississippian) and is underlain by the brownish-black shale of the Clegg Creek Member (equivalent to the upper part of the Grassy Creek Shale of Illinois) of the New Albany Shale. The Mississippian-Devonian boundary has been placed at or slightly below the base of the Falling Run Bed.

The Jacobs Chapel is greenish-gray glauconitic shale. The Henryville is black organic-rich shale that has the highest organic carbon content of all units of the New Albany section and is strongly enriched in heavy metals. The Underwood is greenish-gray shale that is irregularly distributed and varies greatly in thickness. The Falling Run is a bed of nodular phosphate or phosphatic debris high in Ca, P, F, Y, and U. The geochemistry of the Hannibal Member and of its outcrop equivalents is significantly different from that of the underlying members (Devonian) of the New Albany Shale. Statistical analysis shows the Hannibal to be significantly enriched in many trace elements relative to the underlying New Albany members and to many other black shales of North America.

INTRODUCTION

Chemical characterization of the New Albany Shale of Mississippian and Devonian age is one task of the Eastern Gas Shales Project sponsored by the Department of Energy. During the analysis of core and outcrop samples from various locations in the Illinois Basin in Indiana, distinct lateral similarities and vertical differences in chemical composition of the shale, especially the quantities of certain trace elements, were observed. The unique geochemistry and lithology of the Henryville and Falling Run Beds, which are in the upper part of the New Albany Shale in the outcrop area, can be used to correlate the outcrop units with similar units in the Hannibal Member of the New Albany in the subsurface.

Within the Henryville Bed, major element composition is very homogeneous and is similar to the composition of the other black shale units of the New Albany. Organic carbon is distinctly higher, however, and zinc and other heavy metals are enriched with respect to the rest of the New Albany and to other normal black shales as reported by Vine and Tourtelot (1970, p. 261)[1]. This heavy-metal enrichment is consistent within the study area (about 7,000 square miles) and is characteristic of the Henryville Bed. The Falling Run Bed is a highly phosphatic unit different in both major- and trace-element composition from the rest of the New Albany Shale.

In this paper we propose that the name Hannibal Member (the uppermost member of the New Albany Shale in the subsurface) be extended into the outcrop area and that it include the Henryville and Falling Run Beds, as well as the less geochemically distinct Jacobs Chapel and Underwood Beds. These beds were formerly placed by Lineback (1968, p. 1300)[2] in the upper part of the Clegg Creek Member in the outcrop area (Figure 1).

HANNIBAL MEMBER

The Hannibal Shale, named by Keyes (1892, p. 289)[3] for shale exposures near Hannibal Missouri, is present in the subsurface of Illinois and was traced on geophysical-log cross sections into southwestern Indiana by Meents and Swann (1965, Fig. 4)[4]. Becker (1974, p. 48)[5] recognized this shale unit on geophysical logs and in well cuttings in the subsurface of Indiana. He proposed that the name Hannibal Member of the New Albany Shale be applied to the dominantly greenish-gray shale lying between the base of the Rockford Limestone and the top of the black shale that constitutes the main part of the New Albany in the subsurface.

Lineback (1970, p. 42)[6] noted that the Hannibal Shale of Illinois was equivalent to the Jacobs Chapel, Henryville, Underwood, and Falling Run Beds of the New Albany outcrop area in southeastern Indiana. In the present study, beds correlative with the Jacobs Chapel, Henryville, Underwood, and Falling Run Beds have been recognized on many geophysical logs, in some cores, and in well cuttings within the Hannibal interval in the subsurface. On the basis of these observations, outcrop terminology has been extended into the subsurface. Therefore in the subsurface the Jacobs Chapel, Henryville, Underwood, and Falling Run Beds are here recognized in the Hannibal Member. The geochemical and lithologic characteristics of these individual beds in the subsurface are similar to those of the corresponding outcrop units.

Correlation of outcrop and subsurface units is illustrated by comparing lithology and geochemistry of an outcrop exposure (Figure 2) with cores from four wells in the subsurface (Figures 3-6). The Hannibal Member in the subsurface may be identified on both resistivity and gamma-ray logs. Distribution and thickness of the Hannibal Member and outcrop and core locations are shown in Figure 7.

CORRELATION OF OUTCROP UNITS WITH SUBSURFACE UNITS

The Jacobs Chapel is soft gray-green glauconitic shale that underlies the Rockford Limestone in the New Albany Shale outcrop area (Figure 2). This same lithology characterizes the uppermost New Albany lithologic unit in the Clark County (Figure 3), Brown County (Figure 4), and Marion County (Figure 5) cores, but it is not present in the Sullivan County core (Figure 6), which is included here to indicate how both geophysical logs and geochemistry show the absence of the Hannibal sequence where it is not present. Geochemically, the Jacobs Chapel is non-enriched inorganic glauconitic shale. In outcrop the Jacobs Chapel has somewhat elevated zinc content (for example, 788 ppm) that is probably due to upward secondary mobilization of this element from the high-zinc Henryville Bed below. The migration is undoubtedly a weathering phenomenon that does not occur at depth; in the subsurface the Jacobs Chapel is similar to most other non-enriched inorganic glauconitic shales. The correlation is made here on the basis of the similarity of lithology and geochemical composition of both core and outcrop intervals and the similarity in stratigraphic position as defined by geophysical logs and and core studies. Specific geochemical data for outcrop and core samples are given in Tables 1-5.

The aspects of correlative geochemistry that characterize the tight black shale of the Henryville are (1) relatively high organic carbon (>12 percent), (2) high zinc (>3,000 ppm) and other heavy metals, (3) normal P_2O_5 (<0.2 percent), and (4) normal Y (<70 ppm). In the cores the Henryville underlies the Jacobs Chapel Bed within the interval defined by resistivity and gamma-ray logs as Hannibal. These aspects match the stratigraphic position, lithology, and essential geochemistry of outcrop Henryville.

The Underwood Bed is similar to the Jacobs Chapel Bed in that its lithology and geochemistry are not much different from other non-enriched inorganic shales; however, the Underwood is generally less glauconitic. It lies between the Henryville Bed and the underlying Falling Run Bed and has been correlated by means of geophysical logs from the type area into the subsurface. The correlation of the Underwood into the subsurface is also supported by geochemical data (Tables 1-5). In the limited area where the Underwood is present in the New Albany Shale outcrop belt, the unit is thin (Figure 2). But the thickening of the Underwood in the subsurface in central and southwestern Indiana is the principal cause of the increased thickness of the total Hannibal Member in those areas.

The Falling Run is the basal bed of the Hannibal Member in the subsurface and outcrop and consists of

phosphate nodules generally in a matrix of phosphatic pyritic black shale. High P_2O_5 (0.4-20 percent), high Y (100-1,400 ppm) and associated elements are common to both outcrop and core intervals.

In the Phegley core, Sullivan County (Figure 6), beds composing the Hannibal Member are absent. A thin phosphatic interval lies at the base of the New Providence Shale and is underlain by a thin high zinc interval at the top of the Clegg Creek Member. This is not the normal Hannibal geochemical sequence, and the geophysical logs and core lithology confirm the absence of the normal Hannibal sequence. Additional, minor phosphatic zones possibly exist elsewhere in the Hannibal sequence, but these have not been confused with the Falling Run Bed. This is so because the cores and outcrop exposures have been sampled lithologically rather than at arbitrarily fixed intervals and because these intervals with respect to the Falling Run are minor.

CONCLUSIONS

Geochemistry, geophysical characteristics, and core lithology are reliable indicators of Hannibal stratigraphy, and these indicators confirm that the Jacobs Chapel, Henryville, Underwood, and Falling Run Beds as defined in outcrop are traceable into the subsurface and make up the Hannibal Member there. To aid in simplifying and clarifying New Albany stratigraphy, the name Hannibal Member is extended to the southeastern Indiana outcrop area as the uppermost member of the New Albany Shale. The Hannibal Member is composed of the Jacobs Chapel, Henryville, Underwood, and Falling Run Beds (formerly included in the Clegg Creek Member). And where the Hannibal Member exists in the subsurface, it may contain some or all of the Jacobs Chapel, Henryville, Underwood, and Falling Run Beds, similar in lithology and geochemistry to their equivalents as defined in outcrop.

ACKNOWLEDGMENTS

This study was performed under contract EY-76-C-05-5204 Patton of the Department of Energy's Eastern Gas Shales Project. It is published with permission of the State Geologist, Indiana Geological Survey.

REFERENCES

1. Vine, J. D. and E. B. Tourtelot: Geochemistry of black shale deposits - A summary report: Economic Geology, v. 65, 1970, p. 253-272.

2. Lineback, J. A.: Subdivisions and depositional environments of New Albany Shale (Devonian-Mississippian) in Indiana: Am. Assoc. Petroleum Geologists Bull., v. 52, 1968, p. 1291-1303.

3. Keyes, C. R.: Principal Mississippian section: Geol. Soc. America Bull., v. 3, 1892, p. 283-300.

4. Meents, W. F. and Swann, D. H.: Grand Tower Limestone (Devonian) of southern Illinois: Illinois Geol. Survey Circ. 389, 1965, 34 p.

5. Becker, L. E.: Silurian and Devonian rocks in Indiana southwest of the Cincinnati Arch: Indiana Geol. Survey Bull. 50, 1974, 83 p.

6. Lineback, J. A.: Stratigraphy of the New Albany Shale in Indiana: Indiana Geol. Survey Bull. 44, 1970, 73 p.

Table 1. Composition of the Hannibal and associated samples from the outcrop location, Clark County, Indiana.

	Al_2O_3	FeO	MgO	CaO	Na_2O	K_2O	MnO	TiO_2	P_2O_5	C	H	N (percent)
Rockford	3.22	4.88	.66	37.1	.16	.76	.36	.14	.05			
Jacobs Chapel	11.2	3.88	1.05	18.4	.22	2.66	.12	.54	.07	4.02	.35	.11
Henryville	10.9	4.64	1.00	1.10	.31	3.08	.014	.65	.17	19.5	1.88	.56
Underwood	14.5	4.38	1.16	1.17	.50	3.71	.018	.98	.45	.65	.35	.12
Falling Run	1.28	1.17	.12	47.0	.49	.32	.011	.062	21.3	.86	.12	.09
Clegg Creek (TOP)	13.1	4.14	1.02	.96	.38	3.66	.010	.83	.30	15.2	1.58	.37

	Ag	Cd	Cr	Cu	Mo	Ni	Pb	V	Y	Zn (parts per million)
Rockford	1.6	19	30	22	3	40	17	42	54	2990
Jacobs Chapel	.7	9	102	27	<1	105	66	237	61	788
Henryville	6.6	73	202	246	495	772	316	5240	60	2960
Underwood	1.4	10	128	39	50	53	59	643	109	1140
Falling Run	3.4	13	20	36	23	21	49	128	1290	954
Clegg Creek (TOP)	2.2	41	124	207	92	336	95	1170	110	1550

Table 2. Composition of the Hannibal and associated samples from Survey Drill Hole 290, Clark County, Indiana.

	Al_2O_3	FeO	MgO	CaO	Na_2O	K_2O	MnO	TiO_2	P_2O_5	C	H	N (percent)
Jacobs Chapel	12.4	3.49	2.62	8.05	.59	3.44	.14	.67	.10	3.23	.34	.10
Henryville	11.1	4.00	1.14	.37	.54	3.34	.014	.65	.13	20.2	2.18	.62
Falling Run	3.86	2.71	.44	29.3	.52	1.22	.042	.22	11.6	9.18	.95	.28
Clegg Creek (TOP)	11.4	4.15	1.01	.64	.54	3.28	.012	.66	.27	16.1	1.85	.37

	Ag	Cd	Cr	Cu	Mo	Ni	Pb	V	Y	Zn (parts per million)
Jacobs Chapel	4.4	2	103	59	<1	81	68	1080	40	48
Henryville	10.1	79	156	224	635	831	269	4470	37	4690
Falling Run	8.7	125	70	126	378	334	141	1750	537	17300
Clegg Creek (TOP)	4.5	18	124	163	217	307	114	1260	74	1730

Table 3. Composition of the Hannibal and associated samples from Survey Drill Hole 241, Brown County, Indiana.

	Al_2O_3	FeO	MgO	CaO	Na_2O	K_2O	MnO	TiO_2	P_2O_5	C	H	N (percent)
Jacobs Chapel												
Henryville	10.6	4.40	1.26	.35	.53	3.22	.022	.63	.11	18.5	2.00	.60
Falling Run	.78	12.7	.40	18.4	.29	.20	.064	.038	7.3	1.68	.21	.05
Clegg Creek (TOP)	12.8	4.95	1.23	.70	.63	3.29	.019	.66	.27	11.7	1.39	.37

	Ag	Cd	Cr	Cu	Mo	Ni	Pb	V	Y	Zn (parts per million)
Jacobs Chapel										
Henryville	4.6	103	137	183	667	611	197	2770	38	4780
Falling Run	---	412	23	158	111	301	187	88	920	16700
Clegg Creek (TOP)	---	22	119	136	74	212	48	904	83	680

Table 4. Composition of the Hannibal and associated samples from Survey Drill Hole 273, Marion County, Indiana.

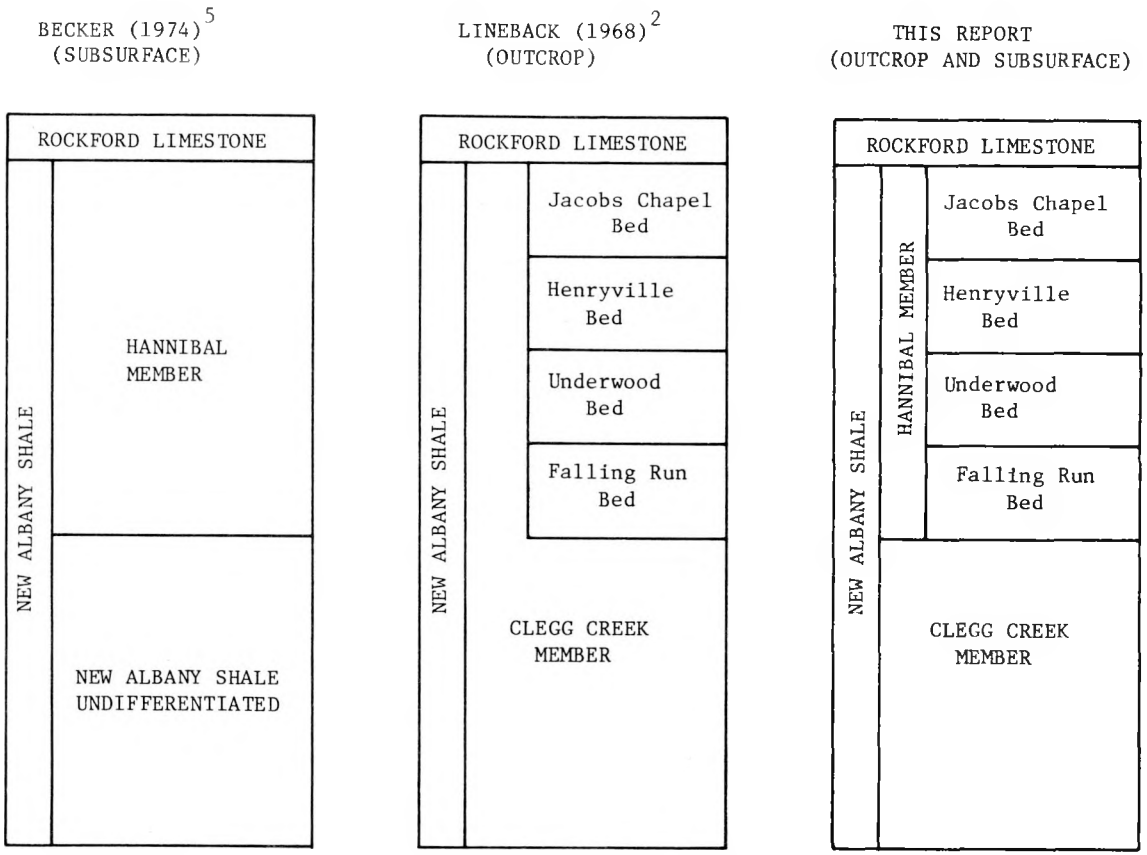
	Al_2O_3	FeO	MgO	CaO	Na_2O	K_2O	MnO	TiO_2	P_2O_5	C	H	N (percent)
Jacobs Chapel	14.0	3.95	2.75	3.94	.74	3.57	.098	.71	.12	1.40	.37	.06
Henryville	10.5	5.00	1.32	.30	.59	2.85	.020	.62	.17	15.5	1.81	.49
Underwood	12.5	4.12	3.52	4.61	.67	3.48	.18	.74	.12	2.52	.39	.17
Falling Run	10.8	3.55	2.63	4.07	.64	3.26	.15	.78	.39	1.44	.30	.14
Clegg Creek (TOP)	13.5	6.95	1.78	.16	.60	2.96	.025	.67	.07	9.57	1.36	.32

	Ag	Cd	Cr	Cu	Mo	Ni	Pb	V	Y	Zn (parts per million)
Jacobs Chapel	14	3	103	32	<1	118	51	403	54	54
Henryville	14	33	126	148	494	327	309	2000	49	2980
Underwood	9	1	82	34	1	39	25	155	46	72
Falling Run	9	2	58	21	<1	29	22	93	123	39
Clegg Creek	9	1	82	70	136	80	25	163	35	63

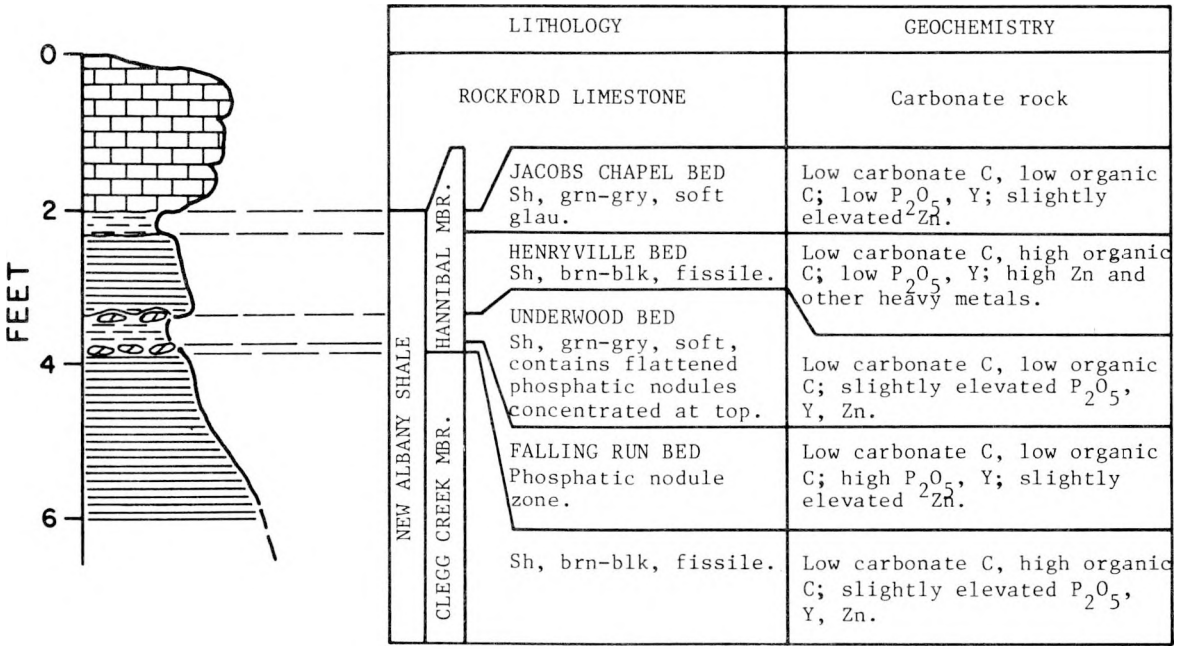
Table 5. Composition of the Phegley Core, Sullivan County, Indiana.

	Al_2O_3	FeO	MgO	CaO	Na_2O	K_2O	MnO	TiO_2	P_2O_5	C	H	N	(percent)
New Providence	18.1	6.13	2.17	.55	.86	5.05	.034	.85	.12	.79	.47	.15	
New Providence (basal)	17.0	5.02	1.69	3.62	.88	4.28	.028	.74	1.71	1.08	.45	.09	
Clegg Creek (TOP)	14.1	3.85	1.56	.49	.55	4.16	.018	.61	.24	12.8	1.59	.38	

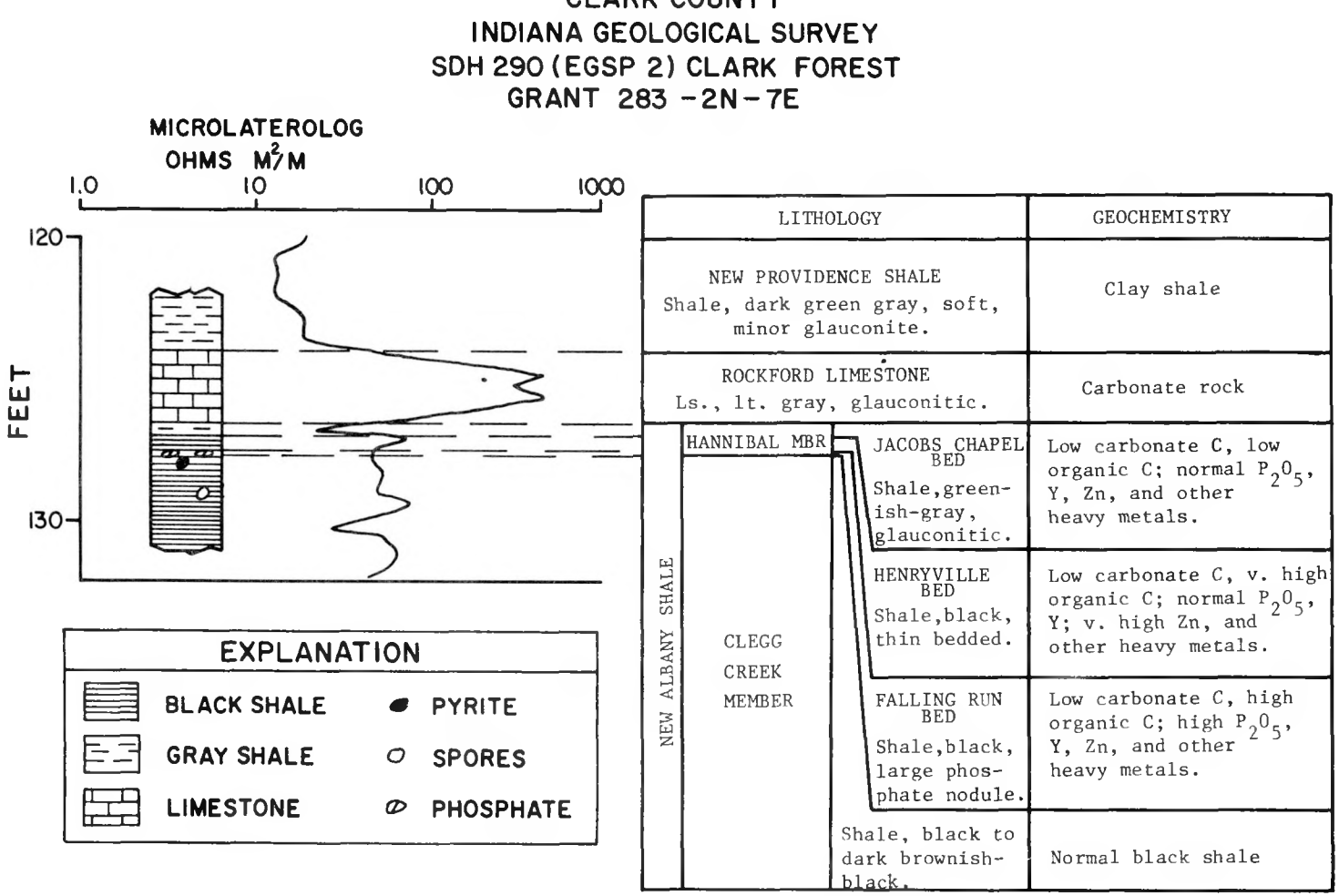
	Ag	Cd	Cr	Cu	Mo	Ni	Pb	V	Y	Zn	(parts per million)
New Providence	8	---	76	31	<1	63	23	166	28	81	
New Providence (basal)	13	---	78	62	<1	319	69	253	107	271	
Clegg Creek (TOP)	11	---	143	130	85	230	58	1250	56	2950	
Clegg Creek	12	---	107	113	46	107	40	919	46	411	



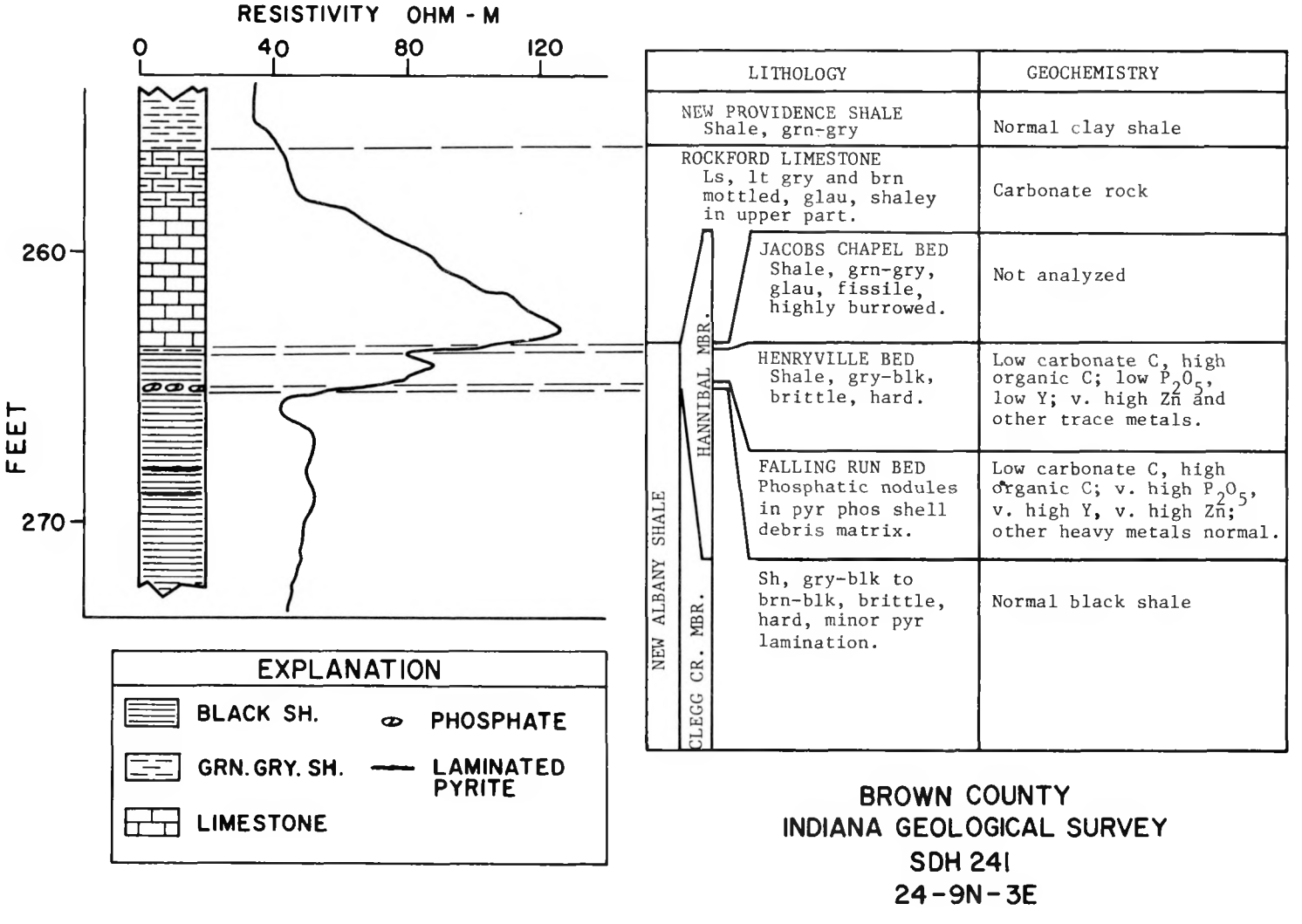
1. **Subdivisions of the New Albany Shale recognized in the subsurface and outcrop area of Indiana.**



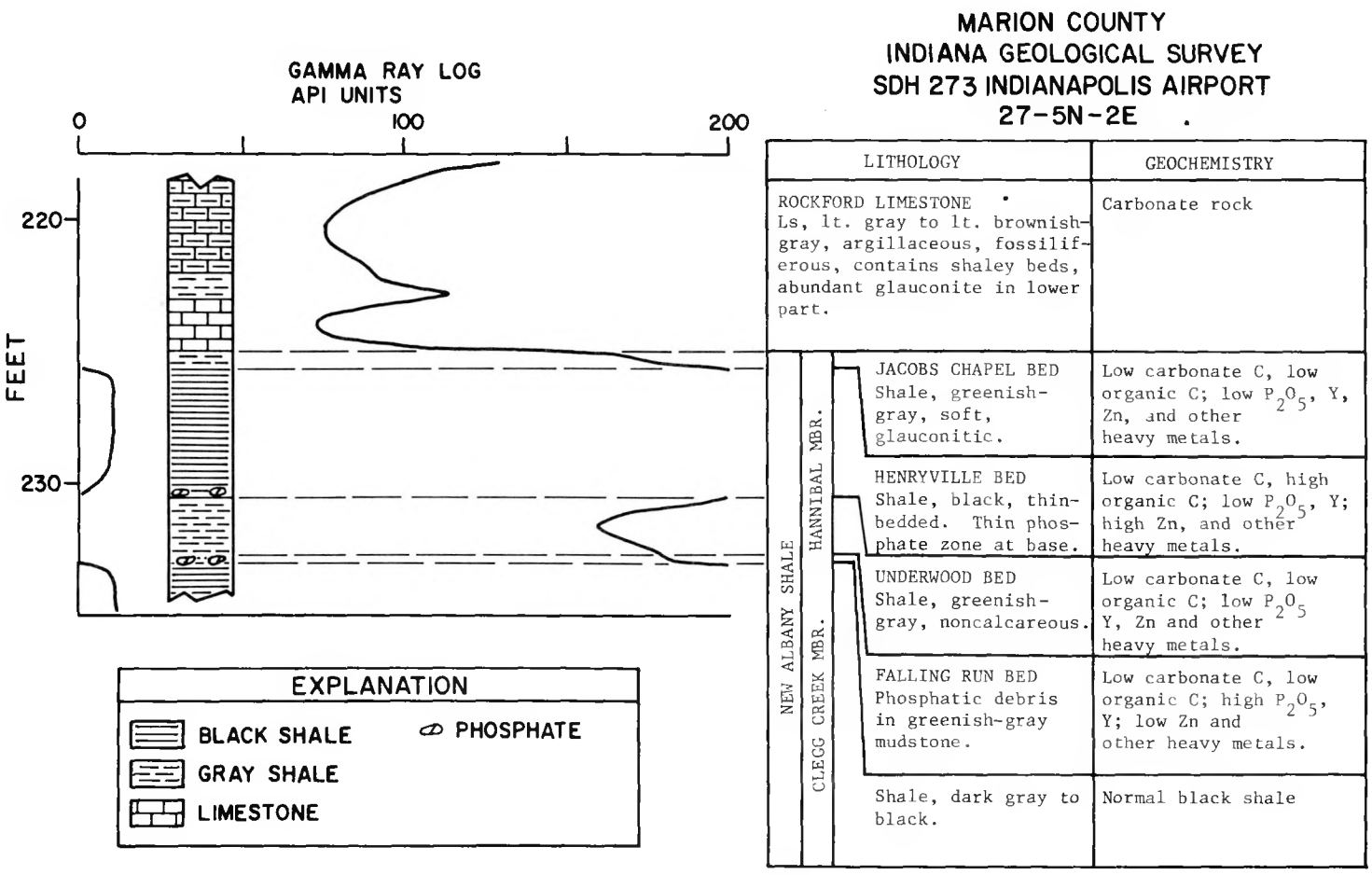
2. Lithology and geochemistry of the Hannibal Member at outcrop in the New Albany type area, Clark County.



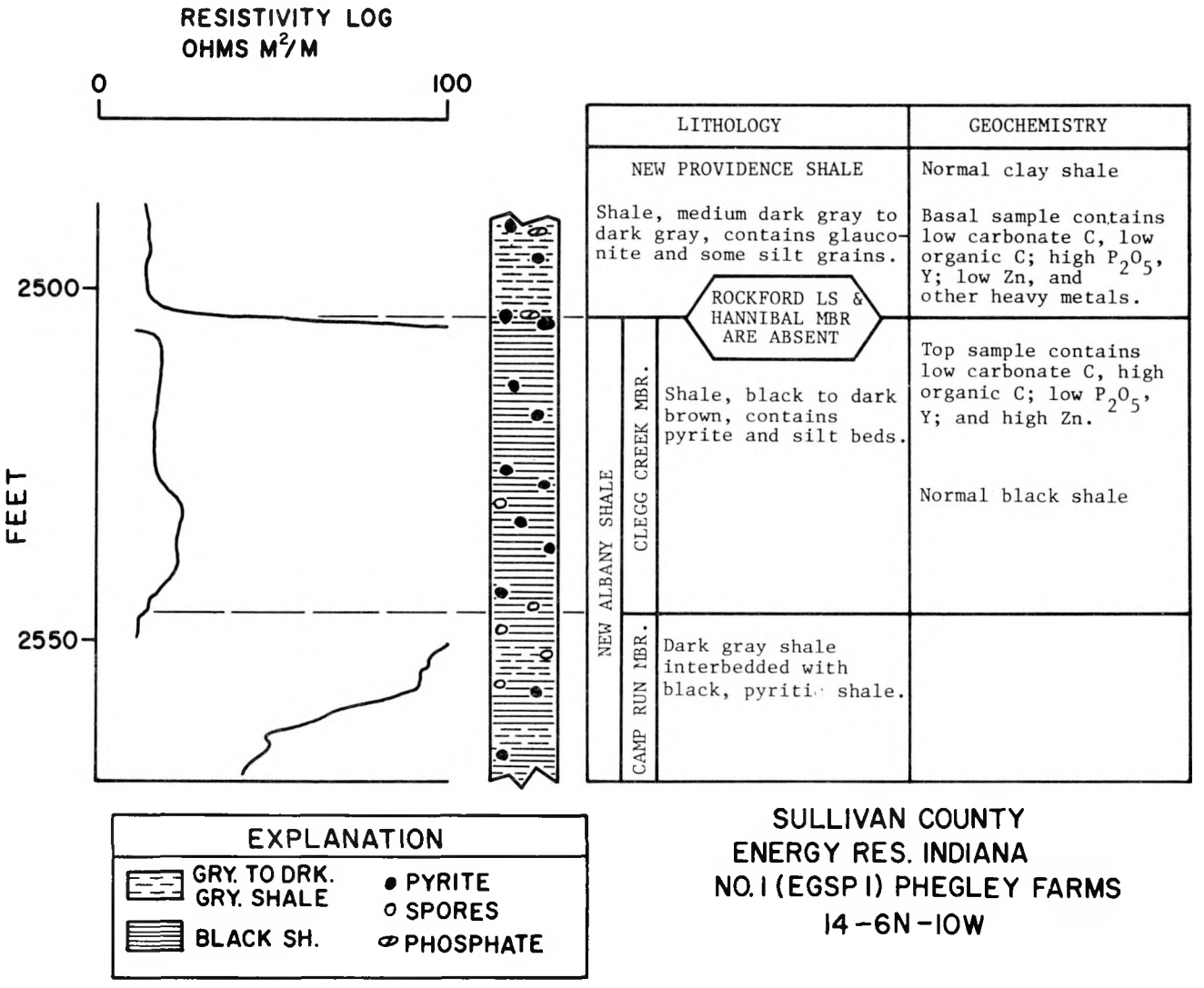
3. Correlation of a geophysical log with the lithology and geochemistry of the Hannibal Member in SDH 290, Clark County.



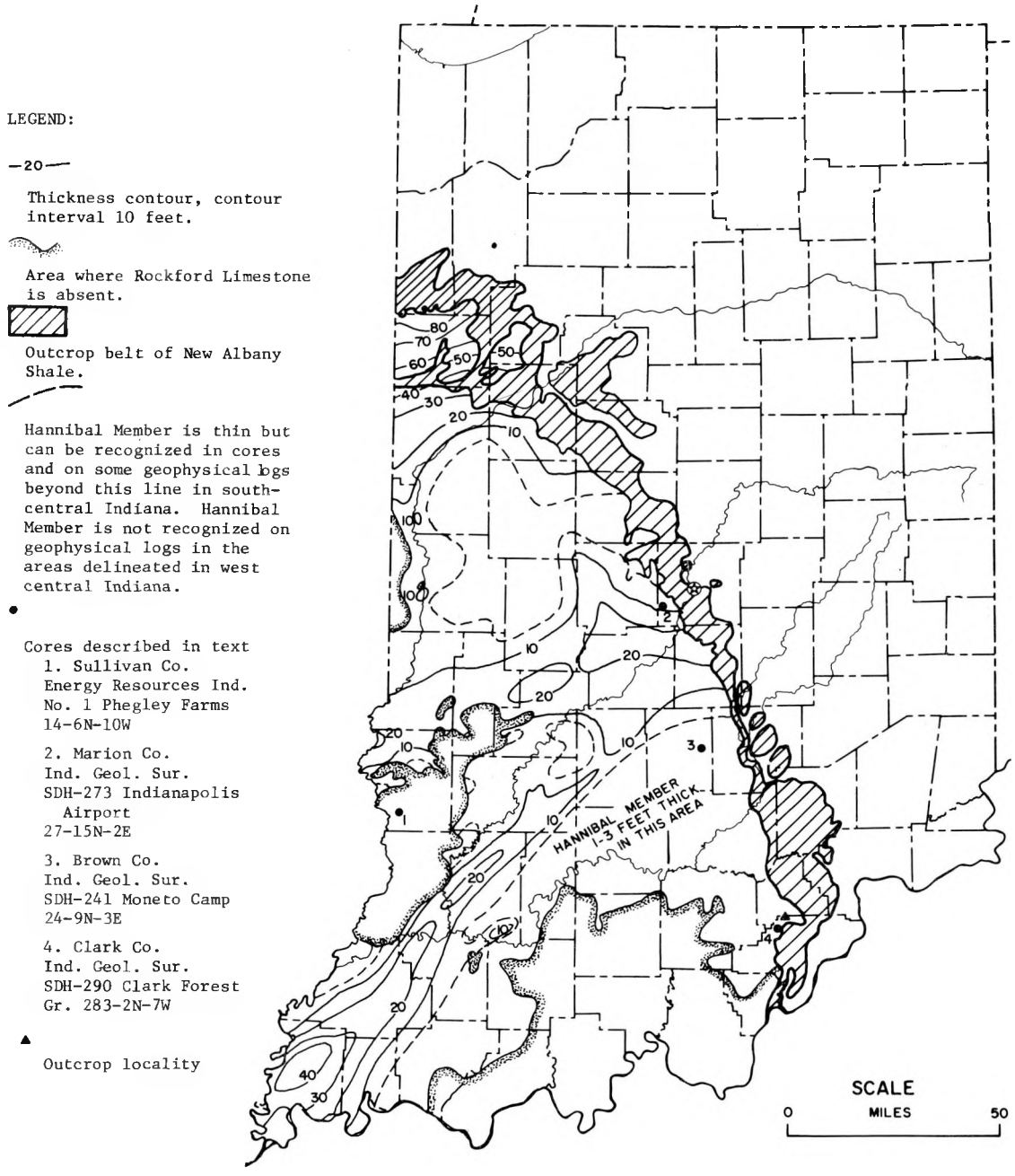
4. Correlation of a geophysical log with the lithology and geochemistry of the Hannibal Member in SDH 241, Brown County.



5. Correlation of a geophysical log with the lithology and geochemistry of the Hannibal Member in SDH 273, Marion County.



6. Correlation of a geophysical log with the lithology and geochemistry of the upper New Albany in Energy Resources of Indiana No. 1 Phegley Farms (EGSP IN 1), Sullivan County.



7. Map of Indiana showing distribution and thickness of the Hannibal Member and the location of cores and outcrop sections described in the text.

ACOUSTIC AND MECHANIC ANALYSIS OF A TRANSVERSE ANISOTROPY IN SHALE

Donald D. Miller and Rex J.E. Johnson

Illinois State Geological Survey, Urbana, IL 61801

ABOUT THE AUTHORS

Donald D. Miller received his B.A. from the Colorado College in 1976 and his M.S. from the University of Illinois at Urbana in 1979. During the past two years he has served on the staff at the Illinois State Geological Survey at Urbana, as a Graduate Research Assistant. Involvement with several mineral exploration projects, including uranium and coal exploration, initiated his interest in geophysical determinations of geological structures. Mr. Miller is now with Mobile Oil Company, Denver, Colorado.

Rex J.E. Johnson received his B.S. in Geology from the University of Illinois at Urbana in 1978. During 1979 he has served on the staff at the Illinois State Geological Survey at Urbana as a Technical Assistant working on the mechanical testing of the New Albany Shale Project. Mr. Johnson is now studying at the Department of Geophysics, University of Michigan, Ann Arbor, Michigan.

ABSTRACT

A transverse anisotropy perpendicular to the bedding planar anisotropy characterizes the mechanical behavior of the New Albany Shale (Devonian-Mississippian) in the structurally faulted area of Christian County, Kentucky. A set of vertical fractures and microfractures in the rock apparently controls the directional behavior of the rock during destructive laboratory tests. A series of tests showed that nondestructive acoustic velocity determinations are unable to consistently detect the anisotropy identified by destructive testing and visual and microscopic examination of the shale. The inability of acoustic velocity testing to detect the known fracture trend and orientation of transverse weakness is thought to be due to the tight, discontinuous nature of microfractures, and mineralization present in some microfractures. These findings do not support the use of acoustic testing as an exploration tool for determining in situ fracture characteristics of shale, such as those tested in this study.

INTRODUCTION

The New Albany Shale (Devonian-Mississippian) is being investigated as a potential hydrocarbon resource in the Illinois Basin. Directional physical properties of the shale were studied to provide information for a geological evaluation of the feasibility of using induced hydrofracture as an economically and environmentally acceptable means of in situ gas recovery from the shale. Directional physical properties of the shale have been investigated through laboratory testing of samples recovered from a number of bore holes located in the basin. Analysis of results obtained from different tests performed on one of the cores has suggested that the ability of some of the laboratory techniques to provide accurate and useful information about directional properties of rock is limited.

A prior knowledge of the expected orientation of hydraulically induced fractures in a reservoir rock is extremely valuable for effective use of the "hydrofrac" process (Komar, 1968; Crawford and Collins, 1964). Anisotropic rock fabric, in the absence of significant differences between principal stresses acting on a rock, will be the prime control on induced fracture orientation (Komar, 1973). For the rocks studied in the Illinois Basin, it is assumed that approximately equal principal stresses are directed horizontally on the rocks in place, and these are much less than the greatest principal stress oriented vertically. Hence, rock fabric that is perpendicular to bedding in the New Albany Shale merits examination. An anisotropy perpendicular to that of the bedding plane is termed transverse anisotropy. The existence of nonuniform directional mechanical properties perpendicular to the bedding planar anisotropy defines a transverse anisotropy.

Laboratory determination of transverse anisotropy has typically relied on measurement of acoustic wave velocities and/or destructive mechanical testing of rock. Directional variation of acoustic geophysical properties of rocks have been previously shown by others to corroborate a mechanical transverse anisotropy detected by destructive testing methods (McWilliams, 1966; Thill, Willard, and Bur, 1969); however, in this study it is shown that acoustic velocity determinations are unable to systematically detect a fracture set and corresponding mechanical strength anisotropy.

Velocities of acoustic waves in rock are in general a function of mineral composition, the distribution of different minerals within a rock, and the crystallographic orientation of anisotropy minerals in a rock. Acoustic velocity in a fractured rock is not only a function of fracture orientation in the rock but also of the fracture filling often associated with fractures. Voids created by fractures can remain open, often becoming saturated by ground water, or they can become filled with sediment or crystalline mineralization such as calcite or quartz. The compressional wave velocities of air, 0.3 km/sec, and water, 1.5 km/sec, are significantly slower than corresponding velocities measured for most rocks (Leet and Birch, 1942); however the anisotropic compression wave velocity for calcite is between 5.6 km/sec and 7.7 km/sec (Foster and Bur, unpublished) and for quartz, between 5.4 km/sec and 7.0 km/sec (McSkimin, 1962). Consequently, acoustic velocities of fractured rock measured across a fracture set that is largely healed by mineralization can equal, if not exceed, acoustic velocities measured in other directions in the rock.

A fracture is defined as a physical discontinuity across which a tensile stress cannot be sustained. A fracture set consists of multiple fractures parallel to one another. In a uniform stress field, small discontinuous fractures can serve as stress risers to decrease the ultimate strength of a material and, perhaps, to act as surfaces of weakness to dictate the direction of failure.

METHODS OF INVESTIGATION

Data presented in this study were compiled from laboratory investigation and testing of approximately 200 feet (60 m) of oriented core of New Albany Shale recovered from a bore hole in Christian County, Kentucky (fig. 1). The oriented core was first examined and special attention was given to natural fractures. Subsequent mechanical testing performed on intact samples of the 10 cm diameter core characterized the shale with respect to the following: (1) orientation of point-load induced fractures perpendicular to bedding, (2) azimuth tensile strength variation in the plane of bedding, and (3) acoustic wave velocity variation in the plane of bedding. Additional methods to examine microscopic thin sections of the shale and x-ray radiographs of core slabs were employed to characterize observable fabric in the shale.

Specimens for mechanical tests, microscopic examination, and radiography were selected from each 10-foot interval of core. This was done to obtain a uniform distribution of samples from the core to determine representative directional characteristics for the whole rock unit. Individual specimens were prepared from the core in accordance with the requirements of the laboratory tests or the method of examination.

The location of this test core in Christian County, Kentucky, was selected to provide information for interpretation of the petrology of the New Albany Shale in the Illinois Basin, for stratigraphic correlation and subsurface stratigraphic mapping of this unit of rock, and for geochemical studies of the shale, as well as to provide materials to test its directional physical properties. As a consequence a great deal of work has been done with descriptive lithologic characteristics of this core. Although the present study is concerned specifically with structure that is normal to bedding in the shale, petrographic data and interpretation are extremely useful in comparing mechanical behavior observed for these rocks with mechanical data for other rock materials. Description of the core is discussed elsewhere, however, and it is not necessary to duplicate that information here (Bergstrom and Shimp, 1977; Harvey et al., 1978).

Natural fractures in the core were studied so that the stress and fracture history of the rock and the effect these have on the fabric of the rock might be interpreted. Systematic examination of fracture trace patterns and markings on the fracture surfaces, both macroscopic and microscopic, attempted to determine the genesis of the observed features (Kulander, Dean, and Barton, 1977). Fractures were classified as either natural fractures or fractures induced by coring or handling operations. Factors suggesting natural fractures include: (1) high angle, (2) smooth surface and continuity, (3) mineralization, and (4) slickensides. Coring induced fractures, handling fractures, and separation parallel to bedding were identified by typical features that include: (1) rough surface, (2) curve to a free face (hook or petal), (3) characteristic propagation flow features, and (4) fresh surface. The position and orientation of all natural fractures were logged.

The *point-load test* was used to determine whether a preferred orientation of fracture weakness exists normal to bedding in the shale. In this test, the load is applied normal to bedding through the central axis of an unconfined disk-shaped segment of the core by means of opposing, coaxial steel points (fig. 2). Although an exact solution of the imposed elastic stress has not been derived, the field is axially symmetric about the point load up to the onset of fractures parallel to the loaded axis of the specimen (Hobbs, 1964). The orientation of the fracture, thus indirectly induced by tensile stresses, represents an orientation of weakness perpendicular to bedding in the specimen. When numerous specimens from an isotropic rock are loaded to failure in this manner and the orientations of the induced fractures are plotted with respect to a common external coordinate system, the trends (strikes) of the fractures on the plane that are normal to the disk axis (or in the plane of bedding) should be randomly distributed. On the other hand, specimens from a rock with an inherent anisotropy should display a preferred orientation of fractures which is directly related to the rock's fabric or structural history.

Standard procedures for point-load testing were used in accordance with USBM (D'Andrea, Fisher, and Fogelson, 1965) and ISRM (1973) standards. Core specimens having a length/diameter ratio of approximately 1:2 were prepared for testing. The significance of the effect of water content, size, and shape on test results was disregarded in accord with standardized procedures used for all test specimens.

The *"Brazilian" indirect tensile test* was used to measure the relative magnitudes of tensile strength at different azimuth directions parallel to bedding in the shale. In the "Brazilian" test, a compressive load is applied diametrally to opposing edges of disk-shaped specimens of core (fig. 3). The compressive load at the edges of the specimen produces a tensile stress field perpendicular to the loading direction, greatest at the center of the disk. Hence, fracture of a relatively homo-

geneous material typically initiates at the center of the disk during loading before propagating along the diameter through which the load is applied (Colback, 1966). Tensile strength (S_t) is determined from the applied load at failure by the formula

$$S_t = \frac{2P}{\pi DT}$$

where P is the maximum load, D is the diameter of the disk, and T is the thickness of the disk. If the rock material contains a "weakness" or a preferred orientation of failure perpendicular to bedding, this orientation is approximately determined through comparison of tensile strength measured for different azimuth directions in the core.

The tensile strength at different azimuth directions in the shale was measured by conducting tests with several specimens, varying the direction of loading for individual samples with respect to the coordinate system marked on the core. At least one "Brazilian" test at each of six different azimuth directions of 30° increment was performed per 10-foot interval of core. Disk-shaped specimens were cut to the same dimensions as point-load test specimens. Flaws in samples, such as scribe grooves, fossils, and pyrile nodules, were oriented to minimize their effects on the theoretical stress fields imposed during the tests.

Acoustic velocity measurements parallel to bedding in the shale were made to examine the variation in velocity when measured in different directions within the bedding. An acoustic bench with a direct pulse transmission technique designed by the U.S. Bureau of Mines was used (Thill, McWilliams, and Bur, 1968). The acoustic bench system measures the travel time required for a wave disturbance initiated by a transducer on one side of a test specimen to traverse a measured distance through the specimen to a receiving transducer located on the opposite side. The wave velocity (V) is determined by the equation

$$V = st^{-1}$$

where s is the distance between the transducers, and t is the time difference between initiation of the disturbance in the sample and its arrival at the receiving transducer.

The velocity of an acoustic wave pulse is dependent on the materials traversed along its path of travel. In rock, the dimension and distribution of different mineral particles along any path controls the acoustic wave velocity along that path. Voids, filled fractures, or fossil fragments affect the velocity in the same manner as other materials encountered in a wave path. Crystallographic orientation of some minerals may also be important where properties vary greatly with direction within a mineral. These rock qualities which affect acoustic velocity, in general, vary with direction in a rock. This variation also defines the fabric of a rock and has been shown to control directional mechanical strength behavior in rock. Hence, methods to compare the velocity of acoustic waves measured in different directions in a rock are used to reflect fabric of a rock and to predict its mechanical failure behavior.

Both compressional wave velocities and shear wave velocities can provide valuable information about the directional properties of a rock. Compressional wave velocities in conjunction with density and shear wave velocity can be used to calculate dynamic elastic constants, and the variation of these velocities with direction in the rock may also be determined. In this study of the New Albany Shale, however, only compressional wave velocities were measured. Highly attenuating characteristics of the shale prevented transmission of shear waves with available equipment.

Velocities were determined for compressional waves transmitted in each of six different directions parallel to bedding in cylindrical core specimens. Longer segments of the core than were used for destructive testing were selected so that signals reflected off of free end surfaces of specimens would not interfere or mask the arrival of a signal traveling directly through the specimen (Thill, McWilliams, and Bur, 1968). A pulsed input generating a wave signal at ~750 khz was used in testing the shale to achieve consistently measurable received signals.

Oriented thin sections and *x-ray radiographs* made from slabs cut from the core were made in three mutually perpendicular orientations. Vertical thin sections and slabs were cut in north-south and east-west orientations. The distribution of distinct features of the shale was observed primarily in horizontal sections and slabs, and the orientation of elongate rock components within the bedding was measured.

The existence of transverse anisotropy and rock fabric perpendicular to bedding in the New Albany Shale was explored using many types of data. Existing megascopic structures in the core were compared with structures observed in thin section and x-ray radiographs. Destructive mechanical tests, the point-load test, and the "Brazilian" indirect tensile test investigated the response of the shale to a large mechanical disturbance that was much greater in magnitude than the disturbance created by transmitted acoustic signals. Comparison of nondestructive acoustic results, destructive test results, and those observed structures perpendicular to bedding provide the analysis of transverse anisotropy.

DATA

Numerous natural fractures were observed in samples of the core from Christian County, Kentucky. Many fractures filled with light-colored calcite mineralization were easily visible in the core (fig. 4). Calcite-filled fractures occur in a broad range of sizes. In addition, several fractures were noted only when the rock was wetted and partially dried. The latter type are generally irregular and discontinuous.

The orientation of larger calcite-filled fractures with separations of 0.5 to 3.0 mm was measured. Most were found to strike in similar orientation, northwest-southeast, and to dip vertically (fig. 5). Most of these fractures are relatively regular planar features; however, individual fractures are not commonly continuous for more than 1 or 2 feet (30 to 60 cm) along the core. More common are subparallel fractures offset from one another where they terminate (fig. 4). Multiple fractures in this type of pattern may occur over a considerable length of core. The trend of natural fractures measured in the core corresponds to the orientation of transverse anisotropy determined through mechanical testing of shale samples from the core. This relationship is discussed in detail later in the report.

Point-load test results from the Kentucky core exhibit a preferred orientation of induced fractures perpendicular to bedding. The predominant number of shale samples tested tended to fail by fracture in a northwest-southeast orientation (fig. 5). Preferred azimuth orientation of fractures ($\bar{\theta}$) was statistically determined using a resultant vector technique (Curray, 1956). This method measures a central tendency or preferred orientation that is independent of origin for a group of fracture data. The scatter in the distribution of fracture orientations is indicated by a "true" standard deviation (σ) calculated for a circular distribution. Central tendency of fracture orientation and standard deviation determined for this sample distribution are:

$$\underset{134^{\circ}}{\bar{\theta}} \qquad \underset{44^{\circ}}{\sigma} \quad \text{(102 samples tested).}$$

The orientation of point-load fractures for this core also generate a second frequency distribution. A "reliability factor" assigned to each point-load test performed is incorporated into fracture orientation data to generate a modified frequency rosette (fig. 5). The "reliability factor" imparts a weighted bias to test results in a systematic manner. In testing a natural material such as shale, flaws inherent in a sample may influence its mechanical test behavior such that it is not representative of the in situ rock unit. Flaws include pyrite nodules, fossils, slaking, slickensiding, jointing, and orientation scribe grooves. Such features can cause irregularities in the surface of vertical induced fractures, irregular orientation of induced fractures, multiple fractures in a sample, or nonvertical fracturing. The influence of flaws in a sample is recorded at the time of each test. Each test is assigned a value between 0.0 and 1.0. If a test is ideally performed and the rock fractures in an ideal manner, a value of 1.0 is assigned. If the mode of failure in a test is extremely irregular and cannot be measured, a 0.0 value is assigned. Intermediate values are assigned to tests where flaws appear to exert only a partial control on fracturing in a sample.

The modified fracture frequency distribution is a summation of "reliability factor" values for each point-load fracture test at the orientation of the test-induced fracture. This frequency distribution shows fracture trends similar to the distribution without "reliability factor" data. Although the number of fractures in the preferred orientation of fracture is slightly diminished by incorporating "reliability" data, the standard deviation of the modified distribution about its central tendency, which is very close to that of raw point-load data, is diminished also (fig. 5). The effect of flaws in test samples is apparently random.

"Brazilian" indirect tensile tests corroborate the orientation of bedding-normal weakness suggested by point-load tests. Lowest tensile strength values were measured for samples tested in the orientation closest to the preferred orientation of point-load induced fractures (fig. 5). This tensile strength refers to the direction perpendicular to the plane of "Brazilian" test fracture. Hence, the least tensile strength of the rock parallel to the bedding is approximately normal to the plane of weakness identified by point-load testing of samples of rock. The greatest tensile strength parallel to bedding in the shale is 16 percent greater than the least tensile strength parallel to bedding. In general, the direction of greatest tensile strength parallel to bedding is orthogonal to the direction of least tensile strength parallel to bedding in samples tested.

Acoustic testing of the shale shows that the velocity of acoustic waves varies in different directions parallel to bedding in the shale. All samples show variation, although actual variation in a sample is between 0.5 percent and 4.0 percent of the average acoustic velocity for that sample. In contrast to destructive test results for the shale, however, acoustic velocities measured parallel to bedding in the shale do not show a systematic variation with azimuth orientation. Acoustic velocities measured for different samples show many different patterns of velocity variation with direction (fig. 6). Fastest or slowest velocity in a sample can be in any one of the six orientations tested. The only pattern exhibited by these data are relatively fast velocities measured approximately northeast in several samples. This pattern is not observed for all samples, and it may or may not be significant. Average velocities at test orientations compiled for all samples is indefinitive:

0°	30°	60°	90°	120°	150°
4.69	4.72	4.74	4.72	4.72	4.72

These values indicate a random variation in acoustic wave velocity with direction in the shale.

Several components of the shale that are observable in thin sections and x-ray radiographs contribute to a random fabric perpendicular to bedding in this core. Primary components of the shale observed in horizontal thin sections, such as approximately equidimensional silt-size mineral grains, preserved spores, and a variety of plant remains other than spores, vary in abundance throughout the core, but are randomly distributed in the plane of bedding. Elongate plant remains were randomly oriented within the bedding planes. Secondary pyrite mineralization observed in a variety of forms in the shale, mostly in x-ray radiographs, also is randomly distributed in the plane of bedding (fig. 7).

In addition to these random fabric elements, several microscopic linear structures observed in horizontal sections of the shale were measured subparallel to one another (fig. 8). Most of these features are very small, 0.1 to 1.0 mm in length. The features vary in appearance and because of their small scale, many have not received positive identification. A number of the features appear as elongate occurrences of carbonate mineralization associated with linear discontinuities in the section. Many appear as linear patterns or linear clusters of carbonate (dolomite) grains associated with discontinuities in the section. There are also many suspect linear patterns of carbonate grains for which discontinuities cannot be identified. The orientation for all these features observed is approximately northwest-southeast.

Also present in a few sections are small-scale linear features (1.0 to 3.0 mm in length), which are filled with massive pyrite mineralization and are oriented northwest-southeast (fig. 8). Some of this mineralization may be siderite. In the examples studied, mineralization tended to obscure detail in the area surrounding the linear feature. The relationship between these and linear features with carbonate mineral associations has not been determined. All examples appear to represent mineralized or partially mineralized fractures in the rock.

All of the oriented linear features were observed in thin sections cut horizontally from the core. None were detected in vertical thin sections. Linear features shown to be mineralized fractures were observed on several horizontal x-ray radiographs. Radiographs provide improved resolution of detail of features only faintly visible in the core; however, features less than 5.0 mm long cannot be identified with certainty in the radiographs.

CONCLUSIONS

The data indicate the existence of a significant anisotropy perpendicular to the bedding in the shale samples tested. Both "Brazilian" tensile tests and point-load tests demonstrate a preferred orientation of weakness and induced fracture, normal to bedding, that strikes northwest-southeast. The results from these destructive tests corroborate a transverse fabric orientation observed in the shale core (fig. 4), thin section, and x-ray radiographs prepared from the core (figs. 7 and 8). This observed fabric consists of a set of vertical, subparallel fractures and microfractures. Although the influence of the fracture-microfracture fabric apparently controls the orientation of destructive test results, it does not produce a distinct correlative variation in acoustic velocities measured in the shale.

The acoustic velocity tests performed are in general unable to detect the transverse anisotropy in the shale that is detected by destructive testing and visual and microscopic observation. The most notable aspect of the variation of acoustic velocity with different test orientations measured in the shale is the nonsystematic patterns of velocity variation measured for different samples. Nevertheless, acoustic signals transmitted parallel to bedding in the shale are expected to experience some influence that is due to the fractures normal to bedding observed in the rock. High relative velocities measured in a direction normal to demonstrated preferred fracture anisotropy in several samples tested suggest that the (carbonate) mineralization that fills microfractures in the northwest-southeast orientation increases the velocity of acoustic signals transmitted across them. Whereas an acoustic signal is more greatly affected by transmission in this orientation through fracture fill material, reflection of wave energy at material boundaries complicates transmission of acoustic signals at low angles to fractures in the rock. However, not all fractures and microfractures, which determine a preferred orientation of mechanical weakness in the shale core, uniformly influence transmitted acoustic signals. Many different types of linear fractures and associated features were observed in the shale. Mineralization present in at least some of the fractures in the rock may increase the velocity of acoustic signals transmitted across them. Yet not all fractures in the shale are mineralized to the same extent, nor are all fractures present in the rock necessarily mineralized. Different fractures traversed by acoustic signals along different paths in the rock determine the nonsystematic velocities measured.

This concept of varying velocities as a function of fracture filling material explains why acoustic geophysical methods of exploration are limited in their application to predict directional mechanical properties of rock. Whereas the mechanical strength across a fracture or set of fractures is lower than that of intact rock, the velocity of an acoustic signal is dependent on whether or not fractures have created voids in the rock and the material that fills them. This study shows that the currently accepted, empirically demonstrated relationship between acoustic velocities and preferred fracture anisotropy in rock is not always true. The significance of acoustic velocity variation in a rock depends on an understanding of components of the rock that combine to influence the variation. Fabric present in some rocks may exhibit characteristics that prevent its detection by acoustic geophysical methods. The need for several methods of investigating rock properties for prediction of in situ rock behavior is therefore demonstrated.

ACKNOWLEDGMENTS

The work reported here was done pursuant to contract number DE-AC21-76-MC05203 with the U.S. Department of Energy.

REFERENCES

Basset, J. L., and N. R. Hasenmueller, 1978, The New Albany Shale and correlative strata in Indiana: Proceedings 1st Eastern Gas Shales Symposium, Oct. 17-19, 1977. Morgantown, West Virginia, U.S. Department of Energy, MERC/SP-77/5, p. 183-194.

Bergstrom, R. E., and N. F. Shimp, 1977, Geologic and geochemical studies of the New Albany Group in Illinois (Devonian black shale) to evaluate its character as a source of hydrocarbons: Illinois State Geological Survey Annual Report, ORO-E-(40-1) 5203-12, Submitted to U.S. Energy Research and Development Administration.

Colback, P. S. B., 1966, An analysis of brittle fracture initiation and propagation in the Brazilian test: Proceedings 1st Congress of International Society for Rock Mechanics, Lisbon, v. 1.

Crawford, P. B., and R. E. Collins, 1964, Estimated effects of vertical fractures on secondary recovery: Transactions American Institute of Mining, Metllurgical, and Petroleum Engineers, v. 201. p. 192-198.

Curray, J. R., 1956, The analysis of two-dimensional orientation data: Journal of Geology, v. 64, p. 117.

D'Andrea, D. V., R. L. Fisher, and D. E. Fogelson, 1965, Production of compressive strength of rock from other rock properties: U.S. Bureau of Mines Report of Investigations 6702.

Foster, E. F., and T. R. Bur, Spatial graphs of longitudinal phase and group velocities for common rock forming minerals: U.S. Bureau of Mines (unpublished open file report).

Harvey, R. D., W. A. White, R. M. Cluff, J. K. Frost, and P. B. DuMontelle, 1978, Petrology of the New Albany Shale Group (Upper Devonian and Kinderhookian) in the Illinois Basin: A preliminary report: First Eastern Gas Shales Symposium, Morgantown Energy Research Center, MERC/SP-77/5, p. 329.

Hobbs, D. W., 1964, The tensile strength of rocks: International Journal of Rock Mechanics and Mining Science, v. 1, p. 385.

ISRM, 1973, Suggested method for determining the point-load strength index: ISRM Committee on Laboratory Tests, Document, v. 1, p. 8-12.

Komar, C. A., 1968, Rock mechanics—Its role in oil recovery: Producers Monthly, v. 32, no. 11, p. 2-7.

Komar, C. A., and K. H. Frohne, 1973, Analysis of factors influencing fracture initiation and orientation in all reservoir sandstone: U.S. Bureau of Mines Report of Investigations 7813.

Kulander, B. R., S. L. Dean, and C. C. Barton, 1977, Fractographic logging for determination of pre-core and core induced fractures: Morgantown Energy Research Center, Contract ME6-P-2820, MERC/CR-77/3.

Leet, L. D., and F. Birch, 1942, Seismic velocities, *in* Birch [ed.], Handbook of physical constants: Geological Society of America Special Paper, no. 36, p. 96.

McSkimin, H. J., 1962, Measurement of the 25°C zero field elastic moduli of quartz by high frequency plane-wave propagation: Journal of Acoustics Society of America, v. 34, p. 1271-1274.

McWilliams, J. R., 1966, Role of microstructure in the physical properties of rock: ASTM STP 402, American Society of Testing and Materials, p. 175.

Schwalb, H. R., and P. E. Potter, 1978, Structure and isopach map of the New Albany-Chattanooga-Ohio Shale (Devonian and Mississippian) in Kentucky: Western Sheet, Kentucky Geological Survey, Series X.

Stevenson, D. L., and L. L. Whiting, 1967, Geologic structure of the Devonian-Silurian Hunton Limestone Megagroup in Illinois: Illinois State Geological Survey, Illinois Petroleum 87, 5 p.

Thill, R. E., J. R. McWilliams, and T. R. Bur, 1968, An acoustical bench for an ultrasonic pulse system: U.S. Bureau of Mines Report of Investigations 7164.

Thill, R. E., R. J. Willard, and T. R. Bur, 1969, Correlation of longitudinal velocity variation with rock fabric: Journal of Geophysical Research, v. 34, p. 4897-4909.

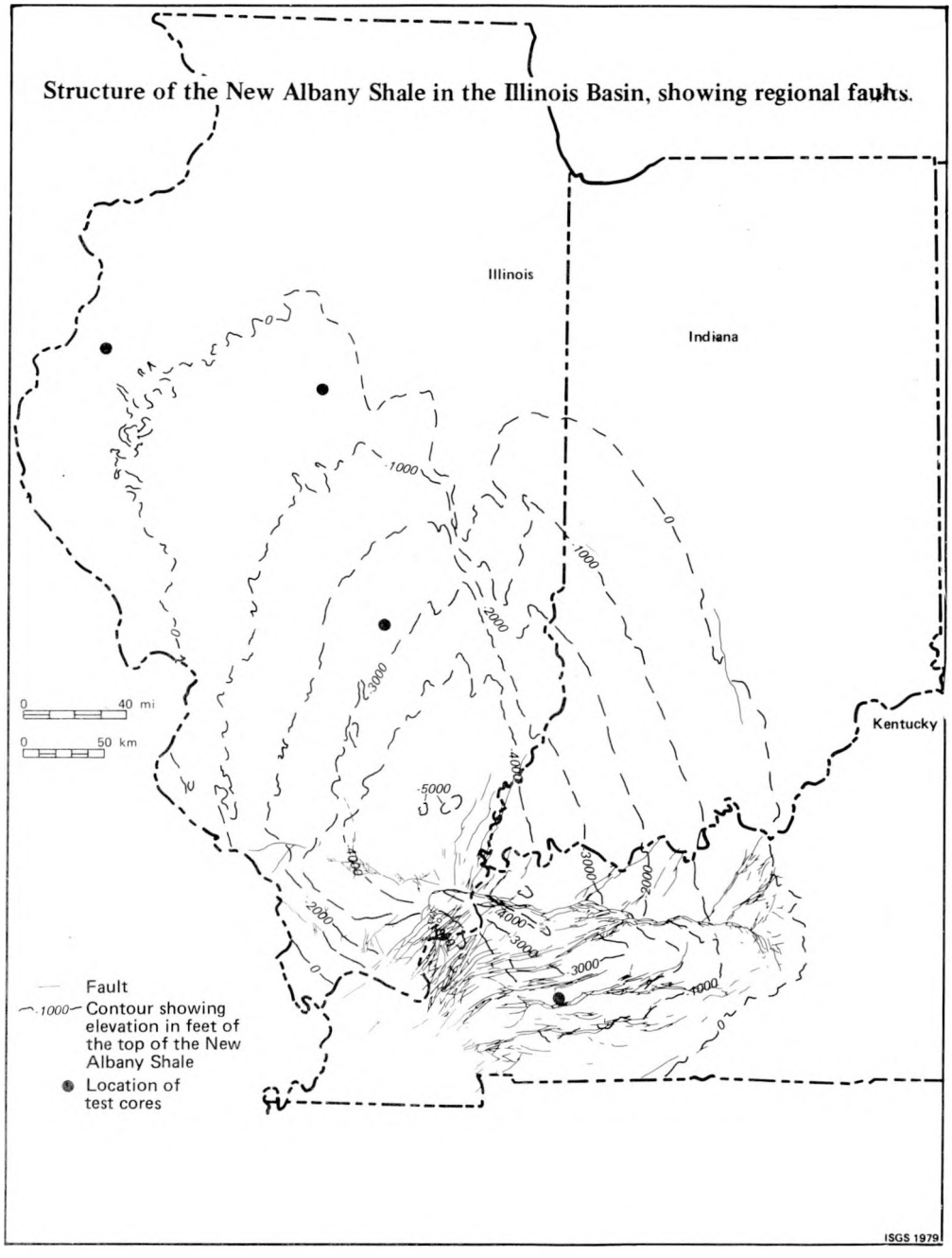


Figure 1. Location of test cores in relation to regional structure of the New Albany Shale (Devonian) in the Illinois Basin (modified from Stevenson and Whiting, 1967; Bassett and Hasenmueller, 1978; and Schwalb and Potter, 1978).

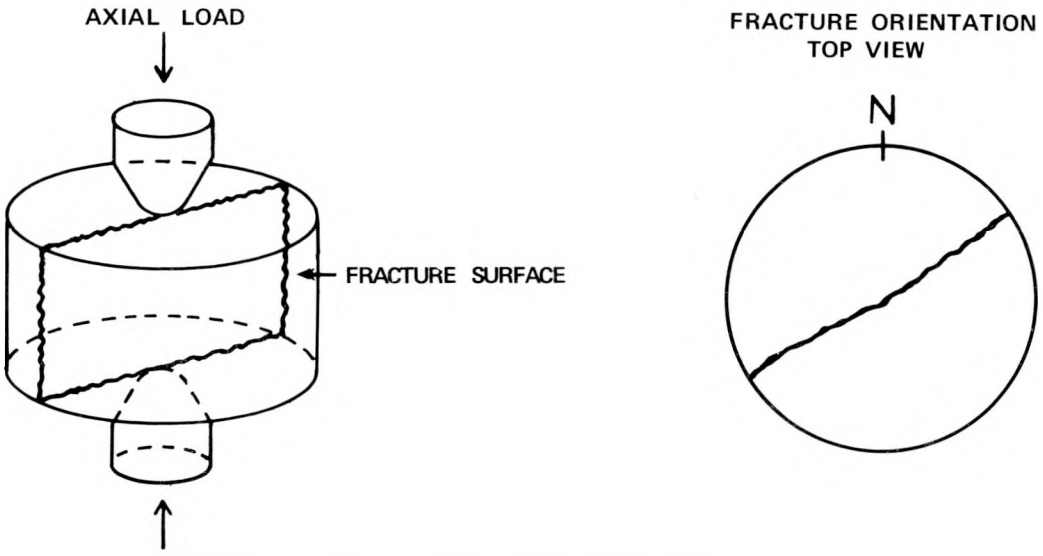


Figure 2. Point load test. Bedding is normal to the applied load direction. Fracture orientation is random unless a "preferred direction" of failure exists in the test specimen.

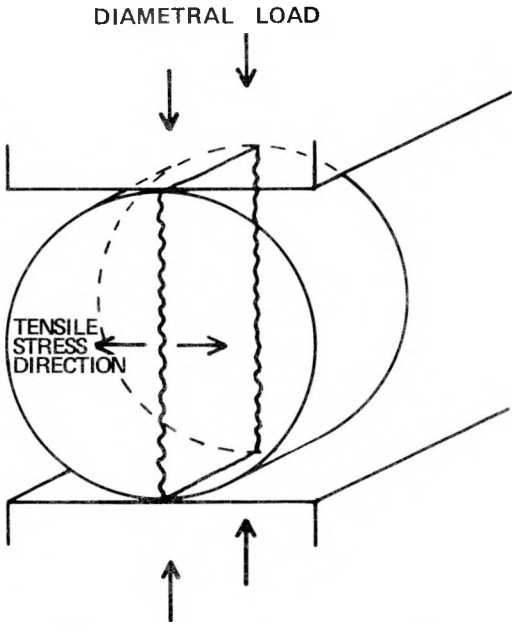
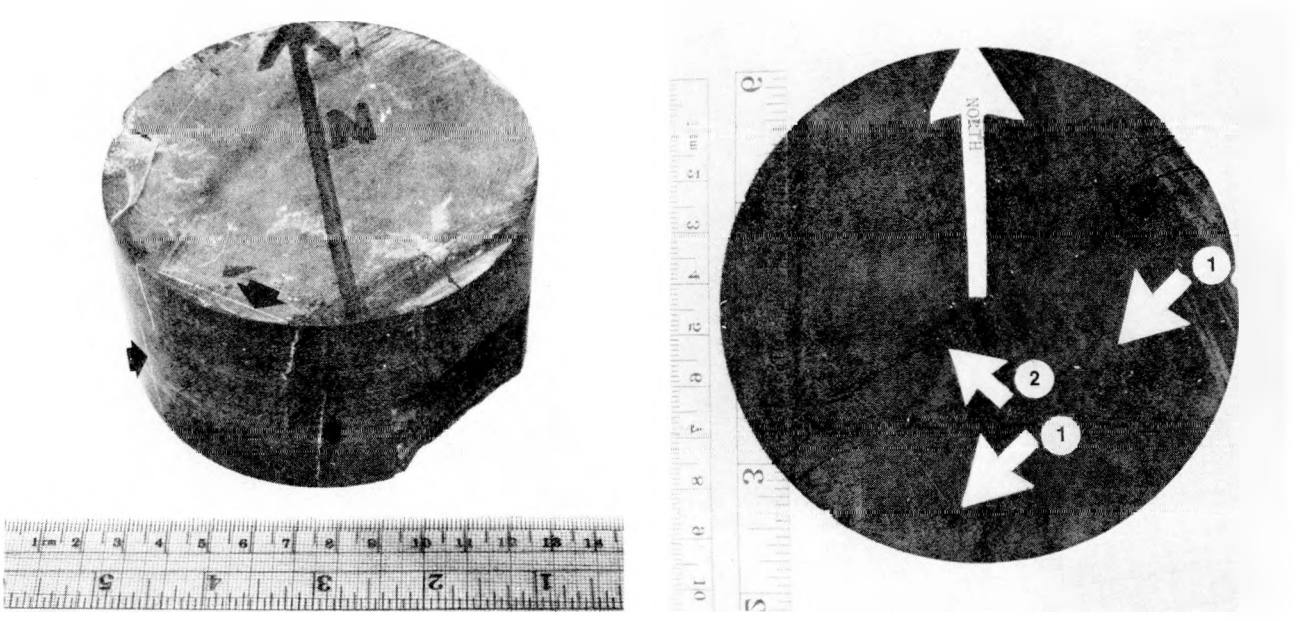


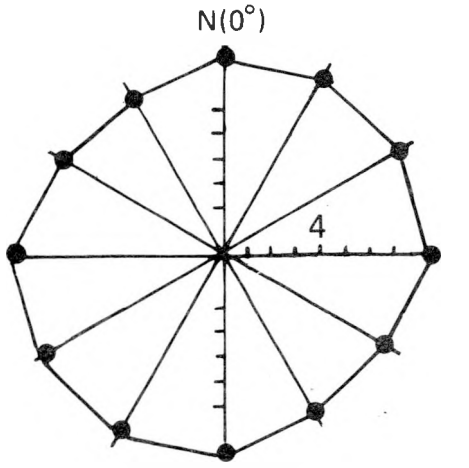
Figure 3. "Brazilian" indirect tensile test. Bedding of the sample is parallel to the plane of the paper.



A. B.

Figure 4. Photographs of calcite-lined natural fractures in core samples of New Albany from Christian County, Kentucky. A) Discontinuous, subvertical natural fractures trending northwest; depth is 2288.0 feet. B) Set of calcite-lined natural fractures trending northwest (1) which cut an earlier northeast trending fracture (2) which is filled by fine grain sediment; northeast trending fracture is enhanced to make it visible in photograph.

TENSILE STRENGTH (MPa) AT TEST ORIENTATION

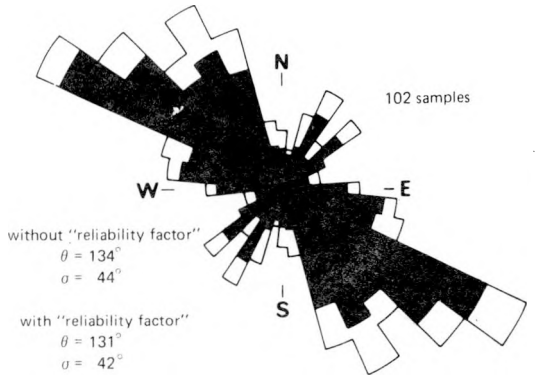


Number of samples/
average tensile strength (MPa)

-60°	-30°	0°	30°	60°	90°
16/7.52	12/7.28	14/8.04	9/8.19	14/8.34	11/8.43

POINT LOAD FRACTURE FREQUENCY PLOT

"reliability factor" superimposed



without "reliability factor"
θ = 134°
σ = 44°

with "reliability factor"
θ = 131°
σ = 42°

Unshaded rosette represents fracture without "reliability factor"; shaded rosette represents fracture data with "reliability factor" incorporated.

NATURAL FRACTURE FREQUENCY PLOT

azimuth orientation of vertical fractures

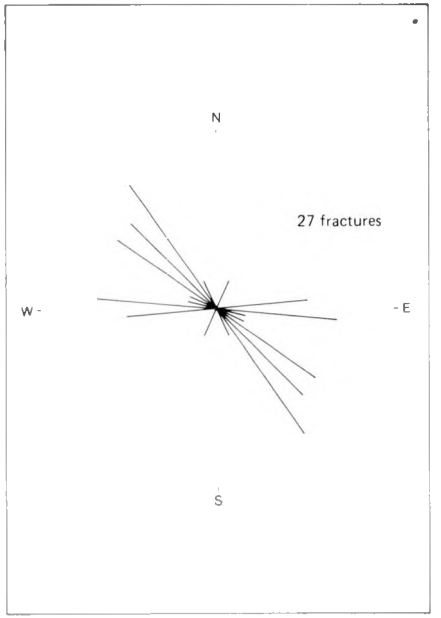


Figure 5. Summary of "Brazilian" tests, point load tests, and natural fractures for New Albany Shale test core, Christian County, Kentucky.

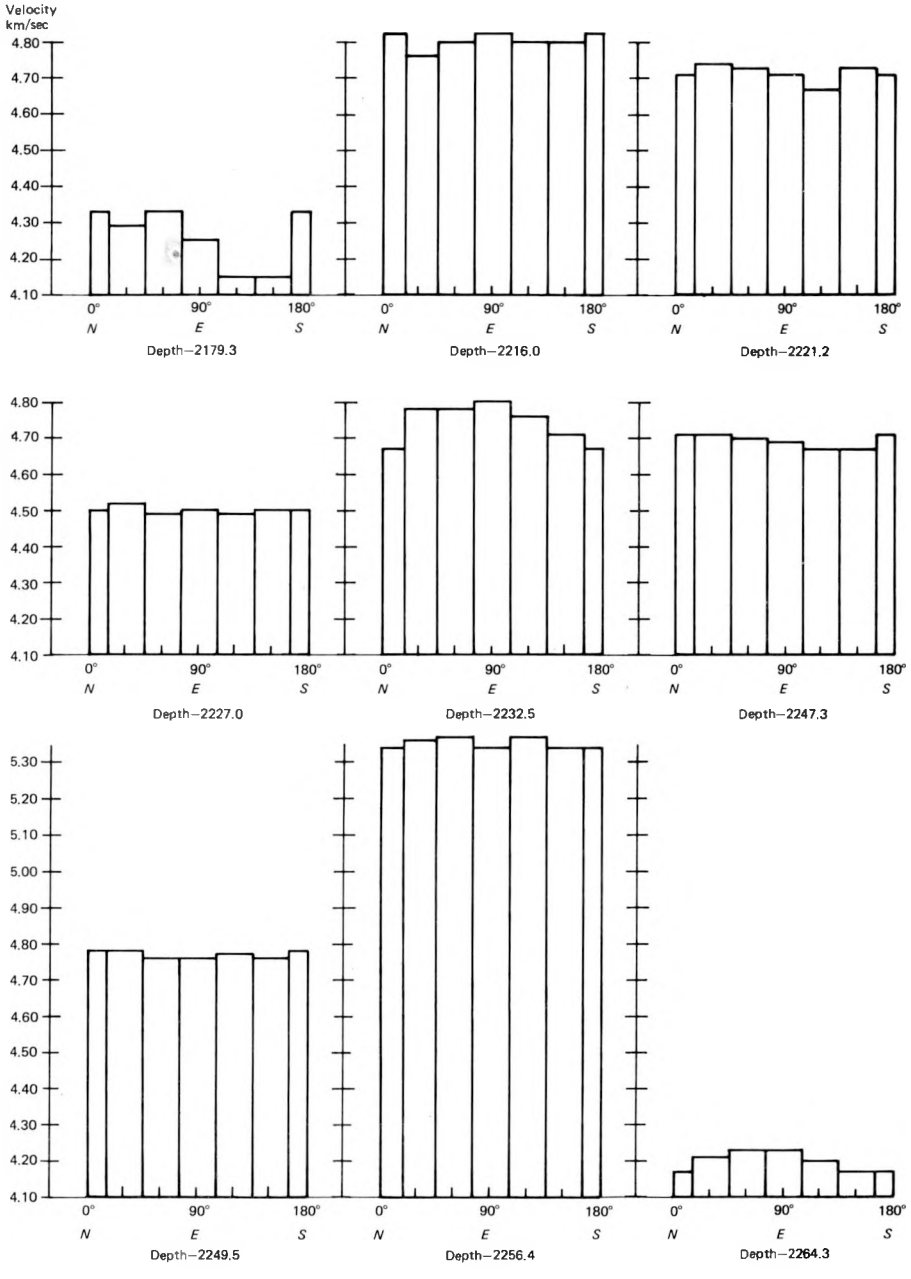


Figure 6. Ultrasonic compressional wave velocity parallel to bedding in cylindrical core specimens of New Albany Shale, Christian County, Kentucky.

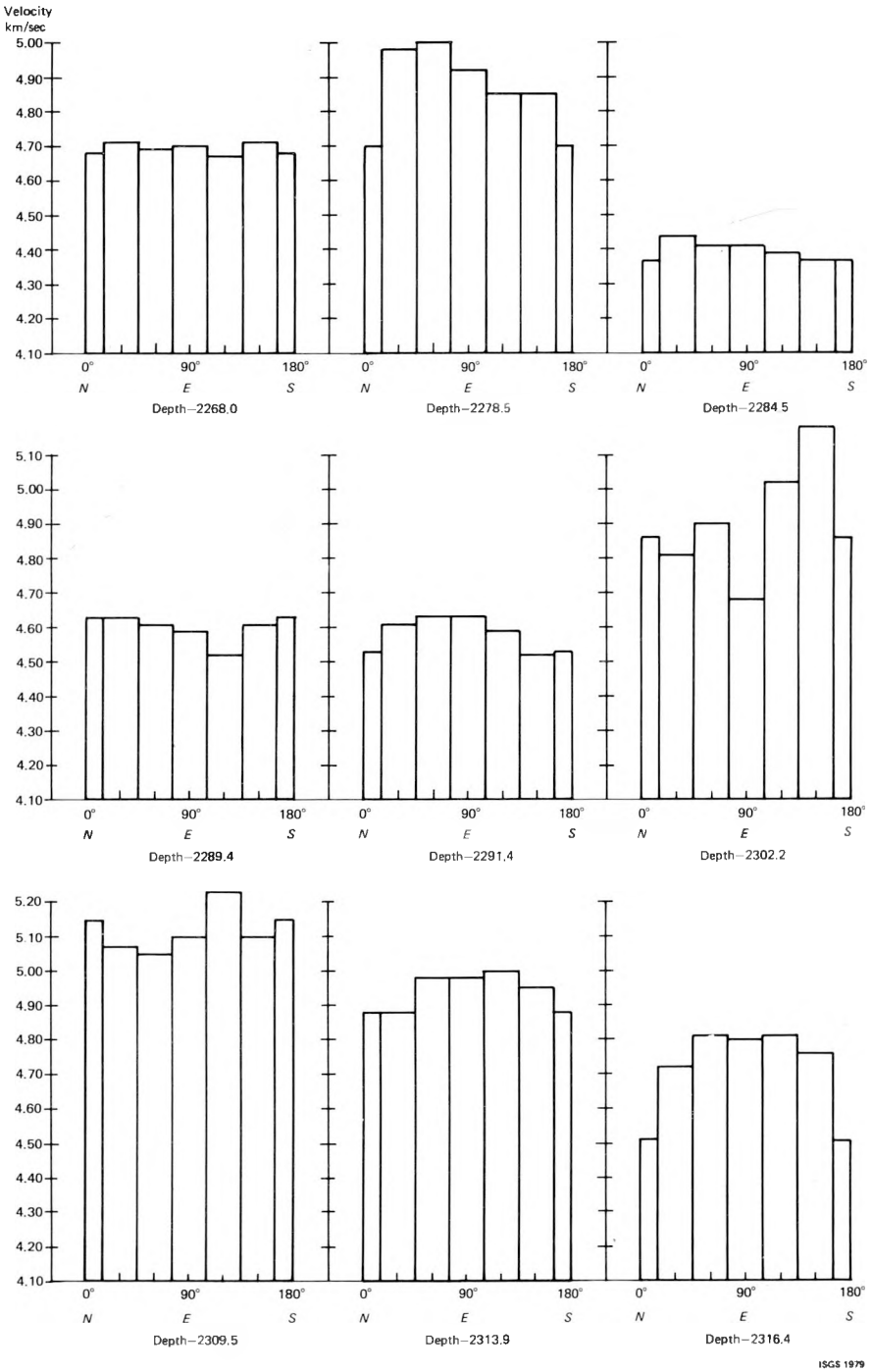
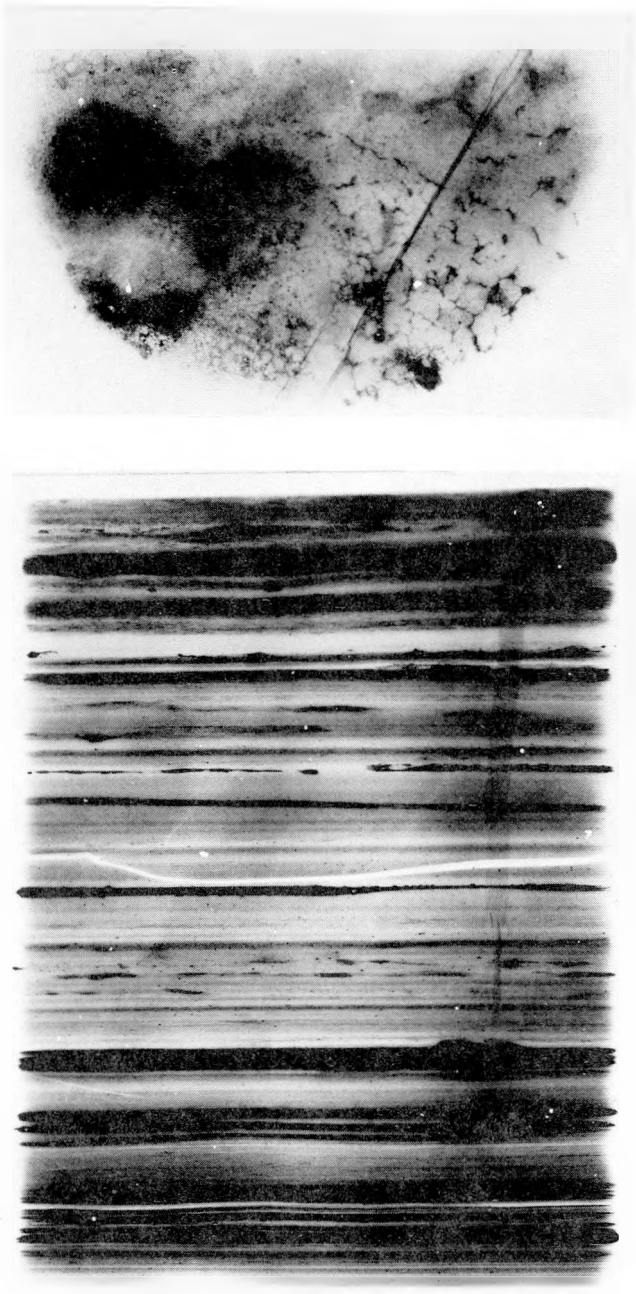


Figure 6. (*Continued*)



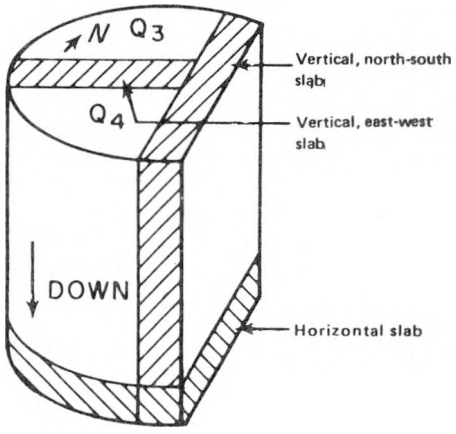


Figure 7. X-ray radiographs of sections of a core segment show a discontinuous mineralized natural fracture trending northwest-southeast. Pyrite is finely dispersed throughout the shale and is concentrated in irregular patches and nodules along coarser grain-size silt rich laminae (vertical section).

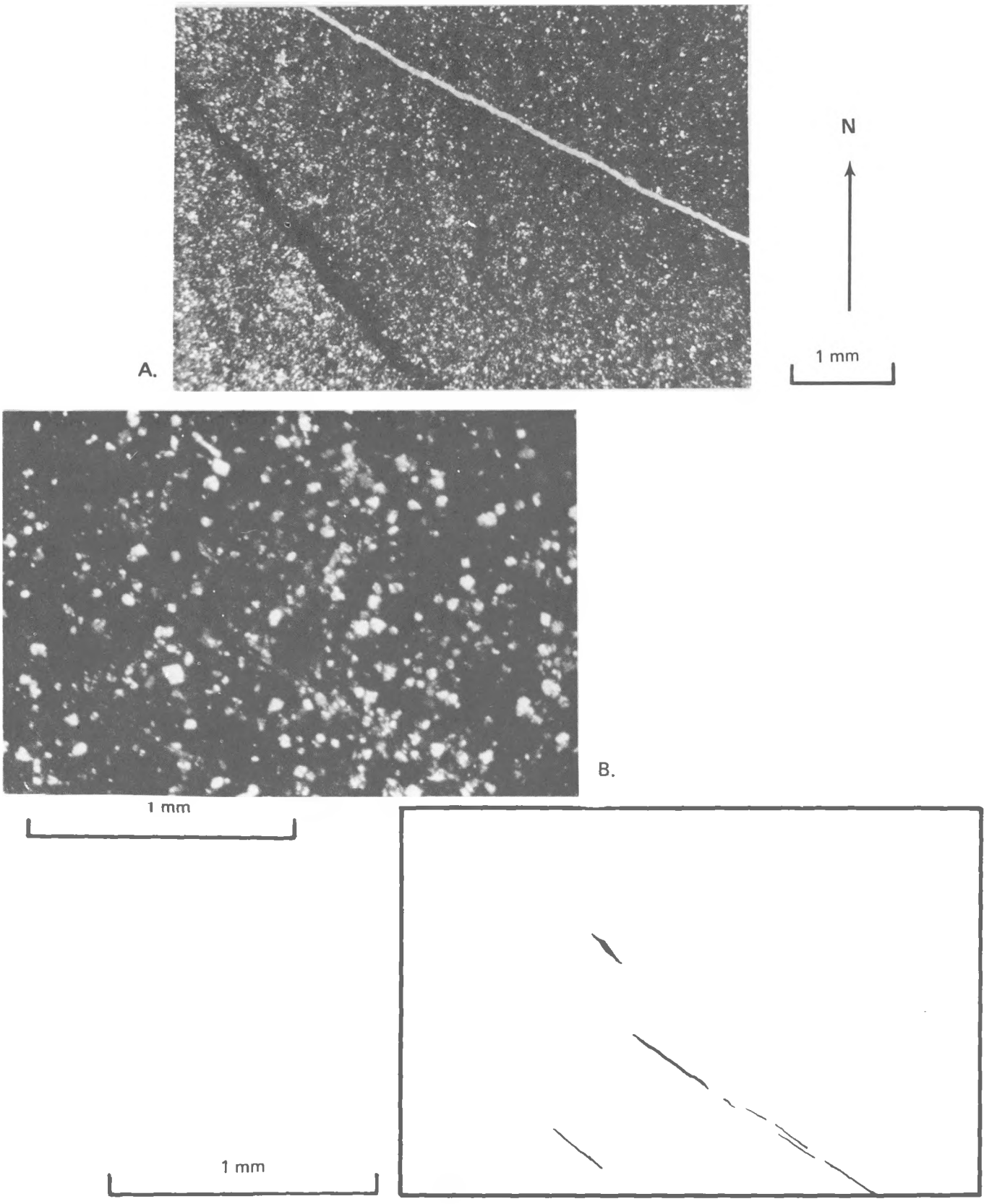


Figure 8. Photomicrographs of oriented microfractures observed in transmitted light sections cut parallel to bedding in New Albany Shale test core, Christian County, Kentucky. A) Pyrite (opaque) filled microfracture trending northwest subparallel to a calcite line natural fracture; depth is 2280 feet. B) Several microfractures show approximate distribution of these features; depth is 2318.9 feet. Accompanying sketch diagram indicates extent of fractures that may be difficult to see in the photomicrograph.

U.S. GOVERNMENT PRINTING OFFICE: 1979—640-092/ 1123